MECHANISMS OF CYTOKINESIS IN EUKARYOTES

EDITED BY: Issei Mabuchi, Fred Chang and Maria Grazia Giansanti
PUBLISHED IN: Frontiers in Cell and Developmental Biology

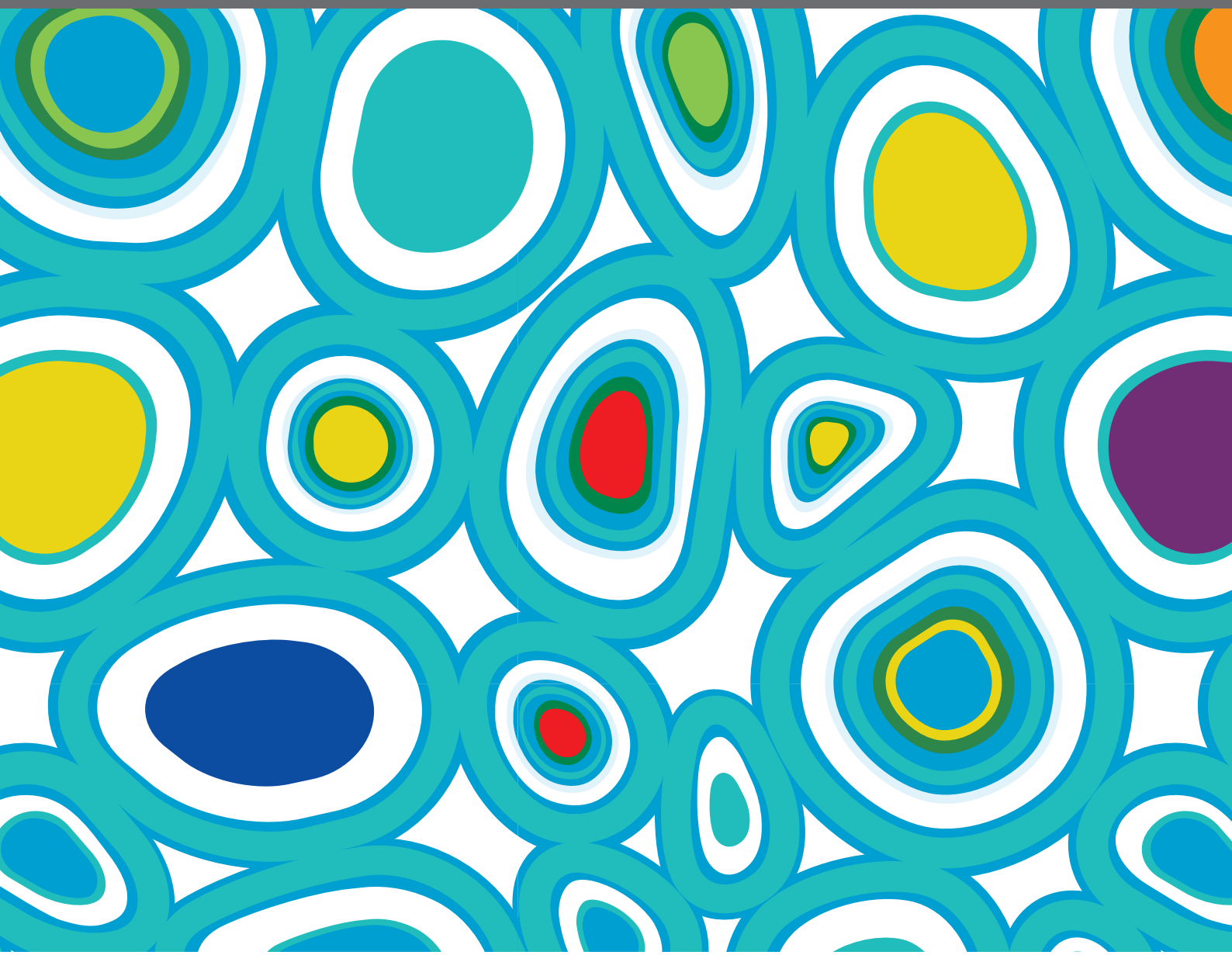

frontiers Research Topics

frontiers

ISSN 1664-8714
ISBN 978-2-88966-758-1
DOI 10.3389/978-2-88966-758-1

About Frontiers

Frontiers is more than just an open-access publisher of scholarly articles: it is a pioneering approach to the world of academia, radically improving the way scholarly research is managed. The grand vision of Frontiers is a world where all people have an equal opportunity to seek, share and generate knowledge. Frontiers provides immediate and permanent online open access to all its publications, but this alone is not enough to realize our grand goals.

Frontiers Journal Series

The Frontiers Journal Series is a multi-tier and interdisciplinary set of open-access, online journals, promising a paradigm shift from the current review, selection and dissemination processes in academic publishing. All Frontiers journals are driven by researchers for researchers; therefore, they constitute a service to the scholarly community. At the same time, the Frontiers Journal Series operates on a revolutionary invention, the tiered publishing system, initially addressing specific communities of scholars, and gradually climbing up to broader public understanding, thus serving the interests of the lay society, too.

Dedication to Quality

Each Frontiers article is a landmark of the highest quality, thanks to genuinely collaborative interactions between authors and review editors, who include some of the world's best academicians. Research must be certified by peers before entering a stream of knowledge that may eventually reach the public - and shape society; therefore, Frontiers only applies the most rigorous and unbiased reviews.
Frontiers revolutionizes research publishing by freely delivering the most outstanding research, evaluated with no bias from both the academic and social point of view. By applying the most advanced information technologies, Frontiers is catapulting scholarly publishing into a new generation.

What are Frontiers Research Topics?

Frontiers Research Topics are very popular trademarks of the Frontiers Journals Series: they are collections of at least ten articles, all centered on a particular subject. With their unique mix of varied contributions from Original Research to Review Articles, Frontiers Research Topics unify the most influential researchers, the latest key findings and historical advances in a hot research area! Find out more on how to host your own Frontiers Research Topic or contribute to one as an author by contacting the Frontiers Editorial Office: frontiersin.org/about/contact

MECHANISMS OF CYTOKINESIS IN EUKARYOTES

Topic Editors:
Issei Mabuchi, University of Tokyo, Japan
Fred Chang, University of California, San Francisco, United States
Maria Grazia Giansanti, Italian National Research Council, Italy

Citation: Mabuchi, I., Chang, F., Giansanti, M. G., eds. (2021). Mechanisms of Cytokinesis in Eukaryotes. Lausanne: Frontiers Media SA.
doi: 10.3389/978-2-88966-758-1

Table of Contents

frontiers in Cell and Developmental Biology

EDITORIAL
published: 19 March 2021
doi: 10.3389/fcell.2021.668705

Editorial: Mechanisms of Cytokinesis in Eukaryotes

Issei Mabuchi[1,2]*, *Maria Grazia Giansanti*[3] and *Fred Chang*[4]

[1] Department of Life Sciences, Graduate School of Arts and Sciences, The University of Tokyo, Tokyo, Japan, [2] Institute of Human Culture Studies, Otsuma Women's University, Tokyo, Japan, [3] Institute of Molecular Biology and Pathology, Italian National Research Council, Rome, Italy, [4] Department of Cell and Tissue Biology, University of California, San Francisco, San Francisco, CA, United States

Keywords: contractile ring, intercellular bridge, abscission, actin, myosin, Rho, Rac, ESCRT

Editorial on the Research Topic

Mechanisms of Cytokinesis in Eukaryotes

The study of cytokinesis, the final stages of cell division, is one of the most active fields in cell biology. This field encompasses investigations on a multitude of diverse cellular processes including cytoskeletal regulation, membrane dynamics, signaling, and cell mechanics, all studied using diverse approaches in model organisms ranging from bacteria and archaea to yeast, plants, and animal cells. This series of articles in Frontiers of Cell and Developmental Biology highlights recent process on our understanding of cytokinesis in eukaryotic cells.

Many eukaryotic cells divide by virtue of constriction of the acto-myosin based contractile ring (CR, **Figure 1**), which was discovered by Schroeder (1968, 1970) using electron microscopy in jellyfish eggs and HeLa cells. Myosin-II is the essential motor for cytokinesis in animal cells (Mabuchi and Okuno, 1977). In this issue, Wang et al. compare the functions of different myosin IIs in cytokinesis in budding yeast, fission yeast and human cells. Budding yeast myosin-II seems to form filaments at the division site, though *in vitro* assembly has not been reported so far. However, it is curious that MYO1 heads (motor domains) are dispensable for division in budding yeast. In fission yeast, the structure/function of the two myosin-IIs (the essential Myo2 and non-essential Myp2) and their roles in the formation and constriction of the CR have been extensively characterized. Myo2 has not been reported to form filaments. Mammalian cells express three non-muscle myosin-IIs (NM-IIA, IIB, and IIC) which all localize to the division site. They form filaments but NM-IIA filaments have recently been reported to form stacks during furrowing, presumably for effective force production (Fenix et al., 2016). Wang et al. claim that the furrowing has two stages. First, the furrow ingresses until it reaches a diameter of 1.5–2 μm (Wang et al., 2019). This process is driven by all the isoforms. Next, IIB causes further constriction to form the thin intercellular bridge that is resolved later by abscission (see below).

A key regulator for cytokinesis is the Rho GTPase, the first regulatory protein factor identified for CR formation (Kishi et al., 1993; Mabuchi et al., 1993). Carim et al. describe roles of two Rho-dependent cytokinetic networks, actin-myosin and anillin-septin networks, both of which are independently anchored to the plasma membrane. They describe a scenario of Rho-dependent formation and contraction of the CR. Specifically, they propose that, during closure of the ring at the point at which its tension reaches a threshold via ring contraction, a Rho-dependent elimination of the membrane microdomains anchored by anillin and septin occurs.

The Rac GTPase, another Rho family member, also contributes to cytokinesis. Pal et al. manipulate the activities of Rac and its effector Arp2/3 during mitotic divisions of early sea urchin embryos, where these factors are dispensable for cytokinesis, as well as in meiotic divisions of sea star oocytes that depend on these proteins for polar body extrusion. In both cases, expression of activated Rac produces an inhibitory effect on cytokinesis that is suppressed by an effector binding

Edited and reviewed by:
Philipp Kaldis,
Lund University, Sweden

***Correspondence:**
Issei Mabuchi
issei.mabuchi@gakushuin.ac.jp

Specialty section:
This article was submitted to Cell Growth and Division, a section of the journal Frontiers in Cell and Developmental Biology

Received: *17 February 2021*
Accepted: *18 February 2021*
Published: *19 March 2021*

Citation:
Mabuchi I, Giansanti MG and Chang F (2021) Editorial: Mechanisms of Cytokinesis in Eukaryotes. Front. Cell Dev. Biol. 9:668705. doi: 10.3389/fcell.2021.668705

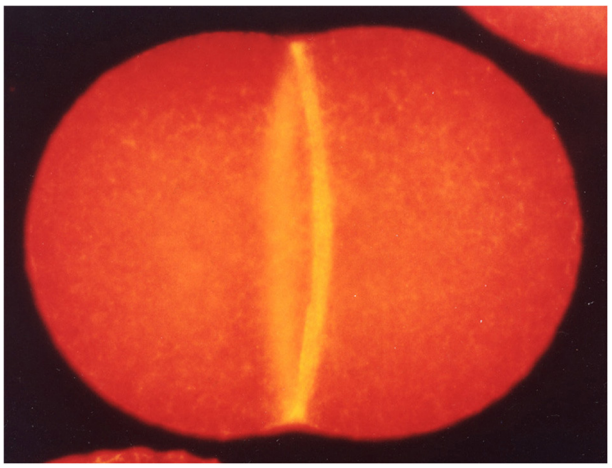

FIGURE 1 | A dividing sea urchin (*Hemicentrotus pulcherrimus*) egg fluorescently stained for F-actin to visualize the CR (Mabuchi, 2008).

mutation or direct inhibition of Arp2/3. These results indicate that the branched actin networks nucleated by Arp2/3 may act as a brake against Rho-dependent contractility at the cleavage site.

A number of mechanisms have been shown to drive contractile ring assembly in different cell types and contexts. In *C. elegans* embryos, cortical flow has been considered to be the main driver of CR formation (Reinann et al., 2016). However, a research article by Leite et al. provides evidence that this is not the case. Instead, they show that the actin filament cross-linker plastin plays a role in the assembly of the ring along with myosin-II.

Although a core set of conserved cytokinesis proteins has been extensively studied (Balasubramanian et al., 2004; Pollard and O'Shaughnessy, 2019), there are still new factors to be found. Nguyen and Robinson review recent discoveries showing proteins that have been implicated previously in other cellular functions also have unexpected roles in cytokinesis. These new cytokinesis players named "unusual suspects" include membrane associated proteins such as discoidin and intracellular chloride channels, RNA-related proteins, the nuclear proteins Importin β, Ran and Lamin B and metabolic enzymes. Investigation of these novel cytokinesis proteins will reveal new cross-talk and network integration and help complete the puzzle of this intricate process.

Successful cytokinesis involves a substantial increase of total surface area, which depends on membrane trafficking from internal stores. However, because of complex geometry of the plasma membrane in animal cells, this increase has been difficult to measure accurately. To eliminate the contribution of small surface membrane reservoirs, Tanaka et al. measure the total increase of surface area in dividing *Dictyostelium* cells flattened by an agar overlay method. Under these conditions, the total surface area increases during cytokinesis by about 20% through an imbalance between exocytosis and endocytosis. In contrast with previous reports, although clathrin-dependent endocytosis was suppressed during cell division, it did not contribute significantly to the changes of cell surface area.

Following the constriction of the CR, the final stage in animal cell cytokinesis is abscission, the process of physical separation of the daughter cells. This step, which can occur significantly after CR constriction, involves the scission of a midbody structure that is densely populated with microtubules and proteins involved in membrane trafficking. The endosomal sorting complex required for transport (ESCRT) pathway is a key factor for this abscission process (Carton and Martin-Serrano, 2007; Morita et al., 2007; Hurley and Hanson, 2010). Horváth and Müller-Reichert review the role of ESCRT in abscission from a structural point of view. Cryo-tomography of the midzone structure reveals the assembly of ESCRTs into remarkable spiral structures surrounding the dense midbody structure. Structural studies provide new insights into the molecular bases for their assembly and regulation of membrane curvature. This review discusses current models for how ESCRT ultimately contributes to membrane deformation and fusion to resolve the intercellular bridge structures.

The ESCRT machinery represents a primordial cytokinetic mechanism that pre-dates the actin-based contractile ring in the evolution of eukaryotes (Lindås et al., 2008; Samson et al., 2008). It mediates cytokinesis in some archaea and is likely to mediate cytokinesis in much of the eukaryotic tree. To test another branch of the tree, a research article from Yagisawa et al. reveals a role for ESCRT in the red algae *C. morelae*, which divides by furrow constriction but without myosin or septins. They show that ESCRT resides at the intercellular bridge, and provide initial evidence that it participates in abscission in this algal cell.

After abscission, the midbody in animal cells can persist as a midbody remnant in the next generation, where it has been shown to have post-mitotic functions such as polarity regulation and stem cell differentiation. This intriguing remnant structure may be internalized to function inside the cell, be released, or be degraded through autophagy. In a research article, Sardina et al. identify a new regulator of midbody remnant, a protein kinase HIPK2 that promotes the removal of the midbody remnant through autophagy.

In summary, this set of articles and reviews illustrates the impressive breadth of the current cytokinesis field in the investigations of the diverse molecular processes responsible for this essential process of cell division.

AUTHOR CONTRIBUTIONS

All authors contributed to both writing and editing the draft.

FUNDING

IM was supported by a grant-in-aid of the Fugaku Trust for Medicinal Research (2020). MGG was supported by a grant from the AIRC - Fondazione AIRC per la Ricerca sul Cancro (AIRC; #IG2017 Id.20779). FC was supported by an NIH grant #GM56836.

ACKNOWLEDGMENTS

We would like to thank the authors for their valuable contributions and the thought provoking manuscripts that they have produced.

REFERENCES

Balasubramanian, M., Bi, E., and Glotzer, M. (2004). Comparative analysis of cytokinesis in budding yeast, fission yeast and animal cells. *Curr. Biol.* 14, R806–818. doi: 10.1016/j.cub.2004.09.022

Carton, J. Z., and Martin-Serrano, J. (2007). Parallels between cytokinesis and retroviral budding: a role for the ESCRT machinery. *Science* 316, 1908–1912. doi: 10.1126/science.1143422

Fenix, A. M., Taneja, N., Buttler, C. A., Lewis, J., Van Engelenburg, S. B., Ohi, R., et al. (2016). Expansion and concatenation of non-muscle myosin IIA filaments drive cellular contractile system formation during interphase and mitosis. *Mol. Biol. Cell* 27, 1465–1478. doi: 10.1091/mbc.E15-10-0725

Hurley, J. H., and Hanson, P. I. (2010). Membrane budding and scission by the ESCRT machinery: it's all in the neck. *Nat. Rev. Mol. Cell Biol.* 11, 556–566. doi: 10.1038/nrm2937

Kishi, K., Sasaki, T., Kuroda, S., Itoh, T., and Takai, Y. (1993). Regulation of cytoplasmic division of *Xenopus* embryo by *rho* p21 and its inhibitory GDP/GTP exchange protein (*rho* GDI). *J. Cell Biol.* 120, 1188–1195. doi: 10.1083/jcb.120.5.1187

Lindås, A-C, Karlsson, E. A., Lindgren, M. T., Ettema, T. J. G., and Bernander, R. (2008). A unique cell division machinery in the Archaea. *Proc. Natl. Acad. Sci. U.S.A.* 105, 18942–18946. doi: 10.1073/pnas.0809467105

Mabuchi, I, (2008). My memorable photo: Fluorescence image of the contractile ring in a sea urchin egg. (written in Japanese). *Cell Technol.* 27, 209.

Mabuchi, I., Hamaguchi, Y., Fujimoto, H., Morii, N., Mishima, M., and Narumiya, S. (1993). A rho-like protein is involved in the organisation of the contractile ring in dividing sand dollar eggs. *Zygote* 1, 325–331. doi: 10.1017/S0967199400001659

Mabuchi, I., and Okuno, M. (1977). The effect of myosin antibody on the division of starfish blastomeres. *J. Cell Biol.* 74, 251–263. doi: 10.1083/jcb.74.1.251

Morita, E., Sandrin, V., Chung, H. Y., Morham, S. G., Gygi, S. P., Rodesch, C. K., et al. (2007). Human ESCRT and ALIX proteins interact with proteins of the midbody and function in cytokinesis. *EMBO J.* 26, 4215–4227. doi: 10.1038/sj.emboj.7601850

Pollard, T. D., and O'Shaughnessy, B. (2019). Molecular mechanism of cytokinesis. *Ann. Rev. Biochem.* 88, 661–689. doi: 10.1146/annurev-biochem-062917-012530

Reinann, A-C., Staniscia, F., Erzberger, A., Salbreux, G., and Grill, S. W. (2016). Cortical flow aligns actin filaments to form a furrow. *eLife* 5:e17807. doi: 10.7554/eLife.17807

Samson, R. Y., Obita, T., Freund, S. M., Williams, R. L., and Bell, S. D. (2008). A role for the ESCRT system in cell division in Archaea. *Science* 322, 1710–1713. doi: 10.1126/science.1165322

Schroeder, T. E. (1968). Cytokinesis: filaments in the cleavage furrow. *Exptl. Cell Res.* 53, 272–276. doi: 10.1016/0014-4827(68)90373-X

Schroeder, T. E. (1970). The contractile ring. I. Fine structure of dividing mammalian (HeLa) cells and the effects of cytochalasin B. *Z. Zellforsch. Mikrosk. Anat.* 109: 431–449. doi: 10.1007/BF00343960

Wang, K., Wloka, C., and Bi, E. (2019). Non-muscle myosin-II is required for the generation of a constriction site for subsequent abscission. *iScience* 13, 69–81. doi: 10.1016/j.isci.2019.02.010

Conflict of Interest: The authors declare that the research was conducted in the absence of any commercial or financial relationships that could be construed as a potential conflict of interest.

frontiers in Cell and Developmental Biology

ORIGINAL RESEARCH
published: 03 April 2020
doi: 10.3389/fcell.2020.00169

ESCRT Machinery Mediates Cytokinetic Abscission in the Unicellular Red Alga *Cyanidioschyzon merolae*

Fumi Yagisawa[1,2†], Takayuki Fujiwara[3,4,5†], Tokiaki Takemura[6,7], Yuki Kobayashi[6], Nobuko Sumiya[3‡], Shin-ya Miyagishima[3,4,5], Soichi Nakamura[8], Yuuta Imoto[9], Osami Misumi[10,11], Kan Tanaka[6], Haruko Kuroiwa[12] and Tsuneyoshi Kuroiwa[12]*

[1] Center for Research Advancement and Collaboration, University of the Ryukyus, Okinawa, Japan, [2] Graduate School of Engineering and Science, University of the Ryukyus, Okinawa, Japan, [3] Department of Gene Function and Phenomics, National Institute of Genetics, Shizuoka, Japan, [4] JST-Mirai Program, Japan Science and Technology Agency, Saitama, Japan, [5] Department of Genetics, The Graduate University for Advanced Studies, Shizuoka, Japan, [6] Laboratory for Chemistry and Life Science, Institute of Innovative Research, Tokyo Institute of Technology, Yokohama, Japan, [7] School of Life Sciences and Technology, Tokyo Institute of Technology, Yokohama, Japan, [8] Laboratory of Cell and Functional Biology, Faculty of Science, University of the Ryukyus, Okinawa, Japan, [9] Department of Cell Biology, Johns Hopkins University School of Medicine, Baltimore, MD, United States, [10] Department of Biological Science and Chemistry, Faculty of Science, Yamaguchi University, Yamaguchi, Japan, [11] Graduate School of Sciences and Technology for Innovation, Yamaguchi University, Yamaguchi, Japan, [12] Department of Chemical and Biological Science, Japan Women's University, Tokyo, Japan

OPEN ACCESS

Edited by:
Issei Mabuchi,
University of Tokyo, Japan

Reviewed by:
Jez Carlton,
King's College London, United Kingdom
Natalie Elia,
Ben-Gurion University of the Negev, Israel

***Correspondence:**
Fumi Yagisawa
yagisawa@lab.u-ryukyu.ac.jp

[†] These authors have contributed equally to this work

[‡] **Present address:**
Nobuko Sumiya,
Department of Biology, Keio University, Yokohama, Japan

Specialty section:
This article was submitted to Cell Growth and Division, a section of the journal Frontiers in Cell and Developmental Biology

Received: 22 October 2019
Accepted: 29 February 2020
Published: 03 April 2020

Citation:
Yagisawa F, Fujiwara T, Takemura T, Kobayashi Y, Sumiya N, Miyagishima S, Nakamura S, Imoto Y, Misumi O, Tanaka K, Kuroiwa H and Kuroiwa T (2020) ESCRT Machinery Mediates Cytokinetic Abscission in the Unicellular Red Alga Cyanidioschyzon merolae. Front. Cell Dev. Biol. 8:169. doi: 10.3389/fcell.2020.00169

In many eukaryotes, cytokinesis proceeds in two successive steps: first, ingression of the cleavage furrow and second, abscission of the intercellular bridge. In animal cells, the actomyosin contractile ring is involved in the first step, while the endosomal sorting complex required for transport (ESCRT), which participates in various membrane fusion/fission events, mediates the second step. Intriguingly, in archaea, ESCRT is involved in cytokinesis, raising the hypothesis that the function of ESCRT in eukaryotic cytokinesis descended from the archaeal ancestor. In eukaryotes other than in animals, the roles of ESCRT in cytokinesis are poorly understood. To explore the primordial core mechanisms for eukaryotic cytokinesis, we investigated ESCRT functions in the unicellular red alga *Cyanidioschyzon merolae* that diverged early in eukaryotic evolution. *C. merolae* provides an excellent experimental system. The cell has a simple organelle composition. The genome (16.5 Mb, 5335 genes) has been completely sequenced, transformation methods are established, and the cell cycle is synchronized by a light and dark cycle. Similar to animal and fungal cells, *C. merolae* cells divide by furrowing at the division site followed by abscission of the intercellular bridge. However, they lack an actomyosin contractile ring. The proteins that comprise ESCRT-I–IV, the four subcomplexes of ESCRT, are partially conserved in *C. merolae*. Immunofluorescence of native or tagged proteins localized the homologs of the five ESCRT-III components [charged multivesicular body protein (CHMP) 1, 2, and 4–6], apoptosis-linked gene-2-interacting protein X (ALIX), the ESCRT-III adapter, and the main ESCRT-IV player vacuolar protein sorting (VPS) 4, to the intercellular bridge. In addition, ALIX was enriched around the cleavage furrow early in cytokinesis. When the ESCRT function was

perturbed by expressing dominant-negative VPS4, cells with an elongated intercellular bridge accumulated—a phenotype resulting from abscission failure. Our results show that ESCRT mediates cytokinetic abscission in *C. merolae*. The fact that ESCRT plays a role in cytokinesis in archaea, animals, and early diverged alga *C. merolae* supports the hypothesis that the function of ESCRT in cytokinesis descended from archaea to a common ancestor of eukaryotes.

Keywords: ESCRT, cytokinesis, cytokinetic abscission, red alga, *Cyanidioschyzon merolae*

INTRODUCTION

Cytokinesis is a fundamental biological phenomenon in all organisms. However, in eukaryotes the mechanisms are diverse. A significant difference exists between a group of animals, fungi, and Amoebozoa (Amorphea; Burki, 2014) and the other groups (Excavates and Diaphoretickes) (**Figure 1A**). Cells of Amorphea generally divide depending on constriction of the contractile ring (Pollard, 2017; **Figure 1A**), whereas those of other eukaryotic groups lack myosin-II, an essential ring component (Mishra et al., 2013; **Figure 1A**). The mechanism of cytokinesis has varied further in each group during evolution. One example is the cytokinesis of land plants whose cells divide by developing cell walls and membranes from the cell center toward the cell periphery (Muller and Jurgens, 2016). Our current knowledge of cytokinesis mostly depends on a limited number of model organisms. However, the mechanisms in different lineages warrant exploration to reveal the eukaryotic history and the core mechanisms of cytokinesis shared by eukaryotes.

In mammalian cells, cytokinesis proceeds by equatorial membrane furrowing followed by abscission of the intercellular bridge. The contractile ring containing actomyosin and septin filaments constricts to furrow the membrane (Green et al., 2012). As the ring closes, the midbody, the platform for the abscission machinery where the plus and minus ends of spindle microtubules overlap, is formed. The actin-capping protein that controls actin polymerization is required for the process (Terry et al., 2018). The intercellular bridge contains the spindle midzone microtubules and midbody. The septin filaments are reorganized into rings in the early intercellular bridge to assist bridge maturation (Renshaw et al., 2014; Karasmanis et al., 2019).

The endosomal sorting complex required for transport (ESCRT), a protein complex conserved among eukaryotes (**Table 1**), contributes to various membrane fusion/fission events such as multivesicular body formation at late endosomes and nuclear envelope fusion (Campsteijn et al., 2016; Schoneberg et al., 2017). In mammalian cells, ESCRT mediates scission of the intercellular bridge (Carlton and Martin-Serrano, 2007; Morita et al., 2007; Elia et al., 2011; Guizetti et al., 2011; Campsteijn et al., 2016; Schoneberg et al., 2017). The proteins comprising ESCRT-I–IV, the four subcomplexes of ESCRT, are sequentially targeted to the midbody. ESCRT-I recruits charged multivesicular body protein (CHMP) 4 in ESCRT-III by binding to CHMP6 in ESCRT-III by itself or through ESCRT-II (Christ et al., 2016). CHMP6 is a nucleation factor for ESCRT-III. A recent study showed that Septin (SEPT) 9, a constituent of the septin ring, associates with the ESCRT-I protein tumor susceptibility gene (TSG) 101 to assist the recruitment of ESCRT-II and demarcate the sites for ESCRT-III assembly (Karasmanis et al., 2019). The septin ring disassembles as ESCRT-III machinery develops (Karasmanis et al., 2019). In addition to ESCRT-I, the ESCRT-III adaptor protein apoptosis-linked gene-2-interacting protein X (ALIX) localizes at the midbody to separately recruit CHMP4 without binding to CHMP6 (Christ et al., 2016).

ESCRT-III consists of CHMP family proteins, which are homologous to each other, and increased sodium tolerance (IST) 1 (**Table 1**). They are coiled-coil proteins suggested to polymerize into spiral filaments beneath the intercellular bridge membrane to narrow abscission sites adjacent to the midbody (Guizetti et al., 2011; Mierzwa et al., 2017; Goliand et al., 2018). ESCRT-III also recruits the microtubule-severing enzyme spastin (Yang et al., 2008; Connell et al., 2009). The intercellular bridge is cleaved after the arrival of vacuolar protein sorting (VPS) 4, the AAA-ATPase in ESCRT-IV, which regulates the turnover of ESCRT-III assembly (Carlton and Martin-Serrano, 2007; Morita et al., 2007; Elia et al., 2011; Schuh and Audhya, 2014; Mierzwa et al., 2017).

ESCRT possibly represents conserved machinery in eukaryotic cytokinesis inherited from the archaeal ancestor. In *Sulfolobus*, a thermophile archaeon, homologs of ESCRT-III proteins and VPS4, and the ESCRT-III scaffold cell division protein (Cdv) A are detected between daughter nucleoids of dividing cells, correlating with the site of membrane ingression (**Table 1**; Lindas et al., 2008; Samson et al., 2008, 2011; Liu et al., 2017). They are necessary for cytokinesis from early to final stages. Whereas ESCRT-dependent cytokinesis is not universal in archaea (Makarova et al., 2010), recent studies support that eukaryotes have diverged from archaea encoding ESCRT (Zaremba-Niedzwiedzka et al., 2017; **Table 1**). However, in eukaryotes other than in animals, whether ESCRT mediates cytokinetic abscission is poorly understood. In the land plant *Arabidopsis thaliana*, *elc* mutation, a mutation of TSG101, results in the production of multinucleated cells (Spitzer et al., 2006). Although the mechanism underlying induction of the phenotype is unclear, it may reflect conserved functions of ESCRT in eukaryotic cytokinetic abscission. Some similarities between the animal midbody and plant phragmoplasts, arrays of microtubules on the division plane, have been indicated in a previous study (Otegui et al., 2005).

Because ESCRT is a conserved multifunctional complex, the presence of ESCRT genes in the genome does not necessarily suggest its involvement in cytokinesis. To determine whether ESCRT is primordial core machinery

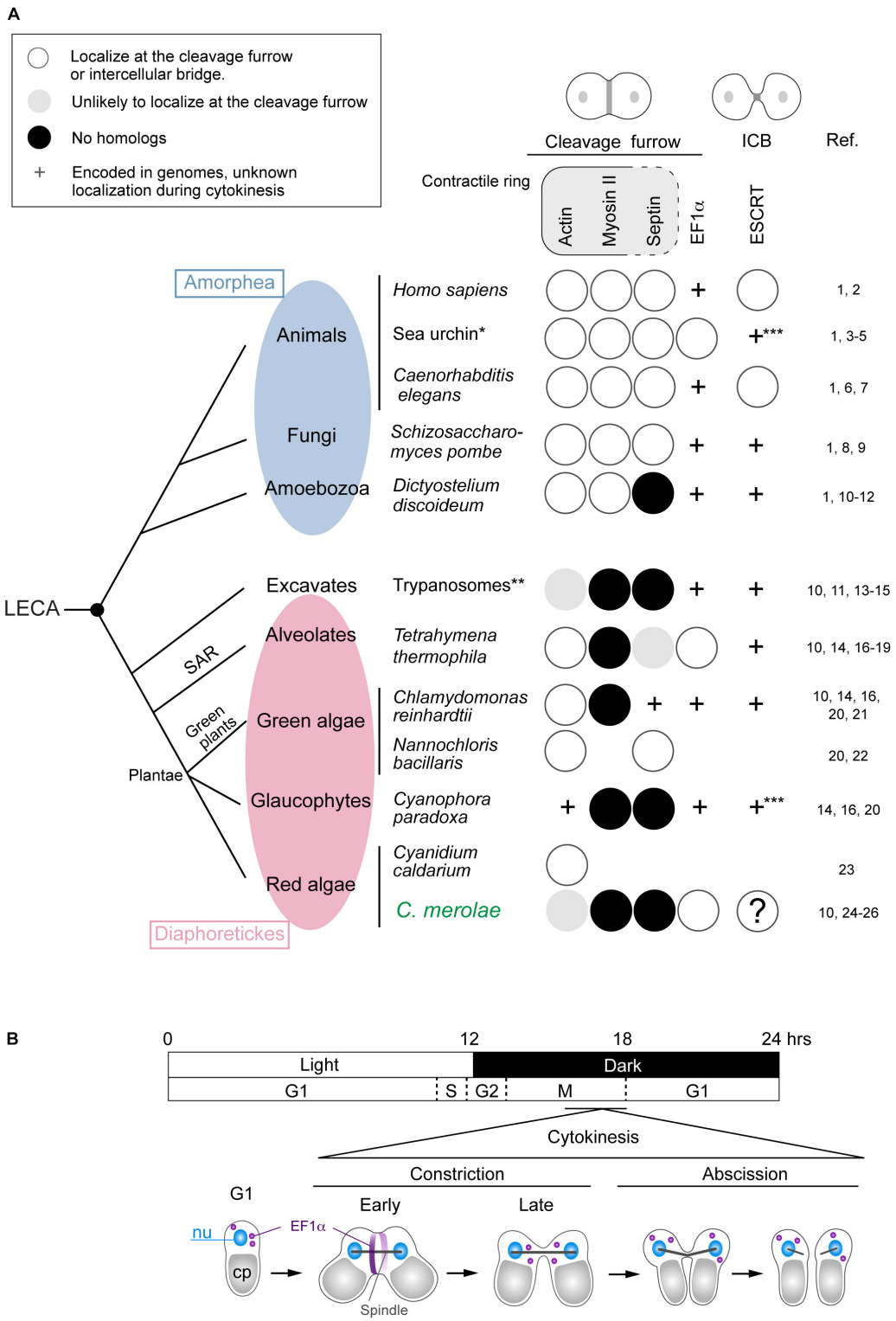

FIGURE 1 | Distribution of representative proteins in the contractile ring, EF1α, and ESCRT in eukaryotes that divide centripetally and a scheme for *C. merolae* cytokinesis. **(A)** The phylogenetic tree is based on Burki (2014). Branch length does not represent evolutionary distance. Amorphea generally divide depending on the actomyosin contractile ring. Other eukaryotes lack myosin-II, an essential component of the contractile ring. Septins are part of the contractile ring in animal cells, whereas in fungal cells, they form separate ring structures. Some contractile ring components are found in the intercellular bridge (ICB), which is not depicted in the figure. Protein localization (to the cleavage furrow or intercellular bridge) or the presence of genes in species were investigated by literature and/or BLAST searching.

(Continued)

FIGURE 1 | Continued
BLAST searching was conducted using the following protein sequences as the query: *Saccharomyces cerevisiae* Act1 for *C. paradoxa* actin, *Saccharomyces cerevisiae* septins (Cdc3, Cdc10, Cdc11, Cdc12, and Shs1) for *C. merolae* septins, *S. cerevisiae* Tef1 for EF1α in the species with " + " marks in the EF1α column, and *S. cerevisiae* Vps2 and Vps4 for ESCRT in sea urchin and *Cyanophora*. References are listed on the right: 1, Pollard, 2017; 2, Campsteijn et al., 2016; 3, Fujimoto and Mabuchi, 2010; 4, Henson et al., 2017; 5, Otto and Schroeder, 1990; 6, Carvalho et al., 2009; 7, Green et al., 2013; 8, Iwaki et al., 2007; 9, Wu et al., 2010; 10, Leung et al., 2008; 11, Nishihama et al., 2011; 12, Reichl et al., 2008; 13, Garcia-Salcedo et al., 2004; 14, Sebe-Pedros et al., 2014; 15, Zhou et al., 2014; 16, Pasha et al., 2016; 17, Hosein et al., 2003; 18, Numata et al., 2000; 19, Wloga et al., 2008; 20, Yamazaki et al., 2013; 21, Cross and Umen, 2015; 22, Yamamoto et al., 2007; 23, Suzuki et al., 1995; 24, Imoto et al., 2011; 25, Matsuzaki et al., 2004; 26, Takahashi et al., 1995. *Information from several sea urchin species, including *Strongylcentrotus purpuratus* and *Hemicentrotus pulcherrimus*, was combined. **Information from *Trypanosoma brucei* and *Trypanosoma cruzi*. ***Both Vps2 and Vps4 homologs were found. Blank, the genome information is unavailable or incomplete. LECA, the last eukaryotic common ancestor. **(B)** A 12 h/12 h light and dark cycle synchronized *C. merolae* cell division. Cytokinesis occurs in the dark period after the nuclear division. EF1α accumulates at the cleavage furrow in the early constriction stage and becomes dispersed in the late constriction stage. Cleavage of the intercellular stage occurs at the abscission stage.

TABLE 1 | Major ESCRT and ESCRT-associated proteins in eukaryotes and archaea.

	Eukaryotes			Archaea		
	Mammals	***Saccharomyces cerevisiae***	***C. merolae***	***Sulfolobus acidocaldarius***	***Sulfolobus islandicus***	**Asgard archaea**
ESCRT-I	TSG101	Vps23	**TSG101/CMK136C**			+ (Steadiness box)
	VPS28*	Vps28	VPS28/CMN120C			+
	VPS37A–D	Vps37	-			
	MVB12A, B	Mvb12	-			
ESCRT-II	EAP20	Vps25	EAP20/CMM195C			+
	EAP30*	Vps22	EAP30/CMO296C			+ (Vps22/36-like)
	EAP45	Vps36	-			
ESCRT-III	CHMP1A, B	Did2/Vps46	**CHMP1/CMQ376C**	CHMP-like:	CHMP-like:	+ (Vps2/24/46-like)
			CHMP1/CMR340C	CdvB,	ESCRT-III,	
	CHMP2A, B	Vps2	**CHMP2/CMB008C**	Saci_0451,	ESCRT-III-1,	
	CHMP3	Vps24	-	Saci_1416,	ESCRT-III-2,	
	CHMP4A-C	Vps32/Snf7	**CHMP4/CMI044C**	Saci_1601	ESCRT-III-3	+ (Vps20/32/60-like)
	CHMP5	Vps60	**CHMP5/VIG1/CML153C**			
	CHMP6	Vps20	**CHMP6/CMQ184C**			
	CHMP7	-	-			
	IST1	Ist1	-			
ESCRT-IV	VPS4A, B	Vps4	**VPS4/CMO281C**	Vps4/CdvC	Vps4/CdvC	+
	LIP5	Vta1	LIP5/CMI268C			
ALIX	ALIX	Bro1	**ALIX/CMC051C**			+ (Bro1 domain)
CdvA	-	-	-	CdvA	CdvA	

*The list of proteins in mammals and S. cerevisiae excluding CdvA is based on Schuh and Audhya (2014). In the C. merolae genome, ESCRT and ALIX homologs were searched by BLAST using S. cerevisiae sequences as queries. The results for ESCRT homologs were consistent with those of Leung et al. (2008). CdvA homologs in eukaryotes were searched by BLAST using the S. acidocaldarius sequence as a query. "–" no detectable homologs. The information of Sulfolobus is based on Lindas et al. (2008); Samson et al. (2008), and Liu et al. (2017). Both Sulfolobus species have four CHMP family proteins. It is unclear which eukaryotic CHMP protein is the closest. "+" indicates that the homologous sequence is present in the genomes of "Asgard" archaea, the group proposed to be the closest to eukaryotes (Zaremba-Niedzwiedzka et al., 2017). Blank indicates that the protein or gene is not mentioned in the above results. Underlined proteins localize at the midbody or intercellular bridge (mammals) or between daughter nucleoids (Sulfolobus). The references are in this legend or the text. *VPS28 and EAP30 are required for midbody localization of TSG101 and EAP20, respectively (Christ et al., 2016). Proteins in bold font were examined in this study.*

for eukaryotic cytokinesis, we explored ESCRT functions in the acidothermophilic unicellular red alga *Cyanidioschyzon merolae* that branched early in eukaryotic evolution (Yoon et al., 2004, 2006). In addition to the phylogenetical position, *C. merolae* provides an excellent experimental system. The cell (∼2 μm in diameter) has a simple structure (Kuroiwa, 1998). The genome (16.5 Mb, 5335 genes) has been completely sequenced (Matsuzaki et al., 2004; Nozaki et al., 2007). Genetic transformation is feasible (Ohnuma et al., 2008; Fujiwara et al., 2013), and a light and dark cycle highly synchronizes cell cycle progression and thus the timing of cytokinesis in a population (Suzuki et al., 1994; **Supplementary Figure S1A**).

Unlike other algae and plants, *C. merolae* does not have a rigid cell wall. It divides through membrane furrowing at the equator (constriction stage) that takes several minutes, followed by scission of the intercellular bridge (abscission stage), a stage that completes within a minute (**Figure 1B**; **Supplementary Figures S1A,B**). *C. merolae* lacks the actomyosin contractile ring and septins (**Figure 1A**). The actin gene does not seem to be expressed

in *C. merolae*, and staining with phalloidin, which detects F-actin, is negative (Suzuki et al., 1995; Takahashi et al., 1995; Matsuzaki et al., 2004). Moreover, no myosin heavy chain gene or septin genes are present in the *C. merolae* genome (Matsuzaki et al., 2004). The only protein that has been linked to *C. merolae* cytokinesis is elongation factor (EF) 1α, which accumulates at the cleavage furrow (**Figure 1B**, **Supplementary Figure S2**; Imoto et al., 2011), as observed in *Tetrahymena* (Numata et al., 2000) and sea urchin eggs (Fujimoto and Mabuchi, 2010). Sea urchin EF1α bundles actin filaments and maintains the contractile ring structure (Fujimoto and Mabuchi, 2010). However, in *C. merolae*, actin filaments are probably absent and thus the function of EF1α in cytokinesis is unclear.

In this study, we investigated localization of ESCRT proteins in *C. merolae* by immunofluorescence and examined the effects of a dominant-negative mutant of VPS4 on cytokinesis. Five homologs of ESCRT-III proteins (CHMP1, CHMP2, and CHMP4–6), ALIX, and VPS4 localized at the intercellular bridge before cytokinetic abscission. ALIX also located close to the cleavage furrow early in the constriction stage. The expression of mutant VPS4 caused abscission failure, indicating that ESCRT mediates cytokinetic abscission in *C. merolae*.

RESULTS

The *C. merolae* genome encodes homologs for 11 ESCRT proteins and ALIX (**Table 1**). We refer to these homologs according to the names of mammalian proteins except for the homolog of mammalian CHMP5, CHMP5/VIG1 (Vacuolar inheritance gene 1), which was previously characterized in *C. merolae* (Fujiwara et al., 2010; Yagisawa et al., 2018). To understand ESCRT functions in cytokinesis, we first examined the localization of ESCRT-III, the structure most directly involved in membrane deformation. We labeled CHMP2 using specific antibodies (**Supplementary Figure S3A**). In a synchronized culture under a light-dark cycle, the protein was expressed throughout the cell cycle with an increased level during the dark period (**Supplementary Figure S3B**). Immunofluorescence showed that CHMP2 localized on the punctate cytoplasmic structures and intercellular bridge of cytokinesis (**Figure 2A**). Next, we examined whether other ESCRT-III components localize with CHMP2 at the intercellular bridge using strains that ectopically expressed proteins fused to hemagglutinin (HA)-tags. *C. merolae* encodes two CHMP1 homologs (CMR340C and CMQ376C; **Table 1**). CHMP1-HA (CMR340C) localized at the intercellular bridge with CHMP2 (**Figure 2B**). CHMP1-HA (CMQ376C) was not expressed consistently with the lack of the expressed sequence tag (EST) of the native gene (data not shown; Matsuzaki et al., 2004). CHMP4-HA, CHMP5/VIG1-HA, and CHMP6-HA localized at the intercellular bridge with CHMP2 (**Figure 2B**).

To further examine the involvement of ESCRT in *C. merolae* cytokinesis, we detected the localization TSG101, a major component of ESCRT-I, and ALIX. TSG101-HA was detected on the cytoplasmic puncta, but not on the intercellular bridge (**Figure 3A**). Although we also tested N-terminally tagged HA-TSG101, it was not expressed (data not shown). In contrast to TSG101, FLAG-tagged ALIX localized to the intercellular bridge (**Figure 3B** and **Supplementary Figures S4A,B**). During early constriction, ALIX-FLAG also located around the cleavage furrow (**Figures 3C,D** and **Supplementary Figures S4A,B**). The signals partially overlapped with those of EF1α (**Figures 3C,D**). In the other stages (G1, M, and late constriction), ALIX-FLAG was mainly localized close to the cell membrane and on some cytoplasmic structures (**Supplementary Figures S4A,B**).

Our attempts to knock out some ESCRT genes were unsuccessful, suggesting that ESCRT disruption is lethal in *C. merolae*. An ATPase-inactive dominant-negative mutant of VPS4 blocks cytokinetic abscission in mammalian cells (Carlton and Martin-Serrano, 2007; Morita et al., 2007). To further clarify the role of ESCRT in cytokinesis, we expressed the corresponding mutant VPS4 (E292Q) in *C. merolae* cells.

When expressed under control of the native promoter sequence, VPS4-HA localized on the intercellular bridge (**Figure 4A**). To assess the effect of the mutation on cytokinesis, wild-type (^{WT}) or the mutant (^{E292Q}) *VPS4-HA* were expressed under the control of a heat-inducible promoter in the synchronized culture. The cells were subjected to heat treatments at the beginning of the dark period (G2/M phase, as shown in **Figures 1B**, **4B,C**). VPS4^{WT}-HA cells completed cell division in 12 h after the onset of heat shock, which was similar to untreated cells (**Figures 4D,E**). In contrast, induction of VPS4^{E292Q}-HA accumulated cells with notably elongated intercellular bridges (**Figures 4D,F–H**). Most of these long intercellular bridges were spanned by the spindle (**Figure 5A**) and positive for VPS4^{E292Q}-HA and CHMP2 (**Figure 5B**).

DISCUSSION

ESCRT potentially represents a component of the most ancient conserved machinery for cytokinetic abscission in eukaryotes. However, little is known about such ESCRT functions in eukaryotes other than in animals. In this study, we revealed that ESCRT is an essential component for cytokinetic abscission in *C. merolae*, an early diverged eukaryote.

We found that five ESCRT-III proteins, CHMP1 (CMR340C), CHMP2, CHMP4, CHMP5/VIG1, and CHMP6, localized at the intercellular bridge of *C. merolae* (**Figures 6A,B**). In mammalian cells, CHMP1–6, including its isoforms (Carlton and Martin-Serrano, 2007; Morita et al., 2007, 2010; Dukes et al., 2008; Yang et al., 2008; Bajorek et al., 2009; Elia et al., 2011; Guizetti et al., 2011; Carlton et al., 2012; Goliand et al., 2014; Christ et al., 2016), and IST1 (Agromayor et al., 2009; Goliand et al., 2018) localize at the midbody. *C. merolae* is devoid of genes encoding CHMP3 and IST1. In addition, ESCRT-III genes, except for *CHMP1*, exist as a single copy. Thus, ESCRT-III machinery in *C. merolae* is simpler in terms of protein composition. Electron microscopy has shown that mammalian ESCRT-III proteins either form or assist in forming a spiral of 17 nm-diameter filaments underlying the intercellular bridge membrane (Guizetti et al., 2011; Mierzwa et al., 2017; Schoneberg et al., 2017). The identification of such a structure is challenging in *C. merolae* because of the short duration of the abscission stage and small size of the intercellular

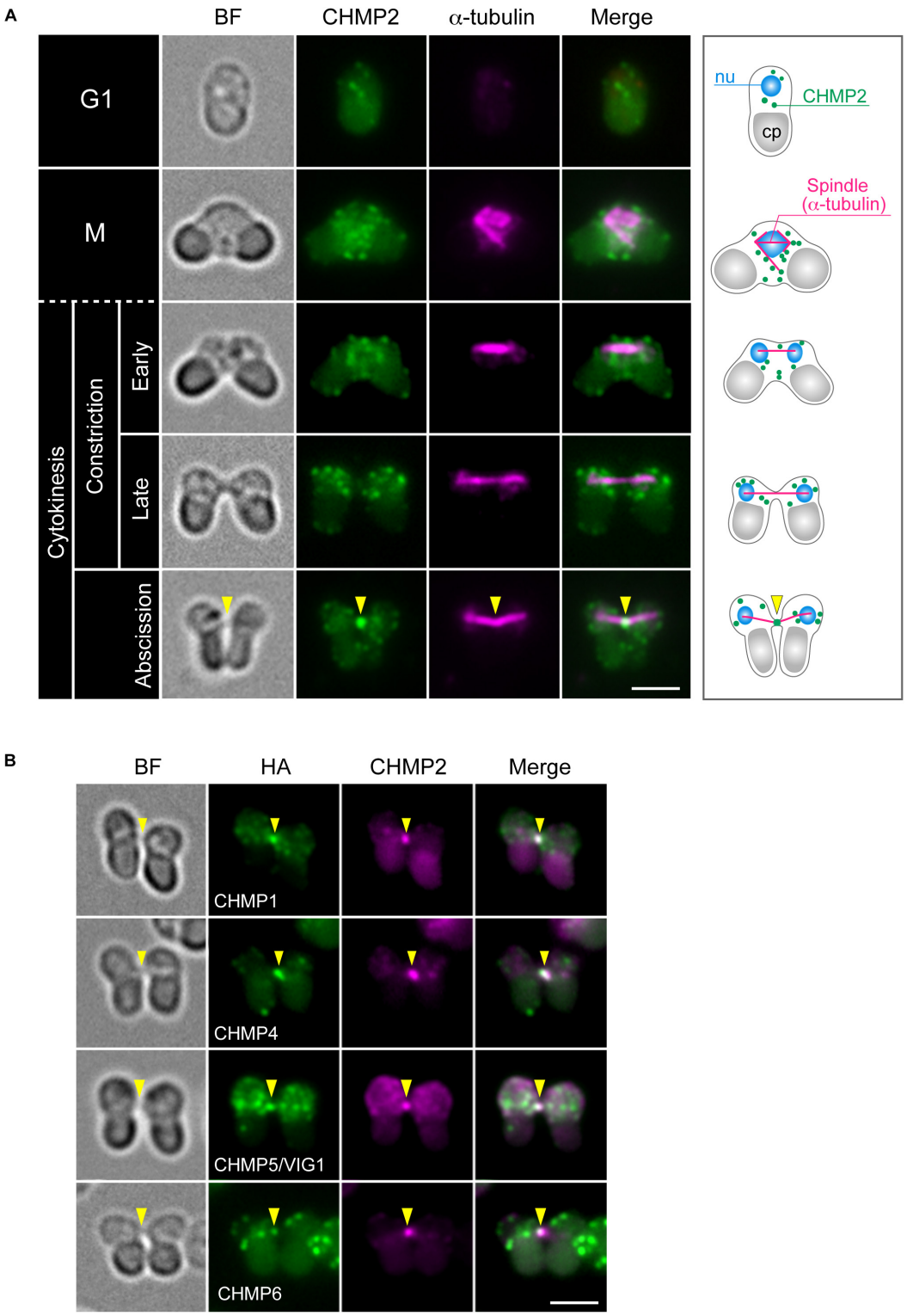

FIGURE 2 | Localization of ESCRT-III proteins. **(A)** WT cells were fixed and labeled with anti-α-tubulin and anti-CHMP2 antibodies. A schematic representation is shown on the right. Because of the short duration of abscission, we found very few cells with the intercellular bridge. CHMP2 localization at the intercellular bridge was confirmed in 10 cells at the abscission stage (a total of three independent experiments). **(B)** Cells expressing CHMP1 (CMR340C)-HA, CHMP4-HA, CHMP5/VIG1-HA, or CHMP6-HA were fixed and labeled with anti-HA and anti-CHMP2 antibodies. Representative cells at the abscission stage are shown. $n \geq 5$ cells were analyzed in two independent experiments for each strain. Arrowheads indicate the position of the intercellular bridge. BF, bright field. nu, cell nucleus; cp, chloroplast. Scale bars, 2 μm.

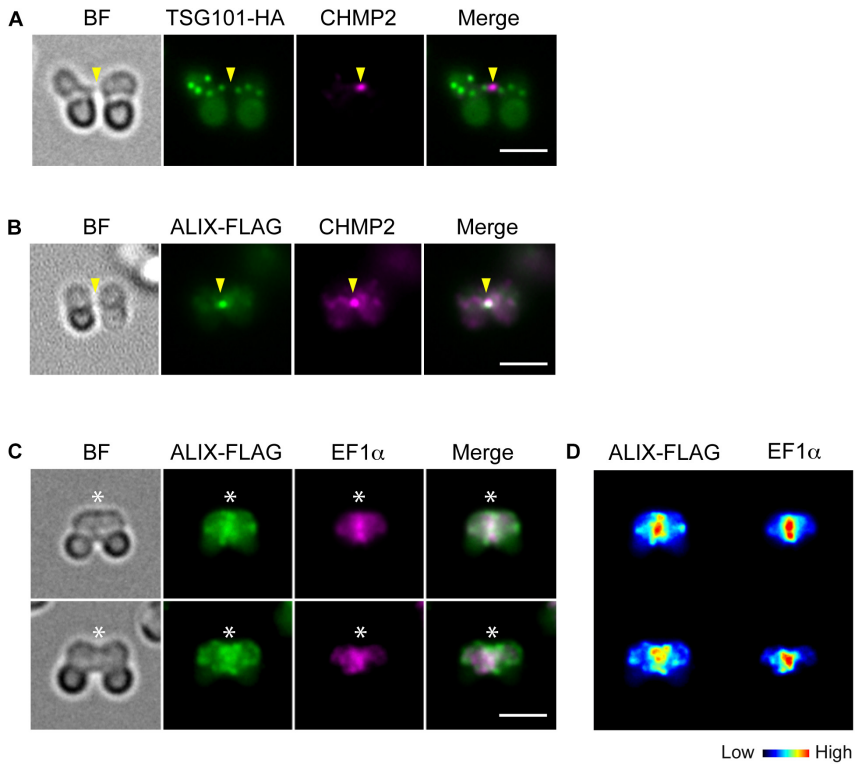

FIGURE 3 | Localization of TSG101 and ALIX. **(A)** Images of a cell expressing TSG101-HA at the abscission stage. The fixed cell was labeled with anti-HA and anti-CHMP2 antibodies. Representative images are shown. Five cells at the abscission stage were analyzed in two independent experiments. **(B)** ALIX-FLAG cells were fixed and labeled with anti-FLAG and anti-CHMP2. Eight cells were analyzed in two independent experiments. **(C)** ALIX-FLAG cells were labeled with anti-FLAG and anti-EF1α antibodies, >30 cells were analyzed in each experiment (n = 2). **(D)** Heat map of the signal intensities in C. Arrowheads, the position of the intercellular bridge. Asterisks, the position of the cleavage furrow where ALIX-FLAG and EF1α localized. BF, bright field. Scale bars, 2 μm.

bridge. Thus, further extensive studies are required to elucidate the structure involved in cytokinetic abscission.

C. merolae TSG101 appeared to be absent from the intercellular bridge. Mammalian ESCRT-I and ALIX localize at the midbody to separately target ESCRT-III (Christ et al., 2016). ESCRT-I depends on CHMP6 to recruit other ESCRT-III proteins, whereas the ALIX route does not (Christ et al., 2016). *C. merolae* CHMP6 resided at the intercellular bridge (**Figures 6A,B**). Thus, it potentially has a role unrelated to ESCRT-I. ESCRT-I is found in all major eukaryotic taxa but was secondarily lost in some species (Williams and Urbe, 2007; Leung et al., 2008). Although we cannot completely rule out the possibility that the addition of epitope-tags altered the localization of the protein or that the antibody could not react with the protein because of poor accessibility, the absence of TSG101 from the intercellular bridge may suggest a major role of ALIX in recruiting ESCRT-III. In mammalian cells, both ESCRT-I and ALIX are recruited by centrosome protein 55 kDa (CEP55), a midbody protein. However, CEP55 is absent in *C. elegans* and *Drosophila melanogaster*, although they depend on ESCRT for cytokinetic abscission (Green et al., 2013; Lie-Jensen et al., 2019). In *Drosophila*, ALIX is recruited to the midbody by Pavarotti, a homolog of human mitotic kinesin-like protein (MKLP) 1 (Lie-Jensen et al., 2019). In *C. merolae*, CEP55 or MKLP1 homologs have not been found. Thus, upstream mechanisms to recruit ESCRT appear to vary among organisms.

In contrast to TSG101, *C. merolae* ALIX was enriched at the intercellular bridge (**Figures 6A,B**). We also detected ALIX around the cleavage furrow early in the constriction stage (**Figure 6A**). Of related interest is CdvA, a scaffold protein for ESCRT-III in the archaea *Sulfolobus* (Lindas et al., 2008; Samson et al., 2011). It localizes to the mid-region of the cell, corresponding to membrane ingression sites from the beginning to final stages of cell division. The localization precedes that of ESCRT-III (Samson et al., 2011). Because *C. merolae* and eukaryotes other than Amorphea lack the actomyosin contractile ring, understanding the role of ALIX or ESCRT in the constriction stage would be of interest for future study.

We found that VPS4 localized to the intercellular bridge (**Figures 6A,B**). The phenotype of cells expressing VPS4^{E292Q}-HA was strikingly similar to that observed after overexpression of VPS4, either WT or dominant-negative forms (Carlton and Martin-Serrano, 2007; Morita et al., 2007), or disruption of spastin (Connell et al., 2009) in mammalian cells. This phenotype is also reminiscent of that in the archaea *Sulfolobus* overexpressing truncated ESCRT-III proteins, which exhibit long intercellular bridges (Liu et al., 2017). Therefore, *C. merolae*

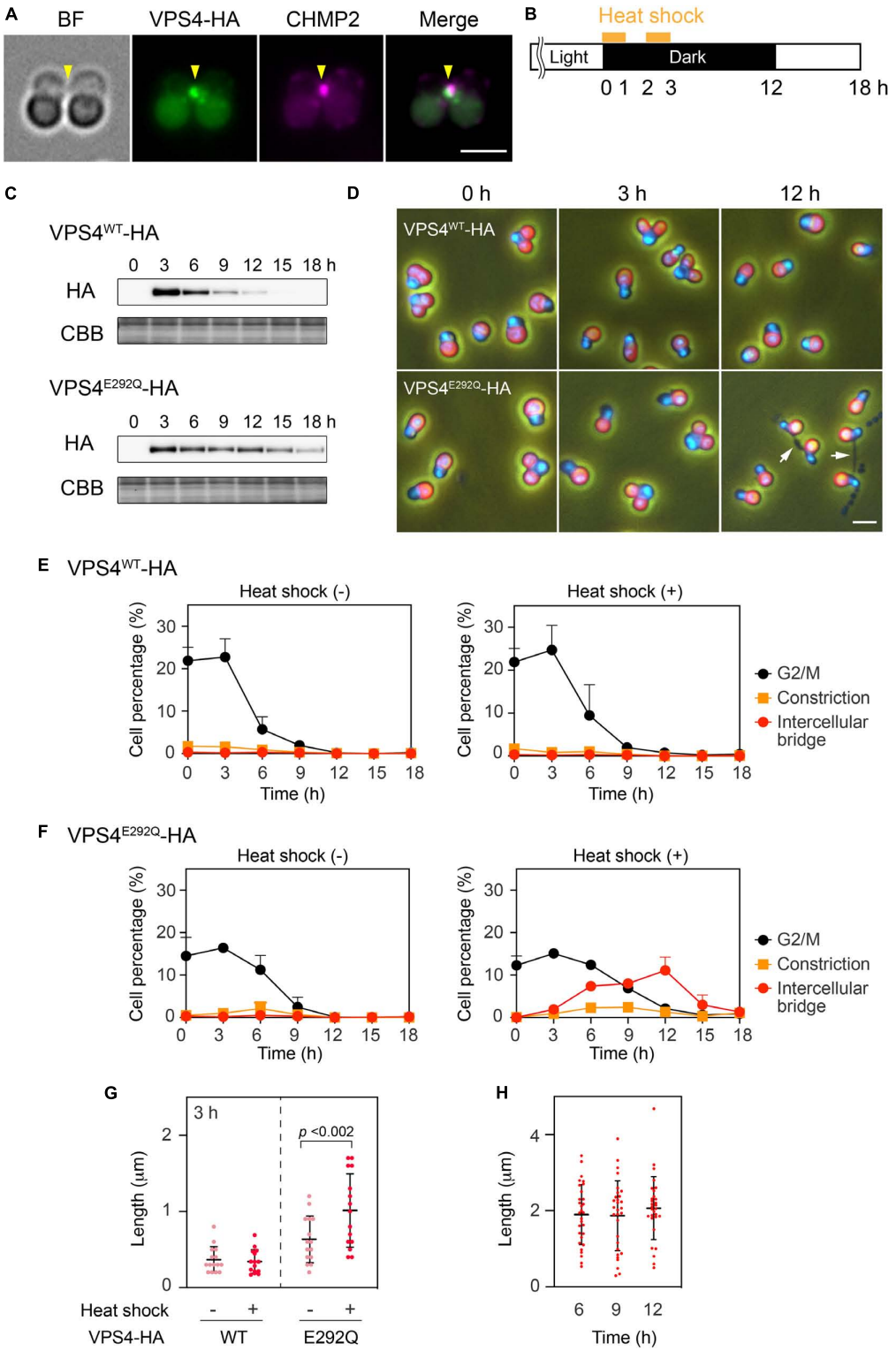

FIGURE 4 | Heat shock induction of the mutant VPS4. **(A)** Immunofluorescence of cells expressing VPS4-HA under control of the native promoter sequence. The fixed cell was labeled with anti-HA and anti-CHMP2 antibodies. Representative images are shown. Five cells were analyzed in two independent experiments. Arrowheads, the position of the intercellular bridge. **(B)** Schematic representation of heat treatments performed in **(C–H)**. Cells harboring the *VPS4*^{WT}*-HA* or *VPS4*^{E292Q}*-HA* gene under the control of the heat-inducible promoter were synchronized by a 12 h light/12 h dark cycle at 42°C, the optimal growth temperature for wildtype cells. The culture was exposed to a higher temperature (50°C) for 1 h twice with a 1 h interval at the beginning of the dark period. **(C)** Immunoblotting of VPS4^{WT}-HA and VPS4^{E292Q}-HA. Proteins were extracted from cells collected at the indicated time point after the onset of the heat shocks. Total proteins were

(Continued)

FIGURE 4 | Continued
loaded in each lane and labeled with anti-HA antibodies. Some of the membrane was stained with Coomassie Brilliant Blue (CBB) as a loading control, $n = 3$. **(D)** DAPI staining of cells harboring heat-inducible *VPS4*^{WT}*-HA* or *VPS4*^{E292Q}*-HA*. The cells were fixed and stained before (0 h) and after the onset of heat shocks (3 and 12 h). Merged images of DAPI (blue), autofluorescence from chloroplasts (red), and phase contrast are shown. White arrows indicate cells with a long intercellular bridge. **(E) and (F)** Percentages of cells at the indicated cell cycle stages among cells harboring the *VPS4*^{WT}*-HA* **(E)** or *VPS4*^{E292Q}*-HA* **(F)**. "Intercellular bridge" includes cells at the abscission stage and those with an elongated intercellular bridge. **(G)** Length of the intercellular bridge at 3 h. Data from 15 cells ($n = 5$, three independent experiments) are shown in each column. Bars indicate the mean ± standard deviation. *p*, *p*-value of the Student's *t*-test. **(H)** Length of the intercellular bridge in cells expressing VPS4^{E292Q}-HA at the indicated time point. Thirty cells ($n = 10$, three independent experiments) were analyzed in each column. Scale bars, 2 μm.

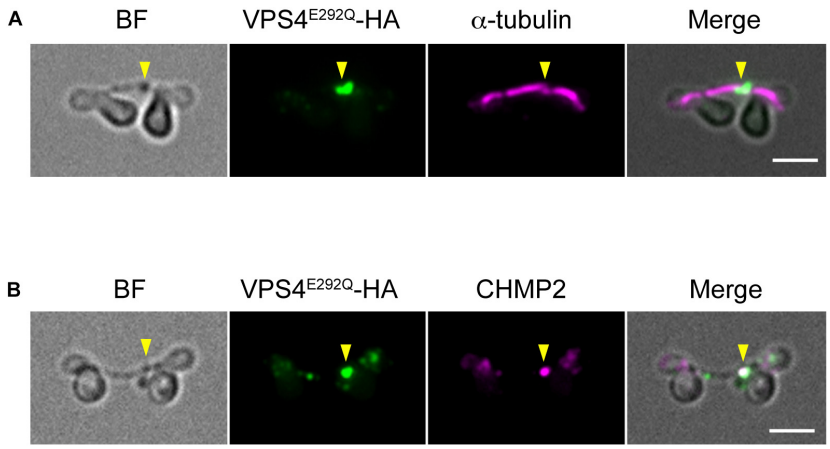

FIGURE 5 | Localization of the spindle, mutant VPS4, and CHMP2. **(A,B)** Cells harboring heat-inducible *VPS4*^{E292Q}*-HA* were fixed at 12 h after the start of heat shocks and then labeled with anti-HA and anti-α-tubulin **(A)** or anti-CHMP2 antibodies **(B)**. Representative images are shown. More than 30 cells with a long intercellular bridge (>1 μm) were imaged in each experiment ($n = 3$). The results showed that 94.5 ± 3.7% of the long intercellular bridges were positive for spindles, and 94.1 ± 5.3% were positive for VPS4^{E292Q}-HA that colocalized with CHMP2. Arrowheads, locations of the VPS4E292Q-HA signal on the long intercellular bridge. BF, bright field. Scale bars, 2 μm.

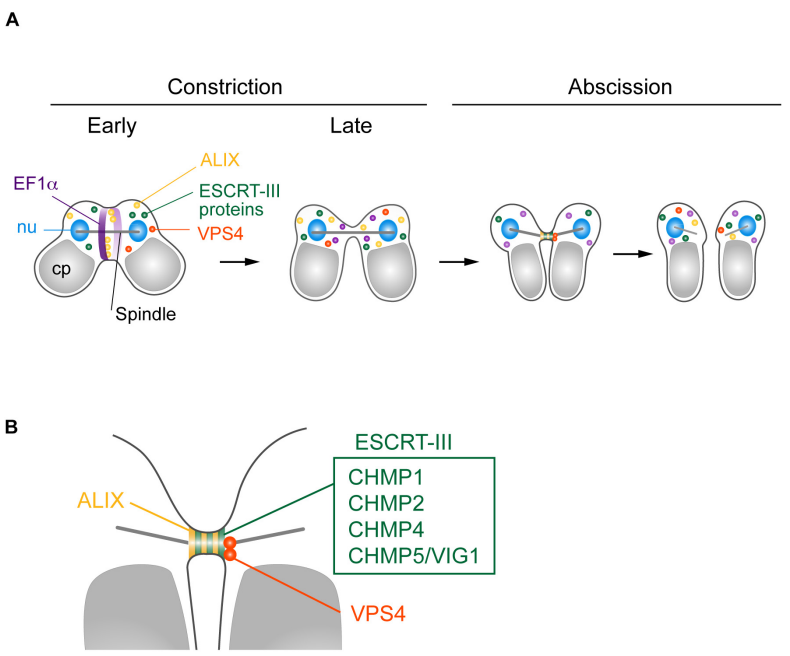

FIGURE 6 | Suggested model for *C. merolae* cytokinesis. **(A)** EF1α and ALIX localized around the cleavage furrow during early constriction and are excluded during late constriction. ALIX, ESCRT-III proteins CHMP1, 2, 4, and 5, and VPS4 colocalized at the intercellular bridge in the abscission stage. **(B)** Enlarged image of the intercellular bridge before abscission.

VPS4 plays a pivotal role in scission of the intercellular bridge, as seen in these organisms. *C. merolae* VPS4^{E292Q}-HA resided with CHMP2 on the long intercellular bridge, suggesting that the dynamics of ESCRT-III regulated by the AAA-ATPase activity of VPS4 are critical for cytokinetic abscission in this organism.

Finally, our data indicate that ESCRT mediates cytokinetic abscission in eukaryotic cells that lack the contractile ring and septins, and in the eukaryotic intercellular bridge that is considerably smaller than that of mammalian cells. In mammalian cells, the contractile ring is required for midbody formation (Hu et al., 2012). The polymerization state of actin controls midbody maturation which is essential for the appropriate assembly of ESCRT-III (Terry et al., 2018). The clearance of F-actin from the intercellular bridge after the furrow closure is also a limiting step in ESCRT-III recruitment (Fremont et al., 2016). Septins function in both the contractile ring and intercellular bridge. They are essential for maturation and stabilization of the intercellular bridge as well as proper ESCRT-III assembly (Renshaw et al., 2014; Addi et al., 2018; Karasmanis et al., 2019). The inhibitory effects of F-actin on ESCRT-III recruitment, and the role of septins in ESCRT-III assembly may be confined to animals or eukaryotic groups in which cell division is dependent on the contractile ring. The mammalian midbody is >1 μm in diameter (Mullins and Biesele, 1977; Green et al., 2012), and ESCRT-III is targeted for >40 min before abscission (Stoten and Carlton, 2018). However, in *C. merolae*, the intercellular bridge is ∼200 nm in diameter and requires less than 1 min to be cleaved (**Supplementary Figure S1B**). Thus, *C. merolae* appears to control cytokinetic abscission more simply than in mammalian cells. Importantly, regardless of these differences and the phylogenetic distance, ESCRT components mediate cytokinetic abscission in these organisms.

In summary, we demonstrate that five ESCRT-III proteins, ALIX, and VPS4 localize at abscission sites to mediate cytokinetic abscission in *C. merolae*. We also show that ESCRT functions in cytokinesis of an organism that lacks the contractile ring and septins. The fact that ESCRT mediates cytokinesis in archaea, animals, and the early diverged red alga *C. merolae* supports the idea that ESCRT is the primordial machinery for cytokinetic abscission in eukaryotes. We expect that exploring other lineages of eukaryotes that undergo ESCRT-mediated cytokinetic abscission and characterization of their mechanisms should further advance our understanding of the conserved mechanisms and evolution of eukaryotic cytokinesis.

MATERIALS AND METHODS

Cell Culture

C. merolae wildtype (10D; Toda et al., 1998) and transformant cells were grown in MA2 medium (Ohnuma et al., 2008) at 30°C under continuous light (30 $\mu E \cdot m^{-2} \cdot s^{-1}$). To synchronize cell division, the cells (OD_{750} = 2–6) were diluted to OD_{750} = 0.4 in 2 × Allen's medium (Allen, 1959) and subjected to a 12 h light (100 $\mu E \cdot m^{-2} \cdot s^{-1}$)/12 h dark cycle at 42°C with bubbling air (300 ml/min). Heat treatments were applied by shifting the synchronized culture to 50°C.

Strain Generation

The primers and plasmids used to generate strains are listed in **Supplementary Table S1**. All strains except for the ALIX-FLAG strain were generated by integration of DNA fragments into the upstream region of the *URA5.3* gene (Fujiwara et al., 2015). To add tags to ESCRT proteins, plasmids containing transformation cassettes, which included the upstream (-2300 to -898 bp) of the *URA5.3* gene (CMK046C), genes encoding ESCRT proteins with their promoter region, 3 × HA-tag, the 3′ UTR of β-tubulin, and the *URA5.3* gene with the promoter region, were generated using an In-Fusion HD Cloning kit (Clontech). For *CHMP2-*, *CHMP4-*, and *CHMP5/VIG1-HA*, PCR products #1, #5 and one of #2–#4 (**Supplementary Table S1**) were used. For other ESCRT proteins, PCR products #6 and one of #7–#11 were used. Plasmids containing a heat shock promoter (Sumiya et al., 2014) and VPS4-HA were generated by fusing PCR products #12 and #13 using the In-Fusion HD cloning kit. The plasmid for dominant-negative *VPS4-HA* (E292Q; a mutation in conserved Walker B motif; Hanson and Whiteheart, 2005) was prepared by In-Fusion cloning of PCR product #14. Transformation of *C. merolae* was conducted as described previously (Ohnuma et al., 2008; Fujiwara et al., 2015). Briefly, the M4 strain (a point mutant of URA5.3; Minoda et al., 2004) was transformed with PCR-amplified cassettes from each plasmid (#15) using a polyethylene glycol-mediated method. The transformants were selected for uracil independence in starch placed on solidified MA2 medium (Fujiwara et al., 2013). Establishment of the strain ALIX-FLAG was performed following the procedures of Takemura et al., 2019a. PCR products #16 and #17, corresponding to the 3′-portion (from + 997 to + 2496, where +1 is the first base position of the initiation codon) and the 3′-downstream region (from +2497 to +3996) of the CMC051C (*ALIX*) ORF, respectively, were inserted into *Stu*I-digested pMKTf (Takemura et al., 2018) to construct the plasmid pMKTf-ALIX-Tagging. Subsequently, transformation cassette #18 was amplified from pMKTf-ALIX-Tagging by PCR and used to transform the uracil-auxotroph T1 strain (Taki et al., 2015) as described previously (Takemura et al., 2019a). Transformants were selected on uracil-free MA2 plates using the top starch method as described previously (Takemura et al., 2019b).

Generation of an Antibody Against *C. merolae* CHMP2

DNA fragments encoding the CMB008C and pQE80 expression vector (Qiagen) were amplified by PCR with the primers listed in **Supplementary Table S2**. The fragments were fused and circularized using the In-Fusion HD cloning kit, resulting in a construct containing the six-histidine tag at the N-terminus of CMB008C. The recombinant proteins were purified with His-Trap columns (GE Healthcare Life Sciences) and used to raise antibodies in rats (T. K. craft, Ltd.).

Time-Lapse Imaging

A synchronized culture at M phase was mounted on coverslips, which had pieces of surgical tape at the corners, and was then incubated for 30 min at room temperature. After removing

excess medium, the coverslips were inverted and placed in glass-bottom dishes. The dishes were transferred into a chamber for live imaging (BZ-H3XD; Keyence) at 40°C. Images were obtained under a microscope (BZ-X700; Keyence) using a ×100 objective.

Microscopy

For immunofluorescence, cells were fixed with methanol containing 1% formaldehyde and 10% DMSO at −20°C overnight. The fixed cells were centrifuged at 1500 × *g* at 4°C, washed once with cold methanol (−20°C), and then twice with PBS. For blocking, the cells were treated with either Blocking One (Nakarai Tesque) for 15 min at 4°C or 5% BSA for 30 min at 37°C. The antibody reaction was performed for 1 h at 4°C. Primary antibodies were diluted in PBS and used at the following dilutions: 1:500 for rat anti-CHMP2, 1:100 for rabbit anti-α-tubulin (Fujiwara et al., 2009), 1:500 for guinea pig anti-EF1α (Imoto et al., 2011), 1:1000 for mouse anti-HA (Clone 16B12; BioLegend), and 1:1000 for mouse anti-DYKDDDDK tag (to detect FLAG-tag; Clone 1E6; Wako). Fluorescent secondary antibodies (Thermo Fisher Scientific) were diluted in PBS and applied at 1:1000 for Alexa Fluor 488 and 1:100 for Alexa Fluor 555. DNA was stained with 1 μg/ml 4′,6-diamidino-2-phenylindole (DAPI). Images were acquired under the BZ-X700 fluorescence microscope using the × 100 objective. For Alexa Fluor 488, the GFP filter was used. The emission filter of the TRITC filter was changed to XF3022 (580DF30; Omega Optical) for Alexa Fluor 555 to avoid signals of chloroplast autofluorescence. To analyze the length of intercellular bridges, cells were fixed with 1% glutaraldehyde and imaged under the BZ-X700 microscope using the × 100 objective. The length was measured using ImageJ software (Schneider et al., 2012). For **Figure 4D**, cells were fixed with 1% glutaraldehyde and stained with 1 μg/ml DAPI. Images were obtained under a fluorescence microscope (BX51; Olympus) with a × 40 objective and CCD camera (C7780, Hamamatsu Photonics). The following filter sets were used: U-MWU2 (Olympus) for DAPI and U-MWIG2 (Olympus) for chloroplast autofluorescence. Heat maps of the signal intensities were generated in Image Lab software (Bio-Rad). All images were adjusted for contrast using Photoshop software (Adobe Systems).

Immunoblotting

C. merolae cells were collected by centrifugation at 1500 × *g* at room temperature. The cell pellets were resuspended in 2 × SDS sample buffer (100 μm Tris, pH 6.8, 12% 2-mercaptoethanol, 4% SDS, and 20% glycerol) and incubated for 3 min at 95°C. After centrifugation at 15000 × *g* for 5 min at 4°C, the protein concentration in the supernatant was measured using an XL-Bradford kit (Aproscience). Total proteins (5 μg) were separated on polyacrylamide gels and then transferred to PVDF membranes. The membranes were blocked with 5% dry skim milk. The antibodies were diluted in 5% dry skim milk and used at the following dilutions: rat anti-CHMP2 (1:10000 for **Supplementary Figure S3A** and 1:2000 for **Supplementary Figure S3B**), rabbit anti-H3S10Ph (1:2000; Merk-Millipore), and mouse anti-HA (1:5000; Clone 16B12, BioLegend). Secondary antibodies were HRP-conjugated anti-rat, anti-rabbit, or anti-mouse IgG (1:20000; Thermo Fisher scientific). The signals were detected using ECL Prime (GE Healthcare) and the imaging system ImageQuant LAS-4000mini (for **Supplementary Figure S3B**; GE Healthcare) or ChemiDoc Touch (Bio-Rad).

DATA AVAILABILITY STATEMENT

The datasets generated for this study are available on reasonable request to the corresponding author.

AUTHOR CONTRIBUTIONS

FY and TF formulated the concept, designed the study, performed the experiments, analyzed and interpreted the data, and drafted the manuscript. TT, YK, and NS performed the experiments, analyzed and interpreted the data, and drafted the manuscript. NS performed the experiments and interpreted the data. SN, YI, OM, and KT designed the study and interpreted the data. SM, HK, and TK contributed to the concept, designed the study, interpreted the data, and drafted the manuscript.

FUNDING

This study was supported by MEXT/JSPS KAKENHI 15H06520, 16K14770, and 19K06742 (to FY), 17K07439 (to YK), 18K06300 (to TF), and 19H03260 (to TK and FY), NIG-JOINT 2016-A1-4, 8A2017, 7A2018, and 31A2019 (to FY), and the University of the Ryukyus Research Project Promotion Grant for Women Researchers (to FY).

ACKNOWLEDGMENTS

We thank Ms. K. Hashimoto and Y. Tanaka of the Miyagishima laboratory for technical support. We are grateful to Dr. Keiji Nishida (Kobe University), Dr. Mio Ohnuma (National Institute of technology, Hiroshima College), Dr. Takema Sasaki (National Institute of Genetics), and Dr. Yoshihisa Oda (National Institute of Genetics) for helpful advice during the study. We also thank the Biomaterials Analysis Division, Tokyo Institute of Technology, for DNA sequencing analysis. Fluorescence microscopy using the Keyence BZ-X700 was performed at the Center for Strategic Research Project of the University of the Ryukyus. We thank Mitchell Arico from Edanz Group for assistance in editing a draft of this manuscript.

SUPPLEMENTARY MATERIAL

The Supplementary Material for this article can be found online at: https://www.frontiersin.org/articles/10.3389/fcell.2020.00169/full#supplementary-material

REFERENCES

Addi, C., Bai, J., and Echard, A. (2018). Actin, microtubule, septin and ESCRT filament remodeling during late steps of cytokinesis. *Curr. Opin. Cell Biol.* 50, 27–34. doi: 10.1016/j.ceb.2018.01.007

Agromayor, M., Carlton, J. G., Phelan, J. P., Matthews, D. R., Carlin, L. M., Ameer-Beg, S., et al. (2009). Essential role of hIST1 in cytokinesis. *Mol. Biol. Cell* 20, 1374–1387. doi: 10.1091/mbc.E08-05-0474

Allen, M. B. (1959). Studies with *Cyanidium caldarium*, an anomalously pigmented Chlorophyta. *Arch. Microbiol.* 32, 270–277. doi: 10.1007/bf00409348

Bajorek, M., Morita, E., Skalicky, J. J., Morham, S. G., Babst, M., and Sundquist, W. I. (2009). Biochemical analyses of human IST1 and its function in cytokinesis. *Mol. Biol. Cell* 20, 1360–1373. doi: 10.1091/mbc.E08-05-0475

Burki, F. (2014). The eukaryotic tree of life from a global phylogenomic perspective. *Cold Spring Harb. Perspect. Biol.* 6:a016147. doi: 10.1101/cshperspect.a016147

Campsteijn, C., Vietri, M., and Stenmark, H. (2016). Novel ESCRT functions in cell biology, spiraling out of control? *Curr Opin Cell Biol.* 41, 1–8. doi: 10.1016/j.ceb.2016.03.008

Carlton, J. G., Caballe, A., Agromayor, M., Kloc, M., and Martin-Serrano, J. (2012). ESCRT-III governs the aurora B-mediated abscission checkpoint through CHMP4C. *Science* 336, 220–225. doi: 10.1126/science.1217180

Carlton, J. G., and Martin-Serrano, J. (2007). Parallels between cytokinesis and retroviral budding, a role for the ESCRT machinery. *Science* 316, 1908–1912. doi: 10.1126/science.1143422

Carvalho, A., Desai, A., and Oegema, K. (2009). Structural memory in the contractile ring makes the duration of cytokinesis independent of cell size. *Cell* 137, 926–937. doi: 10.1016/j.cell.2009.03.021

Christ, L., Wenzel, E. M., Liestol, K., Raiborg, C., Campsteijn, C., and Stenmark, H. (2016). ALIX and ESCRT-I/II function as parallel ESCRT-III recruiters in cytokinetic abscission. *J. Cell Biol.* 212, 499–513. doi: 10.1083/jcb.201507009

Connell, J. W., Lindon, C., Luzio, J. P., and Reid, E. (2009). Spastin couples microtubule severing to membrane traffic in completion of cytokinesis and secretion. *Traffic* 10, 42–56. doi: 10.1111/j.1600-0854.2008.00847.x

Cross, F. R., and Umen, J. G. (2015). The *chlamydomonas* cell cycle. *Plant J.* 82, 370–392. doi: 10.1111/tpj.12795

Dukes, J. D., Richardson, J. D., Simmons, R., and Whitley, P. (2008). A dominant-negative ESCRT-III protein perturbs cytokinesis and trafficking to lysosomes. *Biochem. J.* 411, 233–239. doi: 10.1042/bj20071296

Elia, N., Sougrat, R., Spurlin, T. A., Hurley, J. H., and Lippincott-Schwartz, J. (2011). Dynamics of endosomal sorting complex required for transport (ESCRT) machinery during cytokinesis and its role in abscission. *Proc. Natl. Acad. Sci. U.S.A.* 108, 4846–4851. doi: 10.1073/pnas.1102714108

Fremont, S., Hammich, H., Bai, J., Wioland, H., Klinkert, K., Rocancourt, M., et al. (2016). Oxidation of F-actin controls the terminal steps of cytokinesis. *Nat. Commun.* 8:14528. doi: 10.1038/ncomms14528

Fujimoto, H., and Mabuchi, I. (2010). Elongation factors are involved in cytokinesis of sea urchin eggs. *Genes Cells* 15, 123–135. doi: 10.1111/j.1365-2443.2009.01370.x

Fujiwara, T., Kanesaki, Y., Hirooka, S., Era, A., Sumiya, N., Yoshikawa, H., et al. (2015). A nitrogen source-dependent inducible and repressible gene expression system in the red alga *Cyanidioschyzon merolae*. *Front. Plant Sci.* 6:657. doi: 10.3389/fpls.2015.00657

Fujiwara, T., Kuroiwa, H., Yagisawa, F., Ohnuma, M., Yoshida, Y., Yoshida, M., et al. (2010). The coiled-coil protein VIG1 is essential for tethering vacuoles to mitochondria during vacuole inheritance of *Cyanidioschyzon merolae*. *Plant Cell* 22, 772–781. doi: 10.1105/tpc.109.070227

Fujiwara, T., Ohnuma, M., Yoshida, M., Kuroiwa, T., and Hirano, T. (2013). Gene targeting in the red alga *Cyanidioschyzon merolae*, single- and multi-copy insertion using authentic and chimeric selection markers. *PLoS One* 8:e73608. doi: 10.1371/journal.pone.0073608

Fujiwara, T., Yoshida, Y., and Kuroiwa, T. (2009). Synchronization of cell nuclear, mitochondrial and chloroplast divisions in the unicellular red alga *Cyanidioschyzon merolae*. *Cytologia* 74:1.

Garcia-Salcedo, J. A., Perez-Morga, D., Gijon, P., Dilbeck, V., Pays, E., and Nolan, D. P. (2004). A differential role for actin during the life cycle of *Trypanosoma brucei*. *EMBO J.* 23, 780–789. doi: 10.1038/sj.emboj.7600094

Goliand, I., Adar-Levor, S., Segal, I., Nachmias, D., Dadosh, T., Kozlov, M. M., et al. (2018). Resolving ESCRT-III spirals at the intercellular bridge of dividing cells using 3D STORM. *Cell Rep.* 24, 1756–1764. doi: 10.1016/j.celrep.2018.07.051

Goliand, I., Nachmias, D., Gershony, O., and Elia, N. (2014). Inhibition of ESCRT-II-CHMP6 interactions impedes cytokinetic abscission and leads to cell death. *Mol. Biol. Cell* 25, 3740–3748. doi: 10.1091/mbc.E14-08-1317

Green, R. A., Mayers, J. R., Wang, S., Lewellyn, L., Desai, A., Audhya, A., et al. (2013). The midbody ring scaffolds the abscission machinery in the absence of midbody microtubules. *J. Cell Biol.* 203, 505–520. doi: 10.1083/jcb.201306036

Green, R. A., Paluch, E., and Oegema, K. (2012). Cytokinesis in animal cells. *Annu. Rev. Cell Dev. Biol.* 28, 29–58. doi: 10.1146/annurev-cellbio-101011-155718

Guizetti, J., Schermelleh, L., Mantler, J., Maar, S., Poser, I., Leonhardt, H., et al. (2011). Cortical constriction during abscission involves helices of ESCRT-III-dependent filaments. *Science* 331, 1616–1620. doi: 10.1126/science.1201847

Hanson, P. I., and Whiteheart, S. W. (2005). AAA+ proteins, have engine, will work. *Nat. Rev. Mol. Cell Biol.* 6, 519–529. doi: 10.1038/nrm1684

Henson, J. H., Ditzler, C. E., Germain, A., Irwin, P. M., Vogt, E. T., Yang, S., et al. (2017). The ultrastructural organization of actin and myosin II filaments in the contractile ring, new support for an old model of cytokinesis. *Mol. Biol. Cell* 28, 613–623. doi: 10.1091/mbc.E16-06-0466

Hosein, R. E., Williams, S. A., Haye, K., and Gavin, R. H. (2003). Expression of GFP-actin leads to failure of nuclear elongation and cytokinesis in *Tetrahymena thermophila*. *J. Eukaryot. Microbiol.* 50, 403–408. doi: 10.1111/j.1550-7408.2003.tb00261.x

Hu, C. K., Coughlin, M., and Mitchison, T. J. (2012). Midbody assembly and its regulation during cytokinesis. *Mol. Biol. Cell* 23, 1024–1034. doi: 10.1091/mbc.E11-08-0721

Imoto, Y., Nishida, K., Yagisawa, F., Yoshida, Y., Ohnuma, M., Yoshida, M., et al. (2011). Involvement of elongation factor-1α in cytokinesis without actomyosin contractile ring in the primitive red alga *Cyanidioschyzon merolae*. *Cytologia* 76, 431–437. doi: 10.1508/cytologia.76.431

Iwaki, T., Onishi, M., Ikeuchi, M., Kita, A., Sugiura, R., Giga-Hama, Y., et al. (2007). Essential roles of class E Vps proteins for sorting into multivesicular bodies in *Schizosaccharomyces pombe*. *Microbiology* 153, 2753–2764. doi: 10.1099/mic.0.2007/006072-0

Karasmanis, E. P., Hwang, D., Nakos, K., Bowen, J. R., Angelis, D., and Spiliotis, E. T. (2019). A septin double ring controls the spatiotemporal organization of the escrt machinery in cytokinetic abscission. *Curr. Biol.* 29, 2174–2182. doi: 10.1016/j.cub.2019.05.050

Kuroiwa, T. (1998). The primitive red algae *Cyanidium caldarium* and *Cyanidioschyzon merolae* as model system for investigating the dividing apparatus of mitochondria and plastids. *Bioessays* 20, 344–354. doi: 10.1002/(sici)1521-1878(199804)20:4<344::aid-bies11>3.0.co;2-2

Leung, K. F., Dacks, J. B., and Field, M. C. (2008). Evolution of the multivesicular body ESCRT machinery; retention across the eukaryotic lineage. *Traffic* 9, 1698–1716. doi: 10.1111/j.1600-0854.2008.00797.x

Lie-Jensen, A., Ivanauskiene, K., Malerod, L., Jain, A., Tan, K. W., Laerdahl, J. K., et al. (2019). Centralspindlin recruits ALIX to the midbody during cytokinetic abscission in drosophila via a mechanism analogous to virus budding. *Curr. Biol.* 29, 3538–3548. doi: 10.1016/j.cub.2019.09.025

Lindas, A. C., Karlsson, E. A., Lindgren, M. T., Ettema, T. J., and Bernander, R. (2008). A unique cell division machinery in the Archaea. *Proc. Natl. Acad. Sci. U.S.A.* 105, 18942–18946. doi: 10.1073/pnas.0809467105

Liu, J., Gao, R., Li, C., Ni, J., Yang, Z., Zhang, Q., et al. (2017). Functional assignment of multiple ESCRT-III homologs in cell division and budding in *Sulfolobus islandicus*. *Mol. Microbiol.* 105, 540–553. doi: 10.1111/mmi.13716

Makarova, K. S., Yutin, N., Bell, S. D., and Koonin, E. V. (2010). Evolution of diverse cell division and vesicle formation systems in Archaea. *Nat. Rev. Microbiol.* 8, 731–741. doi: 10.1038/nrmicro2406

Matsuzaki, M., Misumi, O., Shin, I. T., Maruyama, S., Takahara, M., Miyagishima, S. Y., et al. (2004). Genome sequence of the ultrasmall unicellular red alga *Cyanidioschyzon merolae* 10D. *Nature* 428, 653–657. doi: 10.1038/nature02398

Mierzwa, B. E., Chiaruttini, N., Redondo-Morata, L., von Filseck, J. M., Konig, J., Larios, J., et al. (2017). Dynamic subunit turnover in ESCRT-III assemblies is regulated by Vps4 to mediate membrane remodelling during cytokinesis. *Nat. Cell Biol.* 19, 787–798. doi: 10.1038/ncb3559

Minoda, A., Sakagami, R., Yagisawa, F., Kuroiwa, T., and Tanaka, K. (2004). Improvement of culture conditions and evidence for nuclear transformation by

homologous recombination in a red alga, *Cyanidioschyzon merolae* 10D. *Plant Cell Physiol.* 45, 667–671. doi: 10.1093/pcp/pch087

Mishra, M., Kashiwazaki, J., Takagi, T., Srinivasan, R., Huang, Y., Balasubramanian, M. K., et al. (2013). In vitro contraction of cytokinetic ring depends on myosin II but not on actin dynamics. *Nat. Cell Biol.* 15, 853–859. doi: 10.1038/ncb2781

Morita, E., Colf, L. A., Karren, M. A., Sandrin, V., Rodesch, C. K., and Sundquist, W. I. (2010). Human ESCRT-III and VPS4 proteins are required for centrosome and spindle maintenance. *Proc. Natl. Acad. Sci. U.S.A.* 107, 12889–12894. doi: 10.1073/pnas.1005938107

Morita, E., Sandrin, V., Chung, H. Y., Morham, S. G., Gygi, S. P., Rodesch, C. K., et al. (2007). Human ESCRT and ALIX proteins interact with proteins of the midbody and function in cytokinesis. *EMBO J.* 26, 4215–4227. doi: 10.1038/sj.emboj.7601850

Muller, S., and Jurgens, G. (2016). Plant cytokinesis-No ring, no constriction but centrifugal construction of the partitioning membrane. *Semin. Cell Dev. Biol.* 53, 10–18. doi: 10.1016/j.semcdb.2015.10.037

Mullins, J. M., and Biesele, J. J. (1977). Terminal phase of cytokinesis in D-98S cells. *J. Cell Biol.* 73, 672–684. doi: 10.1083/jcb.73.3.672

Nishihama, R., Onishi, M., and Pringle, J. R. (2011). New insights into the phylogenetic distribution and evolutionary origins of the septins. *Biol. Chem.* 392, 681–687. doi: 10.1515/BC.2011.086

Nozaki, H., Takano, H., Misumi, O., Terasawa, K., Matsuzaki, M., Maruyama, S., et al. (2007). A 100%-complete sequence reveals unusually simple genomic features in the hot-spring red alga *Cyanidioschyzon merolae*. *BMC Biol.* 5:28. doi: DOI: 10.1186/1741-7007-5-28

Numata, O., Kurasawa, Y., Gonda, K., and Watanabe, Y. (2000). Tetrahymena elongation factor-1 alpha is localized with calmodulin in the division furrow. *J. Biochem.* 127, 51–56. doi: 10.1093/oxfordjournals.jbchem.a022583

Ohnuma, M., Yokoyama, T., Inouye, T., Sekine, Y., and Tanaka, K. (2008). Polyethylene glycol (PEG)-mediated transient gene expression in a red alga. *Cyanidioschyzon merolae* 10D. *Plant Cell Physiol.* 49, 117–120. doi: 10.1093/pcp/pcm157

Otegui, M. S., Verbrugghe, K. J., and Skop, A. R. (2005). Midbodies and phragmoplasts, analogous structures involved in cytokinesis. *Trends Cell Biol.* 15, 404–413. doi: 10.1016/j.tcb.2005.06.003

Otto, J. J., and Schroeder, T. E. (1990). Association of actin and myosin in the contractile ring. *Ann. N. Y. Acad. Sci.* 582, 179–184. doi: 10.1111/j.1749-6632.1990.tb21678.x

Pasha, S. N., Meenakshi, I., and Sowdhamini, R. (2016). Revisiting myosin families through large-scale sequence searches leads to the discovery of new myosins. *Evol. Bioinform. Online* 12, 201–211. doi: 10.4137/EBO.S39880

Pollard, T. D. (2017). Nine unanswered questions about cytokinesis. *J. Cell Biol.* 216, 3007–3016. doi: 10.1083/jcb.201612068

Reichl, E. M., Ren, Y., Morphew, M. K., Delannoy, M., Effler, J. C., Girard, K. D., et al. (2008). Interactions between myosin and actin crosslinkers control cytokinesis contractility dynamics and mechanics. *Curr. Biol.* 18, 471–480. doi: 10.1016/j.cub.2008.02.056

Renshaw, M. J., Liu, J., Lavoie, B. D., and Wilde, A. (2014). Anillin-dependent organization of septin filaments promotes intercellular bridge elongation and Chmp4B targeting to the abscission site. *Open Biol.* 4:130190. doi: 10.1098/rsob.130190

Samson, R. Y., Obita, T., Freund, S. M., Williams, R. L., and Bell, S. D. (2008). A role for the ESCRT system in cell division in archaea. *Science* 322, 1710–1713. doi: 10.1126/science.1165322

Samson, R. Y., Obita, T., Hodgson, B., Shaw, M. K., Chong, P. L., Williams, R. L., et al. (2011). Molecular and structural basis of ESCRT-III recruitment to membranes during archaeal cell division. *Mol. Cell.* 41, 186–196. doi: 10.1016/j.molcel.2010.12.018

Schneider, C. A., Rasband, W. S., and Eliceiri, K. W. (2012). NIH Image to ImageJ, 25 years of image analysis. *Nat. Methods* 9, 671–675. doi: 10.1038/nmeth.2089

Schoneberg, J., Lee, I. H., Iwasa, J. H., and Hurley, J. H. (2017). Reverse-topology membrane scission by the ESCRT proteins. *Nat. Rev. Mol. Cell Biol.* 18, 5–17. doi: 10.1038/nrm.2016.121

Schuh, A. L., and Audhya, A. (2014). The ESCRT machinery, from the plasma membrane to endosomes and back again. *Crit. Rev. Biochem. Mol. Biol* 49, 242–261. doi: 10.3109/10409238.2014.881777

Sebe-Pedros, A., Grau-Bove, X., Richards, T. A., and Ruiz-Trillo, I. (2014). Evolution and classification of myosins, a paneukaryotic whole-genome approach. *Genome Biol. Evol.* 6, 290–305. doi: 10.1093/gbe/evu013

Spitzer, C., Schellmann, S., Sabovljevic, A., Shahriari, M., Keshavaiah, C., Bechtold, N., et al. (2006). The *Arabidopsis* elch mutant reveals functions of an ESCRT component in cytokinesis. *Development* 133, 4679–4689. doi: 10.1242/dev.02654

Stoten, C. L., and Carlton, J. G. (2018). ESCRT-dependent control of membrane remodelling during cell division. *Semin. Cell Dev. Biol.* 74, 50–65. doi: 10.1016/j.semcdb.2017.08.035

Sumiya, N., Fujiwara, T., Kobayashi, Y., Misumi, O., and Miyagishima, S. Y. (2014). Development of a heat-shock inducible gene expression system in the red alga *Cyanidioschyzon merolae*. *PLoS One* 9:e111261. doi: 10.1371/journal.pone.0111261

Suzuki, K., Ehara, T., Osafune, T., Kuroiwa, H., Kawano, S., and Kuroiwa, T. (1994). Behavior of mitochondria, chloroplasts and their nuclei during the mitotic cycle in the ultramicroalga *Cyanidioschyzon merolae*. *Eur. J. Cell Biol.* 63, 280–288.

Suzuki, K., Kawazu, T., Mita, T., Takahashi, H., Itoh, R., Toda, K., et al. (1995). Cytokinesis by a contractile ring in the primitive red alga *Cyanidium caldarium* RK-1. *Eur. J. Cell Biol.* 67, 170–178.

Takahashi, H., Takano, H., Yokoyama, A., Hara, Y., Kawano, S., Toh-e, A., et al. (1995). Isolation, characterization and chromosomal mapping of an actin gene from the primitive red alga *Cyanidioschyzon merolae*. *Curr. Genet.* 28, 484–490. doi: 10.1007/bf00310820

Takemura, T., Imamura, S., Kobayashi, Y., and Tanaka, K. (2018). Construction of a selectable marker recycling system and the use in epitope tagging of multiple nuclear genes in the unicellular red alga *Cyanidioschyzon merolae*. *Plant Cell Physiol.* 59, 2308–2316. doi: 10.1093/pcp/pcy156

Takemura, T., Imamura, S., Kobayashi, Y., and Tanaka, K. (2019a). Multiple modification of chromosomal loci using URA5.3 selection marker in the unicellular red alga *Cyanidioschyzon merolae*. *Bioprotocol* 9:7. doi: 10.21769/BioProtoc.3204

Takemura, T., Kobayashi, Y., Imamura, S., and Tanaka, K. (2019b). Top starch plating method for the efficient cultivation of unicellular red alga *Cyanidioschyzon merolae*. *Bioprotocol* 9:4. doi: 10.21769/BioProtoc.3172

Taki, K., Sone, T., Kobayashi, Y., Watanabe, S., Imamura, S., and Tanaka, K. (2015). Construction of a URA5.3 deletion strain of the unicellular red alga *Cyanidioschyzon merolae*, A backgroundless host strain for transformation experiments. *J. Gen. Appl. Microbiol.* 61, 211–214. doi: 10.2323/jgam.61.211

Terry, S. J., Dona, F., Osenberg, P., Carlton, J. G., and Eggert, U. S. (2018). Capping protein regulates actin dynamics during cytokinetic midbody maturation. *Proc. Natl. Acad. Sci. U.S.A.* 115, 2138–2143. doi: 10.1073/pnas.1722281115

Toda, K., Takano, H., Miyagishima, S., Kuroiwa, H., and Kuroiwa, T. (1998). Characterization of a chloroplast isoform of serine acetyltransferase from the thermo-acidiphilic red alga *Cyanidioschyzon merolae*. *Biochim. Biophys. Acta* 1403, 72–84. doi: 10.1016/s0167-4889(98)00031-7

Williams, R. L., and Urbe, S. (2007). The emerging shape of the ESCRT machinery. *Nat. Rev. Mol. Cell Biol.* 8, 355–368. doi: 10.1038/nrm2162

Wloga, D., Strzyzewska-Jowko, I., Gaertig, J., and Jerka-Dziadosz, M. (2008). Septins stabilize mitochondria in *Tetrahymena thermophila*. *Eukaryot. Cell* 7, 1373–1386. doi: 10.1128/EC.00085-08

Wu, J. Q., Ye, Y., Wang, N., Pollard, T. D., and Pringle, J. R. (2010). Cooperation between the septins and the actomyosin ring and role of a cell-integrity pathway during cell division in fission yeast. *Genetics* 186, 897–915. doi: 10.1534/genetics.110.119842

Yagisawa, F., Imoto, Y., Fujiwara, T., and Miyagishima, S. (2018). "Single-membrane-bound organelles: division and inheritance," in *Cyanidioschyzon merolae*, eds T. Kuroiwa, et al. (Singapore: Springer), 235–249. doi: 10.1007/978-981-10-6101-1_15

Yamamoto, M., Nishikawa, T., Kajitani, H., and Kawano, S. (2007). Patterns of asexual reproduction in *Nannochloris bacillaris* and *Marvania geminata* (Chlorophyta, Trebouxiophyceae). *Planta* 226, 917–927. doi: 10.1007/s00425-007-0538-7

Yamazaki, T., Owari, S., Ota, S., Sumiya, N., Yamamoto, M., Watanabe, K., et al. (2013). Localization and evolution of septins in algae. *Plant J.* 74, 605–614. doi: 10.1111/tpj.12147

Yang, D., Rismanchi, N., Renvoise, B., Lippincott-Schwartz, J., Blackstone, C., and Hurley, J. H. (2008). Structural basis for midbody targeting of spastin by the ESCRT-III protein CHMP1B. *Nat. Struct. Mol. Biol.* 15, 1278–1286. doi: 10.1038/nsmb.1512

Yoon, H. S., Hackett, J. D., Ciniglia, C., Pinto, G., and Bhattacharya, D. (2004). A molecular timeline for the origin of photosynthetic eukaryotes. *Mol. Biol. Evol.* 21, 809–818. doi: 10.1093/molbev/msh075

Yoon, H. S., Muller, K. M., Sheath, R. G., Ott, F. D., and Bhattacharya, D. (2006). Defining the major lineages of red algae (Rhodophyta). *J. Phycol.* 42, 482–492. doi: 10.1111/j.1529-8817.2006.00210.x

Zaremba-Niedzwiedzka, K., Caceres, E. F., Saw, J. H., Backstrom, D., Juzokaite, L., Vancaester, E., et al. (2017). *Asgard archaea* illuminate the origin of eukaryotic cellular complexity. *Nature* 541, 353–358. doi: 10.1038/nature21031

Zhou, Q., Hu, H., and Li, Z. (2014). New insights into the molecular mechanisms of mitosis and cytokinesis in trypanosomes. *Int. Rev. Cell Mol. Biol.* 308, 127–166. doi: 10.1016/B978-0-12-800097-7.00004-X

Conflict of Interest: The authors declare that the research was conducted in the absence of any commercial or financial relationships that could be construed as a potential conflict of interest.

frontiers in Cell and Developmental Biology

ORIGINAL RESEARCH
published: 08 April 2020
doi: 10.3389/fcell.2020.00238

Regulation of the Total Cell Surface Area in Dividing *Dictyostelium* Cells

*Masahito Tanaka, Koushiro Fujimoto and Shigehiko Yumura**

Graduate School of Sciences and Technology for Innovation, Yamaguchi University, Yamaguchi, Japan

When a cell divides into two daughter cells, the total cell surface area should increase. There are two models for membrane supply to support cell division: (1) unfolding of small surface membrane reservoirs such as microvilli or wrinkles and (2) exocytosis of intracellular vesicles. Here, we precisely measured the total cell surface area in dividing *Dictyostelium* cells, flattened by the agar overlay that eliminated the complexity of unfolding surface membrane reservoirs. Because the cells divided normally under the agar overlay, unfolding of surface membrane reservoirs was not required for cell division. Under the agar overlay, the total cell surface area slightly decreased from the interphase to the metaphase and then increased about 20% during cytokinesis. Both endocytosis and exocytosis were suppressed in the early mitotic phase but recovered during cytokinesis. The imbalance of endocytosis and exocytosis could contribute to the changes observed in the cell surface area. Clathrin-dependent endocytosis was also substantially suppressed during cytokinesis, but contrary to previous reports in cultured animal cells, it did not significantly contribute to the regulation of the cell surface area. Furrowing during cytokinesis was indispensable for the cell membrane increase, and vice versa.

Keywords: cell division, cell membrane, cytokinesis, endocytosis, exocytosis

OPEN ACCESS

Edited by:
Maria Grazia Giansanti, Institute of Molecular Biology and Pathology, National Research Council (CNR), Italy

Reviewed by:
Rytis Prekeris, University of Colorado Denver, United States
Todd Blankenship, University of Denver, United States

****Correspondence:***
Shigehiko Yumura
yumura@yamaguchi-u.ac.jp

Specialty section:
This article was submitted to Cell Growth and Division, a section of the journal Frontiers in Cell and Developmental Biology

Received: *16 January 2020*
Accepted: *20 March 2020*
Published: *08 April 2020*

Citation:
Tanaka M, Fujimoto K and Yumura S (2020) Regulation of the Total Cell Surface Area in Dividing Dictyostelium Cells. Front. Cell Dev. Biol. 8:238. doi: 10.3389/fcell.2020.00238

INTRODUCTION

During cell division, cells vigorously change shape, and their surface area should therefore be changed accordingly. Assuming that a perfectly spherical cell divides into two perfectly spherical daughter cells, the surface area should increase by 26%. Precise measurement of the total cell surface area is difficult because small microvilli or wrinkles of cell surface, which occupy 21–130% of the apparent cell surface area (Schmid-Schonbein et al., 1980; Guillou et al., 2016), complicate the measurement. Recent measurements using fluorescence exclusion (Cadart et al., 2018), microfabricated channels (Varsano et al., 2017), and lattice light-sheet microscopy (Aguet et al., 2016) have enabled more precise cell volume estimation, but it is still difficult to precisely measure the cell surface area. Nevertheless, previous measurements have shown that the total cell surface area changes during cell division (Boucrot and Kirchhausen, 2007; Giansanti et al., 2015; Aguet et al., 2016).

There are two models to explain the regulation of cell surface area: (1) the cell membrane unfolding model and (2) the exocytosis model. In the former model, small microvilli or wrinkles on the cell surface act as membrane reservoirs and unfold to form the required membrane (Knutton et al., 1975; Erickson and Trinkaus, 1976; Figard and Sokac, 2014). In the latter model, exocytosis of intracellular vesicles supplies the necessary membrane (Schmoranzer et al., 2003;

Bretscher, 2008). Migrating cells also need to change the cell surface area by extending and retracting the cell membrane; however, the cell membrane can physically stretch by 2–3% at the most (Mohandas and Evans, 1994). Expansion of the cell surface can be explained by either or both of the two models (Gauthier et al., 2011; Masters et al., 2013).

Endocytosis has been reported to be suppressed during cell division. Clathrin-mediated endocytosis (CME) is halted in dividing Hela cells (Fielding and Royle, 2013), although this is still controversial (Boucrot and Kirchhausen, 2007; Tacheva-Grigorova et al., 2013). Pinocytosis and phagocytosis are also suppressed during mitosis of macrophages and cultured animal cells (Berlin et al., 1978; Raucher and Sheetz, 1999). Suppression of endocytosis may be responsible for the increased cell surface area observed during cell division. Exocytosis also contributes to cytokinesis, although its quantitative information during cell division is unavailable (Goss and Toomre, 2008). Exocyst-dependent membrane addition is required for anaphase cell elongation and cytokinesis in *Drosophila* (Giansanti et al., 2015). In addition, exocytosis contributes to contraction of the cleavage furrow in yeast (Gerien and Wu, 2018) and *Xenopus* eggs (Straight and Field, 2000).

Recently, we showed that *Dictyostelium* cells could migrate by extending large pseudopods when flattened by pressing with an agar sheet; however, the cells exhibited neither wrinkles of the cell membrane nor thin extensions such as filopodia or microvilli. Therefore, even without membrane reservoir unfolding, the cells were able to migrate under the agar overlay (Tanaka et al., 2017). Under this condition, we could precisely measure the cell surface area, without influence of surface membrane reservoirs, and showed that the cell surface area was almost constant during cell migration. Furthermore, by staining the cell membrane with a fluorescent lipid analog, we have shown that the cell membrane is rapidly turned over by endocytosis and exocytosis, in a manner directly dependent on cell migration velocity (Tanaka et al., 2017).

Here, we measured the total cell surface area during cell division by the agar overlay method. Because the cells divide normally under an agar overlay, unfolding of the surface membrane reservoirs is not required for cell division. We found that the total cell surface area increased by about 20% through exocytosis during cytokinesis. The furrowing observed during cytokinesis was indispensable for the cell membrane increase, and vice versa. Both exocytosis and endocytosis are strictly regulated to control the cell shape change during cell division.

MATERIALS AND METHODS

Cell Culture

Dctyostelium discoideum wild-type (AX2) cells and all mutant cells were cultured in HL5 medium (1.3% bacteriological peptone, 0.75% yeast extract, 85.5 mM D-glucose, 3.5 mM Na_2HPO_4, and 3.5 mM KH_2PO_4, pH 6.4) at 22°C. Cells were cultured in suspension at 150 rpm or on plastic dishes. To synchronize the cell cycle and increase the number of mitotic cells, cells were cultured at 10°C for 16 h and then treated with 100 μM TB at 22°C for 3.5 h. To start cell division, TB was removed by centrifugation and media exchange. HS1 cells were originally generated by Manstein et al. (1989). *Chc* null cells and temperature-sensitive *secA* mutant cells were originally generated by Ruscetti et al. (1994) and Zanchi et al. (2010), respectively.

Plasmids and Transformation

Expression vectors containing GFP-ABD (actin-binding domain of filamin), GFP-alpha-tubulin, GFP-clathrin light chain (Fujimoto et al., 2019), or GFP-histone were transformed into AX2 cells by electroporation or laserporation as described previously (Yumura et al., 1995; Yumura, 2016). Positive cells were selected using 10 μg/mL G418 (Wako, Osaka, Japan).

TB Treatment

To completely depolymerize the microtubules of cells at the interphase, the cells were incubated on ice for 30 min in the presence of 100 μM thiabendazole (TB, Tokyo Chemical Industry, Co. Ltd., Tokyo, Japan) and then transferred to incubation at 22°C. Empirically, depolymerization of microtubules in the interphase cells take longer (at least 2 h) at 22°C in the presence of TB. On the other hand, the microtubules in dividing cells quickly depolymerize, even with a lower concentration of TB (20 μM). To observe dividing cells after the application with TB, cells expressing GFP-tubulin were placed on a coverslip (18 mm × 18 mm, No. 1, Matsunami, Inc., Osaka, Japan) and overlaid with a thin agar sheet as described previously (Yumura et al., 1984). A small drop of TB solution was applied to the surface of the agar sheet at a final concentration of 20 μM prior to microscopy.

Microscopy

Cells were placed on a coverslip and overlaid with an agar sheet. After the agar overlay, the cells expressing GFP-ABD were observed under an optical sectioning fluorescence microscope (Deltavision, GE Healthcare Life Science, United Kingdom). Z-axis images with an interval of 0.2–0.3 μm were acquired every 30 s. Each image was processed by deconvolution using the Deltavision system to remove out-of-focus images.

To normalize the cell division stage, MSI was used as described previously (Jahan and Yumura, 2017). MSI was computed from the long axis (L) and short axis (l), where the short axis represents the width of the furrow, using the following formula:

$$MSI = (L - l)/L \quad (1)$$

When the MSI is 0, the cell is round; when the MSI is 1, cell division is completed.

Fixed cells were observed under a fluorescence microscope (TE 300, Nikon, Japan) equipped with regular ultraviolet (UV) and TRITC filter sets. Fluorescence images of live cells expressing GFP-tubulin or GFP-ABD, and membrane uptake in the presence of FM1-43 (Thermo Fisher Scientific, Tokyo, Japan), were observed using a confocal microscope (LSM510, Zeiss, Germany) at a time interval of 20–30 s.

Cells expressing GFP-clathrin (clathrin light chain) were observed using a custom-made TIRF microscope at a time

interval of 2–5 s (Yumura et al., 2008). GFP-clathrin dots were counted manually by ImageJ software[1]. The lifetime of the GFP-clathrin dots was defined as the duration from their appearance to disappearance in the cell cortex.

Measurement of the Cell Surface Area

To measure the cell surface area, we adopted two methods: (1) measurement from the cell outline and (2) measurement using a fluorescent lipid analog.

For the measurement from the cell outline, cells expressing GFP-histone or GFP-ABD were mildly pressed with an agar sheet, and phase-contrast and fluorescence images were captured with an interval of 0.5–1 min under an optical sectioning fluorescence microscope. The total cell surface areas were computed from the dorsoventral and lateral areas as described before (Tanaka et al., 2017). The lateral area of the cell was calculated from the outlines of cell in each optical z-section (7–10 slices). In some cases, we measured the cell surface area after fixation. For the fixation, agar-overlaid cells were fixed by immersing into ethanol containing 1% formaldehyde at −17°C and stained with DAPI (Sigma-Aldrich, Tokyo, Japan) and 50 ng/mL TRITC-conjugated phalloidin (Sigma-Aldrich), as previously described (Yumura et al., 1984).

For the fluorescence measurement using a fluorescent lipid analog, the partially-synchronized cells in suspension were stained with 10 μM FM1-43. Because the nutrient medium hampered the staining, the cells were stained after the medium had been exchanged with 15 mM Na/K phosphate buffer (pH 6.4) containing 0.1M sorbitol. The sorbitol was used to suppress the activities of contractile vacuoles (Zhu and Clarke, 1992). One minute after staining, the fluorescence intensity (excitation at 470 nm and emission at 570 nm) was measured by a fluorescence spectrophotometer (F-2500, Hitachi High-Technologies, Corp., Tokyo, Japan).

Uptake of Cell Membranes

To measure the uptake of cell membranes in single cells, the cells were stained with the FM dye, and the fluorescence images were acquired over time by confocal microscopy. The fluorescence intensities of the cell membrane and the cell interior were calculated as previously described (Tanaka et al., 2017). Briefly, by using the ImageJ software, the integrated fluorescence intensity of a 1 μm-thick outline including the cell membrane was considered as the fluorescence of the cell membrane; the integrated fluorescence inside the outline was considered as the fluorescence of the cell interior.

Scanning Electron Microscopy

The dividing cells were fixed and observed under a scanning electron microscope (SEM) (JSM-6360LA, JEOL, Ltd., Tokyo, Japan), as described previously (Tanaka et al., 2017).

Statistical Analysis

Statistical analysis was performed using GraphPad Prism 7 (GraphPad Software, Inc., San Diego, CA, United States). Data are presented as the mean ± SD and analyzed using Student's *t*-test for comparison between two groups, or by one-way ANOVA with Tukey's multiple comparisons test.

[1]http://rsb.info.nih.gov/ij

RESULTS

Unfolding of Surface Membrane Reservoirs Is Not Required for Cell Division

Like animal cells, *Dictyostelium* cells vigorously change their shape during cell division. When entering the mitotic phase, the cells stop migrating, become spherical, elongate, and constrict the cleavage furrow to separate into two daughter cells. The total cell surface area should be altered during these morphological changes. However, the many projections and wrinkles on the cell surface complicate the accurate measurement of cell surface area. Here, to minimize the small projections and surface wrinkles, the cells were flattened, by pressing with an agar sheet, to expand the cell membrane. Without the agar overlay, the cells were 7–9 μm in thickness, and under the agar overlay, the cells flattened to a thickness of about 2 μm. Even under this condition, the cells divided normally. The surface of the fixed cells was observed using a SEM after removing the agar sheet. While the cells without the agar overlay had many wrinkles and projections on the surface (**Figures 1A,B**), the cells under the agar overlay had flattened shapes and no signs of wrinkles or projections (**Figures 1C,D**). Although there could be wrinkles or folds in the cell membrane that are beyond the resolution of SEM, we have not found any such minute wrinkles or folds even by transmission electron microscopy (Tanaka et al., 2017). Therefore, we concluded that the unfolding of the surface membrane reservoirs is dispensable for cell division.

Total Cell Surface Area During Cell Division

To examine the total surface area of dividing cells, cells expressing green fluorescent protein (GFP)-actin-binding domain of filamin (ABD), a marker of actin filaments, or GFP-histone, were observed under an agar overlay by sectioning microscopy (only GFP-ABD images are shown; **Figure 1E**). The thickness of the cells under the agar overlay remained at about 2 μm during cell division (**Figure 1F**). Because the division time varied between cells, we used the mitosis stage index (MSI; calculated from the long axis and short axis) to normalize the cell division time (Jahan and Yumura, 2017). When the MSI is 0, the cell shape is round, corresponding to the metaphase; when the MSI is 1, the cell separates into two daughter cells. The total cell surface area was measured from the outline and thickness of the cells. **Figure 1G** shows the time course of relative total cell surface area changes from the cell rounding stage (MSI = 0, metaphase) to the completion of cell division (MSI = 1). The total cell surface area showed a subtle increase from the cell rounding stage (metaphase to anaphase) to the elongation stage (MSI = 0.4); thereafter, the surface area increased linearly by about 20% (19.1 ± 4.3%, $n = 83$), from the initiation of furrowing

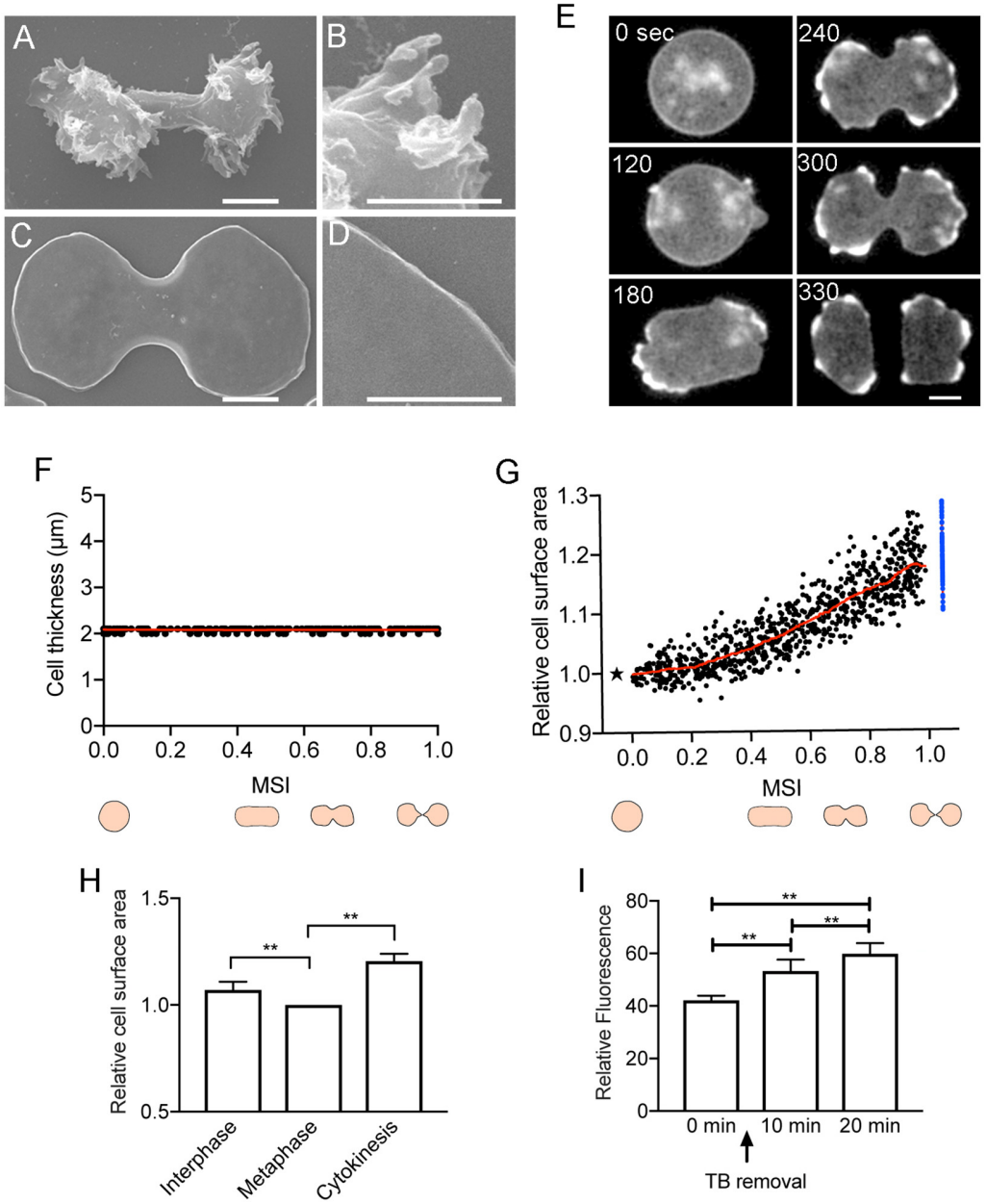

FIGURE 1 | Total cell surface area during cell division. Typical scanning electron micrographs of dividing *Dictyostelium* cells without **(A,B)** and with the agar overlay **(C,D)**. Fixed cells were observed after the agar sheet was removed. **(B,D)** Show enlarged images of **(A,C)**. Bars: 5 μm. **(E)** Time course of cell division of a *Dictyostelium* cell expressing green fluorescent protein (GFP)- actin-binding domain of filamin (ABD). Bar: 10 μm. **(F)** Time course of the thickness of the agar-overlaid cells during cell division, measured by sectioning microscopy (n = 22). The cell division time was normalized according to the mitosis stage index (MSI). **(G)** Time course of the relative cell surface area during cytokinesis (versus MSI). The surface area is normalized to 1 at the metaphase (asterisk). The sum of the surface area of the two daughter cells is represented by blue dots. The red line shows the average. **(H)** Comparison of the relative surface area at the interphase, metaphase, and at end of cytokinesis. Data are presented as the mean ± SD and analyzed by one-way ANOVA with Tukey's multiple comparisons test. $^{**}P \leq 0.001$, n = 15. **(I)** Relative fluorescence intensities of FM1-43-stained cells measured by a fluorescence spectrophotometry. The fluorescence intensity of the stained cells is shown before thiabendazole (TB) removal (0 min) as well as 10 and 20 min after the initiation of cell division. Data are presented as the mean ± SD and analyzed by one-way ANOVA with Tukey's multiple comparisons test. $^{**}P \leq 0.001$, three different experiments.

to the final cell separation (**Figure 1G**). We also compared the surface area between the interphase and metaphase cells, and the surface area decreased slightly during this transition (7.01 ± 3.89%, n = 15). Here, the total cell surface area of the interphase cells was measured immediately before the prophase (**Figure 1H**). In these experiments (**Figures 1A–H**), we used no inhibitor to synchronize the cell division as described below.

To further evaluate the increase in cell surface area, partially synchronized cells were stained with the FM1-43 dye, which is a cell-impermeable fluorescent lipid analog that emits fluorescence when inserted into the outer leaflet of the cell membrane. The fluorescence intensity of the stained cells was measured by a fluorescence spectrophotometer. To synchronize the cells, they were cultured at 10°C for 16 h and then arrested at the metaphase by treating with 100 μM thiabendazole (TB), a microtubule depolymerizer, at 22°C for 3.5 h (Fujimoto et al., 2019). After the removal of TB by centrifugation, most of the cells divided within 20 min. **Figure 1I** shows the relative fluorescence intensities of the stained cells before TB removal (0 min), as well as 10 and 20 min after the initiation of cell division. The fluorescence intensity increased by 30% (29.72 ± 7.01%, three different experiments) over that of the mitosis-arrested cells. This was more than what was observed using the agar overlay method; however, fluorescence spectrophotometry may lead to an overestimation of the surface area because membrane internalized by endocytosis is included in the measurement.

Membrane Uptake Is Suppressed During Cell Division

Endocytosis is suppressed during cell division of cultured animal cells (Berlin et al., 1978; Raucher and Sheetz, 1999; Fielding and Royle, 2013; Aguet et al., 2016), which may explain the increase in cell surface area during cytokinesis. To examine the dynamics of the membrane uptake in dividing *Dictyostelium* cells, the cells were observed in the presence of the FM1-43 dye using confocal microscopy. Although the interphase cells vigorously internalized their membranes (Interphase, **Figure 2A**), mitotic cells showed only few internalized vesicles; during cytokinesis, the number of internalized vesicles gradually increased (Mitosis, **Figure 2A**). The fluorescence intensity time course for internalized membrane, shown in **Figure 2B**, indicates that membrane uptake is substantially suppressed by about 50%.

Microtubules play an important role in membrane trafficking. Interphase cells have approximately 30 microtubules elongating from a centriole associated with the nucleus. Mitotic cells have a mitotic spindle but no astral microtubules from the prophase to the early anaphase. At early anaphase, microtubules begin to elongate, reaching the cell cortex at the late anaphase (Kitanishi-Yumura and Fukui, 1987). In presence of TB, the membrane uptake was not suppressed in the interphase cells (Interphase + TB, **Figures 2A,B**). Interestingly, at interphase, cell size was reduced during the 1 h incubation with TB (**Figure 2C**), and the cell surface area was also significantly decreased (**Figure 2D**). It is plausible that the surface area reduction is caused by the TB-induced inhibition of (microtubule-dependent) exocytosis, while the ongoing endocytosis is unimpaired.

On the other hand, in cells under mitotic arrest, membrane uptake was substantially suppressed in the presence of TB (Mitosis + TB, **Figures 2A,B**), although some membrane uptake was observed. When TB was applied to the anaphase cells expressing GFP-tubulin, the mitotic spindle disappeared, leaving only centrosomes, and the cells failed cytokinesis without furrowing (**Figure 2E**). Interestingly, the total surface area did not change with TB treatment of the anaphase cells (**Figure 2F**), contrary to the result for the interphase cells. Therefore, it is plausible that TB impedes exocytosis because the endocytosis is stalled (**Figure 2B**), which suggests that the exocytosis is dependent on the microtubules in the mitotic phase as well as in the interphase.

To further clarify the contribution of exocytosis to the cell membrane increase, we used temperature-sensitive *secA* (encoding an exocytic protein) mutant cells. These cells show deficient exocytosis at 27.5°C (Zanchi et al., 2010). At the permissive temperature (22°C), cytokinesis proceeded normally, but at the restricted temperature, cytokinesis failed, and the cells became binucleate (**Figure 2G**). The total surface area did not increase in the cells without cytokinesis, contrary to what was observed at the permissive temperature (**Figure 2H**). Therefore, exocytosis is necessary for cytokinesis.

Clathrin-Mediated Endocytosis Is Suppressed During Cell Division

The change in cell surface area during cell division in animal cells has been explained by suppression of CME (Fielding and Royle, 2013; Kaur et al., 2014; Aguet et al., 2016), although this is still controversial (Boucrot and Kirchhausen, 2007; Tacheva-Grigorova et al., 2013). We examined the contribution of CME on the surface area of dividing *Dictyostelium* cells by observing cells expressing GFP-clathrin under a total internal reflection fluorescence (TIRF) microscope. Many fluorescent dots, representing coated pits, were observed in the cell cortex of cells at the interphase and mitotic stages (**Figure 3A**), which confirmed previous observations (Macro et al., 2012; Fujimoto et al., 2019). **Figure 3B** shows a typical time course of individual dots that appeared and then disappeared in the cortex. **Figures 3C,D** show time courses of the fluorescence intensities of these dots in the interphase and mitotic cells, respectively. When dots disappear, endocytic vesicles are considered to be released from the cell membrane (Macro et al., 2012). Unlike the coated pits observed in the interphase cells, those in the dividing cells remained visible for a longer duration in the cortex. **Figure 3E** shows that the lifetime of the coated pits is significantly increased in the cells at the mitotic stage compared with the cells at the interphase ($n > 2000$ dots, each). **Figure 3F** shows that CME in the dividing cells is significantly suppressed at all MSIs compared with CME in the interphase cells. Here, CME was evaluated as the number of disappearing dots per unit area and unit time ($\mu m^{-2}\ min^{-1}$).

Next, we examined the total cell surface area during cytokinesis in *clathrin heavy chain* (*chc*) null cells. Although *chc* null cells show defective cytokinesis in suspension culture (Niswonger and O'Halloran, 1997), most of the cells divide normally in the surface culture. We expected that the cell surface area increased faster in chc null cells than in wild type cells, thereby mutant cells divided faster. However, cell division was slower in the *chc* null cells. The duration increased overall relative to the furrowing (MSI of 0–0.5 and 0.5–1, respectively; **Figure 3G**). However, as shown in **Figure 3H**, the total surface area of the *chc* null cells increased by about 20% (20.39 ± 4.96%,

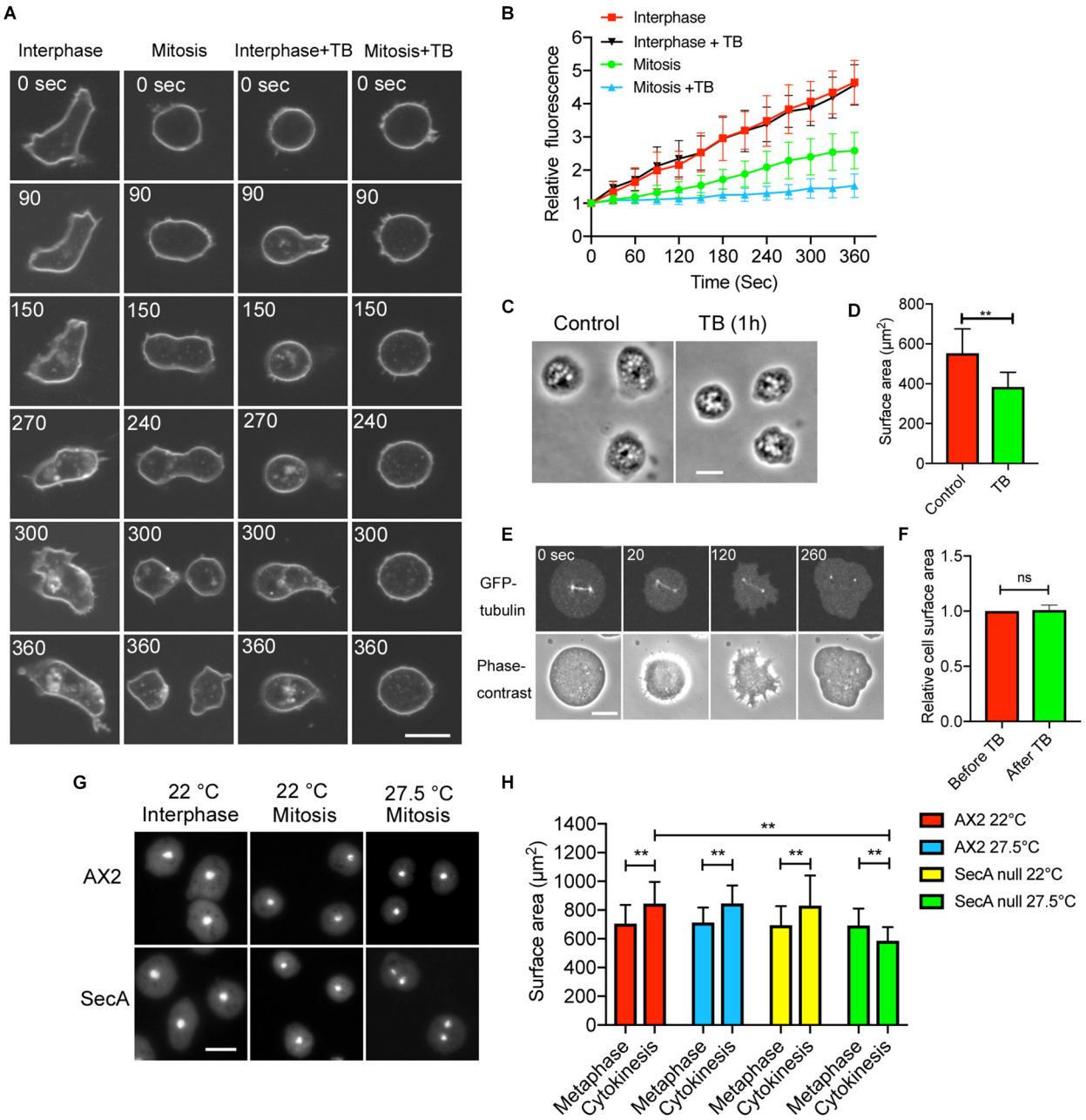

FIGURE 2 | Membrane uptake is suppressed during cell division. **(A)** Time course of typical fluorescence images of cells at the interphase and during mitosis in the presence of FM1-43 (interphase, mitosis, interphase + TB, and mitosis + TB; TB: thiabendazole). In these experiments, the cells were stained without an agar overlay. Bar: 10 μm. **(B)** Time course of the fluorescence intensity of the inside (internalized membrane) of the cells stained with the FM dye in each condition (mean ± SD, $n = 20$). **(C)** Typical phase-contrast images of cells incubated before and 1 h after addition of TB. Bar: 10 μm. **(D)** Surface area of the cells in each condition. Data are presented as the mean ± SD and analyzed by Student's *t*-test. $^{**}P \leq 0.001$, $n \geq 130$. **(E)** Time course of fluorescence and phase-contrast images of the dividing cells expressing GFP-tubulin after the addition of TB. Because TB was added to the surface of the agar block, the cells were transiently raised (therefore, the cells shrunk slightly), but thereafter, the cells became flat. Note that the spindle disappeared 260 s after the addition of TB, and the cells were not able to undergo cytokinesis becoming binucleate. Bar: 10 μm. **(F)** Comparison of the surface area before and after addition of TB. Data are presented as the mean ± SD and analyzed by Student's *t*-test. ns, not significant, $P > 0.05$, $n = 44$. **(G)** Typical fluorescence images of wild type (AX2) and *secA* null cells stained with 4′,6-diamidino-2-phenylindole (DAPI). Interphase cells cultured at 22°C, divided cells immediately after cytokinesis when cultured at 22°C, and divided cells immediately after cytokinesis when cultured at 27.5°C. *secA* null cells failed cytokinesis, resulting in binucleate cells at 27.5°C. Bar: 10 μm. **(H)** Comparison of the total cell surface area in wild type and *secA* null cells at the metaphase, cytokinesis (22°C), or failed cytokinesis (27.5°C). Here, we used TB for cells to be arrested at mitotic stage (Metaphase) and removed TB by media exchange to restart the cell division (Cytokinesis) at each temperature. Because the microtubule structures fully reappeared within 5 min, exocytosis was not affected with TB. Data are presented as the mean ± SD and analyzed by one-way ANOVA with Tukey's multiple comparisons test. $^{**}P \leq 0.001$, $n > 400$.

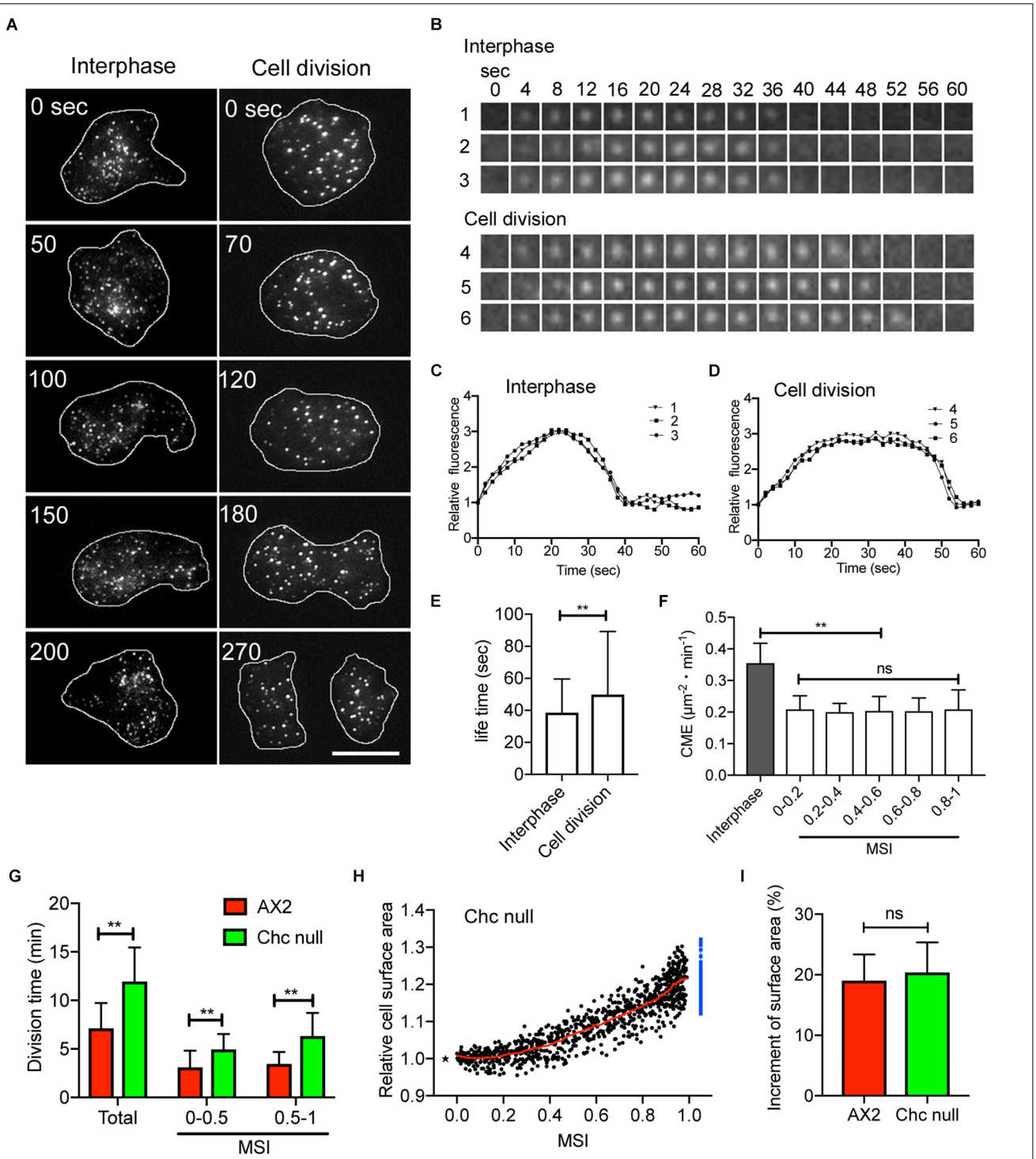

FIGURE 3 | Clathrin-mediated endocytosis (CME) is suppressed during cell division. **(A)** Typical total internal reflection fluorescence (TIRF) microscopic images of cells expressing GFP-clathrin at the interphase and mitosis stage. **(B)** Time courses of typical TIRF images of clathrin dots in cells at the interphase (1, 2, and 3) and mitotic (4, 5, and 6) stages, respectively. **(C,D)** Time courses of fluorescence intensities of the clathrin dots in the cells at the interphase and mitotic stages **(B)**. **(E)** Comparison of the lifetime of clathrin dots between interphase and dividing cells. Data are presented as the mean ± SD and analyzed by Student's *t*-test. $^{**}P < 0.001$, $n > 2{,}000$. **(F)** CME in the interphase and during cell division (MSI 0–0.2, 0.2–0.4, 0.4–0.6, 0.6–0.8, and 0.8–1.0). Here, CME was counted as the number of disappearing dots per unit area and unit time (μm^{-2} min^{-1}). **(G)** Comparison of division duration (Total, MSI 0–0.5, and MSI 0.5–1.0) between wild-type (AX2) and *clathrin heavy chain* (*chc*) null cells. Data are presented as the mean ± SD and analyzed by Student's *t*-test. $^{**}P \leq 0.001$, $n \geq 53$. **(H)** Changes in total cell surface area versus MSI during cytokinesis in *chc* null cells ($n = 53$). The surface area is normalized to 1 at the metaphase (asterisk). The sum of the surface area of the two daughter cells is represented by blue dots. The red line shows the average. **(I)** Comparison of the increase in cell surface area immediately before cytokinesis between wild type (AX2) and *chc* cells. Data are presented as the mean ± SD and analyzed by Student's *t*-test. ns, not significant, $P > 0.05$, $n \geq 53$.

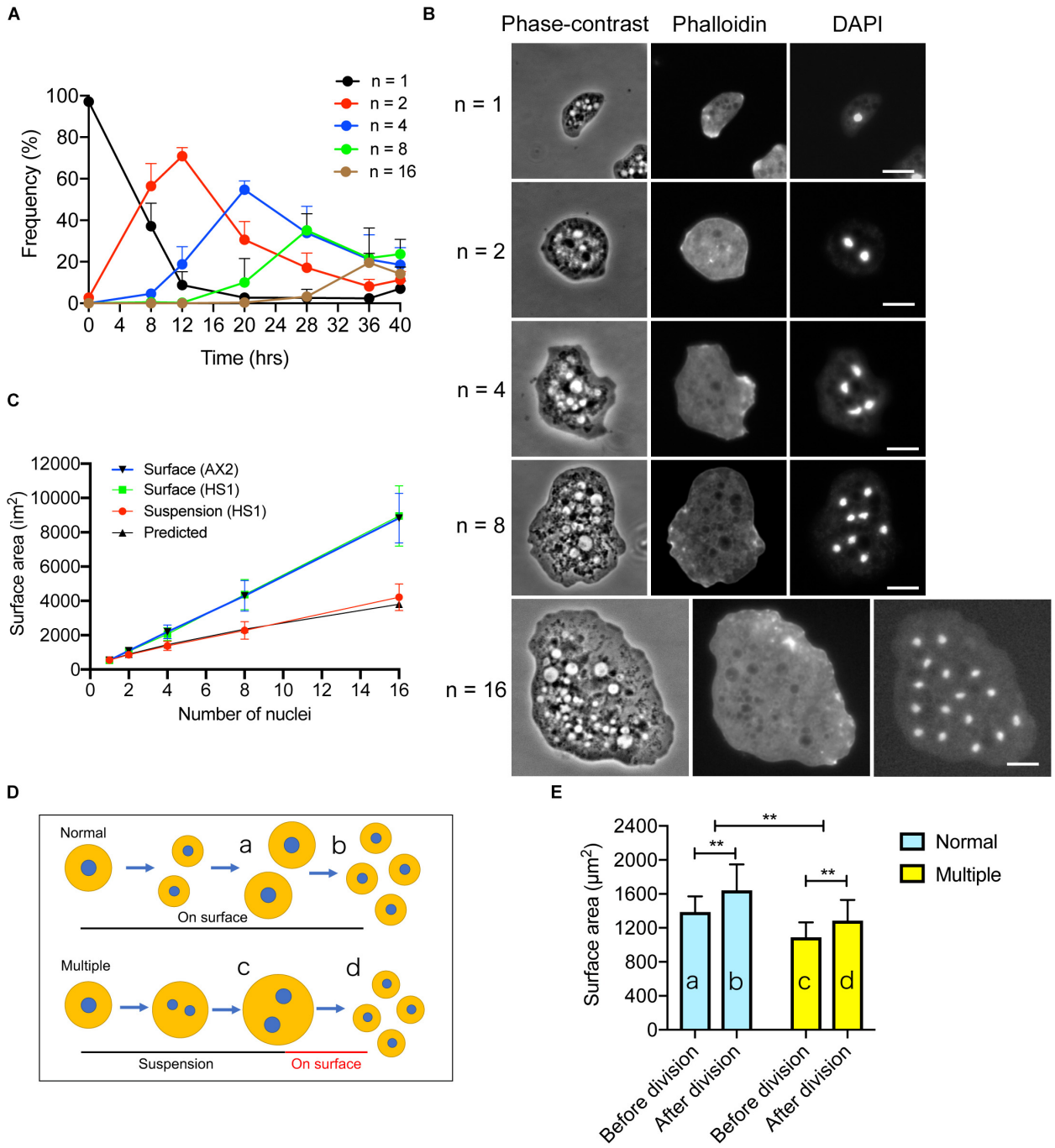

FIGURE 4 | Proper furrowing is required for the increase in surface area. **(A)** Time course of multinucleation of myosin II null (HS1) cells in suspension culture. The frequencies of the cells having a single, 2, 4, 8, or 16 nuclei over time. Although the cells different numbers of nuclei (3, 5, etc.) gradually increased, only the cells with single, 2, 4, 8, and 16 nuclei are plotted (mean ± SD, $n > 500$). **(B)** Typical phase-contrast and fluorescence images of HS1 cells with single, 2, 4, 8, and 16 nuclei at each peak of the graph in **(A)**. The cells were overlaid with agar, fixed, and stained with tetramethylrhodamine isothiocyanate (TRITC) phalloidin and DAPI. Bars: 10 µm. **(C)** Surface area of HS1 cells plotted versus the number of nuclei when cells were cultured in suspension culture (Suspension HS1) and in surface culture (Surface HS1). The surface area of wild type (AX2) cells was also plotted versus the number of nuclei in surface culture (Surface AX2). Data are presented as the mean ± SD, $n > 500$. For the surface culture, the surface area was multiplied by the number of nuclei of the dividing cells such as 2, 4, 8, and 16. The predicted surface area (Predicted) is calculated by subtracting each area that should be incremented during the cytokinesis. **(D)** Scheme to explain the experiments. Multinucleate HS1 cells can divide in surface culture by binary fission (Normal). On the other hand, HS1 cells become multinucleate in suspension culture. The multinucleate cells can then divide by attaching to the surface (Multiple). The cell surface areas were compared before (a,c) and after (b,d) division. **(E)** The cell surface areas in the experiments shown in **(D)** are compared for Normal and Multiple. Data are presented as the mean ± SD and analyzed by Student's *t*-test. $^{**}P \leq 0.001$, $n > 130$.

n = 53), which is not significantly different from that observed in the wild type cells (**Figure 3I**). Therefore, although CME is suppressed during cell division, CME does not appear to contribute significantly to the regulation of cell surface area, which is contrary to previous reports in cultured animal cells (Kaur et al., 2014; Aguet et al., 2016).

Proper Furrowing Is Required for the Surface Area Increase

As described above, membrane surface area increase is necessary for cytokinesis; we therefore examined whether cytokinesis is required for the membrane surface area increase in *Dictyostelium*. Myosin II null (HS1) cells can divide by binary fission in surface culture depending on the opposite traction forces of the daughter halves (Neujahr et al., 1997; Jahan and Yumura, 2017). However, when cultured in suspension, the cell size increases and multiple nuclei are formed by normal nuclear division accompanying spindle formation (Zang et al., 1997; Taira and Yumura, 2017). As the culture duration increased, the number of nuclei increased by a power of two (e.g., 1, 2, 4, 8, and 16, **Figure 4A**). The doubling time of nuclei (about 8 hrs) was similar to the that of cell growth in wild type cells. **Figure 4B** shows typical phase-contrast and fluorescence microscopy images of multinucleate cells stained with tetramethylrhodamine isothiocyanate (TRITC)-conjugated phalloidin and 4′,6-diamidino-2-phenylindole (DAPI). The total surface area of the cells was measured after the agar overlay. When HS1 cells were cultured on an adhesive substratum, their cell surface areas increased linearly in a manner similar to wild type cells (Surface, **Figure 4C**: the surface area of a single cell was multiplied by the number of daughter cells, e.g., 2, 4, 8, or 16). However, the increase in surface area of cells in suspension culture (Suspension, **Figure 4C**) was not consistent with this observation; instead, the increase could be predicted by subtracting each area that should be incremented during each cytokinesis (Predicted, **Figure 4C**). Without furrowing (cytokinesis), about 20% of the membrane increment was lost. Therefore, we concluded that without proper furrowing (cytokinesis), the cell surface area could not increase.

Next, we examined the changes in the surface area upon cell division of multinucleate HS1 cells attached to the adhesive substratum. Within 1 h, the multinucleate cells divided into mononucleate cells, with multiple furrowing, by traction-mediated cytokinesis (**Figures 4Dc,d**). The cell surface area increased by about 20% after cytokinesis (**Figure 4E**, 18.04%, n > 130), in a manner similar to the increase observed during cytokinesis in wild type cells (**Figures 4Da,b**); however, the cell membrane increase did not fully recover to that of the constantly dividing cells on surface. Therefore, independent of the number of nuclei and size of the cells, approximately 20% of the membrane is added during this cytokinesis.

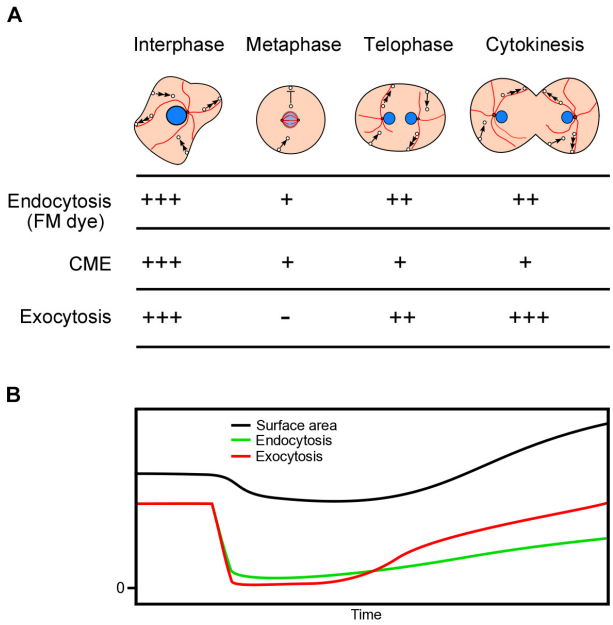

FIGURE 5 | Dynamics of cell membrane surface area during cell division. **(A)** Summary of the dynamics of microtubules, endocytosis, and exocytosis during cell division. In the interphase cells, endocytosis, and exocytosis are balanced to maintain a constant total cell surface area. When the cells enter the prophase, astral microtubules disappear, resulting in the suppression of exocytosis. Exocytosis recovers as astral microtubules reappear during the telophase. Endocytosis is suppressed from the prophase to the metaphase and recovers by half during cytokinesis. CME is suppressed from the prophase to cytokinesis. **(B)** Time course of estimated endocytosis and exocytosis and the relative total cell surface area.

DISCUSSION

Here, we precisely measured the total cell surface area in dividing cells, flattened by the agar overlay method, during which the complex unfolding of surface membrane reservoirs is eliminated. Because the cells divide normally under this condition, unfolding of the surface membrane reservoirs is not required for cell division. Actually, without agar-overlay, the number of projections and wrinkles on the surface of dividing cells was similar to that of interphase cells as far as we observed using SEM (Tanaka et al., 2017).

Using the agar overlay method, we found that the total cell surface area slightly decreased from the interphase to the metaphase, and then increased by about 20% during cytokinesis. The cell surface area seems to be strictly regulated both by endocytosis and exocytosis. **Figure 5** shows a summary of the estimated endocytosis and exocytosis dynamics during cell division. In the interphase cells, endocytosis and exocytosis are balanced to maintain a constant total cell surface area. When entering the mitotic phase, astral microtubules disappear, resulting in suppression of exocytosis due to suspension of microtubule-dependent membrane trafficking. In addition, endocytosis is partially suppressed. Therefore, the total surface area begins to decrease, which may contribute to cell rounding. After the telophase, as astral microtubules reach the cell cortex, the exocytosis and endocytosis recover. During cytokinesis, to increase the total cell surface area, exocytosis should exceed endocytosis.

Based on our previous studies using the agar overlay method, the total cell surface area does not change during cell migration, but the total cell membrane is refreshed with a half-life of 5 min via turnover by endocytosis and exocytosis (Tanaka et al., 2017). Because the membrane uptake of the cytokinetic cells was half of that observed in the interphase cells (**Figure 2B**), the cells should take up 25% of the cell membrane during cytokinesis (5 min). If exocytosis fully recovers as the astral microtubules elongate, it can add 50% of the cell membrane. However, visualization of exocytosis during cell division is required in the future; currently there are no available tools to visualize exocytosis in *Dictyostelium* cells.

Based on the HS1 cell experiments, cytokinetic furrowing is required for the increase in the cell surface area, which is independent of proper spindle formation and nuclear division. Conversely, from the experiments using the *secA* null mutant, the increase in the cell surface is critical for cytokinesis. Previous studies have reported that the delivery of intracellular membrane vesicles to the cell membrane is required for constriction of the cleavage furrow in zebrafish, *C. elegans* embryos, *Drosophila* spermatocytes, and yeast (Li et al., 2006; Robinett et al., 2009; Giansanti et al., 2015; Wang et al., 2016; Kumar et al., 2019). As a candidate of the membrane vesicles source, Golgi-derived vesicles, lysosome, or endosome has been reported (Arden et al., 2007; Boucrot and Kirchhausen, 2007; Goss and Toomre, 2008; Montagnac et al., 2009). Although exocytosis is required for the increase of surface area in cytokinesis, it should be emphasized that the regulation of endocytosis also contributes to the regulation of the cell surface area.

The mechanism underlying suppression of membrane uptake during mitosis has been studied previously; however, these studies focused mainly on the contribution of membrane uptake for cell rounding. Three models for suppression of membrane uptake have been proposed. (1) Phosphorylation of epsin, a clathrin-adaptor protein, blocks the invagination of coated pits during mitosis (Chen et al., 1999). Although phosphorylation of epsin orthologs in *Dictyostelium* has not been reported, cells deficient in epsin have reduced CME (Brady et al., 2010). (2) An increase in membrane tension inhibits endocytosis during mitosis in animal cells (Raucher and Sheetz, 1999). The increase in membrane tension has also been reported to increase during mitosis in *Dictyostelium* cells (Srivastava et al., 2016). (3) Clathrin localizes primarily at the mitotic spindle to stabilize the structure and does not participate in endocytosis in dividing cultured animal cells (Royle et al., 2005). In *Dictyostelium* cells, we have not observed clathrin at the spindle. In *Dictyostelium* cells, clathrin evenly localizes in the cell cortex, whereas dynamin is known to localize at the cleavage furrow (Masud Rana et al., 2013; Fujimoto et al., 2019).

We favor the membrane tension model. As the astral microtubules disappear, exocytosis is suppressed and endocytosis proceeds at a low level, resulting in a reduced cell surface area. This reduction in the cell surface area increases the cell surface tension, resulting in cell rounding, and an increase in the tension beyond a critical level inhibits endocytosis. During cytokinesis, as the astral microtubules elongate, exocytosis recovers, and the membrane tension decreases, resulting in recovered endocytosis.

The contribution of CME to membrane dynamics during cell division is still controversial. CME does not change in dividing Hela or BSC1 cells (Boucrot and Kirchhausen, 2007). On the other hand, CME is inhibited at the early mitotic phase in human breast cancer cells (Aguet et al., 2016). In the present study, we found that CME remained suppressed during the entire cell division, whereas the total membrane uptake recovered during cytokinesis (FM dye experiments). The regulation of CME at the molecular level during cell division should be clarified in future experiments.

If the CME vesicles are 0.1 μm in diameter, and 1,400 vesicles are internalized during cell division, about 4% of the total cell membrane would be internalized. The suppression of CME is not sufficient for the observed membrane increase. Therefore, CME is not a key contributor to the suppression of the total membrane uptake. Incidentally, we could not find any gene homologous to caveolin in the *Dictyostelium* genome that would account for caveola-mediated endocytosis (Fujimoto et al., 2019). Presumably, other endocytosis mechanisms, such as macro-pinocytosis, may also be suppressed.

CONCLUSION

Unfolding of surface membrane reservoirs was not required for cell division. The total cell surface area increased by 20% during cytokinesis. This increase was due to the imbalance between exocytosis and endocytosis. CME was significantly suppressed during cell division but did not significantly contribute to the cell surface area dynamics, contrary to previous reports. The furrowing observed during cytokinesis was indispensable for the increase in the cell membrane, and vice versa. Both exocytosis and endocytosis are strictly regulated to control the cell shape changes during cell division.

DATA AVAILABILITY STATEMENT

The datasets generated for this study are available on request to the corresponding author.

AUTHOR CONTRIBUTIONS

MT and KF were involved in the experimental work and data analysis. SY was involved in the project planning and data analysis. MT, KF, and SY wrote the manuscript.

ACKNOWLEDGMENTS

We are grateful to the members of the *Dictyostelium* research community, the Dicty Stock Center, and the NBRP Nenkin for providing some of the mutants that were used in this study. We thank T. Kitanishi−Yumura for her critical reading and helpful comments. We would like to thank Editage (www.editage.com) for English language editing.

REFERENCES

Aguet, F., Upadhyayula, S., Gaudin, R., Chou, Y. Y., Cocucci, E., He, K., et al. (2016). Membrane dynamics of dividing cells imaged by lattice light-sheet microscopy. *Mol. Biol. Cell* 27, 3418–3435.

Arden, S. D., Puri, C., Au, J. S., Kendrick-Jones, J., and Buss, F. (2007). Myosin VI is required for targeted membrane transport during cytokinesis. *Mol. Biol. Cell* 18, 4750–4761.

Berlin, R. D., Oliver, J. M., and Walter, R. J. (1978). Surface functions during mitosis I: phagocytosis, pinocytosis and mobility of surface-bound Con A. *Cell* 15, 327–341.

Boucrot, E., and Kirchhausen, T. (2007). Endosomal recycling controls plasma membrane area during mitosis. *Proc. Natl. Acad. Sci. U.S.A.* 104, 7939–7944.

Brady, R. J., Damer, C. K., Heuser, J. E., and O'Halloran, T. J. (2010). Regulation of Hip1r by epsin controls the temporal and spatial coupling of actin filaments to clathrin-coated pits. *J. Cell Sci.* 123, 3652–3661.

Bretscher, M. S. (2008). Exocytosis provides the membrane for protrusion, at least in migrating fibroblasts. *Nat. Rev. Mol. Cell Biol.* 9:916.

Cadart, C., Monnier, S., Grilli, J., Saez, P. J., Srivastava, N., Attia, R., et al. (2018). Size control in mammalian cells involves modulation of both growth rate and cell cycle duration. *Nat. Commun.* 9:3275.

Chen, H., Slepnev, V. I., Di Fiore, P. P., and De Camilli, P. (1999). The interaction of epsin and Eps15 with the clathrin adaptor AP-2 is inhibited by mitotic phosphorylation and enhanced by stimulation-dependent dephosphorylation in nerve terminals. *J. Biol. Chem.* 274, 3257–3260.

Erickson, C. A., and Trinkaus, J. P. (1976). Microvilli and blebs as sources of reserve surface membrane during cell spreading. *Exp. Cell Res.* 99, 375–384.

Fielding, A. B., and Royle, S. J. (2013). Mitotic inhibition of clathrin-mediated endocytosis. *Cell Mol. Life Sci.* 70, 3423–3433.

Figard, L., and Sokac, A. M. (2014). A membrane reservoir at the cell surface: unfolding the plasma membrane to fuel cell shape change. *Bioarchitecture* 4, 39–46.

Fujimoto, K., Tanaka, M., Rana, A. Y. K. M. M., Jahan, M. G. S., Itoh, G., Tsujioka, M., et al. (2019). Dynamin-like protein B of *Dictyostelium* contributes to cytokinesis cooperatively with other dynamins. *Cells* 8:781.

Gauthier, N. C., Fardin, M. A., Roca-Cusachs, P., and Sheetz, M. P. (2011). Temporary increase in plasma membrane tension coordinates the activation of exocytosis and contraction during cell spreading. *Proc. Natl. Acad. Sci. U.S.A.* 108, 14467–14472.

Gerien, K. S., and Wu, J. Q. (2018). Molecular mechanisms of contractile-ring constriction and membrane trafficking in cytokinesis. *Biophys. Rev.* 10, 1649–1666.

Giansanti, M. G., Vanderleest, T. E., Jewett, C. E., Sechi, S., Frappaolo, A., Fabian, L., et al. (2015). Exocyst-dependent membrane addition is required for anaphase cell elongation and cytokinesis in *Drosophila*. *PLoS Genet.* 11:e1005632.doi: 10.1371/journal.pgen.1005632

Goss, J. W., and Toomre, D. K. (2008). Both daughter cells traffic and exocytose membrane at the cleavage furrow during mammalian cytokinesis. *J. Cell Biol.* 181:1047.

Guillou, L., Babataheri, A., Saitakis, M., Bohineust, A., Dogniaux, S., Hivroz, C., et al. (2016). T-lymphocyte passive deformation is controlled by unfolding of membrane surface reservoirs. *Mol. Biol. Cell* 27, 3574–3582.

Jahan, M. G. S., and Yumura, S. (2017). Traction force and its regulation during cytokinesis in *Dictyostelium* cells. *Eur. J. Cell Biol.* 96, 515–528.

Kaur, S., Fielding, A. B., Gassner, G., Carter, N. J., and Royle, S. J. (2014). An unmet actin requirement explains the mitotic inhibition of clathrin-mediated endocytosis. *Elife* 3:e00829.

Kitanishi-Yumura, T., and Fukui, Y. (1987). Reorganization of microtubules during mitosis in *Dictyostelium*: dissociation from MTOC and selective assembly/disassembly in situ. *Cell Motil. Cytoskeleton* 8, 106–117.

Knutton, S., Sumner, M. C., and Pasternak, C. A. (1975). Role of microvilli in surface changes of synchronized P815Y mastocytoma cells. *J. Cell Biol.* 66, 568–576.

Kumar, H., Pushpa, K., Kumari, A., Verma, K., Pergu, R., and Mylavarapu, S. V. S. (2019). The exocyst complex and Rab5 are required for abscission by localizing ESCRT III subunits to the cytokinetic bridge. *J. Cell Sci.* 132:jcs226001.

Li, W. M., Webb, S. E., Lee, K. W., and Miller, A. L. (2006). Recruitment and SNARE-mediated fusion of vesicles in furrow membrane remodeling during cytokinesis in zebrafish embryos. *Exp. Cell Res.* 312, 3260–3275.

Macro, L., Jaiswal, J. K., and Simon, S. M. (2012). Dynamics of clathrin-mediated endocytosis and its requirement for organelle biogenesis in *Dictyostelium*. *J. Cell Sci.* 125:5721.

Manstein, D. J., Titus, M. A., De Lozanne, A., and Spudich, J. A. (1989). Gene replacement in *Dictyostelium*: generation of myosin null mutants. *EMBO J.* 8, 923–932.

Masters, T. A., Pontes, B., Viasnoff, V., Li, Y., and Gauthier, N. C. (2013). Plasma membrane tension orchestrates membrane trafficking, cytoskeletal remodeling, and biochemical signaling during phagocytosis. *Proc. Natl. Acad. Sci. U.S.A.* 110, 11875–11880.

Masud Rana, A. Y., Tsujioka, M., Miyagishima, S., Ueda, M., and Yumura, S. (2013). Dynamin contributes to cytokinesis by stabilizing actin filaments in the contractile ring. *Genes Cells.* 18, 621–635.

Mohandas, N., and Evans, E. (1994). Mechanical properties of the red cell membrane in relation to molecular structure and genetic defects. *Annu. Rev. Biophys. Biomol. Struct.* 23, 787–818.

Montagnac, G., Sibarita, J. B., Loubery, S., Daviet, L., Romao, M., Raposo, G., et al. (2009). ARF6 interacts with JIP4 to control a motor switch mechanism regulating endosome traffic in cytokinesis. *Curr. Biol.* 19, 184–195.

Neujahr, R., Heizer, C., and Gerisch, G. (1997). Myosin II-independent processes in mitotic cells of *Dictyostelium discoideum*: redistribution of the nuclei, re-arrangement of the actin system and formation of the cleavage furrow. *J. Cell Sci.* 110, 123–137.

Niswonger, M. L., and O'Halloran, T. J. (1997). A novel role for clathrin in cytokinesis. *Proc. Natl. Acad. Sci. U.S.A.* 94, 8575–8578.

Raucher, D., and Sheetz, M. P. (1999). Membrane expansion increases endocytosis rate during mitosis. *J. Cell Biol.* 144, 497–506.

Robinett, C. C., Giansanti, M. G., Gatti, M., and Fuller, M. T. (2009). TRAPPII is required for cleavage furrow ingression and localization of Rab11 in dividing male meiotic cells of *Drosophila*. *J. Cell Sci.* 122, 4526–4534.

Royle, S. J., Bright, N. A., and Lagnado, L. (2005). Clathrin is required for the function of the mitotic spindle. *Nature* 434, 1152–1157.

Ruscetti, T., Cardelli, J. A., Niswonger, M. L., and O'Halloran, T. J. (1994). Clathrin heavy chain functions in sorting and secretion of lysosomal enzymes in *Dictyostelium discoideum*. *J. Cell Biol.* 126, 343–352.

Schmid-Schonbein, G. W., Shih, Y. Y., and Chien, S. (1980). Morphometry of human leukocytes. *Blood* 56, 866–875.

Schmoranzer, J., Kreitzer, G., and Simon, S. M. (2003). Migrating fibroblasts perform polarized, microtubule-dependent exocytosis towards the leading edge. *J. Cell Sci.* 116, 4513–4519.

Srivastava, V., Iglesias, P. A., and Robinson, D. N. (2016). Cytokinesis: robust cell shape regulation. *Semin. Cell Dev. Biol.* 53, 39–44.

Straight, A. F., and Field, C. M. (2000). Microtubules, membranes and cytokinesis. *Curr. Biol.* 10, R760–R770.

Tacheva-Grigorova, S. K., Santos, A. J., Boucrot, E., and Kirchhausen, T. (2013). Clathrin-mediated endocytosis persists during unperturbed mitosis. *Cell Rep.* 4, 659–668.

Taira, R., and Yumura, S. (2017). A novel mode of cytokinesis without cell-substratum adhesion. *Sci. Rep.* 7:17694.

Tanaka, M., Kikuchi, T., Uno, H., Okita, K., Kitanishi-Yumura, T., and Yumura, S. (2017). Turnover and flow of the cell membrane for cell migration. *Sci. Rep.* 7:12970.

Varsano, G., Wang, Y., and Wu, M. (2017). Probing mammalian cell size homeostasis by channel-assisted cell reshaping. *Cell Rep.* 20, 397–410.

Wang, N., Lee, I. J., Rask, G., and Wu, J. Q. (2016). Roles of the TRAPP-II complex and the exocyst in membrane deposition during fission yeast cytokinesis. *PLoS Biol.* 14:e1002437. doi: 10.1371/journal.pbio.1002437

Yumura, S. (2016). A novel low-power laser-mediated transfer of foreign molecules into cells. *Sci. Rep.* 6:22055.

Yumura, S., Matsuzaki, R., and Kitanishi-Yumura, T. (1995). Introduction of macromolecules into living *Dictyostelium* cells by electroporation. *Cell Struct. Funct.* 20, 185–190.

Yumura, S., Mori, H., and Fukui, Y. (1984). Localization of actin and myosin for the study of ameboid movement in *Dictyostelium* using improved immunofluorescence. *J. Cell Biol.* 99, 894–899.

Yumura, S., Ueda, M., Sako, Y., Kitanishi-Yumura, T., and Yanagida, T. (2008). Multiple mechanisms for accumulation of myosin II filaments at the equator during cytokinesis. *Traffic* 9, 2089–2099.

Zanchi, R., Howard, G., Bretscher, M. S., and Kay, R. R. (2010). The exocytic gene secA is required for *Dictyostelium* cell motility and osmoregulation. *J. Cell Sci.* 123, 3226–3234.

Zang, J. H., Cavet, G., Sabry, J. H., Wagner, P., Moores, S. L., and Spudich, J. A. (1997). On the role of myosin-II in cytokinesis: division of *Dictyostelium* cells under adhesive and nonadhesive conditions. *Mol. Biol. Cell* 8, 2617–2629.

Zhu, Q., and Clarke, M. (1992). Association of calmodulin and an unconventional myosin with the contractile vacuole complex of *Dictyostelium discoideum*. *J. Cell Biol.* 118, 347–358.

Conflict of Interest: The authors declare that the research was conducted in the absence of any commercial or financial relationships that could be construed as a potential conflict of interest.

frontiers in Cell and Developmental Biology

REVIEW
published: 18 June 2020
doi: 10.3389/fcell.2020.00441

The Unusual Suspects in Cytokinesis: Fitting the Pieces Together

Ly T. S. Nguyen[1] *and Douglas N. Robinson*[1,2,3,4,5]*

[1] Department of Cell Biology, Johns Hopkins School of Medicine, Baltimore, MD, United States, [2] Department of Pharmacology and Molecular Sciences, Johns Hopkins School of Medicine, Baltimore, MD, United States, [3] Department of Medicine, Johns Hopkins School of Medicine, Baltimore, MD, United States, [4] Department of Oncology, Johns Hopkins School of Medicine, Baltimore, MD, United States, [5] Chemical and Biomolecular Engineering, Johns Hopkins University Whiting School of Engineering, Baltimore, MD, United States

Cytokinesis is the step of the cell cycle in which the cell must faithfully separate the chromosomes and cytoplasm, yielding two daughter cells. The assembly and contraction of the contractile network is spatially and temporally coupled with the formation of the mitotic spindle to ensure the successful completion of cytokinesis. While decades of studies have elucidated the components of this machinery, the so-called *usual suspects*, and their functions, many lines of evidence are pointing to other unexpected proteins and sub-cellular systems as also being involved in cytokinesis. These we term the *unusual suspects*. In this review, we introduce recent discoveries on some of these new unusual suspects and begin to consider how these subcellular systems snap together to help complete the puzzle of cytokinesis.

Keywords: discoidin, chloride intracellular channels, importins, Ran, helicases, RNP, mmsdh

OPEN ACCESS

Edited by:
Maria Grazia Giansanti,
Italian National Research Council, Italy

Reviewed by:
Roberta Fraschini,
University of Milano-Bicocca, Italy
Giuliano Callaini,
University of Siena, Italy

***Correspondence:**
Douglas N. Robinson
dnr@jhmi.edu

Specialty section:
This article was submitted to Cell Growth and Division, a section of the journal Frontiers in Cell and Developmental Biology

Received: *23 March 2020*
Accepted: *11 May 2020*
Published: *18 June 2020*

Citation:
Nguyen LTS and Robinson DN (2020) The Unusual Suspects in Cytokinesis: Fitting the Pieces Together. Front. Cell Dev. Biol. 8:441. doi: 10.3389/fcell.2020.00441

OVERVIEW OF CYTOKINESIS

The growth and development of cells and tissues depend in part on the segregation of genetic and cytoplasmic components of a mother cell into two daughter cells during cell division. Defects in any step of this process can result in missegregation of genetic material, leading to multinucleation, polyploidy, and eventually aneuploidy, which is associated with many diseases, including cancer (Storchova and Pellman, 2004; Normand and King, 2010). The final step of cell cycle is cytokinesis, when a contractile network (CN) composed of actin filaments, non-muscle myosin II and other necessary factors work to physically divide the mother cell (Fujiwara et al., 2005; Shi and King, 2005; Robinson et al., 2012; Leite et al., 2019; Pollard and O'Shaughnessy, 2019). The CN is the driver and responder to active force production and can be organized into meshworks like those in mammalian and amoeboid cells or rings like those in yeasts (Fishkind and Wang, 1993; Kamasaki et al., 2007; Reichl et al., 2008). Furthermore, the fluid dynamics of the system that are created in part by cortical tension and the cell's viscoelastic properties are also major contributors to cytokinesis (Zhang and Robinson, 2005). Collectively, furrow ingression is driven by active (ATP consuming) contraction from myosin II pulling on actin filaments and the Laplace pressures created by cortical tension and local (cleavage furrow) and global/polar (emerging daughter cell) membrane curvatures (Zhang and Robinson, 2005; Poirier et al., 2012).

The process of the CN formation is spatially and temporally coupled with the assembly of the antiparallel, interdigitating microtubules, which can be formed either by the astral microtubules or the central spindle (Baker et al., 1993; Ding et al., 1993). The central spindle plays multiple roles during cell division, including segregation of chromosomes, positioning of the cleavage furrow, and separation of daughter cells (Straight and Field, 2000). Cytokinesis is completed by the process of abscission, facilitated by the ESCRT-III complexes, resulting in complete physical separation of the two daughter cells (Ettema and Bernander, 2009; Mierzwa and Gerlich, 2014).

While it has been appreciated for decades that cytokinesis is a highly robust and dynamic process, we are beginning to understand some of the mechanisms responsible for this robustness (Kee et al., 2012; Srivastava and Robinson, 2015; Srivastava et al., 2016; Singh et al., 2019). Crosstalk between and integration of various sub-cellular systems exist to ensure fidelity and coordination of the entire cellular system (Kothari et al., 2019a). The field has appropriately focused on what we will term the *usual suspects* – i.e., the players of actomyosin II CN, microtubule-based mitotic spindles, RhoGTPase regulators, and many others (**Figure 1**). However, many lines of evidence are pointing to many unexpected proteins and sub-cellular systems as also being involved in cytokinesis – we term these proteins the *unusual suspects*.

In this review, we focus on recent discoveries implicating some of these new unusual suspects- factors and proteins involved in pathways and networks that are generally assigned different sub-cellular roles, but that appear to be contributing to the cytokinesis machinery too. These unusual suspects are categorized into a total of four groups: membrane-associated proteins, RNA-related proteins, nuclear proteins, and metabolic enzymes. We anticipate that embracing these new players will lead the field to uncover a more holistic understanding of how cytokinesis works. But, perhaps more importantly, they will also guide us to a deeper understanding of how cellular systems are integrated in complex biological processes more broadly. Moreover, we want to state up front that we believe that this list of unusual suspects is just beginning to take off, and therefore, we expect that the list presented here is neither comprehensive nor final.

MEMBRANE-ASSOCIATED PROTEINS

Discoidin

Discoidin I and II are *N*-acetylgalactosamine (GalNAc)-binding lectins found predominantly in the cytoplasm of the amoeba *Dictyostelium discoideum* (Alexander et al., 1992). Classically, the discoidins are considered key to *Dictyostelium* development as their expression increases as the *Dictyostelium* cells enter the developmental stage (Rosen et al., 1973; Frazier et al., 1975). Originally, discoidins were suggested to play a role in mediating cell–cell interaction owing to their lectin properties. However, Discoidin I was recently found to interact genetically and biochemically with a key protein involved in cell contractility and cytokinesis, namely cortexillin I (Robinson and Spudich, 2000; Kothari et al., 2019b). Myosin II and the actin crosslinker Cortexillin I are essential components of the CN and their mechanosensory ability and accumulation at the cleavage furrow were proven to be vital for the progression and completion of cytokinesis (Faix et al., 2001; Zhang and Robinson, 2005; Effler et al., 2007; Kee and Robinson, 2008; Ren et al., 2009). *In vivo* interactions of discoidin I and cortexillin I as well as IQGAP2, an activator of Cortexillin I and Myosin II, were also confirmed using fluorescence cross-correlation spectroscopy. Interestingly, discoidin also acts as a genetic suppressor of *cortexillin I* null mutants through a selection for genetic suppressors where discoidin overexpression could rescue the developmental phenotypes of *cortexillin I* null cells (Robinson and Spudich, 2000). Collectively, discoidin proteins might provide a scaffolding function and help recruit essential components of the CN system to the division site during cytokinesis.

Another possibility is that the discoidins may help to directly connect the CN to the plasma membrane. It is not fully understood in any system how the CN is attached to the membrane, particularly in the context of cytokinesis. Dividing *Dictyostelium* cells show an enrichment of glycosylated proteins at the cleavage furrow membrane as the lectin concanavalin A preferentially labels the cleavage furrow membrane (Faix et al., 2001). Thus, the combination of observations suggests a provocative hypothesis that extracellular discoidin might also interact with the cortical cytoskeleton through a transmembrane domain containing protein. The human discoidin domain receptor (DDR1) protein does exactly this, except it contains a transmembrane domain and interacts with non-muscle myosin IIA (Huang et al., 2009). Invasive tumors and associated metastases show elevated expression of DDR1, suggesting its role as a promoter of tumor cell invasion (Yang et al., 2010; Henriet et al., 2018). However, this type of function would most likely be distinct from discoidin's function in forming complexes with cortexillin and IQGAP2 in the cytoplasm.

Discoidin was not the first sugar-related protein that was speculated to be crucial in cytokinesis-related processes. Mucin is also a glycosylated protein and is a component of ring canals and intercellular bridges, structures formed by incomplete cytokinesis, in various cell types and tissues in *Drosophila melanogaster* (Robinson and Cooley, 1997; Kramerova and Kramerov, 1999). Even though the exact functions of mucinoprotein in ring canal networks are not well-understood, it is possible that it might be an important constituent of a complex or backbone that facilitates the assembly of these structures. Further studies are needed to elaborate on the exact roles and functions of discoidin and other sugar-binding proteins that take part in cytokinesis.

Chloride Intracellular Channels

Another unexpected class of membrane proteins that were found to play a role in cytokinesis are the highly-conserved chloride intracellular channels (CLICs). Comprised of six members that exist primarily as membrane-bound proteins, CLICs are involved in diverse cellular functions, including cell-cell interactions, angiogenesis, and membrane potential regulation (Rual et al., 2005; Singh and Ashley, 2007; Chalothorn et al., 2009). Multiple

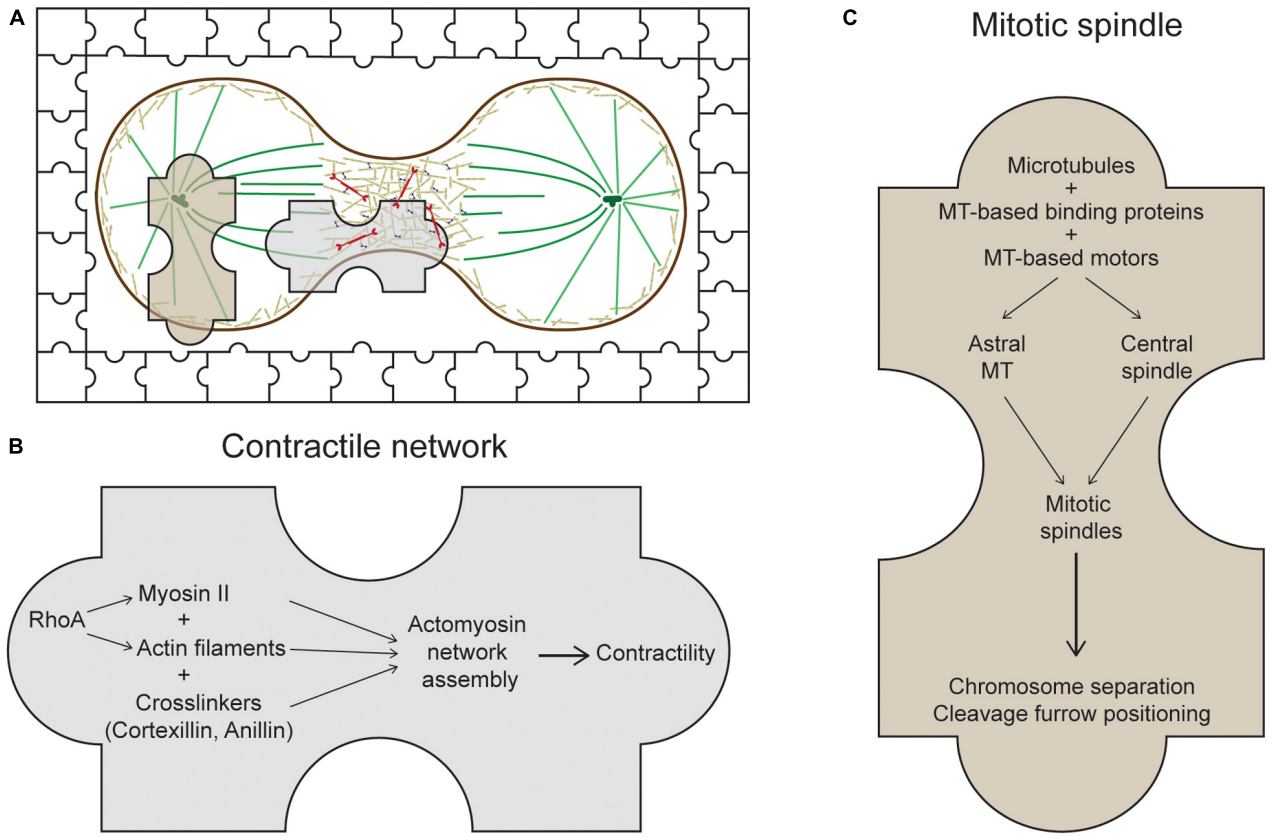

FIGURE 1 | The *usual suspects* of cytokinesis. **(A)** During cytokinesis, the cell cortex contracts at the midzone forming the cleavage furrow. The system at work is presented as a jigsaw puzzle with multiple pieces coming together. Many players of this process can be categorized into two main sets of machinery: the contractile network (CN) and the mitotic spindle, represented by the two large jigsaw pieces. **(B)** The CN consists of actin filaments, myosin II, and actin crosslinkers, which are organized into meshworks or rings and which generate mechanical forces at the cleavage furrow. One major regulator of this CN in metazoans is the RhoA small GTPase (Chircop, 2014). **(C)** The mitotic spindle is composed of antiparallel, interdigitating microtubules that form either the astral microtubules or the central spindle. Along with its binding proteins and motors, the mitotic spindle segregates the chromosomes, positions the cleavage furrow, and helps regulate daughter cell separation.

studies have also implicated CLIC4 in cancer progression. The expression level of CLIC4 was found to be gradually decreased in squamous cancer cells as they transformed from benign to malignant, a prominent indicator of a role in mitosis regulation (Suh et al., 2012).

Growing evidence implicates the function of CLIC4 in actin-mediated processes (Suginta et al., 2001; Singh et al., 2007; Singh, 2010). For instance, CLIC4 is recruited to the plasma membrane and the cleavage furrow upon activation of RhoA in an F-actin-dependent manner (Ponsioen et al., 2009; Argenzio et al., 2018). Additionally, CLIC4 is a direct molecular interactor of profilin-1 and a component in the RhoA-mDia2 signaling pathway that induces cortical actin polymerization (Argenzio et al., 2018). A previous proteomics study investigating the biochemical changes at the cell surface during cell division revealed a significant enrichment of both CLIC4 and CLIC1 on the surface of rounded up mitotic cells compared with flat interphase cells (Ozlu et al., 2015). A recent study comparing the interaction networks of CLIC4 and a CLIC4 mutant version defective in putative substrate binding led to the identification of ezrin, anillin, and ALIX, proteins known to be crucial for cytokinesis, as partners of CLIC4 (Uretmen Kagiali et al., 2020). Furthermore, double knockout of CLIC4 and CLIC1 subsequently impaired the stability of membrane-cortical actin interaction. HeLa cells lacking both CLIC4 and CLIC1 displayed abnormal bleb formation and defective abscission (Uretmen Kagiali et al., 2020). In another study, cells absent of CLIC4 had significantly decreased recruitment of myosin IIA and IIB to the furrow, similarly leading to membrane blebbing and impeding CN maturation (Peterman et al., 2020). It was also previously found that cortical actin controls cell cycle progression, and tumor cells lose their dependence on cortical branched actin (Molinie et al., 2019). Through their role in maintaining cortical and CN stability, CLICs might facilitate normal mitotic progression and prevent the transformation from benignity to malignancy in cancer cells.

Overall, CLIC4 and CLIC1 are two additional membrane-associated proteins that are recruited to the cortex, where they

potentially help anchor the CN, allowing for proper contraction and cell division.

RNA-RELATED PROTEINS

RNA-Binding Proteins

RNPs (ribonucleoproteins) are a large family of RNA-binding proteins that have important roles in mRNA translation and regulation (Ziemienowicz et al., 2003). RNPs commonly localize in nuclei and cytoplasmic mRNP granules. In general, they contain one or more RNA-recognition motifs (RRMs) and often have a predicted intrinsically disorganized region (IDR). While the exact functions of many RNPs are still being defined, studies in some systems indicate that RNPs contribute to cytokinesis.

In *Dictyostelium*, overexpression of RNP-1A suppresses the effect of nocodazole, a microtubule inhibitor, on cellular growth of *Dictyostelium discoideum* (Zhou et al., 2010; Ngo et al., 2016). This protein has protective functions on the microtubule ends, and also localizes to the polar cortex in dividing cells and to the leading edges of migrating cells. These strongly suggest a role of RNP-1A in regulating microtubule dynamics, possibly through stabilizing the linkage between microtubules and the cortex. A later study using proteomics found that a separate RNP, RNP-1B, was a molecular interactor of cortexillin I (Kothari et al., 2019b). In the same study, using fluorescence cross-correlation spectroscopy, RNP-1A was found to interact strongly with cortexillin I. The full significance of these interactions is still under investigation.

The recognition of RNA-binding proteins as potential effectors of cytokinesis was not entirely surprising, as CAR-1, another RNA-binding protein found at P granules and the mitotic spindle during cell division, was identified using an RNA-interference screen for genes essential for cytokinesis in *C. elegans* embryos (Zipperlen et al., 2001; Boag et al., 2005; Squirrell et al., 2006). In *car-1*-depleted embryos, cleavage furrow ingression was significantly disrupted, and the anaphase spindle structure was greatly defective (Audhya et al., 2005). As the study was conducted primarily in early *C. elegans* embryos where tight temporal-spatial regulations of maternally supplied RNAs are critical, the defects found in *car-1*-depleted cells may be due to the local translational incompetence of microtubule components. This effect was similar to a previously characterized RNA-binding protein, CPEB, whose inhibition also results in spindle structural defects (Groisman et al., 2000). Overall, these roles of RNA-binding proteins in cytokinesis regulation elucidates an important crosstalk between local protein translation and steps in cell division. It is tempting to speculate that the unique localization and interactions of these RNP-1 proteins facilitates localized mRNA translation during cytokinesis when cells are undergoing dynamic and robust cell shape changes.

RNA Helicases

Another unusual suspect that falls under the realm of RNA-related proteins are the RNA helicases. The importance of RNA helicases in regulating cell cycle progression and mitosis is not entirely surprising. Indeed, since the progression of the cell cycle requires the coordination of enormous cohorts of differentially expressed proteins through each step, cells need mechanisms to tightly regulate mRNA transcription, translation, and protein degradation to facilitate this dynamic process. For example, RNA helicases have been implicated to play critical roles in mRNA export pathways that are tightly linked to gene products involved in mitosis regulation (Strasser and Hurt, 2001; Herold et al., 2003). Indeed, the RNA helicases UAP56 and URH49 were characterized to form distinct mRNA export machineries to regulate a subset of genes specifically involved in mitosis (Yamazaki et al., 2010). Depletion of these RNA helicases, as a result, leads to mitotic progression defects.

However, unexpected functions of several RNA helicases in cytokinesis independent from its traditional roles in regulating mitotically expressed proteins have been discovered. CGH-1, a DEAD box RNA helicase that localizes to P granules and other possible mRNA–protein particles, was originally identified to be in a multiprotein complex together with CAR-1, another unusual suspect mentioned above, and a localization regulator of CAR-1 in *C. elegans* (Navarro et al., 2001; Audhya et al., 2005). Embryos depleted of *cgh-1* had penetrant sterility while those partially depleted exhibited perturbed localization of CAR-1 and phenocopied *car-1*-depleted cells with defects in microtubule structures. The study suggested that CGH-1 and CAR-1 cooperatively regulate anaphase spindle structure in embryonic cytokinesis.

Interestingly, CGH-1 is the *C. elegans* homolog of DDX6, a member of DEAD box RNA helicase proteins DDXs, which is involved diverse pathways, including mRNP assembly and export, immune response, regulation of cell cycle progression and tumorigenesis (Fuller-Pace, 2013). The exact functions of DDXs in regulating cell cycle and tumorigenesis remain controversial. Knockdown of DDX3 in mice embryonic cells led to reduced growth and proliferation (Li et al., 2014). However, a recent study elucidated a possible mechanism through which DDX3, another member of the DDX family, positively controls cytokinesis and subsequently acts as a tumor suppressor. DDX3 localizes to centrosomes throughout the cell cycle and prevents chromosome misalignment by inactivating and aggregating supernumerary centrosomes (Chen et al., 2017). DDX silencing subsequently led to chromosome misalignment, segregation defects, and eventually cell death. In another study, loss of DDX3 led to enhanced cell proliferation (Chang and Liu, 2010). Moreover, DDX3 localizes to the midbody during late cell division (Chen et al., 2017). These studies support the possibility of novel roles of RNA helicases in maintaining structural integrity of essential mitotic and cytokinesis components, therefore ensuring successful completion of cell division.

NUCLEAR PROTEINS

Importin-β

Importin-β (human transportin/karyopherin b2) acts as a transporter for proteins and complexes, moving them into the

nucleus. Once thought to be exclusively a transporter, importin-β is gradually emerging as a regulator of various other cellular processes, including cell cycle and cytokinesis. For instance, a mutation in the coding gene *Kap104,* which codes for the importin-β homolog in budding yeast, promotes mitotic exit (Asakawa and Toh-e, 2002). Overexpression of importin-β also leads to aberrant spindle formation and delayed mitotic progression (Roscioli et al., 2012).

In the context of cytokinesis, importin-β might function through interacting with anillin – a direct interactor of the cytokinetic regulator RhoA and a scaffolding protein of the CN. Anillin contains a highly conserved nuclear localization signal (NLS) that binds to importin-β and is needed to mediate cortical polarization during cytokinesis; mutating its NLS significantly reduces anillin's affinity for the equatorial cortex (Beaudet et al., 2017). Interestingly, overexpression of importin-β negatively regulates anillin's cortical localization, instead of enhancing it, suggesting that importin-β competes with a cortical receptor for anillin binding. Thus, free importins may function as a molecular ruler, or buffer, for which an optimal level is required to maintain the appropriate cortical recruitment of anillin. Binding of importin-β is directly regulated by Ran-GTP and therefore, the potential functions of importin-β in cytokinesis are likely to be coupled with Ran and its GTP gradient, whose potential cytokinetic functions are discussed next.

RAN

Ras-related nuclear protein (Ran) is a small G-protein involved in transporting various proteins and cellular components in and out of the nucleus through the nuclear pore complex. The function of Ran is tightly regulated by the GTP gradient across the nuclear membrane. Ran has been implicated in numerous cellular processes such as DNA synthesis, nuclear envelope structure, and cell cycle progression (Sazer and Dasso, 2000). Mounting evidence now suggests that Ran also participates in regulating cytokinesis.

Recent studies revealed that chromatin-associated signals can regulate the cortical dynamics during cytokinesis (Norden et al., 2006; Mendoza et al., 2009). Due to its concentration gradient with the peak occurring around the chromatin, chromatin-associated Ran-GTP is potentially also a regulator of the cortex. During meiosis of mouse oocytes, chromatin positioned near the cortex induces the formation of an actin cap via Ran-GTP, and the placement of DNA-coated beads near the cortex induces cortical polarity independent of microtubules (Deng et al., 2007). Active Ran regulates human anillin during anaphase and decreasing Ran-GTP leads to the ectopic localization of anillin and myosin to the cell poles and blocks proper furrowing (Beaudet et al., 2017). These studies suggested that a chromatin-associated Ran-GTP gradient may function as a molecular ruler that helps recruit and organize essential components at the cortex.

In another study, Ran-GTP was found to positively regulate the actomyosin cortex for pseudocleavage furrowing in the early *Drosophila* embryo development (Silverman-Gavrila et al., 2008). Ran controls pseudocleavage furrow organization independently of its role in regulating the microtubule cytoskeleton. Further, disruption of the Ran pathway prevented pseudocleavage furrow formation and restricted the depth and duration of furrow ingression of those pseudocleavage furrows that did form. To further elucidate the mechanism through which Ran-GTP acts to regulate cytokinesis, the authors found that Ran is required for the pseudocleavage furrow localization of the septin, peanut, a protein whose association with anillin contributes to stabilization of the CN. In fact, the direct binding of the nuclear transport receptors importin-α and -β to anillin prevented the binding of peanut to anillin (van Oostende Triplet et al., 2014), and since binding of importin-β is directly regulated by Ran-GTP, Ran appears to be a regulator of anillin and peanut's association. Therefore, Ran-GTP plays an important role in pseudocleavage furrow ingression in syncytial embryos.

Overall, Ran-GTP acts as a microtubule-independent pathway that regulates polarization of contractile protein anillin (a process traditionally thought to require microtubules) to couple signals from the chromatin to the cortex and to ensure robustness of cytokinesis.

Lamin B

Lamins are important constituents of the nuclear lamina in eukaryotes. Apart from their functions in maintaining the structural integrity of the nuclear pores and membranes, lamins are crucial for the assembly and disassembly of the nuclear envelope during mitosis (Lopez-Soler et al., 2001; Gruenbaum et al., 2005). In addition to its canonical roles within the nucleus, lamin B, a ubiquitously expressed type of lamin, helps regulate mitosis. In M-phase-arrested *Xenopus* egg extracts, lamin B associates with the mitotic spindles as well as the surrounding regions of the spindle. When expression of lamin B was reduced using siRNA in HeLa cells, typical spindle defects such as poor spindle morphology and lack of chromosome segregation were detected, suggesting a role for lamin B in facilitating spindle assembly (Tsai et al., 2006). In the same study, the authors also reported that lamin B is also an essential component in the formation of the mitotic matrix, allowing for tethering for other spindle assembly factors. Dominant negative forms of lamin B significantly disrupted this matrix formation, leading to severing of the mitotic spindles and cytokinesis arrest. These results indicate the significant role of lamin B in maintaining the integrity of mitotic spindles during cytokinesis. The prevailing idea to explain these observations is that the disassembled lamin B is dispersed throughout the cytoplasm during mitosis. However, a fraction of lamin B may remain associated with the mitotic spindle and/or mitotic chromosomes (Beaudouin et al., 2002). This pattern of localization of lamin B elucidates its novel role in regulating cytokinesis. Interestingly, association of lamin B with the mitotic spindle is regulated by Ran-GTP, eliciting the possibility of an entirely novel pathway of mitotic spindle regulation involving Ran and its downstream targets (Ma et al., 2007; Cavazza and Vernos, 2015). Strikingly, ESCRT-III-mediated membrane fusion facilitates reintegration of lagging chromosome fragments into micronuclei through lamin-based channels during cytokinesis in *Drosophila*, emphasizing the intricate integration between

the abscission and chromosome segregation machineries during cytokinesis (Warecki et al., 2020).

METABOLIC ENZYMES

Methylmalonate-Semialdehyde Dehydrogenase

Methylmalonate-semialdehyde dehydrogenase (mmsdh) is an enzyme typically thought of being located in the mitochondria and that helps catalyze the production of propionyl- and acetyl-CoA (Kedishvili et al., 2000). Recent studies suggests a possible novel role of mmsdh in regulating cytokinesis. Previously identified in a genetic suppression screen in *Dictyostelium*, over-expression of mmsdh suppressed the dominant-negative phenotype of a myosin II phosphomimetic (Ren et al., 2014). For context, to generate force, the non-muscle myosin II must polymerize into bipolar filaments, and this assembly is regulated by heavy chain phosphorylation. The myosin II phosphomimetic mimics this phosphorylated state and impairs bipolar filament assembly (Egelhoff et al., 1993). Mmsdh promoted myosin II phosphomimetic accumulation at the cortex and cleavage furrow in *myoII* null cells, thus potentially acting as a modulator of myosin II function (Ren et al., 2014).

Importantly, mmsdh showed up again as a molecular interactor of cortexillin I and IQGAP2, core mechanosensory proteins in the contractility system (Kothari et al., 2019b). It is possible that mmsdh functions in cytokinesis through a metabolic pathway that leads to post-translational modification of several contractile enzymes, including myosin II. Mmsdh catalyzes the degradation of valine, leading to the production of propionyl-CoA. Indeed, post-transtional modifications are important in modulating proteins involved in cytokinesis. In mammalian cells, anillin and myosin IIA are acetylated during

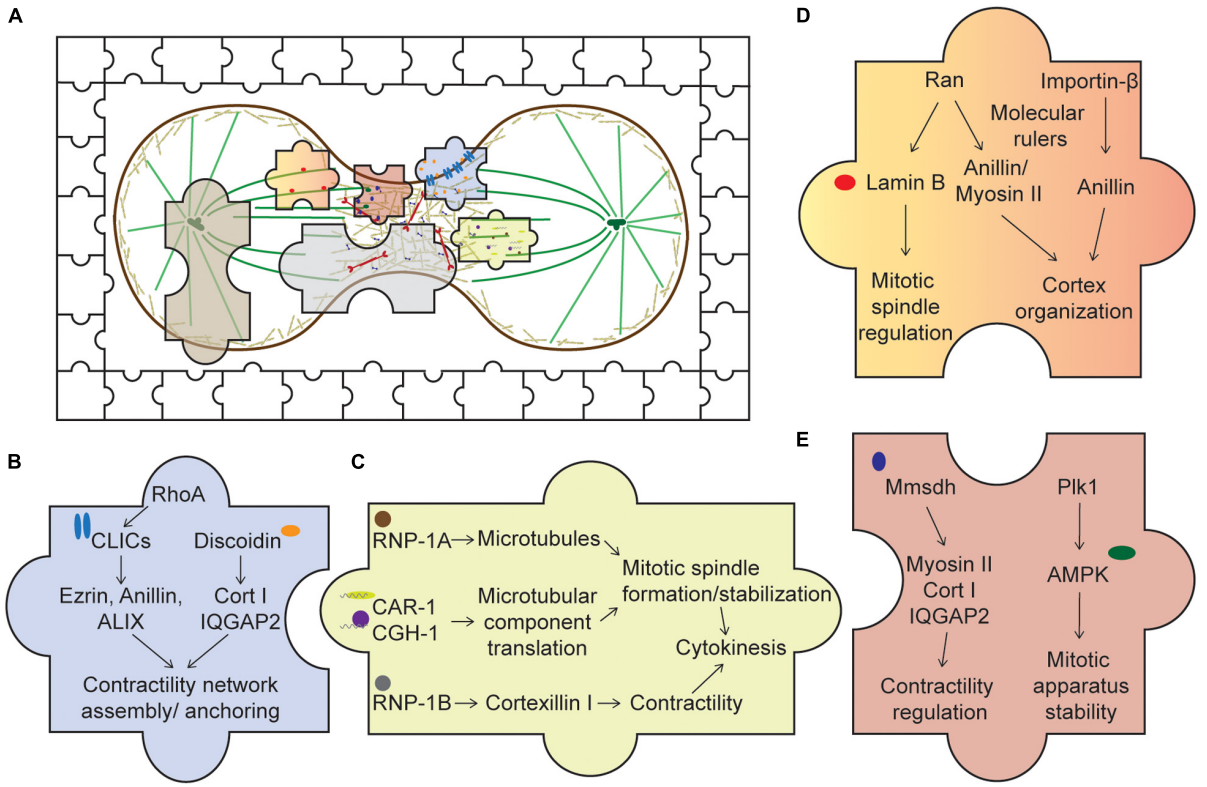

FIGURE 2 | Piecing together the *unusual suspects* of the cytokinesis system. **(A)** An overview of cytokinesis with both the usual and unusual suspects, represented by the jigsaw pieces. Expanding our understanding of cytokinesis by studying these unusual suspects allows us to fully appreciate an intricate cellular system complete with cross talks, redundancy, and network integration. **(B)** Membrane-associated proteins. Upon activation of RhoA, CLICs localize to the cortex where they bind various cortical components, such as profilin-1 and ezrin. Through these interactions, CLICs may help stabilize the cortex and anchor the CN to the membrane. Discoidin, through its interaction with the actin crosslinker cortexillin I and its regulator IQGAP2, might facilitate the assembly of the contractility network. **(C)** RNA-associated proteins. RNP-1A through its protection of microtubules during cytokinesis may stabilize the mitotic spindle, ensuring successful cytokinesis. CAR-1 and CGH-1's roles are proposed to facilitate local translation of microtubule components, ensuring proper formation of the mitotic spindle. On the other hand, RNP-1B interacts with cortexillin I and might play a role in regulating the contractility network. **(D)** Nuclear proteins. Ran and importin-β, through their interactions with various cortical proteins, such as anillin and myosin II, may act as molecular rulers, or buffers, coupled with a GTP gradient to ensure optimal recruitment of these components to the cortex. In addition, lamin B, an interactor of Ran, is crucial for mitotic spindle assembly. **(E)** Metabolic enzymes. Mmsdh appears to help myosin II function and is a biochemical interactor of cortexillin I and IQGAP2. Along with its original known biochemical activity in valine degradation, leading to the production of propionyl- and acetyl-CoA, mmsdh may promote the post-translational modification of contractile proteins, such as myosin II. AMPK is also important for mitotic apparatus assembly and regulation. Activation of AMPK by Plk1 may be important to couple cellular bioenergetic state to cell cycle progression.

cytokinesis, and histone deacetylase (HDAC) inhibitors lead to cytokinetic defects, consistent with this concept (Chuang et al., 2010; Coulton et al., 2010; Marinova et al., 2011).

AMP-Activated Protein Kinase

AMP-activated protein kinase (AMPK) is a highly conserved serine/threonine kinase that plays central roles in metabolic stress sensing that facilitates intracellular ATP preservation in response to energy deprivation (Hardie, 2007; Jones and Thompson, 2009). AMPK is present in the nucleus and cytoplasm, and its intracellular distribution is regulated by stress and cell growth (Kodiha et al., 2007). In addition to its role as an energy sensor, AMPK was found to act as a suppressor of cell proliferation. Enhanced activation of AMPK inhibits tumor growth and oncogenic transformation of several cancer cell lines (Zakikhani et al., 2006; Kuhajda, 2008). Many studies followed to elucidate the mechanisms of AMPK regulating cell division. Substantial evidence now suggests that AMPK plays obligatory role in chromosome segregation and cytokinesis completion. A *Drosophila* genomic screen identifies AMPK as a gene crucial for proper cell cycle progression. S2 cells lacking AMPK expression show strong defects in spindle morphology (Bettencourt-Dias et al., 2004). In human cancer-derived epithelial cells, the active form of AMPK α-catalytic subunit transiently associates with several mitotic structures including centrosomes and central spindle midzone from early stages of mitosis to cytokinetic completion (Vazquez-Martin et al., 2009). Furthermore, kinase activity of Plk1, a major regulator of mitotic progression, regulates localization and activation of AMPK at the mitotic apparatus. Pharmacological inhibition of PLK1 disrupts normal localization and phosphorylation of AMPK at its catalytic site, leading to cytokinesis failure (Vazquez-Martin et al., 2011). Studies in budding yeast reveal similar observations. Loss of Snf1, the budding yeast ortholog of AMPK, caused cells to display aberrant spindle alignment, further highlighting its role in regulating the mitotic spindle (Tripodi et al., 2018). The exact mechanisms and functions of AMPK in the context of cytokinesis regulation remain to be elucidated, but AMPK could be central to physically and temporally tethering the energy state of a cell to cell cycle progression.

CONCLUSION

While substantial progress has been made with regard to the intricacies of the CN and mitotic spindle formation and function, we are now in position to appreciate that cytokinesis results from the function of a truly integrated and collaborative cellular system (**Figure 2**). Further, these examples of unusual suspects in cytokinesis can help motivate us to think beyond the scope of just a few sub-cellular systems and pathways that drive a cellular process. We also should take into consideration that under physiological contexts, a cellular system is under constant environmental pressures that can be chemical and mechanical in nature. Cells are exquisitely exceptional at coping with these challenges. Recent studies have drawn upon this principle to identify new roles of known factors as well as new unknown factors. For instance, a study recently published used mechanically loaded cellular systems to study cytokinesis in the context of mechanics and identified new functions of several factors (Singh et al., 2019). The authors found that factors such as MEL-11 and LIN-5, canonically involved in regulating myosin II function and spindle positioning, respectively, are also involved in regulating cortical rotation, further elucidating how cells simultaneously respond to and create forces during cytokinesis.

Expanding our understanding of cytokinesis by studying these unusual suspects allows us to fully appreciate an intricate cellular system loaded with cross talks, redundancy, and network integration. By doing so, we will begin to better understand how other systems operate. For example, RNPs localize to and help organize P-granules, leading to the concept of phase transitions. It is also important to note that most current scientific methods still focus on cells and tissues in their most optimal culturing or physiological conditions. However, cells in their native contexts, such as in the tissue of an organism, are embedded in a complex 3D environment where they are constantly challenged with stresses and signals from their surroundings. No doubt, the concept of cellular complexes being formed through low affinity, highly dynamic, and responsive interactions is a more general underpinning of highly integrated, robust, and adaptive cellular systems and processes for which cytokinesis is a model example.

AUTHOR CONTRIBUTIONS

LN and DR wrote and edited the review.

FUNDING

This work was supported by the National Institutes of Health (GM66817 and HL124099) and DARPA (HR0011-16-C-0139).

ACKNOWLEDGMENTS

We thank the members of the Robinson lab for providing helpful feedback on the review.

REFERENCES

Alexander, S., Sydow, L. M., Wessels, D., and Soll, D. R. (1992). Discoidin proteins of Dictyostelium are necessary for normal cytoskeletal organization and cellular morphology during aggregation. *Differentiation* 51, 149–161. doi: 10.1111/j.1432-0436.1992.tb00691.x

Argenzio, E., Klarenbeek, J., Kedziora, K. M., Nahidiazar, L., Isogai, T., Perrakis, A., et al. (2018). Profilin binding couples chloride intracellular channel protein CLIC4 to RhoA-mDia2 signaling and filopodium formation. *J. Biol. Chem.* 293, 19161–19176. doi: 10.1074/jbc.RA118.002779

Asakawa, K., and Toh-e, A. (2002). A defect of Kap104 alleviates the requirement of mitotic exit network gene functions in Saccharomyces cerevisiae. *Genetics* 162, 1545–1556.

Audhya, A., Hyndman, F., McLeod, I. X., Maddox, A. S., Yates, J. R. III, Desai, A., et al. (2005). A complex containing the Sm protein CAR-1 and the RNA helicase CGH-1 is required for embryonic cytokinesis in *Caenorhabditis elegans*. *J. Cell Biol.* 171, 267–279. doi: 10.1083/jcb.200506124

Baker, J., Theurkauf, W. E., and Schubiger, G. (1993). Dynamic changes in microtubule configuration correlate with nuclear migration in the preblastoderm *Drosophila embryo*. *J. Cell Biol.* 122, 113–121. doi: 10.1083/jcb.122.1.113

Beaudet, D., Akhshi, T., Phillipp, J., Law, C., and Piekny, A. (2017). Active Ran regulates anillin function during cytokinesis. *Mol. Biol. Cell* 28, 3517–3531. doi: 10.1091/mbc.E17-04-0253

Beaudouin, J., Gerlich, D., Daigle, N., Eils, R., and Ellenberg, J. (2002). Nuclear envelope breakdown proceeds by microtubule-induced tearing of the lamina. *Cell* 108, 83–96. doi: 10.1016/s0092-8674(01)00627-4

Bettencourt-Dias, M., Giet, R., Sinka, R., Mazumdar, A., Lock, W. G., Balloux, F., et al. (2004). Genome-wide survey of protein kinases required for cell cycle progression. *Nature* 432, 980–987. doi: 10.1038/nature03160

Boag, P. R., Nakamura, A., and Blackwell, T. K. (2005). A conserved RNA-protein complex component involved in physiological germline apoptosis regulation in C. elegans. *Development* 132, 4975–4986. doi: 10.1242/dev.02060

Cavazza, T., and Vernos, I. (2015). The RanGTP pathway: from nucleo-cytoplasmic transport to spindle assembly and beyond. *Front. Cell Dev. Biol.* 3:82. doi: 10.3389/fcell.2015.00082

Chalothorn, D., Zhang, H., Smith, J. E., Edwards, J. C., and Faber, J. E. (2009). Chloride intracellular channel-4 is a determinant of native collateral formation in skeletal muscle and brain. *Circ. Res.* 105, 89–98. doi: 10.1161/CIRCRESAHA.109.197145

Chang, T. C., and Liu, W. S. (2010). The molecular evolution of PL10 homologs. *BMC Evol. Biol.* 10:127. doi: 10.1186/1471-2148-10-127

Chen, W. J., Wang, W. T., Tsai, T. Y., Li, H. K., and Lee, Y. W. (2017). DDX3 localizes to the centrosome and prevents multipolar mitosis by epigenetically and translationally modulating p53 expression. *Sci. Rep.* 7:9411. doi: 10.1038/s41598-017-09779-w

Chircop, M. (2014). Rho GTPases as regulators of mitosis and cytokinesis in mammalian cells. *Small GTPases* 5:e29770. doi: 10.4161/sgtp.29770

Chuang, C., Lin, S. H., Huang, F., Pan, J., Josic, D., and Yu-Lee, L. Y. (2010). Acetylation of RNA processing proteins and cell cycle proteins in mitosis. *J. Proteome Res.* 9, 4554–4564. doi: 10.1021/pr100281h

Coulton, A. T., East, D. A., Galinska-Rakoczy, A., Lehman, W., and Mulvihill, D. P. (2010). The recruitment of acetylated and unacetylated tropomyosin to distinct actin polymers permits the discrete regulation of specific myosins in fission yeast. *J. Cell Sci.* 123(Pt 19), 3235–3243. doi: 10.1242/jcs.069971

Deng, M., Suraneni, P., Schultz, R. M., and Li, R. (2007). The Ran GTPase mediates chromatin signaling to control cortical polarity during polar body extrusion in mouse oocytes. *Dev. Cell* 12, 301–308. doi: 10.1016/j.devcel.2006.11.008

Ding, R., McDonald, K. L., and McIntosh, J. R. (1993). Three-dimensional reconstruction and analysis of mitotic spindles from the yeast, Schizosaccharomyces pombe. *J. Cell Biol.* 120, 141–151. doi: 10.1083/jcb.120.1.141

Effler, J. C., Iglesias, P. A., and Robinson, D. N. (2007). A mechanosensory system controls cell shape changes during mitosis. *Cell Cycle* 6, 30–35. doi: 10.4161/cc.6.1.3674

Egelhoff, T. T., Lee, R. J., and Spudich, J. A. (1993). Dictyostelium myosin heavy chain phosphorylation sites regulate myosin filament assembly and localization in vivo. *Cell* 75, 363–371. doi: 10.1016/0092-8674(93)80077-r

Ettema, T. J., and Bernander, R. (2009). Cell division and the ESCRT complex: a surprise from the archaea. *Commun. Integr. Biol.* 2, 86–88. doi: 10.4161/cib.7523

Faix, J., Weber, I., Mintert, U., Kohler, J., Lottspeich, F., and Marriott, G. (2001). Recruitment of cortexillin into the cleavage furrow is controlled by Rac1 and IQGAP-related proteins. *EMBO J.* 20, 3705–3715. doi: 10.1093/emboj/20.14.3705

Fishkind, D. J., and Wang, Y. L. (1993). Orientation and three-dimensional organization of actin filaments in dividing cultured cells. *J. Cell Biol.* 123, 837–848. doi: 10.1083/jcb.123.4.837

Frazier, W. A., Rosen, S. D., Reitherman, R. W., and Barondes, S. H. (1975). Purification and comparison of two developmentally regulated lectins from *Dictyostelium discoideum*. Discoidin I and II. *J. Biol. Chem.* 250, 7714–7721.

Fujiwara, T., Bandi, M., Nitta, M., Ivanova, E. V., Bronson, R. T., and Pellman, D. (2005). Cytokinesis failure generating tetraploids promotes tumorigenesis in p53-null cells. *Nature* 437, 1043–1047. doi: 10.1038/nature04217

Fuller-Pace, F. V. (2013). DEAD box RNA helicase functions in cancer. *RNA Biol.* 10, 121–132. doi: 10.4161/rna.23312

Groisman, I., Huang, Y. S., Mendez, R., Cao, Q., Theurkauf, W., and Richter, J. D. (2000). CPEB, maskin, and cyclin B1 mRNA at the mitotic apparatus: implications for local translational control of cell division. *Cell* 103, 435–447. doi: 10.1016/s0092-8674(00)00135-5

Gruenbaum, Y., Margalit, A., Goldman, R. D., Shumaker, D. K., and Wilson, K. L. (2005). The nuclear lamina comes of age. *Nat. Rev. Mol. Cell Biol.* 6, 21–31. doi: 10.1038/nrm1550

Hardie, D. G. (2007). AMP-activated/SNF1 protein kinases: conserved guardians of cellular energy. *Nat. Rev. Mol. Cell Biol.* 8, 774–785. doi: 10.1038/nrm2249

Henriet, E., Sala, M., Abou Hammoud, A., Tuariihionoa, A., Di Martino, J., Ros, M., et al. (2018). Multitasking discoidin domain receptors are involved in several and specific hallmarks of cancer. *Cell Adh. Migr.* 12, 363–377. doi: 10.1080/19336918.2018.1465156

Herold, A., Teixeira, L., and Izaurralde, E. (2003). Genome-wide analysis of nuclear mRNA export pathways in *Drosophila*. *EMBO J.* 22, 2472–2483. doi: 10.1093/emboj/cdg233

Huang, Y., Arora, P., McCulloch, C. A., and Vogel, W. F. (2009). The collagen receptor DDR1 regulates cell spreading and motility by associating with myosin IIA. *J. Cell Sci.* 122(Pt 10), 1637–1646. doi: 10.1242/jcs.046219

Jones, R. G., and Thompson, C. B. (2009). Tumor suppressors and cell metabolism: a recipe for cancer growth. *Genes Dev.* 23, 537–548. doi: 10.1101/gad.1756509

Kamasaki, T., Osumi, M., and Mabuchi, I. (2007). Three-dimensional arrangement of F-actin in the contractile ring of fission yeast. *J. Cell Biol.* 178, 765–771. doi: 10.1083/jcb.200612018

Kedishvili, N. Y., Goodwin, G. W., Popov, K. M., and Harris, R. A. (2000). Mammalian methylmalonate-semialdehyde dehydrogenase. *Methods Enzymol.* 324, 207–218. doi: 10.1016/s0076-6879(00)24233-x

Kee, Y. S., Ren, Y., Dorfman, D., Iijima, M., Firtel, R., Iglesias, P. A., et al. (2012). A mechanosensory system governs myosin II accumulation in dividing cells. *Mol. Biol. Cell* 23, 1510–1523. doi: 10.1091/mbc.E11-07-0601

Kee, Y. S., and Robinson, D. N. (2008). Motor proteins: myosin mechanosensors. *Curr. Biol.* 18, R860–R862. doi: 10.1016/j.cub.2008.07.071

Kodiha, M., Rassi, J. G., Brown, C. M., and Stochaj, U. (2007). Localization of AMP kinase is regulated by stress, cell density, and signaling through the MEK–>ERK1/2 pathway. *Am. J. Physiol. Cell Physiol.* 293, C1427–C1436. doi: 10.1152/ajpcell.00176.2007

Kothari, P., Johnson, C., Sandone, C., Iglesias, P. A., and Robinson, D. N. (2019a). How the mechanobiome drives cell behavior, viewed through the lens of control theory. *J. Cell Sci.* 132:jcs234476. doi: 10.1242/jcs.234476

Kothari, P., Srivastava, V., Aggarwal, V., Tchernyshyov, I., Van Eyk, J. E., Ha, T., et al. (2019b). Contractility kits promote assembly of the mechanoresponsive cytoskeletal network. *J. Cell Sci.* 132:jcs226704. doi: 10.1242/jcs.226704

Kramerova, I. A., and Kramerov, A. A. (1999). Mucinoprotein is a universal constituent of stable intercellular bridges in *Drosophila melanogaster* germ line and somatic cells. *Dev. Dyn.* 216, 349–360. doi: 10.1002/(SICI)1097-0177(199912)216:4/5<349::AID-DVDY4<3.0.CO;2-X

Kuhajda, F. P. (2008). AMP-activated protein kinase and human cancer: cancer metabolism revisited. *Int. J. Obes. (Lond.)* 32(Suppl 4), S36–S41. doi: 10.1038/ijo.2008.121

Leite, J., Osorio, D. S., Sobral, A. F., Silva, A. M., and Carvalho, A. X. (2019). Network contractility during cytokinesis-from molecular to global views. *Biomolecules* 9:E194. doi: 10.3390/biom9050194

Li, Q., Zhang, P., Zhang, C., Wang, Y., Wan, R., Yang, Y., et al. (2014). DDX3X regulates cell survival and cell cycle during mouse early embryonic development. *J. Biomed. Res.* 28, 282–291. doi: 10.7555/JBR.27.20130047

Lopez-Soler, R. I., Moir, R. D., Spann, T. P., Stick, R., and Goldman, R. D. (2001). A role for nuclear lamins in nuclear envelope assembly. *J. Cell Biol.* 154, 61–70. doi: 10.1083/jcb.200101025

Ma, Y., Cai, S., Lv, Q., Jiang, Q., Zhang, Q., Sodmergen, et al. (2007). Lamin B receptor plays a role in stimulating nuclear envelope production and targeting membrane vesicles to chromatin during nuclear envelope assembly through direct interaction with importin beta. *J. Cell Sci.* 120(Pt 3), 520–530. doi: 10.1242/jcs.03355

Marinova, Z., Leng, Y., Leeds, P., and Chuang, D. M. (2011). Histone deacetylase inhibition alters histone methylation associated with heat shock protein 70 promoter modifications in astrocytes and neurons. *Neuropharmacology* 60, 1109–1115. doi: 10.1016/j.neuropharm.2010.09.022

Mendoza, M., Norden, C., Durrer, K., Rauter, H., Uhlmann, F., and Barral, Y. (2009). A mechanism for chromosome segregation sensing by the NoCut checkpoint. *Nat. Cell Biol.* 11, 477–483. doi: 10.1038/ncb1855

Mierzwa, B., and Gerlich, D. W. (2014). Cytokinetic abscission: molecular mechanisms and temporal control. *Dev. Cell* 31, 525–538. doi: 10.1016/j.devcel.2014.11.006

Molinie, N., Rubtsova, S. N., Fokin, A., Visweshwaran, S. P., Rocques, N., Polesskaya, A., et al. (2019). Cortical branched actin determines cell cycle progression. *Cell Res.* 29, 432–445. doi: 10.1038/s41422-019-0160-9

Navarro, R. E., Shim, E. Y., Kohara, Y., Singson, A., and Blackwell, T. K. (2001). cgh-1, a conserved predicted RNA helicase required for gametogenesis and protection from physiological germline apoptosis in *C. elegans*. *Development* 128, 3221–3232.

Ngo, T., Miao, X., Robinson, D. N., and Zhou, Q. Q. (2016). An RNA-binding protein, RNP-1, protects microtubules from nocodazole and localizes to the leading edge during cytokinesis and cell migration in *Dictyostelium* cells. *Acta Pharmacol. Sin.* 37, 1449–1457. doi: 10.1038/aps.2016.57

Norden, C., Mendoza, M., Dobbelaere, J., Kotwaliwale, C. V., Biggins, S., and Barral, Y. (2006). The NoCut pathway links completion of cytokinesis to spindle midzone function to prevent chromosome breakage. *Cell* 125, 85–98. doi: 10.1016/j.cell.2006.01.045

Normand, G., and King, R. W. (2010). Understanding cytokinesis failure. *Adv. Exp. Med. Biol.* 676, 27–55. doi: 10.1007/978-1-4419-6199-0_3

Ozlu, N., Qureshi, M. H., Toyoda, Y., Renard, B. Y., Mollaoglu, G., Ozkan, N. E., et al. (2015). Quantitative comparison of a human cancer cell surface proteome between interphase and mitosis. *EMBO J.* 34, 251–265. doi: 10.15252/embj.201385162

Peterman, E., Valius, M., and Prekeris, R. (2020). CLIC4 is a cytokinetic cleavage furrow protein that regulates cortical cytoskeleton stability during cell division. *J. Cell Sci.* doi: 10.1242/jcs.241117 [Epub ahead of print].

Poirier, C. C., Ng, W. P., Robinson, D. N., and Iglesias, P. A. (2012). Deconvolution of the cellular force-generating subsystems that govern cytokinesis furrow ingression. *PLoS Comput. Biol.* 8:e1002467. doi: 10.1371/journal.pcbi.1002467

Pollard, T. D., and O'Shaughnessy, B. (2019). Molecular mechanism of cytokinesis. *Annu. Rev. Biochem.* 88, 661–689. doi: 10.1146/annurev-biochem-062917-012530

Ponsioen, B., van Zeijl, L., Langeslag, M., Berryman, M., Littler, D., Jalink, K., et al. (2009). Spatiotemporal regulation of chloride intracellular channel protein CLIC4 by RhoA. *Mol. Biol. Cell* 20, 4664–4672. doi: 10.1091/mbc.E09-06-0529

Reichl, E. M., Ren, Y. X., Morphew, M. K., Delannoy, M., Effler, J. C., Girard, K. D., et al. (2008). Interactions between myosin and actin crosslinkers control cytokinesis contractility dynamics and mechanics. *Curr. Biol.* 18, 471–480. doi: 10.1016/j.cub.2008.02.056

Ren, Y., Effler, J. C., Norstrom, M., Luo, T., Firtel, R. A., Iglesias, P. A., et al. (2009). Mechanosensing through cooperative interactions between myosin II and the actin crosslinker cortexillin I. *Curr. Biol.* 19, 1421–1428. doi: 10.1016/j.cub.2009.07.018

Ren, Y., West-Foyle, H., Surcel, A., Miller, C., and Robinson, D. N. (2014). Genetic suppression of a phosphomimic myosin II identifies system-level factors that promote myosin II cleavage furrow accumulation. *Mol. Biol. Cell* 25, 4150–4165. doi: 10.1091/mbc.E14-08-1322

Robinson, D. N., and Cooley, L. (1997). Genetic analysis of the actin cytoskeleton in the *Drosophila ovary*. *Annu. Rev. Cell Dev. Biol.* 13, 147–170. doi: 10.1146/annurev.cellbio.13.1.147

Robinson, D. N., Kee, Y. S., Luo, T., and Surcel, A. (2012). "Understanding how dividing cells change shape," in *The Comprehensive Biophysics*, Vol. 7, ed. E. H. Egelman (Amsterdam: Elsevier), 48–72. doi: 10.1016/B978-0-12-374920-8.00705-0

Robinson, D. N., and Spudich, J. A. (2000). Dynacortin, a genetic link between equatorial contractility and global shape control discovered by library complementation of a Dictyostelium discoideum cytokinesis mutant. *J. Cell Biol.* 150, 823–838. doi: 10.1083/jcb.150.4.823

Roscioli, E., Di Francesco, L., Bolognesi, A., Giubettini, M., Orlando, S., Harel, A., et al. (2012). Importin-beta negatively regulates multiple aspects of mitosis including RANGAP1 recruitment to kinetochores. *J. Cell Biol.* 196, 435–450. doi: 10.1083/jcb.201109104

Rosen, S. D., Kafka, J. A., Simpson, D. L., and Barondes, S. H. (1973). Developmentally regulated, carbohydrate-binding protein in Dictyostelium discoideum. *Proc. Natl. Acad. Sci. U.S.A.* 70, 2554–2557. doi: 10.1073/pnas.70.9.2554

Rual, J. F., Venkatesan, K., Hao, T., Hirozane-Kishikawa, T., Dricot, A., Li, N., et al. (2005). Towards a proteome-scale map of the human protein-protein interaction network. *Nature* 437, 1173–1178. doi: 10.1038/nature04209

Sazer, S., and Dasso, M. (2000). The ran decathlon: multiple roles of Ran. *J. Cell Sci.* 113(Pt 7), 1111–1118.

Shi, Q., and King, R. W. (2005). Chromosome nondisjunction yields tetraploid rather than aneuploid cells in human cell lines. *Nature* 437, 1038–1042. doi: 10.1038/nature03958

Silverman-Gavrila, R. V., Hales, K. G., and Wilde, A. (2008). Anillin-mediated targeting of peanut to pseudocleavage furrows is regulated by the GTPase Ran. *Mol. Biol. Cell.* 19, 3735–3744. doi: 10.1091/mbc.E08-01-0049

Singh, D., Odedra, D., Dutta, P., and Pohl, C. (2019). Mechanical stress induces a scalable switch in cortical flow polarization during cytokinesis. *J. Cell Sci.* 132:jcs231357. doi: 10.1242/jcs.231357

Singh, H. (2010). Two decades with dimorphic chloride intracellular channels (CLICs). *FEBS Lett.* 584, 2112–2121. doi: 10.1016/j.febslet.2010.03.013

Singh, H., and Ashley, R. H. (2007). CLIC4 (p64H1) and its putative transmembrane domain form poorly selective, redox-regulated ion channels. *Mol. Membr. Biol.* 24, 41–52. doi: 10.1080/09687860600927907

Singh, H., Cousin, M. A., and Ashley, R. H. (2007). Functional reconstitution of mammalian 'chloride intracellular channels' CLIC1, CLIC4 and CLIC5 reveals differential regulation by cytoskeletal actin. *FEBS J.* 274, 6306–6316. doi: 10.1111/j.1742-4658.2007.06145.x

Squirrell, J. M., Eggers, Z. T., Luedke, N., Saari, B., Grimson, A., Lyons, G. E., et al. (2006). CAR-1, a protein that localizes with the mRNA decapping component DCAP-1, is required for cytokinesis and ER organization in *Caenorhabditis elegans* embryos DE. *Mol. Biol. Cell* 17, 336–344. doi: 10.1091/mbc.E05-09-0874

Srivastava, V., Iglesias, P. A., and Robinson, D. N. (2016). Cytokinesis: robust cell shape regulation. *Semin. Cell Dev. Biol.* 53, 39–44. doi: 10.1016/j.semcdb.2015.10.023

Srivastava, V., and Robinson, D. N. (2015). Mechanical stress and network structure drive protein dynamics during cytokinesis. *Curr. Biol.* 25, 663–670. doi: 10.1016/j.cub.2015.01.025

Storchova, Z., and Pellman, D. (2004). From polyploidy to aneuploidy, genome instability and cancer. *Nat. Rev. Mol. Cell Biol.* 5, 45–54. doi: 10.1038/nrm1276

Straight, A. F., and Field, C. M. (2000). Microtubules, membranes and cytokinesis. *Curr. Biol.* 10, R760–R770. doi: 10.1016/s0960-9822(00)00746-6

Strasser, K., and Hurt, E. (2001). Splicing factor Sub2p is required for nuclear mRNA export through its interaction with Yra1p. *Nature* 413, 648–652. doi: 10.1038/35098113

Suginta, W., Karoulias, N., Aitken, A., and Ashley, R. H. (2001). Chloride intracellular channel protein CLIC4 (p64H1) binds directly to brain dynamin I in a complex containing actin, tubulin and 14-3-3 isoforms. *Biochem. J.* 359(Pt 1), 55–64.

Suh, K. S., Malik, M., Shukla, A., Ryscavage, A., Wright, L., Jividen, K., et al. (2012). CLIC4 is a tumor suppressor for cutaneous squamous cell cancer. *Carcinogenesis* 33, 986–995. doi: 10.1093/carcin/bgs115

Tripodi, F., Fraschini, R., Zocchi, M., Reghellin, V., and Coccetti, P. (2018). Snf1/AMPK is involved in the mitotic spindle alignment in Saccharomyces cerevisiae. *Sci. Rep.* 8:5853. doi: 10.1038/s41598-018-24252-y

Tsai, M. Y., Wang, S., Heidinger, J. M., Shumaker, D. K., Adam, S. A., Goldman, R. D., et al. (2006). A mitotic lamin B matrix induced by RanGTP required for spindle assembly. *Science* 311, 1887–1893. doi: 10.1126/science.1122771

Uretmen Kagiali, Z. C., Saner, N., Akdag, M., Sanal, E., Degirmenci, B. S., Mollaoglu, G., et al. (2020). CLIC4 and CLIC1 bridge plasma membrane and cortical actin network for a successful cytokinesis. *Life Sci. Alliance* 3:e201900558. doi: 10.26508/lsa.201900558

van Oostende Triplet, C., Jaramillo Garcia, M., Haji Bik, H., Beaudet, D., and Piekny, A. (2014). Anillin interacts with microtubules and is part of the astral pathway that defines cortical domains. *J. Cell Sci.* 127(Pt 17), 3699–3710. doi: 10.1242/jcs.147504

Vazquez-Martin, A., Oliveras-Ferraros, C., Cufi, S., and Menendez, J. A. (2011). Polo-like kinase 1 regulates activation of AMP-activated protein kinase (AMPK) at the mitotic apparatus. *Cell Cycle* 10, 1295–1302. doi: 10.4161/cc.10.8.15342

Vazquez-Martin, A., Oliveras-Ferraros, C., and Menendez, J. A. (2009). The active form of the metabolic sensor: AMP-activated protein kinase (AMPK) directly binds the mitotic apparatus and travels from centrosomes to the spindle midzone during mitosis and cytokinesis. *Cell Cycle* 8, 2385–2398. doi: 10.4161/cc.8.15.9082

Warecki, B., Ling, X., Bast, I., and Sullivan, W. (2020). ESCRT-III-mediated membrane fusion drives chromosome fragments through nuclear envelope channels. *J. Cell Biol.* 219:e201905091. doi: 10.1083/jcb.201905091

Yamazaki, T., Fujiwara, N., Yukinaga, H., Ebisuya, M., Shiki, T., Kurihara, T., et al. (2010). The closely related RNA helicases, UAP56 and URH49, preferentially form distinct mRNA export machineries and coordinately regulate mitotic progression. *Mol. Biol. Cell* 21, 2953–2965. doi: 10.1091/mbc.E09-10-0913

Yang, S. H., Baek, H. A., Lee, H. J., Park, H. S., Jang, K. Y., Kang, M. J., et al. (2010). Discoidin domain receptor 1 is associated with poor prognosis of non-small cell lung carcinomas. *Oncol. Rep.* 24, 311–319. doi: 10.3892/or_00000861

Zakikhani, M., Dowling, R., Fantus, I. G., Sonenberg, N., and Pollak, M. (2006). Metformin is an AMP kinase-dependent growth inhibitor for breast cancer cells. *Cancer Res.* 66, 10269–10273. doi: 10.1158/0008-5472.CAN-06-1500

Zhang, W., and Robinson, D. N. (2005). Balance of actively generated contractile and resistive forces controls cytokinesis dynamics. *Proc. Natl. Acad. Sci. U.S.A.* 102, 7186–7191. doi: 10.1073/pnas.0502545102

Zhou, Q., Kee, Y. S., Poirier, C. C., Jelinek, C., Osborne, J., Divi, S., et al. (2010). 14-3-3 coordinates microtubules, Rac, and myosin II to control cell mechanics and cytokinesis. *Curr. Biol.* 20, 1881–1889. doi: 10.1016/j.cub.2010.09.048

Ziemienowicz, A., Haasen, D., Staiger, D., and Merkle, T. (2003). Arabidopsis transportin1 is the nuclear import receptor for the circadian clock-regulated RNA-binding protein AtGRP7. *Plant Mol. Biol.* 53, 201–212. doi: 10.1023/B:PLAN.0000009288.46713.1f

Zipperlen, P., Fraser, A. G., Kamath, R. S., Martinez-Campos, M., and Ahringer, J. (2001). Roles for 147 embryonic lethal genes on *C.elegans* chromosome I identified by RNA interference and video microscopy. *EMBO J.* 20, 3984–3992. doi: 10.1093/emboj/20.15.3984

Conflict of Interest: The authors declare that the research was conducted in the absence of any commercial or financial relationships that could be construed as a potential conflict of interest.

frontiers in Cell and Developmental Biology

BRIEF RESEARCH REPORT
published: 15 September 2020
doi: 10.3389/fcell.2020.572094

HIPK2 Is Required for Midbody Remnant Removal Through Autophagy-Mediated Degradation

Francesca Sardina[1], Laura Monteonofrio[2], Manuela Ferrara[1], Fiorenza Magi[2†], Silvia Soddu[2] and Cinzia Rinaldo[1,2*]*

[1] Institute of Molecular Biology and Pathology (IBPM), National Research Council (CNR), c/o Sapienza University of Rome, Rome, Italy, [2] Unit of Cellular Networks and Molecular Therapeutic Targets, IRCCS Regina Elena National Cancer Institute, Rome, Italy

OPEN ACCESS

Edited by:
Fred Chang,
University of California,
San Francisco, United States

Reviewed by:
Costin N. Antonescu,
Ryerson University, Canada
Zhigang Jin,
University of Alberta, Canada

***Correspondence:**
Silvia Soddu
silvia.soddu@ifo.gov.it
Cinzia Rinaldo
cinzia.rinaldo@uniroma1.it

†Present address:
Fiorenza Magi,
Laboratory of Biomedical Research,
Niccolò Cusano University
Foundation, Rome, Italy

Specialty section:
This article was submitted to Cell Growth and Division, a section of the journal Frontiers in Cell and Developmental Biology

Received: 12 June 2020
Accepted: 18 August 2020
Published: 15 September 2020

Citation:
Sardina F, Monteonofrio L, Ferrara M, Magi F, Soddu S and Rinaldo C (2020) HIPK2 Is Required for Midbody Remnant Removal Through Autophagy-Mediated Degradation. Front. Cell Dev. Biol. 8:572094. doi: 10.3389/fcell.2020.572094

At the end of abscission, the residual midbody forms the so-called midbody remnant (MBR), a platform affecting cell fate with emerging key role in differentiation, development, and tumorigenicity. Depending on cell type and pathophysiological context, MBRs undergo different outcomes: they can be retained, released, internalized by nearby cells, or removed through autophagy-mediated degradation. Although mechanisms underlying MBR formation, positioning, and processing have been recently identified, their regulation is still largely unknown. Here, we report that the multifunctional kinase HIPK2 regulates MBR processing contributing to MBR removal. In the process of studying the role of HIPK2 in abscission, we observed that, in addition to cytokinesis failure, HIPK2 depletion leads to significant accumulation of MBRs. In particular, we detected comparable accumulation of MBRs after HIPK2 depletion or treatment with the autophagic inhibitor chloroquine. In contrast, single depletion of the two independent HIPK2 abscission targets, extrachromosomal histone H2B and severing enzyme Spastin, only marginally increased MBR retention, suggesting that MBR accumulation is not just linked to cytokinesis failure. We found that HIPK2 depletion leads to (i) increased levels of CEP55, a key effector of both midbody formation and MBR degradation; (ii) decreased levels of the selective autophagy receptors NBR1 and p62/SQSTM1; and (iii) impaired autophagic flux. These data suggest that HIPK2 contributes to MBR processing by regulating its autophagy-mediated degradation.

Keywords: HIPK2, midbody remnants, abscission, autophagy, nbr1

INTRODUCTION

During the final stage of cell division, daughter cells are connected by an intercellular bridge that contains bundled microtubules that overlap in an antiparallel manner at the midbody. The midbody is an electron-dense structure that works as a platform for the spatiotemporal distribution of specific proteins and lipids that contribute to abscission, the final cut when the intercellular bridge is severed (Hu et al., 2012). In addition to its canonical role to orchestrate abscission, accumulating evidence has indicated postabscission signaling roles of the midbody remnant (MBR), also named midbody derivative, midbody ring derivative, postcytokinesis, or postabscission or postmitotic midbody (Chen et al., 2013; Peterman and Prekeris, 2019). Following abscission, some

of the midbody-localized factors, such as the ESCRT-III recruiters CEP55 and ALIX, persist at the MBR together with several signaling proteins (Willard and Crouch, 2001; Kaplan et al., 2004; Naito et al., 2006; Cho and Kehrl, 2007; Kasahara et al., 2007; Fumoto et al., 2012; Chen et al., 2013). Depending on the cell type and tissue context, MBRs may be released in the extracellular space, inherited by one of the dividing cells, or internalized by interphase cells (Chen et al., 2013; Crowell et al., 2014; Peterman and Prekeris, 2019). These different MBR outcomes have functional consequences in cell-fate determination with key roles in differentiation and development, while their defects can be implicated in different pathological conditions. For example, in neuronal and epithelia morphogenesis, a crucial role is played by MBR positioning that determines cell polarity in neurite outgrowth and in apical lumen formation (Wilcock et al., 2007; Pollarolo et al., 2011; Li et al., 2014; Luján et al., 2016), and such polarity cues have been shown to be required also for ciliogenesis (Bernabé-Rubio et al., 2016). A different example is represented by asymmetrically dividing stem cells and cancer cells in which MBR function is linked to its processing. In these cells, MBRs are long-lived structures that can persist in the cytoplasm for hours mainly due to evasion from autophagic degradation, which is mediated by the binding of the autophagic receptor NBR1 to its ligand CEP55, a key component of both midbodies and MBRs (Kuo et al., 2011; Crowell et al., 2013). In addition to receptor recognition through NBR1/CEP55 complex, MBRs have been shown to be degraded through selective autophagy, a process called autophagy, in which the autophagic factors p62/SQTM1, ALFY, TRAF6 are involved, with the contribution of the E3 ubiquitin-ligase TRIM17 and the autophagy adaptor FYCO-1 (Isakson et al., 2013; Mandell et al., 2016; Dionne et al., 2017). At the functional level, MBR accumulation has been observed in cancer cells and proposed to regulate cell stemness, proliferation, and tumorigenicity. In particular, MBR-enriched subpopulations of cancer cells show higher tumorigenic potential characterized by increase in proliferation, anchorage independent growth, and invadopodia formation (Kuo et al., 2011; Dionne et al., 2017; Peterman et al., 2019). Despite the functional consequences of retention and signaling of MBRs, how their degradation is regulated is poorly understood.

HIPK2 is an evolutionary conserved multifunctional serine/threonine kinase (Calzado et al., 2007; Rinaldo et al., 2007; D'Orazi et al., 2012; Blaquiere and Verheyen, 2017), whose interactors and targets belong to several signal transduction pathways affecting cell fate. HIPK2 is involved in crucial processes, such as development, differentiation, and response to DNA damage and oxidative stress (Calzado et al., 2007; Rinaldo et al., 2007; D'Orazi et al., 2012; Blaquiere and Verheyen, 2017). We previously demonstrated that HIPK2 localizes at the midbody in an Aurora-B–dependent manner and is among the kinases that regulate abscission (Rinaldo et al., 2012; Monteonofrio et al., 2018). In particular, HIPK2-depleted or -null cells undergo abscission delay and failure, accumulating elongated midbodies and binucleated cells, whose uncontrolled proliferation leads to chromosomal instability and increased tumorigenicity (Rinaldo et al., 2012; Valente et al., 2015). Mechanistically, HIPK2 regulates abscission with two apparently parallel mechanisms of action. HIPK2-mediated phosphorylation of the extrachromosomal histone H2B (ecH2B) at Ser14 is not required for its midbody localization but contributes to the formation of the abscission site and is essential for successful cytokinesis (Rinaldo et al., 2012; Monteonofrio et al., 2019). HIPK2-mediated phosphorylation of the microtubule severing enzyme Spastin at Ser268 is required for its midbody localization to cut microtubules and the subsequent physical separation of the two daughter cells (Pisciottani et al., 2019; Gatti et al., 2020).

During our studies on HIPK2 abscission functions, we noticed that HIPK2-depleted cells show a significant accumulation of MBRs. By comparing cells treated with the autophagic inhibitor chloroquine (CQ) or depleted with siRNAs specific for HIPK2 abscission targets, we showed that HIPK2 regulates MBR degradation by controlling CEP55 levels and the autophagic pathway.

MATERIALS AND METHODS

Cells, Culture Conditions, and Treatments

HeLa (a gift of N. Corbi), U2OS (a gift of F. Moretti), HeLa$^{Ctr-Cas9}$, and HeLa$^{HIPK2-Cas9}$ (Ritter and Schmitz, 2019) (a gift M.L. Schmitz) and hTERT RPE-1 (a gift of G. Guarguaglini) were cultured at 5% CO_2 and 37°C in Dulbecco modified eagle medium (DMEM) GlutaMAX supplemented with 10% heat-inactivated fetal bovine serum (FBS) (Life Technologies); mouse motoneuron-like NSC34 cells (a gift of M. Cozzolino) were cultured in DMEM-F12 1:1, supplemented with 10% FBS. Cells were routinely analyzed for mycoplasma contamination. Treatment with CQ (Sigma–Aldrich) or its solvent phosphate-buffered saline (PBS) (Life Technologies) were performed at 10 mM for 72 h.

Brain tissues were explanted from *Hipk2* KO adult mice carrying first conditional-ready allele and their wild-type (WT) counterpart.

RNA Interference and Expression Vector Transfection

In human cells, HIPK2 RNA interference (RNAi) and Spastin RNAi were obtained by using stealth siRNAs as in Pisciottani et al., 2019. Specific prevalidated stealth siRNAs by Life Technologies were used to obtain HIPK2 RNAi in mouse cells and CEP55 RNAi in human cells. In details, cells were transfected with a mix of at least two stealth siRNAs at a final concentration of 40 nM using Lipofectamine RNAi MAX (Life Technologies). Depletion of ecH2B was obtained as in Monteonofrio et al., 2019. Briefly, cells were transfected with a mix of nine siRNAs each at 10 nM in a double pulse, the second one 24 h after the first one. As control, stealth siRNA Negative Medium GC Duplex (Life Technologies) was used with the respective transfection strategies, i.e., single- or double-pulse transfection and siRNA concentration.

Expression vectors were transfected by using Lipofectamine LTX and Plus reagent (Life Technologies). For rescue

experiments, human HeLa siHIPK2 cells were transfected with low doses of vectors expressing GFP-tagged murine HIPK2-WT (D'Orazi et al., 2002) or its empty vector (peGFP-c2; Clontech) as in Pisciottani et al., 2019. Murine HIPK2 protein shows >97% identity with human HIPK2, fully recapitulates its functions, but is resistant to RNAi when human-specific siRNAs were used.

Immunofluorescence Analysis

Cells were seeded onto poly-L-lysine–coated coverslips, fixed in 2% formaldehyde or in ice-cold methanol, permeabilized in 0.25% Triton X-100 in PBS for 10 min, and then blocked in 5% bovine serum albumin in PBS for 1 h before the primary antibody (Ab) was applied. Employed Abs were as follows: anti-ALIX (1:100; #sc-53538; Santa Cruz Biotechnology), anti-CEP55 (1:700; # 00055165-A01; Bionova); anti–β-tubulin-Cy3 (Sigma–Aldrich), secondary 488- or 594-conjugated Abs (1:300; Alexa-Flour, Life Technologies). DAPI (Sigma–Aldrich) was used to stain DNA. Cells were examined under an upright Olympus BX53 microscope equipped with a Lumen 200 Fluorescence Illumination System (Prior Scientific) with a 200-W metal arc lamp, and photographs were taken (× 100 or × 60 objectives) using a cooled camera device (ProgRes MF). Images for each sample were taken selecting the appropriate Olympus filters (DAPI: U-MNU2; FITC: U-MNB2; Texas red: U-MWIY2) at 100% of excitation light intensity with different exposure time for tubulin, CEP55, ALIX, and DAPI, respectively, of 500, 640, 1,264, and 16 ms. For MBR quantification, because CEP55 and ALIX also label centrosome, bonafide MBRs were considered only those clearly showing costaining of CEP55 or ALIX with β-tubulin that is strongly enriched in this subcompartment.

Western Blot

Total cell extracts (TCEs) were prepared in denaturing buffer (50 mM Tris–HCl pH 8.0, 600 mM NaCl, 0.5% sodium deoxycholate, 1% NP40 0.1% sodium dodecyl sulfate, and 1 mM EDTA) supplemented with protease and phosphatase inhibitors (Roche). Proteins were resolved using precast Bolt Novex Bis–Tris Gels 4–12% (Life Technologies), transferred to nitrocellulose membranes (Bio-Rad), and immunoreactivity was determined using ECL (Amersham). Acquisition and densitometric analysis of images were obtained using Image Lab software (Bio-Rad). Employed Abs were as follows: anti-HIPK2 (rat monoclonal Ab C5C6 kindly provided by M. L. Schmitz); anti-Spastin (1:100; #sc-53443), anti-GAPDH (1:1,000; #sc-32233), anti–α-tubulin (1:1,000; #sc-5286), anti-actin (1:1,000; #sc-47778), anti-ALIX (1:200; #sc-53538), anti-p62 (1:1,000; #28359), anti-lamina A/C (1:1,000; #sc-20680) by Santa Cruz Technology; anti-CEP55 (1:1,000; #00055165-A01), and anti-NBR1 (1:500; #H00004077-B01P) by Abnova; anti-TSG101 (1:500: #ab30871) and anti-H2B (1:1,000; #ab52484) by Abcam; anti-LC3 (1:1,000; #L8918 by Sigma–Aldrich) recognizing both the cytosolic LC3-I and lipidated LC3-II forms of LC3. Anti–horseradish peroxidase–conjugated goat anti–mouse #7076, anti–rabbit #7074, and anti–rat #7077 (Cell Signaling Technology).

Autophagy Flux Analysis

Autophagic flux was determined by quantifying the autophagosome marker LC3-II in the presence of CQ to inhibit lysosomal degradation or its solvent, PBS, as described in Kuo et al., 2011. Briefly, siCtr and siHIPK2 cells were treated with CQ or PBS for 24 h, and their TCEs analyzed by Western blot (WB) with anti-LC3 Ab; GAPDH was used as loading control. Data acquisition and densitometric analyses for LC3-II and GAPDH were performed by Image Lab (Bio-Rad). Densitometric values were employed to calculate the LC3-II relative level as LC3-II/GAPDH ratio; the autophagic flux for each condition is the result of the following equation: autophagic flux = 100 - [(PBS LC3-II relative level/CQ LC3-II relative level) × 100)].

Statistical Analysis

Each experiment has been repeated three or five times, and data analyses were performed using the GraphPad Prism software. Statistical significance was assessed by unpaired *t* test; significance was set at $p < 0.05$.

RESULTS

HIPK2 Depletion Leads to MBR Accumulation

To characterize HIPK2 functions in abscission, we previously examined the microtubule stability and the localization of several cytokinesis factors at the intercellular bridge by immunofluorescence (IF) in cells treated with control siRNA (siCtr) or a mix of HIPK2-specific siRNAs (siHIPK2). To evaluate the effect of HIPK2 depletion over more than one cell cycle, cells were transfected with stealth siRNAs that have increased stability in cell culture than standard siRNAs. We showed that HIPK2 depletion delays abscission and induces accumulation of aberrant elongated midbodies and cytokinesis failure (Rinaldo et al., 2012; Pisciottani et al., 2019). During these studies, we also observed the appearance of a large fraction of cells with MBRs in the siHIPK2 cells compared to their relative siCtr (**Figures 1A,B**, and **Supplementary Figure S1**). Quantification of MBRs in fixed HeLa (**Figure 1**) and U2OS (**Supplementary Figure S1**) cells was performed by using the MBR marker CEP55 in combination with β-tubulin enrichment and revealed a significant increase in the percentage of cells carrying one or more than one MBR at days 4 and 5 posttransfection in the siHIPK2 cells (**Figure 1C**). Binucleated cells and cells with abnormally large nuclei were excluded from our analysis to avoid cells that have undergone cytokinesis failure. Similar findings were observed by using an Ab against ALIX, a protein highly concentrated in MBR (**Figure 1D**). Of relevance, we also noticed some MBRs still persisting in siHIPK2 cells at telophase stage (5.3% ± 1.1% in siHIPK2 cells vs. <0.5% in siCtr by analyzing 300 telophases for each condition in three independent experiments) (**Figure 1E**), suggesting that cells underwent new mitosis without degrading the MBR of the previous cell divisions.

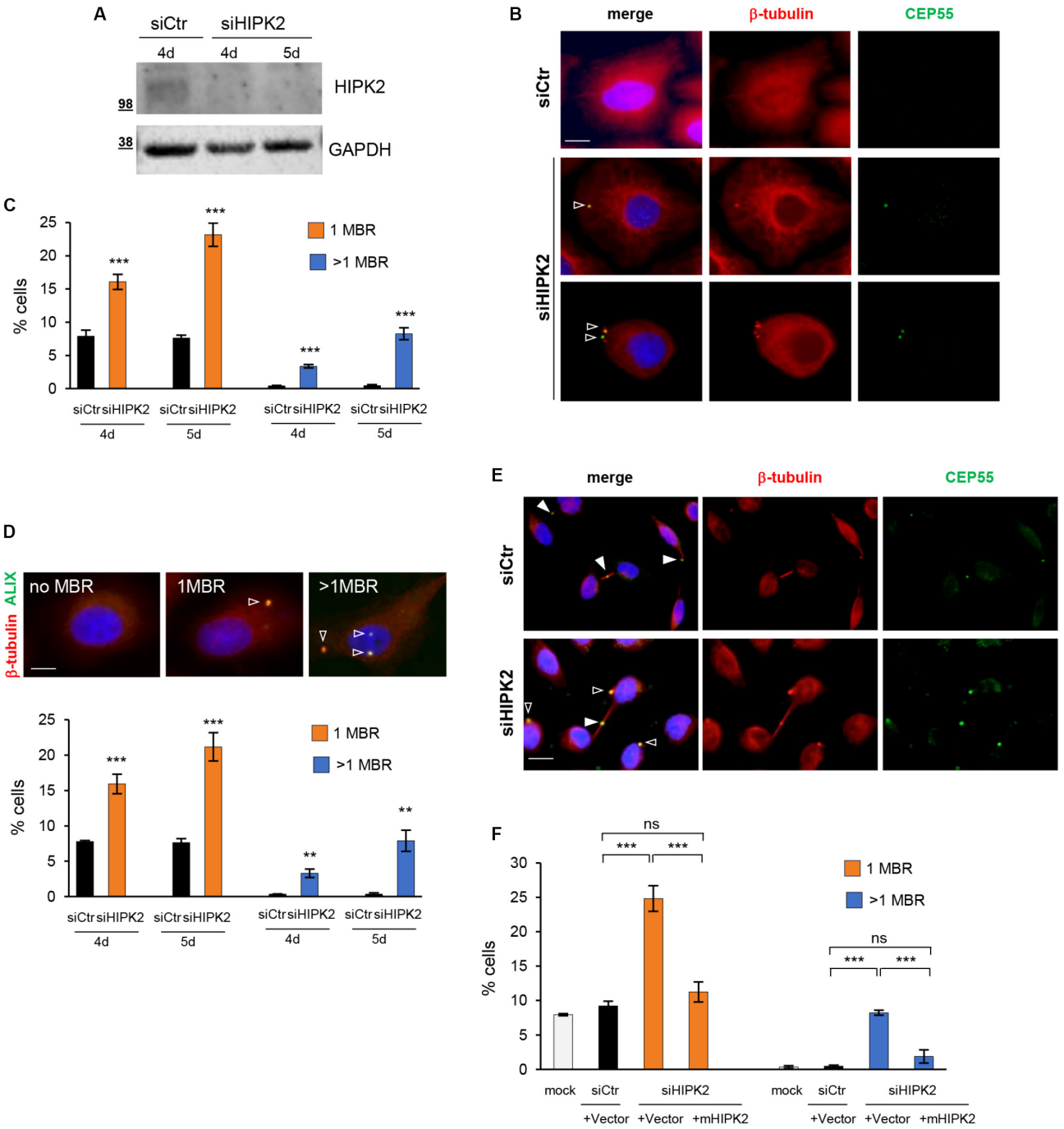

FIGURE 1 | MBR in HIPK2-depleted cells. **(A–D)** HeLa cells were transfected with HIPK2 -specific siRNA or negative universal control and analyzed 4 and 5 days posttransfection by WB with indicated Abs to verify RNAi and by IF for MBR quantification by using CEP55 as MBR marker in combination with β-tubulin costaining. DAPI (blue) was used to stain DNA. Representative WB and images are shown in **(A,B)**, respectively. Scale bar, 5 μM. Here, and in the following images, the empty arrowheads indicate MBR. The percentage of cells with 1 or >1 MBR were reported as mean ± standard deviation (SD) in **(C)** from three independent experiments, in which at least total 3,000 cells per condition were analyzed. ***$p < 0.001$ and **$p < 0.01$, unpaired t test. **(D)** HeLa cells were transfected as in **(A)**, analyzed by IF by using ALIX as MBR marker in combination with β-tubulin costaining and DAPI to stain DNA. Data reported as in **(C)**, are from three independent experiments, in which at least total 3,000 cells per condition were analyzed. ***$p < 0.001$, **$p < 0.01$, unpaired t test. Representative images are shown. Scale bar, 5 μM. **(E)** Representative images of siCtr and siHIPK2 HeLa cells 5 days posttransfection. CEP55 marks MBR as well as the midbody. Here, and in the following images, the full arrowheads indicate CEP55 at midbody. Scale bar, 10 μM. **(F)** HeLa cells 36 h upon transfection with low doses of vectors expressing GFP-tagged murine HIPK2-WT or GFP empty vector and analyzed by IF as in **(C)**. Data are reported as mean ± SD from three independent experiments, in which a total of 2,000 cells per condition were analyzed. Note that the expression of murine HIPK2 protein is not silenced by RNAi because human-specific siRNAs were used in siHIPK2 cells. ***$p < 0.001$, ns = not significant, unpaired t test.

Next, we restored HIPK2 expression in the siHIPK2 cells by transfecting an siRNA-resistant HIPK2 cDNA and showed inhibition of MBR accumulation (**Figure 1F**), excluding RNAi off-target effects.

Overall, these results show that MBRs accumulate and may even persist through successive divisions in HIPK2-depleted cells, suggesting that HIPK2 has a role in controlling MBR fate.

MBR Accumulation Is Only Marginally Detected Upon Depletion of HIPK2 Cytokinesis Targets

HIPK2 has been shown to contribute to cytokinesis through two distinct targets, ecH2B, which contributes to the formation of the abscission site (Monteonofrio et al., 2019), and Spastin, which severs microtubules for the final cut (Pisciottani et al., 2019). Thus, we quantify MBRs also after depletion of Spastin and ecH2B obtained by transfecting HeLa cells with Spastin-specific siRNAs (siSpastin) and H2B-specific siRNAs (si-ecH2B), as reported (Monteonofrio et al., 2019; Pisciottani et al., 2019). Alongside, for each condition, we also evaluated the induction of cytokinesis defects by analyzing the percentage of aberrant midbodies and binucleated cells, as we previously reported (Rinaldo et al., 2012) (**Supplementary Table S1**). As shown in **Figures 2A–D**, compared to their relative siCtr cells, a mild, although significant, accumulation of MBRs was observed in both siSpastin and si-ecH2B cells. However, when compared to siHIPK2 cells, MBR accumulation induced by Spastin and ecH2B depletion was considerably lower (**Figure 2E**). Similar data were observed in human non-transformed RPE-1 cells (**Supplementary Figure S2** and data not shown). These data suggest that HIPK2 depletion might either induce MBR accumulation in a manner that is largely independent of cytokinesis defects or that both Spastin and ecH2B need to be simultaneously knocked down. Because the depletion strategies for Spastin and ecH2B are not compatible (see Materials and Methods), we focused our attention on the first hypothesis.

HIPK2 Regulates MBR Removal Through Autophagy-Mediated Degradation

Autophagy is the main specific degradation mechanism for MBR removal (Pohl and Jentsch, 2009; Kuo et al., 2011; Isakson et al., 2013). Recently, exogenous expression of HIPK2 in primary mouse hepatocytes has been shown to stimulate autophagy (Jiang et al., 2018). Thus, we asked whether HIPK2 might have a role in mediating MBR autophagic degradation. As a first insight, we compared siHIPK2 cells with those treated with the autophagy inhibitor CQ, which inhibits lysosomal activity allowing MBR accumulation (Pohl and Jentsch, 2009). In particular, we evaluated the effect of CQ on MBR accumulation in HeLa cells. Autophagy inhibition by CQ was confirmed by WB detection of the lipidated form of the microtubule-associated protein 1A/1B light chain 3 (LC3-II), whose accumulation is induced when the lysosomal activity is blocked, and the turnover of the LC3-II pool present in the autophagomes is prevented (Klionsky et al., 2008; **Figure 3A**). In the same culture conditions, the percentage of cells with $\geq$1 MBR was measured by IF, as above (**Figure 3B**). Consistent with the possibility that defects in autophagic pathways underlie the MBR accumulation in siHIPK2 cells, comparable fractions of cells with MBR accumulation were observed in CQ-impaired autophagy and HIPK2-depleted cells (**Figure 3C**). Similar results were observed in RPE-1 cells (**Figures 3D,E**).

The autophagic receptors NBR1 and p62 and the CEP55/NBR1 complex have a major role in the autophagy-mediated degradation of MBRs (Pohl and Jentsch, 2009; Kuo et al., 2011; Isakson et al., 2013). In particular, CEP55 overexpression has been proposed to induce MBR accumulation by sequestering its interactor NBR1 in the cytoplasm (Kuo et al., 2011). To more directly evaluate whether HIPK2 regulates MBR fate by affecting the autophagy-mediated MBR degradation, we assessed both autophagy activity and the protein levels of p62, NBR1, and CEP55 in siCtr and siHIPK2 cells. Autophagy activity was evaluated by measuring the changes in the levels of LC3-II (the autophagic flux) in the presence or absence of CQ to inhibit lysosomal degradation and prevent the turnover of the LC3-II pool present in the autophagomes (Klionsky et al., 2008; Kuo et al., 2011). Compared with siCtr cells, the HIPK2-depleted cells showed an impairment of the autophagic flux (**Figures 4A,B**), supporting a role for HIPK2 in autophagy. In agreement with this result, we observed lower levels of p62 and NBR1 and higher levels of CEP55 in the HIPK2-depleted cells compared with the control cells (**Figures 4C,D** and **Supplementary Figures S3A,B**), whereas no major differences where observed for other midbody and MBR proteins, such as ALIX and TGS101 (**Figures 4E–F**). Finally, because of the key role of CEP55 in MBR degradation, we verified whether CEP55 depletion might impair MBR accumulation in HIPK2-depleted cells. To avoid multiple siRNA transfection, transient CEP55 depletion was induced in HIPK2-null cells ($HeLa^{HIPK2-Cas9}$) generated by CRISPR/Cas9-mediated gene editing and in their related controls ($HeLa^{Ctr-Cas9}$) (Ritter and Schmitz, 2019). In these HIPK2-null cells, the increase of CEP55 levels (**Supplementary Figure S4A**) and of MBR accumulation (**Figure 4G**, siCtr columns) was lower compared with the acutely depleted HeLa cells. Still, CEP55 depletion reduced the basal amount of MBRs in the Ctr-Cas9 cells and strongly inhibited MBR accumulation in the HIPK2-Cas9 (**Figure 4G**).

Altogether, these data suggest a model in which HIPK2 regulates MBR fate by acting on the autophagic pathway, both modulating the amount of the autophagic receptors p62 and NBR1 and modulating the activity of NBR1 through its ligand CEP55.

DISCUSSION

Unexpected new means of cellular communications depend on MBR fate, whose regulation is still largely unclear. Here, we show that the multifunctional kinase HIPK2, which localizes at the midbody and controls abscission, might regulate MBR fate by stimulating MBR removal via autophagic degradation.

It has been observed that differentiated cells mainly undergo symmetric bilateral abscission releasing MBR in the extracellular

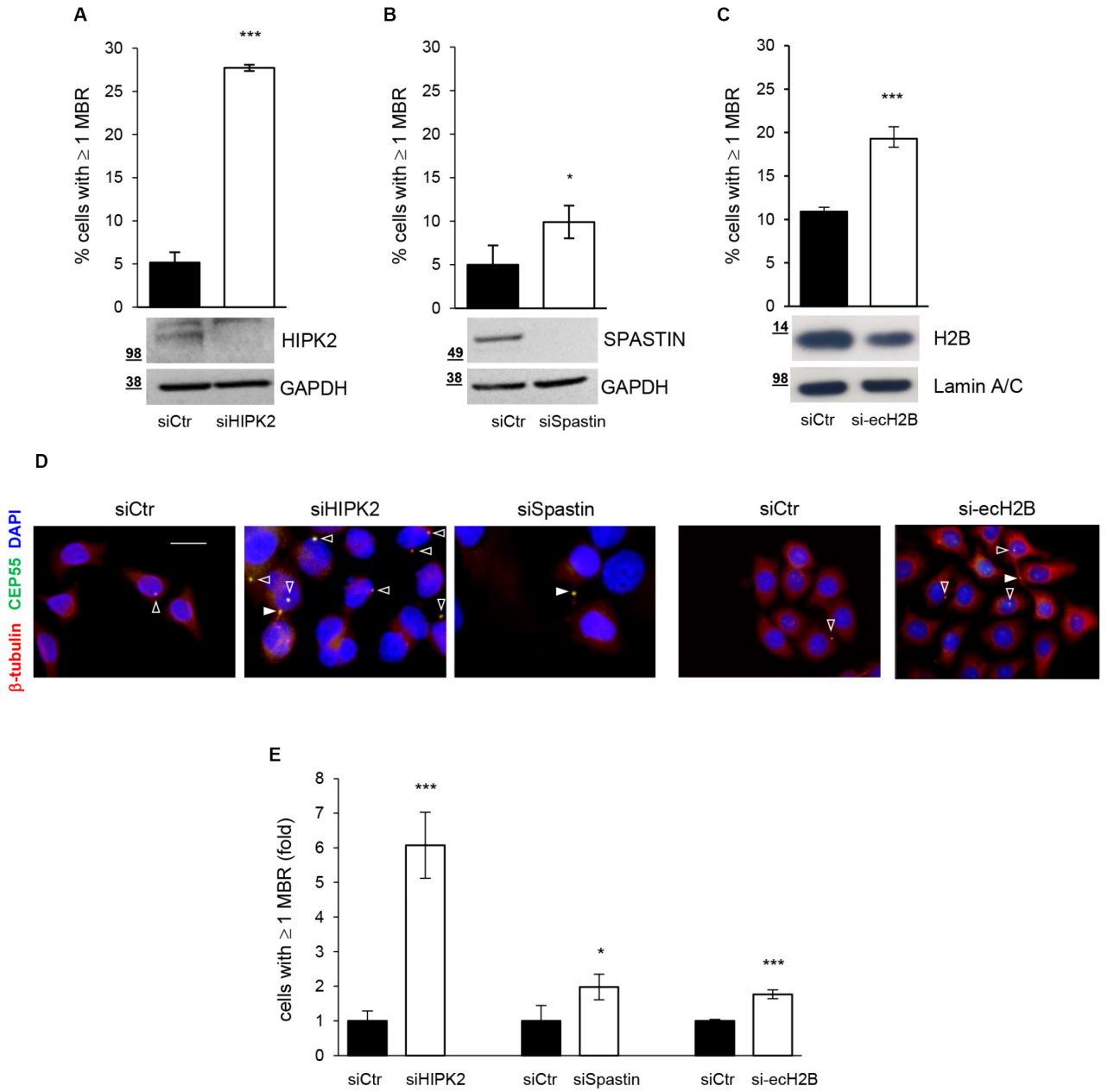

FIGURE 2 | MBR upon depletion of HIPK2 cytokinesis targets. **(A–D)** HeLa cells were transfected with siRNAs specific for HIPK2, Spastin, and H2B or negative control and analyzed by WB with indicated Abs to verify RNAi and by IF to quantify MBR. MBR quantitation, performed as in **Figure 1C**, is reported as mean ± SD from three independent experiments in which at least 1,500 cells per condition were analyzed. Representative WBs are shown below each graph, and representative images are reported in **(D)**. Scale bar, 10 μM. **(E)** MBR quantitation is reported also as fold change relative to siCtr, which was set to 1 for each condition. ***$p < 0.001$ and *$p < 0.05$, unpaired t test.

milieu, and it has been proposed that such event is critical to support a differentiation program by eliminating MBR intracellular signaling or by promoting the release of extracellular cues (Marzesco et al., 2005; Ettinger et al., 2011; Kuo et al., 2011). Stem-like populations and cancer cells, instead, appear more prone to undergo asymmetric abscission and to accumulate MBRs (Ettinger et al., 2011; Kuo et al., 2011). Our findings obtained both in tumor cells and in non-transformed RPE-1 cells show that HIPK2 depletion induces MBR accumulation, whereas depletion of the two known HIPK2 cytokinesis targets, Spastin and ecH2B, has only a marginal effect in MBR accumulation. From one side, these results indicate that the HIPK2 activities at midbody are not required for the following fate of the MBR. Alternatively, it can be speculated that both targets of HIPK2 are required to regulate the MBR fate. However, the observation that at least ecH2B depletion increases CEP55 levels at the midbody

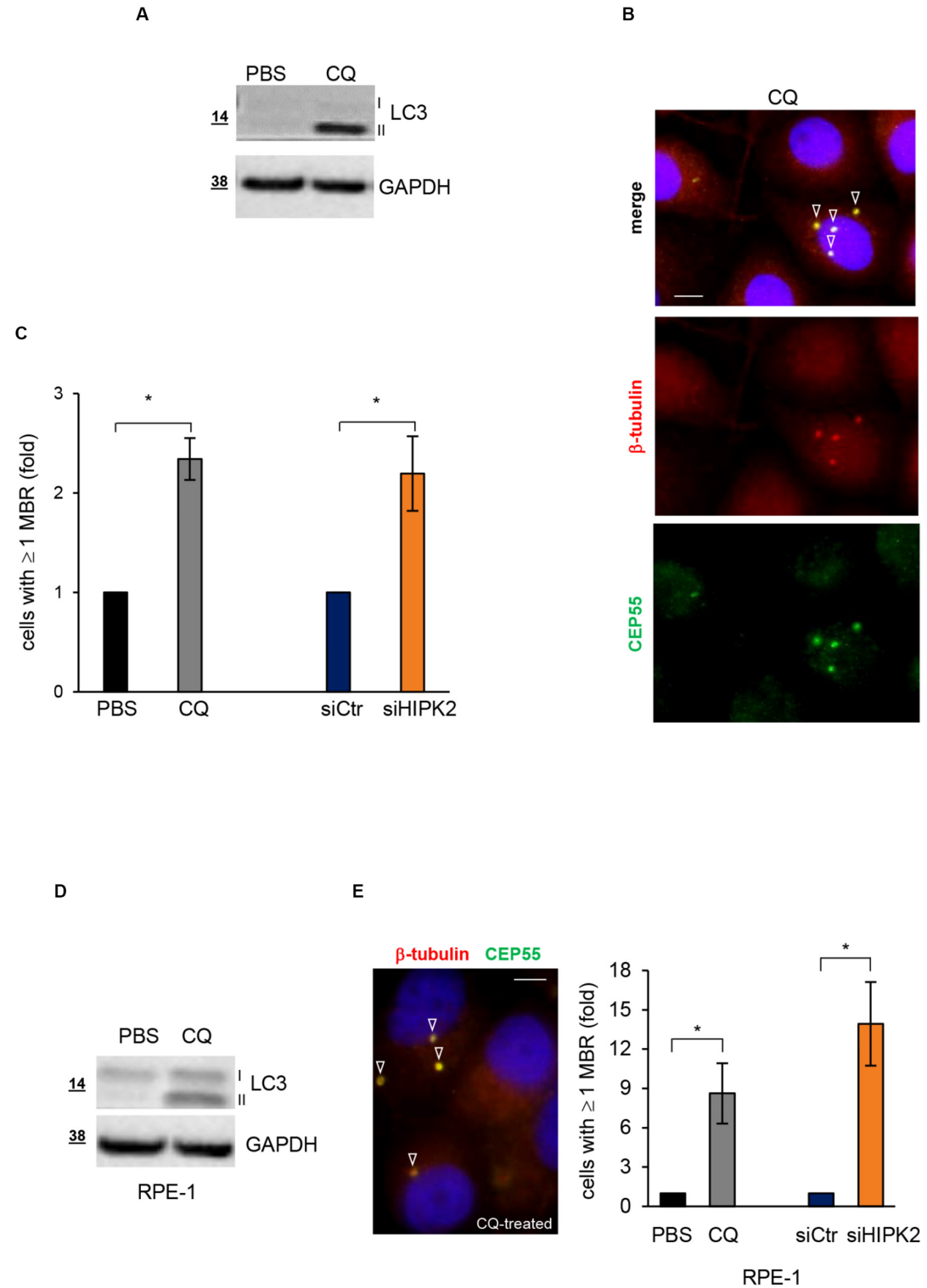

FIGURE 3 | HIPK2-depleted cells show MBR comparable to those of cells treated with the autophagy inhibitor CQ. **(A–C)** HeLa cells were treated with PBS or CQ 10 mM for 3 days and analyzed to verify autophagy inhibition by WB **(A)** and MBR quantitation by IF **(B)**. WB analysis was performed with anti-LC3 Ab that recognizes both cytosolic LC3-I and lipidated LC3-II forms of LC3. IF was performed as in **Figure 1B**. Representative WB and images are shown in **(A,B)**, respectively. Scale bar, 5 μM. In **(C)**, the percentage of cells with ≥1 MBR relative to PBS-treated cells are reported and compared to that of siHIPK2 cells relative to siCtr measured 4 days posttransfection, performed as in **Figures 1A–C**. **(D,E)** RPE-1 cells were treated, analyzed, and compared to siHIPK2 as performed for HeLa cells in **(A–C)**. Representative image of CQ-treated cells is shown. Scale bar, 5 μM. *$p < 0.05$, unpaired t test.

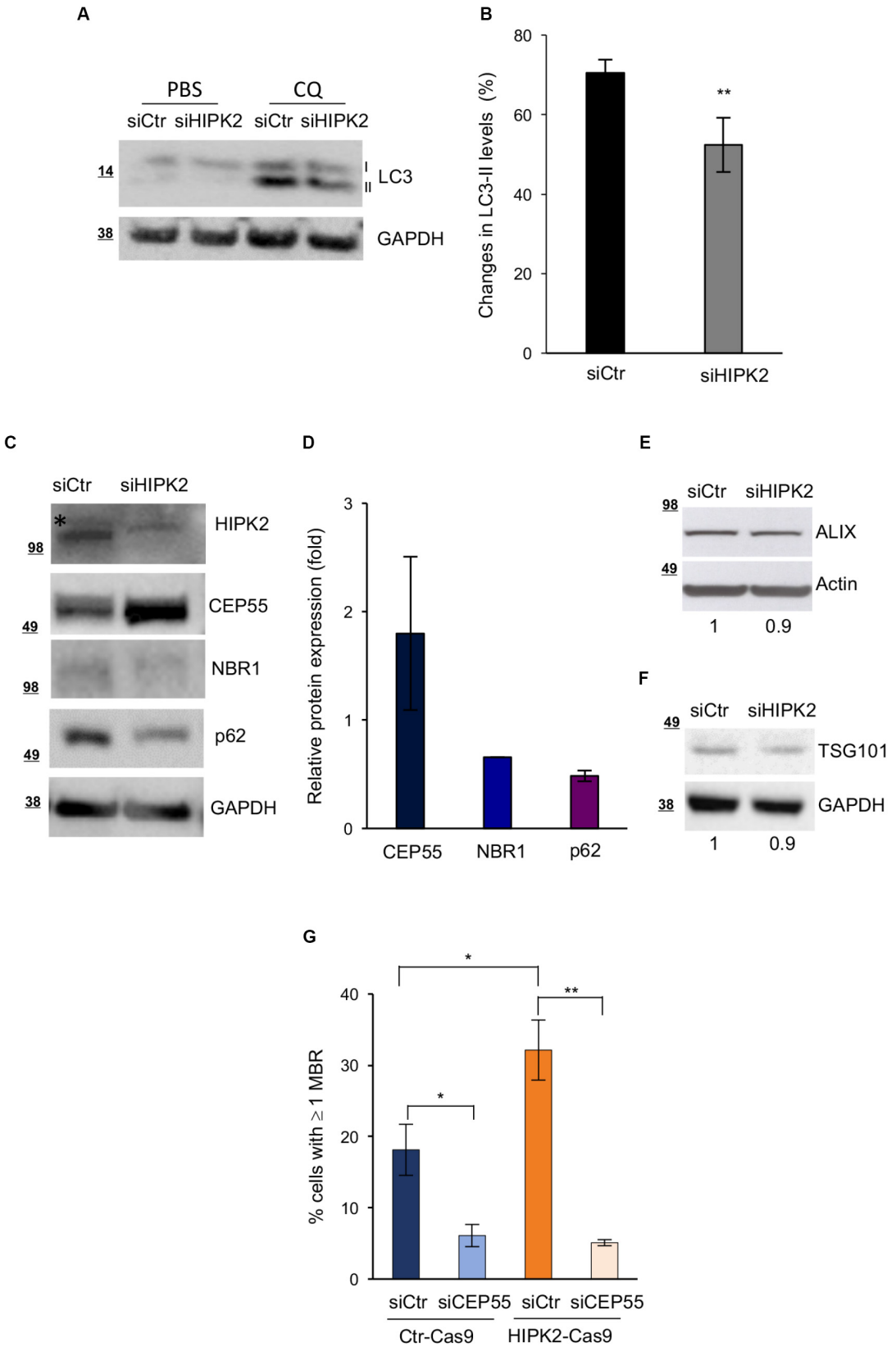

FIGURE 4 | Continued

FIGURE 4 | CEP55 overexpression and reduced autophagic flux after HIPK2-depletion. **(A,B)** HeLa cells were transfected as in **Figure 1A** and treated with PBS or CQ 48 h posttransfection. Autophagic flux was measured by WB 24 h posttreatment, scoring the changes in the levels of LC3-II, in the presence or absence of CQ. Representative WB is shown in A. Data quantification of four experiments is reported as mean ± SD in B. $^{**}p < 0.01$, unpaired *t* test. **(C–F)** HeLa cells were transfected as in **Figure 1A** and analyzed by WB 4 days after transfection with indicated Abs. In **(C,E,F)**, representative WBs are shown. The asterisk marks aspecific band. In D, protein expression of indicated proteins was quantified, normalized to GAPDH and reported as fold relative to siCtr as mean ± SD of two experiments. In **(G)**, $HeLa^{Ctr-Cas9}$ (Ctr-Cas9) and $HeLa^{HIPK2-Cas9}$ (HIPK2-Cas9) were transfected with CEP55-specific (siCEP55) or control (siCtr) siRNAs, and MBR quantitation was performed by using ALIX as MBR markers in combination with β-tubulin costaining and DAPI to stain DNA and reported as in **Figure 1D**.

(LM and SS, unpublished results) favors the first hypothesis and supports the major role for CEP55 in both midbody and MBR regulation. In agreement, we observed that CEP55 depletion in HIPK2-null cells inhibits MBR accumulation. Whether this is due to a rescue of the autophagy activity or it is only linked to the CEP55-NBR1 interaction has to be defined.

HIPK2 has been shown to regulate the expression of a large amount of proteins by acting as cotranscriptional regulator of several promoters or by phosphorylation-dependent modulation of protein stability (Calzado et al., 2007; Rinaldo et al., 2007; Blaquiere and Verheyen, 2017). Based on the increased expression of CEP55 observed in both HIPK2- and ecH2B-depleted cells, we might speculate that HIPK2 controls CEP55 expression at the posttranscriptional levels. However, this hypothesis needs to be specifically addressed. Furthermore, at this point, we cannot exclude that HIPK2 contributes to MBR degradation through direct MBR subcellular localization.

Mechanistically, in different HIPK2-depleted/-null contexts, we found a change in the levels of CEP55 and of the main autophagic receptors involved in autophagy. This, along with the observed autophagic flux reduction, which is in the range of reduction reported between cancer and normal cells (Kuo et al., 2011), supports the hypothesis that HIPK2 modulates the MBR autophagy-mediated degradation. However, we cannot rule out an effect of HIPK2 depletion at least in part also on processes regulating MBR internalization or the choice between asymmetric or symmetric abscission, promoting asymmetric abscission and consequently MBR retention or symmetric abscission and MBR engulfment.

High levels of MBR have been correlated with enhanced tumorigenicity (Kuo et al., 2011; Dionne et al., 2017), and a causal relationship between them and cell proliferation, anchorage independent growth, and survival has been recently demonstrated (Peterman et al., 2019). Most evidence supports HIPK2 as a tumor suppressor, and others suggest HIPK2 as an oncogene and its role in tumor formation/progression appears complex and heterogeneous. In mouse, in transformed fibroblasts and in cancer cells of different origins, HIPK2 inactivation leads to increased tumorigenicity (D'Orazi et al., 2012; Feng et al., 2017). Even if it is difficult to separate effects caused by HIPK2-mediated regulation of MBR persistence from those resulting from the other HIPK2-dependent pathways, MBR regulation might be among the oncosuppressive functions attributed to this kinase. Further work will be needed to better understand and discriminate the consequences of HIPK2 dysfunctions leading to higher MBR levels on cancer formation/progression.

To deeply understand the controversial role of HIPK2, it will be interesting to explore whether HIPK2 is a broad regulator of autophagy. Autophagy consists of several stages, such as initiation, expansion, autophagosome formation, autophagosome–lysosome fusion, and degradation. Each of these steps can be dynamically regulated via a complex network of autophagy-relevant proteins and by posttranslational modifiers including kinases (Stork et al., 2012). It has been suggested that HIPK2 overexpression promotes phagophore expansion and increases mature autophagosome formation in liver sepsis (Jiang et al., 2018). In *Caenorhabditis elegans*, the HIPK-family orthologous HPK-1 is required for inducing autophagosome formation and autophagy gene expression in response to dietary restriction or TORC1 inactivation (Das et al., 2017). Here, we show that HIPK2 depletion impairs the autophagic flux and affects the levels of two major macroautophagy cargo receptors, p62 and NBR1, supporting the hypothesis that HIPK2 is one of the kinases involved in autophagy signaling, which impinges on MBR degradation also indirectly by acting on CEP55 expression.

Autophagy has been implicated not only in cancer but also in neurodegeneration, where autophagy signaling modulation is considered an attractive field of therapeutic intervention. In particular, NBR1 is involved in ensuring ubiquitinated protein degradation, whose inappropriate aggregation is a common feature to numerous neurodegenerative and neuromuscular diseases (Nicot et al., 2014). HIPK2 has been involved in several neurodegenerative diseases, such as Parkinson, Alzheimer, and Lafora disease, mainly because of its role in proapoptotic induction (Lanni et al., 2010; Upadhyay et al., 2015). The HIPK2 role in autophagy regulation opens a scenario in which this kinase might function in the control of cell death and of protein aggregation. Of relevance, we observed a reduction of NBR1 levels and an increase of CEP55 levels also in HIPK2-depleted motoneuron-like cells and in brain tissue from HIPK2 KO mice (**Supplementary Figures S3A,B** and data not shown), supporting the existence of this HIPK2-mediated regulation in neuronal context both *in vitro* and *in vivo*. Thus, it will be interesting to explore mechanisms underlying this novel HIPK2 regulation and its role in normal and pathological conditions.

In conclusion, our data support a model in which, at the end of cell division, HIPK2 controls abscission acting on midbody regulation and MBR removal, this latter at least through autophagy-mediated degradation with clinical implication in cancer and in neurodegenerative diseases.

DATA AVAILABILITY STATEMENT

The datasets generated for this study are available on request to the corresponding authors.

ETHICS STATEMENT

The animal study was reviewed and approved by National Institutes of Health (1056/2015).

AUTHOR CONTRIBUTIONS

CR designed the experiments and wrote the manuscript with the contribution of SS and FS. FS, LM, FM, and MF performed the experiments. CR and SS jointly supervised this work as co-last authors. All authors contributed to the article and approved the submitted version.

FUNDING

This work was supported by grants from AFM-Telethon (#22157), Regione Lazio (85-2017-15348) to CR and Italian Association for Cancer Research (AIRC) (IG #17739) to CR and (IG #14592) to SS.

ACKNOWLEDGMENTS

We are grateful to all people cited in the text for their gifts of cells and reagents. We thank Dr. D. Trisciuoglio for her help and advice and Dr. G. Guarguaglini for her critical reading of the manuscript.

SUPPLEMENTARY MATERIAL

The Supplementary Material for this article can be found online at: https://www.frontiersin.org/articles/10.3389/fcell.2020.572094/full#supplementary-material

FIGURE S1 | MBR accumulation in HIPK2-depleted U2OS cells. **(A–C)** U2OS cells were transfected with HIPK2 -specific siRNA or negative universal control as in 1A and analyzed 5 days post transfection by WB with indicated Abs to verify RNAi and by IF for MBR quantitation as in 1C. Representative WB is shown in **A**. In **B**, the percentage of cells with ≥1 MBR were reported as mean ± SD by analyzing at least total 2000 cells per condition. $^{**}p < 0.01$ and $^{*}p < 0.05$, unpaired *t*-test. In **C**, representative fields are shown. Scale bar, 10 μM.

FIGURE S2 | MBR upon depletion of HIPK2 and its cytokinesis target Spastin in non-transformed cells. **(A,B)** RPE-1 cells were transfected with HIPK2 -specific, Spastin-specific or negative control siRNAs and analyzed 5 days post transfection by WB with indicated Abs to verify RNAi and by IF for MBR quantitation. Representative WB are shown in **(A)**. In **(B)**, MBR quantitation is reported as mean ± SD by analyzing at least total 1000 cells per condition. Representative images are reported in the left panels. Scale bar, 10 μM. $^{**}p < 0.01$, unpaired *t*-test.

FIGURE S3 | NBR1 and CEP55 levels in HIPK2 depleted motorneuron-like cells and *in vivo* in *HIPK2* KO mouse. **(A)** NSC34 cells were transfected with a mix of three murine HIPK2 -specific siRNA or negative universal control and analyzed 4 days post transfection by WB with indicated Abs. **(B)** Cerebellum tissues were explanted from *HIPK2* KO or WT adult mice, protein lysates were obtained and analyzed by WB with indicated Abs. Protein expression of indicated proteins was quantified, normalized to GAPDH and reported below each WB.

FIGURE S4 | CEP55 modulation in Ctr-Cas9 and HIPK2-Cas9 HeLa cells. **(A)** An equal number of Ctr-Cas9 and HIPK2-Cas9 HeLa cells were plated and TCEs were analyzed by WB with indicated Abs 24 h post plating. **(B)** Representative WB to verify CEP55 RNAi in cells analyzed in **Figure 4G**. At variance with **Supplementary Figure S4A**, the amount of CEP55 observed in the Ctr-Cas9 and HIPK2-Cas9 cells upon transfection with control siRNAs is similar. This is possibly due to the different confluence the cells reach after 4 days in culture (see panel in **C**), because of the abscission defects only in the HIPK2-Cas9 cells. **(C)** Representative images of the cells analyzed in **Figure 4G**. Scale bar, 10 μM.

TABLE S1 | Cytokinesis defects were measured by IF in the indicated cells. DAPI was used to mark nuclei and β-tubulin immunostaining was used to identify midbody in telophase and cytoplasm in interphase, as described in Pisciottani et al., 2019 and Monteonofrio et al., 2019. Aberrant midbodies are those filled with microtubules, elongated, and often associated with tubulin-labeled puncta, as previously described in Pisciottani et al., 2019. Data are reported as mean ± SD from three independent experiments, in which at least 500 cells per condition were analyzed.

REFERENCES

Bernabé-Rubio, M., Andrés, G., Casares-Arias, J., Fernández-Barrera, J., Rangel, L., Reglero-Real, N., et al. (2016). Novel role for the midbody in primary ciliogenesis by polarized epithelial cells. *J. Cell Biol.* 214, 259–273. doi: 10.1083/jcb.201601020

Blaquiere, J. A., and Verheyen, E. M. (2017). Homeodomain-interacting protein kinases: diverse and complex roles in development and disease. *Curr. Top. Dev. Biol.* 123, 73–103. doi: 10.1016/bs.ctdb.2016.10.002

Calzado, M. A., Renner, F., Roscic, A., and Schmitz, M. L. (2007). HIPK2: a versatile switchboard regulating the transcription machinery and cell death. *Cell Cycle* 6, 139–143. doi: 10.4161/cc.6.2.3788

Chen, C., Ettinger, A., Huttner, W., and Doxsey, S. (2013). Resurrecting remnants: the lives of post-mitotic midbodies. *Trends Cell Biol.* 23, 118–128. doi: 10.1016/j.tcb.2012.10.012

Cho, H., and Kehrl, J. H. (2007). Localization of Gi alpha proteins in the centrosomes and at the midbody: implication for their role in cell division. *J. Cell Biol.* 178, 245–255. doi: 10.1083/jcb.200604114

Crowell, E. F., Gaffuri, A. L., Gayraud-Morel, B., Tajbakhsh, S., and Echard, A. (2014). Engulfment of the midbody remnant after cytokinesis in mammalian cells. *J. Cell Sci.* 127(Pt 17), 3840–3851. doi: 10.1242/jcs.154732

Crowell, E. F., Tinevez, J. Y., and Echard, A. (2013). A simple model for the fate of the cytokinesis midbody remnant: implications for remnant degradation by autophagy. *Bioessays* 35, 472–481. doi: 10.1002/bies.201200132

Das, R., Melo, J. A., Thondamal, M., Morton, E. A., Cornwell, A. B., Crick, B., et al. (2017). The homeodomain-interacting protein kinase HPK-1 preserves protein homeostasis and longevity through master regulatory control of the HSF-1 chaperone network and TORC1-restricted autophagy in *Caenorhabditis elegans*. *PLoS Genet.* 13:e1007038. doi: 10.1371/journal.pone.1007038

Dionne, L. K., Peterman, E., Schiel, J., Gibieža, P., Skeberdis, V. A., Jimeno, A., et al. (2017). FYCO1 regulates accumulation of post-mitotic midbodies by mediating LC3-dependent midbody degradation. *J. Cell Sci.* 130, 4051–4062. doi: 10.1242/jcs.208983

D'Orazi, G., Cecchinelli, B., Bruno, T., Manni, I., Higashimoto, Y., Saito, S., et al. (2002). Homeodomain-interacting protein kinase-2 phosphorylates p53 at Ser 46 and mediates apoptosis. *Nat. Cell Biol.* 4, 11–19. doi: 10.1038/ncb714

D'Orazi, G., Rinaldo, C., and Soddu, S. (2012). Updates on HIPK2: a resourceful oncosuppressor for clearing cancer. *J. Exp. Clin. Cancer Res.* 31, 63. doi: 10.1186/1756-9966-31-63

Ettinger, A. W., Wilsch-Bräuninger, M., Marzesco, A. M., Bickle, M., Lohmann, A., Maliga, Z., et al. (2011). Proliferating versus differentiating stem and cancer cells exhibit distinct midbody-release behaviour. *Nat. Commun.* 2:503. doi: 10.1038/ncomms1511

Feng, Y., Zhou, L., Sun, X., and Li, Q. (2017). Homeodomain-interacting protein kinase 2 (HIPK2): a promising target for anti-cancer therapies. *Oncotarget* 8, 20452–20461. doi: 10.18632/oncotarget.14723

Fumoto, K., Kikuchi, K., Gon, H., and Kukuchi, A. (2012). Wnt5a signaling controls cytokinesis by correctly positioning ESCRT-III at the midbody. *J. Cell Sci.* 25(Pt 20), 4822–4832. doi: 10.1242/jcs.108142

Gatti, V., Ferrara, M., Virdia, I., Matteoni, S., Monteonofrio, L., Di Martino, S., et al. (2020). An alternative splice variant of HIPK2 with intron retention contributes to cytokinesis. *Cells* 9:484. doi: 10.3390/cells9020484

Hu, C. K., Coughlin, M., and Mitchison, T. J. (2012). Midbody assembly and its regulation during cytokinesis. *Mol. Biol Cell* 23, 1024–1034. doi: 10.1091/mbc.E11-08-0721

Isakson, P., Lystad, A. H., Breen, K., Koster, G., Stenmark, H., and Simonsen, A. (2013). TRAF6 mediates ubiquitination of KIF23/MKLP1 and is required for midbody ring degradation by selective autophagy. *Autophagy* 9, 1955–1964. doi: 10.4161/auto.26085

Jiang, Z., Bo, L., Meng, Y., Wang, C., Chen, T., Wang, C., et al. (2018). Overexpression of homeodomain-interacting protein kinase 2 (HIPK2) attenuates sepsis-mediated liver injury by restoring autophagy. *Cell Death Dis.* 9:847. doi: 10.1038/s41419-018-0838-9

Kaplan, D. D., Meigs, T. E., Kelly, P., and Casey, P. J. (2004). Identification of a role for beta-catenin in the establishment of a bipolar mitotic spindle. *J. Biol. Chem.* 279, 10829–10832. doi: 10.1074/jbc.C400035200

Kasahara, K., Nakayama, Y., Nakazato, Y., Ikeda, K., Kunga, T., and Yamaguchi, N. (2007). Src signaling regulates completion of abscission in cytokinesis through ERK/MAPK activation at the midbody. *J. Biol. Chem.* 282, 5327–5339. doi: 10.1074/jbc.M608396200

Klionsky, D. J., Abeliovich, H., Agostinis, P., Agrawal, D. K., Aliev, G., Askew, D. S., et al. (2008). Guidelines for the use and interpretation of assays for monitoring autophagy in higher eukaryotes. *Autophagy* 4, 151–175. doi: 10.4161/auto.19496

Kuo, T. C., Chen, C. T., Baron, D., Onder, T., Loewer, S., Almeida, S., et al. (2011). Midbody accumulation through evasion of autophagy contributes to cellular reprogramming and tumorigenicity. *Nat. Cell Biol.* 13, 1214–1223. doi: 10.1038/ncb2332

Lanni, C., Nardinocchi, L., Puca, R., Stanga, S., Uberti, D., Memo, M., et al. (2010). Homeodomain interacting protein kinase 2: a target for Alzheimer's beta amyloid leading to misfolded p53 and inappropriate cell survival. *PLoS One* 5:e10171. doi: 10.1371/journal.pone.0010171

Li, D., Mangan, A., Cicchini, L., Margolis, B., and Prekeris, R. (2014). FIP5 phosphorylation during mitosis regulates apical trafficking and lumenogenesis. *EMBO Rep.* 15, 428–437. doi: 10.1002/embr.201338128

Luján, P., Varsano, G., Rubio, T., Hennrich, M. L., Sachsenheimer, T., Gálvez-Santisteban, M., et al. (2016). PRL-3 disrupts epithelial architecture by altering the post-mitotic midbody position. *J. Cell Sci.* 129, 4130–4142. doi: 10.1242/jcs.190215

Mandell, M. A., Jain, A., Kumar, S., Castleman, M. J., Anwar, T., Eskelinen, E. L., et al. (2016). TRIM17 contributes to autophagy of midbodies while actively sparing other targets from degradation. *J. Cell Sci.* 129, 3562–3573. doi: 10.1242/jcs.190017

Marzesco, A. M., Janich, P., Wilsch-Brauninger, M., Dubreuil, V., Langenfeld, K., Corbeil, D., et al. (2005). Release of extracellular membrane particles carrying the stem cell marker prominin-1 (CD133) from neural progenitors and other epithelial cells. *J. Cell Sci.* 118(Pt 13), 2849–2858. doi: 10.1242/jcs.02439

Monteonofrio, L., Valente, D., Ferrara, M., Camerini, S., Miscione, R., Crescenzi, M., et al. (2018). HIPK2 and extrachromosomal histone H2B are separately recruited by Aurora-B for cytokinesis. *Oncogene* 37, 3562–3574. doi: 10.1038/s41388-018-0191-6

Monteonofrio, L., Valente, D., Rinaldo, C., and Soddu, S. (2019). Extrachromosomal histone H2B contributes to the formation of the abscission site for cell division. *Cells* 8:1391. doi: 10.3390/cells811139

Naito, Y., Okada, M., and Yagisawa, H. (2006). Phospholipase C isoforms are localized at the cleavage furrow during cytokinesis. *J. Biochem.* 140, 785–791. doi: 10.1093/jb/mvj209

Nicot, A. S., Lo Verso, F., Ratti, F., Pilot-Storck, F., Streichenberger, N., Sandri, O., et al. (2014). Phosphorylation of NBR1 by GSK3 modulates protein aggregation. *Autophagy* 10, 1036–1053. doi: 10.4161/auto.28479

Peterman, E., Gibieža, P., Schafer, J., Skeberdis, V. A., Kaupinis, A., Valius, M., et al. (2019). The post-abscission midbody is an intracellular signaling organelle that regulates cell proliferation. *Nat. Commun.* 10:3181. doi: 10.1038/s41467-019-10871-0

Peterman, E., and Prekeris, R. (2019). The postmitotic midbody: regulating polarity, stemness, and proliferation. *J. Cell Biol.* 218, 3903–3911. doi: 10.1083/jcb.201906148

Pisciottani, A., Biancolillo, L., Ferrara, M., Valente, D., and Sardina, F. (2019). HIPK2 phosphorylates the microtubule-severing enzyme spastin at S268 for abscission. *Cells* 8:684. doi: 10.3390/cells8070684

Pohl, C., and Jentsch, S. (2009). Midbody ring disposal by autophagy is a post-abscission event of cytokinesis. *Nat. Cell Biol.* 11, 65–70. doi: 10.1038/ncb1813

Pollarolo, G., Schulz, J. G., Munck, S., and Dotti, C. G. (2011). Cytokinesis remnants define first neuronal asymmetry in vivo. *Nat. Neurosci.* 14, 1525–1533. doi: 10.1038/nn.2976

Rinaldo, C., Moncada, A., Gradi, A., Ciuffini, L., D'Eliseo, D., Siepi, F., et al. (2012). HIPK2 controls cytokinesis and prevents tetraploidization by phosphorylating histone H2B at the midbody. *Mol. Cell.* 47, 87–98. doi: 10.1016/j.molcel.2012.04.029

Rinaldo, C., Prodosmo, A., Siepi, S., and Soddu, S. (2007). HIPK2: a multitalented partner for transcription factors in DNA damage response and development. *Biochem. Cell Biol.* 85, 411–418. doi: 10.1139/O07-071

Ritter, O., and Schmitz, M. L. (2019). Differential intracellular localization and dynamic nucleocytoplasmic shuttling of homeodomain-interacting protein kinase family members. *Biochim. Biophys. Acta Mol. Cell Res.* 1866, 1676–1686. doi: 10.1016/j.bbamcr.2019.04.009

Stork, B., Alers, S., Löffler, A. S., and Wesselborg, S. (2012). "Regulation of autophagy by protein phosphorylation," in *Protein Phosphorylation in Human Health*, ed. C. Huang (London: IntechOpen), doi: 10.5772/48502

Upadhyay, M., Gupta, S., Bhadauriya, P., and Ganesh, S. (2015). Lafora disease proteins laforin and malin negatively regulate the HIPK2-p53 cell death pathway. *Biochem. Biophys. Res. Commun.* 464, 106–111. doi: 10.1016/j.bbrc.2015.06.018

Valente, D., Bossi, G., Moncada, A., Tornincasa, M., Indelicato, S., Piscuoglio, S., et al. (2015). HIPK2 deficiency causes chromosomal instability by cytokinesis failure and increases tumorigenicity. *Oncotarget* 6, 10320–10334. doi: 10.18632/oncotarget.3583

Wilcock, A. C., Swedlow, J. R., and Storey, K. G. (2007). Mitotic spindle orientation distinguishes stem cell and terminal modes of neuron production in the early spinal cord. *Development* 134, 1943–1954. doi: 10.1242/dev.002519

Willard, F. S., and Crouch, M. F. (2001). MEK, ERK, and p90RSK are present on mitotic tubulin in Swiss 3T3 cells: a role for the MAP kinase pathway in regulating mitotic exit. *Cell. Signal.* 13, 653–664. doi: 10.1016/s0898-6568(01)00185-1

Conflict of Interest: The authors declare that the research was conducted in the absence of any commercial or financial relationships that could be construed as a potential conflict of interest.

frontiers in Cell and Developmental Biology

ORIGINAL RESEARCH
published: 25 September 2020
doi: 10.3389/fcell.2020.573393

Equatorial Non-muscle Myosin II and Plastin Cooperate to Align and Compact F-actin Bundles in the Cytokinetic Ring

Joana Leite[1,2], Fung-Yi Chan[1,2], Daniel S. Osório[1,2†], Joana Saramago[1,2†], Ana F. Sobral[1,2†], Ana M. Silva[1,2], Reto Gassmann[1,2] and Ana X. Carvalho[1,2]*

[1] Cytoskeletal Dynamics Lab, Instituto de Investigação e Inovação em Saúde (i3S), Universidade do Porto, Porto, Portugal,
[2] Cytoskeletal Dynamics Lab, Instituto de Biologia Molecular e Celular (IBMC), Universidade do Porto, Porto, Portugal

OPEN ACCESS

Edited by:
Maria Grazia Giansanti,
Italian National Research Council, Italy

Reviewed by:
Charles Bradley Shuster,
New Mexico State University,
United States
Giuliano Callaini,
University of Siena, Italy

***Correspondence:**
Ana X. Carvalho
anacarvalho@ibmc.up.pt

† These authors have contributed equally to this work

Specialty section:
This article was submitted to Cell Growth and Division, a section of the journal Frontiers in Cell and Developmental Biology

Received: 16 June 2020
Accepted: 03 September 2020
Published: 25 September 2020

Citation:
Leite J, Chan F-Y, Osório DS, Saramago J, Sobral AF, Silva AM, Gassmann R and Carvalho AX (2020) Equatorial Non-muscle Myosin II and Plastin Cooperate to Align and Compact F-actin Bundles in the Cytokinetic Ring. Front. Cell Dev. Biol. 8:573393. doi: 10.3389/fcell.2020.573393

Cytokinesis is the last step of cell division that physically partitions the mother cell into two daughter cells. Cytokinesis requires the assembly and constriction of a contractile ring, a circumferential array of filamentous actin (F-actin), non-muscle myosin II motors (myosin), and actin-binding proteins that forms at the cell equator. Cytokinesis is accompanied by long-range cortical flows from regions of relaxation toward regions of compression. In the *C. elegans* one-cell embryo, it has been suggested that anterior-directed cortical flows are the main driver of contractile ring assembly. Here, we use embryos co-expressing motor-dead and wild-type myosin to show that cortical flows can be severely reduced without major effects on contractile ring assembly and timely completion of cytokinesis. Fluorescence recovery after photobleaching in the ingressing furrow reveals that myosin recruitment kinetics are also unaffected by the absence of cortical flows. We find that myosin cooperates with the F-actin crosslinker plastin to align and compact F-actin bundles at the cell equator, and that this cross-talk is essential for cytokinesis. Our results thus argue against the idea that cortical flows are a major determinant of contractile ring assembly. Instead, we propose that contractile ring assembly requires localized concerted action of motor-competent myosin and plastin at the cell equator.

Keywords: actomyosin contractility, cytokinesis, non-muscle myosin II, contractile ring, *C. elegans*, cortical flows, plastin/fimbrin

INTRODUCTION

Animal cytokinesis relies on the assembly and constriction of an actomyosin contractile ring at the cell equator, which pinches the plasma membrane inwards, ultimately separating the two daughter cells (reviewed in Leite et al., 2019). The contractile ring is a circumferential array of filamentous actin (F-actin), non-muscle myosin II (hereafter myosin) and actin-binding proteins, including formins and F-actin crosslinkers, such as α-actinin, fimbrin/plastin (hereafter plastin), anillin and septins (reviewed in Green et al., 2012). At cytokinesis onset, RhoA activation at the cell equator triggers the recruitment and activation of downstream effectors to assemble the contractile ring, particularly diaphanous-related formins (Prokopenko et al., 2000;

Großhans et al., 2005; Watanabe et al., 2010; Melak et al., 2017) and Rho kinase, which promote the assembly of linear F-actin and the activation of myosin, respectively (Matsumura, 2005; Vicente-Manzanares, 2009). Experimental evidence from electron microscopy in marine invertebrate and newt eggs and cultured mammalian cells suggests that the contractile ring is a thin layer of closely packed F-actin of mixed polarities (Schroeder, 1968, 1970, 1972; Arnold, 1969; Selman and Perry, 1970; Sanger and Sanger, 1980; Maupin and Pollard, 1986; Mabuchi et al., 1988; Henson et al., 2017) surrounded by a mostly branched network (Henson et al., 2017). How F-actin and myosin accumulate and organize into a circumferential array at the cell equator to form the contractile ring is a central question that remains to be fully resolved. Two main mechanisms have been implicated: equatorial compression due to cortical flows and local RhoA-dependent *de novo* assembly at the equator. According to the former, both F-actin and myosin are advected by flow from the poles towards the equator due to a tension differential between these regions. The persistent convergence at the equator creates a region where filaments are constantly compressed and aligned (White and Borisy, 1983; Salbreux et al., 2009; Turlier et al., 2014; Khaliullin et al., 2018). According to the latter, F-actin and myosin are directly recruited to the equatorial cortex from the cytoplasm, leading to local alignment of F-actin bundles (Kimura et al., 1996; Bement et al., 2005; Vavylonis et al., 2008; Uehara et al., 2010; Spira et al., 2017). The relative contribution of these two mechanisms to cytokinesis has been difficult to ascertain, because flows are myosin-dependent (Reymann et al., 2016) yet myosin perturbations may prevent cytokinesis simply because myosin-dependent force generation at the equator is essential for equatorial deformation and continued furrow ingression (Davies et al., 2014; Osorio et al., 2019). While actomyosin cortical flows towards the cell equator during cytokinesis have been described in several experimental systems, including *C. elegans* (Reymann et al., 2016; Khaliullin et al., 2018; Singh et al., 2019), they are less evident in some mammalian cells and are absent in yeast (Cao and Wang, 1990; Murthy and Wadsworth, 2005; Wu and Pollard, 2005; Vavylonis et al., 2008; Laplante et al., 2015). It remains to be determined whether cortical flows actually drive assembly of a contractile ring or whether they are simply a consequence of the tension differential that arises from equatorial stimulation and polar relaxation.

The involvement of F-actin crosslinkers (hereafter crosslinkers) in contractile ring assembly remains poorly explored. Depending on their size and structure, crosslinkers can form tight and parallel F-actin bundles or loosely crosslinked F-actin networks with distinct architectures and mechanical properties (Faix et al., 1996; Mavrakis et al., 2014; Srivastava and Robinson, 2015). A common feature is that crosslinkers provide interconnectivity, which is important for contractility of actomyosin networks (Ennomani et al., 2016; Descovich et al., 2017). To date, the only crosslinker whose perturbation is known to negatively impact cytokinesis in *C. elegans* embryos is the plastin PLST-1. A *plst-1* loss-of-function mutant decreased F-actin network connectivity and resulted in short-range and erratic F-actin cortical flows (Ding et al., 2017). Plastin is a globular protein that can assemble F-actin into tightly packed bundles with uniform or mixed polarity (Bretscher, 1981; Matsudaira et al., 1983; Skau et al., 2011). Plastin localizes to dense F-actin bundles and is particularly abundant in the cytokinetic ring (Ding et al., 2017), but whether it contributes to the organization and/or stabilization of F-actin bundles in this region is unknown.

We previously generated *C. elegans* expressing motor-dead mutants of myosin (NMY-2) and showed that myosin motor activity is essential for cytokinesis in the one-cell embryo (Osorio et al., 2019). In this study, we use these *nmy-2* mutants, as well as a *plst-1* mutant, to explore the role of cortical flows during cytokinesis in the one-cell *C. elegans* embryo. Our data from quantitative live imaging assays for cortical F-actin and myosin flows, contractile ring assembly and furrow ingression, myosin turnover dynamics, and F-actin bundle alignment at the cell equator, collectively support the idea that contractile ring assembly and furrow ingression requires the concerted action of motor-competent myosin and plastin at the cell equator and is largely independent of compressive cortical flows.

RESULTS

Long-Range Cortical F-actin Flows Are Dispensable for Contractile Ring Formation and Furrow Ingression

To investigate the importance of compressive cortical flows for assembly and constriction of the contractile ring (**Figures 1A,B**), we analyzed F-actin cortical flow profiles in one-cell embryos co-expressing endogenous motor-dead NMY-2(S251A) or NMY-2(R252A) and a transgenic wild-type version of NMY-2 that is mCherry-tagged and RNAi-sensitive (NMY-2::mCherry^{sen}; **Figure 1C**) (Osorio et al., 2019). NMY-2(S251A) and NMY-2(R252A) are unable to translocate F-actin but retain the ability to bind F-actin *in vitro* (Osorio et al., 2019), and embryos expressing endogenous motor-dead myosins fail cytokinesis after penetrant RNAi-mediated depletion of NMY-2::mCherry^{sen} (Osorio et al., 2019). Mild RNAi-mediated depletion of NMY-2::mCherry^{sen} slows but does not prevent cytokinesis.

F-actin flow analysis was performed using transgenic LifeAct::GFP, whose cortical levels are unaffected by myosin inhibition (Osorio et al., 2019). We chose LifeAct::GFP (Silva et al., 2016; Chan et al., 2019; Osorio et al., 2019) rather than LifeAct::mKate2 (Reymann et al., 2016), because in our hands one-cell embryos expressing LifeAct::mKate2 exhibited delayed furrow initiation and had a significantly reduced contractile ring constriction rate when compared to embryos expressing other fluorescent contractile ring components (**Supplementary Figure S1A**). In contrast, cytokinesis kinetics were normal in embryos expressing LifeAct::GFP. Moreover, the cortical distribution of LifeAct::GFP, but not that of LifeAct::mKate2, was similar to the cortical distribution of endogenous PLST-1::GFP (**Supplementary Figure S1B**), which binds all F-actin pools during cytokinesis (Ding et al., 2017).

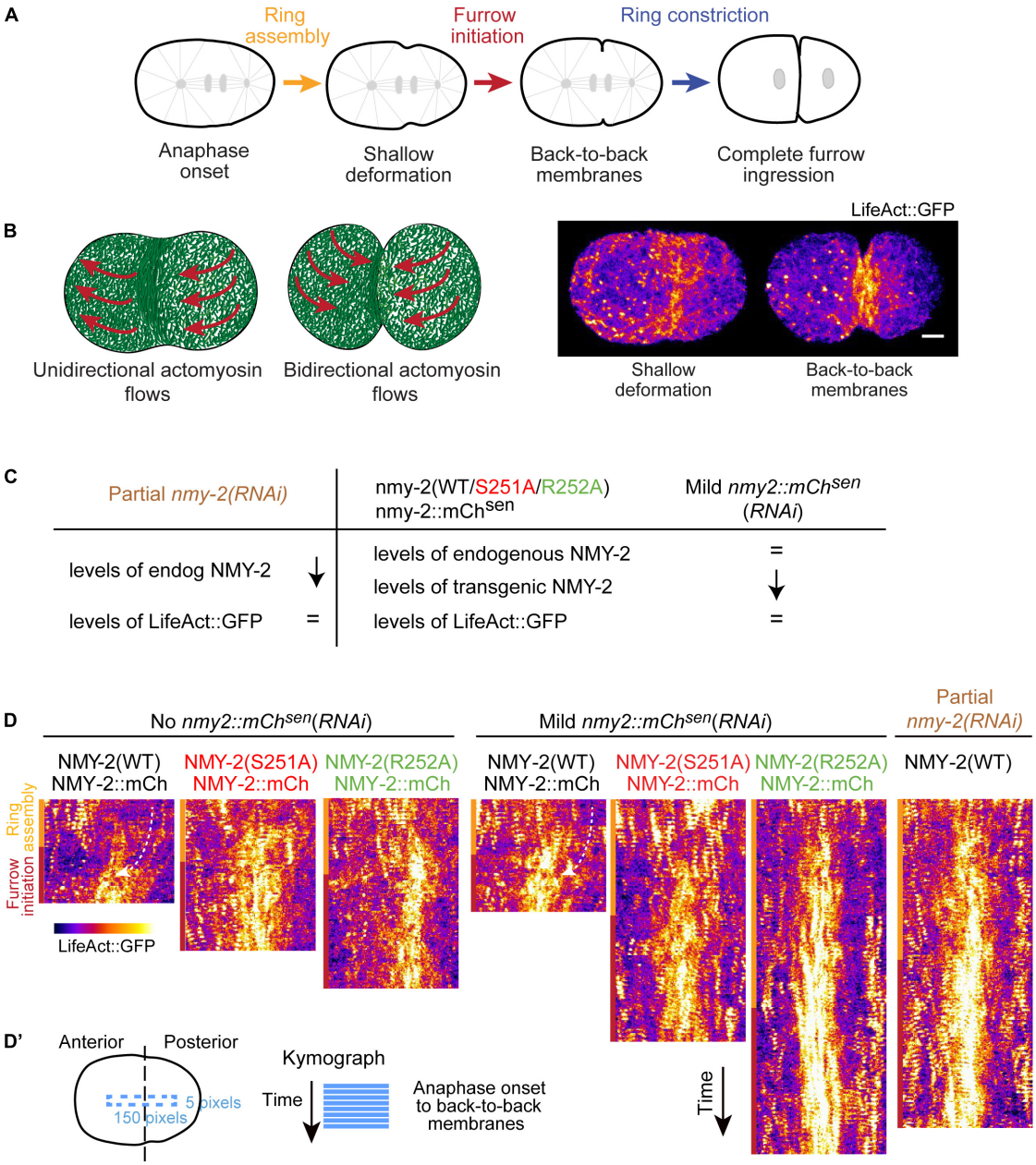

FIGURE 1 | Perturbation of myosin motor activity or reduction of myosin levels lead to significantly reduced cortical F-actin flows. **(A)** Schematic of cytokinesis. Reference points used for measurements of ring assembly and furrow initiation intervals are indicated. Ring assembly: time interval between anaphase onset and the formation of a shallow equatorial deformation, when contractile ring components are being recruited to the cell equator. Furrow initiation: time interval between shallow deformation and the folding of the plasma membrane into a back-to-back configuration. Ring constriction: time interval between back-to-back membrane configuration and full furrow ingression. **(B)** Stills of cortical images of an embryo expressing LifeAct::GFP at shallow deformation and furrow initiation with a schematic illustrating the transition from unidirectional cortical flows during ring assembly to bidirectional flows starting at the onset of ring constriction. **(C)** Perturbations used and their effect on the levels of endogenous and transgenic NMY-2 and LifeAct::GFP relative to controls with no RNAi, as described in Osorio et al. (2019). **(D)** Kymographs of LifeAct::GFP cortical flows along the longitudinal axis in one-cell embryos for the conditions indicated in **(C)**. Yellow and red bars correspond to ring assembly and furrow initiation time intervals, respectively. Curved arrows indicate posterior-anterior flow direction. **(D')** Schematic illustrating the region of the embryo used for the kymographs in **(D)**. Scale bar, 5 μm.

Kymographs of the cortical region between the onset of anaphase and the establishment of a back-to-back plasma membrane configuration revealed F-actin flows directed from the posterior towards the anterior pole in control embryos (**Figures 1A–D**). Even without depletion of transgenic NMY-2::mCherry, flows were barely detectable in *nmy-2(S251A)* and *nmy-2(R252A)* embryos, nor were they evident in embryos partially depleted of endogenous wild-type myosin

(**Figures 1C,D**). To quantitatively analyze cortical flows, we performed particle image velocimetry (PIV) analysis (**Figure 2A**). Flow velocity was calculated by averaging the X- or Y-components (anterior-posterior and dorsal-ventral, respectively) of the velocity vectors in two regions positioned over the anterior and posterior half of the embryo, for each time point between anaphase onset and back-to-back membrane configuration (**Figures 2B,C**). Like reported in Singh et al. (2019), the Y-component was essentially absent when embryos were imaged without compression in an open chamber (**Supplementary Figures S2A,B**; Singh et al., 2019), yet these embryos completed cytokinesis with kinetics that were indistinguishable from those in embryos imaged under compression (**Supplementary Figure S2C**). We therefore focused our attention on the X-component. Negative velocity values indicate posterior-anterior oriented flows and positive velocity values indicate anterior-posterior oriented flows (**Figure 2A**). In agreement with a prior study (Reymann et al., 2016), control embryos presented anterior-directed F-actin cortical flows that started just prior to equatorial shallow deformation, peaked shortly thereafter, and remained high for approximately 50 seconds (**Figure 2B**). In contrast to controls, most vectors detected in *nmy-2(S251A)* and *nmy-2(R252A)* embryos were extremely weak, had no coherent directionality, and did not increase in magnitude after equatorial shallow deformation (**Figures 2B,F**). This flow profile was observed regardless of whether transgenic NMY-2::mCherry^{sen} was mildly depleted by RNAi or not (**Figures 2C,G**). We further analyzed the flow velocity profiles by averaging the X-component of the vectors for each position along the length of the embryo during the first 50 seconds after equatorial shallow deformation, when flows in control embryos showed coherent direction and velocity (region highlighted in gray in **Figure 2B**). In control embryos, flow velocity was higher in the posterior half of the embryo, reaching a maximum velocity of -4.5 μm/min and decreasing toward the anterior pole (**Figure 2D**). In *nmy-2(S251A)* and *nmy-2(R252A)* embryos the flow profile was flat with or without depletion of transgenic NMY-2::mCherry^{sen}, reaching a maximum velocity of -1 μm/min (**Figures 2D,E**). We conclude that endogenous motor-dead myosin has a dominant inhibitory effect on cortical flows in embryos expressing transgenic NMY-2::mCherry^{sen}. Similarly weak flow profiles were observed in embryos after partial depletion of endogenous wild-type NMY-2 (**Figure 2E** and **Supplementary Figures S3C, S6C**).

Analysis of cytokinesis kinetics showed that in the presence of transgenic NMY-2::mCherry^{sen}, *nmy-2(S251A)* and *nmy-2(R252A)* embryos exhibited only minor delays in contractile ring assembly and furrow initiation despite severely impaired cortical flows (**Figure 2F**). In contrast, mild depletion of transgenic NMY-2::mCherry^{sen} in these embryos resulted in substantial delays in cytokinesis and occasional cytokinesis failure, while cortical flows were similar to those observed in the absence of RNAi treatment (**Figure 2G**). We conclude that there is no obvious correlation between perturbed cortical flows and delayed cytokinesis. This argues against the idea that persistent, unidirectional actin cortical flows are a major determinant of cytokinesis.

Cortical Flows Are Dispensable for Accumulation of Myosin in the Ingressing Furrow

To further probe the significance of cortical flows, we sought to evaluate the possibility that flowing myosin generates tension that pushes F-actin to the equator. We first compared cortical flows of LifeAct::GFP and NMY-2::GFP using PIV analysis, which showed that F-actin and myosin flow toward the equator in a concerted manner (**Supplementary Figures S3A,B**): unidirectional cortical flows from the posterior pole toward the anterior side of the embryo initiate shortly after anaphase, and flow velocities increase linearly until a maximum velocity is reached and maintained for ∼50 seconds. This is followed by a period of bidirectional flows starting at constriction onset, in which actin and myosin flow from both poles towards the ingressing furrow (positive flow velocity in the anterior and negative flow velocity in the posterior side of the embryo).

Next, we determined myosin turnover at the cell cortex outside the equator. We reasoned that if flowing myosin actively slides F-actin, myosin turnover should be relatively slow, since myosin is known to be stabilized at sites of increased tension such as the contractile ring (Reichl et al., 2008; Srivastava and Robinson, 2015). We photobleached NMY-2::GFP at the posterior polar region at shallow deformation and followed signal recovery during the period of contractile ring formation and compaction. By the time of shallow deformation, some myosin has already been cleared from the posterior pole (**Supplementary Figures S4A,B**), and therefore confounding effects of flows on the measurement of signal recovery after photobleaching should be reduced. Fluorescence recovery data could be fitted with a single exponential from which we extrapolated a half time of recovery (τ_{half}) of 4.9 ± 2.4 seconds (**Figures 3A,A'**). As a control, we photobleached a region of identical size in the posterior cytoplasm, for which signal recovery was significantly faster (τ_{half} of 2.6 ± 1.8 seconds; $P < 0.05$; **Supplementary Figures S5C,D**). Assuming a diffusion-dominated recovery profile for cortical myosin, we calculated a dissociation constant (k_{off}) of 0.07 ± 0.03 s^{-1} (equation 1 in "Materials and Methods" section). Fast myosin turnover in the polar cortex indicates that flowing myosin is in constant exchange with the cytoplasmic pool before reaching the cell equator.

We next determined the rate at which cortical flow compresses F-actin towards the equatorial region. We measured the flow X-component as a function of the position along the anterior-posterior axis for 10 seconds intervals, from 25 seconds until 95 seconds after anaphase onset, and estimated the compression rate by flow for each time interval by calculating the spatial derivative of the flow velocity for each position (**Figure 3B**). Compression was found to be uniform in the equatorial region (15–25 μm). The average compression rate for the equatorial region increased over time, reaching a maximum of 0.012 ± 0.009 s^{-1} 85 seconds after anaphase onset (**Figure 3C**).

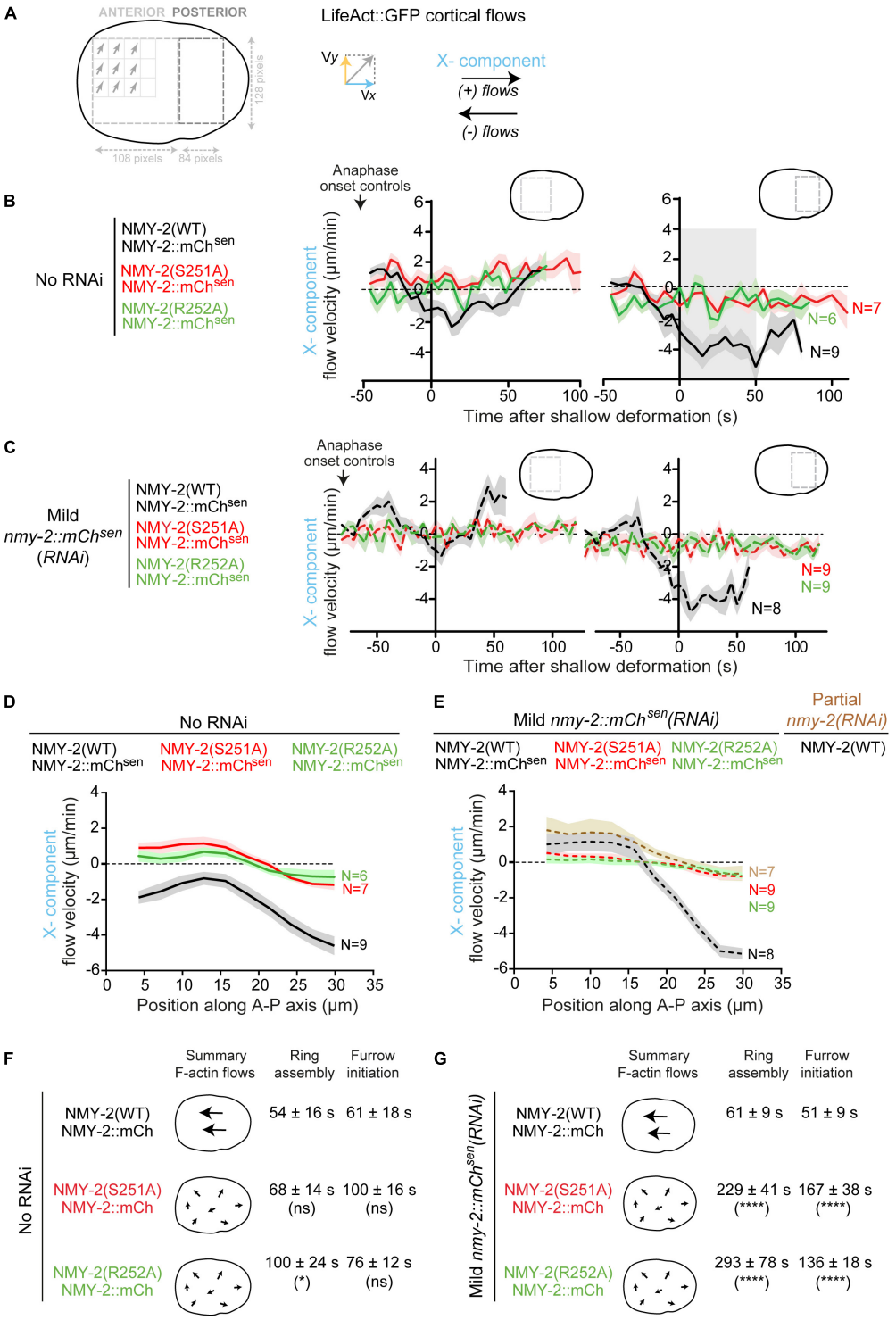

FIGURE 2 | Contractile rings assemble and cytokinesis completes in a timely manner when long-range cortical actin flows are drastically reduced. **(A)** Schematic illustrating how cortical LifeAct::GFP flows were analyzed by particle image velocimetry (PIV; see more details in "Materials and Methods" section). **(B,C)** Longitudinal (X-component) flow velocity (mean ± SEM) over time in the anterior or posterior half of embryos. Curves were aligned to the time of shallow deformation. N is the number of embryos analyzed. Period of consistently strong, posterior-anterior directed flows is indicated in gray. **(D,E)** Longitudinal (X-component) velocity profiles of Lifeact::GFP cortical flows along anterior-posterior (A-P) axis averaged for a period of 50 seconds starting at shallow deformation. Flow profiles show mean X-component velocity ± SEM. N is the number of embryos analyzed. **(F,G)** The schematic on the left summarizes overall flow intensity and directionality (X-component). Ring assembly and furrow initiation time intervals (mean ± SD) are indicated. Statistical significance in (D), (E) was determined using two-way ANOVA for repeated measures, and in (F), (G) using one-way ANOVA followed by Bonferroni's multiple comparison test; $^{*}P < 0.05$, $^{****}P < 0.0001$, ns, not significant.

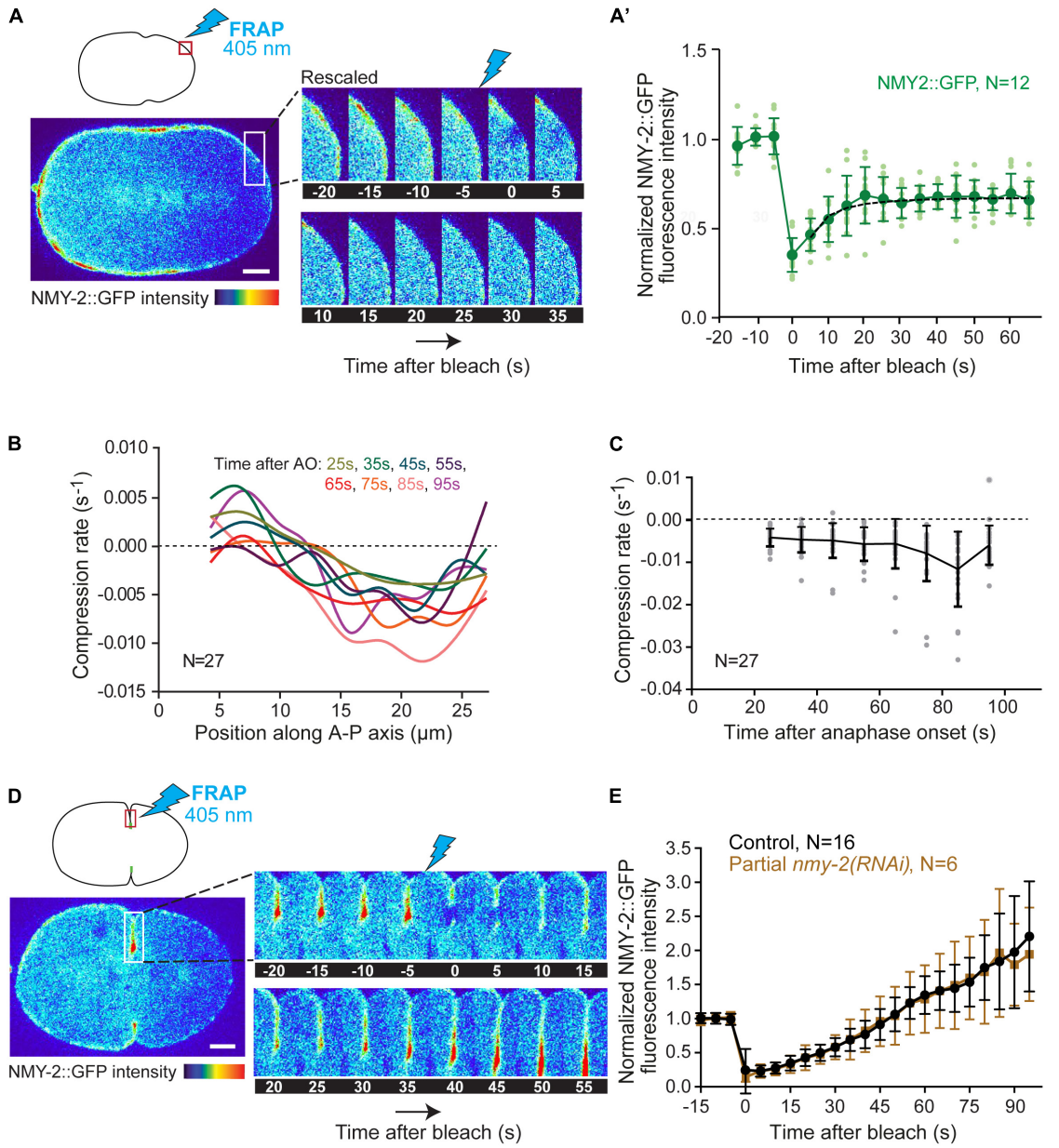

FIGURE 3 | Cortical myosin turnover and flow-induced compression rates. **(A)** Schematic showing the photobleached region at the posterior pole of the embryo at shallow deformation (top left) and selected images from a time-lapse series showing NMY-2::GFP fluorescence over time pre- and post-bleaching. **(A')** Quantification of NMY-2::GFP fluorescence recovery after photobleaching at the posterior pole. Data from individual embryos (light green) and the mean ± SD (dark green) are plotted. The black dashed line is the single exponential fitting curve from which the half time of recovery and myosin k_{off} were extrapolated. **(B)** Average compression rate by flow calculated as the spatial derivative of the longitudinal flow profiles for each position along the anterior-posterior (A-P) axis of the embryo from 25 to 95 seconds after anaphase onset (AO). Compression is uniform in the equatorial region (15–25 µm). Colors represent different time intervals as indicated. **(C)** Average compression rate by flow over time after anaphase onset for the region of equatorial compression (15–25 µm). Data from individual embryos (gray) and the mean ± SD (black) are plotted. **(D)** Schematic showing the photobleached region just behind the tip of the ingressing furrow after back-to-back membrane configuration is achieved (top left) and selected images from a time-lapse series showing the NMY-2::GFP fluorescence over time pre- and post-bleaching. **(E)** Quantification of NMY-2::GFP fluorescence recovery after photobleaching in the ingressing furrow in control and NMY-2 depleted embryos. The mean ± SD is plotted. N is the number of embryos analyzed. Scale bars, 5 µm.

As the maximum compression rate is slower than the rate of myosin dissociation from the cortex, these data argue against the idea that flowing myosin is responsible for F-actin bundle compression at the cell equator.

To confirm this, we assessed myosin turnover in the ingressing furrow. We photobleached a small region just behind the tip of the ingressing furrow and followed NMY-2::GFP signal recovery in the moving region as the furrow continued to

ingress. NMY-2::GFP fluorescence intensity in the bleached region increased until the end of ingression without reaching a plateau (**Figure 3E**). Similar results were obtained when the entire division plane was photobleached at shallow deformation (**Supplementary Figures S5A,B**). These demonstrate that myosin continues to accumulate in the contractile ring during furrow ingression. Myosin could accumulate by incoming flow, by localized recruitment from the cytoplasm, or both. To distinguish between these possibilities, we examined embryos partially depleted of NMY-2, in which the initial unidirectional flows are essentially absent, bidirectional flows are significantly decreased, and cytokinesis still completes (**Supplementary Figure S3C**). Under these conditions, NMY-2::GFP was still visible at the tip of the furrow, which allowed us to perform the photobleaching experiment. Normalized recovery profiles of NMY-2-depleted embryos were identical to those of non-depleted embryos (**Figure 3E**). These results support the idea that the contribution of cortical flows to myosin accumulation at the cell equator is minor and that equatorial myosin is therefore primarily recruited from the cytoplasm. Further support for this idea comes from the observation that the amount of myosin that accumulates at the cell equator after anaphase onset is much higher than the amount of myosin that leaves the polar regions (**Supplementary Figure S4B**).

The F-actin Crosslinker Plastin Cooperates With Myosin to Align F-actin Bundles at the Division Plane

We previously found that *nmy-2(S251A)* and *nmy-2(R252A)* embryos depleted of transgenic NMY-2::mCherry^{sen} accumulated equatorial F-actin bundles with a tilted orientation (Osorio et al., 2019). Based on this observation, we speculated that F-actin crosslinkers could also contribute to the organization of F-actin bundles at the cell equator. The plastin ortholog PLST-1 was a promising candidate, as it localizes in the contractile ring and the surrounding cortex and has been implicated in cytokinesis (Ding et al., 2017).

To determine whether NMY-2 and PLST-1 cooperate to compact and align F-actin bundles at the cell equator, we used genome editing to generate a *plst-1* mutant, *plst-1(prt89)*, which contains a premature stop codon in its open reading frame and is homozygous viable, like another previously described *plst-1* mutant (Ding et al., 2017). Using LifeAct::GFP, we quantified F-actin bundle alignment at the equatorial region over time, starting at anaphase onset (**Figures 4A,B** and **Supplementary Movie S1**). Analysis of F-actin bundle orientation in control embryos revealed fast bundle alignment perpendicular to the longitudinal axis of the embryo with bundles reaching maximum alignment shortly after shallow deformation (deviation from vertical alignment close to 0°). In embryos partially depleted of NMY-2, F-actin bundle alignment was significantly slower and continued throughout furrow initiation. In *plst-1(prt89)* embryos, F-actin bundle alignment was also slower than in control embryos, with F-actin bundles becoming mostly aligned at shallow deformation and reaching maximum alignment just before furrow initiation. In *nmy-2(RNAi);plst-1(prt89)* embryos, F-actin bundles became completely unstable and failed to align, exhibiting oscillating orientations between 20° and 50° relative to vertical alignment.

In *nmy-2(RNAi)* embryos, median contractile ring assembly was delayed threefold (155 seconds *versus* 53 seconds in controls), but 92% of embryos were able to complete cytokinesis (**Figures 4C,E**). In *plst-1(prt89)* embryos, contractile ring assembly was delayed twofold (110 seconds), and cytokinesis was successful in all embryos. Strikingly, contractile ring assembly was delayed sixfold (298 seconds) in *nmy-2(RNAi)*; *plst-1(prt89)* embryos, and 89% of embryos failed to initiate furrowing (**Figures 4C,E**).

We asked whether deficient alignment of F-actin bundles at the cell equator and cytokinesis failure in *nmy-2(RNAi);plst-1(prt89)* embryos could be due to aggravated cortical flows (**Figures 4D,E** and **Supplementary Figure S6**). Using PIV analysis of LifeAct::GFP, we determined flow velocities from anaphase onset until the back-to-back membrane configuration (**Supplementary Figure S6C**). In *plst-1(prt89)* embryos, cortical flows were decreased and erratic compared to controls. There were no periods of unidirectional or bidirectional flows, as the cortex was constantly moving back and forth in opposite directions (**Supplementary Figures S6A,C**). In *nmy-2(RNAi)*; *plst-1(prt89)* embryos, there was no further aggravation of flow profiles compared to the single perturbations. Analysis of flow velocity along the anterior-posterior axis for the period of persistent unidirectional flow, as defined in control embryos (50 seconds starting at shallow deformation), revealed that *plst-1(prt89)* embryos showed an intermediate profile between that of control and *nmy-2(RNAi)* embryos, with a maximum flow velocity at the posterior pole of −2.5 μm/min (**Figure 4D**). In *nmy-2(RNAi)*; *plst-1(prt89)* embryos, flow velocities were similar to those observed in *nmy-2(RNAi)* embryos. We further investigated the correlation between vectors as a function of the distance between them for the period of persistent unidirectional flows (**Supplementary Figure S6B**; equation 2 in "Materials and Methods" section). The closer the cosine similarity is to 1, the higher the correlation between vectors and the more coherent the flow directionality. In control embryos, the cosine similarity was close to 1 for neighboring vectors and decayed gradually as the distance between vectors increased, approaching a minimum of 0.7 for vectors located on opposite poles. In *nmy-2(RNAi)* embryos, the cosine similarity decayed significantly faster, reaching a minimum of approximately 0.2 for the maximum distance between vectors. The correlation was even worse for *plst-1(prt89)* embryos, with minimum values approaching 0, meaning that vectors were pointing in opposite directions. In *nmy-2(RNAi)*; *plst-1(prt89)* embryos, cosine similarity was identical to that in *plst-1(prt89)* embryos, revealing similar problems in flow directionality. We conclude that cytokinesis failure in *nmy-2(RNAi);plst-1(prt89)* embryos is unlikely to be caused by an aggravation of cortical flows.

We also inspected the behavior of NMY-2::mCherry signal in the single and double perturbations (**Supplementary Movie S1**). Interestingly, we observed that residual myosin in *nmy-2(RNAi);plst-1(prt89)* embryos accumulates at the equator more

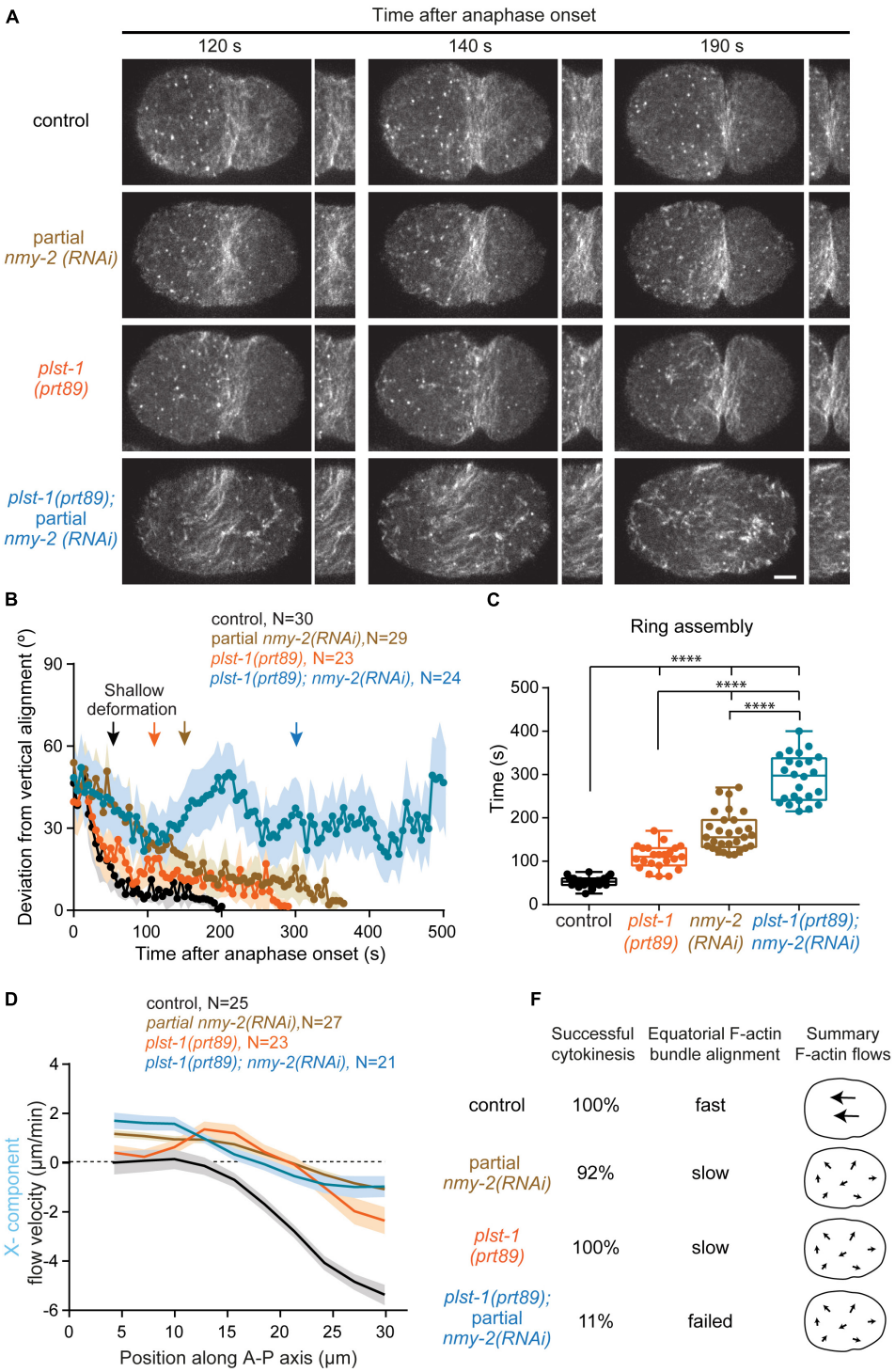

FIGURE 4 | The F-actin crosslinker plastin cooperates with myosin to align F-actin bundles at the division plane. **(A)** Images of the cortical plane of embryos expressing LifeAct::GFP showing the evolution of the equatorial F-actin band relative to anaphase onset. Also see **Supplementary Movie S1**. **(B)** Deviation from vertical alignment of F-actin bundles at the equatorial cortex relative to anaphase onset (mean ± SEM). **(C)** Boxplots showing the dispersion of contractile ring assembly times. In each box, the central line is the median, the boundaries of the box are the 25th and 75th percentiles; the whiskers extend to include the maximum and minimum values. **(D)** Longitudinal (X-component) velocity profiles of Lifeact::GFP cortical flows along anterior-posterior (A-P) axis averaged for a period of 50 seconds starting at shallow deformation. Flow profiles show mean X-component velocity ± SEM. **(E)** Values on the left indicate percentage of embryos that completed cytokinesis successfully. On the right, a summary of F-actin bundle alignment at the equator and overall flow intensity and directionality (X-component). N is the number of embryos analyzed. Statistical significance of ring assembly times in (C) was determined using one-way ANOVA followed by Bonferroni's multiple comparison test. ****$P < 0.0001$. Scale bar, 5 µm.

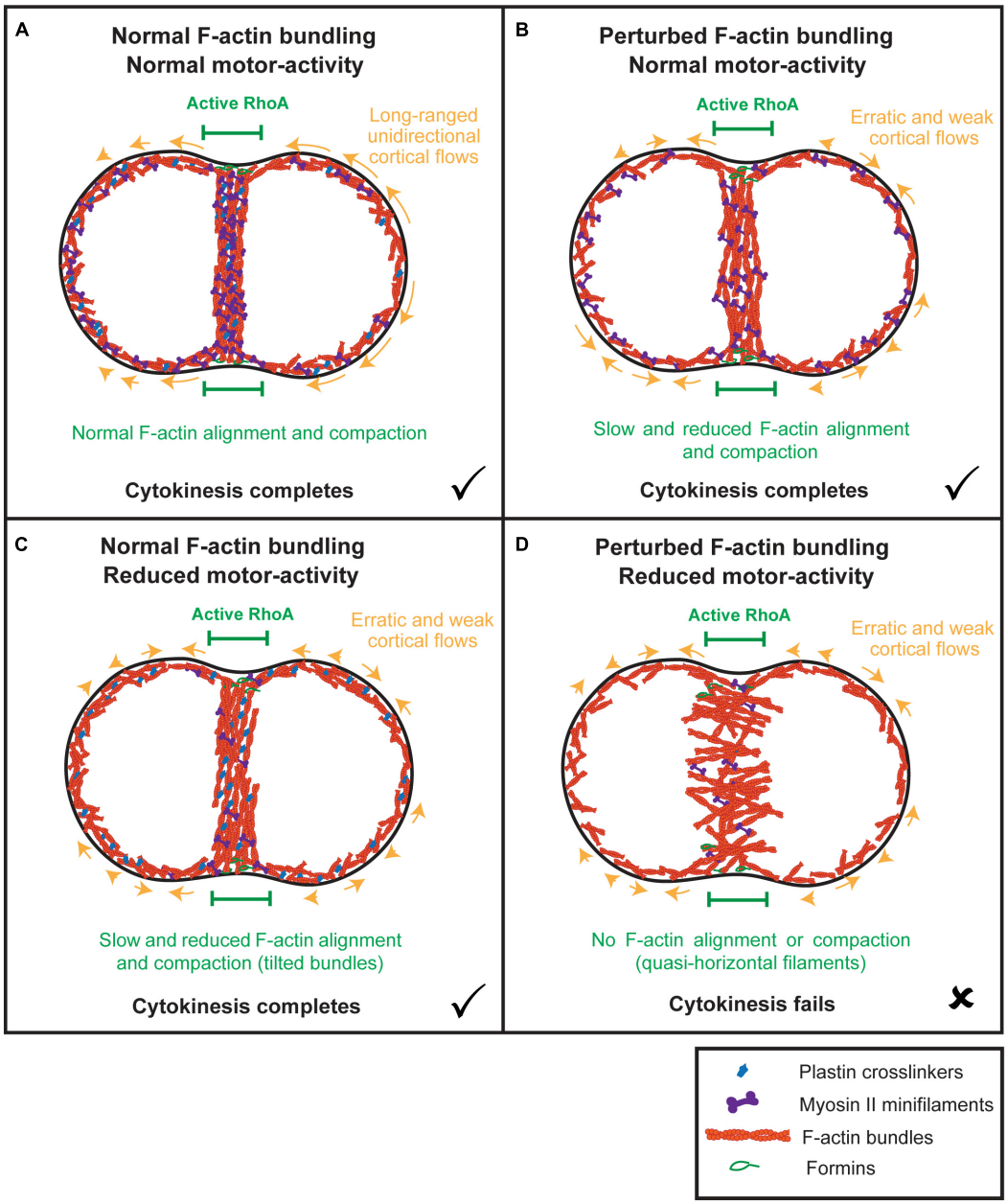

FIGURE 5 | Model: the combined synergistic action of plastin and myosin aligns and compacts F-actin at the division plane independently of actomyosin cortical flows. **(A)** When both plastin and myosin accumulate at the equator, F-actin bundles are properly connected, and myosin is able to efficiently align and compact them into a circumferential array to maximize tension. Early actomyosin flows are unidirectional and long-ranged. **(B)** In the absence of plastin-mediated bundling, myosin struggles to align and compact F-actin bundles, initially spending energy on filament sorting instead of filament sliding. Cortical flows are reduced and erratic and cytokinesis completes with delays in F-actin alignment and contractile ring formation. **(C)** In the presence of plastin-mediated F-actin bundling and decreased myosin levels, F-actin bundles are connected to each other but tilt and struggle to orient along the division plane and to compact because of insufficient motor-activity. Cortical flows are severely reduced and erratic and cytokinesis completes with delays in F-actin alignment and contractile ring formation. **(D)** When both plastin-mediated bundling and myosin levels are decreased, equatorial actin filaments become unstable and start rotating and oscillating, adopting a quasi-horizontal orientation. Cortical flows are reduced and erratic, as in the individual plastin and myosin perturbations. F-actin bundles never align to form the contractile ring and cytokinesis fails.

slowly than in *nmy-2(RNAi)* embryos. These results suggest that PLST-1, in addition to its role in promoting connectivity throughout the cell cortex, has a localized role at the cell equator independently of cortical flows. We conclude that localized synergistic action of NMY-2 and PLST-1 at the division plane is critical for F-actin alignment and compaction into a circumferential array that is capable of sustaining furrow ingression.

DISCUSSION

Unidirectional Long-Range Cortical Flows Play a Minor Role During Cytokinesis

Several models have been proposed to explain how the cell shape changes that occur during cytokinesis are triggered. The first theories date back to the 1950s and considered cleavage as an integrated process involving reorganization of the entire cell surface. While Mitchison (1952); Mitchison and Swann (1955), and Swann and Mitchison (1958) proposed that cytokinetic furrow formation was a passive event resulting from an active expansion at the poles that would spread toward the equator, Marsland proposed that the furrow region was itself contractile, independently of the poles (Marsland, 1950, 1956a,b). Wolpert's astral relaxation theory specifically proposed that a negative signal from the astral microtubules would make the poles relax, allowing the equator to contract (Wolpert, 1960). While the molecular mechanisms for polar relaxation have only recently started to be unraveled (Mangal et al., 2018; Chapa-y-lazo et al., 2020), it has become widely accepted that cytokinesis requires a positive signal from the central spindle that activates the small GTPase RhoA, which in turn promotes the accumulation of contractile ring components, F-actin and myosin, at the cell equator. F-actin alignment and accumulation via flow-driven equatorial compression and RhoA-dependent local recruitment are the two main mechanisms thought to drive the assembly of a circumferentially aligned contractile ring.

A recent study showed that F-actin cortical flows are myosin-dependent and that compression by flow, equatorial F-actin alignment, and furrow ingression show similar spatiotemporal dynamics in the one-cell *C. elegans* embryo (Reymann et al., 2016). The authors proposed that persistent, unidirectional compressive flows towards the cell equator dictate the timing of equatorial F-actin alignment and furrow formation. We find that embryos co-expressing similar amounts of endogenous motor-dead and transgenic wild-type myosin have severely decreased F-actin cortical flows, yet contractile ring assembly and furrow initiation still occur in a timely manner, and cytokinesis completes. Lowering the levels of transgenic wild-type myosin in these embryos results in substantial cytokinesis delays with no additional effects on cortical flows. While these results show that both long-range cortical flows and cytokinesis require myosin motor activity, they suggest that cortical flows are neither essential for cytokinesis nor a major determinant of cytokinesis kinetics.

Apart from the cytokinetic furrow, *C. elegans* one-cell embryos also form a transient furrow, which partially ingresses and then regresses, during the period of polarity establishment that precedes the first mitotic division. Unlike cytokinesis, pseudocleavage lacks equatorial accumulation of active RhoA, F-actin and myosin (Mayer et al., 2010; Reymann et al., 2016). Moreover, counter-rotating flows in the two halves of the embryo occur during pseudocleavage initiation that do not occur during cytokinetic furrow initiation (Naganathan et al., 2014). While our results argue that cortical flows play a relatively minor role in furrow formation during cytokinesis, it remains possible that cortical flows are essential for furrow formation during pseudocleavage, as proposed by Reymann et al. (2016).

Myosin Accumulation at the Cell Equator Occurs Primarily by Recruitment From the Cytoplasm

There is evidence that myosin and other crosslinkers become stabilized and immobilized in regions of increased tension, such as the contractile ring (Reichl et al., 2008; Srivastava and Robinson, 2015). Our experiments of fluorescence recovery after photobleaching and measurements of flow-driven equatorial F-actin compression suggest that the rate of myosin turnover at the cortex outside the cell equator is significantly faster than the rate at which cortical flow compresses the actomyosin network toward the equator. The results agree with findings in *D. discoideum* cells, where cortical myosin did not move all the way to the equator, but rather appeared and disappeared shortly after from the cortex (Yumura et al., 2008). This indicates that flowing myosin may not be able to generate substantial amounts of compressing force. Thus, tension generated by equatorial myosin activity is likely more relevant for the alignment and compaction of F-actin bundles, which is in agreement with sustained RhoA positive signaling at this location. It also indicates that compression and alignment of the equatorial F-actin bundles may occur independently of flows. We show that unidirectional and bidirectional cortical flows can be severely reduced without affecting the recovery profile of photobleached myosin in the ingressing furrow. This suggests that cortical flows may not be the main source of myosin loading onto the contractile ring, in contrast to a previous model (Khaliullin et al., 2018). We propose that myosin accumulates at the furrow primarily by direct recruitment from the cytoplasm to the cell equator and largely independently of cortical flows.

Plastin-Mediated Bundling and Myosin Motor Activity Are Locally Required for F-actin Alignment at the Division Plane and Deformation of the Equator

The contractile ring must produce sufficient force to deform the plasma membrane against the overall cell shape. Actomyosin contractility must therefore be optimized at the cell equator, which involves the organization of F-actin in circumferentially aligned and compacted linear bundles. An F-actin network architecture composed of modules of antiparallel F-actin bundles is optimal for contraction, as filaments are already aligned and oriented such that myosin-dependent filament sliding is facilitated and tension can be readily propagated across the network (Ennomani et al., 2016). It is still unclear, however, whether F-actin bundles in the contractile ring are organized in an antiparallel manner (reviewed in Pinto et al., 2013;

Murrell et al., 2015) and whether contractile modules exist (Carvalho et al., 2009; Silva et al., 2016). In fact, *in vitro* reconstituted circular actomyosin networks have been shown to contract in the absence of a modular organization, as long as F-actin crosslinkers are present (Ennomani et al., 2016; Wollrab et al., 2019). Our *in vivo* data show that myosin struggles to align and compact equatorial F-actin at the cell equator without the crosslinking activity of plastin in *plst-1(prt89)* embryos. We envision that plastin facilitates myosin-driven alignment by organizing formin-nucleated linear F-actin into tight bundles, so that tension can be efficiently amplified and propagated throughout the network to rapidly compact it into a circumferential array (**Figure 5**). Without plastin, myosin may initially spend energy on sorting randomly oriented F-actin instead of productive filament sliding. When myosin levels are reduced in the presence of plastin (partial depletion of NMY-2), F-actin bundles also struggle to align and compact, likely because of insufficient motor activity to produce tension in the network. When both F-actin bundling and myosin levels are reduced in *nmy-2(RNAi);plst-1(prt89)* embryos, equatorial F-actin bundles become unstable and never orient along the division plane. Consequently, contractile ring assembly fails altogether. The enhanced defects in the plastin/myosin double perturbation cannot be ascribed to aggravated cortical flows, since these are already severely affected in the single perturbations, in which a contractile ring assembles and cytokinesis completes. This strongly suggests that myosin and plastin cooperate locally at the cell equator.

Interestingly, the observation that residual myosin in *nmy-2(RNAi)*; *plst-1(prt89)* embryos accumulates at the equator more slowly than in *nmy-2(RNAi)* embryos suggests that plastin-dependent F-actin bundling may stabilize myosin at the equatorial cortex. This is not the first time cooperation between a passive and an active crosslinker has been observed. In *C. elegans*, a previous study demonstrated that plastin provides the connectivity for coalescence and maturation of myosin foci from distant nascent filaments in the cortex, amplifying the range of contractile domains during polarity establishment (Ding et al., 2017). In *D. discoideum*, myosin and the crosslinker cortexillin have been proposed to stabilize each other at sites of increased mechanical load: cortexilin I, as a long-lived crosslinker, anchors F-actin in the network so that myosin can exert more tension, and this promotes accumulation of yet more myosin and cortexillin (Ren et al., 2009). Whether a similar mechanosensing mechanism between myosin and plastin operates during cytokinesis in *C. elegans* embryos is an interesting hypothesis to test in the future.

CONCLUSION

In conclusion, while cortical flows may help compress and align F-actin at the equator, our results argue that this is not the main mechanism that drives contractile ring assembly. Instead, we propose that contractile ring assembly requires the localized and concerted action of myosin and the F-actin bundler plastin.

MATERIALS AND METHODS

C. elegans Strains

Strains used in this study are listed in **Supplementary Table S1** and were maintained at 20°C on nematode growth medium (NGM) plates seeded with OP50 *E. coli*.

NMY-2 motor-dead mutants and the RNAi-sensitive wild-type nmy-2 transgene fused to mCherry are described in a previous study (Osorio et al., 2019). To generate the allele *plst-1(prt89)*, the endogenous locus of *plst-1* was modified using CRISPR/Cas9-mediated genome editing. An extra nucleotide and a *Nhe*I restriction site were introduced to cause a frameshift and premature stop at the beginning of the *plst-1* coding sequence. Note that the *plst-1* sequence in WormBase (version WS276) lacks the first part of the gene corresponding to the EF hands and CH1 domain of the PLST-1 protein (Ding et al., 2017). The premature stop codon that we introduced occurs after amino acid 262 in the CH2 domain of PLST-1 (Ding et al., 2017). The repair template for this modification was the following:

5′*ctctgaaaatccacaaatttccagactgctccgcgacggtgaaactcttgaagatctc*
aggcgtctgtccccagaagaaattctcatgAaga**gctagc**tgggttaattatcatttagaacg
tgctag*aactcaacgtcgcctacacaatttcacatcagatattgtcgattcagagatttatac*-
3′, where the extra nucleotide is in uppercase, the *Nhe*I restriction site for diagnostic PCR of the genomic edit is in bold, silent mutations introduced to avoid repair template recognition by Cas9 are underlined, and flanking 58 bp homology regions are in italics. Three single guide RNAs (sgRNAs) were chosen using the online tool http://crispr.mit.edu and cloned into the pDD162 vector (Dickinson et al., 2013): 5′-TTCTTCTGGGGACAGACGCCGG-3′, 5′-ATTATCATTTGGAACGTGCTGG-3′ and 5′-AGATGGGTTAATTATCATTTGG-3′. Underlined in the sgRNAs are the PAM sequences, which were not included in the pDD162 vector. The single-stranded repair template (IDT) and pDD162 were mixed together and injected into gonads of young adults N2 hermaphrodites. To facilitate the identification of positive animals, the injection mix also contained a sgRNA and a repair template to generate the R92C mutation in DPY-10, which causes a dominant roller phenotype (Levy et al., 1993; Arribere et al., 2014). To screen for animals carrying the desired modification in the *plst-1* locus, amplification of a plst-1 gene fragment was performed using the primers 5′ CATGGCCTAGAAACCACTTT 3′ and 5′ GCTTCTCGGCTTCATCTAAC 3′, followed by digestion with the *Nhe*I restriction enzyme that recognizes the restriction site present in modified animals only. The modification was confirmed by DNA sequencing. To remove potential off-target mutations, the mutant was subjected to six rounds of outcrossing with N2 animals, before crossing with animals expressing LifeAct::GFP or LifeAct::GFP and NMY-2::mCherry. Although expression of the PLST-1 protein was not assessed by immunoblotting, the defects in *plst-1(prt89)* embryos are similar to those observed for *plst-1(tm4255)*, which is a null mutant (Ding et al., 2017).

RNA Interference

RNAi-mediated NMY-2 depletion was performed by feeding hermaphrodites with bacteria that express double stranded RNA (dsRNA) targeting *nmy-2*. The dsRNAs nmy-2_RNA#1 and nmy-2_RNA#2 (**Supplementary Table S2**) are described in Osorio et al. (2019). Expression of dsRNAs in transformed HT115 *E. coli* was induced with 1 mM IPTG and the bacteria were fed to hermaphrodites as described below.

In experiments where specific depletion of transgenic NMY-2::mCherry^{sen} was desired [labeled as *nmy-2::mCherry^{sen}(RNAi)* in **Figures 1D**, **2C,E,G**], nmy-2_RNA#3 was used in GCP22, GCP618 or GCP592 L4 hermaphrodites. Mild depletions (22–26 h of RNAi treatment at 20°C) were used in **Figures 1D**, **2C,E,F**. In experiments whose purpose was to deplete endogenous NMY-2 to an extent that did not preclude cytokinesis [labeled as partial *nmy-2*(*RNAi*)], nmy-2_RNA#1 (29–31 h of RNAi treatment at 20°C) was used in GCP113 L4 hermaphrodites for **Figures 3D,E** and **Supplementary Figure S3C**, and nmy-2_RNA#2 (23–27 h of RNAi treatment at 20°C) was used in GCP21, GCP22, and GCP927 L4 hermaphrodites for **Figures 1D**, **2E**, **4A–E**, and **Supplementary Figure S6**.

Live Imaging

Gravid hermaphrodites were dissected and one-cell embryos were mounted in a drop of M9 (86 mM NaCl, 42 mM Na_2HPO_4, 22 mM KH_2PO_4, and 1 mM $MgSO_4$) on 2% agarose pads overlaid with a coverslip. Live imaging of cytokinesis was performed at 20°C. Images were acquired on a spinning disk confocal system (Andor Revolution XD Confocal System; Andor Technology) with a confocal scanner unit (CSU-X1; Yokogawa Electric Corporation) mounted on an inverted microscope (Ti-E, Nikon) equipped with a 60x NA 1.4 oil-immersion Plan-Apochromat objective, and solid-state lasers of 405 nm (60 mW), 488 nm (50 mW), and 561 nm (50 mW). For image acquisition, an electron multiplication back-thinned charge-coupled device camera (iXon; Andor Technology) was used. For photobleaching experiments, a FRAPPA photobleaching module (Andor Technology) placed between the spinning disk head and the microscope was used. Photobleaching was performed by 3 sweeps of a 405 nm laser with 100% power and 100 μs dwell time in the posterior cortex, ingressing furrow and division plane (**Figure 3** and **Supplementary Figures S5A,B**) or 10 sweeps and 40 μs dwell time in the posterior cytoplasm (**Supplementary Figure S5C**). Acquisition parameters, shutters, focus and photobleaching parameters and regions to be photobleached were controlled using Andor iQ3 software. For central plane imaging in one-cell embryos (**Figure 3** and **Supplementary Figure S1A**), 5 × 1 μm z-stacks were collected in the 488 nm channel every 5 seconds for strains GCP113, GCP21, RZB213 and OD26, and in the 561 nm channel every 5 seconds for strain SWG001. For photobleaching experiments in the posterior cytoplasm (**Supplementary Figures S5C,D**), 5 × 1 μm z stacks were collected in the 488 nm channel every 0.78 seconds. For cortical dual-color imaging in one-cell embryos, 7 × 0.5 μm z-stacks were collected every 5 seconds for strains GCP21, GCP22, GCP592, and GCP618 (**Figures 1**, **2** and **Supplementary Figures S1, S2**), strains GCP21 and GCP113 (**Figure 3** and **Supplementary Figures S3–S5**), and strains GCP22 and GCP927 (**Figure 4** and **Supplementary Figure S6**). For cortical imaging in one-cell embryos of strains RZB213 and SWG001 (**Supplementary Figure S1B**), 7 × 0.5 μm z-stacks were collected in the 488 nm or 561 nm channels every 5 seconds, respectively.

Fluorescence Intensity Measurements

Before quantification, each time-lapse movie was corrected for fluorescence intensity decay using the simple ratio method in ImageJ's bleach correction tool. Quantification of fluorescence recovery after photobleaching in **Figures 3A',E** was performed using 3 different ROIs to quantify mean fluorescence intensity over time. ROI 1 is the bleached region (5 × 5 pixel for the posterior cortex and posterior cytoplasm; 5 × 15 pixel for the ingressing furrow and 15 × 200 pixel for the whole division plane). ROI 2 is the whole embryo and corrects for overall photobleaching of the sample resulting from acquisition and photobleaching sweeps (oval: 305 × 205 pixels). ROI 3 is the camera background, measured outside fluorescent regions (20 × 20 pixels). After background subtraction and photobleaching correction, the data was normalized using the double normalization method, and curve fitting was performed to extrapolate the half time of recovery. All operations were performed automatically using easyFRAP software (see below).

For quantification of NMY-2::GFP levels at the equator versus poles in **Supplementary Figure S4B**, images of the central plane of dividing one-cell embryos were used. A line was traced at the poles and at the equator and the mean intensity was determined after subtraction of the camera background.

Calculation of Myosin Dissociation Rate

Assuming a diffusion-dominated recovery profile, the myosin dissociation rate (k_{off}) in **Figure 3A'** was calculated from FRAP data using the following equation (Bernetti et al., 2019):

$$k_{off} = \frac{\log(2)}{\tau_{1/2}}, \quad (1)$$

where $\tau_{1/2}$ is the half time recovery measured from FRAP fitting curves.

Cortical Flows Quantification

Cortical flow dynamics were analyzed in one-cell embryos of strains GCP21, GCP22, GCP113, GCP562, GCP618, and GCP927 between anaphase onset and back-to-back membrane configuration. In **Figures 2B–E**, **4D** and **Supplementary Figures S2B, S3B,C, S6C**, magnitude and direction of cortical flows were quantified using an Iterative Particle Image Velocimetry (PIV) plugin for ImageJ, https://sites.google.com/site/qingzongtseng/piv (Tseng et al., 2011). A 192 × 128 pixel (34.1 × 22.8 μm) region of interest was applied to all embryos to standardize the cortex area and exclude cortical curved peripheries. To average the maximum particle displacement with better resolution, two iterations were performed, in which the application of a larger interrogation window of 64 × 64 pixels (first

iteration) was followed by a smaller interrogation window of 32 × 32 pixels (second iteration). Consecutive interrogation windows overlapped by 50%. After flow field generation, the 192 × 128 pixel region was divided in two adjacent sub-regions along the anterior-posterior axis of the embryo for quantification: anterior cortex (1st-108th pixel; 0.2–19.2 μm) and posterior cortex (109th-192nd pixel; 19.4–34.1 μm). Each velocity vector was resolved into components along the anterior-posterior axis, Vx, and the dorsal-ventral axis, Vy. The mean Vx and Vy were estimated for each time point and plotted as a function of time to trace the cortical flow profiles in **Figures 2B,C** and **Supplementary Figures S2B, S3B,C, S6C**.

To plot longitudinal flow profiles (Vx) along the anterior-posterior axis in **Figures 2D,E**, **4D**, all vectors along the dorsal-ventral axis with the same x-coordinate (corresponding to the longitudinal position) were averaged and plotted as a function of the position along the anterior-posterior axis.

The cosine similarity analysis measures the correlation between every vector pair of the flow fields as a function of the distance between them for the period of persistent unidirectional flow. A cosine similarity of 1 means the vectors are totally correlated. Cosine similarities between two vectors shown in **Supplementary Figure S6B** was computed using a custom MATLAB script, according to the following formula:

$$cosine\ similarity\left(\overrightarrow{w_i}, \overrightarrow{w_j}\right) = \frac{\overrightarrow{w_i} \cdot \overrightarrow{w_j}}{||\overrightarrow{w_i}||||\overrightarrow{w_j}||} \quad (2)$$

Calculation of Cortical Compression Rates

Longitudinal cortical compression rates in **Figures 3B,C** were estimated from cortical flow profiles along the anterior-posterior axis by approximating the spatial derivative for each position using a custom MATLAB script. Cortical compression rates were plotted as a function of both position along the anterior-posterior axis and time relative to anaphase onset in 10 seconds intervals, starting at 25 seconds (when a noticeable region of compression could be identified) and stopping at 95 seconds (start of furrow ingression) after anaphase onset.

Analysis of Bundle Alignment at the Equatorial Cortex

Deviation from vertical alignment over time in **Figure 4B** was measured using the Directionality plugin for ImageJ. A region of 30 × 70 pixels corresponding to the furrow region was selected for each movie. The average directionality (angle α, in degrees), was calculated for every frame of each movie using the local gradient orientation method. Deviation from vertical alignment (in degrees) was calculated for each angle α by subtracting the value of this angle from 90°. Absolute numbers were plotted.

Image Analysis, Quantifications, and Statistics

Image processing and image analysis were performed using Fiji (ImageJ; National Institutes of Health) (Schindelin et al., 2019) and MATLAB (MathWorks). Z-stacks acquired on the cell cortex were projected using Fiji's maximum intensity projection tool. Images within each panel were scaled equally. Flow kymographs shown in **Figure 1D** and **Supplementary Figures S3A**, **S6A** were created by tracing a 150 × 5 pixel rectangle positioned at the center of the embryo on the cortical plane and mounted using Fiji's Make Montage tool, as illustrated in **Figure 1D'**. Graph plotting, linear regressions and statistical analyses were performed with Prism 6.0 (GraphPad Software). Photobleaching experiments were analyzed using easyFRAP, https://easyfrap.vmnet.upatras.gr (Koulouras et al., 2018). Measurements for cytokinetic analysis in **Supplementary Figure S1A** were performed as previously reported (Chan et al., 2019). Error bars represent the standard-deviation (SD), standard-error of the mean (SEM), or 95% confidence interval (95% CI), and statistical significance tests were performed using one-way ANOVA with Bonferroni correction, as indicated in figure legends. Statistical significance of flow profiles was performed using two-way ANOVA for repeated measures.

DATA AVAILABILITY STATEMENT

The raw data supporting the conclusions of this article will be made available by the authors, without undue reservation.

AUTHOR CONTRIBUTIONS

AXC and JL: conceptualization. JL: methodology and software. JL, F-YC, DSO, JS, and AFS: validation. JL and F-YC: formal analysis. JL, F-YC, DSO, JS, AFS, and AMS: investigation. JL and AXC: writing – original draft. JL, F-YC, DSO, JS, AFS, AMS, RG, and AXC: writing – review and editing. JL, F-YC, DSO, and AXC: visualization. AXC and RG: supervision. AXC: funding acquisition.

FUNDING

The research leading to these results was funded by the European Research Council under the European Union's Horizon 2020 Research and Innovation Programme (grant agreement 640553 – ACTOMYO). AXC and RG hold Principal Investigator positions from the Portuguese Foundation for Science and Technology (FCT) (CEECIND/01967/2017 and CEECIND/00333/2017, respectively). F-YC and AMS hold FCT junior researcher positions (DL 57/2016/CP1355/CT0013 and DL 57/2016/CP1355/CT0017, respectively). AFS holds an FCT Ph.D. scholarship (SFRH/BD/121874/2016). The funders had no role in study design, data collection and analysis, decision to publish, or preparation of the manuscript.

ACKNOWLEDGMENTS

We thank Stephan Grill, Ronen Zaidel-Bar, and Karen Oegema for providing strains.

SUPPLEMENTARY MATERIAL

The Supplementary Material for this article can be found online at: https://www.frontiersin.org/articles/10.3389/fcell.2020.573393/full#supplementary-material

SUPPLEMENTARY FIGURE S1 | Delayed cytokinesis in embryos expressing LifeAct::mKate2. **(A)** Intervals for ring assembly/furrow initiation and ring constriction rate (mean ± 95% CI). N is the number of embryos analyzed. Statistical significance was determined using one-way ANOVA followed by Bonferroni's multiple comparison test. ****$P < 0.0001$, ns, not significant. **(B)** Cortical images of embryos expressing different fluorescent probes for actin. Scale bar, 10 μm.

SUPPLEMENTARY FIGURE S2 | Rotational flows are a consequence of embryo compression. **(A)** Time projections of control embryos expressing LifeAct::GFP imaged under compression (top) or without compression (bottom). Rotational (Y-component) flows are indicated by curved arrows. Scale bar, 10 μm. **(B)** Rotational (Y-component) flow velocity (mean ± SEM) in the anterior (left) or posterior (right) half of embryos imaged with (black) or without (gray) compression. **(C)** Intervals for ring assembly/furrow initiation and ring constriction rate (mean ± 95% CI) measured in embryos imaged with (black) or without (gray) compression. N is the number of embryos analyzed.

SUPPLEMENTARY FIGURE S3 | F-actin and myosin cortical flow profiles are similar. **(A)** Kymographs depicting Lifeact::GFP (top) and NMY-2::GFP (bottom) longitudinal cortical flows from anaphase onset until complete ingression. **(B)** Longitudinal (X-component) and rotational (Y-component) flow velocities (mean ± SEM) for LifeAct::GFP and NMY-2::GFP in the anterior or posterior half of embryos, plotted over time starting at anaphase onset. The depicted interval covers both the period of unidirectional and the period of bidirectional flows. **(C)** Longitudinal (X-component) LifeAct::GFP flow velocities (mean ± SEM) over time for control and NMY-2-depleted embryos from anaphase onset until complete ingression. Arrows indicate average time of shallow deformation (darker tone) or furrow initiation (lighter tone). N is the number of embryos analyzed.

SUPPLEMENTARY FIGURE S4 | The amount of myosin that accumulates at the cell equator is higher than the amount that leaves the cortical poles. **(A)** Images of the central and cortical planes of a dividing one-cell embryo expressing NMY-2::GFP at different time points in cytokinesis, revealing a decrease of myosin levels at the cortical poles and an increase at the cell equator. Scale bar, 5 μm. **(B)** Quantification of NMY-2::GFP levels (mean ± SD) on the anterior pole, posterior pole, and equator at the time points indicated in **(A)**, determined as indicated in the schematic on the right. N is the number of embryos analyzed.

SUPPLEMENTARY FIGURE S5 | Fluorescence recovery after photobleaching of the entire division plane indicates that myosin continues to accumulate in the contractile ring during furrow ingression. **(A)** Schematic showing the photobleached region of the entire division plane at shallow deformation (top left) and selected images from a time-lapse series showing NMY-2::GFP fluorescence over time pre- and post-bleaching. **(B)** Quantification of NMY-2::GFP fluorescence recovery after photobleaching the entire division plane at shallow deformation. Data from individual embryos (light gray) and the mean ± SD (black) are plotted. **(C)** Quantification of NMY-2::GFP fluorescence recovery after photobleaching in the posterior cytoplasm. **(D)** Boxplots showing the dispersion of half-time recovery for the posterior cytoplasm and the posterior cortex. In each box, the central line is the median, the boundaries of the box are the 25th and 75th percentiles; the whiskers extend to include the maximum and minimum values. N is the number of embryos analyzed. Statistical significance of half-time recovery in (D) was determined using unpaired Student's *t*-test: *$P < 0.05$.

SUPPLEMENTARY FIGURE S6 | Cortical flows are not aggravated in *nmy-2(RNAi);plst-1(prt89)* embryos. **(A)** Kymographs of LifeAct::GFP cortical flow profiles along the longitudinal axis of the embryos. Yellow, red, and blue bars correspond to contractile ring assembly, furrow initiation, and ring constriction intervals, respectively. Kymographs were built as described in **Figure 1D'**. **(B)** Cosine similarity between two vectors as a function of the distance between them. **(C)** Longitudinal (X-component) average flow velocity (mean ± SEM) over time after anaphase onset for LifeAct::GFP in the anterior or posterior half of the embryos. Arrows indicate the time of shallow deformation. In panels (B), (C), N is the number of embryos analyzed.

SUPPLEMENTARY TABLE S1 | List of *C. elegans* strains used in this study.

SUPPLEMENTARY TABLE S2 | List of dsRNAs used in this study.

SUPPLEMENTARY MOVIE S1 | Plastin and myosin cooperate to align F-actin bundles at the division plane. Time-lapse series of the cell cortex in dividing one-cell embryos of the indicated genotypes expressing LifeAct::GFP and NMY-2::mCherry. Cortical images are maximum intensity projections of seven z-sections 0.5 μm apart acquired every 5 seconds from anaphase onset (0:00). Frame rate is 6 frames per second, timestamp is minutes:seconds. Scale bar, 5 μm.

REFERENCES

Arnold, J. M. (1969). Cleavage furrow formation in a telolecithal egg (Loligo Pealii): I. Filaments in early furrow formation. *J. Cell Biol.* 41, 894–904. doi: 10.1083/jcb.41.3.894

Arribere, J. A., Bell, R. T., Fu, B. X. H., Artiles, K. L., Hartman, P. S., and Fire, A. Z. (2014). Efficient marker-free recovery of custom genetic modifications with CRISPR/Cas9 in *Caenorhabditis elegans*. *Genetics* 198, 837–846. doi: 10.1534/genetics.114.169730

Bement, W. M., Benink, H. A., and Von Dassow, G. (2005). A microtubule-dependent zone of active RhoA during cleavage plane specification. *J. Cell Biol.* 170, 91–101. doi: 10.1083/jcb.200501131

Bernetti, M., Masetti, M., Rocchia, W., and Cavalli, A. (2019). Kinetics of Drug Binding and Residence Time. *Annu. Rev. Phys. Chem.* 70, 143–171. doi: 10.1146/annurev-physchem-042018-052340

Bretscher, A. (1981). Fimbrin is a cytoskeletal protein that crosslinks F-actin in vitro. *Proc. Natl. Acad. Sci. U.S.A.* 78, 6849–6853. doi: 10.1073/pnas.78.11.6849

Cao, L. G., and Wang, Y. L. (1990). Mechanism of the formation of contractile ring in dividing cultured animal cells. II. Cortical movement of microinjected actin filaments. *J. Cell Biol.* 111, 1905–1911. doi: 10.1083/jcb.111.5.1905

Carvalho, A., Desai, A., and Oegema, K. (2009). Structural Memory in the Contractile Ring Makes the Duration of Cytokinesis Independent of Cell Size. *Cell* 137, 926–937. doi: 10.1016/j.cell.2009.03.021

Chan, F., Silva, A. M., Saramago, J., Pereira-Sousa, J., Brighton, H. E., Pereira, M., et al. (2019). The ARP2/3 complex prevents excessive formin activity during cytokinesis. *Mol. Biol. Cell* 30, 96–107. doi: 10.1091/mbc.E18-07-0471

Chapa-y-lazo, B., Hamanaka, M., Wray, A., Balasubramanian, M. K., and Mishima, M. (2020). Polar relaxation by dynein-mediated removal of cortical myosin II. *J. Cell Biol.* 219:e201903080. doi: 10.1083/jcb.201903080

Davies, T., Jordan, S. N., Chand, V., Sees, J. A., Laband, K., Carvalho, A. X., et al. (2014). High-Resolution temporal analysis reveals a functional timeline for the molecular regulation of cytokinesis. *Dev. Cell* 30, 209–223. doi: 10.1016/j.devcel.2014.05.009

Descovich, C. P., Cortes, D. B., Ryan, S., Nash, J., Zhang, L., Maddox, P. S., et al. (2017). Cross-linkers both drive and brake cytoskeletal remodeling and furrowing in cytokinesis. *Mol. Biol. Cell* 2, 3–4. doi: 10.1091/mbc.E17-06-0392

Dickinson, D. J., Ward, J. D., Reiner, D. J., and Goldstein, B. (2013). Engineering the Caenorhabditis elegans genome using Cas9-triggered homologous recombination. *Nat. Methods* 10, 1028–1034. doi: 10.1038/nmeth.2641

Ding, W. Y., Ong, H. T., Hara, Y., Wongsantichon, J., Toyama, Y., Robinson, R. C., et al. (2017). Plastin increases cortical connectivity to facilitate robust polarization and timely cytokinesis. *J. Cell Biol.* 216, 1371–1386. doi: 10.1083/jcb.201603070

Ennomani, H., Letort, G., Guérin, C., Martiel, J. L., Cao, W., Nédeléc, F., et al. (2016). Architecture and Connectivity Govern Actin Network Architecture and Connectivity. *Curr. Biol.* 26, 616–626. doi: 10.1016/j.cub.2015.12.069

Faix, J., Steinmetz, M., Boves, H., Kammerer, R. A., Lottspeich, F., Mintert, U., et al. (1996). Cortexillins, major determinants of cell shape and size, are actin-bundling proteins with a parallel coiled-coil tail. *Cell* 86, 631–642. doi: 10.1016/S0092-8674(00)80136-1

Green, R. A., Paluch, E. K., and Oegema, K. (2012). Cytokinesis in Animal Cells. *Annu. Rev. Cell Dev. Biol.* 28, 29–58. doi: 10.1146/annurev-cellbio-101011-155718

Großhans, J., Wenzl, C., Herz, H. M., Bartoszewski, S., Schnorrer, F., Vogt, N., et al. (2005). RhoGEF2 and the formin Dia control the formation of the furrow canal by directed actin assembly during *Drosophila cellularisation*. *Development* 132, 1009–1020. doi: 10.1242/dev.01669

Henson, J. H., Ditzler, C. E., Germain, A., Irwin, P. M., Vogt, E. T., Yang, S., et al. (2017). The ultrastructural organization of actin and myosin II filaments in the contractile ring: new support for an old model of cytokinesis. *Mol. Biol. Cell* 28, 613–623. doi: 10.1091/mbc.E16-06-0466

Khaliullin, R. N., Green, R. A., Shi, L. Z., Gomez-Cavazos, J. S., Berns, M. W., Desai, A., et al. (2018). A positive-feedback-based mechanism for constriction rate acceleration during cytokinesis in *Caenorhabditis elegans*. *eLife* 7:e36073. doi: 10.7554/eLife.36073

Kimura, K., Ito, M., Amano, M., Chihara, K., Fukata, Y., Nakafuku, M., et al. (1996). Regulation of myosin phosphatase by Rho and Rho-associated kinase (Rho-kinase). *Science* 273, 245–248. doi: 10.1126/science.273.5272.245

Koulouras, G., Panagopoulos, A., Rapsomaniki, M. A., Giakoumakis, N. N., Taraviras, S., and Lygerou, Z. (2018). EasyFRAP-web: a web-based tool for the analysis of fluorescence recovery after photobleaching data. *Nucleic Acids Res.* 46, W467–W472. doi: 10.1093/nar/gky508

Laplante, C., Berro, J., Karatekin, E., Hernandez-Leyva, A., Lee, R., and Pollard, T. D. (2015). Three myosins contribute uniquely to the assembly and constriction of the fission yeast cytokinetic contractile ring. *Curr. Biol.* 25, 1955–1965. doi: 10.1016/j.cub.2015.06.018

Leite, J., Osorio, D. S., Sobral, A. F., Silva, A. M., and Carvalho, A. X. (2019). Network Contractility during Cytokinesis - From Molecular to Global Views. *Biomolecules* 9:194. doi: 10.3390/biom9050194

Levy, A. D., Yang, J., and Kramer, J. M. (1993). Molecular and genetic analyses of the *Caenorhabditis elegans* dpy-2 and dpy-10 collagen genes : a variety of molecular alterations affect organismal morphology. *Mol. Biol. Cell* 4, 803–817. doi: 10.1091/mbc.4.8.803

Mabuchi, I., Tsukita, S., Tsukita, S., and Sawai, T. (1988). Cleavage furrow isolated from newt eggs : contraction, organization of the actin filaments, and protein components of the furrow. *Proc. Natl. Acad. Sci. U.S.A.* 85, 5966–5970. doi: 10.1073/pnas.85.16.5966

Mangal, S., Sacher, J., Kim, T., Osório, D. S., Motegi, F., Carvalho, A. X., et al. (2018). TPXL-1 activates Aurora A to clear contractile ring components from the polar cortex during cytokinesis. *J. Cell Biol.* 217, 837–848. doi: 10.1083/jcb.201706021

Marsland, D. (1950). The mechanisms of celldivision; temperature-pressure experiments on the cleaving eggs of *Arbacia punctulata*. *J. Cell Comp. Physiol.* 36, 205–227. doi: 10.1002/jcp.1030360207

Marsland, D. (1956a). Protoplasmic contractility in relation to cytokinesis. *Pubblicazioni Della Stazione Zoologica Di Napoli* 28, 182–203.

Marsland, D. (1956b). Protoplasmic contractility in relation to gel structure: temperature - pressure experiments on cytokinesis and amoeboid movement. *Int. Rev. Cytol.* 5, 199–227. doi: 10.1016/S0074-7696(08)62571-1

Matsudaira, P., Mandelkow, E., Renner, W., Hesterberg, L. K., and Weber, K. (1983). Role of fimbrin and villin in determining the interfilament distances of actin bundles. *Nature* 301, 209–214. doi: 10.1038/301209a0

Matsumura, F. (2005). Regulation of myosin II during cytokinesis in higher eukaryotes. *Trends Cell Biol.* 15, 371–377. doi: 10.1016/j.tcb.2005.05.004

Maupin, P., and Pollard, T. D. (1986). Arrangement of actin filaments and myosin-like filaments in the contractile ring and of actin-like filaments in the mitotic spindle of dividing HeLa cells. *J. Ultrastruc. Mol. Struct. Res.* 94, 92–103. doi: 10.1016/0889-1605(86)90055-8

Mavrakis, M., Azou-gros, Y., Tsai, F., Alvarado, J., Bertin, A., Iv, F., et al. (2014). Septins promote F-actin ring formation by crosslinking actin filaments into curved bundles. *Nat. Cell Biol.* 16, 322–334. doi: 10.1038/ncb2921

Mayer, M., Depken, M., Bois, J. S., Jülicher, F., and Grill, S. W. (2010). Anisotropies in cortical tension reveal the physical basis of polarizing cortical flows. *Nature* 467, 617–621. doi: 10.1038/nature09376

Melak, M., Plessner, M., and Grosse, R. (2017). Actin visualization at a glance. *J. Cell Sci.* 130, 525–530. doi: 10.1242/jcs.189068

Mitchison, J. (1952). Cell membranes and cell division. *Symp. Soc. Exp. Biol.* 6, 105–127.

Mitchison, J. M., and Swann, M. (1955). The mechanical properties of the cell surface: III.The sea-urchin egg from fertilization to cleavage. *J. Exp. Biol.* 32, 734–750. doi: 10.1016/0021-9290(80)90043-3

Murrell, M., Oakes, P. W., Lenz, M., and Gardel, M. L. (2015). Forcing cells into shape: the mechanics of actomyosin contractility. *Nat. Rev. Mol. Cell Biol.* 16, 486–498. doi: 10.1038/nrm4012

Murthy, K., and Wadsworth, P. (2005). Myosin-II-dependent localization and dynamics of F-actin during cytokinesis. *Curr. Biol.* 15, 724–731. doi: 10.1016/j.cub.2005.02.055

Naganathan, S., Fürthauer, S., Rodriguez, J., Fievet, B. T., Ahringer, J., Cannistraci, C. V., et al. (2014). Morphogenetic degeneracies in the actomyosin cortex. *eLife* 7:e37677. doi: 10.7554/eLife.37677

Osorio, D. S., Chan, F., Saramago, J., Leite, J., Silva, A. M., Sobral, A. F., et al. (2019). Crosslinking activity of non-muscle myosin II is not sufficient for embryonic cytokinesis in *C. elegans*. *Development* 146:dev179150. doi: 10.1242/dev.179150

Pinto, I. M., Rubinstein, B., and Li, R. (2013). Force to divide: structural and mechanical requirements for actomyosin ring contraction. *Biophys. J.* 105, 547–554. doi: 10.1016/j.bpj.2013.06.033

Prokopenko, S. N., Saint, R., and Bellen, H. J. (2000). Untying the Gordian Knot of Cytokinesis : role of Small G Proteins and Their Regulators. *J. Cell Biol.* 148, 843–848. doi: 10.1083/jcb.148.5.843

Reichl, E. M., Ren, Y., Morphew, M. K., Delannoy, M., Effler, J. C., Girard, K. D., et al. (2008). Interactions between myosin and actin crosslinkers control cytokinesis contractility dynamics and mechanics. *Curr. Biol.* 18, 471–480. doi: 10.1016/j.cub.2008.02.056

Ren, Y., Effler, J. C., Norstrom, M., Luo, T., Firtel, R. A., Iglesias, P. A., et al. (2009). Mechanosensing through cooperative interactions between myosin II and the actin crosslinker cortexillin I. *Curr. Biol.* 19, 1421–1428. doi: 10.1016/j.cub.2009.07.018

Reymann, A. C., Staniscia, F., Erzberger, A., Salbreux, G., and Grill, S. W. (2016). Cortical flow aligns actin filaments to form a furrow. *eLife* 5, 1–25. doi: 10.7554/eLife.17807

Salbreux, G., Prost, J., and Joanny, J. F. (2009). Hydrodynamics of cellular cortical flows and the formation of contractile rings. *Phys. Rev. Lett.* 103:058102. doi: 10.1103/PhysRevLett.103.058102

Sanger, J. M., and Sanger, J. W. (1980). Banding and polarity of actin filaments in interphase and cleaving cells. *J. Cell Biol.* 86, 568–575. doi: 10.1083/jcb.86.2.568

Schindelin, J., Arganda-Carreras, I., Frise, E., Kaynig, V., Longair, M., Pietzsch, T., et al. (2019). Fiji : an open-source platform for biological-image analysis. *Nat. Methods* 28, 676–682. doi: 10.1038/nmeth.2019

Schroeder, T. E. (1968). Cytokinesis: filaments in the cleavage furrow. *Exp. Cell Res.* 53, 272–276. doi: 10.1016/0014-4827(68)90373-x

Schroeder, T. E. (1970). The contractile ring: I. Fine structure of dividing mammalian (HeLa) cells and the effects of cytochalasin B. *Z Zellforsch Mikrosk Anat.* 109, 431–449. doi: 10.1007/BF00343960

Schroeder, T. E. (1972). The contractile ring: II. Determining its brief existence, volumetric changes, and vital role in cleaving arbacia eggs. *J. Cell Biol.* 53, 419–434. doi: 10.1083/jcb.53.2.419

Selman, G. G., and Perry, M. M. (1970). Ultrastructural changes in the surface layers of the newt's egg in relation to the mechanism of its cleavage. *J. Cell Sci.* 6, 207–227.

Silva, A. M., Osório, D., Pereira, A. J., Maiato, H., Pinto, I. M., Rubinstein, B., et al. (2016). Robust gap repair in the contractile ring ensures timely completion of cytokinesis. *J. Cell Biol.* 215, 789–799. doi: 10.1083/jcb.201605080

Singh, D., Odedra, D., Dutta, P., and Pohl, C. (2019). Mechanical stress induces a scalable switch in cortical flow polarization during cytokinesis. *J. Cell Sci.* 132, jcs231357. doi: 10.1242/jcs.231357

Skau, C. T., Courson, D. S., Bestul, A. J., Winkelman, J. D., Rock, R. S., Sirotkin, V., et al. (2011). Actin filament bundling by fimbrin is important for endocytosis, cytokinesis, and polarization in fission yeast. *J. Biol. Chem.* 286, 26964–26977. doi: 10.1074/jbc.M111.239004

Spira, F., Cuylen-haering, S., Mehta, S., Samwer, M., Reversat, A., Verma, A., et al. (2017). Cytokinesis in vertebrate cells initiates by contraction of an equatorial

actomyosin network composed of randomly oriented filaments. *eLife* 6:e30867. doi: 10.7554/eLife.30867

Srivastava, V., and Robinson, D. N. (2015). Mechanical stress and network structure drive protein dynamics during cytokinesis. *Curr. Biol.* 25, 663–670. doi: 10.1016/j.cub.2015.01.025

Swann, M. M., and Mitchison, J. M. (1958). The mechanism of cleavage in animal cells. *Biol. Rev. Camb. Philos. Soc.* 33, 103–135. doi: 10.1111/j.1469-185X.1958.tb01409.x

Tseng, Q., Duchemin-Pelletier, E., Deshiere, A., Balland, M., Guillou, H., Filhol, O., et al. (2011). Spatial organization of the extracellular matrix regulates cell-cell junction positioning. *Proc. Natl. Acad. Sci. U.S.A.* 109, 1506–1511. doi: 10.1073/pnas.1106377109

Turlier, H., Audoly, B., Prost, J., and Joanny, J. F. (2014). Furrow constriction in animal cell cytokinesis. *Biophys. J.* 106, 114–123. doi: 10.1016/j.bpj.2013.11.014

Uehara, R., Goshima, G., Mabuchi, I., Vale, R. D., Spudich, J. A., and Griffis, E. R. (2010). Determinants of Myosin II Cortical Localization during Cytokinesis. *Curr. Biol.* 20, 1080–1085. doi: 10.1016/j.cub.2010.04.058

Vavylonis, D., Wu, J. Q., Hao, S., O'Shaughnessy, B., and Pollard, T. D. (2008). Assembly mechanism of the contractile ring for cytokinesis by fission yeast. *Science* 319, 97–100. doi: 10.1126/science.1151086

Vicente-Manzanares, M. (2009). Non-muscle myosin II takes centre stage in cell adhesion and migration. *Nat. Rev. Mol. Cell Biol.* 10, 778–790. doi: 10.1038/nrm2786

Watanabe, S., Okawa, K., Miki, T., Sakamoto, S., Morinaga, T., Segawa, K., et al. (2010). Rho and Anillin-dependent Control of mDia2 Localization and Function in Cytokinesis. *Mol. Biol. Cell* 21, 3193–3204. doi: 10.1091/mbc.e10-04-0324

White, J. G., and Borisy, G. G. (1983). On the mechanisms of cytokinesis in animal cells. *J. Theor. Biol.* 101, 289–316. doi: 10.1016/0022-5193(83)90342-9

Wollrab, V., Belmonte, J. M., Baldauf, L., Leptin, M., Nédeléc, F., and Koenderink, G. H. (2019). Polarity sorting drives remodeling of actin-myosin networks. *J. Cell Sci.* 132, 1–14. doi: 10.1242/jcs.219717

Wolpert, L. (1960). The mechanics and mechanism of cleavage. *Int. Rev. Cytol.* 10, 163–216.

Wu, J. Q., and Pollard, T. D. (2005). Cell biology: counting cytokinesis proteins globally and locally in fission yeast. *Science* 310, 310–314. doi: 10.1126/science.1113230

Yumura, S., Ueda, M., Sako, Y., Kitanishi-Yumura, T., and Yanagida, T. (2008). Multiple mechanisms for accumulation of myosin II filaments at the equator during cytokinesis. *Traffic* 9, 2089–2099. doi: 10.1111/j.1600-0854.2008.00837.x

Conflict of Interest: The authors declare that the research was conducted in the absence of any commercial or financial relationships that could be construed as a potential conflict of interest.

frontiers in Cell and Developmental Biology

HYPOTHESIS AND THEORY
published: 07 October 2020
doi: 10.3389/fcell.2020.575226

Animal Cell Cytokinesis: The Rho-Dependent Actomyosin-Anilloseptin Contractile Ring as a Membrane Microdomain Gathering, Compressing, and Sorting Machine

Sabrya C. Carim[1†], Amel Kechad[1†] and Gilles R. X. Hickson[1,2]*

[1] CHU Sainte-Justine Research Center, Université de Montréal, Montréal, QC, Canada, [2] Département de Pathologie et Biologie Cellulaire, Faculté de Médecine, Université de Montréal, Montréal, QC, Canada

OPEN ACCESS

Edited by:
Maria Grazia Giansanti, Institute of Molecular Biology and Pathology, Italian National Research Council, Italy

Reviewed by:
Clemens Cabernard, University of Washington, United States
William Trimble, Hospital for Sick Children, Canada
Alisa Piekny, Concordia University, Canada

***Correspondence:**
Gilles R. X. Hickson
gilles.hickson@umontreal.ca

† These authors have contributed equally to this work

Specialty section:
This article was submitted to Cell Growth and Division, a section of the journal Frontiers in Cell and Developmental Biology

Received: 22 June 2020
Accepted: 07 September 2020
Published: 07 October 2020

Citation:
Carim SC, Kechad A and Hickson GRX (2020) Animal Cell Cytokinesis: The Rho-Dependent Actomyosin-Anilloseptin Contractile Ring as a Membrane Microdomain Gathering, Compressing, and Sorting Machine. Front. Cell Dev. Biol. 8:575226. doi: 10.3389/fcell.2020.575226

Cytokinesis is the last step of cell division that partitions the cellular organelles and cytoplasm of one cell into two. In animal cells, cytokinesis requires Rho-GTPase-dependent assembly of F-actin and myosin II (actomyosin) to form an equatorial contractile ring (CR) that bisects the cell. Despite 50 years of research, the precise mechanisms of CR assembly, tension generation and closure remain elusive. This hypothesis article considers a holistic view of the CR that, in addition to actomyosin, includes another Rho-dependent cytoskeletal sub-network containing the scaffold protein, Anillin, and septin filaments (collectively termed anillo-septin). We synthesize evidence from our prior work in *Drosophila* S2 cells that actomyosin and anillo-septin form separable networks that are independently anchored to the plasma membrane. This latter realization leads to a simple conceptual model in which CR assembly and closure depend upon the micro-management of the membrane microdomains to which actomyosin and anillo-septin sub-networks are attached. During CR assembly, actomyosin contractility gathers and compresses its underlying membrane microdomain attachment sites. These microdomains resist this compression, which builds tension. During CR closure, membrane microdomains are transferred from the actomyosin sub-network to the anillo-septin sub-network, with which they flow out of the CR as it advances. This relative outflow of membrane microdomains regulates tension, reduces the circumference of the CR and promotes actomyosin disassembly all at the same time. According to this hypothesis, the metazoan CR can be viewed as a membrane microdomain gathering, compressing and sorting machine that intrinsically buffers its own tension through coordination of actomyosin contractility and anillo-septin-membrane relative outflow, all controlled by Rho. Central to this model is the abandonment of the dogmatic view that the plasma membrane is always readily deformable by the underlying cytoskeleton. Rather, the membrane resists compression to build tension. The notion that the CR might generate tension through resistance

to compression of its own membrane microdomain attachment sites, can account for numerous otherwise puzzling observations and warrants further investigation using multiple systems and methods.

Keywords: cytokinesis, anillin, septin, membrane microdomains, membrane cytoskeleton, rho (Rho GTPase), contractile ring tension, contractile ring mechanism

INTRODUCTION

Cytokinesis of animal cells begins during anaphase with the formation of a cleavage furrow at the cell equator, between the separating chromosomes. At the base of this furrow is a "contractile ring" (CR) (Schroeder, 1972, 1990) that exerts force (Rappaport, 1977) to dramatically reduce the circumference of the cell's plasma membrane and form a midbody ring, which then orchestrates abscission. Pioneering electron microscopy of sea urchin embryos by Schroeder showed that the CR contains circumferential actin filaments (Schroeder, 1972). This was quickly followed by studies showing that the CR contains myosin (Schroeder, 1973; Fujiwara and Pollard, 1976; Mabuchi and Okuno, 1977). It was initially thought that the CR might have a muscle sarcomere-like organization and close like a purse-string. However, the actin filaments of the CR are not organized as in sarcomeres, but are rather organized as a meshwork of filaments in a random order of mixed polarity (Sanger and Sanger, 1980; Fishkind and Wang, 1993; Mabuchi, 1994; Mabuchi et al., 1988; Kamasaki et al., 2007; Spira et al., 2017). An additional class of cytoskeletal filaments, the septins, was discovered as membrane-associated filaments of the budding yeast CR (Byers and Goetsch, 1976; Haarer and Pringle, 1987). Septins are conserved components of CRs from yeast to humans, yet the roles that they play there and how they interact with actomyosin filaments remain unclear (Caudron and Barral, 2009; Mostowy and Cossart, 2012; Bridges and Gladfelter, 2015; Addi et al., 2018; Marquardt et al., 2019). It has been evident since the work of Schroeder (Schroeder, 1972), and more recently Carvalho (Carvalho et al., 2009), that the CR disassembles as it closes, since its closure results in a decrease in its circumference but does not increase its thickness or width. From many studies since these pioneering works, we have learned much about the CR, its constituent parts and their biochemical activities (Eggert et al., 2006; Green et al., 2012). Yet we still do not understand how those components are organized and coordinated with one another to promote CR assembly and closure, particularly in animal cells. Indeed, some of the most enduring and fundamental questions in the field that remain unanswered include: How does the CR generate tension? How does the CR maintain tension while closing and disassembling at the same time? How is the CR anchored to the plasma membrane? How are the different filament systems of the CR (F-actin, myosin II, septins) coordinated with one another (Green et al., 2012; Pollard, 2017; Gerien and Wu, 2018; O'Shaughnessy and Thiyagarajan, 2018; Leite et al., 2019; Mangione and Gould, 2019; Pollard and O'Shaughnessy, 2019)? This article seeks to address these questions. The following sections will briefly summarize the current state of knowledge of the key players involved in CR assembly and function, before describing novel models for how the actomyosin and septin sub-networks of the CR collaborate to generate tension during CR assembly and regulate it to drive CR closure.

Rho: The Master Activator of Cytokinesis

The small molecular weight GTPase Rho has emerged as the master activator of cytokinesis, and specifically, CR assembly. From the onset of cytokinesis, RhoA (Rho1 in *Drosophila*) undergoes dynamic cycles of activation/inactivation at the equatorial plasma membrane (Drechsel et al., 1997; Bement et al., 2005, 2015; Miller et al., 2008; Miller and Bement, 2009; Basant and Glotzer, 2018) with activation through GDP to GTP exchange catalyzed by a specific guanine nucleotide exchange factor (GEF), ECT2 (Miki et al., 1993; Tatsumoto et al., 1999; Kimura et al., 2000) Pebble in *Drosophila* (Lehner, 1992; Somers and Saint, 2003) and inactivation promoted by GTP hydrolysis catalyzed by GTPase activating proteins (GAPs). ECT2/Pebble forms a complex with the centralspindlin complex (Somers and Saint, 2003; Yuce et al., 2005; Kamijo et al., 2006; Nishimura and Yonemura, 2006), comprising kinesin-6 (MKLP1/KIF23 in mammals, Pavarotti in *Drosophila*, ZEN4 in *C. elegans*) and RacGAP (MgcRacGAP in mammals, Tumbleweed/RacGAP50C in *Drosophila*, CYK4 in *C. elegans*), which is required both to activate the GEF activity (via the RacGAP component) and localize it to the equator (via the kinesin-6 component) (Glotzer, 2009; Mishima, 2016). Although centralspindlin-ECT2/Pebble complexes localize to the central spindle at the cell interior, ECT2/Pebble is specifically active as a Rho GEF only at the plasma membrane (Kotynkova et al., 2016; Basant and Glotzer, 2018; Chen M. et al., 2020). There, active Rho-GTP in turn binds and activates specific effector proteins (described below), while RhoGAPs stimulate GTP hydrolysis to rapidly inactivate Rho. Although ECT2/Pebble clearly controls the major Rho-dependent events during cytokinesis, the RhoGAPs responsible for inactivation of specific Rho-effector complexes are less clear. The RacGAP component of the centralspindlin complex required for ECT2/Pebble activation has long been a candidate and its involvement in Rho inactivation is supported by the analysis of GAP-defective MgcRacGAP in *Xenopus* embryos (Miller and Bement, 2009). However, RacGAP exhibits preferential GAP activity toward Rac and Cdc42 rather than Rho *in vitro* (Toure et al., 1998; Bastos et al., 2012; Jantsch-Plunger et al., 2000). Genetic experiments in *C. elegans* embryos have led to conflicting models (discussed in Basant and Glotzer, 2017) in which the CYK4 GAP domain either targets Rac (Canman et al., 2008; Zhuravlev et al., 2017), or acts non-canonically to activate Rho (Loria et al., 2012; Zhang and Glotzer, 2015). Another candidate GAP for

Rho inactivation at the CR is p190RhoGAP-A/ARHGAP35 (Mikawa et al., 2008; Su et al., 2009; Manukyan et al., 2015). M-phase GAP (MP-GAP:ARHGAP11A in mammals, RGA-3/4 in *C. elegans*) also acts to globally suppress Rho and restrict cortical contractility to the equator (Zanin et al., 2013), although no ortholog exists in *Drosophila*. Finally, an additional level of regulation of the Rho GTPase cycle comes from guanine nucleotide dissociation inhibitors (GDIs), which can directly extract active Rho from the plasma membrane (Golding et al., 2019).

While our understanding of the dynamic control of Rho activity is far from complete, it is clear that active Rho-GTP binds and activates multiple effectors that are essential for cytokinesis. These include Diaphanous-related formins, which polymerize unbranched actin filaments (Castrillon and Wasserman, 1994; Otomo et al., 2005; Watanabe et al., 2008, 2010, 2013b). Rho-GTP also activates Rho-kinase, which in turn activates myosin II (Kosako et al., 1999, 2000; Piekny and Mains, 2002; Matsumura, 2005; Hickson et al., 2006), through both stimulatory phosphorylation of the myosin regulatory light chain (MRLC) and inhibitory phosphorylation of the myosin phosphatase (Kawano et al., 1999; Matsumura, 2005). Together, these Rho-dependent events provide the textbook description for actomyosin-based CR assembly (Morgan, 2006).

However, Rho controls a more expansive network than just formins and Rho-kinase (**Figure 1**). Rho-GTP also binds and recruits to the CR Anillin (Hickson and O'Farrell, 2008b; Piekny and Glotzer, 2008; Sun et al., 2015; El-Amine et al., 2019) and Citron kinase (called Sticky in *Drosophila* (Madaule et al., 1995, 1998; Di Cunto et al., 1998; Eda et al., 2001; Gai et al., 2011; Watanabe et al., 2013a; El-Amine et al., 2019). As described in the next section, Anillin is a conserved scaffold protein that has emerged as a master organizer of the CR (reviewed in Hickson and O'Farrell, 2008a; D'Avino, 2009; Piekny and Maddox, 2010). Citron kinase/Sticky does not appear to play important roles at the CR but becomes essential for formation of the subsequent midbody ring (MR) (Di Cunto et al., 2002; D'Avino et al., 2004; Echard et al., 2004; Naim et al., 2004; Dean and Spudich, 2006; Bassi et al., 2011, 2013; Gai et al., 2011; El Amine et al., 2013, El-Amine et al., 2019; Watanabe et al., 2013a; McKenzie et al., 2016; D'Avino, 2017; Dema et al., 2018). The MR is a stable cortical ring structure that forms after CR closure at the center of the intercellular bridge, where it encircles the densely packed zone of interdigitating microtubule plus-ends of the midbody (Steigemann and Gerlich, 2009; Green et al., 2012; Hu et al., 2012; D'Avino et al., 2015). Although the mechanisms of MR formation are poorly defined, MRs contain numerous CR-derived proteins including Anillin, Citron kinase/Sticky, myosin, centralspindlin, as well as CEP55 in mammalian cells. The MR persists after the midbody microtubules have depolymerized and it recruits ESCRT proteins to mediate abscission (Carlton and Martin-Serrano, 2007; Elia et al., 2011; Guizetti et al., 2011).

Thus Rho activates at least four downstream effector pathways that must collaborate at the CR and MR: the formin Diaphanous, Rho-kinase, Citron kinase and Anillin.

Anillin: The Master Organizer of Cytokinesis

Anillin is an integral component of all cytokinetic CRs (Field and Alberts, 1995; Giansanti et al., 1999). Through conserved domains, it can bind a host of other essential CR components, including F-actin, which it bundles (Field and Alberts, 1995; Oegema et al., 2000; Tian et al., 2015; Jananji et al., 2017) and myosin II (Straight et al., 2005). Accordingly, Anillin is often framed as an actomyosin crosslinker. However, Anillin can also bind many other components including Rho-GTP (Sun et al., 2015; Budnar et al., 2019), Citron kinase/Sticky (Gai et al., 2011; El-Amine et al., 2019), membrane phospholipids (Liu et al., 2012) and septins (Oegema et al., 2000; Kinoshita et al., 2002; **Figure 1**).

Septins form palindromic, hetero-oligomeric rod-like complexes that polymerize end-on to form non-polar filaments that can in turn assemble into higher-ordered structures (Sirajuddin et al., 2007; Mostowy and Cossart, 2012; Bridges and Gladfelter, 2015; Spiliotis, 2018; Mendonça et al., 2019; Soroor et al., 2019). In *Drosophila*, the prototypic complex is a hexamer comprising two copies each of Peanut (mammalian SEPT7 ortholog), Sep1 (mammalian SEPT2) and Sep2 (mammalian SEPT1) (Field et al., 1996). According to the recent data of Mendonça and Soroor, the order of the hexamer is likely Sep1-Sep2-Peanut-Peanut-Sep2-Sep1. Septins bind PIP2 (Zhang et al., 1999; Tanaka-Takiguchi et al., 2009; Mendonça et al., 2019; Soroor et al., 2019) which stimulates septin polymerization (Bertin et al., 2010) and septin filaments are often found in tight association with the plasma membrane, where they can form membrane diffusion barriers (Takizawa et al., 2000; Dobbelaere and Barral, 2004; Caudron and Barral, 2009) and contribute to cortical rigidity (Gilden and Krummel, 2010; Mostowy and Cossart, 2011). In both worm and fly cells, the recruitment of septins to the CR depends on Anillin (Maddox et al., 2005; Hickson and O'Farrell, 2008b). Yet, despite conservation from yeast to humans, the precise roles played by the septin cytoskeleton at the CR remain obscure.

Over the past 12 + years, we have studied the Rho1-dependent cytokinetic network in *Drosophila* S2 cells, with an emphasis on Anillin function. Our work has revealed that Anillin (Kechad et al., 2012; El Amine et al., 2013), together with its binding partner Citron kinase/Sticky mediates the "CR-to-MR transition" (El Amine et al., 2013, El-Amine et al., 2019). Rather than the traditional view of the MR and CR as entirely separate structures, our work suggests that Anillin promotes the maturation of the CR into the MR. Indeed, analysis of truncation mutants revealed that Anillin can localize to and organize two separable, Rho1-dependent sub-networks: the actomyosin cytoskeleton via its N-terminus, and the membrane-anchored septin cytoskeleton via its C-terminus (Kechad et al., 2012; El Amine et al., 2013). We further showed that the CR-to-MR transition reflects a balance between two opposing mechanisms acting simultaneously on Anillin: one of cortical retention (mediated by the Anillin N-terminus and Citron kinase/Sticky), the other of membrane-associated removal (mediated by the Anillin C-terminus and septins, Kechad et al., 2012; El Amine et al., 2013) and **Figures 2C,D**. These works not only demonstrate the central importance of Anillin during cytokinetic progression, but they

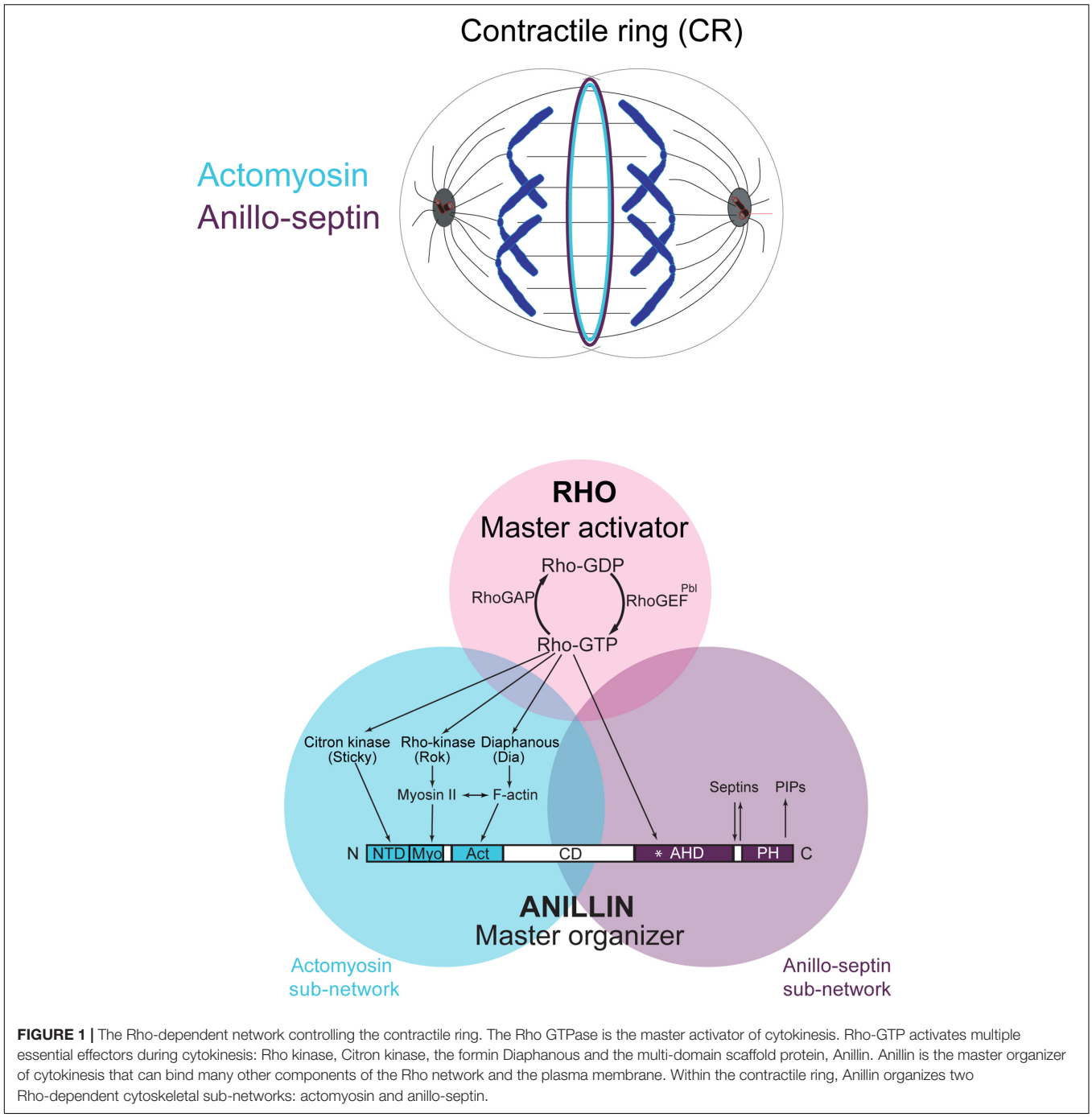

FIGURE 1 | The Rho-dependent network controlling the contractile ring. The Rho GTPase is the master activator of cytokinesis. Rho-GTP activates multiple essential effectors during cytokinesis: Rho kinase, Citron kinase, the formin Diaphanous and the multi-domain scaffold protein, Anillin. Anillin is the master organizer of cytokinesis that can bind many other components of the Rho network and the plasma membrane. Within the contractile ring, Anillin organizes two Rho-dependent cytoskeletal sub-networks: actomyosin and anillo-septin.

also highlight how Anillin can be used as a tool to break down the complex cytokinetic network into more manageable and observable sub-networks.

In this *Hypothesis and Theory* article, we revisit several key observations that, together with multiple iterations of "night science" (Yanai and Lercher, 2019), have led us to a more global view of the CR than is often described. A more expansive view considers not only actomyosin, but also Anillin, septins and, crucially, the plasma membrane microdomain attachment sites to which all of these cytoskeletal elements are anchored. We do not attempt to provide an exhaustive review of the literature on the CR, as this has already been expertly done recently (Glotzer, 2017; O'Shaughnessy and Thiyagarajan, 2018; Leite et al., 2019; Mangione and Gould, 2019; Pollard and O'Shaughnessy, 2019). We rather seek to expose a novel conceptual framework, in which the plasma membrane plays a much more active role in regulating the tension of the CR than has generally been considered. The insight gained from our Anillin-centric experimental approach leads to a simple yet compelling model for how the global Rho GTPase network

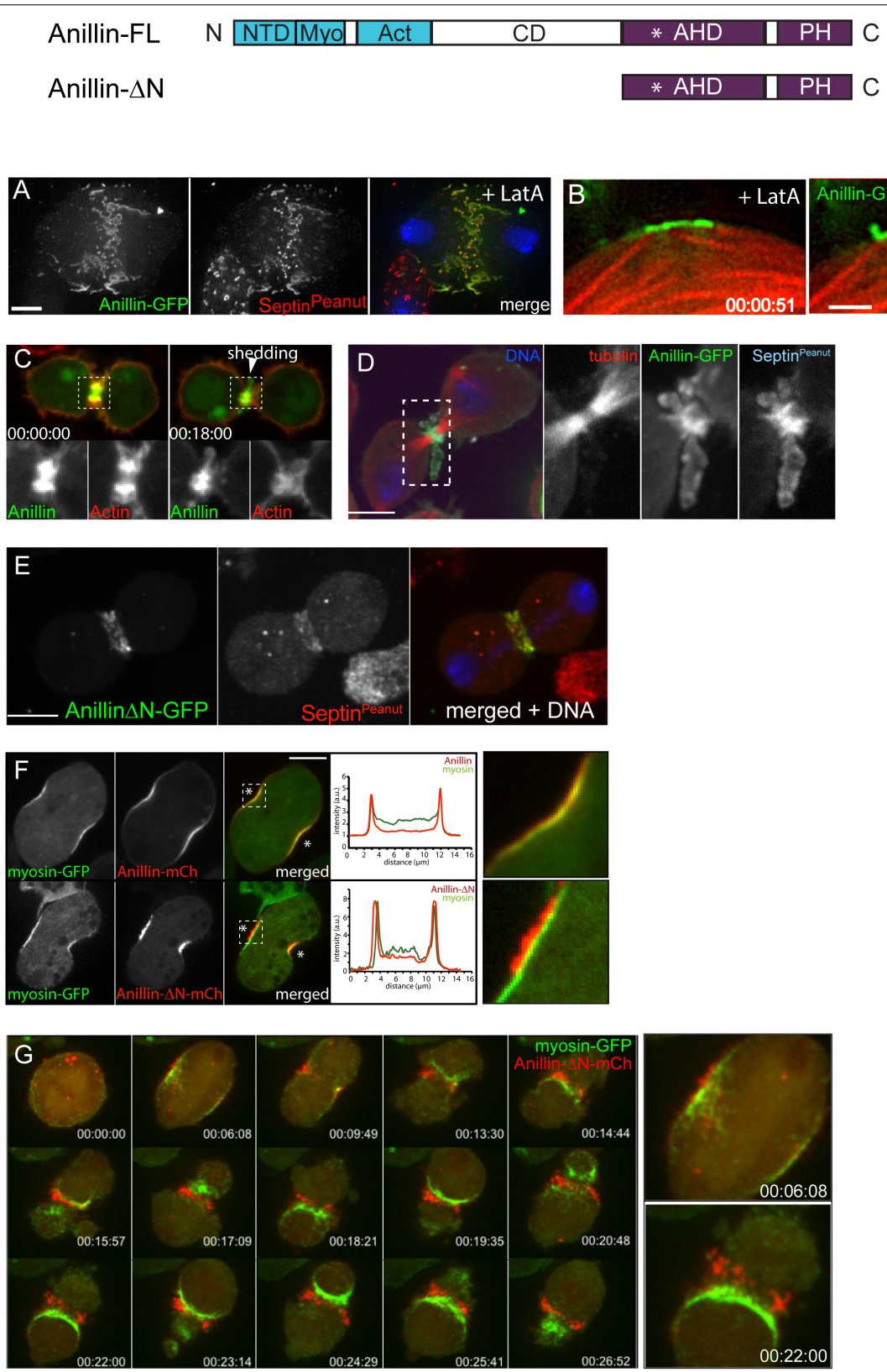

FIGURE 2 | Actomyosin and anillo-septin are independently anchored to the plasma membrane and can laterally separate from one another. **(A)** Rho1 drives assembly of anillo-septin structures directly at the equatorial plasma membrane in the presence of the F-actin inhibitor, Latrunculin A. Maximum intensity projection of a fixed S2 cell expressing Anillin-GFP, stained for endogenous septin (Peanut) and DNA. Similar behavior of anillo-septin is observed upon additional inhibition of

(Continued)

FIGURE 2 | Continued
myosin activation (not shown). **(B)** Actin-independent assembly of anillo-septin sequesters the plasma membrane. Time-lapse frames of close-ups of the cell cortex of an S2 cell co-expressing Anillin-GFP (green) and mCherry-tubulin (red) treated with Latrunculin A and progressing through anaphase. The nascent anillo-septin structures reorient from parallel to perpendicular to the cell surface as they envelop themselves in plasma membrane. This envelopment and reorientation suggest that, as the anillo-septin complexes bind and sequester the membrane microdomains, the resulting tubular structures can deform the membrane to make it fit their shape. Time is shown as h:min:s from anaphase, scale bar, 2 μm. **(C)** Anillin-mCherry (mCh, green) shedding from the late contractile ring/nascent midbody ring (indicated by the white arrowhead) of a *Drosophila* S2 cell co-expressing the F-actin probe Lifeact-GFP (red), which does not shed). Split channels of the dashed boxed region are shown magnified below. **(D)** Shed material contains Anillin and Peanut. Fixed cells expressing Anillin-GFP (green), mCh-tubulin (red) and stained for endogenous Peanut (cyan) and DNA (Hoechst, blue). **(E)** The Anillin C-terminus (Anillin-ΔN) and the septin, Peanut, are co-recruited to the CR. Fixed *Drosophila* S2 cell expressing Anillin-ΔN-GFP, stained for endogenous Peanut and DNA (Hoechst, blue). **(F)** *Drosophila* S2 cell during early furrowing co-expressing myosin-GFP (green) and either Anillin-mCherry (top) or the Anillin C-terminus (Anillin-ΔN-mCherry, red, bottom). Intensity profiles along a line drawn between the asterisks are shown and white dashed boxed regions are shown magnified on the right. While Anillin-mCherry localization closely follows that of myosin-GFP, Anillin-ΔN-mCherry appears in puncta that extrude outward toward the cell exterior. **(G)** Frames from a time-lapse sequence of an S2 cell co-expressing myosin-GFP (green) and Anillin-ΔN-mCh (red) and depleted of endogenous Anillin. Anillin-ΔN (anillo-septin) forms punctate structures that herniate the membrane outward, whilst myosin (actomyosin) undergoes back-and-forth, lateral oscillations beneath these distinct structures. This clearly shows that actomyosin and anillo-septin are separate from one another (at least when the Anillin N-terminus is missing) and that they are independently anchored to the plasma membrane. The 00:06:08 and 00:22:00 time points are shown magnified on the right. Times are h:min:s from anaphase. **(A)** adapted and **(B)** reproduced from © 2008 Hickson and O'Farrell originally published in Journal of Cell Biology: https://doi.org/10.1083/jcb.200709005 which is available under a Creative Commons License (Attribution–Non-commercial–Share Alike 4.0 Unported license, as described at http://creativecommons.org/licenses/by-nc-sa/4.0/) and for which we retain copyright (Hickson and O'Farrell, 2008b). **(C,D)** adapted from© 2013 El-Amine et al., originally published in Journal of Cell Biology: https://doi.org/10.1083/jcb.201305053, which is available under a Creative Commons License (Attribution–Non-commercial–Share Alike 3.0 Unported license, as described at http://creativecommons.org/licenses/by-nc-sa/3.0/) and for which we retain copyright (El Amine et al., 2013). **(E–G)** are adapted from Kechad et al. (2012), originally published in Current Biology with permission from Elsevier (publisher) license number: 4844230307942 (obtained on June 08th, 2020) https://doi.org/10.1016/j.cub.2011.11.062.

and the plasma membrane influence one another during CR assembly and closure.

Organization of the CR Involves Two Rho-Dependent Sub-Networks

Determining the organization of CRs by direct visualization is challenging because of dynamicity, the degree of compaction of components, and the limits of resolution afforded by light microscopy. In-built redundancy and robustness of the components have also hampered the dissection of the molecular circuitry of the system. However, we found that Anillin truncations can be used as tools to effectively split the CR into two separable and resolvable sub-structures, representing two distinct Rho-dependent sub-networks that Anillin ordinarily localizes to: an actomyosin-based sub-network and a septin-based sub-network (**Figure 1**; Kechad et al., 2012; El Amine et al., 2013). Considering the CR as a dynamic marriage of these two Rho-dependent, Anillin-organized sub-networks is what led to the model elaborated below.

A Rho-Dependent Actomyosin Sub-Network Organized by the Anillin N-Terminus

During CR formation Rho activation drives actomyosin assembly through formin-mediated F-actin polymerization and Rho-kinase-dependent myosin II activation. Actomyosin-driven CRs can assemble without Anillin, but such Anillin-deficient CRs are defective. In fly and human cells, Anillin-depleted CRs fail to close completely, and become unstable and prone to lateral oscillation (Straight et al., 2005; Zhao and Fang, 2005; Hickson and O'Farrell, 2008b; Piekny and Glotzer, 2008; Goldbach et al., 2010; Kechad et al., 2012). In larger *C. elegans* zygotes, Anillin-depleted CRs successfully close but they are abnormally sensitive to reduced myosin levels (Maddox et al., 2007) and they exhibit higher levels of F-actin (Jordan et al., 2016). But although the actomyosin elements of the CR can assemble independently of Anillin, Anillin does connect to this actomyosin sub-network and it does so using its N-terminal half. This region harbors conserved domains for binding F-actin (Field and Alberts, 1995; Tian et al., 2015; Jananji et al., 2017; Matsuda et al., 2020) and myosin II (Straight et al., 2005), and the Anillin N-terminus (Anillin-ΔC) is sufficient to co-localize with actomyosin at the CR in a similar manner to full-length Anillin (e.g., Kechad et al., 2012; El Amine et al., 2013). Disrupting the actin cytoskeleton with Latrunculin A (LatA) disrupts the cortical localization of the Anillin N-terminus (Anillin-ΔC) during anaphase (unpublished data), indicating that F-actin is required to recruit the Anillin N-terminus to the actomyosin sub-network of the CR. Within that sub-network, Anillin's F-actin cross-linking ability may contribute to tension generation within the CR (Field and Alberts, 1995; Tian et al., 2015; Jananji et al., 2017; Matsuda et al., 2020) and it also enhances formin-mediated F-actin polymerization (Chen et al., 2017). Anillin−myosin interactions presumably also play a role at the CR (Straight et al., 2005), although these have not been directly tested. Finally, interactions with Dia-related formin (Watanabe et al., 2010) and Citron-kinase/Sticky (El Amine et al., 2013, El-Amine et al., 2019) that also reportedly occur in the Anillin N-terminus, likely also impinge on this actomyosin-based sub-network, which the Anillin N-terminus coordinates. Regardless of any other potential contributions, the N-terminal half of Anillin, and by extension the actomyosin sub-network that it participates in, can only provide partial functionality to the CR. Indeed, although expressing the Anillin N-terminus (Anillin-ΔC) in *Drosophila* S2 cells depleted of endogenous Anillin rescued the oscillating CR phenotype (the only animal system where, to our knowledge, such a construct has been examined), the resulting Anillin N-terminus-organized CRs closed slowly and displayed aberrant membrane blebbing in their flanking furrows (Kechad et al., 2012). Thus, for their proper function, CRs must

require additional Anillin-dependent activities associated with its C-terminus.

A Rho-Dependent Anillo-Septin Sub-Network Organized by the Anillin C-Terminus

Anillin recruitment is also Rho-dependent, and the requirement for ECT2/Pebble indicates that "active Rho" is required (Hickson and O'Farrell, 2008b; Piekny and Glotzer, 2008). This recruitment mechanism occurs via the C-terminus of Anillin (Piekny and Glotzer, 2008; Kechad et al., 2012), which contains a conserved Rho binding domain within its Anillin Homology Domain (Piekny and Glotzer, 2008; Tse et al., 2012; Sun et al., 2015; Nishikawa et al., 2017; Michaux et al., 2018; Budnar et al., 2019), as well as a PH domain that can bind both membrane phospholipids (Liu et al., 2012) and septins (Oegema et al., 2000; Field C.M. et al., 2005). Indeed, Anillin is required to recruit septins to the CR in *C. elegans* embryos (Maddox et al., 2005), fly cells and embryos (Field C.M. et al., 2005; Hickson and O'Farrell, 2008b), and human cells via a region that includes the PH domain (Liu et al., 2012). Reciprocally, robust recruitment of the fly C-terminal AH/PH domains (Anillin-ΔN) depends on septins (Kechad et al., 2012), indicating that this region of Anillin is more than a simple Rho-GTP binding domain.

The existence of a distinct active-Rho, Anillin and septin sub-network is particularly evident in cells in which the actin cytoskeleton has been completely disrupted using LatA (Hickson and O'Farrell, 2008b). In this case, Rho1, Anillin and septins are co-recruited to the plasma membrane, independently of actomyosin, where they form long tubular structures that become enveloped in plasma membrane, consistent with avid membrane binding (**Figures 2A,B**; Hickson and O'Farrell, 2008b). For simplicity, and in keeping with the accepted convention of the term "acto-myosin," we will subsequently use the term "anillo-septin" to describe the Anillin and septin sub-network of the CR.

Thus, in addition to active Rho promoting actomyosin assembly (which can occur independently of anillo-septin), active Rho also promotes anillo-septin assembly (which can occur independently of actomyosin). These separable sub-networks must somehow coexist, interwoven within the CR.

Actomyosin and Anillo-Septin Are Independently Anchored to the CR Membrane and Can Separate From One Another

Thus, Anillin can localize to both actomyosin (with which it interacts via its N-terminus) and septin-based (via its C-terminus) sub-networks. But crucially, our work shows that Anillin allows these two sub-networks to separate, laterally in the plane of the membrane during CR closure. This physical separation of anillo-septin from actomyosin can be readily observed during the natural progression of the CR-to-MR transition. Curiously, we found that the late CR extrudes and sheds membranes enriched for Rho1-Anillin-septin but lacking actomyosin (El Amine et al., 2013; **Figures 2C,D**), and others have documented similar phenomena of shedding in other cell types (Mullins and Biesele, 1977; Dubreuil et al., 2007; Renshaw et al., 2014). However, an analogous separation of anillo-septin from actomyosin can also be observed earlier during CR assembly and ingression, upon the experimental truncation of Anillin. While full-length Anillin (or the Anillin N-terminus, Anillin-ΔC) faithfully tracked with the actomyosin components of the CR during the early stages of furrow ingression (**Figure 2F**), the truncated Anillin C-terminus (Anillin-ΔN) was recruited to the equatorial plasma membrane, independently of actomyosin. Indeed, it was recruited together with Rho1- and septins (**Figure 2E**) to punctate, membrane-associated structures that rapidly resolved themselves during furrow ingression as being distinct from the actomyosin network, and from which they herniated outward (**Figures 2F,G**; Kechad et al., 2012). This separation was all the more clear in cells depleted of endogenous Anillin: actomyosin formed unstable CRs that oscillated laterally back and forth across the equator, while the punctate anillo-septin structures remained firmly anchored to the equatorial membrane (**Figure 2G**). Thus membrane-anchored actomyosin and anillo-septin can clearly separate from one another, both naturally (during shedding from the late CR/nascent MR) and experimentally (at the early CR following truncation of the Anillin N-terminus). It is therefore logical to surmise that, in the context of a normal CR, the actomyosin and anillo-septin sub-networks might be independently anchored to neighboring patches of plasma membrane, as depicted in **Figure 3D**. Because in the resolved structures we never saw actomyosin co-localizing with anillo-septin, this suggests that either the two sub-networks utilize different membrane attachment sites (i.e., membrane microdomains) or that they somehow compete for the same membrane microdomains binding them in a mutually exclusive manner. We strongly favor the latter, for reasons discussed below, but the important point here is that the lateral separation of actomyosin and anillo-septin sub-networks drives the lateral separation of their associated membrane microdomains: i.e., neighboring membrane microdomains within the CR membrane can potentially slide past one another, depending on which cytoskeletal sub-network they are anchored to. Consideration of these findings, leads us to propose a simple two-stage model for cytokinetic furrowing (**Figure 3**): (1) CR assembly, during which tension is generated to a threshold, and (2) CR closure by disassembly, during which tension is maintained at that threshold.

A Model for CR Assembly and Tension Generation: Rho-Dependent Actomyosin Contractility Gathers and Compresses Membrane Microdomains at the Cell Equator

We envision that, prior to the initiation of cytokinesis (i.e., at metaphase), the plasma membrane contains specific raft-like microdomains that are evenly dispersed within the more fluid phospholipid bilayer, spaced apart through dynamic connections to the isotropic mitotic actomyosin cortex. During anaphase, Rho activation at the equator is triggered by centralspindlin-delivered

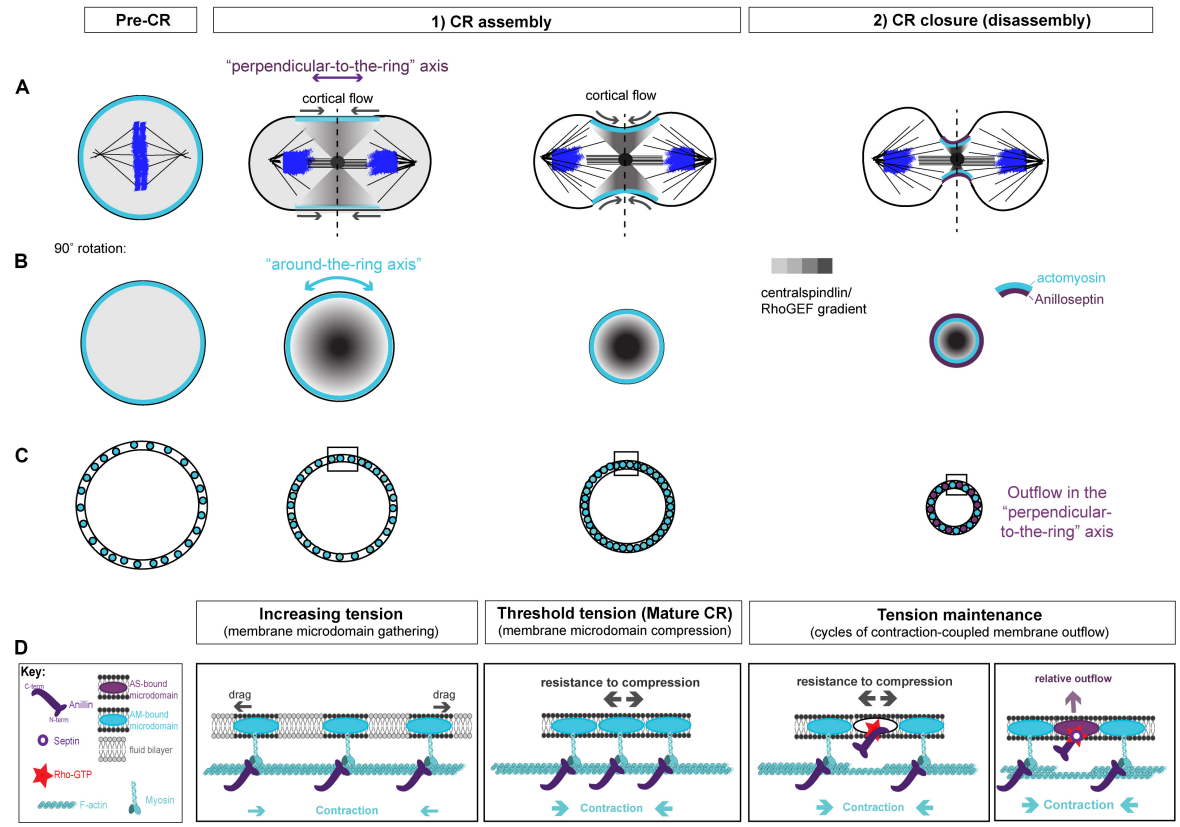

FIGURE 3 | Two-stage model for CR assembly and closure. **(A)** Cartoons of the conventional view of cytokinesis in the "perpendicular-to-the-ring" axis, showing how the architecture of the spindle establishes a gradient of centralspindlin/RhoGEF that peaks at the equator and at the cell center to promote cortical flow during CR assembly and closure. **(B)** 90° rotations of the dotted lines in panel **(A)** showing the "around-the-ring" axis. **(C)** Cartoons in the "around-the-ring" axis to illustrate the proposed concept of how membrane microdomain attachment sites of the CR oppose contractility to generate tension during CR assembly, and regulate tension during CR closure/disassembly. At a certain density of microdomain compaction, which represents a certain tension threshold, the CR becomes "mature" and shifts from the assembly stage to the disassembly stage, which involves relative outflow of microdomains in the "perpendicular-to-the-ring" axis. **(D)** More detailed views of the boxed regions in panel **(C)**, showing the hypothetical arrangement of actomyosin, anillo-septin and their associated membrane microdomains. *Note: The "actomyosin sub-network" comprises numerous components and membrane anchors (not least for F-actin nucleating formins and for myosin II motors), but it is purposefully depicted as one entity here for clarity. Similarly, the stoichiometry and scaling of depicted components are for illustrative purposes only.*

ECT2/Pebble, but only at specific membrane microdomains (likely PIP2-rich) that can accept the ECT2 PH domain and promote the activation of its GEF activity (Kotynkova et al., 2016; Chen M. et al., 2020). ECT2-stimulated Rho-GTP then recruits effectors for actin and myosin to individual membrane microdomains. Because of the architecture of the spindle, centralspindlin concentrates at the cell equator, first at the central spindle, but then in a disc that emanates outward toward the cortex. This delivers ECT2/Pebble and therefore Rho-GTP to the plasma membrane, in a gradient that peaks at the equator and trails off toward the poles (**Figure 3A**). In response to this gradient of Rho activation, the actomyosin sub-network contracts in a graded fashion, maximally at the equator, which initiates cortical flow toward the equator. This cortical flow pulls the actomyosin-attached membrane microdomains into the equator also, where they begin to become compressed, again in a gradient that is maximal at the equator (**Figures 3A–C**). The cortical flow also reinforces and maintains the equatorial peak of the ECT2/Pebble gradient (and downstream components) that was first established by the spindle. During this initial phase of CR assembly, actomyosin and Anillin are connected to one another via Anillin's N-terminus. The gradient of actomyosin contractility powers the coalescence of associated membrane microdomain attachment sites, gathering them into an increasingly compact ring at the equator (**Figures 3A–C**). This gathering of cytoskeletal elements appears conceptually similar to the "search, capture, pull, release" model that accounts for the coalescence of pre-CR nodes in *S. pombe* cytokinesis, and where the Anillin-like Mid1 plays a pivotal role (Vavylonis et al., 2008; Ojkic et al., 2011; Rincon and Paoletti, 2012; Bidone et al., 2014; Mangione and Gould, 2019). It is also similar to the compression feedback described by Khaliullin et al. (2018). However, these models do not satisfactorily account for how the nascent CR might generate tension.

Yet as the CR forms, it must generate tension. Tension can be defined as a strained state resulting from forces acting in opposition to each other. As the actomyosin network contracts and pulls on itself, through the coordination of

formin-polymerized F-actin and myosin motors/mini-filaments, it pulls its membrane microdomain attachment sites toward each other, gathering them at the expense of the unbound intervening constituents of the phospholipid bilayer that previously separated them (this intervening membrane may also be extruded as microvillus-like projections). Initially, drag forces oppose this gathering of membrane microdomains (**Figure 3D**), but as the components become increasingly compacted, we postulate that a much greater force will oppose the actomyosin contractility to generate tension within the CR: that of increasing resistance to compression of the membrane microdomain attachment sites themselves (**Figure 3D**). According to this idea, tension mounts within the nascent CR membrane and associated cortex in response to intra-membrane resistance to compression, which opposes the actomyosin contractility. An analogy for this proposed mechanism of tension generation can be found in the architecture of a traditional wine barrel, which is made of separate wooden staves held together by metal hoops, all under tension. However, the metal hoops are only under tension because of the resistance to compression of the wooden staves, while the wooden staves are only under tension because of the resistance to expansion of the metal hoops. At the CR, actomyosin acts like a tightening metal hoop (except it is on the inside rather than the outside), while the membrane microdomains to which it is anchored are like the wooden staves, resisting compression. It is the opposition of these forces that generate the tension (**Figures 3C,D**).

We propose that as the nascent CR gathers a certain density of CR-anchored membrane microdomains, their compression reaches a certain threshold in tension, and can now be considered "mature" (**Figures 3C,D**). This mature CR now transitions from an assembly stage to a disassembly stage, which drives its full closure (**Figures 3C,D**). According to this model, the assembly stage of the nascent CR is driven primarily by actomyosin, while Anillin follows, bound to actomyosin via its N-terminus.

A Model for CR Closure by Disassembly: Actomyosin Contractility Pumps Out Anillo-Septin-Bound Membrane Microdomains to Reduce the Circumference of the CR

At this point it is useful to consider the mature CR from its two axes, as described by Khaliullin et al. (2018): the circumferential "around-the-ring" axis and the "perpendicular-to-the-ring" axis (**Figure 3**). The cortical and membrane flow described above during CR assembly is best envisioned in the "perpendicular-to-the-ring" axis, while the resistance to compression is best envisioned in the "around-the-ring" axis. While the "CR assembly" stage can account for the initiation of furrowing, full closure of the mature CR requires a reduction in its circumference in the "around-the-ring" axis. To achieve this, we propose that ratchet-like cycles of actomyosin contraction (building tension) are coupled to anillo-septin-bound membrane outflow (releasing tension) as the CR advances toward the cell interior and shrinks in circumference. Together, these opposing activities regulate tension such that it can be maintained at the appropriate threshold as the CR closes. Central to this model is the inference that actomyosin and anillo-septin must share the same pool of membrane microdomains, but in a mutually exclusive manner. Only this can satisfactorily accommodate the facts that CRs operate over a wide range cell sizes, using an equivalent starting cortex, and that the relative proportions of each sub-network remain largely constant throughout closure, regardless of initial cell size (Carvalho et al., 2009; Khaliullin et al., 2018).

Indeed we make the specific prediction that, within the mature CR, actomyosin loses its membrane microdomains to anillo-septin, which sequesters them and allows them to flow out of the CR, depriving the actomyosin of the opportunity to reassemble. The net result of such a cycle is net depolymerization of actomyosin, a progressive reduction in the total number of membrane microdomains within the CR, and a concomitant reduction in the circumference of the CR, i.e., CR closure. A useful analogy of this proposed mechanism of ring closure is the party game of musical chairs, where participants (actomyosin) jog around a circle of chairs (membrane micro-domains) to music. When the music is abruptly stopped, the participants must compete for chairs (of which there is 1 fewer than the number of participants) and the person left standing, is eliminated. The music restarts, the participants jog again and the organizer (anillo-septin) removes a chair. Repeated cycles of elimination ensue until there is only one chair and the winner. According to this analogy, anillo-septin (the organizer) removes membrane microdomains (chairs) away from dynamic actomyosin (participants), resulting in a progressive loss of membrane microdomains and a concomitant reduction in the circumference of the contractile ring (the number of participants and chairs progressively declines and the circle closes in).

A hypothetical series of steps for how the loss of membrane microdomains could operate at the CR is presented in **Figure 4**. In the first step, contraction in the "around-the-ring" axis of actomyosin-elements bound to two separate membrane microdomains compresses the intervening membrane microdomains. We propose that this compression creates conditions for anillo-septin assembly at the intervening membrane microdomains (**Figure 4A**) and then squeezes anillo-septin-bound membrane out in the "perpendicular-to-the-ring" axis (**Figure 4B**). How might this work molecularly? In addition to compressing the intervening membrane microdomains, contraction of actomyosin elements anchored to two membrane microdomains will compress any intervening actomyosin elements that are not directly participating in this contraction event (**Figure 4C**). Somewhat counter-intuitively for a CR under high tension, this contraction will locally reduce tension on the intervening actomyosin, to which Anillin is bound via its N-terminus. We predict this will provide the opportunity for anillo-septin to assemble on microdomains transiently vacated by actomyosin (**Figures 4C,D**). Such anillo-septin assembly could potentially involve some sequence of disengagement of Anillin from actomyosin, disengagement of actomyosin from the membrane microdomain, Rho-GTP-mediated recruitment

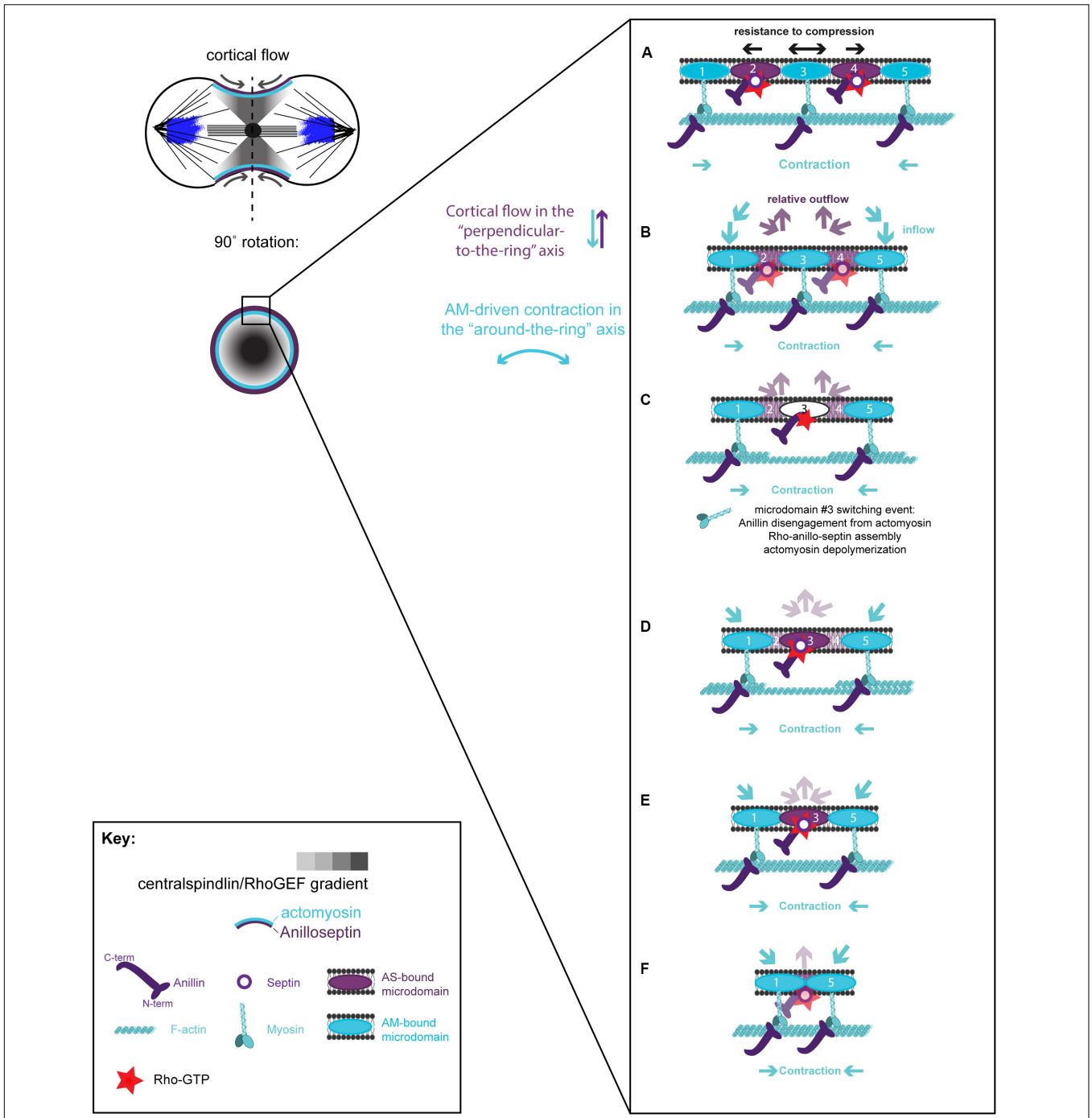

FIGURE 4 | Hypothetical steps in the contraction-coupled anillo-septin membrane sorting model for CR closure, viewed down the spindle/"perpendicular-to-the-ring" axis. **(A)** Actomyosin elements anchored to microdomains 1 and 5 contract in the circumferential, "around-the-ring" axis, compressing the intervening membrane microdomains. Anillin is connected to the membrane either indirectly via actomyosin (microdomains 1, 3, and 5), or directly as anillo-septin (microdomains 2 and 4), but not via both mechanisms at the same time. **(B,C)** Continued contraction advances microdomains 1 and 5 toward the viewer, while the intervening microdomains stay behind (relative outflow). Microdomains 2 and 4 are the latest additions to a growing anillo-septin filament that projects back away from the viewer. Continued contraction pulls microdomains 1 and 5 closer together squeezing them forward, past the intervening microdomains. **(C,D)** Contraction of actomyosin anchored to microdomains 1 and 5, also compresses the intervening actomyosin (reducing its tension) that is anchored to microdomain 3. This in turn allows Rho/Anillin to displace actomyosin (which depolymerizes) and assemble Anillo-septin on microdomain 3, thereby extending the growing anillo-septin filament. **(E,F)** Further contraction pulls microdomains 1 and 5 both closer together and closer to the viewer, past the end of the nascent anillo-septin filament, thereby equilibrating the tension and reducing the circumference of the CR. Thus, the CR closes by contraction-coupled membrane sorting, in which membrane enters and advances the ring with actomyosin but stays behind and exits with anillo-septin. Thus, it disassembles in a bifurcated fashion: actomyosin depolymerization and anillo-septin-membrane outflow.

of the Anillin C-terminus and septins to the microdomain, and actomyosin depolymerization (**Figure 4C**). Whatever the precise mechanism and order of events, anillo-septin assembles on microdomains vacated by actomyosin, thereby sequestering them and providing them the opportunity to exit the ring in the "perpendicular-to-the-ring" axis, as part of a growing, membrane-anchored Anillo-septin filament that is then squeezed out of the ring upon continued contraction of the actomyosin (**Figures 4D–F**). Anillin is perfectly placed to effectively displace actomyosin from its membrane microdomains because it is bound to actomyosin via its N-terminus, ready to disengage and, via its C-terminus, co-assemble with Rho-GTP and septins at the membrane when the conditions are favorable (i.e., tension-regulated). The predicted relative outflow of anillo-septin-bound membrane microdomains provides a means for regulating the tension within the CR (like a pressure release valve), while the predicted sequestration of shared microdomains prevents re-assembly of actomyosin, therefore promoting net actomyosin disassembly. Thus, CR closure proceeds by a kind of "bifurcated disassembly": actomyosin depolymerization coupled to anillo-septin-membrane outflow, all operating at a certain threshold in tension (**Figure 5A**).

According to this model, Anillin flows into the CR bound to actomyosin (but not Rho/septins/membrane), but then exits the CR bound to Rho/septins/membrane (but not actomyosin). From the perspective of the membrane microdomains, they flow into the ring bound to the actomyosin sub-network, then switch to the anillo-septin network (**Figures 4C,D**), with which they flow out, or rather stay behind in the wake of the CR as it continues its onward journey toward the cell interior. Implicit to the model is the prediction that Anillin's interactions with Rho/septins (via the C-terminus) and Anillin's interactions with actomyosin (via the N-terminus) are mutually exclusive, such that Anillin disengages from actomyosin as it switches to the septin network (and displaces actomyosin from its membrane microdomains). For the proposed mechanisms of tension dissipation to be effective, anillo-septin must remain disconnected from actomyosin, at least transiently, to allow the associated membrane microdomains of each sub-network to flow past one another, as this is required to reduce the resistance to compression of the membrane and therefore tension. Super-resolution (fPALM) microscopy of the fission yeast CR cortex has shown it to comprise at least 3 distinct layers with septins occupying the most membrane-proximal layer and F-actin the most membrane-distal layer (McDonald et al., 2017). Perhaps the distance between these layers is ordinarily too great for Anillin to span, until for example an F-actin filament to which it is bound buckles under compression (or depolymerizes), as one expects once the local cortex has reached its threshold in tension. Although highly speculative, this illustrates one of many possibilities for how the system could be organized in a mechanosensitive fashion, regulated by the local tension.

Additional views of the proposed model for CR closure are provided in **Figures 5B,C**, where the "perpendicular-to-the-ring" axis is projected into a flattened image so that both axes can be visualized simultaneously. These show more clearly the proposed mechanism of actomyosin-dependent inflow of membrane microdomains (blue arrows), and contraction-coupled anillo-septin-dependent outflow of membrane microdomains (purple arrows). The membrane microdomains are color-coded based on the network to which they are attached, to show how they "switch" from the actomyosin sub-network (blue) to the anillo-septin sub-network (purple) at the CR front where the tension is highest (**Figures 5B,C**). The microdomains are individually numbered to depict their relative movements over a hypothetical time-course in **Figure 5C**. This arrangement invokes the analogy of mini-caterpillar^{TM} tracks (or conveyor belts) of membrane microdomains flowing forward bound to actomyosin and backward (relatively, i.e., static) bound to anillo-septin. **Figure 5C** also shows how nascent anillo-septin filaments are predicted to form in the "perpendicular-to-the-ring" axis, with new filament assembly occurring just at/behind the CR front (i.e., the site of maximal tension), utilizing the newly switched membrane microdomains. Thus, while septin filaments are non-polar in the traditional, spatial sense, they may exhibit temporal polarity in cells with "new" ends at the CR and "old" ends projecting toward the poles. To facilitate closure of the CR and prevent it from becoming stuck on itself as the ring circumference shortens, some of these anillo-septin filaments and associated membrane microdomains must presumably disengage from the CR (not shown) and stay behind as the CR advances (i.e., relative outflow).

The Anillo-Septin Network: Grease for the Actomyosin Network Within the CR?

The described model posits that crosstalk between actomyosin-anilloseptin sub-networks regulates tension and facilitates CR closure through membrane microdomain micro-management. Further support for the model comes from the realization that it provides plausible explanations for otherwise puzzling phenotypes observed upon disruption of the anillo-septin sub-network. Anillin depletion can lead to unstable, oscillating furrows and a failure of CR closure in small cells such as human and fly tissue culture cells (Straight et al., 2005; Zhao and Fang, 2005; Hickson and O'Farrell, 2008b; Piekny and Glotzer, 2008; Kechad et al., 2012) and fly spermatocytes (Goldbach et al., 2010). According to the model, these phenotypes could reflect perturbations in the ability of the CR to sequester and remove its membrane microdomain attachment sites, release tension, disassemble actomyosin and thus close (**Figure 6A**). Anillo-septin depletion is predicted to lead to unregulated, above-threshold, tension because actomyosin membrane microdomains accumulate, fail to be extruded, and thus impede CR closure. Continued cortical flow toward this stalling CR could destabilize the CR, potentially by widening it, and lead to its oscillation (**Figure 6A**). In cells expressing the C-terminus (Anillin-ΔN) as their only source of Anillin, actomyosin clearly still oscillates (**Figure 2G**), indicating that the coupling between Anillin and actomyosin is crucial for the system to function, as predicted by the conceptual model (**Figure 4**). In other words, the Anillin N-terminus ensures that Anillin is at the right place (at the CR front) to be able to sequester the appropriate membrane microdomains needed to reduce tension and dissassemble the ring. In the case of Anillin-ΔN, the ectopic, uncoupled formation

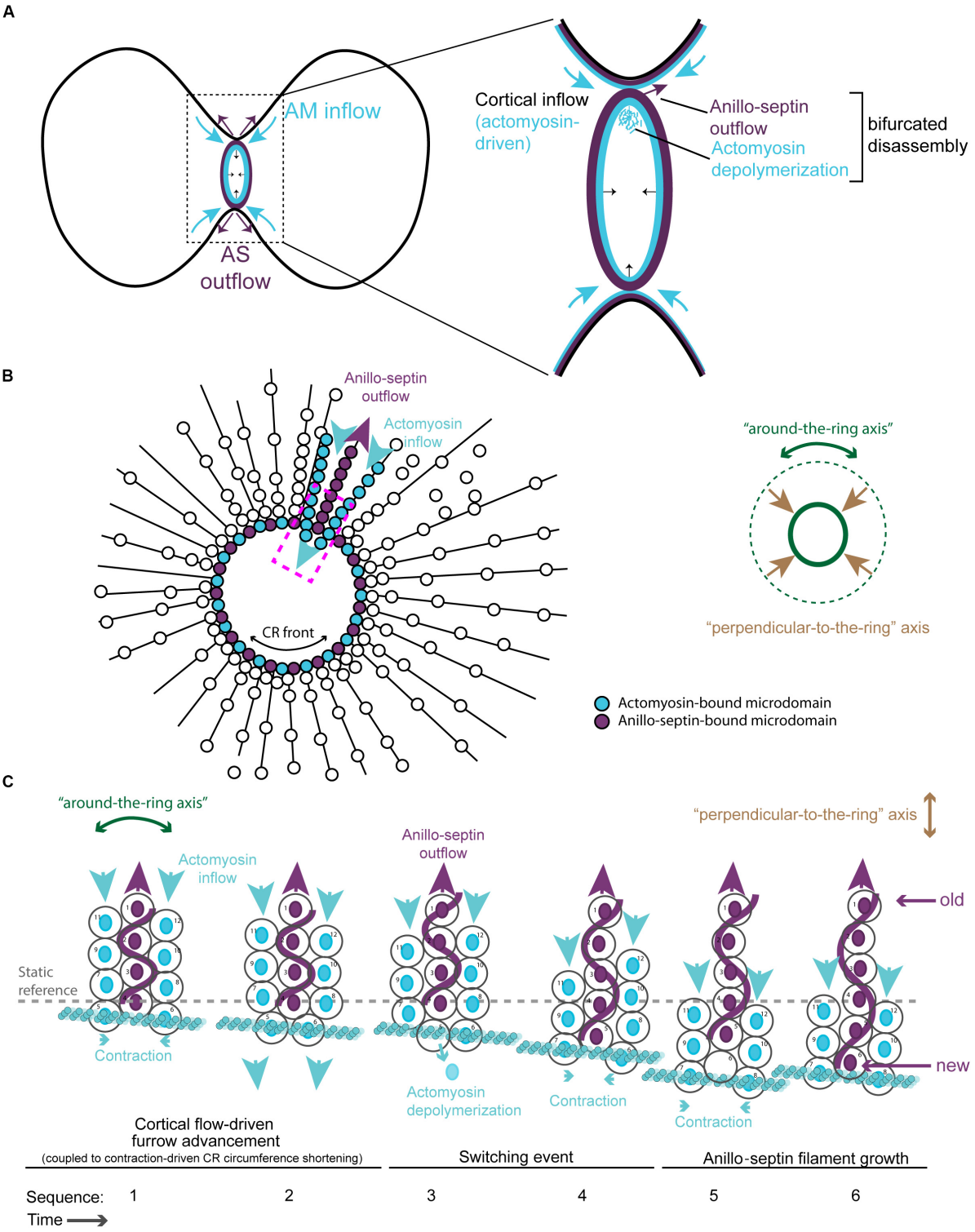

FIGURE 5 | Different viewing perspectives of the contraction-coupled membrane sorting model for CR closure. **(A)** Cartoon showing the proposed relative inflow/outflow of actomyosin/anillo-septin and the concept of closure by bifurcated disassembly, in which the CR sheds components both by depolymerization (actomyosin) and by membrane-anchored outflow (anillo-septin). **(B)** Flattened image viewed down the spindle axis showing both the "around-the-ring" and the "perpendicular-to-the-ring" axes. Arrows depict the relative flow of actomyosin-bound microdomains into the ring (blue) and anillo-septin-bound microdomains out of the ring (purple) as it advances in the "perpendicular-to-the-ring" axis and shrinks in the "around-the-ring" axis. **(C)** Close-up view of the magenta boxed region in panel **(B)**, showing the proposed inflow of actomyosin-bound membrane microdomains, and switching events, as they transfer to nascent anillo-septin filaments that emanate back into the flanks of the furrow. The membrane microdomains are numbered to be able to follow their shifting positions in the time sequence.

of anillo-septin occurs at membrane that already trails the CR front. It therefore cannot regulate the tension and closure of the CR front, which is essentially depleted of Anillin. Therefore actomyosin-driven compression of membrane microdomains causes tension to mount to above the usual threshold, resulting in furrow oscillations (**Figure 6B**).

The Anillin N-Terminus: A Scaffold for the Actomyosin Network as Well as a Regulator of Anillo-Septin Assembly

According to the model for CR closure (**Figure 4**), its amino terminus brings Anillin to the mature CR front and is required to position Anillin appropriately for the tension-regulated assembly of the Anillo-septin sub-network that is deposited just behind the CR. However, the N-terminus of Anillin likely also directly scaffolds the actomyosin sub-network, through its domains for binding F-actin, myosin, and Citron kinase (**Figure 1**), thereby regulating actomyosin contractility. In *Drosophila* S2 cells, expression of the Anillin N-terminus (Anillin-ΔC) suppressed CR oscillations that can occur upon Anillin depletion, but CR closure was still greatly slowed and the furrow membrane exhibited excessive membrane blebbing (Kechad et al., 2012). Similarly, depletion of the septin, Peanut, did not cause furrow oscillations on its own, but it did slow the rate (and limited the full extent) of furrowing (Hickson and O'Farrell, 2008b; Kechad et al., 2012). These results argue that furrow oscillations (and by extension CR tension imbalance) induced by loss of Anillin cannot solely be due to a failure to coordinate anillo-septin assembly with actomyosin, and suggest that Anillin N-terminus-dependent scaffolding of actomyosin also plays a role in furrow stability and therefore tension regulation. Indeed, our prior work suggests that Citron kinase/Sticky contributes to this actomyosin-scaffolding role of the Anillin N-terminus, since Sticky is required for robust recruitment of Anillin-ΔC, and co-depletion of Sticky and the septin Peanut induced unstable furrows reminiscent of Anillin depletion, a phenotype not observed upon single depletions (El Amine et al., 2013). Therefore, Anillin plays a dual role in regulating furrow stability, by regulating both components of the tension balance: actomyosin contraction and intra-membrane resistance to compression.

Actomyosin crosslinking by the Anillin N-terminus may dampen actomyosin contractility at the CR front, so that loss of septin-mediated membrane removal (in the context of Anillin-ΔC) is better tolerated than full depletion of Anillin (less of a tension imbalance). Complete loss of Anillin should accordingly have both enhanced contractility and a reduced means to remove membrane. Failure to remove membrane also enhances contractility by reducing the ability of actomyosin to disassemble. This is consistent with the Anillin-depleted CRs being under the greatest tension and therefore the most prone to oscillation. However, we note that other interactions that Anillin participates in are likely also important for furrow stability, for example those with Tum/RacGAP50c, microtubules and importins (Sisson et al., 2000; D'Avino et al., 2008; Gregory et al., 2008; Hickson and O'Farrell, 2008a; Silverman-Gavrila et al., 2008; Beaudet et al., 2017, 2020).

MODEL SUMMARY

Stage 1: Actomyosin-Dependent CR Assembly

- Rho activation at the cell equator drives inward cortical flow of actomyosin-bound microdomains in the "perpendicular-to-the-ring" axis.
- Anillin is bound to actomyosin through its N-terminus (but not to the membrane).
- Cortical flow and contraction of actomyosin in the circumferential, "around-the-ring" axis compresses actomyosin-bound microdomains.
- Resistance to compression of the membrane microdomains generates tension.
- The CR "matures" at a certain density of microdomains, and threshold in tension, and shifts from the assembly stage to the closure/disassembly stage.

Stage 2: Actomyosin- and Anillo-Septin-Dependent CR Closure and Disassembly

- Localized compression of actomyosin triggers Anillin disengagement from actomyosin.
- Freed Anillin binds directly to Rho-GTP at the plasma membrane and recruits septins via its C-terminus. This occurs on a membrane microdomain transiently liberated by actomyosin.
- Newly assembled anillo-septin sequesters its membrane microdomain and incorporates into an anillo-septin filament growing in the "perpendicular-to-the-ring" axis.
- Anillo-septin-bound microdomains exit the CR as actomyosin-bound membrane microdomains squeeze past.
- Relative outflow of anillo-septin-bound microdomains releases tension, promotes actomyosin disassembly and allows CR closure.
- Ratchet-like cycles of actomyosin contraction coupled to anillo-septin-bound membrane outflow ensure CR closure and disassembly at the tension threshold.

DISCUSSION

Tension Generation Within the CR

Contractile rings must generate tension from forces acting in opposition to each other. The underlying mechanisms of tension generation at CRs have long been elusive, but most consideration has been paid to how the cytoskeletal elements of the CR interact with each other. The other key component of CRs, the plasma membrane itself, seems to have been overlooked as a significant potential contributor to tension generation (besides

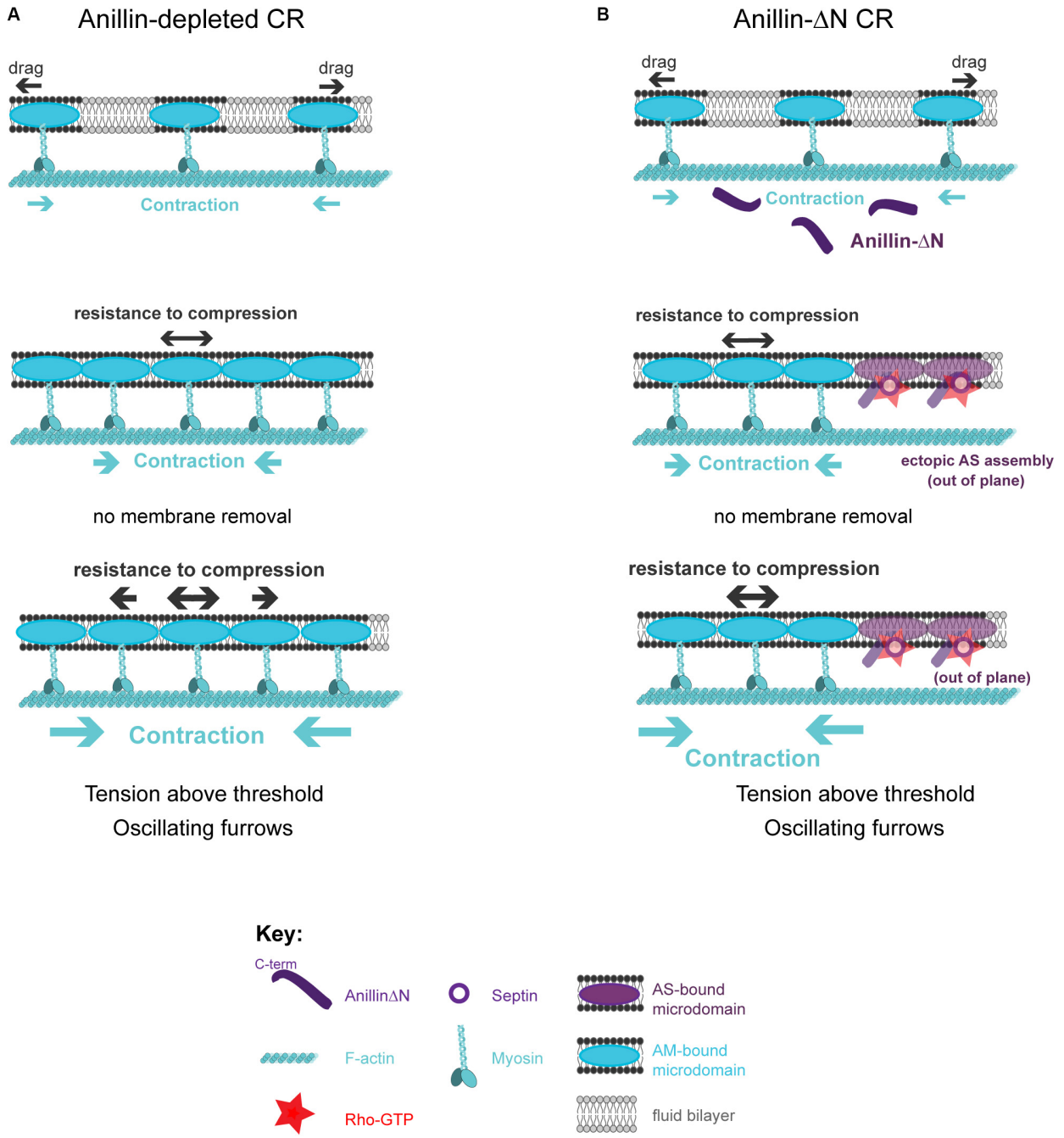

FIGURE 6 | How the proposed model can account for phenotypes observed upon loss of anillo-septin or its coupling to actomyosin. **(A)** Anillin-depleted CR. Actomyosin assembly and contractility persists and is able to gather and compress its own membrane microdomains. However, in the absence of anillo-septin to facilitate membrane microdomain outflow, CR closure stalls because the membrane microdomains impede it and actomyosin cannot disassemble. Tension mounts within the CR to above the usual threshold and this leads to furrow instability and oscillations in the "perpendicular-to-the-ring" axis. **(B)** Deletion of the Anillin N-terminus uncouples anillo-septin from actomyosin. Anillo-septin sequesters membrane, but in a manner that is no longer coupled to actomyosin contractility and at patches of cortex that already trail the CR. Disconnected from Anillin, actomyosin contracts without the means to regulate tension or its own disassembly because it cannot appropriately hand over membrane microdomains to anillo-septin for them to be removed, again leading to stalled CR closure, furrow instability and lateral oscillations.

drag forces) because of the pervasive assumption that membranes are always fluid and always readily deformable by the underlying cytoskeleton. While this assumption may be generally true in many contexts, we argue that it is categorically false in the case of the CR. Indeed, the central tenet of the current model is that the membrane of the CR is anything but compliant: it resists

compression by actomyosin contractility, thereby generating tension, and must be actively managed to permit CR closure. Tension generation during CR assembly results largely from the opposing forces of actomyosin contractility and intra-membrane resistance to compression, analogous to the tension holding a wine barrel together.

If CR tension is a balance between cytoskeletal contraction and intra-membrane resistance to compression, then Anillin appears to operate on both sides of that balance. It dampens contractility (both through scaffolding and promotion of depolymerization by membrane sequestration) and reduces resistance to compression of the membrane (through membrane outflow). Thus Anillin reduces the tension required for CR closure, acting like molecular grease. Without Anillin, higher tension results (and is needed) because of both high contractility and high resistance to compression.

This view might explain why different levels of Anillin either speed up or slow down CR closure in *C. elegans* zygotes, with intermediate levels promoting the fastest rate (Descovich et al., 2018). Different levels of Anillin might influence the two sides of the tension-balancing system slightly differently. *C. elegans* zygote CRs still complete ingression after anillo-septin depletion, but the rate of closure is slowed and higher levels of myosin are required (Maddox et al., 2007). Furthermore, this elevated myosin appears to spread more uniformly around the ring (Maddox et al., 2007). Thus, these anillo-septin-depleted CRs require more actomyosin contractility to close, presumably under higher tension. Anillo-septin depletion in the same cells also leads to enhanced recruitment of an F-actin probe to the CR (Jordan et al., 2016), which may reflect impaired actomyosin disassembly. Intriguingly, Anillo-septin depletion was also shown to rescue cytokinesis failure in temperature-sensitive formin mutants (Jordan et al., 2016). In light of our model, it is tempting to speculate that formin-deficient CRs might be defective at generating and maintaining tension when wild-type anillo-septin is present because the latter removes the CR membrane microdomains too effectively, causing tension to drop below a minimum threshold for CR closure. Conversely, anillo-septin depletion might allow formin-deficient CRs to close successfully by making them reliant on a less-effective mechanism of membrane removal, such that the defective actomyosin sub-network can now sustain enough tension to maintain CR integrity. Collectively, these data appear to support, and do not refute, the view that a balance between actomyosin-driven membrane compression and anillo-septin-dependent membrane removal are central to tension control within the CR, with the former sub-network building tension, the latter dissipating it.

The proposed intra-membrane resistance to compression can explain other diverse phenomena, such as why CRs isolated from fission yeast "ghosts" (permeabilized protoplasts lacking a cell wall) display sections of actomyosin that are not anchored to the membrane and that shorten at a rate 30 times faster than that of adjacent, membrane-anchored sections (Jochova et al., 1991; Mishra et al., 2013; Stachowiak et al., 2014; Wang and O'Shaughnessy, 2019). It also can explain why CR closure is much slower than one would predict from the velocities of load-free myosin *in vitro* (Stark et al., 2010; Mishra et al., 2013; Alonso-Matilla et al., 2019). In both cases, the intra-membrane resistance to compression of the CR-anchored membrane microdomains may impede actomyosin contractility.

The CR Is "*Consumed by Its Own Contractility*"

Once formed, how does a mature CR close? Again the poorly understood connections to the plasma membrane are seldom considered. However, Schroeder recognized their central importance and, based on the rapidity of the disruptive effects of the actin inhibitor cytochalasin B, surmised that "*individual filament-membrane attachments are firm but of brief duration*" (Schroeder, 1990). Schroeder also noted from his seminal electron microscopy studies that "*the furrow membrane neither folds nor buckles, and any microvilli in the furrow do not become especially concentrated, suggesting that they migrate out. Evidently, therefore, membrane "flows" or shears away from the bottom of the furrow out to the walls or shoulders, leaving the contractile ring behind. Somehow the contractile ring maintains its mechanical purchase on the membrane despite a "fluid" attachment*" (Schroeder, 1990). Our model is entirely consistent with Schroeder's visionary inferences: the Rho-dependent anillo-septin sub-network provides the means for the membrane attachment sites to flow out from the CR, thereby relaxing the tension built-up by actomyosin contractility. Our live imaging observations indicate that the actomyosin network can effectively "step over" the membrane-bound anillo-septin structures formed by the anillin C-terminus (Anillin-ΔN), since it neither drags them along as it oscillates, nor is it slowed down as it passes (Kechad et al., 2012; **Figure 2G**). This is consistent with dynamic on/off binding of the plasma membrane by actomyosin, which is also supported by the rapidity of the effects of actin drugs (Schroeder, 1972; Hickson and O'Farrell, 2008b), as well as numerous FRAP studies indicating that CR components turn over rapidly (seconds) (Guha et al., 2005; Murthy and Wadsworth, 2005; Uehara et al., 2010; Kondo et al., 2011; Beaudet et al., 2020). Indeed, at the mature CR we envision membrane microdomains shuttling from the actomyosin sub-network to the anillo-septin network, where they are sequestered and deposited behind the CR as it continues its onward journey, while closing at the same time. This proposed contraction-coupled outflow of anillo-septin-bound membrane microdomains finally provides a plausible mechanistic explanation for how the CR sheds its components (by bifurcated disassembly) and is "*consumed by its own contractility*" (Schroeder, 1972).

Composition of Membrane Microdomains and Protein Anchors

For the CR membrane attachment sites to be able to resist compression induced by actomyosin contractility and/or crosslinking they need to be of sufficient size and rigidity. We envision them as membrane microdomains, such as cholesterol- and sphingolipid-rich lipid rafts (Lingwood and Simons, 2010; Neto et al., 2011). Several observations suggest the importance of lipid rafts to cytokinesis: cholesterol and other raft components accumulate during cytokinesis (Ng et al., 2005; Atilla-Gokcumen

et al., 2014; Makino et al., 2015), and cytokinesis is impaired upon depletion of these components (Feng et al., 2002; Fernandez et al., 2004; Szafer-Glusman et al., 2008; Atilla-Gokcumen et al., 2011, 2014; Abe et al., 2012).

The phosphoinositide phosphatidyl-inositol (4,5) bisphosphate (PIP2) is a strong candidate receptor at the plasma membrane that is known to bind many components of the cortical cytoskeleton (Logan and Mandato, 2006). Although PIP2 localization to lipid rafts is still debated, PIP2 can form clusters with cations, basic peptides and other lipids (Wang et al., 2014; Brown, 2015), and has been observed in 64 nm wide membrane microdomains as measured by stochastic optical reconstruction microscopy (STORM) (Wang and Richards, 2012). PIP2 accumulates in the cleavage furrows of human cells (Field S.J. et al., 2005), in a manner that depends on cholesterol and sphingomyelin (Abe et al., 2012). Perturbing PIP2 through overexpression of PIP2-binding domains or PIP2 phosphatase decreased RhoA levels at the furrow and caused separation of F-actin from the plasma membrane, consistent with a role for PIP2 in anchoring the CR (Field S.J. et al., 2005; Abe et al., 2012).

Anillin and septins are known to bind to PIP2 (Tanaka-Takiguchi et al., 2009; Bertin et al., 2010; Liu et al., 2012). Conversely, the mechanisms by which actomyosin are anchored to the CR membrane are poorly understood, although myosin II can localize to the plasma membrane independently of F-actin and Anillin in fly and human cells (Dean et al., 2005; Kamijo et al., 2006; Hickson and O'Farrell, 2008b). PIP2 is an attractive candidate membrane component for binding both the actomyosin and anillo-septin sub-networks. However, it is also conceivable that different lipids/proteins within the microdomains, which are likely to have a heterogeneous composition (Neto et al., 2011; Echard, 2012; Atilla-Gokcumen et al., 2014), could bind different components of each sub-network (actomyosin versus anillo-septin) while still maintaining mutually exclusive binding. Despite the undoubted complexity of the lipid composition of the CR membrane (Neto et al., 2011; Echard, 2012; Atilla-Gokcumen et al., 2014), our model makes the simple prediction that, at the mature CR, discrete membrane microdomains switch from the actomyosin sub-network to the anillo-septin sub-network, allowing furrow advancement (in the "perpendicular-to-the-ring" axis) and CR closure (in the "around-the-ring" axis).

Although we refer to actomyosin as one entity for simplicity and clarity, this sub-network must itself be anchored to the membrane through at least two mechanisms: one for F-actin and one for myosin, and likely multiple others. Further elaboration of the concept will therefore require the consideration of additional microdomain attachments: for F-actin, myosin and anillo-septin. Rho-kinase and Citron kinase/Sticky are also present and presumably bound to the membrane, although the latter is not required for CR closure in *Drosophila* S2 cells, and nor is the former so long as myosin is active (Echard et al., 2004; Dean and Spudich, 2006; Hickson et al., 2006). The anillo-septin-independent mechanisms of membrane anchoring of actomyosin likely involve direct lipid binding in the case of myosin (Li et al., 1994; Murakami et al., 1994, 1995; Liu et al., 2016) and the formin, Diaphanous, in the case of F-actin (Ramalingam et al., 2010; Bucki et al., 2019). Diaphanous-related formins can bind and cluster PIP2 within cholesterol microdomains (Bucki et al., 2019). Other proteins may also participate as membrane anchors linking actomyosin to the plasma membrane independently of anillo-septin. Candidates include ezrin-radixin-moesin (ERM) family proteins that bind both F-actin and PIP2 and maintain cortical stability during mitosis and cytokinesis (Carreno et al., 2008; Roubinet et al., 2011; Kunda et al., 2012; Hiruma et al., 2017). Interestingly, Anillin depletion in human cells has been shown to enhance ERM localization to the furrow, although ERMs did not track well with the resulting oscillating furrows (Hiruma et al., 2017). Supervillin, which can bind F-actin, myosin and the plasma membrane, is another candidate auxilliary anchor protein that acts during cytokinesis (Pestonjamasp et al., 1995, 1997; Fang et al., 2010; Smith et al., 2010, 2013; Hiruma et al., 2017).

Anillo-Septin Regulation and Function

The proposed model has a number of implications regarding the regulation and function of Anillo-septin. Firstly, although Anillin is well known to bundle and cross-link actomyosin, this model highlights the fact that actomyosin crosslinking is not the only important role for Anillin at the CR. The robust and polymorphic interactions between Anillin and actomyosin (Field and Alberts, 1995; Straight et al., 2005; Jananji et al., 2017; Matsuda et al., 2020) also serve to ensure that Anillin molecules are always appropriately positioned at the right place and time to effectively sequester membrane microdomains from actomyosin at the CR to release tension. Anillin-actomyosin interactions are also important for regulating the later transition to the midbody ring, after CR closure, which is coupled to actin disassembly and requires the Anillin N-terminus (Kechad et al., 2012; El Amine et al., 2013).

Although septin−myosin interactions have been reported in human cells (Joo et al., 2007) and septin−actin interactions are clearly observed in *Drosophila* embryos and *in vitro* (Mavrakis et al., 2014), our observations and model suggest that, at least at the CR of S2 cells, septins are linked to F-actin and myosin only via Anillin, if at all. Septins are clearly not recruited to actomyosin rings depleted of Anillin in *Drosophila* S2 cells or *C. elegans* zygotes (Maddox et al., 2005, 2007; Hickson and O'Farrell, 2008b). Indeed, as elaborated above, we propose that Anillin is bound either to actomyosin or to septin, but not to both at the same time (at least at the mature CR). This may seem counter to observations in human cells, where Anillin has been shown to recruit septins to actin bundles (Kinoshita et al., 2002), but those cells were in interphase, the actin bundles cytoplasmic, and Rho was likely not involved. Clearly, further work is needed to understand the full complement of interactions between septins, actomyosin, and Anillin, and how Rho and membranes modulate them throughout cytokinetic progression.

Septins have been shown to bind preferentially to membranes of a positive, micron-scale curvature (Bridges et al., 2016; Beber et al., 2019; Cannon et al., 2019; McMurray, 2019). Although the CR undoubtedly harbor regions of changing membrane curvature, the Rho/Anillin-dependent recruitment of septins to the plasma membrane that we have observed occurs just as effectively in cells treated

with LatA (where no such curvature exists) as in cells with a constricting actomyosin ring. Indeed in LatA, Rho1, Anillin and septins form tubular structures that envelop themselves in membrane: i.e., that membrane becomes curved (Hickson and O'Farrell, 2008b). Perhaps Rho/Anillin binding induces septin rods and/or filaments to adopt a particular curvature that enhances membrane binding, while promoting higher-order assemblies capable of inducing membrane deformation?

We view the primary role of anillo-septin assembly as a robust mechanism to sequester membrane from actomyosin, opposing its contractility so that tension can be maintained around an optimal threshold. In cells treated with LatA (i.e., without tension), anillo-septin forms tubular structures (**Figures 2A,B**; Hickson and O'Farrell, 2008b). It seems most logical to consider that these structures represent unrestricted anillo-septin assembly forming supramolecular coils via septin polymerization at their base, zippering up membrane microdomains as they assemble. In the absence of F-actin, these putative coils represent the relaxed state of anillo-septin, like springs under zero tension. However, in the presence of F-actin, we envision that nascent anillo-septin filaments that trail the advancing CR to which they are connected are being stretched out under tension by the advancing CR, as depicted in **Figure 5C**. Accordingly, we predict that the anillo-septin filaments that project radially out from the CR accumulate stored energy and a spring-like quality, ready to recoil back up the flanks of the furrow upon disconnection from the CR front. Such a recoil mechanism could be dependent on anillo-septin filament length (and therefore age) since tension along the anillo-septin filament could increase with length (and age). Such a putative recoil mechanism would facilitate anillo-septin-dependent membrane microdomain removal from the closing CR, thereby promoting local reduction of tension in the "around-the-ring" axis. Tensile springs of anillo-septin filaments could also rigidify the furrow membrane and stabilize its ingression. This hypothetical mechanism can explain why the furrows of cells depleted of anillo-septin exhibit excessive membrane blebbing (Somma et al., 2002; Kechad et al., 2012; El Amine et al., 2013) and are prone to oscillation. It can also begin to explain our observations that anillo-septin drives the extrusion and shedding of plasma membrane tubules from the nascent midbody ring as the CR F-actin disassembles (El Amine et al., 2013).

Although our model predicts that actomyosin and anillo-septin are not directly connected with one another, an important concept arises in which the two sub-networks can influence one another indirectly through their underlying membrane microdomains. The radially organized, anillo-septin-bound membrane microdomains emanating from the CR into the flanks of the furrow should be relatively static (at least until the predicted outward recoil) and could therefore form the walls of channels within the lipid bilayer, through which actomyosin-anchored membrane microdomains can flow into the CR as they advance it (**Figure 5**). This concept seems relevant to the enigma of the hourglass-to-double ring transition of septin filaments that has been described for budding yeast CRs (Vrabioiu and Mitchison, 2006), and that is regulated by the anillin-like Bud4 (Ong et al., 2014; Chen X. et al., 2020). Intra-membrane flow of microdomains anchored to actomyosin CR components could help orient the differentially membrane-anchored septin filaments of the hourglass, while a reduction/cessation of that flow could allow a 90-degree rotation of the septin filaments to a "preferred" circumferential arrangement.

The Rho Network Micro-Manages Its Own Membrane Microdomain Attachment Sites

What makes the contraction-coupled membrane sorting model particularly compelling is that both actomyosin and anillo-septin sub-networks are directly controlled by the Rho GTPase. This means that the system can be wired to locally and intrinsically balance actomyosin contractility (which drives CR assembly) with relative anillo-septin membrane outflow (which drives CR disassembly and closure). However, this raises additional, intriguing questions regarding how the Rho GTPase might control the system.

A recent series of creative experiments using engineered chimeric proteins expressed at cell junctions and cleavage furrows of MCF-7 cells, has led Yap and colleagues to propose that the human Anillin AH domain is required to promote actomyosin activity by cyclically "resetting" Rho-GTP at the membrane, dynamically binding and releasing it, thereby prolonging its cortical residency in a manner that promotes activation of effectors for actomyosin assembly (Budnar et al., 2019; Munro, 2019; Morris et al., 2020). However, some aspects of that model appear incongruous with ours. Firstly, Anillin-depleted furrows do not appear to be defective in activating actomyosin effectors in *Drosophila* S2 cells (Hickson and O'Farrell, 2008b; Kechad et al., 2012), or HeLa cells (Straight et al., 2005; Zhao and Fang, 2005; Piekny and Glotzer, 2008). Secondly, actomyosin and anillo-septin (Anillin-ΔN) become so spatially segregated from one another (Piekny and Glotzer, 2008; Kechad et al., 2012) that it is difficult to imagine how they could share a pool of Rho as proposed by Budnar et al. In S2 cells, Rho1 is enriched in Anillin-ΔN structures, LatA-induced structures and in the anillo-septin-dependent membranes extruded from the nascent MR (Hickson and O'Farrell, 2008b; Kechad et al., 2012; El Amine et al., 2013). Although we have not directly monitored the Rho1 effectors Dia and Rok, one assumes they would track with actomyosin, which is excluded from the anillo-septin-specific structures.

Rather than Anillin sharing Rho1-GTP with effectors for actomyosin assembly, our model is more consistent with sequential transfer of Rho1 from actomyosin effectors to Anillin. This latter idea fits well with the current model's proposed sequential transfer of membrane microdomains from actomyosin to anillo-septin, but it rather implies that anillo-septin sequesters Rho1 and membrane away from actomyosin (but only after actomyosin has been activated and served its purpose).

Anillin reportedly binds Rho-GTP with much less affinity than other effectors (Blumenstein and Ahmadian, 2004; Sun et al., 2015), yet it is clearly very competent to access Rho-GTP at the equatorial membrane, even when many of its other modes

of recruitment are absent, as exemplified by Anillin-AHPH (Anillin C-terminus), which can no longer bind F-actin, myosin or Citron kinase/Sticky. The recruitment of the Anillin-AHPH is Rho-dependent and Anillin itself is required for the major fraction of detectable RhoA at the CR of human cells (Piekny et al., 2005; Piekny and Glotzer, 2008; Budnar et al., 2019). Thus perhaps Anillin sustains a pool of Rho-GTP and PIP2, as elegantly shown by Budnar et al. (2019), not so much to promote actomyosin activation, but rather to prolong the lifetime of the Anillo-septin sub-network itself, as it trails behind the advancing actomyosin. According to this view, Anillo-septin-bound Rho might reflect a temporal record of Rho activation, with "new" Rho-GTP closest to the CR and "old" Rho-GTP emanating further into the flanks of the furrow (rather like the vapor trails marking the passage of an aircraft). This can explain why furrow-associated Rho levels are much lower in cells depleted of Anillin (Piekny and Glotzer, 2008). Actomyosin contractility might persist in Anillin-depleted furrows, because actomyosin is ordinarily always activated first, ahead of Anillin. Anillin may then be positioned to accept the Rho-GTP, presumably as Anillin disengages from actomyosin and assembles onto the switching membrane microdomains. This view implies that Rho may be sequentially transferred through its different effectors, starting with the actomyosin activators and ending with anillo-septin. The RhoGEF ECT2/Pebble, which activates the entire Rho-dependent network, also needs to access the membrane to function (Kotynkova et al., 2016). A recent structural study indicates that allosteric binding of Rho-GTP to the ECT2 PH domain is needed to relieve autoinhibition on the adjacent DH domain and fully activate its GEF activity (Chen M. et al., 2020). Conceivably, as the "older" Rho-Anillo-septin network begins to break down (and/or is stretched out to a certain point prior to recoil), it could release some Rho-GTP to re-activate ECT2/Pebble and/or actomyosin. Thus Anillin-dependent prolongation of Rho-GTP lifetime, as shown by Budnar et al. (2019), could potentially act as a controlled-release mechanism to sustain an expanded Rho-zone behind the CR. This could help maintain the anillo-septin sub-network and boost cortical/membrane flow back in toward the CR to maintain the appropriate tension there. Anillin-dependent positive feedback on Rho activity has been proposed before (Piekny and Glotzer, 2008; Frenette et al., 2012; Budnar et al., 2019), but this putative time-resolved mechanism fits particularly well with the analogy that the CR comprises self-sustaining conveyor belts, or "caterpillar^{TM} tracks," of membrane microdomains that are continually flowing in (with actomyosin) and out (with anillo-septin) in the "perpendicular-to-the-ring" axis, with net loss of material from the CR front as it shrinks in the "around-the-ring" axis.

Membrane Growth During CR Closure

For cleavage furrows to ingress, the plasma membrane must "grow" inward toward the cell interior, yet where the membrane comes from and how the membrane growth occurs has been far from clear. There is an extensive body of literature suggesting that the addition of new membrane (i.e., from internal stores) is required for furrow ingression (Bluemink and de Laat, 1973; de Laat and Bluemink, 1974; Shuster and Burgess, 2002) and/or completion of cytokinesis (reviewed in Albertson et al., 2005; Prekeris and Gould, 2008; Neto et al., 2011; D'Avino et al., 2015; Fremont and Echard, 2018; Gerien and Wu, 2018). Membrane delivery by exocytosis can certainly occur in the flanks of the furrow to increase surface area, for example through polarized secretion via the exocyst complex (Giansanti et al., 2015). However, addition of membrane by exocytosis to the CR front seems incompatible with the density of components and tension there, and there is no good evidence for it (e.g., Schroeder's electron micrographs). Rather, we propose that the membrane ingresses in an orderly fashion by being physically reeled in by the contracting CR (in the "around-the-ring" axis), while being compressed by cortical flow (in the "perpendicular-to-the-ring" axis).

Implications for Controlling the Rate of CR Closure

A recent study of *C. elegans* zygote cytokinesis by Khaliullin et al. (2018) showed that CRs accelerate their per-unit-length constriction rate as they close, and in a manner that can be explained by an exponential increase in Rho network components (such as myosin and Anillin). Based on these experimental data and mathematical modeling a "constriction-coupled disassembly with compression feedback" model was proposed, in which actomyosin cortical flow promotes more cortical flow through positive feedback (Khaliullin et al., 2018). While bearing similarity to the current proposal in terms of cortex compression, that study did not consider the overlying plasma membrane, which is central to the proposed contraction-coupled membrane microdomain sorting model. This posits that actomyosin-driven membrane microdomain flow into the CR is balanced by relative outflow of anillo-septin-bound membrane microdomains, through tension-regulated membrane microdomain switching events (from actomyosin to anillo-septin). The membrane inflow promotes furrow advancement in the "perpendicular-to-the-ring" axis while relative outflow of promotes CR closure in the "around-the-ring" axis. Increased rates of per-unit-length constriction of the "around-the-ring" axis might therefore reflect more frequent membrane microdomain switching events occurring at higher tension (or at higher tension production potential). Such conditions might also cause microdomain switching events to occur further back into the "perpendicular-to-the-ring" axis, promoting faster removal of membrane in the "around-the-ring" axis and faster advancement in the perpendicular axis. The deposited anillo-septin may in turn promote additional cortical flow through releasing Rho-GTP in an expanded Rho-zone, while its underlying membrane domains provide conduits to channel actomyosin-bound membrane domains forward. We also note that centralspindlin, required to activate the RhoGEF Pebble/ECT2 at the membrane, becomes increasingly concentrated there as the furrow ingresses (see **Figure 3A**). This may also expand the Rho zone to accelerate the rate of CR closure.

It has also been shown in early *C. elegans* embryos that larger cells close their CRs at a faster rate than their smaller progeny, such that the total time of furrowing stays constant (Carvalho et al., 2009). Larger cells presumably have a greater pool of centralspindlin/ECT2 such that, as furrowing progresses, their spindles and furrows will accumulate a more concentrated bolus of the Rho activation machinery than smaller cells do. Larger cells may also build more tension in their CRs sooner than small cells because of a more expansive cortical network with which to fuel the cortical flow required for generating and sustaining tension.

Relevance to the Symmetry of CR Closure and Unilateral Furrows

A widespread property of CRs is their tendency to close asymmetrically, such that the center of the CR (viewed down the spindle/"perpendicular-to-the-ring" axis) is displaced during closure (Maddox et al., 2007). In the most extreme cases, unilateral furrows can ingress from one side of the cell before the CR is fully assembled (e.g., Rappaport and Conrad, 1963; Savoian et al., 1999). In *C. elegans* embryos, the asymmetry of closure was shown to require Anillin and septins (Maddox et al., 2007), since Anillin (ANI-1) or septin (UNC-59 and UNC-61) depletion led to symmetric closure. Furthermore, these anillo-septin-deficient CRs were shown to be sensitive to reductions in myosin levels/activity that are usually tolerated (Maddox et al., 2007). Myosin levels increase in anillo-septin-deficient rings (see Figure 3B in Maddox et al., 2007). Mathematical modeling has led to the suggestion that feedback among membrane curvature, cytoskeletal alignment, and contractility is responsible for asymmetric CR closure (Dorn et al., 2016). However, an alternative model has also been proposed in which radially asymmetric cortical flows account for the asymmetric closure (Menon et al., 2017). This model is supported by the observations that cortical flows are sufficient to align actin filaments in the circumferential, "around-the-ring" axis and are attenuated in anillin/ANI-1-depleted embryos (Reymann et al., 2016). Our observations and model are also consistent with this view and further predict that radially asymmetric outflow (i.e., non-uniform around the CR) of anillo-septin-membrane microdomains is a driving factor also, that should go hand-in-hand with asymmetric cortical inflow (actomyosin-dependent), since both are co-dependent on active Rho (Michaux et al., 2018). The tight coupling between actomyosin contraction and anillo-septin outflow could amplify any local asymmetries in Rho activation or in resistance within the membrane, or both since they are likely inter-dependent. In the case of a mature CR, if tension were evenly maintained throughout the ring (which is not necessarily the case), then membrane microdomains would only need to flow out of the region of least resistance to promote closure. And once outflow starts in a given region, the same region might continue to offer the least resistance leading to asymmetric closure of the CR.

The proposed membrane microdomain compression and sorting mechanism can accommodate conditions where there is no complete ring, such as rings cut with lasers, which recover and close (Silva et al., 2016), and unilateral furrows. Indeed, because the proposed tension regulation occurs on membrane microdomains that are compressed between those anchored to contracting actomyosin, it should be able to operate at any discrete region of cortex where Rho is locally activated. Indeed optogenetic activation of RhoA anywhere at the plasma membrane of HeLa cells is sufficient to initiate furrowing (Wagner and Glotzer, 2016), including unilateral furrowing (Kotynkova et al., 2016). The model supports the view that the CR should not really be considered as a single entity, but rather as a collection of (semi)-independent contractile modules that congregate into a ring and contract (semi)-autonomously yet in unison (Silva et al., 2016).

Relevance to Other Species and Processes

While mechanistic details likely exist between systems and species, we propose that regulated membrane microdomain micromanagement will be a conserved feature of CR assembly, tension regulation and closure. Indeed the concept of tension generation through cytoskeleton-regulated membrane microdomain compression may also be relevant to diverse, yet mechanistically related processes such as apical constriction and would healing. Apical constriction of epithelial cells proceeds via a ratchet-like mechanism driven by pulsed actomyosin contractions (Martin et al., 2009; Mason et al., 2013; Acharya et al., 2017). Epithelial wounds heal via contraction of a supracellular actomyosin cable that forms at the wound edges (Rothenberg and Fernandez-Gonzalez, 2019), and involves collaboration between actomyosin and septins (Shindo et al., 2018). Considering these processes from the perspective of the membrane microdomains to which the cytoskeleton is attached, as we have done here, will likely yield important mechanistic insight. Single-cell wound healing, as observed in *Xenopus* oocytes and syncytial *Drosophila* embryos (Bement et al., 1999, 2006; Abreu-Blanco et al., 2011), is another process particularly analogous to cytokinesis. After an initial rapid resealing of the ruptured plasma membrane by exocytosis, an actomyosin-based CR forms around the wound site, in a structure resembling the cartoon of **Figure 5B** (McNeil et al., 2000; Boucher and Mandato, 2015; Davenport et al., 2016). This CR then closes over several minutes, driven by cortical flow powered by an analogous Rho-dependent network. These CRs are under substantial tension as evidenced by the observation that flow-transported microtubules buckle and break as they slam into the CRs (Mandato and Bement, 2003). Yet, it remains unclear why the rings close so slowly, especially if the membrane is already sealed. In light of our model, it seems logical to suggest that the tension reflects resistance to compression of the underlying membrane microdomains that become jammed into a ring within the bilayer at the wound site. Accordingly, closure of these CRs could depend on an analogous sorting of membrane microdomains, allowing them to slide/jostle past one another and invade the virgin membrane (devoid of appropriate microdomains) that temporarily plugged the wound. Thus, we suggest that cytoskeletal micromanagement of membrane

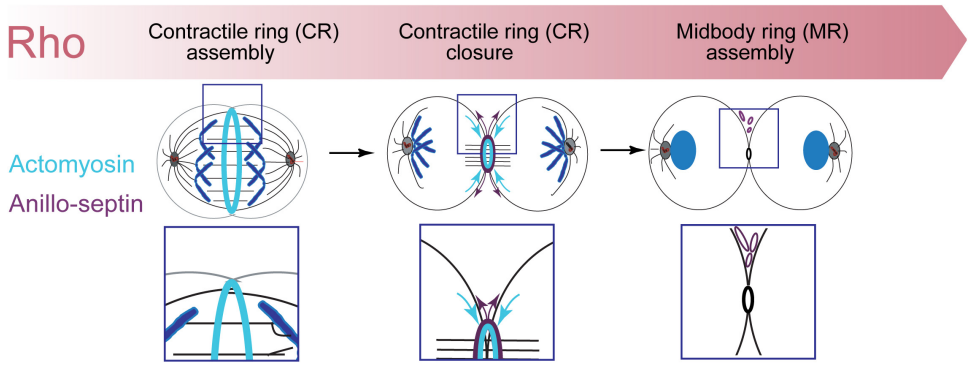

FIGURE 7 | The Rho-dependent network drives cytokinetic progression from CR assembly, through closure/disassembly and to midbody ring assembly.

microdomain attachment sites may be key for diverse contractile arrays beyond cytokinesis (Bement, 2002, Bement et al., 2006).

CONCLUSION

In summary, we propose that the widely accepted concept of the Rho-dependent actomyosin CR be extended to include the Rho-dependent actomyosin-anilloseptin, membrane-anchored ring (the AMAS ring), controlled by Rho and organized by Anillin. The AMAS ring buffers its own tension, building it through actomyosin gathering and compressing the CR's membrane microdomain attachment sites and releasing it through anillo-septin removing the CR's membrane microdomains. The AMAS ring has two stages: assembly and disassembly/closure. Assembly occurs by compressing membrane microdomains within the plane of the bilayer in the "perpendicular-to-the ring" axis, generating tension. Closure then occurs by bifurcated disassembly, whereby ratchet-like cycles of actomyosin contraction in the "around-the-ring" axis squeeze anillo-septin-bound microdomains out of the ring in the "perpendicular-to-the ring" axis, thereby regulating tension, reducing the circumference of the ring and promoting net depolymerization of actomyosin, all at the same time. Considering the dynamic properties of this more inclusive AMAS ring, which places crucial emphasis on the membrane microdomain attachment sites, provides a novel and detailed conceptual framework for understanding the inner workings of CRs. This concept needs to be rigorously tested using a variety of systems and techniques from cell biology to physics and mathematical modeling.

Finally, in considering the different Rho-dependent sub-networks (**Figure 1**), our observations also provide insight into the bigger picture view of how cytokinetic ring structures mature during successive stages of cytokinetic progression. The actomyosin sub-network drives CR assembly and closure, while the anillo-septin sub-network promotes CR closure and disassembly. Finally, an Anillin-Citron kinase sub-network promotes MR formation (**Figure 7**). Thus, maturation of the cell cortex during cytokinesis reflects a shifting importance of different sub-networks controlled by the master activator, Rho, and coordinated by the master organizer, Anillin. Mapping how these different sub-networks are integrated with one another throughout cytokinetic progression remains an important challenge.

DATA AVAILABILITY STATEMENT

All datasets generated for this study are included in the article.

AUTHOR CONTRIBUTIONS

GH wrote the manuscript, with significant input from SC and AK, who both contributed equally to the conceptualization and refinement of the proposed hypothesis and how it fits with published literature. GH and SC wrote the abstract. AK assembled the **Figures 1**, **7**. SC assembled the **Figures 2–6**. All authors read and edited the submitted version of the manuscript.

FUNDING

GH is a senior scholar of the FRQS and work in the lab has been supported by grants from Canadian Institutes for Health Research (CIHR) (MOP-97788), the Natural Sciences and Engineering Research Council (NSERC) (RGPIN-2014-05083), the Canadian Fund for Innovation (CFI), and the Cole Foundation. SC thanks Sainte-Justine Foundation for a postdoctoral fellowship. AK thanks Fonds de recherche du Québec – Santé (FRQS) for a doctoral fellowship.

ACKNOWLEDGMENTS

We thank past and present members of the Hickson lab, especially Silvana Jananji, Nour El-amine, and Denise Wernike for many discussions and work that has contributed to this work. GH thanks Jean-Claude Labbé, Greg Fitzharris, and Lia Paim for recent discussions and comments on an early draft of the manuscript, and Quynh Nguyen for inspiration while running. We regret not being able to cite all of the outstanding contributions by our colleagues in the field.

REFERENCES

Abe, M., Makino, A., Hullin-Matsuda, F., Kamijo, K., Ohno-Iwashita, Y., Hanada, K., et al. (2012). A role for sphingomyelin-rich lipid domains in the accumulation of phosphatidylinositol-4,5-bisphosphate to the cleavage furrow during cytokinesis. *Mol. Cell. Biol.* 32, 1396–1407. doi: 10.1128/mcb.06113-11

Abreu-Blanco, M. T., Verboon, J. M., and Parkhurst, S. M. (2011). Cell wound repair in Drosophila occurs through three distinct phases of membrane and cytoskeletal remodeling. *J. Cell Biol.* 193, 455–464. doi: 10.1083/jcb.201011018

Acharya, B. R., Wu, S. K., Lieu, Z. Z., Parton, R. G., Grill, S. W., Bershadsky, A. D., et al. (2017). Mammalian diaphanous 1 mediates a pathway for E-cadherin to stabilize epithelial barriers through junctional contractility. *Cell Rep.* 18, 2854–2867. doi: 10.1016/j.celrep.2017.02.078

Addi, C., Bai, J., and Echard, A. (2018). Actin, microtubule, septin and ESCRT filament remodeling during late steps of cytokinesis. *Curr. Opin. Cell Biol.* 50, 27–34. doi: 10.1016/j.ceb.2018.01.007

Albertson, R., Riggs, B., and Sullivan, W. (2005). Membrane traffic: a driving force in cytokinesis. *Trends Cell Biol.* 15, 92–101. doi: 10.1016/j.tcb.2004.12.008

Alonso-Matilla, R., Thiyagarajan, S., and O'Shaughnessy, B. (2019). Sliding filament and fixed filament mechanisms contribute to ring tension in the cytokinetic contractile ring. *Cytoskeleton* 76, 611–625. doi: 10.1002/cm.21558

Atilla-Gokcumen, G. E., Bedigian, A. V., Sasse, S., and Eggert, U. S. (2011). Inhibition of glycosphingolipid biosynthesis induces cytokinesis failure. *J. Am. Chem. Soc.* 133, 10010–10013. doi: 10.1021/ja202804b

Atilla-Gokcumen, G. E., Muro, E., Relat-Goberna, J., Sasse, S., Bedigian, A., Coughlin, M. L., et al. (2014). Dividing cells regulate their lipid composition and localization. *Cell* 156, 428–439. doi: 10.1016/j.cell.2013.12.015

Basant, A., and Glotzer, M. (2017). A GAP that divides. *F1000Res*. 6:1788. doi: 10.12688/f1000research.12064.1

Basant, A., and Glotzer, M. (2018). Spatiotemporal regulation of RhoA during cytokinesis. *Curr. Biol.* 28, R570–R580.

Bassi, Z. I., Audusseau, M., Riparbelli, M. G., Callaini, G., and D'Avino, P. P. (2013). Citron kinase controls a molecular network required for midbody formation in cytokinesis. *Proc. Natl. Acad. Sci. U.S.A.* 110, 9782–9787. doi: 10.1073/pnas.1301328110

Bassi, Z. I., Verbrugghe, K. J., Capalbo, L., Gregory, S., Montembault, E., Glover, D. M., et al. (2011). Sticky/Citron kinase maintains proper RhoA localization at the cleavage site during cytokinesis. *J. Cell Biol.* 195, 595–603. doi: 10.1083/jcb.201105136

Bastos, R. N., Penate, X., Bates, M., Hammond, D., and Barr, F. A. (2012). CYK4 inhibits Rac1-dependent PAK1 and ARHGEF7 effector pathways during cytokinesis. *J. Cell Biol.* 198, 865–880. doi: 10.1083/jcb.201204107

Beaudet, D., Akhshi, T., Phillipp, J., Law, C., and Piekny, A. (2017). Active Ran regulates anillin function during cytokinesis. *Mol. Biol. Cell* 28, 3517–3531. doi: 10.1091/mbc.e17-04-0253

Beaudet, D., Pham, N., Skaik, N., and Piekny, A. (2020). Importin binding mediates the intramolecular regulation of anillin during cytokinesis. *Mol. Biol. Cell* 31, 1124–1139. doi: 10.1091/mbc.e20-01-0006

Beber, A., Taveneau, C., Nania, M., Tsai, F. C., Di Cicco, A., Bassereau, P., et al. (2019). Membrane reshaping by micrometric curvature sensitive septin filaments. *Nat. Commun.* 10:420.

Bement, W. M. (2002). Actomyosin rings: the riddle of the sphincter. *Curr. Biol.* 12, R12–R14.

Bement, W. M., Benink, H. A., and von Dassow, G. (2005). A microtubule-dependent zone of active RhoA during cleavage plane specification. *J. Cell Biol.* 170, 91–101. doi: 10.1083/jcb.200501131

Bement, W. M., Leda, M., Moe, A. M., Kita, A. M., Larson, M. E., Golding, A. E., et al. (2015). Activator-inhibitor coupling between Rho signalling and actin assembly makes the cell cortex an excitable medium. *Nat. Cell Biol.* 17, 1471–1483. doi: 10.1038/ncb3251

Bement, W. M., Mandato, C. A., and Kirsch, M. N. (1999). Wound-induced assembly and closure of an actomyosin purse string in Xenopus oocytes. *Curr. Biol.* 9, 579–587. doi: 10.1016/s0960-9822(99)80261-9

Bement, W. M., Miller, A. L., and von Dassow, G. (2006). Rho GTPase activity zones and transient contractile arrays. *Bioessays* 28, 983–993. doi: 10.1002/bies.20477

Bertin, A., McMurray, M. A., Thai, L., Garcia, G. III, Votin, V., Grob, P., et al. (2010). Phosphatidylinositol-4,5-bisphosphate promotes budding yeast septin filament assembly and organization. *J. Mol. Biol.* 404, 711–731. doi: 10.1016/j.jmb.2010.10.002

Bidone, T. C., Tang, H., and Vavylonis, D. (2014). Dynamic network morphology and tension buildup in a 3D model of cytokinetic ring assembly. *Biophys. J.* 107, 2618–2628. doi: 10.1016/j.bpj.2014.10.034

Bluemink, J. G., and de Laat, S. W. (1973). New membrane formation during cytokinesis in normal and cytochalasin B-treated eggs of *Xenopus laevis*. I. Electron microscope observations. *J. Cell Biol.* 59, 89–108. doi: 10.1083/jcb.59.1.89

Blumenstein, L., and Ahmadian, M. R. (2004). Models of the cooperative mechanism for Rho effector recognition: implications for RhoA-mediated effector activation. *J. Biol. Chem.* 279, 53419–53426. doi: 10.1074/jbc.m409551200

Boucher, E., and Mandato, C. A. (2015). Plasma membrane and cytoskeleton dynamics during single-cell wound healing. *Biochim. Biophys. Acta* 1853, 2649–2661. doi: 10.1016/j.bbamcr.2015.07.012

Bridges, A. A., and Gladfelter, A. S. (2015). Septin form and function at the cell cortex. *J. Biol. Chem.* 290, 17173–17180. doi: 10.1074/jbc.r114.634444

Bridges, A. A., Jentzsch, M. S., Oakes, P. W., Occhipinti, P., and Gladfelter, A. S. (2016). Micron-scale plasma membrane curvature is recognized by the septin cytoskeleton. *J. Cell Biol.* 213, 23–32. doi: 10.1083/jcb.201512029

Brown, D. A. (2015). PIP2Clustering: from model membranes to cells. *Chem. Phys. Lipids* 192, 33–40. doi: 10.1016/j.chemphyslip.2015.07.021

Bucki, R., Wang, Y. H., Yang, C., Kandy, S. K., Fatunmbi, O., Bradley, R., et al. (2019). Lateral distribution of phosphatidylinositol 4,5-bisphosphate in membranes regulates formin- and ARP2/3-mediated actin nucleation. *J. Biol. Chem.* 294, 4704–4722. doi: 10.1074/jbc.ra118.005552

Budnar, S., Husain, K. B., Gomez, G. A., Naghibosadat, M., Varma, A., Verma, S., et al. (2019). Anillin promotes cell contractility by cyclic resetting of RhoA residence kinetics. *Dev. Cell* 49, 894–906.e12.

Byers, B., and Goetsch, L. (1976). A highly ordered ring of membrane-associated filaments in budding yeast. *J. Cell Biol.* 69, 717–721. doi: 10.1083/jcb.69.3.717

Canman, J. C., Lewellyn, L., Laband, K., Smerdon, S. J., Desai, A., Bowerman, B., et al. (2008). Inhibition of Rac by the GAP activity of centralspindlin is essential for cytokinesis. *Science* 322, 1543–1546. doi: 10.1126/science.1163086

Cannon, K. S., Woods, B. L., Crutchley, J. M., and Gladfelter, A. S. (2019). An amphipathic helix enables septins to sense micrometer-scale membrane curvature. *J. Cell Biol.* 218, 1128–1137. doi: 10.1083/jcb.201807211

Carlton, J. G., and Martin-Serrano, J. (2007). Parallels between cytokinesis and retroviral budding: a role for the ESCRT machinery. *Science* 316, 1908–1912. doi: 10.1126/science.1143422

Carreno, S., Kouranti, I., Glusman, E. S., Fuller, M. T., Echard, A., and Payre, F. (2008). Moesin and its activating kinase Slik are required for cortical stability and microtubule organization in mitotic cells. *J. Cell Biol.* 180, 739–746. doi: 10.1083/jcb.200709161

Carvalho, A., Desai, A., and Oegema, K. (2009). Structural memory in the contractile ring makes the duration of cytokinesis independent of cell size. *Cell* 137, 926–937. doi: 10.1016/j.cell.2009.03.021

Castrillon, D. H., and Wasserman, S. A. (1994). Diaphanous is required for cytokinesis in Drosophila and shares domains of similarity with the products of the limb deformity gene. *Development* 120, 3367–3377.

Caudron, F., and Barral, Y. (2009). Septins and the lateral compartmentalization of eukaryotic membranes. *Dev. Cell* 16, 493–506. doi: 10.1016/j.devcel.2009.04.003

Chen, A., Arora, P. D., McCulloch, C. A., and Wilde, A. (2017). Cytokinesis requires localized beta-actin filament production by an actin isoform specific nucleator. *Nat. Commun.* 8:1530.

Chen, M., Pan, H., Sun, L., Shi, P., Zhang, Y., Li, L., et al. (2020). Structure and regulation of human epithelial cell transforming 2 protein. *Proc. Natl. Acad. Sci. U.S.A.* 117, 1027–1035. doi: 10.1073/pnas.1913054117

Chen, X., Wang, K., Svitkina, T., and Bi, E. (2020). Critical Roles of a RhoGEF-Anillin module in septin architectural remodeling during cytokinesis. *Curr. Biol.* 30, 1477–1490.e3.

Davenport, N. R., Sonnemann, K. J., Eliceiri, K. W., and Bement, W. M. (2016). Membrane dynamics during cellular wound repair. *Mol. Biol. Cell* 27, 2272–2285. doi: 10.1091/mbc.e16-04-0223

D'Avino, P. P. (2009). How to scaffold the contractile ring for a safe cytokinesis - lessons from Anillin-related proteins. *J. Cell Sci.* 122, 1071–1079. doi: 10.1242/jcs.034785

D'Avino, P. P. (2017). Citron kinase - renaissance of a neglected mitotic kinase. *J. Cell Sci.* 130, 1701–1708. doi: 10.1242/jcs.200253

D'Avino, P. P., Giansanti, M. G., and Petronczki, M. (2015). Cytokinesis in animal cells. *Cold Spring Harb. Perspect. Biol.* 7:a015834.

D'Avino, P. P., Savoian, M. S., and Glover, D. M. (2004). Mutations in sticky lead to defective organization of the contractile ring during cytokinesis and are enhanced by Rho and suppressed by Rac. *J. Cell Biol.* 166, 61–71. doi: 10.1083/jcb.200402157

D'Avino, P. P., Takeda, T., Capalbo, L., Zhang, W., Lilley, K. S., Laue, E. D., et al. (2008). Interaction between Anillin and RacGAP50C connects the actomyosin contractile ring with spindle microtubules at the cell division site. *J. Cell Sci.* 121, 1151–1158. doi: 10.1242/jcs.026716

de Laat, W. S., and Bluemink, J. G. (1974). New membrane formation during cytokinesis in normal and cytochalasin B-treated eggs of *Xenopus laevis*. II. Electrophysiological observations. *J. Cell Biol.* 60, 529–540. doi: 10.1083/jcb.60.3.529

Dean, S. O., Rogers, S. L., Stuurman, N., Vale, R. D., and Spudich, J. A. (2005). Distinct pathways control recruitment and maintenance of myosin II at the cleavage furrow during cytokinesis. *Proc. Natl. Acad. Sci. U.S.A.* 102, 13473–13478. doi: 10.1073/pnas.0506810102

Dean, S. O., and Spudich, J. A. (2006). Rho kinase's role in myosin recruitment to the equatorial cortex of mitotic Drosophila S2 cells is for myosin regulatory light chain phosphorylation. *PLoS One* 1:e131. doi: 10.1371/journal.pone.0000131

Dema, A., Macaluso, F., Sgro, F., Berto, G. E., Bianchi, F. T., Chiotto, A. A., et al. (2018). Citron kinase-dependent F-actin maintenance at midbody secondary ingression sites mediates abscission. *J. Cell Sci.* 131:jcs209080. doi: 10.1242/jcs.209080

Descovich, C. P., Cortes, D. B., Ryan, S., Nash, J., Zhang, L., Maddox, P. S., et al. (2018). Cross-linkers both drive and brake cytoskeletal remodeling and furrowing in cytokinesis. *Mol. Biol. Cell* 29, 622–631. doi: 10.1091/mbc.e17-06-0392

Di Cunto, F., Calautti, E., Hsiao, J., Ong, L., Topley, G., Turco, E., et al. (1998). Citron rho-interacting kinase, a novel tissue-specific ser/thr kinase encompassing the Rho-Rac-binding protein Citron. *J. Biol. Chem.* 273, 29706–29711. doi: 10.1074/jbc.273.45.29706

Di Cunto, F., Imarisio, S., Camera, P., Boitani, C., Altruda, F., and Silengo, L. (2002). Essential role of citron kinase in cytokinesis of spermatogenic precursors. *J. Cell Sci.* 115, 4819–4826. doi: 10.1242/jcs.00163

Dobbelaere, J., and Barral, Y. (2004). Spatial coordination of cytokinetic events by compartmentalization of the cell cortex. *Science* 305, 393–396. doi: 10.1126/science.1099892

Dorn, J. F., Zhang, L., Phi, T. T., Lacroix, B., Maddox, P. S., Liu, J., et al. (2016). A theoretical model of cytokinesis implicates feedback between membrane curvature and cytoskeletal organization in asymmetric cytokinetic furrowing. *Mol. Biol. Cell* 27, 1286–1299. doi: 10.1091/mbc.e15-06-0374

Drechsel, D. N., Hyman, A. A., Hall, A., and Glotzer, M. (1997). A requirement for Rho and Cdc42 during cytokinesis in Xenopus embryos. *Curr. Biol.* 7, 12–23. doi: 10.1016/s0960-9822(06)00023-6

Dubreuil, V., Marzesco, A. M., Corbeil, D., Huttner, W. B., and Wilsch-Brauninger, M. (2007). Midbody and primary cilium of neural progenitors release extracellular membrane particles enriched in the stem cell marker prominin-1. *J. Cell Biol.* 176, 483–495. doi: 10.1083/jcb.200608137

Echard, A. (2012). Phosphoinositides and cytokinesis: the "PIP" of the iceberg. *Cytoskeleton* 69, 893–912. doi: 10.1002/cm.21067

Echard, A., Hickson, G. R., Foley, E., and O'Farrell, P. H. (2004). Terminal cytokinesis events uncovered after an RNAi screen. *Curr. Biol.* 14, 1685–1693. doi: 10.1016/j.cub.2004.08.063

Eda, M., Yonemura, S., Kato, T., Watanabe, N., Ishizaki, T., Madaule, P., et al. (2001). Rho-dependent transfer of Citron-kinase to the cleavage furrow of dividing cells. *J. Cell Sci.* 114, 3273–3284.

Eggert, U. S., Mitchison, T. J., and Field, C. M. (2006). Animal cytokinesis: from parts list to mechanisms. *Annu. Rev. Biochem.* 75, 543–566. doi: 10.1146/annurev.biochem.74.082803.133425

El Amine, N., Kechad, A., Jananji, S., and Hickson, G. R. (2013). Opposing actions of septins and Sticky on Anillin promote the transition from contractile to midbody ring. *J. Cell Biol.* 203, 487–504. doi: 10.1083/jcb.201305053

El-Amine, N., Carim, S. C., Wernike, D., and Hickson, G. R. X. (2019). Rho-dependent control of the Citron kinase. Sticky, drives midbody ring maturation. *Mol. Biol. Cell* 30, 2185–2204. doi: 10.1091/mbc.e19-04-0194

Elia, N., Sougrat, R., Spurlin, T. A., Hurley, J. H., and Lippincott-Schwartz, J. (2011). Dynamics of endosomal sorting complex required for transport (ESCRT) machinery during cytokinesis and its role in abscission. *Proc. Natl. Acad. Sci. U.S.A.* 108, 4846–4851. doi: 10.1073/pnas.1102714108

Fang, Z., Takizawa, N., Wilson, K. A., Smith, T. C., Delprato, A., Davidson, M. W., et al. (2010). The membrane-associated protein, supervillin, accelerates F-actin-dependent rapid integrin recycling and cell motility. *Traffic* 11, 782–799. doi: 10.1111/j.1600-0854.2010.01062.x

Feng, B., Schwarz, H., and Jesuthasan, S. (2002). Furrow-specific endocytosis during cytokinesis of zebrafish blastomeres. *Exp. Cell Res.* 279, 14–20. doi: 10.1006/excr.2002.5579

Fernandez, C., Lobo Md Mdel, V., Gomez-Coronado, D., and Lasuncion, M. A. (2004). Cholesterol is essential for mitosis progression and its deficiency induces polyploid cell formation. *Exp. Cell Res.* 300, 109–120. doi: 10.1016/j.yexcr.2004.06.029

Field, C. M., al-Awar, O., Rosenblatt, J., Wong, M. L., Alberts, B., and Mitchison, T. J. (1996). A purified Drosophila septin complex forms filaments and exhibits GTPase activity. *J. Cell Biol.* 133, 605–616. doi: 10.1083/jcb.133.3.605

Field, C. M., and Alberts, B. M. (1995). Anillin, a contractile ring protein that cycles from the nucleus to the cell cortex. *J. Cell Biol.* 131, 165–178. doi: 10.1083/jcb.131.1.165

Field, C. M., Coughlin, M., Doberstein, S., Marty, T., and Sullivan, W. (2005). Characterization of anillin mutants reveals essential roles in septin localization and plasma membrane integrity. *Development* 132, 2849–2860. doi: 10.1242/dev.01843

Field, S. J., Madson, N., Kerr, M. L., Galbraith, K. A., Kennedy, C. E., Tahiliani, M., et al. (2005). PtdIns(4,5)P2 functions at the cleavage furrow during cytokinesis. *Curr. Biol.* 15, 1407–1412. doi: 10.1016/j.cub.2005.06.059

Fishkind, D. J., and Wang, Y. L. (1993). Orientation and three-dimensional organization of actin filaments in dividing cultured cells. *J. Cell Biol.* 123, 837–848. doi: 10.1083/jcb.123.4.837

Fremont, S., and Echard, A. (2018). Membrane traffic in the late steps of cytokinesis. *Curr. Biol.* 28, R458–R470.

Frenette, P., Haines, E., Loloyan, M., Kinal, M., Pakarian, P., and Piekny, A. (2012). An anillin-Ect2 complex stabilizes central spindle microtubules at the cortex during cytokinesis. *PLoS One* 7:e34888. doi: 10.1371/journal.pone.0034888

Fujiwara, K., and Pollard, T. D. (1976). Fluorescent antibody localization of myosin in the cytoplasm, cleavage furrow, and mitotic spindle of human cells. *J. Cell Biol.* 71, 848–875. doi: 10.1083/jcb.71.3.848

Gai, M., Camera, P., Dema, A., Bianchi, F., Berto, G., Scarpa, E., et al. (2011). Citron kinase controls abscission through RhoA and anillin. *Mol. Biol. Cell* 22, 3768–3778. doi: 10.1091/mbc.e10-12-0952

Gerien, K. S., and Wu, J. Q. (2018). Molecular mechanisms of contractile-ring constriction and membrane trafficking in cytokinesis. *Biophys. Rev.* 10, 1649–1666. doi: 10.1007/s12551-018-0479-3

Giansanti, M. G., Bonaccorsi, S., and Gatti, M. (1999). The role of anillin in meiotic cytokinesis of Drosophila males. *J. Cell Sci.* 112(Pt 14), 2323–2334.

Giansanti, M. G., Vanderleest, T. E., Jewett, C. E., Sechi, S., Frappaolo, A., Fabian, L., et al. (2015). Exocyst-dependent membrane addition is required for anaphase cell elongation and cytokinesis in Drosophila. *PLoS Genet.* 11:e1005632. doi: 10.1371/journal.pgen.1005632

Gilden, J., and Krummel, M. F. (2010). Control of cortical rigidity by the cytoskeleton: emerging roles for septins. *Cytoskeleton* 67, 477–486.

Glotzer, M. (2009). The 3Ms of central spindle assembly: microtubules, motors and MAPs. *Nat. Rev. Mol. Cell Biol.* 10, 9–20. doi: 10.1038/nrm2609

Glotzer, M. (2017). Cytokinesis in Metazoa and Fungi. *Cold Spring Harb. Perspect. Biol.* 9:a022343. doi: 10.1101/cshperspect.a022343

Goldbach, P., Wong, R., Beise, N., Sarpal, R., Trimble, W. S., and Brill, J. A. (2010). Stabilization of the actomyosin ring enables spermatocyte cytokinesis in Drosophila. *Mol. Biol. Cell* 21, 1482–1493. doi: 10.1091/mbc.e09-08-0714

Golding, A. E., Visco, I., Bieling, P., and Bement, W. M. (2019). Extraction of active RhoGTPases by RhoGDI regulates spatiotemporal patterning of RhoGTPases. *eLife* 8:e50471.

Green, R. A., Paluch, E., and Oegema, K. (2012). Cytokinesis in animal cells. *Annu. Rev. Cell Dev. Biol.* 28, 29–58.

Gregory, S. L., Ebrahimi, S., Milverton, J., Jones, W. M., Bejsovec, A., and Saint, R. (2008). Cell division requires a direct link between microtubule-bound RacGAP and Anillin in the contractile ring. *Curr. Biol.* 18, 25–29. doi: 10.1016/j.cub.2007.11.050

Guha, M., Zhou, M., and Wang, Y. L. (2005). Cortical actin turnover during cytokinesis requires myosin II. *Curr. Biol.* 15, 732–736. doi: 10.1016/j.cub.2005.03.042

Guizetti, J., Schermelleh, L., Mantler, J., Maar, S., Poser, I., Leonhardt, H., et al. (2011). Cortical constriction during abscission involves helices of ESCRT-III-dependent filaments. *Science* 331, 1616–1620. doi: 10.1126/science.1201847

Haarer, B. K., and Pringle, J. R. (1987). Immunofluorescence localization of the *Saccharomyces cerevisiae* CDC12 gene product to the vicinity of the 10-nm filaments in the mother-bud neck. *Mol. Cell. Biol.* 7, 3678–3687. doi: 10.1128/mcb.7.10.3678

Hickson, G. R., Echard, A., and O'Farrell, P. H. (2006). Rho-kinase controls cell shape changes during cytokinesis. *Curr. Biol.* 16, 359–370. doi: 10.1016/j.cub.2005.12.043

Hickson, G. R., and O'Farrell, P. H. (2008a). Anillin: a pivotal organizer of the cytokinetic machinery. *Biochem. Soc. Trans.* 36, 439–441. doi: 10.1042/bst0360439

Hickson, G. R., and O'Farrell, P. H. (2008b). Rho-dependent control of anillin behavior during cytokinesis. *J. Cell Biol.* 180, 285–294. doi: 10.1083/jcb.200709005

Hiruma, S., Kamasaki, T., Otomo, K., Nemoto, T., and Uehara, R. (2017). Dynamics and function of ERM proteins during cytokinesis in human cells. *FEBS Lett.* 591, 3296–3309. doi: 10.1002/1873-3468.12844

Hu, C. K., Coughlin, M., and Mitchison, T. J. (2012). Midbody assembly and its regulation during cytokinesis. *Mol. Biol. Cell* 23, 1024–1034. doi: 10.1091/mbc.e11-08-0721

Jananji, S., Risi, C., Lindamulage, I. K. S., Picard, L. P., Van Sciver, R., Laflamme, G., et al. (2017). Multimodal and Polymorphic Interactions between Anillin and Actin: their Implications for Cytokinesis. *J. Mol. Biol.* 429, 715–731. doi: 10.1016/j.jmb.2017.01.020

Jantsch-Plunger, V., Gonczy, P., Romano, A., Schnabel, H., Hamill, D., Schnabel, R., et al. (2000). CYK-4: a Rho family gtpase activating protein (GAP) required for central spindle formation and cytokinesis. *J. Cell Biol.* 149, 1391–1404.

Jochova, J., Rupes, I., and Streiblova, E. (1991). F-actin contractile rings in protoplasts of the yeast Schizosaccharomyces. *Cell. Biol. Int. Rep.* 15, 607–610. doi: 10.1016/0309-1651(91)90007-6

Joo, E., Surka, M. C., and Trimble, W. S. (2007). Mammalian SEPT2 is required for scaffolding nonmuscle myosin II and its kinases. *Dev. Cell* 13, 677–690. doi: 10.1016/j.devcel.2007.09.001

Jordan, S. N., Davies, T., Zhuravlev, Y., Dumont, J., Shirasu-Hiza, M., and Canman, J. C. (2016). Cortical PAR polarity proteins promote robust cytokinesis during asymmetric cell division. *J. Cell Biol.* 212, 39–49. doi: 10.1083/jcb.201510063

Kamasaki, T., Osumi, M., and Mabuchi, I. (2007). Three-dimensional arrangement of F-actin in the contractile ring of fission yeast. *J. Cell Biol.* 178, 765–771. doi: 10.1083/jcb.200612018

Kamijo, K., Ohara, N., Abe, M., Uchimura, T., Hosoya, H., Lee, J. S., et al. (2006). Dissecting the role of Rho-mediated signaling in contractile ring formation. *Mol. Biol. Cell* 17, 43–55. doi: 10.1091/mbc.e05-06-0569

Kawano, Y., Fukata, Y., Oshiro, N., Amano, M., Nakamura, T., Ito, M., et al. (1999). Phosphorylation of myosin-binding subunit (MBS) of myosin phosphatase by Rho-kinase *in vivo*. *J. Cell Biol.* 147, 1023–1038. doi: 10.1083/jcb.147.5.1023

Kechad, A., Jananji, S., Ruella, Y., and Hickson, G. R. (2012). Anillin acts as a bifunctional linker coordinating midbody ring biogenesis during cytokinesis. *Curr. Biol.* 22, 197–203. doi: 10.1016/j.cub.2011.11.062

Khaliullin, R. N., Green, R. A., Shi, L. Z., Gomez-Cavazos, J. S., Berns, M. W., Desai, A., et al. (2018). A positive-feedback-based mechanism for constriction rate acceleration during cytokinesis in *Caenorhabditis elegans*. *eLife* 7:e36073.

Kimura, K., Tsuji, T., Takada, Y., Miki, T., and Narumiya, S. (2000). Accumulation of GTP-bound RhoA during cytokinesis and a critical role of ECT2 in this accumulation. *J. Biol. Chem.* 275, 17233–17236. doi: 10.1074/jbc.c000212200

Kinoshita, M., Field, C. M., Coughlin, M. L., Straight, A. F., and Mitchison, T. J. (2002). Self- and actin-templated assembly of Mammalian septins. *Dev. Cell* 3, 791–802. doi: 10.1016/s1534-5807(02)00366-0

Kondo, T., Hamao, K., Kamijo, K., Kimura, H., Morita, M., Takahashi, M., et al. (2011). Enhancement of myosin II/actin turnover at the contractile ring induces slower furrowing in dividing HeLa cells. *Biochem. J.* 435, 569–576. doi: 10.1042/bj20100837

Kosako, H., Goto, H., Yanagida, M., Matsuzawa, K., Fujita, M., Tomono, Y., et al. (1999). Specific accumulation of Rho-associated kinase at the cleavage furrow during cytokinesis: cleavage furrow-specific phosphorylation of intermediate filaments. *Oncogene* 18, 2783–2788. doi: 10.1038/sj.onc.1202633

Kosako, H., Yoshida, T., Matsumura, F., Ishizaki, T., Narumiya, S., and Inagaki, M. (2000). Rho-kinase/ROCK is involved in cytokinesis through the phosphorylation of myosin light chain and not ezrin/radixin/moesin proteins at the cleavage furrow. *Oncogene* 19, 6059–6064. doi: 10.1038/sj.onc.1203987

Kotynkova, K., Su, K. C., West, S. C., and Petronczki, M. (2016). Plasma Membrane Association but Not Midzone Recruitment of RhoGEF ECT2 Is Essential for Cytokinesis. *Cell Rep.* 17, 2672–2686. doi: 10.1016/j.celrep.2016.11.029

Kunda, P., Rodrigues, N. T., Moeendarbary, E., Liu, T., Ivetic, A., Charras, G., et al. (2012). PP1-mediated moesin dephosphorylation couples polar relaxation to mitotic exit. *Curr. Biol.* 22, 231–236. doi: 10.1016/j.cub.2011.12.016

Lehner, C. F. (1992). The pebble gene is required for cytokinesis in Drosophila. *J. Cell Sci.* 103(Pt 4), 1021–1030.

Leite, J., Osorio, D. S., Sobral, A. F., Silva, A. M., and Carvalho, A. X. (2019). Network contractility during cytokinesis-from molecular to global views. *Biomolecules* 9:194. doi: 10.3390/biom9050194

Li, D., Miller, M., and Chantler, P. D. (1994). Association of a cellular myosin II with anionic phospholipids and the neuronal plasma membrane. *Proc. Natl. Acad. Sci. U.S.A.* 91, 853–857. doi: 10.1073/pnas.91.3.853

Lingwood, D., and Simons, K. (2010). Lipid rafts as a membrane-organizing principle. *Science* 327, 46–50. doi: 10.1126/science.1174621

Liu, J., Fairn, G. D., Ceccarelli, D. F., Sicheri, F., and Wilde, A. (2012). Cleavage furrow organization requires PIP(2)-mediated recruitment of anillin. *Curr. Biol.* 22, 64–69. doi: 10.1016/j.cub.2011.11.040

Liu, X., Shu, S., Billington, N., Williamson, C. D., Yu, S., Brzeska, H., et al. (2016). Mammalian Nonmuscle Myosin II Binds to Anionic Phospholipids with Concomitant Dissociation of the Regulatory Light Chain. *J. Biol. Chem.* 291, 24828–24837. doi: 10.1074/jbc.m116.739185

Logan, M. R., and Mandato, C. A. (2006). Regulation of the actin cytoskeleton by PIP2 in cytokinesis. *Biol. Cell* 98, 377–388. doi: 10.1042/bc20050081

Loria, A., Longhini, K. M., and Glotzer, M. (2012). The RhoGAP domain of CYK-4 has an essential role in RhoA activation. *Curr. Biol.* 22, 213–219. doi: 10.1016/j.cub.2011.12.019

Mabuchi, I. (1994). Cleavage furrow: timing of emergence of contractile ring actin filaments and establishment of the contractile ring by filament bundling in sea urchin eggs. *J. Cell Sci.* 107(Pt 7), 1853–1862.

Mabuchi, I., and Okuno, M. (1977). The effect of myosin antibody on the division of starfish blastomeres. *J. Cell Biol.* 74, 251–263. doi: 10.1083/jcb.74.1.251

Mabuchi, I., Tsukita, S., and Sawai, T. (1988). Cleavage furrow isolated from newt eggs: contraction, organization of the actin filaments, and protein components of the furrow. *Proc. Natl. Acad. Sci. U.S.A.* 85, 5966–5970. doi: 10.1073/pnas.85.16.5966

Madaule, P., Eda, M., Watanabe, N., Fujisawa, K., Matsuoka, T., Bito, H., et al. (1998). Role of citron kinase as a target of the small GTPase Rho in cytokinesis. *Nature* 394, 491–494. doi: 10.1038/28873

Madaule, P., Furuyashiki, T., Reid, T., Ishizaki, T., Watanabe, G., Morii, N., et al. (1995). A novel partner for the GTP-bound forms of rho and rac. *FEBS Lett.* 377, 243–248. doi: 10.1016/0014-5793(95)01351-2

Maddox, A. S., Habermann, B., Desai, A., and Oegema, K. (2005). Distinct roles for two *C. elegans* anillins in the gonad and early embryo. *Development* 132, 2837–2848. doi: 10.1242/dev.01828

Maddox, A. S., Lewellyn, L., Desai, A., and Oegema, K. (2007). Anillin and the septins promote asymmetric ingression of the cytokinetic furrow. *Dev. Cell* 12, 827–835. doi: 10.1016/j.devcel.2007.02.018

Makino, A., Abe, M., Murate, M., Inaba, T., Yilmaz, N., Hullin-Matsuda, F., et al. (2015). Visualization of the heterogeneous membrane distribution of sphingomyelin associated with cytokinesis, cell polarity, and sphingolipidosis. *FASEB J.* 29, 477–493. doi: 10.1096/fj.13-247585

Mandato, C. A., and Bement, W. M. (2003). Actomyosin transports microtubules and microtubules control actomyosin recruitment during Xenopus oocyte wound healing. *Curr. Biol.* 13, 1096–1105. doi: 10.1016/s0960-9822(03)00420-2

Mangione, M. C., and Gould, K. L. (2019). Molecular form and function of the cytokinetic ring. *J. Cell Sci.* 132:jcs226928. doi: 10.1242/jcs.226928

Manukyan, A., Ludwig, K., Sanchez-Manchinelly, S., Parsons, S. J., and Stukenberg, P. T. (2015). A complex of p190RhoGAP-A and anillin modulates RhoA-GTP and the cytokinetic furrow in human cells. *J. Cell Sci.* 128, 50–60. doi: 10.1242/jcs.151647

Marquardt, J., Chen, X., and Bi, E. (2019). Architecture, remodeling, and functions of the septin cytoskeleton. *Cytoskeleton* 76, 7–14. doi: 10.1002/cm.21475

Martin, A. C., Kaschube, M., and Wieschaus, E. F. (2009). Pulsed contractions of an actin-myosin network drive apical constriction. *Nature* 457, 495–499. doi: 10.1038/nature07522

Mason, F. M., Tworoger, M., and Martin, A. C. (2013). Apical domain polarization localizes actin-myosin activity to drive ratchet-like apical constriction. *Nat. Cell Biol.* 15, 926–936. doi: 10.1038/ncb2796

Matsuda, K., Sugawa, M., Yamagishi, M., Kodera, N., and Yajima, J. (2020). Visualizing dynamic actin cross-linking processes driven by the actin-binding protein anillin. *FEBS Lett.* 594, 1237–1247. doi: 10.1002/1873-3468.13720

Matsumura, F. (2005). Regulation of myosin II during cytokinesis in higher eukaryotes. *Trends Cell Biol.* 15, 371–377. doi: 10.1016/j.tcb.2005.05.004

Mavrakis, M., Azou-Gros, Y., Tsai, F. C., Alvarado, J., Bertin, A., Iv, F., et al. (2014). Septins promote F-actin ring formation by crosslinking actin filaments into curved bundles. *Nat. Cell Biol.* 16, 322–334. doi: 10.1038/ncb2921

McDonald, N. A., Lind, A. L., Smith, S. E., Li, R., and Gould, K. L. (2017). Nanoscale architecture of the Schizosaccharomyces pombe contractile ring. *eLife* 6:e28865.

McKenzie, C., Bassi, Z. I., Debski, J., Gottardo, M., Callaini, G., Dadlez, M., et al. (2016). Cross-regulation between Aurora B and Citron kinase controls midbody architecture in cytokinesis. *Open Biol.* 6:160019. doi: 10.1098/rsob.160019

McMurray, M. A. (2019). The long and short of membrane curvature sensing by septins. *J. Cell Biol.* 218, 1083–1085. doi: 10.1083/jcb.201903045

McNeil, P. L., Vogel, S. S., Miyake, K., and Terasaki, M. (2000). Patching plasma membrane disruptions with cytoplasmic membrane. *J. Cell Sci.* 113(Pt 11), 1891–1902.

Mendonça, D. C., Macedo, J. N., Guimaraes, S. L., Barroso da Silva, F. L., Cassago, A., Garratt, R. C., et al. (2019). A revised order of subunits in mammalian septin complexes. *Cytoskeleton* 76, 457–466. doi: 10.1002/cm.21569

Menon, V. V., Soumya, S. S., Agarwal, A., Naganathan, S. R., Inamdar, M. M., and Sain, A. (2017). Asymmetric flows in the intercellular membrane during cytokinesis. *Biophys. J.* 113, 2787–2795. doi: 10.1016/j.bpj.2017.10.011

Michaux, J. B., Robin, F. B., McFadden, W. M., and Munro, E. M. (2018). Excitable RhoA dynamics drive pulsed contractions in the early *C. elegans* embryo. *J. Cell Biol.* 217, 4230–4252. doi: 10.1083/jcb.201806161

Mikawa, M., Su, L., and Parsons, S. J. (2008). Opposing roles of p190RhoGAP and Ect2 RhoGEF in regulating cytokinesis. *Cell Cycle* 7, 2003–2012. doi: 10.4161/cc.7.13.6128

Miki, T., Smith, C. L., Long, J. E., Eva, A., and Fleming, T. P. (1993). Oncogene ect2 is related to regulators of small GTP-binding proteins. *Nature* 362, 462–465. doi: 10.1038/362462a0

Miller, A. L., and Bement, W. M. (2009). Regulation of cytokinesis by Rho GTPase flux. *Nat. Cell Biol.* 11, 71–77. doi: 10.1038/ncb1814

Miller, A. L., von Dassow, G., and Bement, W. M. (2008). Control of the cytokinetic apparatus by flux of the Rho GTPases. *Biochem. Soc. Trans.* 36, 378–380. doi: 10.1042/bst0360378

Mishima, M. (2016). Centralspindlin in Rappaport's cleavage signaling. *Semin. Cell Dev. Biol.* 53, 45–56. doi: 10.1016/j.semcdb.2016.03.006

Mishra, M., Kashiwazaki, J., Takagi, T., Srinivasan, R., Huang, Y., Balasubramanian, M. K., et al. (2013). In vitro contraction of cytokinetic ring depends on myosin II but not on actin dynamics. *Nat. Cell Biol.* 15, 853–859. doi: 10.1038/ncb2781

Morgan, D. O. (2006). *The Cell Cycle: Principles of Control*. Sunderland, MA: Sinauer Associates Inc, 297.

Morris, R. G., Husain, K. B., Budnar, S., and Yap, A. S. (2020). Anillin: The First Proofreading-like Scaffold? *Bioessays* 10:e2000055.

Mostowy, S., and Cossart, P. (2011). Septins as key regulators of actin based processes in bacterial infection. *Biol. Chem.* 392, 831–835. doi: 10.1515/bc.2011.078

Mostowy, S., and Cossart, P. (2012). Septins: the fourth component of the cytoskeleton. *Nat. Rev. Mol. Cell Biol.* 13, 183–194. doi: 10.1038/nrm3284

Mullins, J. M., and Biesele, J. J. (1977). Terminal phase of cytokinesis in D-98s cells. *J. Cell Biol.* 73, 672–684. doi: 10.1083/jcb.73.3.672

Munro, E. (2019). Anillin Puts RhoA in Touch with PIP2. *Dev. Cell* 49, 819–820. doi: 10.1016/j.devcel.2019.05.042

Murakami, N., Elzinga, M., Singh, S. S., and Chauhan, V. P. (1994). Direct binding of myosin II to phospholipid vesicles via tail regions and phosphorylation of the heavy chains by protein kinase C. *J. Biol. Chem.* 269, 16082–16090.

Murakami, N., Singh, S. S., Chauhan, V. P., and Elzinga, M. (1995). Phospholipid binding, phosphorylation by protein kinase C, and filament assembly of the COOH terminal heavy chain fragments of nonmuscle myosin II isoforms MIIA and MIIB. *Biochemistry* 34, 16046–16055. doi: 10.1021/bi00049a019

Murthy, K., and Wadsworth, P. (2005). Myosin-II-dependent localization and dynamics of F-actin during cytokinesis. *Curr. Biol.* 15, 724–731. doi: 10.1016/j.cub.2005.02.055

Naim, V., Imarisio, S., Di Cunto, F., Gatti, M., and Bonaccorsi, S. (2004). Drosophila citron kinase is required for the final steps of cytokinesis. *Mol. Biol. Cell* 15, 5053–5063. doi: 10.1091/mbc.e04-06-0536

Neto, H., Collins, L. L., and Gould, G. W. (2011). Vesicle trafficking and membrane remodelling in cytokinesis. *Biochem. J.* 437, 13–24. doi: 10.1042/bj20110153

Ng, M. M., Chang, F., and Burgess, D. R. (2005). Movement of membrane domains and requirement of membrane signaling molecules for cytokinesis. *Dev. Cell* 9, 781–790. doi: 10.1016/j.devcel.2005.11.002

Nishikawa, M., Naganathan, S. R., Julicher, F., and Grill, S. W. (2017). Controlling contractile instabilities in the actomyosin cortex. *eLife* 6:e19595.

Nishimura, Y., and Yonemura, S. (2006). Centralspindlin regulates ECT2 and RhoA accumulation at the equatorial cortex during cytokinesis. *J. Cell Sci.* 119, 104–114. doi: 10.1242/jcs.02737

Oegema, K., Savoian, M. S., Mitchison, T. J., and Field, C. M. (2000). Functional analysis of a human homologue of the Drosophila actin binding protein anillin suggests a role in cytokinesis. *J. Cell Biol.* 150, 539–552. doi: 10.1083/jcb.150.3.539

Ojkic, N., Wu, J. Q., and Vavylonis, D. (2011). Model of myosin node aggregation into a contractile ring: the effect of local alignment. *J. Phys. Condens. Matter.* 23:374103. doi: 10.1088/0953-8984/23/37/374103

Ong, K., Wloka, C., Okada, S., Svitkina, T., and Bi, E. (2014). Architecture and dynamic remodelling of the septin cytoskeleton during the cell cycle. *Nat. Commun.* 5:5698.

O'Shaughnessy, B., and Thiyagarajan, S. (2018). Mechanisms of contractile ring tension production and constriction. *Biophys. Rev.* 10, 1667–1681. doi: 10.1007/s12551-018-0476-6

Otomo, T., Otomo, C., Tomchick, D. R., Machius, M., and Rosen, M. K. (2005). Structural basis of Rho GTPase-mediated activation of the formin mDia1. *Mol. Cell* 18, 273–281. doi: 10.1016/j.molcel.2005.04.002

Pestonjamasp, K., Amieva, M. R., Strassel, C. P., Nauseef, W. M., Furthmayr, H., and Luna, E. J. (1995). Moesin, ezrin, and p205 are actin-binding proteins associated with neutrophil plasma membranes. *Mol. Biol. Cell* 6, 247–259. doi: 10.1091/mbc.6.3.247

Pestonjamasp, K. N., Pope, R. K., Wulfkuhle, J. D., and Luna, E. J. (1997). Supervillin (p205): a novel membrane-associated, F-actin-binding protein in the villin/gelsolin superfamily. *J. Cell Biol.* 139, 1255–1269. doi: 10.1083/jcb.139.5.1255

Piekny, A., Werner, M., and Glotzer, M. (2005). Cytokinesis: welcome to the Rho zone. *Trends Cell Biol.* 15, 651–658. doi: 10.1016/j.tcb.2005.10.006

Piekny, A. J., and Glotzer, M. (2008). Anillin is a scaffold protein that links RhoA, actin, and myosin during cytokinesis. *Curr. Biol.* 18, 30–36. doi: 10.1016/j.cub.2007.11.068

Piekny, A. J., and Maddox, A. S. (2010). The myriad roles of Anillin during cytokinesis. *Semin. Cell Dev. Biol.* 21, 881–891. doi: 10.1016/j.semcdb.2010.08.002

Piekny, A. J., and Mains, P. E. (2002). Rho-binding kinase (LET-502) and myosin phosphatase (MEL-11) regulate cytokinesis in the early *Caenorhabditis elegans* embryo. *J. Cell Sci.* 115, 2271–2282.

Pollard, T. D. (2017). Nine unanswered questions about cytokinesis. *J. Cell Biol.* 216, 3007–3016. doi: 10.1083/jcb.201612068

Pollard, T. D., and O'Shaughnessy, B. (2019). Molecular Mechanism of Cytokinesis. *Annu. Rev. Biochem.* 88, 661–689. doi: 10.1146/annurev-biochem-062917-012530

Prekeris, R., and Gould, G. W. (2008). Breaking up is hard to do - membrane traffic in cytokinesis. *J. Cell Sci.* 121, 1569–1576. doi: 10.1242/jcs.018770

Ramalingam, N., Zhao, H., Breitsprecher, D., Lappalainen, P., Faix, J., and Schleicher, M. (2010). Phospholipids regulate localization and activity of mDia1 formin. *Eur. J. Cell Biol.* 89, 723–732. doi: 10.1016/j.ejcb.2010.06.001

Rappaport, R. (1977). Tensiometric studies of cytokinesis in cleaving sand dollar eggs. *J. Exp. Zool.* 201, 375–378. doi: 10.1002/jez.1402010304

Rappaport, R., and Conrad, G. W. (1963). An experimental analysis of unilateral cleavage in invertebrate eggs. *J. Exp. Zool.* 153, 99–112. doi: 10.1002/jez.1401530203

Renshaw, M. J., Liu, J., Lavoie, B. D., and Wilde, A. (2014). Anillin-dependent organization of septin filaments promotes intercellular bridge elongation and Chmp4B targeting to the abscission site. *Open Biol.* 4:130190. doi: 10.1098/rsob.130190

Reymann, A. C., Staniscia, F., Erzberger, A., Salbreux, G., and Grill, S. W. (2016). Cortical flow aligns actin filaments to form a furrow. *eLife* 5:e17807.

Rincon, S. A., and Paoletti, A. (2012). Mid1/anillin and the spatial regulation of cytokinesis in fission yeast. *Cytoskeleton* 69, 764–777. doi: 10.1002/cm.21056

Rothenberg, K. E., and Fernandez-Gonzalez, R. (2019). Forceful closure: cytoskeletal networks in embryonic wound repair. *Mol. Biol. Cell* 30, 1353–1358. doi: 10.1091/mbc.e18-04-0248

Roubinet, C., Decelle, B., Chicanne, G., Dorn, J. F., Payrastre, B., Payre, F., et al. (2011). Molecular networks linked by Moesin drive remodeling of the cell cortex during mitosis. *J. Cell Biol.* 195, 99–112. doi: 10.1083/jcb.201106048

Sanger, J. W., and Sanger, J. M. (1980). Surface and shape changes during cell division. *Cell Tissue Res.* 209, 177–186. doi: 10.1016/b978-0-08-091747-4.50013-8

Savoian, M. S., Khodjakov, A., and Rieder, C. L. (1999). Unilateral and wandering furrows during mitosis in vertebrates: implications for the mechanism of cytokinesis. *Cell Biol. Int.* 23, 805–812. doi: 10.1006/cbir.1999.0477

Schroeder, T. E. (1972). The contractile ring. II. Determining its brief existence, volumetric changes, and vital role in cleaving Arbacia eggs. *J. Cell Biol.* 53, 419–434.

Schroeder, T. E. (1973). Actin in dividing cells: contractile ring filaments bind heavy meromyosin. *Proc. Natl. Acad. Sci. U.S.A.* 70, 1688–1692. doi: 10.1073/pnas.70.6.1688

Schroeder, T. E. (1990). The contractile ring and furrowing in dividing cells. *Ann. N. Y. Acad. Sci.* 582, 78–87. doi: 10.1111/j.1749-6632.1990.tb21669.x

Shindo, A., Audrey, A., Takagishi, M., Takahashi, M., Wallingford, J. B., and Kinoshita, M. (2018). Septin-dependent remodeling of cortical microtubule drives cell reshaping during epithelial wound healing. *J. Cell Sci.* 131:jcs212647. doi: 10.1242/jcs.212647

Shuster, C. B., and Burgess, D. R. (2002). Targeted new membrane addition in the cleavage furrow is a late, separate event in cytokinesis. *Proc. Natl. Acad. Sci. U.S.A.* 99, 3633–3638. doi: 10.1073/pnas.052342699

Silva, A. M., Osorio, D. S., Pereira, A. J., Maiato, H., Pinto, I. M., Rubinstein, B., et al. (2016). Robust gap repair in the contractile ring ensures timely completion of cytokinesis. *J. Cell Biol.* 215, 789–799. doi: 10.1083/jcb.201605080

Silverman-Gavrila, R. V., Hales, K. G., and Wilde, A. (2008). Anillin-mediated targeting of peanut to pseudocleavage furrows is regulated by the GTPase Ran. *Mol. Biol. Cell* 19, 3735–3744. doi: 10.1091/mbc.e08-01-0049

Sirajuddin, M., Farkasovsky, M., Hauer, F., Kuhlmann, D., Macara, I. G., Weyand, M., et al. (2007). Structural insight into filament formation by mammalian septins. *Nature* 449, 311–315. doi: 10.1038/nature06052

Sisson, J. C., Field, C., Ventura, R., Royou, A., and Sullivan, W. (2000). Lava lamp, a novel peripheral golgi protein, is required for Drosophila melanogaster cellularization. *J. Cell Biol.* 151, 905–918. doi: 10.1083/jcb.151.4.905

Smith, T. C., Fang, Z., and Luna, E. J. (2010). Novel interactors and a role for supervillin in early cytokinesis. *Cytoskeleton* 67, 346–364.

Smith, T. C., Fridy, P. C., Li, Y., Basil, S., Arjun, S., Friesen, R. M., et al. (2013). Supervillin binding to myosin II and synergism with anillin are required for cytokinesis. *Mol. Biol. Cell* 24, 3603–3619. doi: 10.1091/mbc.e12-10-0714

Somers, W. G., and Saint, R. (2003). A RhoGEF and Rho family GTPase-activating protein complex links the contractile ring to cortical microtubules at the onset of cytokinesis. *Dev. Cell* 4, 29–39. doi: 10.1016/s1534-5807(02)00402-1

Somma, M. P., Fasulo, B., Cenci, G., Cundari, E., and Gatti, M. (2002). Molecular dissection of cytokinesis by RNA interference in Drosophila cultured cells. *Mol. Biol. Cell* 13, 2448–2460. doi: 10.1091/mbc.01-12-0589

Soroor, F., Kim, M. S., Palander, O., Balachandran, Y., Collins, R., Benlekbir, S., et al. (2019). Revised subunit order of mammalian septin complexes explains their in vitro polymerization properties. *bioRxiv* [Preprint]. doi: 10.1101/569871

Spiliotis, E. T. (2018). Spatial effects - site-specific regulation of actin and microtubule organization by septin GTPases. *J. Cell Sci.* 131:jcs207555. doi: 10.1242/jcs.207555

Spira, F., Cuylen-Haering, S., Mehta, S., Samwer, M., Reversat, A., Verma, A., et al. (2017). Cytokinesis in vertebrate cells initiates by contraction of an equatorial actomyosin network composed of randomly oriented filaments. *eLife* 6:e30867.

Stachowiak, M. R., Laplante, C., Chin, H. F., Guirao, B., Karatekin, E., Pollard, T. D., et al. (2014). Mechanism of cytokinetic contractile ring constriction in fission yeast. *Dev. Cell* 29, 547–561. doi: 10.1016/j.devcel.2014.04.021

Stark, B. C., Sladewski, T. E., Pollard, L. W., and Lord, M. (2010). Tropomyosin and myosin-II cellular levels promote actomyosin ring assembly in fission yeast. *Mol. Biol. Cell* 21, 989–1000. doi: 10.1091/mbc.e09-10-0852

Steigemann, P., and Gerlich, D. W. (2009). Cytokinetic abscission: cellular dynamics at the midbody. *Trends Cell Biol.* 19, 606–616. doi: 10.1016/j.tcb.2009.07.008

Straight, A. F., Field, C. M., and Mitchison, T. J. (2005). Anillin binds nonmuscle myosin II and regulates the contractile ring. *Mol. Biol. Cell* 16, 193–201. doi: 10.1091/mbc.e04-08-0758

Su, L., Pertz, O., Mikawa, M., Hahn, K., and Parsons, S. J. (2009). p190RhoGAP negatively regulates Rho activity at the cleavage furrow of mitotic cells. *Exp. Cell Res.* 315, 1347–1359. doi: 10.1016/j.yexcr.2009.02.014

Sun, L., Guan, R., Lee, I. J., Liu, Y., Chen, M., Wang, J., et al. (2015). Mechanistic insights into the anchorage of the contractile ring by anillin and Mid1. *Dev. Cell* 33, 413–426. doi: 10.1016/j.devcel.2015.03.003

Szafer-Glusman, E., Giansanti, M. G., Nishihama, R., Bolival, B., Pringle, J., Gatti, M., et al. (2008). A role for very-long-chain fatty acids in furrow ingression during cytokinesis in Drosophila spermatocytes. *Curr. Biol.* 18, 1426–1431. doi: 10.1016/j.cub.2008.08.061

Takizawa, P. A., DeRisi, J. L., Wilhelm, J. E., and Vale, R. D. (2000). Plasma membrane compartmentalization in yeast by messenger RNA transport and a septin diffusion barrier. *Science* 290, 341–344. doi: 10.1126/science.290.5490.341

Tanaka-Takiguchi, Y., Kinoshita, M., and Takiguchi, K. (2009). Septin-mediated uniform bracing of phospholipid membranes. *Curr. Biol.* 19, 140–145. doi: 10.1016/j.cub.2008.12.030

Tatsumoto, T., Xie, X., Blumenthal, R., Okamoto, I., and Miki, T. (1999). Human ECT2 is an exchange factor for Rho GTPases, phosphorylated in G2/M phases, and involved in cytokinesis. *J. Cell Biol.* 147, 921–928. doi: 10.1083/jcb.147.5.921

Tian, D., Diao, M., Jiang, Y., Sun, L., Zhang, Y., Chen, Z., et al. (2015). Anillin regulates neuronal migration and neurite growth by linking RhoG to the actin cytoskeleton. *Curr. Biol.* 25, 1135–1145. doi: 10.1016/j.cub.2015.02.072

Toure, A., Dorseuil, O., Morin, L., Timmons, P., Jegou, B., Reibel, L., et al. (1998). MgcRacGAP, a new human GTPase-activating protein for Rac and Cdc42 similar to Drosophila rotundRacGAP gene product, is expressed in male germ cells. *J. Biol. Chem.* 273, 6019–6023. doi: 10.1074/jbc.273.11.6019

Tse, Y. C., Werner, M., Longhini, K. M., Labbe, J. C., Goldstein, B., and Glotzer, M. (2012). RhoA activation during polarization and cytokinesis of the early *C. elegans* embryo are differentially dependent on NOP-1 and CYK-4. *Mol. Biol. Cell* 23, 4020–4031. doi: 10.1091/mbc.e12-04-0268

Uehara, R., Goshima, G., Mabuchi, I., Vale, R. D., Spudich, J. A., and Griffis, E. R. (2010). Determinants of myosin II cortical localization during cytokinesis. *Curr. Biol.* 20, 1080–1085. doi: 10.1016/j.cub.2010.04.058

Vavylonis, D., Wu, J. Q., Hao, S., O'Shaughnessy, B., and Pollard, T. D. (2008). Assembly mechanism of the contractile ring for cytokinesis by fission yeast. *Science* 319, 97–100. doi: 10.1126/science.1151086

Vrabioiu, A. M., and Mitchison, T. J. (2006). Structural insights into yeast septin organization from polarized fluorescence microscopy. *Nature* 443, 466–469. doi: 10.1038/nature05109

Wagner, E., and Glotzer, M. (2016). Local RhoA activation induces cytokinetic furrows independent of spindle position and cell cycle stage. *J. Cell Biol.* 213, 641–649. doi: 10.1083/jcb.201603025

Wang, J., and Richards, D. A. (2012). Segregation of PIP2 and PIP3 into distinct nanoscale regions within the plasma membrane. *Biol. Open* 1, 857–862. doi: 10.1242/bio.20122071

Wang, S., and O'Shaughnessy, B. (2019). Anchoring of actin to the plasma membrane enables tension production in the fission yeast cytokinetic ring. *Mol. Biol. Cell* 30, 2053–2064. doi: 10.1091/mbc.e19-03-0173

Wang, Y. H., Slochower, D. R., and Janmey, P. A. (2014). Counterion-mediated cluster formation by polyphosphoinositides. *Chem. Phys. Lipids* 182, 38–51. doi: 10.1016/j.chemphyslip.2014.01.001

Watanabe, S., Ando, Y., Yasuda, S., Hosoya, H., Watanabe, N., Ishizaki, T., et al. (2008). mDia2 induces the actin scaffold for the contractile ring and stabilizes its position during cytokinesis in NIH 3T3 cells. *Mol. Biol. Cell* 19, 2328–2338. doi: 10.1091/mbc.e07-10-1086

Watanabe, S., De Zan, T., Ishizaki, T., and Narumiya, S. (2013a). Citron kinase mediates transition from constriction to abscission through its coiled-coil domain. *J. Cell Sci.* 126, 1773–1784. doi: 10.1242/jcs.116608

Watanabe, S., De Zan, T., Ishizaki, T., Yasuda, S., Kamijo, H., Yamada, D., et al. (2013b). Loss of a Rho-regulated actin nucleator, mDia2, impairs cytokinesis during mouse fetal erythropoiesis. *Cell Rep.* 5, 926–932. doi: 10.1016/j.celrep.2013.10.021

Watanabe, S., Okawa, K., Miki, T., Sakamoto, S., Morinaga, T., Segawa, K., et al. (2010). Rho and anillin-dependent control of mDia2 localization and function in cytokinesis. *Mol. Biol. Cell* 21, 3193–3204. doi: 10.1091/mbc.e10-04-0324

Yanai, I., and Lercher, M. (2019). Night science. *Genome Biol.* 20:179.

Yuce, O., Piekny, A., and Glotzer, M. (2005). An ECT2-centralspindlin complex regulates the localization and function of RhoA. *J. Cell Biol.* 170, 571–582. doi: 10.1083/jcb.200501097

Zanin, E., Desai, A., Poser, I., Toyoda, Y., Andree, C., Moebius, C., et al. (2013). A conserved RhoGAP limits M phase contractility and coordinates with microtubule asters to confine RhoA during cytokinesis. *Dev. Cell* 26, 496–510. doi: 10.1016/j.devcel.2013.08.005

Zhang, D., and Glotzer, M. (2015). The RhoGAP activity of CYK-4/MgcRacGAP functions non-canonically by promoting RhoA activation during cytokinesis. *eLife* 4:e08898.

Zhang, J., Kong, C., Xie, H., McPherson, P. S., Grinstein, S., and Trimble, W. S. (1999). Phosphatidylinositol polyphosphate binding to the mammalian septin H5 is modulated by GTP. *Curr. Biol.* 9, 1458–1467. doi: 10.1016/s0960-9822(00)80115-3

Zhao, W. M., and Fang, G. (2005). Anillin is a substrate of anaphase-promoting complex/cyclosome (APC/C) that controls spatial contractility of myosin during late cytokinesis. *J. Biol. Chem.* 280, 33516–33524. doi: 10.1074/jbc.m504657200

Zhuravlev, Y., Hirsch, S. M., Jordan, S. N., Dumont, J., Shirasu-Hiza, M., and Canman, J. C. (2017). CYK-4 regulates Rac, but not Rho, during cytokinesis. *Mol. Biol. Cell* 28, 1258–1270. doi: 10.1091/mbc.e17-01-0020

Conflict of Interest: The authors declare that the research was conducted in the absence of any commercial or financial relationships that could be construed as a potential conflict of interest.

frontiers in Cell and Developmental Biology

MINI REVIEW
published: 09 November 2020
doi: 10.3389/fcell.2020.586880

A Structural View on ESCRT-Mediated Abscission

Péter Horváth and Thomas Müller-Reichert**

Experimental Center, Faculty of Medicine Carl Gustav Carus, Technische Universität Dresden, Dresden, Germany

The endosomal sorting complex required for transport (ESCRT) mediates cellular processes that are related to membrane remodeling, such as multivesicular body (MVB) formation, viral budding and cytokinesis. Abscission is the final stage of cytokinesis that results in the physical separation of the newly formed two daughter cells. Although abscission has been investigated for decades, there are still fundamental open questions related to the spatio-temporal organization of the molecular machinery involved in this process. Reviewing knowledge obtained from *in vitro* as well as *in vivo* experiments, we give a brief overview on the role of ESCRT components in abscission mainly focussing on mammalian cells.

Keywords: endosomal sorting complexes required for transport (ESCRT), cytokinesis, abscission, microtubules, membranes, electron microscopy, electron tomography, 3D reconstruction

OPEN ACCESS

Edited by:
Maria Grazia Giansanti,
Italian National Research Council, Italy

Reviewed by:
Pier Paolo D'Avino,
University of Cambridge,
United Kingdom
John McCullough,
The University of Utah, United States

****Correspondence:***
Thomas Müller-Reichert
mueller-reichert@tu-dresden.de
Péter Horváth
peter.horvath@tu-dresden.de

Specialty section:
This article was submitted to Cell Growth and Division, a section of the journal Frontiers in Cell and Developmental Biology

Received: *24 July 2020*
Accepted: *16 October 2020*
Published: *09 November 2020*

Citation:
Horváth P and Müller-Reichert T (2020) A Structural View on ESCRT-Mediated Abscission. Front. Cell Dev. Biol. 8:586880. doi: 10.3389/fcell.2020.586880

INTRODUCTION

Cytokinesis, the physical separation of newly formed daughter cells, is a very sophisticated process that is precisely coordinated and controlled by a complex molecular machinery. Proteome analysis revealed 577 proteins in purified intact midbodies of Chinese hamster ovary (CHO) cells (Skop et al., 2004) and 1730 proteins in the midbody interactome of HeLa cells (Capalbo et al., 2019). In addition, the midbody remnant in HeLa cells consisted of 1732 proteins (Addi et al., 2020). To systematically analyze cytokinesis, it is practical to break this complex process into the following discrete steps: assembly and ingression of the contractile actin ring to achieve a primary constriction leading to the formation of the intercellular bridge; rearrangement of microtubules during bridge formation; and secondary constriction of the intercellular bridge culminating in abscission (Bhutta et al., 2014). There are distinct processes controlling the order of events in abscission of animal cells: formation, stabilization and severing of microtubules at the intercellular bridge and membrane constriction followed by a scission event as the closing step.

The endosomal sorting complex required for transport (ESCRT) machinery has been linked to the process of abscission (Carlton and Martin-Serrano, 2007; Morita et al., 2007; Carlton et al., 2008; Guizetti and Gerlich, 2010). In addition to cytokinesis (Glotzer, 2001; Eggert et al., 2006; Barr and Gruneberg, 2007), the ESCRTs are also involved in a variety of other processes, such as multivesicular body (MVB) biogenesis (Teis et al., 2008; Tang et al., 2016), viral budding (Garrus et al., 2001) and nuclear membrane reformation (Stoten and Carlton, 2018). The common aspect of all these processes is that they are all related to membrane remodeling. The core of the ESCRT machinery consists of ESCRT-0, ESCRT-I, ESCRT-II, and ESCRT-III complexes and vacuolar protein sorting-associated protein 4 (VPS4) (Olmos and Carlton, 2016; Christ et al., 2017; Zhu et al., 2017; Gatta and Carlton, 2019). In eukaryotes, ESCRT-III and VPS4 are involved in the late phases of cytokinesis (Adell and Teis, 2011; Vietri et al., 2015). This is in contrast to the role of ESCRT-I and ESCRT-II, which coordinate the assembly of downstream complexes necessary

for cytokinesis (Schmidt and Teis, 2012). Reporting on the role of the ESCRT-III complex and associated protein components, we provide here an structural view on abscission focusing mainly on mammalian cells.

FORMATION OF THE INTERCELLULAR BRIDGE

The initiation of mitotic exit is based on cyclin-dependent kinase (CDK1), a universal protein kinase regulator. Cytokinesis is associated with down-regulation of CDK1 activity by phosphoregulation carried out by the coordinated action of kinases, counteracting phosphatases and association with cyclins (Hunt, 1991). Misregulation of CDK1 can prevent cytokinesis presumably because of its role in guiding and maintaining cleavage signals (Wheatley and Wang, 1996; Wheatley et al., 1997). Besides CDK1, Aurora B-dependent phosphorylation of the mitotic kinesin-like protein 1 (MKLP1) (Guse et al., 2005) is also essential for cytokinesis (Eggert et al., 2006). After furrow ingression both Aurora B and MKLP1 localize to the midbody, suggesting that the two proteins are involved subsequently in the regulation of abscission. Timing of abscission is regulated by Aurora B through phosphorylation of the human ESCRT-III subunit, charged multivesicular body protein 4C (CHMP4C) (Capalbo et al., 2012) in concert with VPS4 and abscission/NoCut checkpoint regulator (ANCHR) (Thoresen et al., 2014).

Concomitant with the rearrangement of the mitotic spindle into the central spindle, the actomyosin ring induces furrow ingression, thus leading to the formation of the intercellular bridge containing the midbody (**Figure 1A**). Actomyosin-driven contraction of the cleavage furrow continues until the intercellular bridge with the midbody at its center has been formed (Mierzwa and Gerlich, 2014). The ingressed furrow then needs to be stabilized to prevent furrow regression. Centralspindlin was identified as a protein complex with plasma membrane tethering activity. The C1 domain of the centralspindlin subunit, male germ cell rac GTPase-activating protein (MgcRacGAP) associates with phosphoinositide lipids (Lekomtsev et al., 2012). This link is thought to have a stabilizing role to secure the final steps of cytokinesis in animal cells. An additional protein with a stabilizing function of the midspindle is protein regulator of cytokinesis 1 (PRC1) (Lee et al., 2015). Centralspindlin and PRC1 show microtubule binding activities. Both proteins co-localize to the midbody and recruit additional factors, such as Kruppel-like factor (KLF4) (Lee et al., 2015). PRC1 is required for midzone formation, and KLF4 is necessary for organization of the central spindle (Kurasawa et al., 2004). The contractile ring protein, anillin was also proposed to play a role in stabilizing the membrane invagination after myosin II-mediated force production ceases (Field and Alberts, 1995). Furthermore, anillin recruits septins, involved in the formation of the constriction sites (Renshaw et al., 2014). The C-terminus of anillin can bind septins, linking anillin and septins to membrane stabilization (Kinoshita et al., 2002; Menon and Gaestel, 2015; Karasmanis et al., 2019).

MODELS OF ABSCISSION

The physical separation of post-mitotic daughter cells is accompanied by a continuous decrease in the diameter of the intercellular bridge at the two opposing sides of the midbody. Initiated by furrow ingression, abscission is the net result of many complex and precisely orchestrated subprocesses (Agromayor and Martin-Serrano, 2013; Henne et al., 2013; Mierzwa and Gerlich, 2014; Frémont and Echard, 2018; Karasmanis et al., 2019). According to the vesicle-mediated model, midbody ring-localized secretory vesicles fuse with each other and with the plasma membrane. Release of the vesicle content is thought to be mediated by synaptosomal-associated protein 23/25 (SNAP23/25) and vesicle-associated snap receptor (v-SNARE) (Takahashi et al., 2004). Thus, abscission is proposed to take place at the site of vesicle fusion (Gromley et al., 2005). The caveat is that vesicles were no longer detectable within the intercellular bridge by the time abscission occured (Guizetti et al., 2011). In contrast to the vesicle-mediated model, the mechanical force model suggests that traction based forces generated by adherent cells induce abscission. Based on a comparison to the *Xenopus* oocyte, this model suggests a "wound-induced closure" mechanism at late cytokinesis (Darenfed and Mandato, 2005; Schiel and Prekeris, 2010).

In the following sections, we will focus on the role of ESCRT proteins and their spatial distribution in cell division. ESCRT-III components are primary candidates for the completion of cytokinesis (Wollert et al., 2009). Secondary constriction sites develop either at both sides of the midbody or in some cases only at one side (Mullins and Biesele, 1977; Schiel et al., 2012). In search of interacting partners of ESCRT-III, it was found that tumor susceptibility gene 101 protein (TSG101), a subunit of ESCRT-I, binds the centrosomal protein of 55 kDa (CEP55) (Fabbro et al., 2005) and the apoptosis-linked gene 2-interacting protein x (ALIX) (Morita et al., 2007; Carlton et al., 2008). In fact, CEP55 recruits TSG101 and ALIX to the midbody (Lee et al., 2008). Depletion of ALIX by RNA interference resulted in a 14-fold increase in multinucleated cells compared to control cells, suggesting a role for ALIX in cytokinesis (Carlton and Martin-Serrano, 2007). ALIX acts as an adaptor molecule connecting CEP55 with ESCRT-III to initiate completion of cytokinesis (Carlton et al., 2008). The CHMP4 subunits of ESCRT-III localize next to the midbody and polymerize toward the direction of the constriction site (Guizetti et al., 2011). In support of this observation, membrane deforming and interaction properties of ESCRT-III components were documented (Darenfed and Mandato, 2005; Hanson et al., 2008; Malerød and Stenmark, 2009). Based on studies of syndecan–syntenin–ALIX interaction in the case of exosome formation (Baietti et al., 2012), a recent study suggested a two-phase recruitment of ESCRT-III, involving a tripartite module (ALIX-syntenin-syndecan-4) to be essential for localization and abscission. ALIX-syntenin anchors ESCRT-III to the membrane, while syndecan-4 stabilizes ESCRT-III polymers at the abscission site (Addi et al., 2020).

Importantly, ESCRT-III–mediated secondary constriction requires synchronization with the disassembly of microtubules within the intercellular bridge. Increased concentration of the

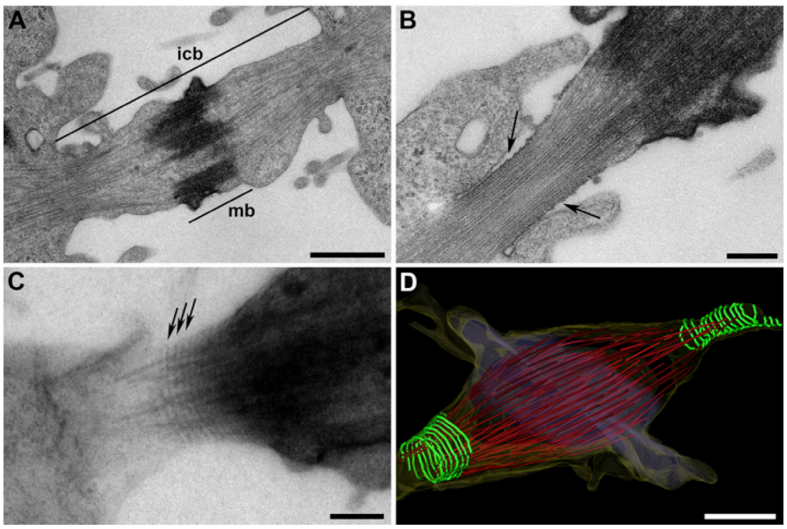

FIGURE 1 | Ultrastructure of the abscission machinery in HeLa cells. **(A)** Thin-section electron micrograph of a chemically fixed intercellular bridge (icb). This overview image also shows the midbody (mb). **(B)** Visualization of a secondary constriction site. Image of a chemically fixed intercellular bridge showing a typical "ruffled zone" with membrane thickening (arrows). **(C)** Semi-thick serial section of a high-pressure frozen, freeze substituted and plastic-embedded sample as visualized by electron tomography. Filamentous structures (arrows) oriented perpendicular to the long axis of the bridge are shown. **(D)** 3D model of an intercellular bridge revealed by serial-section electron tomography. 3D rendering of ESCRT-III-dependent filaments (green), microtubules (red) and the cell membrane (yellow). The filaments show different degrees of constriction as previously reported (Guizetti et al., 2011). Scale bars **(A,D)**, 1 μm; **(B,C)**, 250 nm.

microtubule-severing enzyme, spastin can be measured at the site where microtubule disassembly takes place (Yang et al., 2008; Connell et al., 2009; Guizetti et al., 2011). How the components of the ESCRT-III machinery are orchestrated during abscission *in vivo* remains largely elusive. One possibility is that plasma membrane-attached ESCRT-III filaments increase their curvature as they extend from the midbody, constricting the membrane until scission takes place (Guizetti et al., 2011). Another possibility involves an increase in constriction by remodeling ESCRT-III subunits by Vps4 (Mierzwa et al., 2017). It has also been proposed that filaments may slide along the intercellular bridge and exert constriction determined by the elastic forces in the membrane (Elia et al., 2012).

STRUCTURAL STUDIES ON ISOLATED ESCRT COMPONENTS

The ESCRT machinery is conserved from archaea to humans (Hurley and Emr, 2006; Lindås et al., 2008; Schöneberg et al., 2017; Gupta et al., 2020). The 12 human homologs of ESCRT-III and VPS4 were shown to contribute to cytokinesis (Carlton and Martin-Serrano, 2007; Morita et al., 2007; Caballe and Martin-Serrano, 2011; Schöneberg et al., 2017). The ESCRT-III proteins show structural variance, but the four N-terminal helices are homologous. The C-terminal truncated CHMP38–183 crystal structure with a truncated C-terminal acidic domain (Muzioł et al., 2006) served as a search model for molecular replacement of CHMP38–222 (Bajorek et al., 2009).

Depending on the composition of the lipid monolayer and the interacting ESCRT-III subunits, self-assembled ESCRT-III heteropolymers can adopt structures of variable dynamics and architectures such as rings, spirals, helices or linear polymers (Hanson et al., 2008; Henne et al., 2012). As an example, yeast vacuolar-sorting protein ($Snf7^{CHMP4A;B;C}$), a core component of ESCRT-III polymerizes into spirals at the surface of lipid bilayers, mediating membrane deformation and fission (Chiaruttini et al., 2015). In addition the ESCRT-III subunits isolated from yeast, $Vps2^{CHMP2A,B}$, $Vps20^{CHMP6}$, $Vps24^{CHMP3}$, and also Snf7 were proposed to form filaments and deform membranes (Cashikar et al., 2014). Although Snf7 by itself is unable to induce buckling on artificial lipid membranes, Vps2/Vps24 drive the formation of spirals (Henne et al., 2012) and form a parallel strand through electrostatic interaction with Snf7 (Mierzwa et al., 2017; Mandal et al., 2020). Incubation of Snf7/Vps2/Vps24 with detergent-solubilized lipids resulted in helices of different forms (Moser von Filseck et al., 2020).

A recent cryo-electron microscopy (cryo-EM) study at 3.2 Å resolution showed a double-stranded helical arrangement of Vps24. Lipids were shown to assist in the disassembly of the filaments. This study further revealed the following three important aspects of Vps24 function: First, apolar Vps24 integrates into linear polar Snf7 polymers, thereby neutralizing the polarity so that opposite polarity filaments can combine (Huber et al., 2020). Second, it was shown that Vps24 has an intrinsical helical property. Under defined conditions, Vps24 is capable of inducing curvature in flat Snf7 polymers (Henne et al., 2012; Tang et al., 2015). Third, Vps24 consists of two protofilaments. Based on a lateral association of Vps2/Vps24 and Snf7, this could allow a combination of multiple linear Snf7 filaments (Mierzwa et al., 2017; Huber et al., 2020). All this suggested that Vps24 is a candidate for

an adaptor complex that connects ESCRT-III homopolymers (Huber et al., 2020).

In a study of ESCRT-III-driven shaping of positively curved membranes, the membrane-bound complex CHMP1B-IST1 was shown to constrict the underlying membrane bilayer nearly to the fission point by a two-component sequential polymerization mechanism (Nguyen et al., 2020). Spontaneous co-assembly between CHMP1 and truncated IST1 frequently resulted in conical helix shapes with decreasing diameter under low ionic strength, whereas an increasing ionic strength favored the monomeric form of the subunits (McCullough et al., 2015). The other way round, membrane shape was also reported to influence the assembly of ESCRT-III subunits. In contrast to *in vivo* conditions, *in vitro* experiments showed that CHMP2B and CHMP2A/CHMP3 assemble on positively curved but not on negatively curved membranes. This suggests that these complexes don't assemble inside membrane structures (negative curvature) but rather on the outside surface (positive curvature). Moreover, CHMP4B has a preference to bind either to flat membranes or to tubes with positive mean curvature (Bertin et al., 2020). Last but not least, it is important to note that polymeric structures can also form even in the absence of membranes (Henne et al., 2012; Banjade et al., 2019). Therefore, it will be crucial in future studies to verify the reported molecular shapes and membrane interactions of the various ESCRT-III components within the cellular context of abscission.

ROLE OF VPS4 IN REGULATING ESCRT-III

Vps4 is a member of the meiotic clade AAA-ATPase and a key component of the ESCRT pathway (Monroe and Hill, 2016). Its N-terminus consists of a microtubule interacting and trafficking (MIT) domain, which interacts with carboxy-terminal peptide, MIT interaction motifs (MIM) in ESCRT-III proteins (Obita et al., 2007; Stuchell-Brereton et al., 2007; Kieffer et al., 2008). This is followed by a linker region (Shestakova et al., 2013) and an AAA-ATPase cassette that consists of a large ATPase and a small ATPase domain, a beta domain and a C-terminal helix (Scott et al., 2005; Gonciarz et al., 2008). Vps4 also binds the activator vacuolar protein sorting-associated protein (Vta1) (Yeo et al., 2003; Shestakova et al., 2010), which contacts the beta domain and regulates assembly of Vps4 and ATPase activity (Azmi et al., 2006). In the cytosol, Vps4 is present mainly as a monomer but it forms hexamers in its activated form (Monroe et al., 2014; Adell et al., 2017). The hexamers are associated to each ESCRT-III filament by the MIT-MIM interaction. The cryo-EM structure at 4.3 Å resolution revealed that Vps4 is highly asymmetric and stabilized by ATP and Vta1 binding. One end of the Vps4 molecule grows and hydrolyzes ATP, while the other end disassembles (Monroe et al., 2017). The disassembled subunits were reported to move to the growing site, creating a "walking" motion of Vps4 along the ESCRT-III filament, pulling it through the pore of the hexamer and therefore disassembling the filament (Yang et al., 2015; Adell et al., 2017; Monroe et al., 2017).

While regulating assembly and disassembly of ESCRT-III complexes, Vps4 can also promote shape adaptations to membranes with different curvatures (Mierzwa et al., 2017), allowing Vps4 to function in a wide range of processes. High-speed atomic force microscopy (HS-AFM) imaging of Vps4 with Vps2, Vps24, and Snf7 on lipid bilayers showed ESCRT-III spirals with reduced diameter in the presence of ATP. From this observation it was concluded that Vps4 is responsible for a dynamic subunit turnover and that Vps2, Vps24 subunits function as inhibitors (Mierzwa et al., 2017). Vps24 induced curvature when mixed with flat Snf7 filament polymers (Henne et al., 2012; Tang et al., 2015). Vps2/Vps24 subunits of ESCRT-III formed side by side filaments with Snf7 (Mierzwa et al., 2017). Furthermore, Vps2/Vps24 is crucial for Vps4–mediated remodeling. Polymerized Snf7 on membranes mixed with Vps4 and ATP didn't induce remodeling of the Snf7 filaments. However, the combination of Snf7, Vps2/Vps24, Vps4, and ATP resulted in both shrinking and growth of ESCRT-III spirals (Mierzwa et al., 2017). This dynamic remodeling of ESCRT-III argues against the previously proposed "cut and slide" model, which suggested a single cut by VPS4 to trigger constriction (Elia et al., 2012).

STRUCTURAL APPROACHES TO STUDY THE FUNCTION OF ESCRTs *IN VIVO*

Structural analysis of cytokinesis is challenging given that the spatial organization of the abscission machinery is complex and the interactions of the different components are dynamic and possibly transient. In order to reduce the complexity, cytokinesis has been studied predominantly under *in vitro* conditions. This approach allows the assessment of the roles of specific components of the machinery by taking them out of the physiological context and placing them into a defined artificial environment. As a result of the "resolution revolution", cryo-EM is now the method of choice for the determination of 3D structures of large macromolecular assemblies *in vitro* at near atomic resolution (Callaway, 2020). Ultimately, however, cytokinesis should also be studied within the cellular context.

The first *in vivo* study on cytokinesis used fixed HeLa cells and revealed an elongated intercellular bridge (Byers and Abramson, 1968). The elongated bridge showed membrane thickenings, called "waves." These waves were claimed to relate to translational forces acting along arrays of microtubules. Concerted waves passing from the midbody to the cell were thought to exert forces on the connected cells, resulting in a separation of the cell pair (Byers and Abramson, 1968). Using D-98S cells, it was possible to quantify the change in the diameter of the intercellular bridge over time. The reduction in diameter was attributed to two subprocesses (Mullins and Biesele, 1977): first, a systematic breakdown of the midbody structure, and second a constriction causing a disintegration and a spatial rearrangement of microtubules. Along the narrowed plasma membrane of cellular bridges, wave-like ripples on both sides adjacent to the midbody were also observed in this experiment analyzing chemically fixed cells (see also **Figure 1B** for an example in HeLa cells). However, there was no evident sub-cellular structure visible by thin-section electron microscopy causing these ripples. Stretching of the intercellular bridge was

hypothesized to cause the final cut by reaching a "point of breakage" (Mullins and Biesele, 1977).

Membrane ripples were later observed by serial-section electron tomography of high-pressure frozen and freeze substituted intercellular bridges in HeLa cells (Guizetti et al., 2011). This study revealed intertwined helical filaments causing cortical constriction. The visualized filaments at the secondary constriction sites were 17.3 ± 2.5 nm wide and showed a helical pitch of 35.3 ± 4.1 nm (**Figures 1C,D**). Based on the helical properties of filaments assembled *in vitro* (Ghazi-Tabatabai et al., 2008; Hanson et al., 2008; Lata et al., 2008) and by comparison of wild-type and CHMP2A-depleted HeLa cells (Hanson et al., 2008; Guizetti et al., 2011), it was suggested that the *in vivo* observed filaments are polymerized ESCRT-III core components (Guizetti et al., 2011). However, a direct labeling of these ESCRT-III-dependent filaments, for instance by immuno-EM, has not been reported so far.

In terms of labeling, the antibody-stained ESCRT-III-subunit IST1 was visualized by stochastic optical reconstruction microscopy (STORM). It was shown that rings emanate parallel to the dark zone of the midbody. In later stages of abscission, spirals of IST1 were extending toward the abscission site with decreasing diameter and width (Goliand et al., 2018). Structural analysis of Madin-Darby canine kidney cells (MDCK) by soft X-ray cryo-tomography (Sherman et al., 2016) confirmed previous results regarding the membrane bulging from the midbody (Elia et al., 2011; Guizetti et al., 2011; Schiel et al., 2011; Crowell et al., 2014) and also showed membrane extrusions from the vicinity of the pre-abscission site. Three cortical rings were visualized with an average diameter of 1.43 ± 0.25 μm. Furthermore, three intertwined helices were imaged with an average diameter of 556 ± 15 nm, one of the helices extended to the abscission site (Sherman et al., 2016).

OUTLOOK

A number of *in vitro* ultrastructural studies of ESCRT-III components are based on single-particle analyses by cryo-EM (Su et al., 2017; Maity et al., 2019; Bertin et al., 2020; Huber et al., 2020; Moser von Filseck et al., 2020; Nguyen et al., 2020; Pfitzner et al., 2020). While *in vitro* experiments provide useful structural information about the building blocks of the abscission machinery under artificial conditions, it is difficult to correlate this information with the dynamic attributes of the cytokinetic apparatus under physiological conditions. In addition, isolated components may form artificial structures, thus leading to molecular mechanisms that may not fully represent the molecular processes as observed within cells. Along this line, *in vitro* purification can cause aggregation of ESCRT-III proteins (Wollert et al., 2009), induce dramatic conformational changes, diverse morphologies (Schöneberg et al., 2017) and non-physiological interactions of interdependent subunits. Furthermore, another problematic issue of *in vitro* studies is the lack of biomimetic substrates that capture the *in vivo* conditions on which ESCRT-III components can act upon. For all these reasons, an *in vitro* reconstruction of the abscission machinery might therefore be insufficient to explain the complexity of abscission within cells. Moreover, cellular crowding and local concentrations of the ESCRT-III components may have significant effects on the mechanism of abscission, inasmuch as time-dependent aspects need to be considered when analyzing the cytokinetic apparatus.

Interestingly, the number of *in vivo* ultrastructural analyses on cytokinesis is currently very small (Elia et al., 2011; Guizetti et al., 2011; Sherman et al., 2016; Mierzwa et al., 2017; Goliand et al., 2018). In fact, a systematic time-resolved study on the ultrastructure of abscission has never been performed. In addition, models on ESCRT-III function deduced from *in vitro* experiments need to be benchmarked against cellular conditions. Certainly, more *in vivo* structural studies would result in a better understanding of the abscission machinery in cells and clarify some fundamental questions such as: How does the geometry of ESCRT-III change during the elongation of the intercellular bridge? What are the interacting partners of ESCRT-III? How do they interact and coordinate with each other during cytokinesis? How do other cytoskeletal components cooperate with ESCRT-III proteins and how does RNAi silencing of helix forming subunits affect the ultrastructure of the abscission machinery? Moreover, how are the 17-nm cortical filaments anchored to the plasma membrane? To answer these questions, additional 3D analyses of intercellular bridges at defined time points need to be performed. Such time-resolved 4D studies will give important information on the development of the abscission machinery and the process of constriction.

In summary, while many high-resolution structures of subunits involved in abscission were solved under *in vitro* conditions, very little is known about the spatial organization and function of these subunits inside the cell. Therefore, *in vivo* ultrastructural studies should play an essential role in uncovering the discrete time-dependent steps of late cytokinesis. Subsequently, high-resolution structures should then be fitted into the electron density map of the abscission machinery. Thus, both *in vitro* and *in vivo* studies should be performed in parallel to grasp the full complexity of abscission across different imaging scales.

AUTHOR CONTRIBUTIONS

All authors listed have made a substantial, direct and intellectual contribution to the work, and approved it for publication.

FUNDING

TM-R received funding from the German Research Foundation (DFG grant MU 1423/12-1).

ACKNOWLEDGMENTS

The authors are grateful to Dr. Beata Mierzwa (UCSD), Dr. Julia Mahamid (EMBL Heidelberg), and Dr. Erin Tranfield (Instituto Gulbenkian de Ciencia) for a critical reading of the manuscript.

REFERENCES

Addi, C., Presle, A., Frémont, S., Cuvelier, F., Rocancourt, M., Milin, F., et al. (2020). The Flemmingsome reveals an ESCRT-to-membrane coupling via ALIX/syntenin/syndecan-4 required for completion of cytokinesis. *Nat. Commun.* 11:1941. doi: 10.1038/s41467-020-15205-z

Adell, M. A., and Teis, D. (2011). Assembly and disassembly of the ESCRT-III membrane scission complex. *FEBS Lett.* 585, 3191–3196. doi: 10.1016/j.febslet.2011.09.001

Adell, M. A. Y., Migliano, S. M., Upadhyayula, S., Bykov, Y. S., Sprenger, S., Pakdel, M., et al. (2017). Recruitment dynamics of ESCRT-III and Vps4 to endosomes and implications for reverse membrane budding. *eLife* 6:e31652. doi: 10.7554/eLife.31652

Agromayor, M., and Martin-Serrano, J. (2013). Knowing when to cut and run: mechanisms that control cytokinetic abscission. *Trends Cell Biol.* 23, 433–441. doi: 10.1016/j.tcb.2013.04.006

Azmi, I., Davies, B., Dimaano, C., Payne, J., Eckert, D., Babst, M., et al. (2006). Recycling of ESCRTs by the AAA-ATPase Vps4 is regulated by a conserved VSL region in Vta1. *J. Cell Biol.* 172, 705–717. doi: 10.1083/jcb.200508166

Baietti, M. F., Zhang, Z., Mortier, E., Melchior, A., Degeest, G., Geeraerts, A., et al. (2012). Syndecan-syntenin-ALIX regulates the biogenesis of exosomes. *Nat. Cell Biol.* 14, 677–685. doi: 10.1038/ncb2502

Bajorek, M., Schubert, H. L., McCullough, J., Langelier, C., Eckert, D. M., Stubblefield, W. M., et al. (2009). Structural basis for ESCRT-III protein autoinhibition. *Nat. Struct. Mol. Biol.* 16, 754–762. doi: 10.1038/nsmb.1621

Banjade, S., Tang, S., Shah, Y. H., and Emr, S. D. (2019). Electrostatic lateral interactions drive ESCRT-III heteropolymer assembly. *eLife* 8:e46207. doi: 10.7554/eLife.46207

Barr, F. A., and Gruneberg, U. (2007). Cytokinesis: placing and making the final cut. *Cell* 131, 847–860. doi: 10.1016/j.cell.2007.11.011

Bertin, A., de Franceschi, N., de la Mora, E., Maity, S., Alqabandi, M., Miguet, N., et al. (2020). Human ESCRT-III polymers assemble on positively curved membranes and induce helical membrane tube formation. *Nat. Commun.* 11:2663. doi: 10.1038/s41467-020-16368-5

Bhutta, M. S., McInerny, C. J., and Gould, G. W. (2014). ESCRT function in cytokinesis: location, dynamics and regulation by mitotic kinases. *Int. J. Mol. Sci.* 15, 21723–21739. doi: 10.3390/ijms151221723

Byers, B., and Abramson, D. H. (1968). Cytokinesis in HeLa: post-telophase delay and microtubule-associated motility. *Protoplasma* 66, 413–435. doi: 10.1007/BF01255868

Caballe, A., and Martin-Serrano, J. (2011). ESCRT machinery and cytokinesis: the road to daughter cell separation. *(2011). Traffic* 12, 1318–1326. doi: 10.1111/j.1600-0854.2011.01244.x

Callaway, E. (2020). 'It opens up a whole new universe': revolutionary microscopy technique sees individual atoms for first time. *Nature* 582, 156–157. doi: 10.1038/d41586-020-01658-1

Capalbo, L., Bassi, Z. I., Geymonat, M., Todesca, S., Copoiu, L., Enright, A. J., et al. (2019). The midbody interactome reveals unexpected roles for PP1 phosphatases in cytokinesis. *Nat. Commun.* 10:4513. doi: 10.1038/s41467-019-12507-9

Capalbo, L., Montembault, E., Takeda, T., Bassi, Z. I., Glover, D. M., and D'Avino, P. P. (2012). The chromosomal passenger complex controls the function of endosomal sorting complex required for transport-III Snf7 proteins during cytokinesis. *Open Biol.* 2:120070. doi: 10.1098/rsob.120070

Carlton, J. G., Agromayor, M., and Martin-Serrano, J. (2008). Differential requirements for Alix and ESCRT-III in cytokinesis and HIV-1 release. *Proc. Natl. Acad. Sci. U.S.A.* 105, 10541–10546. doi: 10.1073/pnas.0802008105

Carlton, J. G., and Martin-Serrano, J. (2007). Parallels between cytokinesis and retroviral budding: a role for the ESCRT machinery. *Science* 316, 1908–1912. doi: 10.1126/science.1143422

Cashikar, A. G., Shim, S., Roth, R., Maldazys, M. R., Heuser, J. E., and Hanson, P. I. (2014). Structure of cellular ESCRT-III spirals and their relationship to HIV budding. *eLife* 3:e02184. doi: 10.7554/eLife.02184

Chiaruttini, N., Redondo-Morata, L., Colom, A., Humbert, F., Lenz, M., Scheuring, S., et al. (2015). Relaxation of loaded ESCRT-III spiral springs drives membrane deformation. *Cell* 163, 866–879. doi: 10.1016/j.cell.2015.10.017

Christ, L., Raiborg, C., Wenzel, E. M., Campsteijn, C., and Stenmark, H. (2017). Cellular functions and molecular mechanisms of the ESCRT membrane-scission machinery. *Trends Biochem. Sci.* 42, 42–56. doi: 10.1016/j.tibs.2016.08.016

Connell, J. W., Lindon, C., Luzio, J. P., and Reid, E. (2009). Spastin couples microtubule severing to membrane traffic in completion of cytokinesis and secretion. *Traffic* 10, 42–56. doi: 10.1111/j.1600-0854.2008.00847.x

Crowell, E. F., Gaffuri, A. L., Gayraud-Morel, B., Tajbakhsh, S., and Echard, A. (2014). Engulfment of the midbody remnant after cytokinesis in mammalian cells. *J. Cell Sci.* 127, 3840–3851. doi: 10.1242/jcs.154732

Darenfed, H., and Mandato, C. A. (2005). Wound-induced contractile ring: a model for cytokinesis. *Biochem. Cell Biol.* 83, 711–720. doi: 10.1139/o05-164

Eggert, U. S., Mitchison, T. J., and Field, C. M. (2006). Animal cytokinesis: from parts list to mechanisms. *Annu. Rev. Biochem.* 75, 543–566. doi: 10.1146/annurev.biochem.74.082803.133425

Elia, N., Fabrikant, G., Kozlov, M. M., and Lippincott-Schwartz, J. (2012). Computational model of cytokinetic abscission driven by ESCRT-III polymerization and remodeling. *Biophys. J.* 102, 2309–2320. doi: 10.1016/j.bpj.2012.04.007

Elia, N., Sougrat, R., Spurlin, T. A., Hurley, J. H., and Lippincott-Schwartz, J. (2011). Dynamics of endosomal sorting complex required for transport (ESCRT) machinery during cytokinesis and its role in abscission. *Proc. Natl. Acad. Sci. U.S.A.* 108, 4846–4851. doi: 10.1073/pnas.1102714108

Fabbro, M., Zhou, B. B., Takahashi, M., Sarcevic, B., Lal, P., Graham, M. E., et al. (2005). Cdk1/Erk2- and Plk1-dependent phosphorylation of a centrosome protein, Cep55, is required for its recruitment to midbody and cytokinesis. *Dev. Cell* 9, 477–488. doi: 10.1016/j.devcel.2005.09.003

Field, C. M., and Alberts, B. M. (1995). Anillin, a contractile ring protein that cycles from the nucleus to the cell cortex. *J. Cell Biol.* 131, 165–178. doi: 10.1083/jcb.131.1.165

Frémont, S., and Echard, A. (2018). Membrane traffic in the late steps of cytokinesis. *Curr. Biol.* 28, R458–R470. doi: 10.1016/j.cub.2018.01.019

Garrus, J. E., von Schwedler, U. K., Pornillos, O. W., Morham, S. G., Zavitz, K. H., Wang, H. E., et al. (2001). Tsg101 and the vacuolar protein sorting pathway are essential for HIV-1 budding. *Cell* 107, 55–65. doi: 10.1016/s0092-8674(01)00506-2

Gatta, A. T., and Carlton, J. G. (2019). The ESCRT-machinery: closing holes and expanding roles. *Curr. Opin. Cell Biol.* 59, 121–132. doi: 10.1016/j.ceb.2019.04.005

Ghazi-Tabatabai, S., Saksena, S., Short, J. M., Pobbati, A. V., Veprintsev, D. B., Crowther, R. A., et al. (2008). Structure and disassembly of filaments formed by the ESCRT-III subunit Vps24. *Structure* 16, 1345–1356. doi: 10.1016/j.str.2008.06.010

Glotzer, M. (2001). Animal cell cytokinesis. *Annu. Rev. Cell Dev. Biol.* 17, 351–386. doi: 10.1146/annurev.cellbio.17.1.351

Goliand, I., Adar-Levor, S., Segal, I., Nachmias, D., Dadosh, T., Kozlov, M. M., et al. (2018). Resolving ESCRT-III spirals at the intercellular bridge of dividing cells using 3D STORM. *Cell Rep.* 24, 1756–1764. doi: 10.1016/j.celrep.2018.07.051

Gonciarz, M. D., Whitby, F. G., Eckert, D. M., Kieffer, C., Heroux, A., Sundquist, W. I., et al. (2008). Biochemical and structural studies of yeast Vps4 oligomerization. *J. Mol. Biol.* 384, 878–895. doi: 10.1016/j.jmb.2008.09.066

Gromley, A., Yeaman, C., Rosa, J., Redick, S., Chen, C. T., Mirabelle, S., et al. (2005). Centriolin anchoring of exocyst and SNARE complexes at the midbody is required for secretory-vesicle-mediated abscission. *Cell* 123, 75–87. doi: 10.1016/j.cell.2005.07.027

Guizetti, J., and Gerlich, D. W. (2010). Cytokinetic abscission in animal cells. *Semin. Cell Dev. Biol.* 21, 909–916. doi: 10.1016/j.semcdb.2010.08.001

Guizetti, J., Schermelleh, L., Mäntler, J., Maar, S., Poser, I., Leonhardt, H., et al. (2011). Cortical constriction during abscission involves helices of ESCRT-III-dependent filaments. *Science* 331, 1616–1620. doi: 10.1126/science.1201847

Gupta, T. K., Klumpe, S., Gries, K., Heinz, S., Wietrzynski, W., and Ohnishi, N. (2020). Structural basis for VIPP1 oligomerization and maintenance of thylakoid membrane integrity. *bioRxiv* doi: 10.1101/2020.08.11.243204

Guse, A., Mishima, M., and Glotzer, M. (2005). Phosphorylation of ZEN-4/MKLP1 by aurora B regulates completion of cytokinesis. *Curr. Biol.* 15, 778–786. doi: 10.1016/j.cub.2005.03.041

Hanson, P. I., Roth, R., Lin, Y., and Heuser, J. E. (2008). Plasma membrane deformation by circular arrays of ESCRT-III protein filaments. *J. Cell Biol.* 180, 389–402. doi: 10.1083/jcb.200707031

Henne, W. M., Buchkovich, N. J., Zhao, Y., and Emr, S. D. (2012). The endosomal sorting complex ESCRT-II mediates the assembly and architecture of ESCRT-III helices. *Cell* 151, 356–371. doi: 10.1016/j.cell.2012.08.039

Henne, W. M., Stenmark, H., and Emr, S. D. (2013). Molecular mechanisms of the membrane sculpting ESCRT pathway. *Cold Spring Harb. Perspect. Biol.* 5:a016766. doi: 10.1101/cshperspect.a016766

Huber, S. T., Mostafavi, S., Mortensen, S. A., and Sachse, C. (2020). Structure and assembly of ESCRT-III helical Vps24 filaments. *Sci. Adv.* 6:eaba4897. doi: 10.1126/sciadv.aba4897

Hunt, T. (1991). Cell biology. Destruction's our delight. *Nature* 349, 100–101. doi: 10.1038/349100a0

Hurley, J. H., and Emr, S. D. (2006). The ESCRT complexes: structure and mechanism of a membrane-trafficking network. *Annu. Rev. Biophys. Biomol. Struct.* 35, 277–298. doi: 10.1146/annurev.biophys.35.040405.102126

Karasmanis, E. P., Hwang, D., Nakos, K., Bowen, J. R., Angelis, D., and Spiliotis, E. T. (2019). A septin double ring controls the spatiotemporal organization of the ESCRT machinery in cytokinetic abscission. *Curr. Biol.* 29, 2174.e7–2182.e7. doi: 10.1016/j.cub.2019.05.050

Kieffer, C., Skalicky, J. J., Morita, E., De Domenico, I., Ward, D. M., Kaplan, J., et al. (2008). Two distinct modes of ESCRT-III recognition are required for VPS4 functions in lysosomal protein targeting and HIV-1 budding. *Dev. Cell* 15, 62–73. doi: 10.1016/j.devcel.2008.05.014

Kinoshita, M., Field, C. M., Coughlin, M. L., Straight, A. F., and Mitchison, T. J. (2002). Self- and actin-templated assembly of Mammalian septins. *Dev. Cell* 3, 791–802. doi: 10.1016/s1534-5807(02)00366-0

Kurasawa, Y., Earnshaw, W. C., Mochizuki, Y., Dohmae, N., and Todokoro, K. (2004). Essential roles of KIF4 and its binding partner PRC1 in organized central spindle midzone formation. *Embo J.* 23, 3237–3248. doi: 10.1038/sj.emboj.7600347

Lata, S., Schoehn, G., Jain, A., Pires, R., Piehler, J., Gottlinger, H. G., et al. (2008). Helical structures of ESCRT-III are disassembled by VPS4. *Science* 321, 1354–1357. doi: 10.1126/science.1161070

Lee, H. H., Elia, N., Ghirlando, R., Lippincott-Schwartz, J., and Hurley, J. H. (2008). Midbody targeting of the ESCRT machinery by a noncanonical coiled coil in CEP55. *Science* 322, 576–580. doi: 10.1126/science.1162042

Lee, K. Y., Esmaeili, B., Zealley, B., and Mishima, M. (2015). Direct interaction between centralspindlin and PRC1 reinforces mechanical resilience of the central spindle. *Nat. Commun.* 6:7290. doi: 10.1038/ncomms8290

Lekomtsev, S., Su, K. C., Pye, V. E., Blight, K., Sundaramoorthy, S., Takaki, T., et al. (2012). Centralspindlin links the mitotic spindle to the plasma membrane during cytokinesis. *Nature* 492, 276–279. doi: 10.1038/nature11773

Lindås, A. C., Karlsson, E. A., Lindgren, M. T., Ettema, T. J., and Bernander, R. (2008). A unique cell division machinery in the Archaea. *Proc. Natl. Acad. Sci. U.S.A.* 105, 18942–18946. doi: 10.1073/pnas.0809467105

Maity, S., Caillat, C., Miguet, N., Sulbaran, G., Effantin, G., Schoehn, G., et al. (2019). VPS4 triggers constriction and cleavage of ESCRT-III helical filaments. *Sci Adv.* 5:eaau7198. doi: 10.1126/sciadv.aau7198

Malerød, L., and Stenmark, H. (2009). ESCRTing membrane deformation. *Cell* 136, 15–17. doi: 10.1016/j.cell.2008.12.029

Mandal, T., Lough, W., Spagnolie, S. E., Audhya, A., and Cui, Q. (2020). Molecular simulation of mechanical properties and membrane activities of the ESCRT-III complexes. *Biophys. J.* 118, 1333–1343. doi: 10.1016/j.bpj.2020.01.033

McCullough, J., Clippinger, A. K., Talledge, N., Skowyra, M. L., Saunders, M. G., Naismith, T. V., et al. (2015). Structure and membrane remodeling activity of ESCRT-III helical polymers. *Science* 350, 1548–1551. doi: 10.1126/science.aad8305

Menon, M. B., and Gaestel, M. (2015). Sep(t)arate or not – how some cells take septin-independent routes through cytokinesis. *J. Cell Sci.* 128, 1877–1886. doi: 10.1242/jcs.164830

Mierzwa, B., and Gerlich, D. W. (2014). Cytokinetic abscission: molecular mechanisms and temporal control. *Dev. Cell* 31, 525–538. doi: 10.1016/j.devcel.2014.11.006

Mierzwa, B. E., Chiaruttini, N., Redondo-Morata, L., Moser, von Filseck, J., König, J., et al. (2017). Dynamic subunit turnover in ESCRT-III assemblies is regulated by Vps4 to mediate membrane remodelling during cytokinesis. *Nat. Cell Biol.* 19, 787–798. doi: 10.1038/ncb3559

Monroe, N., Han, H., Gonciarz, M. D., Eckert, D. M., Karren, M. A., Whitby, F. G., et al. (2014). The oligomeric state of the active Vps4 AAA ATPase. *J. Mol. Biol.* 426, 510–525. doi: 10.1016/j.jmb.2013.09.043

Monroe, N., Han, H., Shen, P. S., Sundquist, W. I., and Hill, C. P. (2017). Structural basis of protein translocation by the Vps4-Vta1 AAA ATPase. *eLife* 6:e24487. doi: 10.7554/eLife.24487

Monroe, N., and Hill, C. P. (2016). Meiotic clade AAA ATPases: protein polymer disassembly machines. *J. Mol. Biol.* 428, 1897–1911. doi: 10.1016/j.jmb.2015.11.004

Morita, E., Sandrin, V., Chung, H. Y., Morham, S. G., Gygi, S. P., Rodesch, C. K., et al. (2007). Human ESCRT and ALIX proteins interact with proteins of the midbody and function in cytokinesis. *Embo J.* 26, 4215–4227. doi: 10.1038/sj.emboj.7601850

Moser von Filseck, J., Barberi, L., Talledge, N., Johnson, I. E., Frost, A., Lenz, M., et al. (2020). Anisotropic ESCRT-III architecture governs helical membrane tube formation. *Nat. Commun.* 11:1516. doi: 10.1038/s41467-020-15327-4

Mullins, J. M., and Biesele, J. J. (1977). Terminal phase of cytokinesis in D-98s cells. *J. Cell Biol.* 73, 672–684. doi: 10.1083/jcb.73.3.672

Muzioł, T., Pineda-Molina, E., Ravelli, R. B., Zamborlini, A., Usami, Y., Göttlinger, H., et al. (2006). Structural basis for budding by the ESCRT-III factor CHMP3. *Dev. Cell* 10, 821–830. doi: 10.1016/j.devcel.2006.03.013

Nguyen, H. C., Talledge, N., McCullough, J., Sharma, A., Moss, F. R. III, Iwasa, J. H., et al. (2020). Membrane constriction and thinning by sequential ESCRT-III polymerization. *Nat. Struct. Mol. Biol.* 27, 392–399. doi: 10.1038/s41594-020-0404-x

Obita, T., Saksena, S., Ghazi-Tabatabai, S., Gill, D. J., Perisic, O., Emr, S. D., et al. (2007). Structural basis for selective recognition of ESCRT-III by the AAA ATPase Vps4. *Nature* 449, 735–739. doi: 10.1038/nature06171

Olmos, Y., and Carlton, J. G. (2016). The ESCRT machinery: new roles at new holes. *Curr. Opin. Cell Biol* 38, 1–11. doi: 10.1016/j.ceb.2015.12.001

Pfitzner, A. K., Mercier, V., Jiang, X., Moser, von Filseck, J., Baum, B., et al. (2020). An ESCRT-III polymerization sequence drives membrane deformation and fission. *Cell* 182, 1140.e18–1155.e18. doi: 10.1016/j.cell.2020.07.021

Renshaw, M. J., Liu, J., Lavoie, B. D., and Wilde, A. (2014). Anillin-dependent organization of septin filaments promotes intercellular bridge elongation and Chmp4B targeting to the abscission site. *Open Biol.* 4:130190. doi: 10.1098/rsob.130190

Schiel, J. A., Park, K., Morphew, M. K., Reid, E., Hoenger, A., and Prekeris, R. (2011). Endocytic membrane fusion and buckling-induced microtubule severing mediate cell abscission. *J. Cell Sci.* 124, 1411–1424. doi: 10.1242/jcs.081448

Schiel, J. A., and Prekeris, R. (2010). Making the final cut - mechanisms mediating the abscission step of cytokinesis. *Sci. World J.* 10, 1424–1434. doi: 10.1100/tsw.2010.129

Schiel, J. A., Simon, G. C., Zaharris, C., Weisz, J., Castle, D., Wu, C. C., et al. (2012). FIP3-endosome-dependent formation of the secondary ingression mediates ESCRT-III recruitment during cytokinesis. *Nat. Cell Biol.* 14, 1068–1078. doi: 10.1038/ncb2577

Schmidt, O., and Teis, D. (2012). The ESCRT machinery. *Curr. Biol.* 22, 116–120. doi: 10.1016/j.cub.2012.01.028

Schöneberg, J., Lee, I. H., Iwasa, J. H., and Hurley, J. H. (2017). Reverse-topology membrane scission by the ESCRT proteins. *Nat. Rev. Mol. Cell Biol.* 18, 5–17. doi: 10.1038/nrm.2016.121

Scott, A., Chung, H. Y., Gonciarz-Swiatek, M., Hill, G. C., Whitby, F. G., Gaspar, J., et al. (2005). Structural and mechanistic studies of VPS4 proteins. *Embo J.* 24, 3658–3669. doi: 10.1038/sj.emboj.7600818

Sherman, S., Kirchenbuechler, D., Nachmias, D., Tamir, A., Werner, S., Elbaum, M., et al. (2016). Resolving new ultrastructural features of cytokinetic abscission with soft-X-ray cryo-tomography. *Sci Rep.* 6:27629. doi: 10.1038/srep27629

Shestakova, A., Curtiss, M., Davies, B. A., Katzmann, D. J., and Babst, M. (2013). The linker region plays a regulatory role in assembly and activity of the Vps4 AAA ATPase. *J. Biol. Chem.* 288, 26810–26819. doi: 10.1074/jbc.M113.497032

Shestakova, A., Hanono, A., Drosner, S., Curtiss, M., Davies, B. A., Katzmann, D. J., et al. (2010). Assembly of the AAA ATPase Vps4 on ESCRT-III. *Mol. Biol. Cell* 21, 1059–1071. doi: 10.1091/mbc.e09-07-0572

Skop, A. R., Liu, H., Yates, J. III, Meyer, B. J., and Heald, R. (2004). Dissection of the mammalian midbody proteome reveals conserved cytokinesis mechanisms. *Science* 305, 61–66. doi: 10.1126/science.1097931

Stoten, C. L., and Carlton, J. G. (2018). ESCRT-dependent control of membrane remodelling during cell division. *Semin. Cell Dev. Biol.* 74, 50–65. doi: 10.1016/j.semcdb.2017.08.035

Stuchell-Brereton, M. D., Skalicky, J. J., Kieffer, C., Karren, M. A., and Ghaffarian, S. (2007). Sundquist W.I. ESCRT-III recognition by VPS4 ATPases. *Nature* 449, 740–744. doi: 10.1038/nature06172

Su, M., Guo, E. Z., Ding, X., Li, Y., Tarrasch, J. T., Brooks, C. L. III, et al. (2017). Mechanism of Vps4 hexamer function revealed by cryo-EM. *Sci. Adv.* 3:e1700325. doi: 10.1126/sciadv.1700325

Takahashi, N., Hatakeyama, H., Okado, H., Miwa, A., Kishimoto, T., Kojima, T., et al. (2004). Sequential exocytosis of insulin granules is associated with redistribution of SNAP25. *J. Cell Biol.* 165, 255–262. doi: 10.1083/jcb.200312033

Tang, S., Buchkovich, N. J., Henne, W. M., Banjade, S., Kim, Y. J., and Emr, S. D. (2016). ESCRT-III activation by parallel action of ESCRT-I/II and ESCRT-0/Bro1 during MVB biogenesis. *eLife* 5:e15507. doi: 10.7554/eLife.15507

Tang, S., Henne, W. M., Borbat, P. P., Buchkovich, N. J., Freed, J. H., Mao, Y., et al. (2015). Structural basis for activation, assembly and membrane binding of ESCRT-III Snf7 filaments. *eLife* 4:e12548. doi: 10.7554/eLife.12548

Teis, D., Saksena, S., and Emr, S. D. (2008). Ordered assembly of the ESCRT-III complex on endosomes is required to sequester cargo during MVB formation. *Dev. Cell* 15, 578–589. doi: 10.1016/j.devcel.2008.08.013

Thoresen, S. B., Campsteijn, C., Vietri, M., Schink, K. O., Liestøl, K., Andersen, J. S., et al. (2014). ANCHR mediates Aurora-B-dependent abscission checkpoint control through retention of VPS4. *Nat. Cell Biol.* 16, 550–560. doi: 10.1038/ncb2959

Vietri, M., Schink, K. O., Campsteijn, C., Wegner, C. S., Schultz, S. W., Christ, L., et al. (2015). Spastin and ESCRT-III coordinate mitotic spindle disassembly and nuclear envelope sealing. *Nature* 522, 231–235. doi: 10.1038/nature14408

Wheatley, S. P., Hinchcliffe, E. H., Glotzer, M., Hyman, A. A., Sluder, G., and Wang, Y. L. (1997). CDK1 inactivation regulates anaphase spindle dynamics and cytokinesis in vivo. *J. Cell Biol.* 138, 385–393. doi: 10.1083/jcb.138.2.385

Wheatley, S. P., and Wang, Y. (1996). Midzone microtubule bundles are continuously required for cytokinesis in cultured epithelial cells. *J. Cell Biol.* 135, 981–989. doi: 10.1083/jcb.135.4.981

Wollert, T., Wunder, C., Lippincott-Schwartz, J., and Hurley, J. H. (2009). Membrane scission by the ESCRT-III complex. *Nature* 458, 172–177. doi: 10.1038/nature07836

Yang, B., Stjepanovic, G., Shen, Q., Martin, A., and Hurley, J. H. (2015). Vps4 disassembles an ESCRT-III filament by global unfolding and processive translocation. *Nat. Struct. Mol. Biol.* 22, 492–498. doi: 10.1038/nsmb.3015

Yang, D., Rismanchi, N., Renvoisé, B., Lippincott-Schwartz, J., Blackstone, C., and Hurley, J. H. (2008). Structural basis for midbody targeting of spastin by the ESCRT-III protein CHMP1B. *Nat. Struct. Mol. Biol.* 15, 1278–1286. doi: 10.1038/nsmb.1512

Yeo, S. C., Xu, L., Ren, J., Boulton, V. J., Wagle, M. D., Liu, C., et al. (2003). Vps20p and Vta1p interact with Vps4p and function in multivesicular body sorting and endosomal transport in Saccharomyces cerevisiae. *J. Cell Sci.* 116, 3957–3970. doi: 10.1242/jcs.00751

Zhu, L., Jorgensen, J. R., Li, M., Chuang, Y. S., and Emr, S. D. (2017). ESCRTs function directly on the lysosome membrane to downregulate ubiquitinated lysosomal membrane proteins. *eLife* 6:e26403. doi: 10.7554/eLife.26403

Conflict of Interest: The authors declare that the research was conducted in the absence of any commercial or financial relationships that could be construed as a potential conflict of interest.

frontiers in Cell and Developmental Biology

ORIGINAL RESEARCH
published: 17 November 2020
doi: 10.3389/fcell.2020.591141

Rac and Arp2/3-Nucleated Actin Networks Antagonize Rho During Mitotic and Meiotic Cleavages

*Debadrita Pal[1], Andrea Ellis[1], Silvia P. Sepúlveda-Ramírez[1], Torey Salgado[1], Isabella Terrazas[1], Gabriela Reyes[1], Richard De La Rosa[1], John H. Henson[2] and Charles B. Shuster[1]**

[1] Department of Biology, New Mexico State University, Las Cruces, NM, United States, [2] Department of Biology, Dickinson College, Carlisle, PA, United States

In motile cells, the activities of the different Rho family GTPases are spatially segregated within the cell, and during cytokinesis there is evidence that this may also be the case. But while Rho's role as the central organizer for contractile ring assembly is well established, the role of Rac and the branched actin networks it promotes is less well understood. To characterize the contributions of these proteins during cytokinesis, we manipulated Rac and Arp2/3 activity during mitosis and meiosis in sea urchin embryos and sea star oocytes. While neither Rac nor Arp2/3 were essential for early embryonic divisions, loss of either Rac or Arp2/3 activity resulted in polar body defects. Expression of activated Rac resulted in cytokinesis failure as early as the first division, and in oocytes, activated Rac suppressed both the Rho wave that traverses the oocyte prior to polar body extrusion as well as polar body formation itself. However, the inhibitory effect of Rac on cytokinesis, polar body formation and the Rho wave could be suppressed by effector-binding mutations or direct inhibition of Arp2/3. Together, these results suggest that Rac- and Arp2/3 mediated actin networks may directly antagonize Rho signaling, thus providing a potential mechanism to explain why Arp2/3-nucleated branched actin networks must be suppressed at the cell equator for successful cytokinesis.

Keywords: cytokinesis, Rac, Rho, Arp2/3, meiosis, sea urchin, sea star, contractile ring

OPEN ACCESS

Edited by:
Issei Mabuchi,
The University of Tokyo, Japan

Reviewed by:
Yibo Luo,
The University of Toledo, United States
Yukako Nishimura,
National University of Singapore, Singapore
Amy Maddox,
The University of North Carolina at Chapel Hill, United States

****Correspondence:***
Charles B. Shuster
cshuster@nmsu.edu

Specialty section:
This article was submitted to Cell Growth and Division, a section of the journal Frontiers in Cell and Developmental Biology

Received: *03 August 2020*
Accepted: *20 October 2020*
Published: *17 November 2020*

Citation:
Pal D, Ellis A, Sepúlveda-Ramírez SP, Salgado T, Terrazas I, Reyes G, De La Rosa R, Henson JH and Shuster CB (2020) Rac and Arp2/3-Nucleated Actin Networks Antagonize Rho During Mitotic and Meiotic Cleavages. Front. Cell Dev. Biol. 8:591141. doi: 10.3389/fcell.2020.591141

INTRODUCTION

Cytokinesis is the final phase of cell division where in animal and fungal cells, a transient assemblage of actin and myosin II assembles at the former metaphase plate to effect the partitioning of the two daughter cells. Due to the unique spatiotemporal parameters that drive contractile ring assembly, cytokinesis is often considered distinct from other motility events in animal cells, yet parallels exist between cytokinesis and polarized cell migration, especially in regard to the Rho family GTPases. In crawling cells, there is a symmetry-breaking event that drives the localized activation of the small GTPases Rac and/or Cdc42, which in turn promote the elaboration of viscoelastic, branched actin networks at the leading edge to effect forward protrusion (Blanchoin et al., 2014; Schaks et al., 2019). In contrast, Rho activity at the rear promotes contractility and retraction of the trailing edge (Machacek et al., 2009). During cytokinesis, there is an analogous spatial segregation of Rho GTPase activity, with Rho activated at the cell equator (Yoshizaki et al., 2003; Bement et al., 2005), whereas Rac/Cdc42 activity is cleared from the cell equator and enriched in domains of

cytoplasm undergoing post-mitotic spreading (Yoshizaki et al., 2003). There are multiple potential mechanisms by which Rho and Rac may antagonize one another (Guilluy et al., 2011), and there is evidence that mutual Rho-Rac antagonism may be a fundamental aspect of polarized cell migration (Byrne et al., 2016). Whether a Rho-Rac negative regulatory circuit plays a functional role during cytokinesis has not been firmly established.

Following anaphase onset and the initiation of mitotic exit, symmetry is broken by the mitotic apparatus, which specifies the equatorial position of Rho activation and contractile ring assembly (Basant and Glotzer, 2018). The primary component of the signaling apparatus that determines the cleavage plane is the centralspindlin complex, comprised of the Mitotic Kinesin Like Protein (MKLP1) and Cyk4/MgcRacGAP, which not only plays a role in organizing the post-anaphase central spindle (Mishima et al., 2002) but also recruits the RhoGEF Ect2 (Yüce et al., 2005) to activate Rho at the cell equator. The precise role of GAP activity of Cyk4 has been difficult to elucidate, and there have been multiple proposed roles for Cyk4 that invoke RhoGAP activity, RacGAP activity, or indirect promotion of Rho activation (Canman et al., 2008; Miller et al., 2008; Loria et al., 2012; Tse et al., 2012; Breznau et al., 2015; Zhang and Glotzer, 2015; Zhuravlev et al., 2017). The notion of a negative regulatory role for Rac has been supported by studies in cultured mammalian cells (Yoshizaki et al., 2004; Bastos et al., 2012; Cannet et al., 2014), *Drosophila* (D'Avino et al., 2004) and *Caenorhabditis elegans* embryos (Canman et al., 2008; Zhuravlev et al., 2017). There are multiple effector pathways by which activated Rac might antagonize cytokinesis (Jordan and Canman, 2012), and there is evidence that Rac may disrupt cytokinesis through PAK-mediated promotion of cell adhesion (Bastos et al., 2012) or through WAVE-mediated activation of Arp2/3 (Canman et al., 2008; Cannet et al., 2014). While these studies implicate Rac as a negative regulator of cytokinesis, a common mechanism by which Rac antagonizes Rho-mediated contractile ring assembly yet to emerge.

To further explore the notion that the spatiotemporal regulation of cytokinesis might involve antagonism between Rac and Rho, we modulated Rac activity during mitotic divisions in early sea urchin embryos and meiotic divisions in sea star oocytes. In contrast to symmetrical divisions, polar body formation exemplifies a highly asymmetric division that involves a (1) surface contraction wave (SCW) that terminates at the site of polar body formation, (2) protrusion of the anaphase spindle and (3) centralspindlin-mediated ring constriction (Zhang et al., 2008; Maddox et al., 2012; Satoh et al., 2013), and both Rac and Arp2/3 have been directly or indirectly implicated in this process (Maddox et al., 2012). Live cell imaging of sea urchin zygotes revealed that while neither Rac nor Arp2/3 were not required for cell division in the early embryo, expression of activated mutants of Rac disrupted both cytokinesis and normal actin dynamics throughout the embryo. However, the effect of dysregulated Rac activity could be suppressed by effector-binding mutations or direct inhibition of Arp2/3-mediated actin polymerization. During oocyte maturation, Rac and Arp2/3 were required for spindle docking at the cortex, but dysregulated Rac activity suppressed polar body formation in an Arp2/3-dependent manner by directly suppressing the wave of Rho activity that drives the SCW during anaphase I. Together, our results suggest that Rac-stimulated branched actin networks may act as a direct antagonist to Rho activity, which may provide an additional layer of spatial regulation to promote efficient daughter cell partitioning during cytokinesis.

RESULTS

Actin Organization in the Sea Urchin Zygote

To better understand the respective roles of Rho and Rac in regulating cell shape change and cytokinesis, we first employed live cell imaging of actin during the first division of the sea urchin embryo to establish a baseline by which further perturbations could be compared (**Figure 1**). Injection of recombinant Lifeact-GFP labeled actin filaments throughout the cortex and cytoplasm without compromising cell viability, with embryos surviving through gastrulation. During interphase, there was a bright, perinuclear rim of EGFP-Lifeact that increased in intensity until nuclear envelope breakdown (**Figures 1A,F**). Lifeact labeled the dense array of microvilli and microvillar rootlets that extended into the cytoplasm. Following nuclear envelope breakdown, the rootlets retracted and microvilli remained short and dense (**Figures 1A,B**) up until the metaphase-anaphase transition, at which time microvilli elongated (**Figures 1C,K,M**), consistent with previous observations made in fixed specimens (Wong et al., 1997). Submembranous cortical actin, obscured by microvilli earlier in mitosis, could be observed undergoing a transient thinning at the metaphase-anaphase transition, followed by an isotropic thickening just prior to the onset of cytokinesis (**Figures 1C,K,M** and **Supplementary Movie S1**). There was also an elaboration of actin filaments in the cytoplasm that peaked after anaphase onset and dissipated during cytokinesis, which appeared in kymographs as parallel streaks (**Figures 1D,E,L** and **Supplementary Movie S1**). Lastly, inactivation of Rho with C3 transferase blocked cytokinesis (**Figures 1F−K**), but had no overt qualitative effects on the different actin populations. However, Rho inactivation did result in an increase in the accumulation of cytoplasmic actin (**Figure 1L**) and disrupted the thickening of the cortex during mitotic exit (**Figures 1H−K,M** and **Supplementary Movie S2**). Thus, of all the different actin populations identified by live cell imaging, Rho appeared to be only required for the thickening of the cell cortex during mitotic exit as well as its well-characterized role in contractile ring formation (Mabuchi et al., 1993).

Inactivation of Rac Is Required for Cytokinesis

In the sea urchin zygote, Rac transcript levels are seven-fold higher than Cdc42 (Tu et al., 2014) and given the proposed antagonistic role of Rac during cytokinesis (Canman et al., 2008), efforts were focused on Rac. Microinjection of mRNA encoding wild type or dominant-negative (T17N)

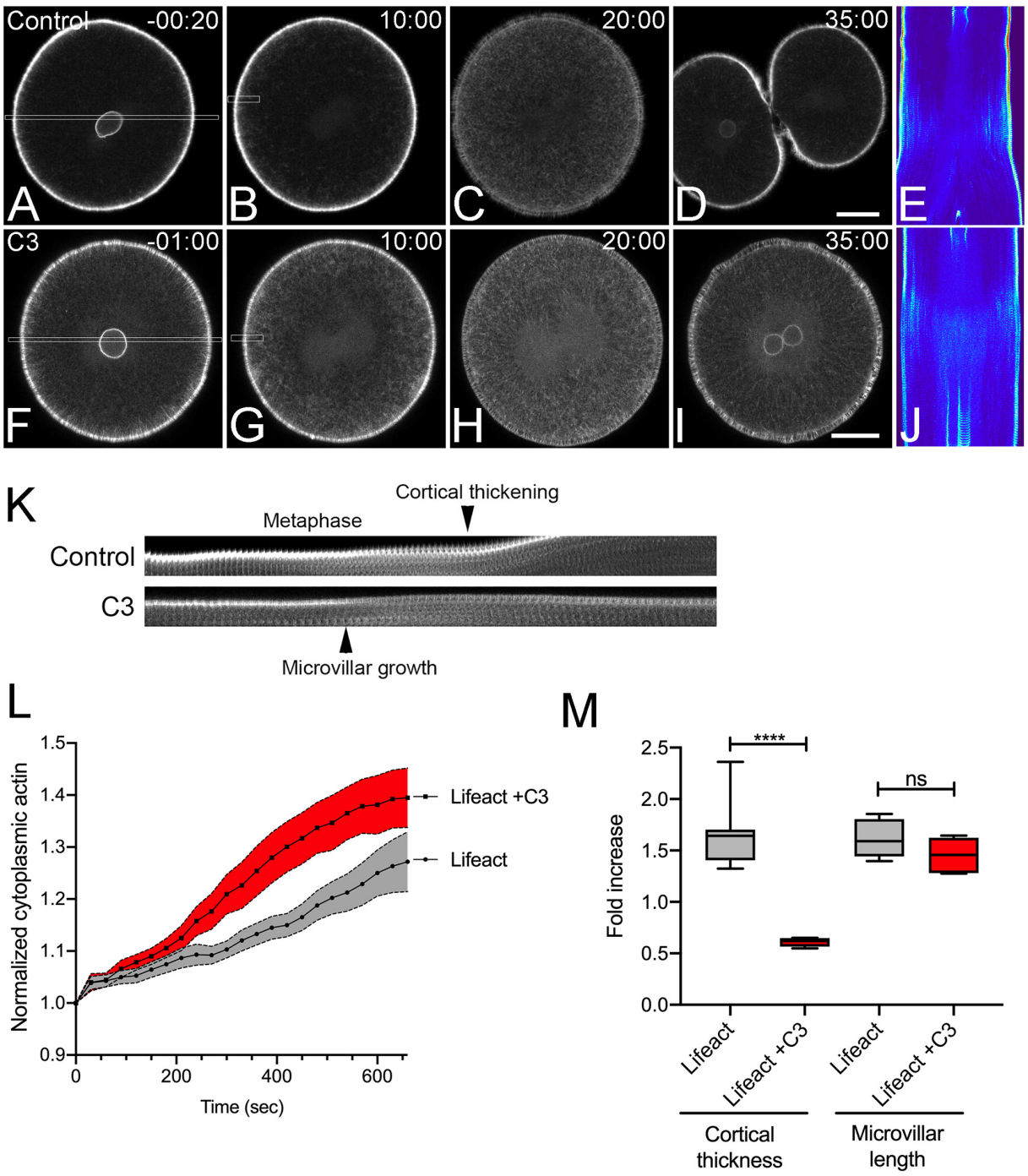

FIGURE 1 | Actin dynamics in the dividing sea urchin embryo. Frames from time-lapse movies of *L. variegatus* embryos injected with either recombinant Lifeact-GFP (**A–E**, final intracellular concentration of 0.21 μM) or Lifeact-GFP and C3 Transferase (**F–J**, final intracellular concentration 0.27 μM). Bar, 30 μm. Time points denote minutes post-nuclear envelope breakdown (NEB). **(E,J)** Corresponding kymographs of sections taken through the long axis of the spindle as denoted by the rectangles in panels **(A,F)**. Prior to nuclear envelope breakdown a bright rim of perinuclear actin is visible **(A,F)**. Upon mitotic entry, microvilli and their rootlets shorten, and there is a gradual increase in deep cytoplasmic actin initiating at the cortex and accumulating inward up until anaphase onset **(C,E,H,J)**. **(K)** Kymograph of cortical microvillar dynamics in the polar regions of control- and C3-injected embryos, taken from regions denoted by the small rectangles in Panels **(B,G)**. **(L)** Quantification of cytoplasmic actin levels beginning 1 min post-NEB up until the metaphase-anaphase transition (Mean ± SEM, $n = 6$ cells per condition). While there was not a qualitative effect of Rho inactivation on cytoplasmic actin, there was a significant increase in cytoplasmic Lifeact fluorescence in C3-injected embryos. **(M)** Quantitation of the increases in cortical thickness and microvillar length that accompanies the metaphase-anaphase transition in control and C3-injected embryos ($n = 6$ cells per condition, whiskers denote minimum and maximum values), where a value of 1.0 represents length or thickness 1 min prior to the metaphase-anaphase transition. While there was no significant difference in the growth of microvilli, Rho inactivation blocked the thickening of actin cortex. ****$p < 0.0001$.

Rac together with EGFP-Lifeact into sea urchin embryos resulted in morphologically indistinguishable mesenchymal blastulae (**Supplementary Figure S1B**), suggesting that Rac was dispensable for at least the first ten cleavages. To further explore the notion that Rac may play an antagonistic role in cytokinesis, a constitutively active (Q61L) form of sea urchin Rac was generated as well as an effector-binding mutant that blocked interaction with the WAVE complex (F37A) and thus the downstream activation of Arp2/3 (Lamarche et al., 1996). The activities of these mutants were validated in cultured cells (**Supplementary Figure S1C**) and then expressed in *Lytechinus variegatus* embryos during the first cell cycle (**Figure 2**). In contrast to wild-type (WT) Rac (**Figures 2A–C** and **Supplementary Movie S3**), Q61L Rac had a strong negative effect on cytokinesis at the first division, with Q61L Rac expressing cells failing to initiate furrowing (**Figure 2B**, **Supplementary Movie S3**). However, the effector-binding F37A mutation suppressed the inhibitory effect of constitutively active Rac, both in terms of the overall success rates of cleavage (**Figure 2A**) as well as the rate of furrow ingression where WT and Q61L/F37A expressing embryos had superimposable furrowing rates (**Figure 2B**). Examination of actin dynamics in Q61L Rac embryos revealed no gross disruptions in actin organization during the first cell cycle (**Figure 2C** and **Supplementary Movie S3**), although in later divisions, actin organization was more dramatically altered, with pseudopodial processes extending and retracting from the cell surface (**Supplementary Movie S4**). Quantification of actin dynamics revealed that the accumulation of cytoplasmic actin, thickening of the actin cortex and microvillar elongation were all significantly disrupted in Q61L-expressing embryos, but suppressed in embryos expressing Q61L/F37A Rac (**Figures 2D–F** and **Supplementary Movie S3**). Thus, in addition to the two Rho-independent actin populations (microvillar and cytoplasmic actin), dysregulated Rac significantly suppressed Rho-dependent cortical thickening and contractile ring formation, and this effect appeared to be dependent on effectors that were sensitive to the F37A mutation.

Direct Inhibition of the Arp2/3 Complex Rescues Furrowing in Q61L-Expressing Cells

Constitutively active Rac blocked cytokinesis through effectors sensitive to the F37A mutation (**Figure 2**), which has been previously reported to affect WAVE activation and Arp2/3-mediated actin polymerization (Lamarche et al., 1996). Indeed, immuno-labeling of Arp3 in *Strongylocentrotus purpuratus* embryos revealed that Arp2/3 is isotropically distributed throughout the polar and equatorial cortices of anaphase embryos, but as cytokinesis progressed, Arp2/3 was increasingly cleared from the equatorial plane (**Figures 3A,B**). Pharmaceutical inhibition of Arp2/3 with the small molecule inhibitor CK-666 (Nolen et al., 2009) did not inhibit cytokinesis during the first cleavage, but did slow the rate of furrowing (**Figure 3C**) such that the time required to reach 50% ingression was increased by approximately 90 s (**Figure 3D**). Quantification of the different actin populations revealed that while a depression of cytoplasmic actin could be observed in CK-666 treated embryos (**Figure 3E**), there were no significant differences in the increases in cortical thickness and microvillar length in Arp2/3-inhibited embryos (**Figure 3F**).

Introduction of the F37A mutation neutralized the ability of constitutively active Rac to block cytokinesis (**Figure 2**). To further explore the potential role of Arp2/3, embryos expressing WT or Q61L Rac were scored for cleavage in the absence or presence of the Arp2/3 inhibitor. Direct inhibition of the Arp2/3 complex rescued cytokinesis in Q61L Rac-expressing embryos (**Figure 3G**). And while CK-666 did not affect the dynamics of cytoplasmic actin in Q61L Rac embryos (**Figure 3H**), Arp2/3 inhibition did rescue Rho-dependent thickening of the cortical layer (**Figure 3I**). Thus, while Rac is capable of activating a variety of downstream effector pathways (Jordan and Canman, 2012), Rac's promotion of Arp2/3-mediated branched actin networks appeared to be what was responsible for Rac's deleterious effects on cytokinesis.

Rac and Arp2/3 Involvement in Polar Body Formation in Starfish Oocytes

Expression of constitutively active Rac had a strong, inhibitory effect on cytokinesis in sea urchin zygotes (**Figure 2**), in agreement with studies in cultured cells (Yoshizaki et al., 2004). However, both Rac and Arp2/3 are required for meiotic divisions in mouse oocytes, through the regulation of cytoplasmic streaming and spindle migration (Halet and Carroll, 2007; Leblanc et al., 2011; Sun et al., 2011a; Chaigne et al., 2013, 2016; Yi et al., 2013; Wang et al., 2014). Polar body formation during meiotic maturation is thought to occur through a combination of a SCW, a localized protrusion of the cortex induced by the meiotic spindle, and the canonical cytokinetic signaling apparatus (Maddox et al., 2012; Satoh et al., 2013; Bischof et al., 2017; Klughammer et al., 2018). To investigate the potentially opposing roles of Rac in meiotic cytokinesis, *Patiria miniata* oocytes expressing markers for actin, Rho activity and the Arp2/3 complex were imaged during first meiosis. Polar body extrusion begins at the vegetal pole with a SCW that traverses the egg and terminates at the site of polar body extrusion, where the centralspindlin complex organizes a contractile ring (**Figure 4A** and **Supplementary Movies S5–S7**). This wave could be easily observed with either Lifeact or rGBD-GFP, a rhotekin-based biosensor that labels zones of active Rho (Benink and Bement, 2005). In contrast to these probes as well as the formin Diaphanous (Ucar et al., 2013) that label the constricting neck of the polar body protrusion, the Arp2/3 subunit ArpC1 only weakly labeled the cortex until the initiation of polar body extrusion, when it could be observed at the cortex in association with the protruding spindle pole (**Figure 4A**, arrowhead and **Supplementary Movie S7**). The meiotic spindles of sea star oocytes form near the site of polar body extrusion, and in contrast to controls, Arp2/3 inhibition resulted a failure in the spindle to induce a protrusion and polar body formation failed (**Figures 4B,C** and **Supplementary Movie S8**). Of the 15 cells observed by time-lapse microscopy, five oocytes displayed spindles that failed to dock at the cortex; and of the other 10

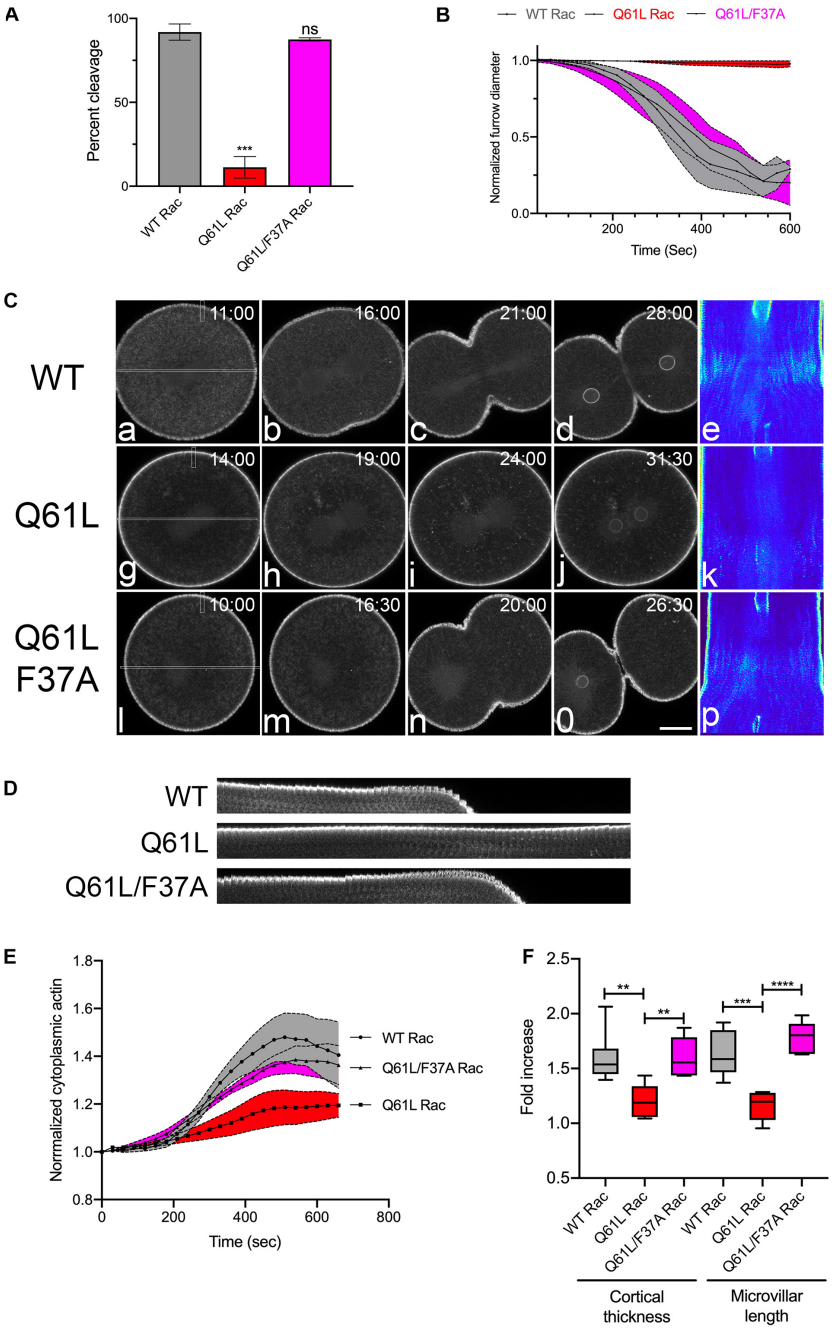

FIGURE 2 | Activated Rac suppresses actin dynamics and cytokinesis. **(A)** Cleavage rates for *L. variegatus* embryos injected with WT, Q61L or Q61L/F37A Rac mRNA (final intracellular concentration 2.5 μg/ml) and recombinant Lifeact-GFP (final intracellular concentration 0.2 μM) immediately after fertilization and cultured at 20°C until un-injected controls completed cytokinesis. Mean ± SEM for three experimental replicates, with >21 cells per experiment. ***$p < 0.001$. **(B)** Furrow ingression profiles for injected cells, beginning at the initiation of furrowing (mean ± SEM, $n = 5$ per condition). **(C)** Frames from time-lapse movies of *L. variegatus* embryos injected with mRNA encoding WT or mutant Rac. Time points denote minutes post-NEB. Bar, 30 μm. Rectangles in panels **(a,g,l)** denote the region used to generate the kymographs in panels **(e,k,p)**. Small rectangles denote regions used to generate the kymographs in panel **(D)**. Bar, 30 μm. **(D)** Kymograph highlighting microvillar growth and cortical actin dynamics during mitotic exit in WT or mutant Rac-expressing cells. **(E)** Quantification of cytoplasmic actin levels beginning 1 min post-NEB up until the metaphase-anaphase transition (Mean ± SEM, $n = 6$ cells per condition). Activated Rac (Q61L, red) suppressed the increase in cytoplasmic actin in comparison to WT (gray), whereas activated Rac containing the effector-binding mutation F37A (Q61L/F37A, magenta) had no effect on cytoplasmic actin levels. **(F)** Quantitation of the increases in cortical thickness and microvillar length that accompanies the metaphase-anaphase transition in embryos expressing WT and mutant Rac ($n = 6$ cells per condition, whiskers denote minimum and maximum values), where a value of 1.0 represents length or thickness 1 min prior to the metaphase-anaphase transition. Activated Rac blocked both cortical thickening and microvillar elongation, but these actin dynamics were rescued in embryos expressing the double mutant that is incapable of promoting WAVE-mediated Arp2/3 activation. **$p < 0.005$, ****$p < 0.0001$.

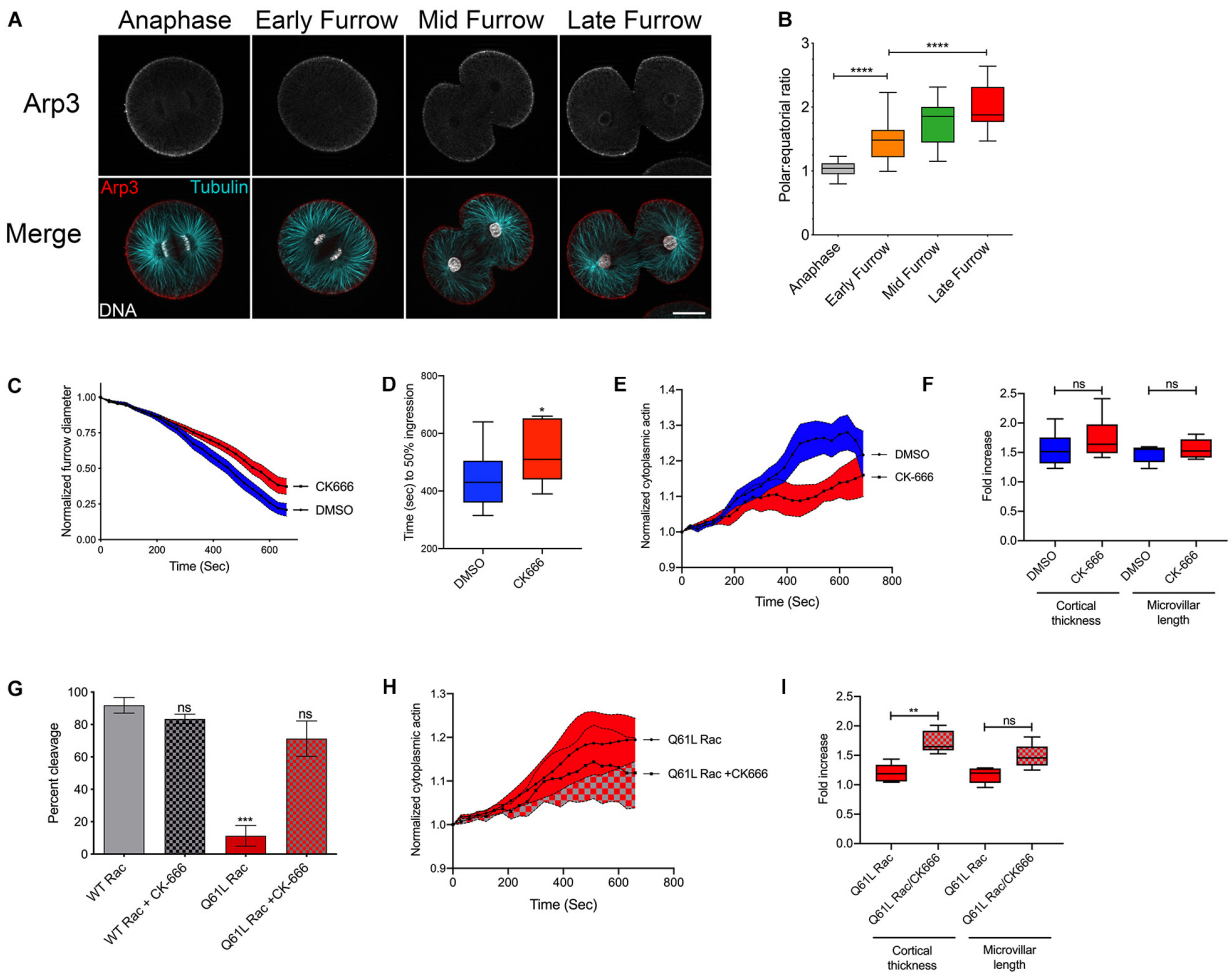

FIGURE 3 | Activated Rac suppresses cytokinesis through Arp2/3. **(A,B)** *S. purpuratus* embryos probed for Arp3 (top row in grayscale, red in the merged image), tubulin (cyan), and DNA (White). Bar, 30 μm. As cytokinesis progresses, Arp2/3 is increasingly excluded from the furrow region. ****$p < 0.0001$. **(C)** Arp2/3 delays but does not block cytokinesis. Embryos were treated with 0.1% DMSO or 100 μM CK-666 prior to nuclear envelope breakdown, and furrow diameter was measured by Nomarski/DIC starting at the initiation of furrowing (mean ± SEM, $n = 13$ for DMSO, $n = 12$ for CK-666). **(D)** Comparison of the rates of furrowing (time to 50% ingression), *$p < 0.05$. **(E)** Quantification of cytoplasmic actin levels in either DMSO- or CK-666-treated embryos beginning 1 min post-NEB up until the metaphase-anaphase transition (Mean ± SEM, $n = 6$ cells per condition). **(F)** Quantitation of the increases in cortical thickness and microvillar length that accompanies the metaphase-anaphase transition in DMSO or CK-666-treated embryos expressing ($n = 6$ cells per condition, whiskers denote minimum and maximum values), where a value of 1.0 represents length or thickness 1 min prior to the metaphase-anaphase transition. No significant differences were detected for either actin population. **(G)** Arp2/3 inhibition rescues cytokinesis in embryos expressing activated Rac. Q61L Rac data replicated from **Figure 2A**. Mean ± SEM for three experimental replicates, >24 cells per experiment. ***$p < 0.001$. **(H)** Cytoplasmic actin levels in embryos expressing Q61L Rac in the absence or presence of CK-666, beginning 1 min post-NEB up until the metaphase-anaphase transition (Mean ± SEM, $n = 6$ cells per condition). **(I)** Quantitation of the increases in cortical thickness and microvillar length that accompanies the metaphase-anaphase transition in embryos expressing Q61L Rac in the absence or presence of CK-666 ($n = 6$ cells per condition, whiskers denote minimum and maximum values), where a value of 1.0 represents length or thickness 1 min prior to the metaphase-anaphase transition. **$p = 0.005$.

samples, eight oocytes failed to form a protrusion and two were able to form a shallow protrusion which was absorbed back into the cytoplasm. Similar results were observed in oocytes expressing dominant-negative (T17N) Rac (**Figures 4D,E**) but in most cases (10 of 12 oocytes), the spindle failed to dock at the animal cortex, and instead drifted deep into the cytoplasm (**Supplementary Movie S9**). Thus, in contrast to the mitotic divisions in the sea urchin embryo, Rac and Arp2/3 were required for proper spindle docking and polar body extrusion in sea star oocytes.

Expression of constitutively active Rac suppressed polar body extrusion without affecting spindle migration or rotation (**Figures 5A,C** and **Supplementary Movie S10**). Interestingly, active Rac did not block Rho activity associated with the central spindle in oocytes that failed to form a protrusion, with bright foci of rGBD-GFP observed at the spindle midzone of anaphase I spindles (**Figures 5C,D**). Polar body extrusion also failed in the Q61L/F37A mutant (**Figures 5A,C** and **Supplementary Movie S11**), possibly due to a dominant-negative effect that has been reported for this mutation (Schwartz et al., 1998).

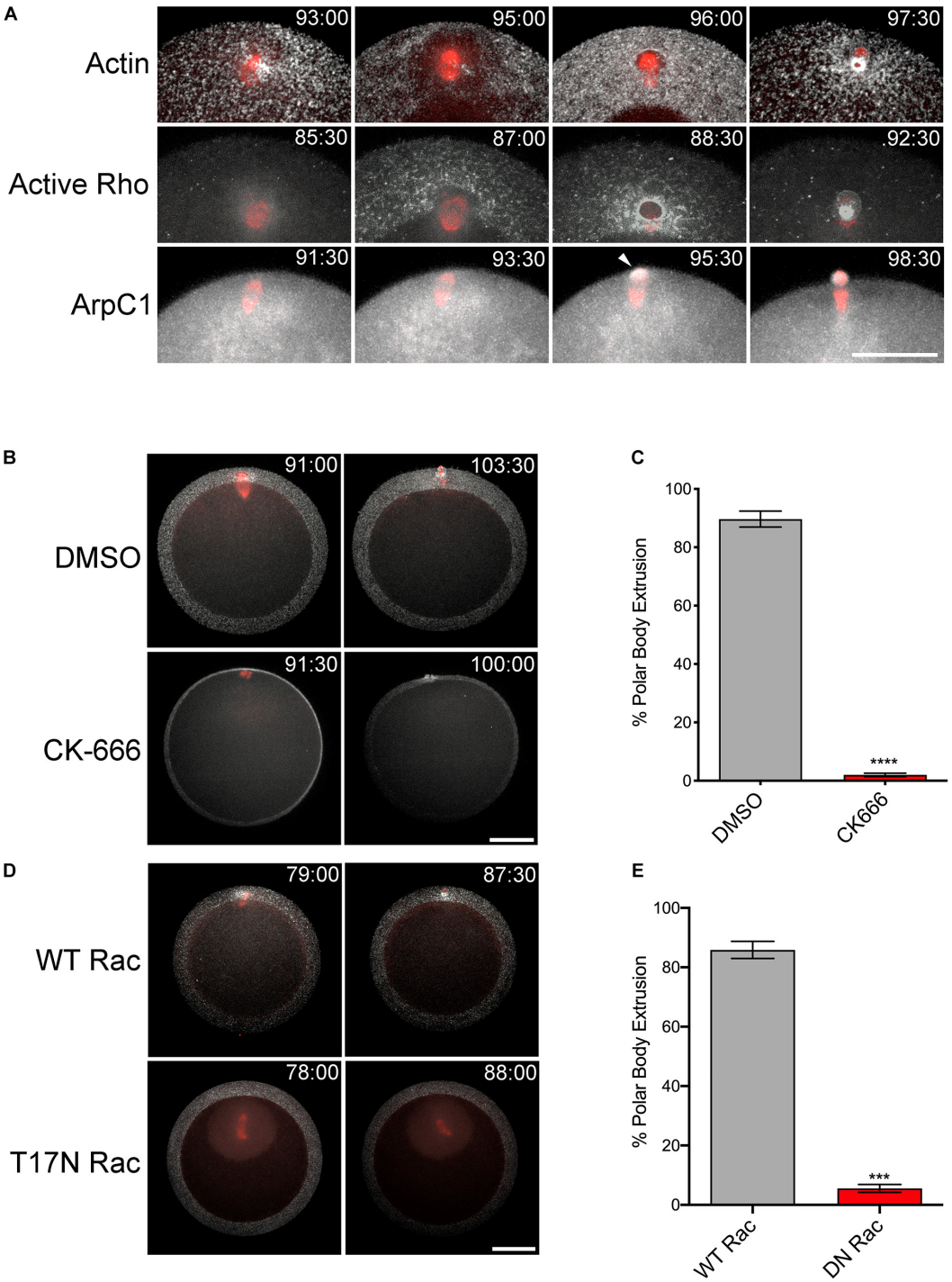

FIGURE 4 | Rac and Arp2/3 are required for polar body extrusion in sea star oocytes. **(A)** First polar body extrusion in *P. miniata* oocytes co-expressing Lifeact (white) and GFP-tubulin (red), rGBD-GFP (white) and mCherry-EMTB (red), and ArpC-GFP (white) and mCherry-EMTB (red). Time points indicate minutes post-hormone activation. Arrow denotes protruding polar body. Bar, 50 μm. **(B)** *P. miniata* oocytes co-expressing Lifeact (white) and GFP-tubulin (red) were activated with maturation hormone and 40 min following germinal vesicle breakdown, were treated with 0.1% DMSO or 100 μM CK-666. The spindle in the CK-666 sample is positioned in the *Z* axis of the image. The spindle failed to rotate or form a polar body protrusion. Bar, 50 μm **(C)** Quantification of polar body formation in DMSO or CK-666 samples for three experimental replicates, 100 oocytes scored per condition per experiment (Mean ± SEM, $^{****}p < 0.0001$). **(D)** *P. miniata* oocytes co-expressing Lifeact (white), GFP-tubulin (red) and either wild-type (WT) or dominant-negative (T17N) Rac. In contrast to WT Rac-injected oocytes, T17N Rac-expressing oocytes failed in polar body formation after spindles failed to dock at the cortex. Bar, 50 μm. **(E)** Quantification of polar body formation in WT or T17N Rac-expressing oocytes for three experimental replicates, 100 oocytes scored per condition per experiment (Mean ± SEM, $^{***}p < 0.001$).

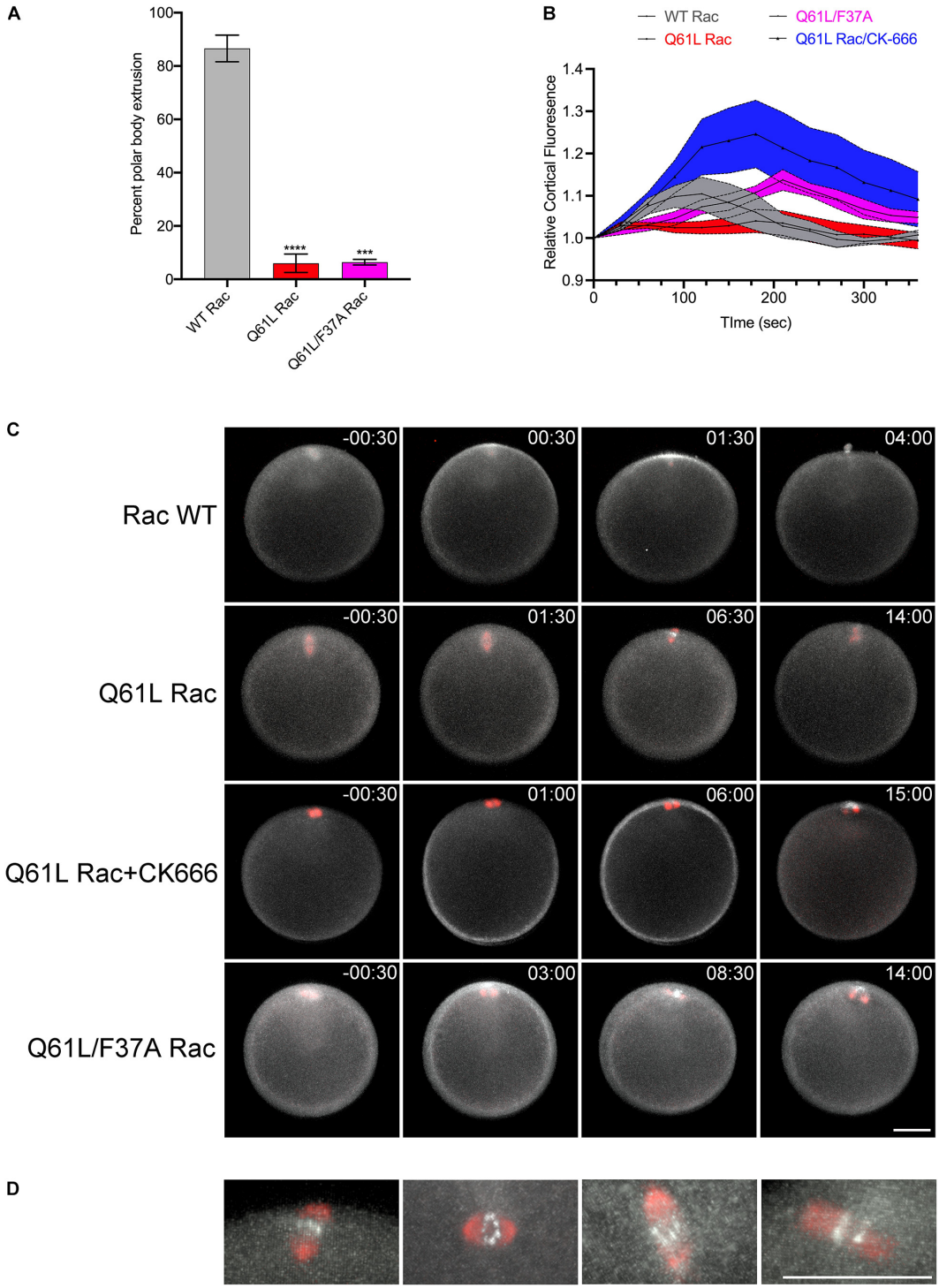

FIGURE 5 | Rac and Arp2/3 directly antagonizes Rho activation during meiosis I. **(A)** Quantification of polar body formation in *P. miniata* oocytes injected WT, Q61L or Q61L/F37A Rac (final intracellular concentration 1.8 μg/ml), 200 oocytes scored per condition per experiment (Mean ± SEM, $^{***}p < 0.001$; $^{****}p < 0.0001$). **(B)** Cortical Rho activity during the surface contraction wave (SCW) in oocytes expressing WT Rac (gray), Q61L Rac (red), Q61L/F37A Rac (magenta) or Q61L Rac oocytes treated with 100 μM CK-666 (blue). Rhotekin-GFP fluorescence was measured for the entire cortex, where time 0 denotes the initiation of the SCW at the vegetal pole. Mean ± SEM, 7 oocytes per condition. **(C)** SCW and polar body extrusion in *P. miniata* oocytes co-expressing rGBD-GFP (white), mCherry-EMTB (red) and Rac variants described in panel **(B)**. Time point indicate minutes post-initiation of the SCW. Bar, 50 μm. **(D)** Examples of Rho activity associated with meiotic spindles after cytokinesis failure in Q61L Rac-expressing cells. The first panel is the same cell shown in panel **(B)**. Bar, 50 μm.

As mentioned above, polar body extrusion initiates with a Rho-dependent SCW triggered at the vegetal pole (Bement et al., 2015; Bischof et al., 2017), and quantification of cortical Rho activity revealed that the Rho wave observed in controls was suppressed in Q61L Rac-expressing oocytes (**Figures 5B,C** and **Supplementary Movie S10**). However, the wave of Rho activity associated with the SCW could be rescued in cells expressing Q61L/F37A Rac, albeit with a delay (**Figures 5B,C** and **Supplementary Movie S11**). Further, treatment of Q61L Rac-expressing oocytes with CK-666 dramatically enhanced the Rho wave relative to oocytes expressing WT Rac alone (**Figures 5B,C** and **Supplementary Movie S12**). This enhancement of cortical Rho activity could be replicated in oocytes treated with CK-666 in the absence of ectopic Rac (**Supplementary Figures S2E−I** and **Supplementary Movie S13**), suggesting that inhibition of branched actin networks may affect the amplitude and dynamics of Rho activation in these cells.

DISCUSSION

There is now a general consensus that Rappaport's "cleavage stimulus" involves the Chromosomal Passenger, PRC1/Kif4A, and centralspindlin complexes that organize the post-anaphase central spindle and direct the local activation of Rho (Glotzer, 2009; Mishima, 2016; Basant and Glotzer, 2018). The notion of negative regulatory cues have a long history (Wolpert, 1960) and there is evidence supporting the idea that there are antagonistic signals or mechanisms for clearing contractile proteins from the polar regions (Murthy and Wadsworth, 2008; Kunda et al., 2012; Rodrigues et al., 2015; Mangal et al., 2018; Chapa-Y-Lazo et al., 2020). Rac has also been implicated as a negative regulator for cytokinesis (D'Avino et al., 2004; Yoshizaki et al., 2004; Canman et al., 2008; Cannet et al., 2014), with proposed downstream effectors including PAK-mediated cell adhesion (Bastos et al., 2012) and the Arp2/3 complex (Canman et al., 2008). In this report, we explored Rac and Arp2/3 function in sea urchin zygotes, where these factors are dispensable for cytokinesis as well as in sea star oocytes, where both factors are required for polar body extrusion. In both cases, dysregulated Rac blocked cytokinesis in an Arp2/3-dependent manner, and in the case of the SCW, Arp2/3 directly suppresses Rho activity. Together, these results suggest a novel mechanism by which branched actin networks may act as a break against Rho-dependent contractility, which may be applicable not only to canonical cleavages, but to other cell polarization events as well.

Rac and Cytokinesis in the Sea Urchin Zygote

Considered a "classic" model for studying cell division, echinoid embryos continue to provide mechanistic insights into cytokinesis (Mabuchi et al., 1993; Bement et al., 2005; Foe and von Dassow, 2008; von Dassow et al., 2009; Argiros et al., 2012; Su et al., 2014; Henson et al., 2017). A baseline characterization of actin dynamics revealed a series of dynamic changes in actin-based structures that occur throughout mitosis and cytokinesis, including dramatic changes in deep cytoplasmic actin, cortical actin, and microvilli (**Figure 1** and **Supplementary Movie S1**). However, of the actin populations visible by diffraction-limited imaging, only the global increase in cortical actin preceding furrow initiation was Rho-dependent (**Figures 1H,K,M** and **Supplementary Movie S2**), consistent with prior observations of Rho-dependent increases in cortical stiffness accompanying the metaphase-anaphase transition in these cells (Lucero et al., 2006).

Constitutively active Rac had a strong, negative effect on cytokinesis (**Figures 2A−C** and **Supplementary Movie S3**), and suppressed cytoplasmic actin, microvillar and cortical actin dynamics (**Figures 2E,F**). Normal actin dynamics and cytokinesis were rescued if constitutively active Rac contained second, effector-binding domain that blocks WAVE activation (**Figures 2A,E,F** and **Supplementary Movie S3**), suggesting that Rac's effects on cell division were due its downstream effector, Arp2/3. Arp2/3 is progressively cleared from the cell equator in dividing embryos (**Figures 3A−B**), and inhibition of Arp2/3 slows but does not inhibit cytokinesis (**Figures 3C,D,G**). While Arp2/3 was no essential for furrow formation, direct inhibition of Arp2/3 in Q61L-expressing embryos rescued both cytokinesis as well as cortical thickening (**Figures 3G,I**), suggesting that Arp2/3 was antagonizing Rho-dependent processes. In *C. elegans*, it has been proposed that Rac-activated Arp2/3 might compete with formins for actin monomers (Canman et al., 2008). However, at the level of resolution used for these live cell imaging experiments, it is not clear that activated Rac was significantly shifting the equilibrium between branched and unbranched actin populations (**Figures 2E,F**, **3E,F**). Together, our findings that deregulated activated Rac strongly suppresses cytokinesis in an Arp2/3-dependent manner, supporting the notion that under control conditions, centralspindlin promotes equatorial ring assembly while suppressing Rac and branched actin assembly (**Figure 6A**; Canman et al., 2008; Cannet et al., 2014; Zhuravlev et al., 2017). Further exploration of the relationship between Rho and Arp2/3 in other cell types will reveal whether this is a general phenomenon.

Role of Rac and Arp2/3 During Polar Body Extrusion

In addition to representing a highly asymmetric cell division, polar body formation differs from conventional cell divisions in that the Rho signal originates not from the central spindle, but at opposite end of the oocyte, where the initiation of CDK1 inactivation triggers a Rho-dependent SCW (Bischof et al., 2017). Coupled with a protrusion induced by the meiotic spindle, the SCW converges at the animal pole, where central spindle signaling organizes the contractile ring to pinch off the polar body. Polar body formation also differs from mitotic cleavages in its requirement for Rac and Arp2/3. The protrusion of the polar body is thought to be a function of Cdc42 (Zhang et al., 2008), but we and others have shown that Rac functions in polar body formation (**Figure 4A**; Halet and Carroll, 2007), and Arp2/3 has been implicated in both spindle migration and polar body formation (Sun et al., 2011a,b; Chaigne et al., 2013; Yi et al., 2013; Wang et al., 2014, 2016). Indeed, Arp2/3 is enriched in the forming polar body (**Figure 4A**) as well as

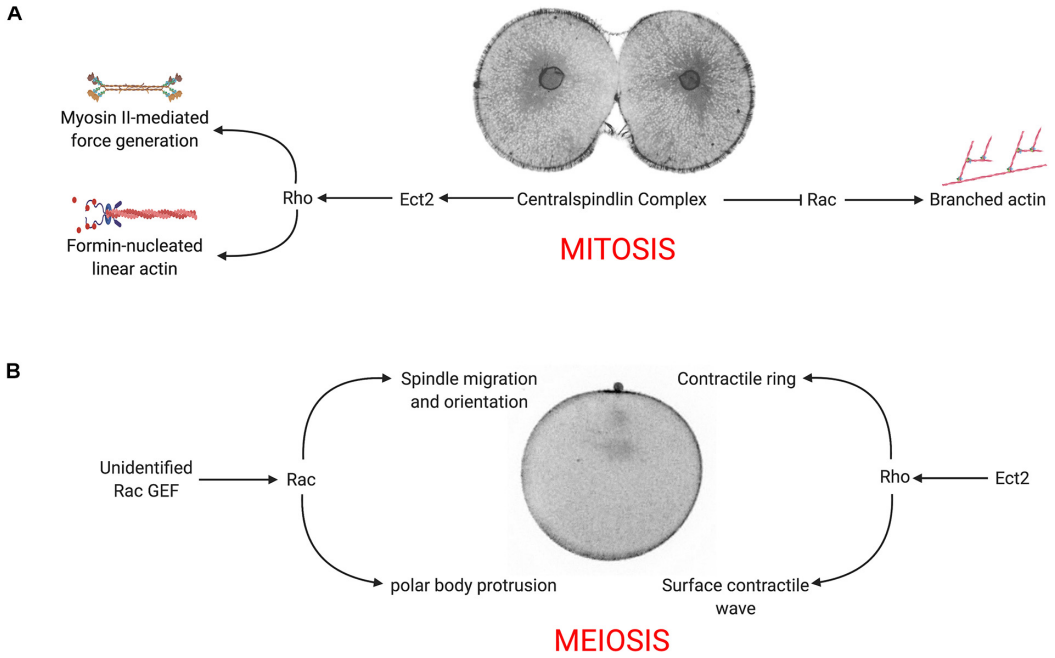

FIGURE 6 | Model for Rac-Arp2/3 signaling during mitotic and meiotic divisions. **(A)** In the presence of WT Rac, the centralspindlin complex recruits Ect2 to promote equatorial Rho activity, which in turn stimulates formin-nucleated actin, myosin II activation and contractile ring assembly. Simultaneously, centralspindlin blocks Rac and Arp2/3 activity, downregulating branched actin networks at the cell equator. **(B)** During meiosis, Rho is activated at the vegetal pole, inducing a surface contractile wave that converges on the animal pole where the centralspindlin complex organizes the ring that completes cytokinesis and polar body extrusion. Rac (activated by an unidentified exchange factor) promotes Arp2/3-mediated branched actin that is required for proper positioning of the spindle and polar body protrusion.

following polar body extrusion (Toledo-Jacobo et al., 2019). Inhibition of either Rac or Arp2/3 blocks spindle alignment and polar body extrusion (**Figures 4B–E**), and while many of these failures can be attributed to spindle migration defects, membrane bulge formation still fails even when the spindle is immediately subjacent to the membrane (**Figure 4B** and **Supplementary Movie S8**). Thus, under normal conditions, both Rho and Rac play essential roles in polar body formation, where Rho provides contractile force through the SCW and contractile ring, and Rac promotes spindle anchoring to the cortex and promotes bulge formation (**Figure 6B**).

The SCW provided an ability to examine Rac and Rho antagonism independently of the central spindle. In oocytes, activated Rac blocked polar body formation, but also depressed the Rho wave (**Figures 5A–C**), raising the possibility that active Rac could block polar body extrusion by suppressing the Rho-dependent SCW, consistent with the models for polar body extrusion where cortical contractility is coupled with protrusive activity (Zhang et al., 2008; Satoh et al., 2013). Although polar body extrusion was not rescued under these conditions, both the F37A effector-binding mutation and the Arp2/3 inhibitor rescued the Rho wave in the presence of activated Rac (**Figures 5B,C**), and in the case of direct Arp2/3 inhibition, the amplitude and persistence of the Rho wave was dramatically increased (**Figures 5A–C** and **Supplementary Movie S12**). Further, Arp2/3 inhibition alone increased the amplitude and duration of the Rho wave (**Supplementary Figure S2** and **Supplementary Movie S13**), arguing that Rac indirectly antagonizes Rho through Arp2/3. The notion that actin networks may downregulate Rho has been observed in these same cells, where pulsatile waves of Rho and actin induced by Ect2 overexpression are propagated through a negative feedback loop (Bement et al., 2015). Given that Ect2 is thought to be the exchange factor involved in Rho waves in sea star oocytes (Bement et al., 2015), it is possible then that Arp2/3 nucleated actin may directly interfere with Ect2 activity.

Arp2/3 may modulate contractility by regulating Rho activity, but these experiments do not address the possibility that branched actin networks may act more directly to serve as a break for myosin contractility. There is an abundance of evidence demonstrating that crosslinking proteins tune actomyosin contractility during cytokinesis (Girard et al., 2004; Zhang and Robinson, 2005; Mukhina et al., 2007; Ennomani et al., 2016; Ding et al., 2017; Descovich et al., 2018). In reconstituted systems, disordered networks generated by the inclusion of Arp2/3 are less contractile than ordered bundles (Ennomani et al., 2016), and in living cells, Arp2/3 has been shown to restrict myosin II contractility in growth cones (Yang et al., 2012). More recently, it has been demonstrated that in mollusk embryos, Arp2/3 defines the domain of vegetal cortex that is sequestered by a the polar lobe, a transient constriction that forms at an angle normal to the cleavage plane (Toledo-Jacobo et al., 2019). Thus, regardless of the exact mechanism by which Arp2/3 affects Rho-mediated contractility, branched actin networks may represent

an additional mechanism by which cells may spatially control contractility during cell shape change.

MATERIALS AND METHODS

Procurement and Culture of Echinoderm Gametes and Embryos

Lytechinus pictus and *S. purpuratus* sea urchins were obtained from Marinus Scientific and Point Loma Marine, and were maintained in a chilled saltwater aquarium at 11–14°C. The sea urchin *L. variegatus* was obtained from Reeftopia and maintained at 20°C. Gametes were obtained by intracoelomic injection of 0.5 M of KCl, and eggs were collected by inverting the urchin over a small beaker of Artificial Sea Water (ASW) while the sperm was collected dry and used immediately or stored at 4°C. Eggs were fertilized with a 1:10,000 dilution of sperm in artificial seawater containing 1 mM 3-amino-triazole, and fertilization envelopes were then removed by passing embryos through Nitex mesh. Embryos were then cultured at 14°C for *S. purpuratus* and *L. pictus* and 20°C for *L. variegatus* until use.

The bat star *P. miniata* was obtained from Marinus and kept in a chilled aquarium as described above. To obtain fully grown, immature oocytes, an incision was made on the ventral surface of an arm, and a small amount of ovary tissue was removed and washed twice in chilled calcium-free artificial sea water (CaFASW) for 15 min to remove follicle cells. Ovary tissue was then placed in 10 μM acetylcholine-ASW for 8–10 min to promote extrusion of oocytes. Oocytes were then placed in fresh ASW containing 100 μg/ml gentamycin, where they could be cultured at 14°C for 3–5 days without any loss of viability. Oocyte maturation was induced by addition of 1–2 μM 1-methyladenine (Acros #AC201310250), where germinal vesicle breakdown (GVBD) occurred after 20–30 min, and first polar body extrusion occurred about 90 min post-hormone addition.

Reagents and Small Molecule Inhibitors

Unless otherwise specified, all chemicals and reagents were purchased from Sigma. C3 transferase was obtained from Cytoskeleton (#CT03), The Arp2/3 inhibitor CK-666 was purchased from Tocris (#3950), resuspended in Dimethyl Sulfoxide at a stock concentration of 100 mM, and aliquoted stocks stored at −80°C.

Recombinant Proteins

Recombinant Lifeact-EGFP (Gift from David Burgess, Boston College) was expressed in BL21(DE3) STAR cells (Thermo Fisher Scientific #C601003) and recombinant protein expression was induced for 6 h with 1 mM IPTG. Cells were harvested by centrifugation and protein purified using a Qiagen Ni NTA kit (#30600). Protein fractions were then dialyzed in Phosphate-Buffered Saline (PBS) + 10% glycerol overnight at 4°C, snap frozen in liquid nitrogen and stored at −80°C.

Immunofluorescence

To visualize Arp2/3 in dividing sea urchin embryos, embryos were fixed in Millonig's fixative (200 mM NaH_2PO_4, 136 NaCl, pH 7.0, 3.7% Formaldehyde) and processed for immunolocalization as previously described (Argiros et al., 2012). Arp2/3 was labeled using a mouse anti-Arp3 monoclonal antibody (Sigma, #A5979) diluted 1:100; and affinity purified rabbit anti-sea urchin MKLP1 (Argiros et al., 2012) was used at a dilution of 1:100. Microtubules were labeled with 1:1000 rat anti-tubulin (YL1/2; Santa Cruz Biotechnology, #sc-53029), and primary antibodies were detected using Alexa Fluor-labeled secondary antibodies (Thermo Fisher Scientific # A-21441, A-11031, and A-21247). Hoescht 33342 (Thermo Fisher Scientific # 62249) was included in the secondary antibody to label DNA.

Molecular Cloning and Mutagenesis

Unless specified otherwise, all molecular reagents were purchased from New England Biolabs, and PCR primers from Integrated DNA Technologies (IDT). The open reading frames for *S. purpuratus* and *P. miniata* Rac were amplified from either random-primed cDNA (*S. purpuratus*) or a synthetic Gblock (*P. miniata*) and subcloned into XhoI-linearized pCS2P+ (gift from Marc Kirschner Addgene, plasmid # 17095) using In-Fusion cloning (Takara, #638912). Constitutively active (Q61L), dominant-negative (T17N), and effector-binding SpRac mutant (F37A) were generated using the QuickChange II XL site-directed mutagenesis kit (Agilent, #200521) in accordance to the manufacturer's specifications.

To confirm the effects of Rac mutations on actin organization, *S. purpuratus* WT and mutant Rac was subcloned into pLAGFP2A, a pCS2P+ derivative where GFP-lifeact and Rac are expressed as a single open reading frame separated by a 21-residue viral 2A peptide, which upon translation, results in two separate polypeptides (Sepúlveda-Ramírez et al., 2018). Constructs were transfected into human Retinal Pigmented Epithelial (RPE1) cells using Lipofectamine (Life Technologies, #L3000001), and serum-starved overnight to reduce serum-stimulated actin polymerization. Prior to fixation, cells were treated with SIR-actin (Cytoskeleton, #CY-SC001) for 30 min. Coverslips were then fixed and processed for fluorescence imaging as previously described (Shrestha et al., 2012).

In vitro Transcription

The following pCS2-based constructs: Echinoderm WT and Rac mutants, EMTB-mCherry (gift from William Bement, Addgene # 26742), GFP-rGBD (gift from William Bement, Addgene # 26732), and pLAGFP2A-GFP-Tubulin (Sepúlveda-Ramírez et al., 2019) were linearized with Not I, and capped, poly-adenylated mRNAs synthesized *in vitro* using the SP6 mMessage mMachine and Poly(A) tailing kits (Thermo Fisher Scientific, #AM1340, AM1350). RNA was precipitated with Lithium chloride, suspended in nuclease-free water, quantified by spectrophotometry and stored at −80°C. Lifeact-GFP in pSP64T (gift from Mamiko Yajima, Brown University) was linearized with SalI and transcribed as detailed above. ArpC1 in pGEMHE (gift from Peter Lenart), (Max Planck Institute for Biophysical Chemistry) was *in vitro* transcribed with T7 mMessage mMachine (Thermo Fisher

Scientific # AM1344) and poly-adenylated and precipitated as described above.

Microinjection

Sea urchin eggs were fertilized, stripped of fertilization envelopes, and then transferred to a 35-mm glass bottom culture dish (World Precision Instruments, #FD35). Cells were microinjected with glass capillary micropipettes (World Precision Instruments, #TW100F-3) backfilled with *in vitro* transcribed RNA (500 μg/ml for short term experiments in sea urchin embryos, 300 μg/ml for oocytes). For experiments in sea urchins, recombinant Lifeact-EGFP was co-injected to label the actin cytoskeleton. *P. miniata* oocytes were injected in a 35 mm culture dish with 180 μm Nitex mesh adhered to bottom of the dish to immobilize the oocytes. All injections were carried out on a Zeiss Axiovert 200 M inverted microscope with a Brook temperature stage set to 14°C, using a Parker-Hannifin Picospritzer II pressure injection system with Leica M micromanipulators. Embryos were either imaged immediately (for the first mitotic division) or cultured overnight at 14°C.

Image Acquisition and Processing

Wide-field epi-fluorescent and DIC time-lapse imaging was performed on a Zeiss Axiovert 200 M inverted microscope equipped with standard epi-fluorescence and Apotome structured illumination imaging, Leica M and Narishige micromanipulators and a Brook temperature-controlled stage. Images were obtained with an AxioCam MRm CCD camera driven by AxioVision 4.8 software.

Sea urchin embryos were imaged using a Leica TCS SP5 II confocal microscope driven by Leica Application Suite software. 512 × 512 images were acquired in resonant scanning mode, which allowed for rapid scanning and averaging. *P. miniata* oocytes were imaged using an Andor Dragonfly 505 spinning disk confocal system mounted on an Olympus IX83 inverted microscope equipped with an Oko Touch microscope stage incubator set to 14°C. 20 μm slabs (40 images at 0.5 μm intervals) were acquired every 30 s using a 60× Aprochromat silicon objective (NA 1.30) and an Andor iXon 888 EMCCD camera driven by Andor Fusion software. Images were compiled and processed using Fusion and Imaris (v9.0.2) software.

Image Analysis

Image stack manipulations, maximum intensity projections and kymographs were generated using FIJI (ImageJ, National Institutes of Health). To measure the relative cortical distribution of Arp2/3 in fixed sea urchin embryos, fluorescence intensity measurements were made of cross section images using a 45 × 8 pixel ROI for each polar and equatorial surface and a polar: equatorial ratio was calculated per cell for a total of 20 cells were measured per stage. Changes in cortical thickness and microvillar length were measured using ImageJ, taking measurements prior to the metaphase-anaphase transition, and then just prior to the normal timing of furrow initiation at 4 locations on the cortex and the fold increase of thickness was calculated and averaged for each cell. To quantify changes in cytoplasmic actin during mitosis and cortical Rho activity during meiosis, the cytoplasmic fluorescence intensity of Lifeact-GFP and the cortical fluorescence intensity of the Rhotekin biosensor (GFP-rGBD) were measured in time-lapse sequences using the QuimP plugin for ImageJ (Piotr et al., 2018). The resulting fluorescence intensity values for cytoplasmic actin was then normalized to the image frame corresponding to 1 min past NEB. For cortical Rho activity, fluorescence intensity was normalized to the image frame 30 s before the first detection of the surface contractile wave.

Statistical Analysis

Statistical significance was determined using paired one or two-way Analysis of Variance (ANOVA) tests followed by Tukey-Kramer *post hoc* test with a 95% confidence interval. For frequency data, data were arcsin-square root transformed followed by two-way ANOVA and a Tukey-Kramer *post hoc* test. *T*-tests were used for pairwise comparisons, with a 95% confidence level. All statistics and graphs were generated using GraphPad Prism 8.

DATA AVAILABILITY STATEMENT

The raw data supporting the conclusion of this article will be made available by the authors, without undue reservation, to any qualified researcher.

AUTHOR CONTRIBUTIONS

CS, JH, DP, and AE contributed to the conceptualization and development of the project. AE, DP, SS-R, TS, RD, IT, and GR all contributed to the experimentation and data analysis. IT, GR, AE, DP, and SS-R all contributed to the figure preparation and visualization. CS, JH, AE, GR, SS-R, and DP contributed to the writing and editing of the manuscript. CS and JH secured funding. All authors contributed to the article and approved the submitted version.

FUNDING

This work was supported by the National Science Foundation awards MCB-1917976 (JH) and MCB-1917983 (CS), and IT was supported by the New Mexico Alliance for Minority Participation NSF HRD 1826758. RD and TS were supported by the Maximizing Access to Research Careers program at NMSU (NIH T34 GM007667).

ACKNOWLEDGMENTS

The authors would like to thank the David Burgess (Boston College) and Peter Lenart (Max Planck) for sharing the Lifeact-GFP and ArpC1-GFP, respectively, and Cory Sicard, Anthony Alvarez, and Anne Meyer-Meyer for their assistance.

SUPPLEMENTARY MATERIAL

The Supplementary Material for this article can be found online at: https://www.frontiersin.org/articles/10.3389/fcell.2020.591141/full#supplementary-material

Supplementary Figure S1 | Characterization of sea urchin Rac mutants. **(A)** Sequence alignment of *Strongylocentrotus purpuratus* (SpRac), *Lytechinus variegatus* (LvRac), *P. miniata* (PmRac) and *Homo sapiens* Rac1. Positions of dominant-negative (T17N), constitutively active (Q61) and effector binding domain (F37) mutants are highlighted in yellow, gray and cyan, respectively. **(B)** Rac is dispensable for early sea urchin development. WT or T17N Rac was injected into fertilized *S. purpuratus* eggs, and embryos were scored for developmental defects at 24 h post-fertilization, when the embryos are normally at the mesenchyme blastula stage **(panel a)**. With increasing amounts of injected RNA, a range of phenotypes were observed such as **(panel b)** a lack of epithelial-mesenchymal transition by the primary mesenchyme cells (PMCs); **(panel c)** embryos with dispersed and dying PMCs; **(panel d)** a lack of blastocoel expansion; and **(panel e)** embryos that did not develop past the cleavage stage. Although dose-dependent trends could be seen (particularly in blastulae containing disorganized PMCs in the blastocoel, orange), there was no significant difference in viability between WT and T17N Rac expressing embryos. Mean ± SEM for a minimum of three experimental replicates, with >24 cells per experiment. ***$p < 0.001$. **(C)** Ectopic expression of sea urchin Rac in serum-starved hTERT-immortalized RPE1 cells. Transfected cells are marked by Lifeact-GFP, with all cells highlighted with SIR-actin (white) and Hoescht 33342 (blue). Note that presence of lamellipodia in serum-starved, Q61L Rac expressing cells **(C, panels d–f)**. Bar, 25 μm.

Supplementary Figure S2 | Arp2/3 inhibition amplifies the Rho wave in sea star oocytes. **(A–H)** Surface contraction wave (SCW) and polar body extrusion in *P. miniata* oocytes co-expressing rGBD-GFP (white) and mCherry-EMTB (red) and treated with either 0.1% DMSO **(A–D)** or 100 μM CK-666 **(E–H)**. Bar, 50 μm. Whereas the Rho activity in DMSO controls traversed as a wave and terminated with polar body extrusion, CK-666 treated oocytes exhibited a delayed and dramatically elevated Rho wave. **(I)** Rhotekin-GFP fluorescence was measured for the entire cortex in DMSO and CK-666 treated oocytes, where time 0 denotes the initiation of the SCW at the vegetal pole. Mean ± SEM, 7 oocytes per condition.

Supplementary Movie S1 | Actin dynamics during the first mitotic division the sea urchin embryo. Single plane time-lapse movie of a *L. pictus* embryo injected with recombinant Lifeact-GFP. Images were acquired every 20 s and played back at 10 frames/second.

Supplementary Movie S2 | C3 Transferase blocks cytokinesis without affecting cytoplasmic or microvillar actin dynamics. Single plane time-lapse movie of a *L. pictus* embryo co-injected with recombinant Lifeact-GFP and C3 transferase. Images were acquired every 30 s and played back at 10 frames/second.

Supplementary Movie S3 | Actin dynamics and cytokinesis in embryos expressing wild-type or mutant Rac. *L. variegatus* embryos were co-injected with Lifeact-GFP and either WT, Q61L, or Q61L/F37A Rac mRNA and imaged during the first division. Images were acquired every 30 s and played back at 10 frames/second.

Supplementary Movie S4 | Aberrant actin dynamics in a multinucleate embryo expressing constitutively active Rac. *L. variegatus* embryos were co-injected with Q61L Rac mRNA and recombinant Lifeact-GFP and imaged during the third division. Images were acquired every 30 s and played back at 10 frames/second.

Supplementary Movie S5 | Actin dynamics during the first polar body formation. Time-lapse movie of a *P. miniata* oocyte injected with bicistronic mCherry-Lifeact-GFP tubulin mRNA RNA to simultaneously image actin (white) and microtubules (red). A 20 μm surface image was acquired at 0.5 μm intervals every 60 s and played back at 5 frames/second.

Supplementary Movie S6 | Active Rho dynamics during the first polar body formation. Time-lapse movie of a *P. miniata* oocyte injected with rGBD-GFP and mCherry-ETMB mRNA to image active Rho (white) and microtubules (red). A 20 μm medial slab was acquired at 0.5 μm intervals every 30 s and played back at 10 frames/second.

Supplementary Movie S7 | Arp2/3 dynamics during the first polar body formation. Time-lapse movie of a *P. miniata* oocyte, co-injected with ArpC1-GFP and mchETMB mRNA to image the Arp2/3 complex (white) and microtubules (red). A 20 μm medial slab was acquired at 0.5 μm intervals every 30 s and played back at 10 frames/second.

Supplementary Movie S8 | Polar body extrusion fails in presence of the Arp2/3 inhibitor CK-666. Time-lapse movie of a *P. miniata* oocyte injected with bicistronic mCherry-Lifeact-GFP tubulin mRNA to simultaneously image actin (white) and microtubules (red) in the presence of 0.1% DMSO or 100 μM CK-666. A 20 μm medial slab was acquired at 0.5 μm intervals every 30 s and played back at 10 frames/second.

Supplementary Movie S9 | Polar body extrusion fails in an oocyte expressing dominant negative Rac. Time-lapse movie of a *P. miniata* oocyte injected co-injected with either WT Rac or T17N Rac and bicistronic mCherry-Lifeact-GFP tubulin mRNA to simultaneously image actin (white) and microtubules (red). A 20 μm medial slab was acquired at 0.5 μm intervals every 30 s and played back at 10 frames/second.

Supplementary Movie S10 | Suppression of the Rho wave and failure of polar body extrusion in an oocyte expressing constitutively active Rac. Time-lapse movie of a *P. miniata* oocyte injected with either WT Rac or Q61L Rac with rGBD-GFP and mCherry-ETMB RNA to simultaneously image active Rho (white) and microtubules (red). A 20 μm medial slab was acquired at 0.5 μm intervals every 30 s and played back at 10 frames/second.

Supplementary Movie S11 | Rescue of the Rho wave but failure of polar body extrusion in an oocyte expressing Q61L/F37A Rac. Time-lapse movie of a *P. miniata* oocyte injected with Q61L/F37A Rac, rGBD-GFP and mCherry-ETMB RNA to simultaneously image active Rho (white) and microtubules (red) A 20 μm medial slab was acquired at 0.5 μm intervals every 30 s and played back at 10 frames/second.

Supplementary Movie S12 | Arp2/3 inhibition rescues the Rho wave but not polar body extrusion in an oocyte expressing constitutively active Rac. Time-lapse movie of a *P. miniata* oocyte injected with Q61L Rac, rGBD-GFP and mCherry-ETMB RNA to simultaneously image active Rho (white) and microtubules (red) in presence of 100 μM CK-666. Images were acquired every 30 s and played back at 10 frames/second. A 20 μm medial slab was acquired at 0.5 μm intervals every 30 s and played back at 10 frames/second.

Supplementary Movie S13 | Arp2/3 inhibition enhances the Rho wave during surface contraction during polar body extrusion. Time-lapse movie of a *P. miniata* oocyte injected with rGBD-GFP and mCherry-ETMB RNA to simultaneously image active Rho (white) and microtubules (red) in presence of either 0.1% DMSO or 100 μM CK-666. A 20 μm medial slab was acquired at 0.5 μm intervals every 30 s and played back at 10 frames/second.

REFERENCES

Argiros, H., Henson, L., Holguin, C., Foe, V., and Shuster, C. B. (2012). Centralspindlin and chromosomal passenger complex behavior during normal and Rappaport furrow specification in echinoderm embryos. *Cytoskeleton* 69, 840–853. doi: 10.1002/cm.21061

Basant, A., and Glotzer, M. (2018). Spatiotemporal regulation of RhoA during cytokinesis. *Curr. Biol.* 28, R570–R580. doi: 10.1016/j.cub.2018.03.045

Bastos, R. N., Penate, X., Bates, M., Hammond, D., and Barr, F. A. (2012). CYK4 inhibits Rac1-dependent PAK1 and ARHGEF7 effector pathways during cytokinesis. *J. Cell Biol.* 198, 865–880. doi: 10.1083/jcb.201204107

Bement, W. M., Benink, H. A., and von Dassow, G. (2005). A microtubule-dependent zone of active RhoA during cleavage plane specification. *J. Cell Biol.* 170, 91–101. doi: 10.1083/jcb.200501131

Bement, W. M., Leda, M., Moe, A. M., Kita, A. M., Larson, M. E., Golding, A. E., et al. (2015). Activator-inhibitor coupling between Rho signalling and

actin assembly makes the cell cortex an excitable medium. *Nat. Cell Biol.* 17, 1471–1483. doi: 10.1038/ncb3251

Benink, H. A., and Bement, W. M. (2005). Concentric zones of active RhoA and Cdc42 around single cell wounds. *J. Cell Biol.* 168, 429–439. doi: 10.1083/jcb.200411109

Bischof, J., Brand, C. A., Somogyi, K., Májer, I., Thome, S., Mori, M., et al. (2017). A cdk1 gradient guides surface contraction waves in oocytes. *Nat. Commun.* 8:849.

Blanchoin, L., Boujemaa-Paterski, R., Sykes, C., and Plastino, J. (2014). Actin dynamics, architecture, and mechanics in cell motility. *Physiol. Rev.* 94, 235–263. doi: 10.1152/physrev.00018.2013

Breznau, E. B., Semack, A. C., Higashi, T., and Miller, A. L. (2015). MgcRacGAP restricts active RhoA at the cytokinetic furrow and both RhoA and Rac1 at cell-cell junctions in epithelial cells. *Mol. Biol. Cell* 26, 2439–2455. doi: 10.1091/mbc.e14-11-1553

Byrne, K. M., Monsefi, N., Dawson, J. C., Degasperi, A., Volinsky, N., Birtwistle, M. R., et al. (2016). Bistability in the Rac1, PAK, and RhoA signaling network drives actin cytoskeleton dynamics and cell motility switches. *Cell Syst.* 2, 38–48. doi: 10.1016/j.cels.2016.01.003

Canman, J. C., Lewellyn, L., Laband, K., Smerdon, S. J., Desai, A., and Bowerman, B. (2008). Inhibition of Rac by the GAP activity of centralspindlin is essential for cytokinesis. *Science* 322, 1543–1546. doi: 10.1126/science.1163086

Cannet, A., Schmidt, S., Delaval, B., and Debant, A. (2014). Identification of a mitotic Rac-GEF, Trio, that counteracts MgcRacGAP function during cytokinesis. *Mol. Biol. Cell* 25, 4063–4071. doi: 10.1091/mbc.e14-06-1153

Chaigne, A., Campillo, C., Gov, N. S., Voituriez, R., Azoury, J., Almonacid, M., et al. (2013). A soft cortex is essential for asymmetric spindle positioning in mouse oocytes. *Nat. Cell Biol.* 15, 958–966. doi: 10.1038/ncb2799

Chaigne, A., Campillo, C., Voituriez, R., Gov, N. S., Sykes, C., Verlhac, M. H., et al. (2016). F-actin mechanics control spindle centring in the mouse zygote. *Nat. Commun.* 7:10253. doi: 10.1038/ncomms10253

Chapa-Y-Lazo, B., Hamanaka, M., Wray, A., Balasubramanian, M. K., and Mishima, M. (2020). Polar relaxation by dynein-mediated removal of cortical myosin II. *J. Cell Biol.* 219:e201903080. doi: 10.1083/jcb.201903080

D'Avino, P. P., Savoian, M. S., and Glover, D. M. (2004). Mutations in sticky lead to defective organization of the contractile ring during cytokinesis and are enhanced by Rho and suppressed by Rac. *J. Cell Biol.* 166, 61–71. doi: 10.1083/jcb.200402157

Descovich, C. P., Cortes, D. B., Ryan, S., Nash, J., Zhang, L., Maddox, P. S., et al. (2018). Cross-linkers both drive and brake cytoskeletal remodeling and furrowing in cytokinesis. *Mol. Biol. Cell* 29, 622–631. doi: 10.1091/mbc.e17-06-0392

Ding, W. Y., Ong, H. T., Hara, Y., Wongsantichon, J., Toyama, Y., and Robinson, R. C. (2017). Plastin increases cortical connectivity to facilitate robust polarization and timely cytokinesis. *J. Cell Biol.* 216, 1371–1386. doi: 10.1083/jcb.201603070

Ennomani, H., Letort, G., Guérin, C., Martiel, J. L., Cao, W., and Nédélec, F. (2016). Architecture and connectivity govern actin network contractility. *Curr. Biol.* 26, 616–626. doi: 10.1016/j.cub.2015.12.069

Foe, V. E., and von Dassow, G. (2008). Stable and dynamic microtubules coordinately shape the myosin activation zone during cytokinetic furrow formation. *J. Cell Biol.* 183, 457–470. doi: 10.1083/jcb.200807128

Girard, K. D., Chaney, C., Delannoy, M., Kuo, S. C., and Robinson, D. N. (2004). Dynacortin contributes to cortical viscoelasticity and helps define the shape changes of cytokinesis. *EMBO J.* 23, 1536–1546. doi: 10.1038/sj.emboj.7600167

Glotzer, M. (2009). The 3Ms of central spindle assembly: microtubules, motors and MAPs. *Nat. Rev. Mol. Cell Biol.* 10, 9–20. doi: 10.1038/nrm2609

Guilluy, C., Garcia-Mata, R., and Burridge, K. (2011). Rho protein crosstalk: another social network? *Trends Cell Biol.* 21, 718–726. doi: 10.1016/j.tcb.2011.08.002

Halet, G., and Carroll, J. (2007). Rac activity is polarized and regulates meiotic spindle stability and anchoring in mammalian oocytes. *Dev. Cell* 12, 309–317. doi: 10.1016/j.devcel.2006.12.010

Henson, J. H., Ditzler, C. E., Germain, A., Irwin, P. M., Vogt, E. T., Yang, S., et al. (2017). The ultrastructural organization of actin and myosin II filaments in the contractile ring: new support for an old model of cytokinesis. *Mol. Biol. Cell* 28, 613–623. doi: 10.1091/mbc.e16-06-0466

Jordan, S. N., and Canman, J. C. (2012). Rho GTPases in animal cell cytokinesis: an occupation by the one percent. *Cytoskeleton* 69, 919–930. doi: 10.1002/cm.21071

Klughammer, N., Bischof, J., Schnellbächer, N. D., Callegari, A., Lénárt, P., and Schwarz, U. S. (2018). Cytoplasmic flows in starfish oocytes are fully determined by cortical contractions. *PLoS Comput. Biol.* 14:e1006588. doi: 10.1371/journal.pcbi.1006588

Kunda, P., Rodrigues, N. T., Moeendarbary, E., Liu, T., Ivetic, A., and Charras, G. (2012). PP1-mediated moesin dephosphorylation couples polar relaxation to mitotic exit. *Curr. Biol.* 22, 231–236. doi: 10.1016/j.cub.2011.12.016

Lamarche, N., Tapon, N., Stowers, L., Burbelo, P. D., Aspenström, P., and Bridges, T. (1996). Rac and Cdc42 induce actin polymerization and G1 cell cycle progression independently of p65PAK and the JNK/SAPK MAP kinase cascade. *Cell* 87, 519–529. doi: 10.1016/s0092-8674(00)81371-9

Leblanc, J., Zhang, X., McKee, D., Wang, Z. B., Li, R., Ma, C., et al. (2011). The small GTPase Cdc42 promotes membrane protrusion during polar body emission via ARP2-nucleated actin polymerization. *Mol. Hum. Reprod.* 17, 305–316. doi: 10.1093/molehr/gar026

Loria, A., Longhini, K. M., and Glotzer, M. (2012). The RhoGAP domain of CYK-4 has an essential role in RhoA activation. *Curr. Biol.* 22, 213–219. doi: 10.1016/j.cub.2011.12.019

Lucero, A., Stack, C., Bresnick, A. R., and Shuster, C. B. (2006). A global, myosin light chain kinase-dependent increase in myosin II contractility accompanies the metaphase-anaphase transition in sea urchin eggs. *Mol. Biol. Cell* 17, 4093–4104. doi: 10.1091/mbc.e06-02-0119

Mabuchi, I., Hamaguchi, Y., Fujimoto, H., Morii, N., Mishima, M., and Narumiya, S. (1993). A Rho-like protein is involved in the organisation of the contractile ring in dividing sand dollar eggs. *Zygote* 1, 325–331. doi: 10.1017/s0967199400001659

Machacek, M., Hodgson, L., Welch, C., Elliott, H., Pertz, O., Nalbant, P., et al. (2009). Coordination of Rho GTPase activities during cell protrusion. *Nature* 461, 99–103. doi: 10.1038/nature08242

Maddox, A. S., Azoury, J., and Dumont, J. (2012). Polar body cytokinesis. *Cytoskeleton* 69, 855–868. doi: 10.1002/cm.21064

Mangal, S., Sacher, J., Kim, T., Motegi, F., Carvalho, A. X., and Oegema, K. (2018). TPXL-1 activates aurora A to clear contractile ring components from the polar cortex during cytokinesis. *J. Cell Biol.* 217, 837–848. doi: 10.1083/jcb.201706021

Miller, A. L., von Dassow, G., and Bement, W. M. (2008). Control of the cytokinetic apparatus by flux of the Rho GTPases. *Biochem. Soc. Trans.* 36(Pt 3), 378–380. doi: 10.1042/BST0360378

Mishima, M. (2016). Centralspindlin in Rappaport's cleavage signaling. *Semin. Cell Dev. Biol.* 53, 45–56. doi: 10.1016/j.semcdb.2016.03.006

Mishima, M., Kaitna, S., and Glotzer, M. (2002). Central spindle assembly and cytokinesis require a kinesin-like protein/RhoGAP complex with microtubule bundling activity. *Dev. Cell* 2, 41–54. doi: 10.1016/s1534-5807(01)00110-1

Mukhina, S., Wang, Y. L., and Murata-Hori, M. (2007). Alpha-actinin is required for tightly regulated remodeling of the actin cortical network during cytokinesis. *Dev. Cell* 13, 554–565. doi: 10.1016/j.devcel.2007.08.003

Murthy, K., and Wadsworth, P. (2008). Dual role for microtubules in regulating cortical contractility during cytokinesis. *J. Cell Sci.* 121(Pt 14), 2350–2359. doi: 10.1242/jcs.027052

Nolen, B. J., Tomasevic, N., Russell, A., Pierce, D. W., Jia, Z., McCormick, C. D., et al. (2009). Characterization of two classes of small molecule inhibitors of Arp2/3 complex. *Nature* 460, 1031–1034. doi: 10.1038/nature08231

Piotr, B., Sharon, C., and Till, B. (2018). QuimP: analyzing trans- membrane signalling in highly deformable cells. *Bioinformatics* 34, 2695–2697. doi: 10.1093/bioinformatics/bty169

Rodrigues, N. T., Lekomtsev, S., Jananji, S., Kriston-Vizi, J., Hickson, G. R., and Baum, B. (2015). Kinetochore-localized PP1-Sds22 couples chromosome segregation to polar relaxation. *Nature* 524, 489–492. doi: 10.1038/nature14496

Satoh, S. K., Tsuchi, A., Satoh, R., Miyoshi, H., Hamaguchi, M. S., and Hamaguchi, Y. (2013). The tension at the top of the animal pole decreases during meiotic cell division. *PLoS One* 8:e79389. doi: 10.1371/journal.pone.0079389

Schaks, M., Giannone, G., and Rottner, K. (2019). Actin dynamics in cell migration. *Essays Biochem.* 63, 483–495. doi: 10.1042/EBC20190015

Schwartz, M. A., Meredith, J. E., and Kiosses, W. B. (1998). An activated Rac mutant functions as a dominant negative for membrane ruffling. *Oncogene* 17, 625–629. doi: 10.1038/sj.onc.1201977

Sepúlveda-Ramírez, S. P., Toledo-Jacobo, L., Garno, C., Pal, D., Ross, C., Ellis, A., et al. (2019). Live-cell fluorescence imaging of echinoderm embryos. *Methods Cell Biol.* 151, 379–397. doi: 10.1016/bs.mcb.2018.10.006

Sepúlveda-Ramírez, S. P., Toledo-Jacobo, L., Henson, J. H., and Shuster, C. B. (2018). Cdc42 controls primary mesenchyme cell morphogenesis in the sea urchin embryo. *Dev. Biol.* 437, 140–151. doi: 10.1016/j.ydbio.2018.03.015

Shrestha, S., Wilmeth, L. J., Eyer, J., and Shuster, C. B. (2012). PRC1 controls spindle polarization and recruitment of cytokinetic factors during monopolar cytokinesis. *Mol. Biol. Cell* 23, 1196–1207. doi: 10.1091/mbc.e11-12-1008

Su, K. C., Bement, W. M., Petronczki, M., and von Dassow, G. (2014). An astral simulacrum of the central spindle accounts for normal, spindle-less, and anucleate cytokinesis in echinoderm embryos. *Mol. Biol. Cell* 25, 4049–4062. doi: 10.1091/mbc.e14-04-0859

Sun, S. C., Wang, Z. B., Xu, Y. N., Lee, S. E., Cui, X. S., and Kim, N. H. (2011a). Arp2/3 complex regulates asymmetric division and cytokinesis in mouse oocytes. *PLoS One* 6:e18392. doi: 10.1371/journal.pone.0018392

Sun, S. C., Xu, Y. N., Li, Y. H., Lee, S. E., Jin, Y. X., Cui, X. S., et al. (2011b). WAVE2 regulates meiotic spindle stability, peripheral positioning and polar body emission in mouse oocytes. *Cell Cycle* 10, 1853–1860. doi: 10.4161/cc.10.11.15796

Toledo-Jacobo, L., Henson, J. H., and Shuster, C. B. (2019). Cytoskeletal polarization and cytokinetic signaling drives polar lobe formation in spiralian embryos. *Dev. Biol.* 456, 201–211. doi: 10.1016/j.ydbio.2019.08.020

Tse, Y. C., Werner, M., Longhini, K. M., Labbe, J. C., Goldstein, B., and Glotzer, M. (2012). RhoA activation during polarization and cytokinesis of the early *Caenorhabditis elegans* embryo is differentially dependent on NOP-1 and CYK-4. *Mol. Biol. Cell* 23, 4020–4031. doi: 10.1091/mbc.e12-04-0268

Tu, Q., Cameron, R. A., and Davidson, E. H. (2014). Quantitative developmental transcriptomes of the sea urchin *Strongylocentrotus purpuratus*. *Dev. Biol.* 385, 160–167. doi: 10.1016/j.ydbio.2013.11.019

Ucar, H., Tachibana, K., and Kishimoto, T. (2013). The Mos-MAPK pathway regulates Diaphanous-related formin activity to drive cleavage furrow closure during polar body extrusion in starfish oocytes. *J. Cell Sci.* 126(Pt 22), 5153–5165. doi: 10.1242/jcs.130476

von Dassow, G., Verbrugghe, K. J., Miller, A. L., Sider, J. R., and Bement, W. M. (2009). Action at a distance during cytokinesis. *J. Cell Biol.* 187, 831–845. doi: 10.1083/jcb.200907090

Wang, F., Zhang, L., Zhang, G. L., Wang, Z. B., Cui, X. S., Kim, N. H., et al. (2014). WASH complex regulates Arp2/3 complex for actin-based polar body extrusion in mouse oocytes. *Sci. Rep.* 4:5596. doi: 10.1038/srep05596

Wang, Z. B., Ma, X. S., Hu, M. W., Jiang, Z. Z., Meng, T. G., Dong, M. Z., et al. (2016). Oocyte-specific deletion of N-WASP does not affect oocyte polarity, but causes failure of meiosis II completion. *Mol. Hum. Reprod.* 22, 613–621. doi: 10.1093/molehr/gaw046

Wolpert, L. (1960). The mechanics and mechanism of cleavage. *Int. Rev. Cytol.* 10, 163–216.

Wong, G. K., Allen, P. G., and Begg, D. A. (1997). Dynamics of filamentous actin organization in the sea urchin egg cortex during early cleavage divisions: implications for the mechanism of cytokinesis. *Cell Motil. Cytoskeleton* 36, 30–42. doi: 10.1002/(sici)1097-0169(1997)36:1<30::aid-cm3>3.0.co;2-l

Yang, Q., Zhang, X. F., Pollard, T. D., and Forscher, P. (2012). Arp2/3 complex-dependent actin networks constrain myosin II function in driving retrograde actin flow. *J. Cell Biol.* 197, 939–956. doi: 10.1083/jcb.201111052

Yi, K., Rubinstein, B., Unruh, J. R., Guo, F., Slaughter, B. D., and Li, R. (2013). Sequential actin-based pushing forces drive meiosis I chromosome migration and symmetry breaking in oocytes. *J. Cell Biol.* 200, 567–576. doi: 10.1083/jcb.201211068

Yoshizaki, H., Ohba, Y., Kurokawa, K., Itoh, R. E., Nakamura, T., Mochizuki, N., et al. (2003). Activity of Rho-family GTPases during cell division as visualized with FRET-based probes. *J. Cell Biol.* 162, 223–232. doi: 10.1083/jcb.200212049

Yoshizaki, H., Ohba, Y., Parrini, M. C., Dulyaninova, N. G., Bresnick, A. R., Mochizuki, N., et al. (2004). Cell type-specific regulation of RhoA activity during cytokinesis. *J. Biol. Chem.* 279, 44756–44762. doi: 10.1074/jbc.M402292200

Yüce, O., Piekny, A., and Glotzer, M. (2005). An ECT2-centralspindlin complex regulates the localization and function of RhoA. *J. Cell Biol.* 170, 571–582. doi: 10.1083/jcb.200501097

Zhang, D., and Glotzer, M. (2015). The RhoGAP activity of CYK-4/MgcRacGAP functions non-canonically by promoting RhoA activation during cytokinesis. *eLife* 4:e08898. doi: 10.7554/eLife.08898

Zhang, W., and Robinson, D. N. (2005). Balance of actively generated contractile and resistive forces controls cytokinesis dynamics. *Proc. Natl. Acad. Sci. U.S.A.* 102, 7186–7191. doi: 10.1073/pnas.0502545102

Zhang, X., Ma, C., Miller, A. L., Katbi, H. A., Bement, W. M., and Liu, X. J. (2008). Polar body emission requires a RhoA contractile ring and Cdc42-mediated membrane protrusion. *Dev. Cell* 15, 386–400. doi: 10.1016/j.devcel.2008.07.005

Zhuravlev, Y., Hirsch, S. M., Jordan, S. N., Dumont, J., Shirasu-Hiza, M., and Canman, J. C. (2017). CYK-4 regulates Rac, but not Rho, during cytokinesis. *Mol. Biol. Cell* 28, 1258–1270. doi: 10.1091/mbc.e17-01-0020

Conflict of Interest: The authors declare that the research was conducted in the absence of any commercial or financial relationships that could be construed as a potential conflict of interest.

frontiers in Cell and Developmental Biology

REVIEW
published: 19 November 2020
doi: 10.3389/fcell.2020.593400

Comparative Analysis of the Roles of Non-muscle Myosin-IIs in Cytokinesis in Budding Yeast, Fission Yeast, and Mammalian Cells

*Kangji Wang†, Hiroki Okada† and Erfei Bi**

Department of Cell and Developmental Biology, Perelman School of Medicine, University of Pennsylvania, Philadelphia, PA, United States

The contractile ring, which plays critical roles in cytokinesis in fungal and animal cells, has fascinated biologists for decades. However, the basic question of how the non-muscle myosin-II and actin filaments are assembled into a ring structure to drive cytokinesis remains poorly understood. It is even more mysterious why and how the budding yeast *Saccharomyces cerevisiae*, the fission yeast *Schizosaccharomyces pombe*, and humans construct the ring structure with one, two, and three myosin-II isoforms, respectively. Here, we provide a comparative analysis of the roles of the non-muscle myosin-IIs in cytokinesis in these three model systems, with the goal of defining the common and unique features and highlighting the major questions regarding this family of proteins.

Keywords: Myo1, Myo2, Myp2, non-muscle myosin-II, cytokinesis, budding yeast, fission yeast, mammalian cells

OPEN ACCESS

Edited by:
Maria Grazia Giansanti, Italian National Research Council, Italy

Reviewed by:
Saravanan Palani, Indian Institute of Science (IISc), India
Gang Dong, Medical University of Vienna, Austria

***Correspondence:**
Erfei Bi
ebi@pennmedicine.upenn.edu

† These authors have contributed equally to this work

Specialty section:
This article was submitted to Cell Growth and Division, a section of the journal Frontiers in Cell and Developmental Biology

Received: *10 August 2020*
Accepted: *30 October 2020*
Published: *19 November 2020*

Citation:
Wang K, Okada H and Bi E (2020) Comparative Analysis of the Roles of Non-muscle Myosin-IIs in Cytokinesis in Budding Yeast, Fission Yeast, and Mammalian Cells. Front. Cell Dev. Biol. 8:593400. doi: 10.3389/fcell.2020.593400

INTRODUCTION

Non-muscle myosin-IIs (NM-IIs) play critical roles in many fundamental processes including cytokinesis, cell adhesion, cell migration, exocytosis, and tissue morphogenesis (Vicente-Manzanares et al., 2009; Shutova and Svitkina, 2018). Interestingly, the budding yeast *Saccharomyces cerevisiae*, the fission yeast *Schizosaccharomyces pombe*, and humans possess one, two, and three isoforms of the NM-IIs, respectively (Watts et al., 1987; Bezanilla et al., 1997; Kitayama et al., 1997; May et al., 1997; Motegi et al., 1997; Bi et al., 1998; Lippincott and Li, 1998; Golomb et al., 2004). While the *in vitro* assembly of the mammalian NM-IIs and its regulation by phosphorylation have been studied and reviewed extensively (Trybus, 1991; Tan et al., 1992; Ronen and Ravid, 2009; Vicente-Manzanares et al., 2009; Shutova and Svitkina, 2018), the *in vivo* assembly, architecture, function, and regulation of these NM-IIs are not well understood. Much less is known about myosin-II assembly or its lack thereof in both yeasts. Here, we compare and contrast the roles of the NM-IIs in cytokinesis in budding yeast, fission yeast, and humans to define the commonalities and differences for this important family of proteins.

Cytokinesis in fungal and animal cells requires concerted actions of an actomyosin ring (AMR), targeted vesicle fusion, and localized ECM remodeling (Balasubramanian et al., 2004; Pollard and Wu, 2010; Meitinger and Palani, 2016; Bhavsar-Jog and Bi, 2017; Pollard and O'Shaughnessy, 2019). The AMR consists of NM-IIs and actin filaments and is thought to produce a contractile

force that drives cleavage furrow ingression. In both budding and fission yeast, the AMR also guides exocytosis and localized cell wall synthesis (equivalent of ECM remodeling in animal cells) (Vallen et al., 2000; Schmidt et al., 2002; Fang et al., 2010; Proctor et al., 2012; Thiyagarajan et al., 2015; Palani et al., 2017; Okada et al., 2019). Reciprocally, the newly synthesized ECM at the division site stabilizes the AMR (Bi, 2001; Schmidt et al., 2002; Verplank and Li, 2005). Whether a similar AMR–ECM relationship exists in mammalian cells remains unknown. It is also a central mystery as to why and how cytokinesis is driven by one NM-II (defined by the heavy chain gene *MYO1*) in budding yeast, two (*MYO2* and *MYP2*) in fission yeast, and three (*MYH9*, *MYH10*, and *MYH14*) in mammalian cells. Here, we attempt to shed some light on this mystery by comparative analysis of the roles of the NM-IIs in cytokinesis in these diverse model systems.

MYO1: THE SOLE MYOSIN-II HEAVY CHAIN IN BUDDING YEAST

The budding yeast *S. cerevisiae* has only one myosin-II heavy chain Myo1 (a misnomer for a historical reason) (**Figure 1**), one essential light chain (ELC) Mlc1, and one regulatory light chain (RLC) Mlc2 (Luo et al., 2004). Mlc1 is also a light chain for the myosin-V Myo2 as well as for the sole IQGAP Iqg1 in budding yeast (Stevens and Davis, 1998; Boyne et al., 2000; Shannon and Li, 2000; Luo et al., 2004). Deletion of *MYO1* causes pronounced defects in cytokinesis and cell separation but not cell lethality in most strain backgrounds (Watts et al., 1987; Rodriguez and Paterson, 1990; Bi et al., 1998; Lippincott and Li, 1998). Thus, the budding yeast is ideally suited for dissecting the structure–function relationship of a NM-II, especially in the context of cytokinesis.

The Structure and Assembly of Myo1

Myo1 consists of 1,928 amino acids, with a predicted globular head (aa1–855) containing an actin-binding site and ATPase domain, two IQ motifs (aa795–850) where the ELC and RLC bind, and a coiled-coil (CC) tail (aa856–1,928) (**Figure 1**; Luo et al., 2004). Remarkably, deletion of the IQ1 and IQ2 motifs does not cause any obvious defects in cytokinesis (Luo et al., 2004). Myo1 tail is also predicted to contain two non-helical regions (NHRs), an internal NHR (residues 1,224–1,397) that contains seven helix-breaking proline residues and a C-terminal NHR (residues 1,914–1,928) (Fang et al., 2010; Wloka et al., 2013). Studies of Myo1 purified from yeast by rotary-shadowing electron microscopy (EM) indicate that Myo1 forms a two-headed structure with a rod tail, similar to the NM-IIs in other organisms (Fang et al., 2010). The Myo1 tail forms a kink at the position corresponding to the internal NHR (Fang et al., 2010). Analysis of the native septin architectures at the division site during the cell cycle by platinum-replica EM (PREM) suggests that Myo1 forms filaments during cytokinesis (Ong et al., 2014; Chen et al., 2020), although it remains unknown whether Myo1 forms bipolar filaments *in vitro* without the assistance of some accessary factors.

Localization and Dynamics of Myo1 During the Cell Cycle

Myo1 localizes to the division site in a biphasic pattern (Fang et al., 2010; **Figure 2**). Before anaphase, Myo1 is recruited to the division site by the septin-binding protein Bni5 (**Figure 2**; Fang et al., 2010). Bni5 binds to both the minimal targeting domain 1 (mTD1, aa991–1,180) in the Myo1 tail (**Figure 1**) and the C-terminal tails of the septins Cdc11 and Shs1 (Lee et al., 2002; Fang et al., 2010; Finnigan et al., 2015). The mTD1 is necessary and sufficient for Myo1 localization to the division site before anaphase (Fang et al., 2010). During telophase or cytokinesis, Myo1 is maintained at the division site by Iqg1 (Fang et al., 2010), the sole and essential IQGAP in budding yeast (**Figure 2**; Epp and Chant, 1997; Lippincott and Li, 1998). As the neck localization of Iqg1 depends on Mlc1 (Boyne et al., 2000; Shannon and Li, 2000), not surprisingly, the maintenance of Myo1 at the division site during cytokinesis also depends on Mlc1 (**Figure 2**; Fang et al., 2010). Strikingly, the targeting domain 2 (TD2, aa1,224–1,397) in the Myo1 tail, which is essentially the internal NHR, is necessary and sufficient for Myo1 localization at the division site during cytokinesis (**Figure 1**; Fang et al., 2010). While the localization dependency is clear, no direct interaction between Myo1 or its TD2 and Iqg1 has been detected (Fang et al., 2010). The Bni5- and Iqg1-mediated mechanisms for Myo1 targeting presumably overlap during anaphase, with the Bni5 mechanism dampening and the Iqg1 mechanism strengthening (Fang et al., 2010; **Figure 2**). The switch between the two mechanisms is regulated largely at the level of Bni5 degradation and Iqg1 expression during the cell cycle (Epp and Chant, 1997; Lippincott and Li, 1998; Lee et al., 2002).

Because Mlc1, the ELC for Myo1 (Luo et al., 2004), is also a light chain for Myo2 and Iqg1 (Stevens and Davis, 1998; Boyne et al., 2000; Shannon and Li, 2000), its localization mechanism appears more complex. The localization of Mlc1 to the division site before cytokinesis depends on the septin hourglass (Boyne et al., 2000; Shannon and Li, 2000; Luo et al., 2004) and this targeting mechanism is chiefly mediated by the binding of Mlc1 to Myo1 (Feng et al., 2015). The maintenance of Mlc1 at the division site during cytokinesis depends on filamentous actin (F-actin) and the formin Bni1 (Feng et al., 2015), which localizes to the division site during cytokinesis (Pruyne et al., 2004; Buttery et al., 2007). Mlc1 fails to localize to the division site when the septin structure and F-actin are simultaneously disrupted (Feng et al., 2015). In contrast, the localization of the RLC Mlc2 to the division site completely depends on its binding to Myo1 (Luo et al., 2004).

Fluorescence recovery after photo-bleaching (FRAP) analysis indicates that prior to anaphase, there is little or no exchange of Myo1 between the division site and the cytosol, suggesting that nearly all the Myo1 molecules are localized to the division site. However, Myo1 is highly dynamic within the division site (Dobbelaere and Barral, 2004; Wloka et al., 2013; **Figure 2**). This dynamic pattern of Myo1 is similar to that of its binding partner and recruiter Bni5, suggesting that the dynamics of Myo1, in addition to its localization, at this stage of the cell cycle is likely regulated by Bni5 (Wloka et al., 2013). Interestingly, after

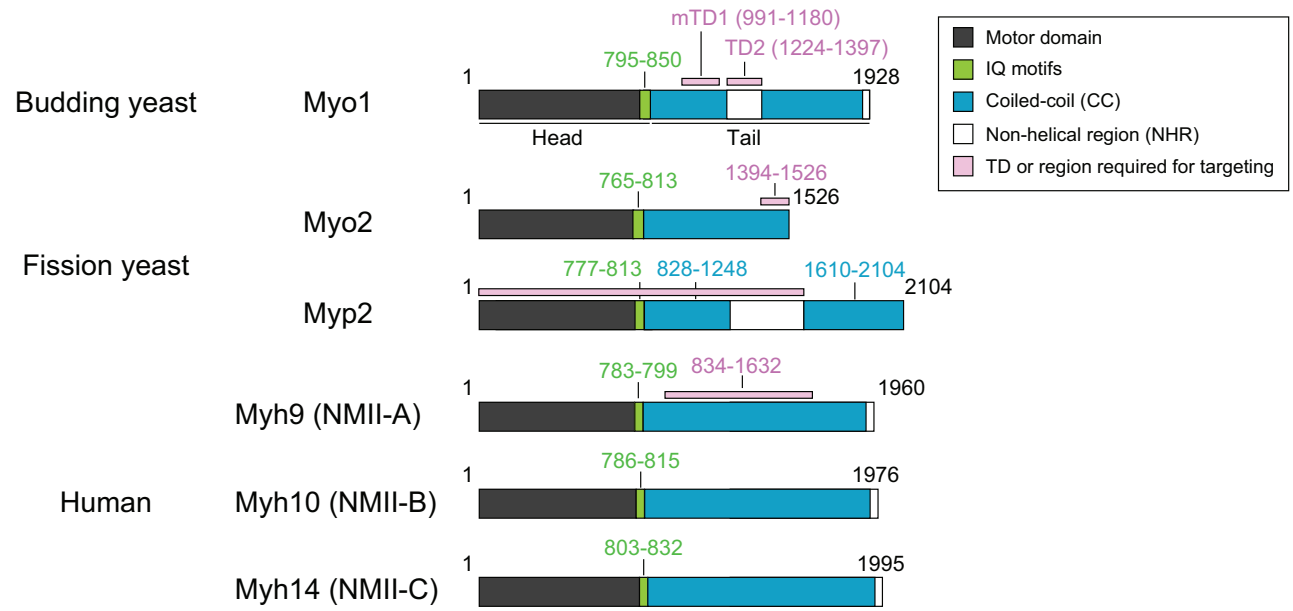

FIGURE 1 | Common features of myosin-II isoforms in *S. cerevisiae*, *S. pombe*, and *H. sapiens*. Motor, motor domain with ATPase and actin-binding sites; IQ, IQ1, and IQ2 motifs—the binding sites for the essential light chain (ELC) and regulatory light chain (RLC), respectively. CC, coiled-coil region; NHR, non-helical region; TD, targeting domain, which is defined as the region of a protein that is both necessary and sufficient for its localization to the division site.

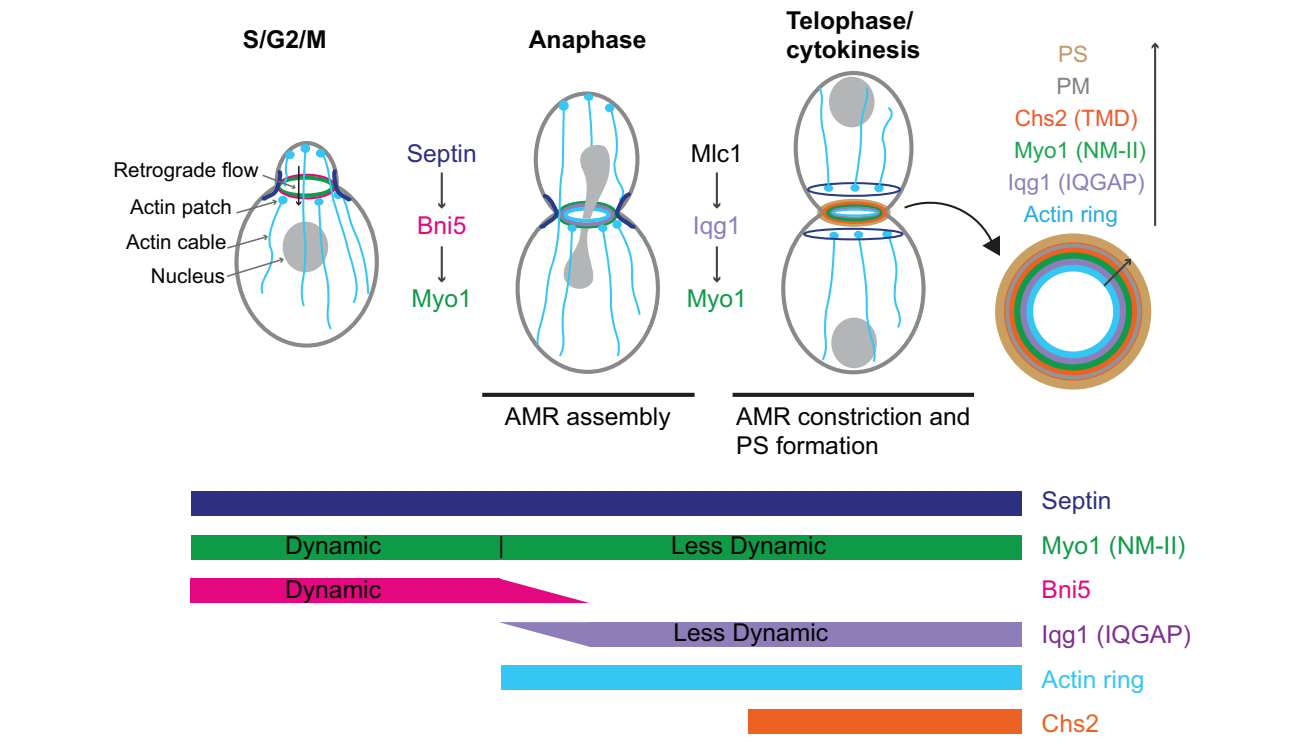

FIGURE 2 | Localization, dynamics, function, and regulation of Myo1 during the cell cycle in budding yeast. AMR, actomyosin ring; PS, primary septum; PM, plasma membrane; Chs2 (TMD), chitin synthase-II (transmembrane domain protein). See text for details.

the onset of anaphase, Myo1 is progressively immobilized, going from a partially "frozen" state during anaphase to a completely frozen state during cytokinesis (**Figure 2**; Dobbelaere and Barral, 2004; Wloka et al., 2013). Not surprisingly, Mlc1 and Iqg1, the stabilizers of Myo1 at the division site during this stage of the cell cycle, begin to localize to the division site after anaphase and are frozen during their entire durations at the division site (Wloka et al., 2013). Remarkably, Mlc1 and Iqg1 become dynamic in the absence of Myo1, suggesting that the immobility of Myo1 is foundational to the immobility of other cytokinetic proteins (Wloka et al., 2013). These observations also suggest that Mlc1/Iqg1 and Myo1 regulate each other during cytokinesis, with Mlc1/Iqg1 being required for Myo1 localization while Myo1 being required for Mlc1/Iqg1 organization or turnover. In contrast to the ELC Mlc1, the RLC Mlc2 displays a similar change in dynamics during the cell cycle as Myo1 does (Wloka et al., 2013). This is not surprising, as Mlc2 binds to Myo1 and this binding is essential for its localization to the division site throughout the cell cycle (Luo et al., 2004). Further analysis indicates that the head domain of Myo1 is not required for its frozen state (Wloka et al., 2013). However, a small truncation at its C-terminus [e.g., Myo1-(aa1–1,798)] makes Myo1 at this stage dynamic again (Wloka et al., 2013). Collectively, these observations suggest that Myo1 might form a highly ordered structure during cytokinesis and the tail region near its C-terminal end is required for this assembly (Wloka et al., 2013). Alternatively, the C-terminal truncations may not abolish Myo1 assembly, but might make the assembled structures more mobile at the division site, perhaps due to a weakened C-terminus-mediated association with the plasma membrane (PM). As five distinct C-terminal truncations of Myo1, including Myo1-(aa1–1,798), were isolated from the synthetic-lethal screen with the deletion of *HOF1*, which encodes an F-BAR protein involved in cytokinesis, the C-terminal region of Myo1 must be important for its function (Nishihama et al., 2009; Wloka et al., 2013).

The Functions of Myo1 in Cytokinesis and Beyond

Myo1 localizes to the presumptive bud site and then to the bud neck from bud emergence to the completion of cytokinesis (i.e., membrane closure between the mother and daughter cells). However, actin filaments join Myo1 at the bud neck to form an AMR only after the onset of anaphase. Thus, the function of Myo1 during the cell cycle can be divided into two stages: before and after anaphase.

The Function of Myo1 in Retrograde Flow of Actin Cables Before Anaphase

Myo1 facilitates the retrograde flow of actin cables before anaphase (**Figure 2**; Huckaba et al., 2006). Retrograde flow is a process conserved from yeast to mammalian cells. In mammalian cells, actin retrograde flow promotes receptor recycling and cell migration, and this process requires actin polymerization and myosin-II activity (Lin et al., 1997; Yang et al., 2012; Yi et al., 2012; Swaminathan et al., 2017). In budding yeast, the actin cables nucleated by the formin Bni1 at the bud cortex undergo retrograde flow that is involved in the inward movement of actin patches, the sites of endocytosis, and endosomes as well as in mitochondrial inheritance (Fehrenbacher et al., 2004; Huckaba et al., 2004). The same actin cables are also required for the anterograde transport of various cargoes including secretory vesicles, mRNAs, vacuoles, and nucleus that are powered by myosin-Vs (Bretscher, 2003). Thus, actin cables are engaged in bidirectional transport in budding yeast. Myo1 at the bud neck binds to actin cables via its motor domain, which generates a pulling force to increase the rate of the retrograde flow by twofold (Huckaba et al., 2006). This function requires the motor activity as well as the bud-neck localization of Myo1 (Huckaba et al., 2006). By anchoring to the septin hourglass, a diffusion barrier at the bud neck, and moving on the actin cables, Myo1 might help cargoes go through the septin barrier and the narrow bud neck more efficiently (Huckaba et al., 2006). As Bni5 is the linker between Myo1 and the septin hourglass, it is also expected to function in the retrograde flow of actin cables (Fang et al., 2010), a possibility that should be investigated in the future.

The Function of Myo1 in Cytokinesis After Anaphase

In budding yeast, AMR constriction is closely followed by the centripetal growth of a primary septum (PS) that is catalyzed by the chitin synthase II (Chs2) (**Figure 2**; Fang et al., 2010). These two processes are interdependent and act in concert to drive efficient cleavage-furrow ingression (Schmidt et al., 2002). The AMR guides PS formation whereas the PS stabilizes the AMR during its constriction (Vallen et al., 2000; Bi, 2001; Schmidt et al., 2002; Verplank and Li, 2005). In this context, Myo1 plays both motor-dependent and-independent roles in cytokinesis. The head domain of Myo1, including the binding sites for the ELC and RLC, accounts for 25–30% of the constriction rate of the AMR (Lord et al., 2005; Fang et al., 2010). When the head domain is deleted, the Myo1 tail is able to direct the assembly of a "headless AMR" that can largely accomplish cytokinesis by guiding the PS formation (Fang et al., 2010). How the Myo1 tail interacts with actin filaments to assemble the headless AMR remains unknown. It is also unknown whether and how the headless AMR drives furrow ingression through cell-cycle triggered disassembly of Myo1 tail and actin filaments or Chs2-mediated PS synthesis or both.

Major Unanswered Questions Regarding Myo1 in Budding Yeast

FRAP analysis suggests that Myo1 is organized into a stable structure during cytokinesis (Dobbelaere and Barral, 2004; Wloka et al., 2013). Indeed, PREM analysis suggests that Myo1 might form filaments in the middle region of a transitional septin hourglass at the onset of cytokinesis (Ong et al., 2014; Chen et al., 2020). However, the precise architecture of the AMR, especially the pattern of Myo1 organization, before and during AMR constriction remains unknown. It is also unknown whether Myo1 can form any kind of filaments *in vitro* and whether its filament assembly *in vivo* is regulated by cell cycle-controlled phosphorylation and/or by trans-acting factors such as other cytokinetic proteins.

Finally, it remains unclear how Myo1 is spatiotemporally coupled to polarized exocytosis and Chs2-mediated PS formation during cytokinesis.

MYO2 AND MYP2: THE TWO MYOSIN-II HEAVY CHAINS IN FISSION YEAST

The rod-shaped fission yeast, *S. pombe*, evolutionally diverged from its fungal relative, the budding yeast *S. cerevisiae*, ∼420 million years ago (Sipiczki, 2000). Similar to that in budding yeast, cytokinesis in fission yeast requires spatiotemporal coupling of AMR constriction with PS formation (Balasubramanian et al., 2004; Pollard and Wu, 2010; Willet et al., 2015; Zhou et al., 2015; Okada et al., 2019). In contrast, however, *S. pombe* has two myosin-II heavy chains, the major isoform Myo2 (Kitayama et al., 1997; May et al., 1997) and the minor isoform Myp2/Myo3 (hereafter Myp2) (**Figure 1**; Bezanilla et al., 1997; Motegi et al., 1997). Both Myo2 and Myp2 share the ELC Cdc4 and the RLC Rlc1, and both localize to the division site (Mccollum et al., 1995; Le Goff et al., 2000; Naqvi et al., 2000; D'souza et al., 2001). Similar to budding yeast, Cdc4 in fission yeast is also a light chain for the IQGAP Rng2 and myosin-V Myo51 (D'souza et al., 2001). Myo2 is indispensable for viability and cytokinesis, while Myp2 is only required for survival under stressful conditions such as high salt (Bezanilla et al., 1997; Kitayama et al., 1997; May et al., 1997; Motegi et al., 1997). Thus, the fission yeast is an ideal model system for dissecting the differentiated roles of different myosin-II isoforms in cytokinesis.

The Structure and Assembly of Myo2 and Myp2

Myo2 and Myp2 share the same basic domains as myosin-IIs in other organisms: a head domain harboring ATPase activity and an actin-binding site, two IQ motifs that bind to ELC and RLC, and a tail domain that is made of CCs, with a NHR in the middle of Myp2 tail (**Figure 1**; Bezanilla et al., 1997; Kitayama et al., 1997; May et al., 1997; Motegi et al., 1997; D'souza et al., 2001). Similar to Myo1 in budding yeast (Luo et al., 2004), deletion of the IQ1 and IQ2 motifs in Myo2 abolishes the ELC (Cdc4) and RLC (Rlc1) binding, but, surprisingly, does not cause any obvious defects in cytokinesis, even in the absence of Myp2 (D'souza et al., 2001). Analysis of Myo2 and Myp2 chimera indicates that the tail domain determines the protein-specific regulation and function (Bezanilla and Pollard, 2000; Lord et al., 2005).

Myo2 has a short tail with 711 residues, which is predicted to contain α-helical rod followed by a flexible, less-ordered region due to the presence of proline residues within the last ∼150 residues (**Figures 1**, **3A**). This was validated by rotary-shadowing EM showing that Myo2 forms a two-headed structure with an 85–90 nm rod tail (Bezanilla and Pollard, 2000; Pollard et al., 2017; Friend et al., 2018). In contrast to myosin-IIs in animals and amoebas, purified Myo2 does not form filaments or mini-filaments under a wide range of salt concentrations, including physiological concentration (Pollard et al., 2017; Friend et al., 2018). This is consistent with its unipolar organization in the cytokinesis nodes, as revealed by quantitative high-speed fluorescence photoactivation localization microscopy (FPALM) (**Figure 3B**; Laplante et al., 2016). In addition, cytosolic Myo2 in interphase cells also exists as a non-filament form (Friend et al., 2018).

Myp2 has a long tail with 1,336 residues, which contains two CC regions separated by a medial proline-rich NHR (**Figures 1**, **3A**). Recombinant Myp2 tail sediments as a monomer and the tail length is 60 nm, which is about half of the length estimated by the residues (∼130 nm), suggesting that Myp2 is a single-headed myosin-II with its tail folded back to form a short rod consisting of antiparallel CCs (Bezanilla and Pollard, 2000). This would essentially place the C-terminal end of Myp2 next to its head domain. However, a recent study by super-resolution microscopy indicates that N- and C-terminal ends of Myp2 are ∼90 nm apart in the assembled AMR (**Figure 3B**; Mcdonald et al., 2017), suggesting that Myp2 unlikely exists as a single-headed myosin with a folded-back tail *in vivo*. Interestingly, the tail of Myo1 in *S. cerevisiae* has a similar domain structure (two CC regions separated by a proline-rich NHR) (**Figure 1**). However, Myo1 forms a two-headed structure with "kink" at the proline region (Fang et al., 2010). Moreover, Myo1 appears to form filaments at the division site (Ong et al., 2014; Chen et al., 2020). It is tempting to speculate that Myp2 might also exist as a two-headed monomer that assembles into bipolar filament as proposed in a simulated model of *S. pombe* cytokinesis (**Figure 3B**; Nguyen et al., 2018).

The assemblies and spatial organization patterns of Myo2 and Myp2 within the contractile ring are distinct (**Figure 3B**). There is a total of ∼5,000 myosin-II molecules at the division site (3,000 of Myo2 and 2,000 of Myp2) (Wu and Pollard, 2005). Myo2 is thought to assemble into an AMR by a search, capture, pull, and release (SCPR) mechanism, which drives the coalescence of the cytokinetic nodes into a ring structure during metaphase and anaphase A (Vavylonis et al., 2008). After the onset of mitosis, Myo2 is incorporated into the nodes by forming a bouquet of Myo2 molecules (**Figure 3B**), with their head domains exposed to the cytoplasm and their tails anchored to the PM via the anillin-like protein Mid1, the central organizer of the nodes (Laporte et al., 2011; Laplante et al., 2016; Mcdonald et al., 2017). The Myo2 tails are also associated with several other key cytokinetic proteins including the IQGAP Rng2, the F-BAR protein Cdc15, and the formin Cdc12 in the nodes (Laporte et al., 2011; Laplante et al., 2016). Cdc12 nucleates the assembly of linear actin filaments, which will be captured and pulled by the Myo2 heads in the nearby nodes, resulting in the coalescence of the nodes into a ring structure (Vavylonis et al., 2008). The pulling force inhibits the activity of Cdc12, preventing node entanglement by an excess of actin filaments (Zimmermann et al., 2017). According to the SCPR model (Vavylonis et al., 2008), both the ATPase and the actin-binding activities of Myo2 should be essential for AMR assembly, and, presumably, for constriction as well.

While the assembly of Myo2 in the cytokinetic nodes or ring is best understood among all the NM-IIs, the assembly of Myp2 is far from clear. Disruption of F-actin by Latrunculin A (LatA) abolishes Myp2, but not Myo2, localization, suggesting that Myp2 localizes to and maintains at the division site by binding to actin filaments or other proteins whose localizations

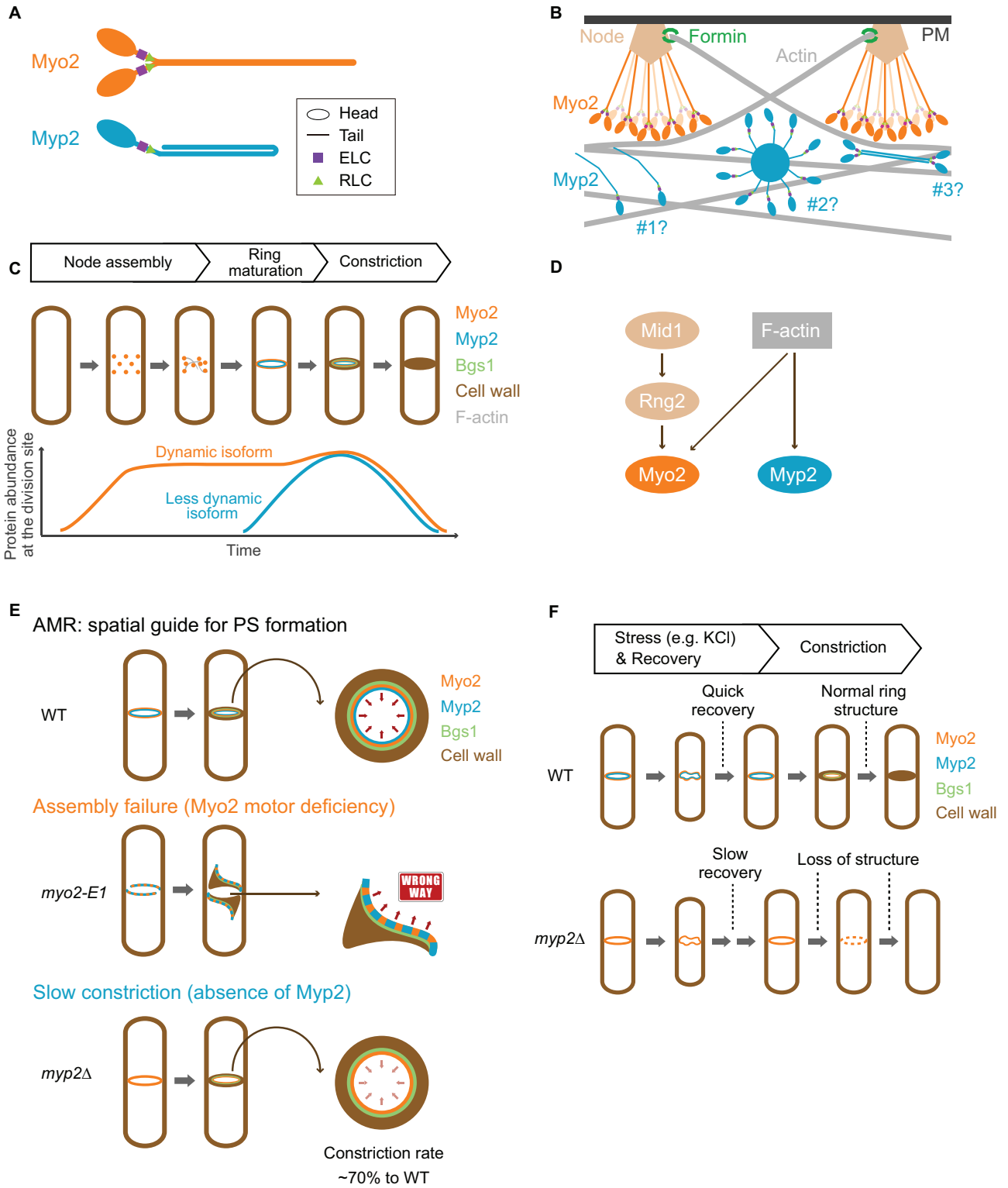

FIGURE 3 | Structure, assembly, localization, dynamics, and function of Myo2 and Myp2 during the cell cycle in fission yeast. **(A)** Molecular structure of Myo2 and Myp2. **(B)** Assembly of Myo2 and Myp2. Modified from Laporte et al. (2011); Takaine et al. (2015), Laplante et al. (2016), and Nguyen et al. (2018). **(C)** Localization of Myo2 and Myp2 during the cell cycle. **(D)** Targeting mechanisms of Myo2 and Myp2. **(E)** The role of the AMR in guiding PS formation. Modified from Okada et al. (2019). **(F)** Stress response of the AMR. See text for details.

depend on F-actin (Wu et al., 2003). This is further corroborated by recent nanoscale analysis of Myp2 in the pre-constricted AMR (Mcdonald et al., 2017). The head domain of Myp2 lies within the F-actin network, ∼210 nm deep from the PM, while the C-terminal tail lies ∼125 nm away from the PM (**Figure 3B**, scenario #1; Mcdonald et al., 2017). Myp2 was also proposed to form clusters with a kernel that is assembled by Myp2 tails. These clusters could presumably interact with actin filaments persistently, therefore, contributing to the consolidation of and stable association with the actin ring (**Figure 3B**, scenario #2; Takaine et al., 2015). However, the uniform distribution of Myp2 in the pre-constricted AMR argues against this possibility (Mcdonald et al., 2017). Alternatively, Myp2 might form bipolar filaments, as suggested by computational modeling (Nguyen et al., 2018), which can explain the previous observation that F-actin bundles containing Myp2 are peeled off from the main ring during constriction (**Figure 3B**, scenario #3; Laplante et al., 2015). However, this possibility does not easily reconcile with the observed distance (∼90 nm) between the N- and C-terminal ends of Myp2 in relation to the PM (Mcdonald et al., 2017). Regardless of the scenarios, overexpression or deletion of the tail region disrupts the Myp2 function (Bezanilla and Pollard, 2000; Takaine et al., 2015; Okada et al., 2019), suggesting that the tail is critical for Myp2 assembly and function.

Localization and Dynamics of Myo2 and Myp2 During the Cell Cycle

Both Myo2 and Myp2 in *S. pombe* localize to the division site during mitosis but at distinct times (**Figure 3C**). Upon mitotic entry, Myo2 localizes to the cell equator as a band of nodes, which are membrane-associated precursors of the contractile ring (Wu et al., 2003, 2006). These nodes are subsequently coalesced into a ring during metaphase and anaphase A (Bezanilla et al., 2000; Motegi et al., 2000; Wu et al., 2003; Vavylonis et al., 2008). At the onset of cytokinesis in anaphase B, long before the spindle breakage (Cortes et al., 2018), the Myo2 ring starts to constrict slowly, and then switches to a fast-phase constriction after the spindle breakage or the onset of telophase (Okada et al., 2019). Structural and functional analysis indicates that a 133-aa C-terminal fragment (residues 1,394–1,526) of Myo2 serves as a TD that is necessary and sufficient for its localization to the division site (**Figure 1**; Motegi et al., 2004). In interphase cells, Myo2 exists in the cytosol (Kitayama et al., 1997; Bezanilla et al., 2000). It was proposed that, upon entry into mitosis, Myo2 is dephosphorylated at Ser1444 within its localization domain, which enables Myo2 to localize to the division site (Motegi et al., 2004). Myo2 localizes to the division site in both F-actin-dependent and -independent manners (**Figure 3D**; Wu et al., 2003; Motegi et al., 2004; Takaine et al., 2014). Mid1 and its downstream component Rng2 are essential for the F-actin-independent localization of Myo2 or its C-terminal targeting domain to the cytokinetic nodes prior to actin ring assembly (Laporte et al., 2011; Padmanabhan et al., 2011; Takaine et al., 2014). This may involve the interactions between Mid1, Rng2, and the localization domain of Myo2, which were detected by co-immunoprecipitation experiments, but not detected by direct protein-binding assays using purified proteins or their fragments (Motegi et al., 2004; Padmanabhan et al., 2011; Takaine et al., 2014). Mid1 disappears from the division site at the time of actin ring assembly (Padmanabhan et al., 2011; Takaine et al., 2014). Afterward, Rng2 is required for the maintenance of F-actin-independent Myo2 at the division site (Takaine et al., 2014). This Rng2-dependent targeting of Myo2 and the potential interaction between Rng2 and the targeting domain of Myo2 is remarkably similar to the Iqg1-mediated Myo1 localization during cytokinesis in budding yeast (Fang et al., 2010).

Myp2 is recruited to the division site during anaphase B, after the actin ring assembly (Wu et al., 2003). Despite its later arrival than Myo2 at the division site, the Myp2 ring constricts slightly earlier than the Myo2 ring (Mcdonald et al., 2017; Okada et al., 2019). This might account for the geometric separation of the myosin-II isoforms in the constricting ring in which the Myp2 ring is located inside of the Myo2 ring (Laplante et al., 2015; Mcdonald et al., 2017). Myp2 localization to the division site completely depends on F-actin (**Figure 3D**; Wu et al., 2003) and requires the collective contributions of its head domain, the first CC region, and the NHR (residues 1–1,615) (**Figure 1**; Takaine et al., 2015; Okada et al., 2019). In interphase cells, Myp2 forms "spots" next to the nucleus at high temperature (Wu et al., 2006). The formation of the spot depends on the second CC region of the Myp2 tail, and these spots may be associated with the γ-tubulin complex (Okada et al., 2019), although the function and regulation of these spots remain unknown.

Myo2, the formin Cdc12, and actin filaments in the contractile ring are dynamic, turning over in 30–60 s (Pelham and Chang, 2002; Clifford et al., 2008; Yonetani et al., 2008; Stachowiak et al., 2014). A number of *in silico* and *in vivo* analyses indicates that proper turnover is required for tension generation and uniform constriction of the ring components (Stachowiak et al., 2014; Oelz et al., 2015; Thiyagarajan et al., 2017; Alonso-Matilla et al., 2019; Cheffings et al., 2019). In contrast to Myo2, Myp2 is largely immobile during cytokinesis (Wloka et al., 2013; Takaine et al., 2015; Okada et al., 2019). Similar to Myo1 in *S. cerevisiae* (Wloka et al., 2013), truncation of a C-terminal region in Myp2 abolishes its immobility (Okada et al., 2019). The same C-terminal region of Myp2 also renders Myo2 less dynamic when it is fused to the tail of Myo2 (Okada et al., 2019). Thus, the C-terminal region of Myp2 is critical for its immobility, and, importantly, fully accounts for the contribution of Myp2 to the rate of AMR constriction (Okada et al., 2019). How the immobility of Myp2 is established remains unknown. As the C-terminal region of a myosin-II is generally required for its self-assembly, we hypothesize that the loss of the C-terminal region in Myp2 might prevent its assembly into a higher-order structure such as the kernel of a Myp2 cluster, as proposed previously (Takaine et al., 2015). Alternatively, but not mutually exclusively, the loss of the C-terminal region in Myp2 could abolish its interaction with other proteins or subcellular structures such as the post-anaphase array (PAA), a microtubule array formed at the division site during cytokinesis (Samejima et al., 2010). Strikingly, Myp2 lacking the C-terminal fragment or the 2nd CC region is able to localize to the division site with the same efficiency as the full-length Myp2 and fully mediates its role in high-salt response

(Bezanilla and Pollard, 2000; Takaine et al., 2015; Okada et al., 2019). Thus, distinct regions of Myp2 are responsible for its localization and dynamics during the cell cycle.

The Functions of Myo2 and Myp2 in Cytokinesis

Roles of Myo2 and Myp2 in Cytokinesis Under Normal Growth Conditions

Myo2 plays an essential role in cell viability and cytokinesis (Kitayama et al., 1997; May et al., 1997), and this role requires both its head and tail domains (Lord et al., 2005). In contrast, Myp2 plays a fine-tuning role in cytokinesis under normal growth conditions and this role can be visualized only when the Myo2 function is compromised (Laplante et al., 2015; Palani et al., 2017; Okada et al., 2019). This role must also require both the head and tail domains of Myp2, as both domains are essential for its localization to the division site (Takaine et al., 2015; Okada et al., 2019).

The AMR in permeabilized fission yeast cells or "cell ghosts" constricted in an ATP- and myosin-II-dependent manner (Mishra et al., 2013). This constriction was completely blocked by blebbistatin, a specific inhibitor of myosin-IIs, suggesting that the collective motor activities of Myo2 and Myp2 are essential for the AMR constriction (Mishra et al., 2013). This is supported by the analyses of motor-domain mutations in both Myo2 and Myp2 (Mishra et al., 2013; Takaine et al., 2015; Pollard and O'Shaughnessy, 2019), as *myo2-E1* and *myp2-R694C* display additive effects on ring constriction (Takaine et al., 2015). Using this cell-ghost system, the rates of ring constriction in *myp2*Δ and *myo2-E1* cell were determined to be approximately 2/3 and 1/3 of the rate in WT cells, respectively (Mishra et al., 2013). However, the rings in the cell ghosts of the *myp2*Δ *myo2-E1* double mutant were frequently fragmented or deformed and failed to undergo ATP-dependent constriction, suggesting that the motor activity of Myo2 is required for the assembly and/or maintenance of the AMR (Mishra et al., 2013). When spheroplasts (i.e., the cells after the removal of cell walls) and micropipette aspiration were used to measure membrane tension, the average ring tensions of the WT, *myp2*Δ, and *myo2-E1* cells were ∼640, 400, and 220 pN, respectively (Pollard and O'Shaughnessy, 2019). Again, the ring tensions in *myp2*Δ and *myo2-E1* cells were about 2/3 and ∼1/3 of the ring tension in WT cells, respectively (Pollard and O'Shaughnessy, 2019). Thus, two independent studies came to the same conclusion that both Myo2 and Myp2 contribute to the ring constriction in fission yeast, with Myo2 playing a more prominent role (Pollard and O'Shaughnessy, 2019). This conclusion is further supported by the measurements of the relative contributions of the myosin-II isoforms to ring constriction in intact cells, which indicates that Myp2 accounts for ∼30% of the rate of constriction (Okada et al., 2019). Strikingly, Myp2 lacking the last ∼200 residues (i.e., the C-terminal portion of the 2nd CC region) does not affect the accumulation kinetics of Myp2 at the division site, but reduces the rate of constriction to the same level as *myp2* null does (Okada et al., 2019). This observation suggests that the last portion of Myp2 tail might be required for the appropriate organization of Myp2 in the contractile ring in order for its motor domain to function in constriction. Despite significant progress in experimental and modeling studies, how Myo2 and Myp2 act in concert to drive AMR assembly and constriction *in vivo* remains unclear (Pollard and O'Shaughnessy, 2019).

AMR constriction is thought to depend on the binding and sliding of actin filaments by myosin-II. The relative contributions of the binding and sliding to AMR assembly and constriction were determined through the genetic and biochemical analysis of the motor-deficient allele *myo2-E1* and its suppressor (Palani et al., 2017). The *myo2-E1* is temperature-sensitive for growth and division. The mutated amino acid (G345R) in the *myo2-E1* allele induces a steric hindrance that causes deficiencies in ATPase activity and actin-filament binding *in vitro* (Balasubramanian et al., 1998; Lord and Pollard, 2004; Stark et al., 2013; Palani et al., 2017, 2018). The fact that the *myo2-E1* cells can grow and divide reasonably well at the permissive temperature whereas *myo2* null is inviable suggests that a motor-independent function of Myo2 likely exists. A genetic screen for the suppressors of the temperature-sensitive growth of the *myo2-E1* cells has led to the identification of an intragenic suppressor (Sup1) that contains two amino-acid changes, Q640H and F641I (Palani et al., 2017). Surprisingly, the gene product of *myo2-E1-Sup1* can bind, but cannot slide, actin filaments *in vitro*, and the isolated AMRs from the *myo2-E1-Sup1* cells fail to undergo ATP-dependent contraction (Palani et al., 2017). Thus, *myo2-E1-Sup1* defines an actin translocation-defective allele (Palani et al., 2017). While the *myo2-E1-Sup1* cells can grow and divide at the high temperature that is restrictive for *myo2-E1*, the AMR assembly is delayed, and the rate of ring constriction is decreased (Palani et al., 2017). These observations suggest that the binding of Myo2 to actin filaments is sufficient for AMR assembly and constriction *in vivo*, and the motor or filament-sliding activity of Myo2 is required for efficiency (Palani et al., 2017). Likewise, mutational analysis of the Myp2 motor domain suggests that the ability to bind actin filaments is more important than the motor activity for its function (Takaine et al., 2015). Given that the actin translocation activity of myosin-II is dispensable for cytokinesis in mammalian COS-7 cells (Ma et al., 2012), the essential role of myosin-II in cytokinesis appears to be dictated by its ability to bind and cross-link the actin filaments whereas the motor activity makes the processes of ring assembly and constriction more efficient. This is fundamentally the same as the headless Myo1 in budding yeast, which can direct AMR assembly and constriction, although with decreased efficiency (Fang et al., 2010). In the absence of the motor activity, the AMR constriction is perhaps driven, at least in part, by cell cycle-triggered actin depolymerization, as suggested previously (Mendes Pinto et al., 2012).

Because the AMR is incapable of generating sufficient tension to overcome the turgor pressure and cell wall stiffness (Proctor et al., 2012; Stachowiak et al., 2014), the contractility of the ring is unlikely to be the direct driving force for furrow ingression. Alternatively, the rate of PS synthesis determines the rate of constriction (**Figure 3E**; Stachowiak et al., 2014). The PS in *S. pombe* consists of linear β-1,3-glucan synthesized by Bgs1/Cps1, hereafter Bgs1 (Cortes et al., 2007). Conditional inactivation of PS synthesis in the temperature-sensitive *cps1-191*

mutant does not prevent AMR assembly but attenuates its constriction (Liu et al., 1999; Dundon and Pollard, 2020). Thus, PS formation is required for efficient AMR constriction and furrow ingression. Bgs1 appears to anchor to the AMR (Arasada and Pollard, 2014; Davidson et al., 2016; Sethi et al., 2016; Martin-Garcia et al., 2018). Moreover, Bgs1 and its nascent product strictly follow the constriction of the AMR structure (Mulvihill and Hyams, 2003a; Cortes et al., 2007; Okada et al., 2019). Thus, the AMR might play a pivotal role in cytokinesis by acting as "scaffold" or "compass" that guides PS formation, whereas the contractile force produced by the AMR might play a supportive role in cytokinesis by regulating Bgs1 activity (Thiyagarajan et al., 2015) or by generating a tiny space between the cell wall and the PM at the leading edge of the ingressing furrow for efficient PS synthesis.

The mechanisms underlying the roles of Myo2 and Myp2 in guiding PS formation remain poorly understood. The depletion of Myo2 leads to haphazard deposition of PS materials at the division site, suggesting that Myo2 plays a critical role in guiding PS formation (Okada et al., 2019). A previous analysis indicates that a defect in AMR assembly can be suppressed by a block in PS formation, suggesting that the arrival of Bgs1 and PS formation before the completion of AMR assembly compromises later aspects of cytokinesis (Huang et al., 2008). In support of this conclusion, when the AMR assembly is compromised (e.g., *myo2-E1* at the restrictive temperature), Bgs1 localizes to the misoriented myosin-II cables, instead of a ring structure, at the medial region and starts synthesizing the PS materials by following the myosin cables (**Figure 3E**; Okada et al., 2019). Thus, myosin-II can guide PS formation even when it is not incorporated into a ring structure. However, timely and correct AMR assembly is essential for "centripetal" PS formation (Okada et al., 2019). It is worth noting that the guiding role of Myo2 does not require its motor activity, as the actin translocation-defective allele of *myo2*$^{+}$ (i.e., *myo2-E1-Sup1*) can largely accomplish cytokinesis and guide PS formation (Palani et al., 2017). This is strikingly similar to the headless Myo1, which does the same in budding yeast (Fang et al., 2010).

Myp2 may also play a role in guiding PS formation. Myp2 starts to constrict earlier than Myo2, and is internal to Myo2 during ring constriction (Laplante et al., 2015; Okada et al., 2019). Deletion of *myp2*$^{+}$ delays the onset of constriction and decreases the rate of constriction (**Figure 3E**; Laplante et al., 2015; Okada et al., 2019). Myp2 is also required for AMR assembly and maintenance when the motor activity of Myo2 is inactivated (e.g., in the *myo2-E1* or *myo2-E1-Sup1* mutant) (Takaine et al., 2015; Palani et al., 2017). Furthermore, Myp2 is immobile (Wloka et al., 2013; Takaine et al., 2015; Okada et al., 2019), similar to Myo1 in budding yeast that acts as scaffold during cytokinesis (Wloka et al., 2013). Taken together, it is tempting to speculate that Myp2 might play a role in guiding PS formation by reinforcing the AMR structure and controlling its timely and fast constriction at the leading edge of the ingressing membrane.

F-actin is also involved in guiding the PS formation, but is only required during the early phase of ring constriction. Association of Bgs1 with the myosin-II and the activation of PS formation can occur in a F-actin-independent manner (Okada et al., 2019). However, F-actin is required for the confinement of Bgs1 at the membrane edge during the early phase of ring constriction (Ramos et al., 2019), but is dispensable for Bgs1 localization and cytokinesis during the second half of ring constriction (Proctor et al., 2012; Okada et al., 2019). Further analysis indicates that F-actin is required for maintaining Myo2 at the division site during the first half of ring constriction. Afterward, Myo2 can maintain its localization at the division site in the absence of F-actin (Okada et al., 2019). Thus, F-actin is indirectly involved in guiding PS formation by concentrating and organizing Myo2 at the division site during the early phase of ring constriction (Okada et al., 2019).

The Interplay of Myo2 and Myp2 in Cytokinesis During Stress Response

Deletion of *myp2*$^{+}$, but not the *myo2-E1* mutant, leads to loss of viability and defects in cytokinesis in the presence of high salt (Bezanilla and Pollard, 2000; Fujita et al., 2002; Baker et al., 2016), suggesting that Myp2 plays a unique role in coping with environmental stresses. Myosin-II behavior in stress response has been under-studied. Recent time-lapse imaging analysis, coupled with microfluidic devices, indicates different responses of Myo2 and Myp2 upon high salt stress (Okada et al., 2019). Importantly, Myp2 is required for the dynamic disassembly and stability of the AMR during stress response (**Figure 3F**; Okada et al., 2019), but the underlying mechanism remains unknown. The cells lacking calcineurin, a conserved Ca^{2+}- and calmodulin-dependent protein phosphatase, show a similar phenotype to *myp2*Δ cells such as defective cytokinesis and high salt sensitivity (Sugiura et al., 1998). A constitutive-active form of calcineurin suppresses salt sensitivity of the *myp2*Δ cells, suggesting that Myp2 might be required for ion homeostasis and/or activation of calcineurin (Fujita et al., 2002). Myp2 interacts with Ste20 (not the homologue of the PAK Ste20 in budding yeast), the rictor subunit of the TOR complex 2 (TORC2), that is required for cell viability in high salt (Matsuo et al., 2007; Baker et al., 2016). Myp2 and Ste20 are interdependent for their localization, and Ste20 is required for efficient cytokinesis (Baker et al., 2016). Given the importance of TORC2 in general stress responses, Myp2 may be required for stress adaptation of cytokinesis via TORC2-mediated pathways.

Major Unanswered Questions Regarding Myo2 and Myp2 in Fission Yeast

Despite significant progress made in recent years, many key aspects of the structure, function, and regulation of myosin-IIs in fission yeast remain unclear. The organizational patterns of Myo2 and Myp2 at the division site must be determined, as they are essential for understanding the mechanisms of AMR assembly and tension generation. The motor-dependent and -independent functions of myosin-IIs in cytokinesis require further investigation, as this is crucial for understanding the relative contributions of the binding, sliding, and disassembly of actin filaments to the rate of ring constriction. It also remains largely unknown how PS formation, the primary driving force of ingression, is regulated by the AMR. More specifically, it remains

unclear whether and how the AMR interacts with Bgs1 to achieve uniform ingression during cytokinesis.

It is also a mystery how Myo2 and Myp2 act in concert to drive AMR assembly and constriction under normal and stressed conditions. While the structure and organization of Myo2 at the division site has been extensively analyzed, even the basic questions regarding Myp2 remain unanswered: is Myp2 a single-headed myosin, as suggested by the *in vitro* study (Bezanilla and Pollard, 2000)? How is its immobility established during cytokinesis? How does it generate tension or act as a scaffold to facilitate furrow ingression? Of particular interest is how Myp2 is regulated to render the division machinery resistant to various stresses. Finally, the existence of proline residues in the middle portion of the myosin tail is conserved among fungal species (Mulvihill and Hyams, 2003b), but the function and mechanism of this NHR is not well understood. In budding yeast, this region, also called TD2, is required for Iqg1-mediated Myo1 localization at the division site during cytokinesis (Fang et al., 2010). The NHR in Myp2 is also required for its localization to the division site (Takaine et al., 2015), but the underlying mechanism remains unknown.

MYH9, MYH10, AND MYH14: THE THREE NON-MUSCLE MYOSIN-II HEAVY CHAINS IN MAMMALIAN CELLS

Humans diverged from the budding yeast and fission yeast almost a billion years ago (Hoffman et al., 2015; Liu et al., 2017). Along the way, the human genome has evolved to encode three NM-II heavy chains Myh9, Myh10, and Myh14 that define the NM-II isoforms IIA, IIB, and IIC, respectively (**Figure 1**; Conti and Adelstein, 2008; Vicente-Manzanares et al., 2009; Heissler and Sellers, 2015). Each heavy chain binds an ELC (Mlc3nm or Mlc1sa) encoded by either *MYL6* or *MYL6B*, and an RLC (Mlc2, Mlc2B, or Mlc2A) encoded by *MYL9*, *MYL12A*, or *MYL12B* (Heissler and Sellers, 2015). Similar to budding yeast and fission yeast, the ELC in mammalian cells also binds to IQGAPs, but the function of this binding remains unknown (Weissbach et al., 1998; Atcheson et al., 2011; Pathmanathan et al., 2011). Different cell types usually express two or three of the isoforms (Golomb et al., 2004; Ma et al., 2010; Pecci et al., 2018). Deletions of different NM-II isoforms in mice cause distinct phenotypes. Deletion of NM-IIA causes embryonic lethality at day 6.5 and defects in cell adhesion and endoderm formation (Conti et al., 2004). Deletion of NM-IIB causes embryonic lethality at day 14.5 and defects in heart and brain functions including cardiac myocyte cytokinesis (Ma et al., 2010). Deletion of NM-IIC alone does not cause lethality or obvious defects, but, when combined with decreased level of NM-IIB, causes lethality and karyokinesis in cardiac myocytes by affecting microtubule dynamics (Tullio et al., 1997; Ma et al., 2010). Studies using the mouse model and different cell lines indicate that NM-IIs play critical roles in tissue morphogenesis, cell migration, cytokinesis, and exocytosis (Conti and Adelstein, 2008; Vicente-Manzanares et al., 2009; Shutova and Svitkina, 2018). Despite decades of research, the answers to the major questions of how different isoforms are elaborately regulated to achieve an appropriate ratio and how these isoforms act in concert to carry out specific functions in a given cell type just began to emerge. Here, we will focus on the roles of the NM-II isoforms in cytokinesis.

The Structure and Assembly of the NM-IIA, -IIB, and -IIC

The NM-II heavy chains Myh9, Myh10, and Myh14 in mammalian cells share a similar domain organization as the myosin-II heavy chains in budding yeast and fission yeast, a globular head domain with actin-binding and ATPase activities, IQ1 and IQ2 motifs where an ELC and an RLC bind, respectively, and a rod-shaped tail that is made of CCs, followed by a small NHR in each isoform (**Figure 1**). Similar to the myosin-IIs in budding yeast (Luo et al., 2004) and fission yeast (D'souza et al., 2001), deletion of the IQ2 motif in NM-IIA does not appear to compromise its ability to localize to the division site or to drive cytokinesis (Beach and Egelhoff, 2009). The biochemical property of each NM-II isoform, its monomer structure and its assembly into bipolar filaments, and the regulation of its filament assembly by RLC and heavy chain phosphorylation as well as by interacting proteins have been studied extensively *in vitro* as well as in the context of cell adhesion, polarization, and migration (Vicente-Manzanares et al., 2009; Shutova and Svitkina, 2018). In addition, specific mutations in the NM-IIA gene, which cause *MYH9*-related diseases, have been analyzed in terms of their impact on IIA structure and functions in developmental processes as well as in the pathogenesis of the relevant diseases (Vicente-Manzanares et al., 2009; Pecci et al., 2018). These subjects have been reviewed comprehensively in several recent articles (Vicente-Manzanares et al., 2009; Pecci et al., 2018; Shutova and Svitkina, 2018). Here, we only describe some salient features of the NM-IIA, -IIB, and -IIC in relation to their roles in cytokinesis.

The structure and organization of these NM-IIs were studied using both native myosin and sf9 expressed proteins (Pollard et al., 1974; Niederman and Pollard, 1975; Billington et al., 2013; Liu et al., 2018). Like Myo1 in budding yeast and Myo2 in fission yeast, the monomers of all three NM-II isoforms are heterohexamers that consist of two heavy chains, two ELCs, and two RLCs (**Figure 4A**; Billington et al., 2013). These monomers can further polymerize into bipolar filaments of ∼300 nm in length *in vitro*, although with isoform-specific features. The bare zone length of IIC is much longer than that of IIA or IIB, but the width of IIC filaments is smaller than that of IIA or IIB (Billington et al., 2013; Liu et al., 2018). IIA and IIB filaments each contain ∼30 myosin monomers whereas IIC filaments contain ∼16 myosin monomers (Billington et al., 2013; Melli et al., 2018). *In vitro* analysis suggests that NM-II filament assembly starts with folded monomers that interact with each other to form folded antiparallel dimers, which assemble into folded antiparallel tetramers that are unfolded via RLC phosphorylation to form a bipolar tetramer (Liu et al., 2018). The unfolded bipolar tetramers associate with each other to form bipolar filaments (**Figure 4A**; Liu et al., 2018). *In vivo* analyses indicate that NM-II bipolar filaments assemble into "stacks," presumably, to increase their capacity for force production

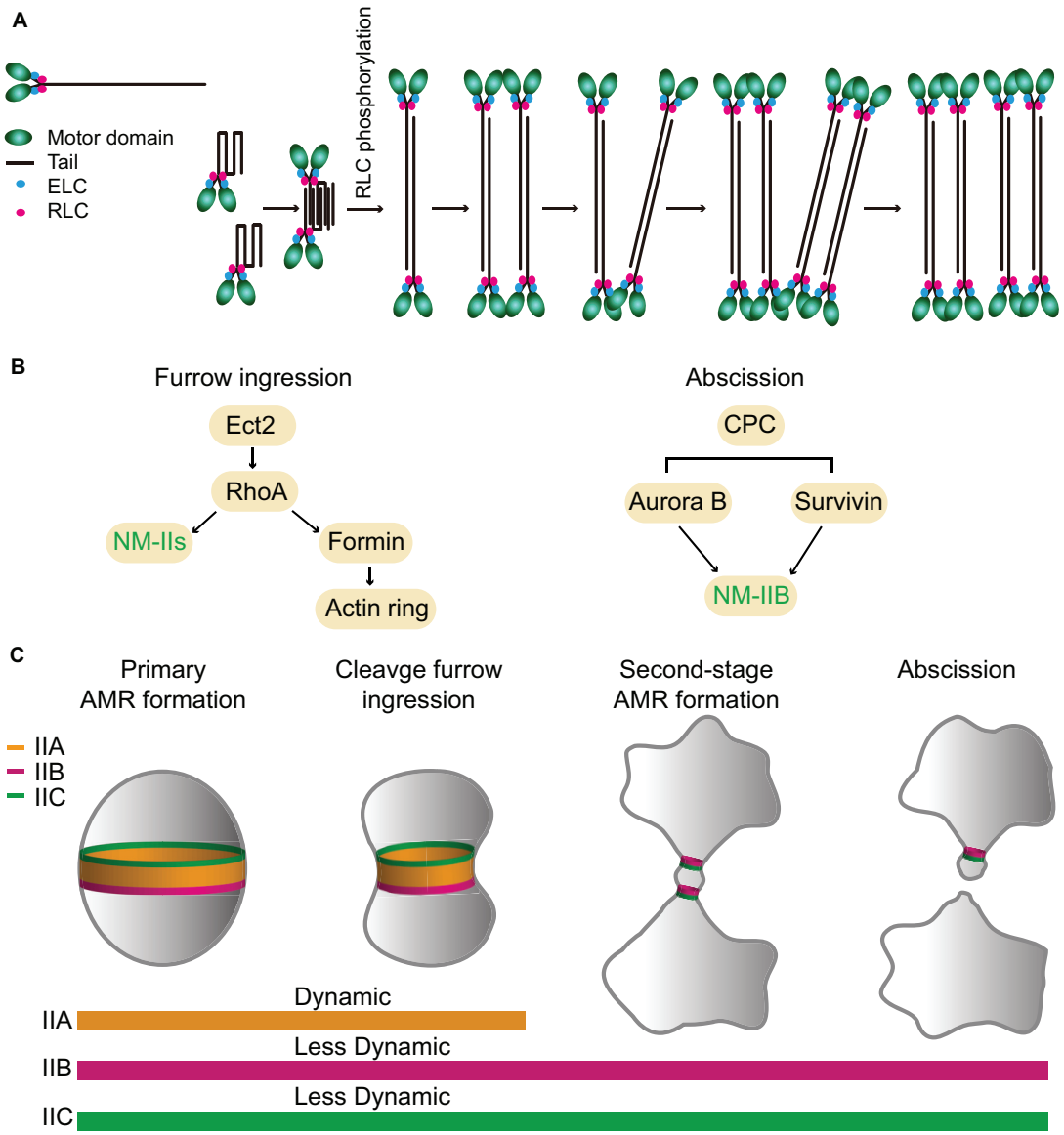

FIGURE 4 | Assembly, localization, dynamics, and function of NM-IIA, -IIB, and -IIC during cytokinesis in mammalian cells. **(A)** A model for NM-IIA assembly. Modified from Fenix et al. (2016); Beach et al. (2017), and Liu et al. (2018). **(B)** Targeting mechanisms of NM-IIs during furrow ingression and abscission. **(C)** Localization patterns and dynamics of different NM-II isoforms during furrow ingression and abscission. See text for details.

(**Figure 4A**; Verkhovsky et al., 1995, 1999; Fenix et al., 2016; Fenix and Burnette, 2018). Time-lapse analysis by super-resolution microscopy suggests that the assembly of IIA filament stacks follows the same pathway or the "expansion model" at the leading edge of a motile cell (U2-OS) or at the cleavage furrow of a dividing cell (HeLa): the bipolar filaments first recruit other bipolar filaments to become thicker, and then a part of the thick filament bundle branches out to recruit more bipolar filaments, and, eventually, form a IIA filament stack (**Figure 4A**; Fenix et al., 2016; Fenix and Burnette, 2018). Further live-cell imaging by super-resolution microscopy of mouse fibroblasts carrying a knock-in EGFP-NM-IIA indicates that IIA filaments nucleate at the cell periphery, grow, split, expand, and stack up as they move deeper into the cell to form large-scale actomyosin structures and this process depends on actin dynamics (Beach et al., 2017). Similar conclusions on myosin filament stacking and its dependency on actin organization have been reached by an independent study (Hu et al., 2017; Titus, 2017). It remains unknown whether IIB and IIC form stacks in the same way.

The stack-like organization of the IIA filaments at the division site in HeLa cells (Fenix et al., 2016) shows some similarities and differences to the organization of the NM-II filaments at the division site in sea urchin embryos (Henson et al., 2017). Both appear to organize into arrays of myosin filaments along the circumference of the division site, which is consistent with the classic "purse-string model" of cytokinesis (Schroeder, 1972;

Rappaport, 1996). However, the registration of the head and tail domains of the bipolar filament assemblages in sea urchin embryos is not as ordered as that in HeLa cells (Fenix et al., 2016; Henson et al., 2017). In addition, NM-II appears to form discrete clusters at the division site during early stage of cytokinesis in sea urchin embryos (Henson et al., 2017). These clusters coalesce into myosin filament arrays over time, a process that resembles the node-to-ring assembly process in fission yeast. Whether the assemblies of mammalian NM-IIs go through a similar process during cytokinesis remains unknown.

Localization and Dynamics of the NM-IIA, -IIB, and -IIC During Cytokinesis

The expression levels of the three NM-II isoforms vary greatly in HeLa-Kyoto cells. IIA is expressed 16-fold and 135-fold higher than IIB and IIC, respectively (Maliga et al., 2013). During cytokinesis, they localize to the division site for different periods of time. IIA localizes to the division site only during furrow ingression and disappears at the midbody stage, whereas IIB and IIC localize to the division site during both the furrowing and the abscission stages (Wang et al., 2019). The endogenous IIB and IIC localize to the constriction sites in HeLa-Kyoto cells and A549 (human lung tumor cells), respectively, before abscission (Jana et al., 2006; Wang et al., 2019). During furrow ingression, the localization of IIA and IIB at the division site depends on local RhoA activation by its guanine-nucleotide-exchange factor Ect2 whose localization is, in turn, dictated by the centraspindlin complex (**Figure 4B**; Yuce et al., 2005; Piekny and Glotzer, 2008; Zhou and Wang, 2008; Frenette et al., 2012). Active RhoA also controls actin ring assembly via formins (**Figure 4B**; Watanabe et al., 2008). Thus, RhoA is required for AMR assembly in mammalian cells (**Figure 4B**; Basant and Glotzer, 2018; Verma et al., 2019). The chromosomal passenger complex (CPC), including its components Aurora B and survivin, appears to regulate IIB localization during the abscission stage (**Figure 4B**; Kondo et al., 2013; Babkoff et al., 2019). Similar to Myo1 in budding yeast (Fang et al., 2010), the central region of the IIA tail (residues 834–1,632) is required for its localization to the division site (**Figure 1**), but its tethering factor at the division site remains unknown (Beach and Egelhoff, 2009). Because the septin-binding protein Bni5 and the IQGAP Iqg1 in budding yeast (Fang et al., 2010) and the anillin-like protein Mid1 and the IQGAP Rng2 in fission yeast (Motegi et al., 2004; Laporte et al., 2011; Padmanabhan et al., 2011; Takaine et al., 2014) are required for the targeting of myosin-II heavy chain to the division site during the cell cycle, similar proteins such as anillin and/or IQGAPs might be involved in the localization of NM-IIA to the division site in mammalian cells. The C-terminal region of IIA (residues 1,633–1,960) is able to localize to the division site only by interacting with the endogenous IIA or IIB in the cell (Beach and Egelhoff, 2009), which is strikingly similar to the behavior of the C-terminal "putative assembly domain" of Myo1 in budding yeast (Fang et al., 2010; Wloka et al., 2013). How RhoA and other factors control the localization of different isoforms at the division site during different stages of cytokinesis requires further investigation.

FRAP analysis indicates that IIA is highly dynamic, whereas IIB and IIC are less dynamic during cytokinesis (**Figure 4C**; Kondo et al., 2011; Wang et al., 2019). The differential turnover of IIA and IIB at the division site is similar to that of IIA and IIB during cell migration (Sandquist and Means, 2008). This isoform-specific behavior appears to be dictated by a C-terminal region in their respective tails (Sandquist and Means, 2008). As both IIA and IIB assemble into bipolar filaments of similar size and shape *in vitro* (Billington et al., 2013), it remains unclear how their turnover is differentially regulated *in vivo*.

The Functions of NM-IIA, -IIB, and -IIC in Cytokinesis

Mammalian cytokinesis is divided into two stages: furrow ingression and abscission. During furrow ingression, the diameter of the cell at the division site shrinks from its initial size (∼10–20 μm for most cell types) to the diameter of the intercellular bridge (ICB) between the daughter cells at the time of the midbody formation (1.5–2 μm) (Mullins and Biesele, 1973, 1977). The prevalent idea is that furrow ingression is driven by the contractile ring, which disassembles at the midbody stage, whereas abscission is carried out by the endosomal sorting complex required for transport-III (ESCRT-III) (Elia et al., 2011; Guizetti et al., 2011; Agromayor and Martin-Serrano, 2013). However, the ESCRT-III complex is known to act on membrane tubes with much smaller dimension (∼100–300 nm in diameter) (Henne et al., 2012; Agromayor and Martin-Serrano, 2013; Chiaruttini et al., 2015; Alonso et al., 2016). Thus, the ICB must be further thinned significantly in order to permit the ESCRT-III to fulfill its role in abscission.

Differential Requirements of NM-IIs in Furrow Ingression and Abscission

During furrow ingression, all three isoforms localize to the division site and play redundant or overlapping roles, as depletion of IIA or IIB alone or in combination did not block furrowing in HeLa-Kyoto cells, but the addition of 25 μM blebbistatin, a specific inhibitor of myosin-IIs (Straight et al., 2003; Zhang et al., 2017), completely arrested cytokinesis at the furrowing stage (Wang et al., 2019). Strikingly, the addition of a lower dosage of blebbistatin (7.5 μM) allowed furrowing, but significantly delayed or blocked abscission (Wang et al., 2019). Thus, the motor activity of NM-II plays a critical role in abscission, not just at the furrowing stage (Wang et al., 2019). Importantly, GFP-tagged IIB and IIC, but not IIA, still localize to the division site during the abscission stage (**Figure 4C**; Wang et al., 2019). Further analysis indicates that the endogenous IIB (but not IIA), F-actin, and Sept9 localize to the constriction sites during the early midbody stage whereas the ESCRT-III components arrive there only during the late midbody stage (Wang et al., 2019). Strikingly, the addition of the lower dosage of blebbistatin completely abolished the constriction site formation at either side of the midbody and prevented the normal localization of the above-mentioned factors at the constriction sites (Wang et al., 2019). Together, these observations suggest that NM-IIs are not only required for furrow ingression, but also for abscission. Furthermore, these observations suggest that different NM-II

isoforms play differential roles in abscission, with IIB (and IIC) playing a local and direct role in the formation of the constriction sites and IIA playing a more global and indirect role in abscission by exerting cortical tension to drive the daughter cells apart (Wang et al., 2019).

It has become increasingly clear that there are two spatiotemporally separated actomyosin rings that operate during mammalian cytokinesis (**Figure 4C**; Wang et al., 2019). The primary AMR drives furrow ingression and it requires all NM-II isoforms whereas the second-stage AMRs drive the formation of the constriction sites for the subsequent abscission (Wang et al., 2019). These second-stage rings consist of similar components as those in the primary AMR, e.g., RhoA, formins, F-actin, anillin, and septins, with the exception that the second-stage rings contain IIB and likely IIC, but not IIA (Jana et al., 2006; Hu et al., 2012; Renshaw et al., 2014; Dema et al., 2018; Karasmanis et al., 2019; Wang et al., 2019). Thus, the isoforms of NM-IIs define a difference between the primary and second-stage AMRs, which presumably account for their distinct roles in furrow ingression and abscission during cytokinesis. It is noteworthy that the IIB-based second-stage AMR is remarkably similar to the Myo1-based AMR in budding yeast in terms of size, composition, and myosin-II dynamics.

Distinct Biochemical Properties of NM-IIs May Account for Their Distinct Roles in Furrow Ingression and Abscission

Several recent studies indicate that IIA generates cortical tension and drives furrow ingression during cytokinesis, whereas IIB controls cortical stability and cytokinetic fidelity, perhaps by attenuating the IIA-dependent rate of rapid ingression (Yamamoto et al., 2019; Taneja et al., 2020). These observations are consistent with the distinct biochemical properties of IIA and IIB, i.e., IIA is "designed" for rapid motility whereas IIB is best for maintaining static tension (Golomb et al., 2004; Kovacs et al., 2007; Zhang et al., 2017; Melli et al., 2018). These observations are also consistent with the differential localization patterns and dynamics of IIA and IIB at the division site (Wang et al., 2019). Besides cytokinesis, IIA and IIB also play distinct roles in cell migration and cell–cell adhesion (Sandquist and Means, 2008; Shutova et al., 2014; Shutova and Svitkina, 2018; Heuze et al., 2019). In migrating cells, IIA is preferentially localized to the leading edge where it displays rapid turnover. In contrast, IIB is incorporated into actomyosin structures at the rear end and displays much less turnover than IIA does (Sandquist and Means, 2008; Shutova et al., 2014; Shutova and Svitkina, 2018). During the early stage of adherent junction formation in epithelial cells, IIA binds to the actin bundles that are in parallel to the adherent junctions (Efimova and Svitkina, 2018; Heuze et al., 2019) and functions to elongate the junctions by producing a contractile force (Heuze et al., 2019). In contrast, IIB localizes to the branched actin network that might serve as a cross linker of the junctional actin network to maintain the rigidity of the structure (Heuze et al., 2019). These functions of IIA and IIB are also consistent with the general notion that IIA is specialized for force production whereas IIB is specialized for maintaining tension. Together, these observations suggest that the distinct biochemical properties of NM-IIs may account for their distinct roles in furrow ingression and abscission during cytokinesis.

Major Questions Regarding the Roles of Different Isoforms in Mammalian Cytokinesis

While the NM-II isoforms in mammalian cells are best studied for their *in vitro* behaviors such as in motility and filament assembly, their mechanisms of action for their *in vivo* roles such as in cytokinesis remain poorly understood. There are many outstanding questions. For example, it remains unknown how and why different isoforms are regulated to achieve a cell type-specific ratio to drive furrow ingression and abscission. What is the architecture of the primary and second-stage AMRs? Is the myosin-II organization in the contractile ring nearly identical to that in stress fibers, as suggested by a recent analysis of IIA at the division site in HeLa cells (Fenix et al., 2016)? It is also unknown whether different NM-II isoforms are co-assembled into the same bipolar filaments, as seen in the LLC-Pk1 cells (Beach et al., 2014), or the co-assembly merely represents an intermediate stage for sorting IIA and IIB into distinct filaments at distinct locations (Beach et al., 2014; Shutova et al., 2014). Are IIA and IIB filaments spatially segregated at the division site as Myo2 and Myp2 in fission yeast or in other spatial patterns (e.g., the edge vs. the center of the cleavage furrow)? How are the primary and second-stage AMRs assembled during the cell cycle? Does the furrow ingression depend on the motor activity, as suggested by the blebbistatin experiments (Straight et al., 2003; Wang et al., 2019) or is it mainly dictated by the binding of myosin heads to the actin filaments not their sliding on the filaments, as suggested by the behavior of an actin translocation-defective mutation in IIB in COS-7 cells (Ma et al., 2012)? Both motor-dependent and-independent activities of myosin-IIs are known to play a role in cytokinesis in budding yeast (Lord et al., 2005; Fang et al., 2010) and fission yeast (Mishra et al., 2013; Palani et al., 2017).

CONCLUSION AND PERSPECTIVE

Several important lessons are learned through the comparative analysis of the roles of the NM-II isoforms in cytokinesis in budding yeast, fission yeast, and mammalian cells. First, the commonalities regarding the roles of the NM-IIs in cytokinesis in different systems seem to be far more significant than their differences. The NM-IIs in all three systems assemble into a functional AMR in anaphase and constrict to drive furrow ingression. Their differences in the timing of arrival at the division site, which seems to be over-emphasized in the literature, may have nothing to do with cytokinesis or are only involved in fine-tuning the division process. For example, Myo1 in budding yeast localizes to the division site in the absence of an actin ring from bud emergence (G/S) to the onset of anaphase (Bi et al., 1998; Lippincott and Li, 1998). This portion of Myo1 localization is responsible for its role in the retrograde flow of actin cables (Huckaba et al., 2006), and erasing Myo1 localization at the division site before anaphase by deleting Bni5, the linker protein between the septin hourglass and Myo1, does not cause

any obvious defects in cytokinesis (Fang et al., 2010). Similarly, Myo2 in fission yeast localizes to the cytokinetic nodes in the absence of an actin ring upon entry into mitosis (Wu et al., 2003, 2006). These nodes are presumably involved in linking nuclear position (usually at the mid-point of the cell) to the division site (Sohrmann et al., 1996; Bahler et al., 1998; Paoletti and Chang, 2000). However, these nodes are not essential for cytokinesis, as abolishing the nodes by deleting the anillin-like protein Mid1 only affects the location and efficiency of the AMR assembly, and once the AMR is assembled, cytokinesis can occur normally (Huang et al., 2008). Thus, starting in anaphase when the AMR assembly occurs in budding yeast, fission yeast, and mammalian cells, the roles of NM-IIs in cytokinesis appear to be very similar in all three systems. The pre-anaphase NM-II structures at the division site in the two yeast species are presumably evolved to fit the lifestyle of each organism, i.e., budding and binary fission.

Second, it is remarkable that, in all three systems, cytokinesis can largely occur in the absence of the motor activity of the NM-IIs or when the motor activity is severely compromised, but the execution of cytokinesis requires the binding of the NM-IIs to the actin filaments. This is demonstrated abundantly clear by the behaviors of the headless AMR in budding yeast (Lord et al., 2005; Fang et al., 2010), and of the actin translocation-defective NM-IIs in fission yeast (Palani et al., 2017) and mammalian cells (Ma et al., 2012). Thus, the assembly of an AMR and the tension generated by the myosin–actin interaction in the ring are critical for cytokinesis whereas the motor activity merely makes the process more efficient. This raises an important question: how does furrow ingression occur in the absence of the motor activity? One possibility is that the cell cycle-triggered actin and myosin filament disassembly drives furrow ingression in all three systems. Additionally, in the case of the budding yeast and fission yeast, the AMR in the absence of the motor activity can still guide PS formation, which, in turn, could drive furrow ingression (Fang et al., 2010; Proctor et al., 2012; Palani et al., 2017; Okada et al., 2019).

Finally, why do the budding yeast, fission yeast, and mammalian cells possess one, two, and three NM-II isoforms, respectively? There are a number of possibilities. First, it may be related to the dimension of the division site in different systems (Fang et al., 2010). The division sites in budding yeast, fission yeast, and the mammalian cells are 1, 3.5, and > 10 μm in diameter, respectively (Mitchison, 1957; Bi et al., 1998; Lippincott and Li, 1998; Straight et al., 2003; Carvalho et al., 2009). In order to accomplish cytokinesis in a defined window of time during the cell cycle, the fission yeast and mammalian cells may have acquired a fast-turnover NM-II (Myo2 in fission yeast and IIA in mammalian cells) that is specialized in rapid contraction whereas the more "ancient" NM-IIs are probably the slow-turnover ones (e.g., Myo1 in budding yeast, Myp2 in fission yeast, and IIB and IIC in mammalian cells) that are kept to maintain the cortical stability of the division site (Okada et al., 2019; Wang et al., 2019). These slow-turnover NM-IIs may scaffold PS formation in budding yeast (Fang et al., 2010; Wloka et al., 2013) and fission yeast (Proctor et al., 2012; Palani et al., 2017; Okada et al., 2019) or the assembly of the abscission machinery in mammalian cells (Wang et al., 2019). Second, more than one NM-II isoform in fission yeast and mammalian cells might be evolved to enable cytokinesis under environmental stresses such as the fission yeast Myp2 in dealing with survival under high-salt stress at the low temperature (Bezanilla and Pollard, 2000; Okada et al., 2019). Another possibility is that the additional isoforms of NM-II are evolved to expand the repertoire of their functions. For example, IIA and IIB play distinct roles not only in cytokinesis, but also in cell migration, junctional complex formation, exocytosis, and many other processes (Sandquist and Means, 2008; Shutova et al., 2014; Milberg et al., 2017; Efimova and Svitkina, 2018; Shutova and Svitkina, 2018; Heuze et al., 2019). Regardless of the possibilities, the core questions of how different NM-II isoforms are elaborately regulated to achieve a cell type-specific ratio and how different isoforms are assembled into a specific architecture to drive cytokinesis in different cell types require extensive investigation.

AUTHOR CONTRIBUTIONS

KW and HO wrote the initial draft. EB revised the manuscript. All authors read and approved the final manuscript.

FUNDING

This work was supported by the NIH Grant GM115420.

ACKNOWLEDGMENTS

We thank Joseph Marquardt and Xi Chen for crtically reading the manuscript.

REFERENCES

Agromayor, M., and Martin-Serrano, J. (2013). Knowing when to cut and run: mechanisms that control cytokinetic abscission. *Trends Cell Biol.* 23, 433–441. doi: 10.1016/j.tcb.2013.04.006

Alonso, Y. A. M., Migliano, S. M., and Teis, D. (2016). ESCRT-III and Vps4: a dynamic multipurpose tool for membrane budding and scission. *FEBS J.* 283, 3288–3302. doi: 10.1111/febs.13688

Alonso-Matilla, R., Thiyagarajan, S., and O'Shaughnessy, B. (2019). Sliding filament and fixed filament mechanisms contribute to ring tension in the cytokinetic contractile ring. *Cytoskeleton* 76, 611–625. doi: 10.1002/cm.21558

Arasada, R., and Pollard, T. D. (2014). Contractile ring stability in *S. pombe* depends on F-BAR protein Cdc15p and Bgs1p transport from the Golgi complex. *Cell Rep.* 8, 1533–1544. doi: 10.1016/j.celrep.2014.07.048

Atcheson, E., Hamilton, E., Pathmanathan, S., Greer, B., Harriott, P., and Timson, D. J. (2011). IQ-motif selectivity in human IQGAP2 and IQGAP3: binding of calmodulin and myosin essential light chain. *Biosci. Rep.* 31, 371–379. doi: 10.1042/bsr20100123

Babkoff, A., Cohen-Kfir, E., Aharon, H., Ronen, D., Rosenberg, M., Wiener, R., et al. (2019). A direct interaction between survivin and myosin II is required for cytokinesis. *J. Cell Sci.* 132:jcs233130. doi: 10.1242/jcs.233130

Bahler, J., Steever, A. B., Wheatley, S., Wang, Y., Pringle, J. R., Gould, K. L., et al. (1998). Role of polo kinase and Mid1p in determining the site of cell division in fission yeast. *J. Cell Biol.* 143, 1603–1616. doi: 10.1083/jcb.143.6.1603

Baker, K., Kirkham, S., Halova, L., Atkin, J., Franz-Wachtel, M., Cobley, D., et al. (2016). TOR complex 2 localises to the cytokinetic actomyosin ring and controls the fidelity of cytokinesis. *J. Cell Sci.* 129, 2613–2624. doi: 10.1242/jcs.190124

Balasubramanian, M. K., Bi, E., and Glotzer, M. (2004). Comparative analysis of cytokinesis in budding yeast, fission yeast and animal cells. *Curr. Biol.* 14, R806–R818.

Balasubramanian, M. K., Mccollum, D., Chang, L., Wong, K. C., Naqvi, N. I., He, X., et al. (1998). Isolation and characterization of new fission yeast cytokinesis mutants. *Genetics* 149, 1265–1275.

Basant, A., and Glotzer, M. (2018). Spatiotemporal regulation of RhoA during cytokinesis. *Curr. Biol.* 28, R570–R580.

Beach, J. R., Bruun, K. S., Shao, L., Li, D., Swider, Z., Remmert, K., et al. (2017). Actin dynamics and competition for myosin monomer govern the sequential amplification of myosin filaments. *Nat. Cell Biol.* 19, 85–93. doi: 10.1038/ncb3463

Beach, J. R., and Egelhoff, T. T. (2009). Myosin II recruitment during cytokinesis independent of centralspindlin-mediated phosphorylation. *J. Biol. Chem.* 284, 27377–27383. doi: 10.1074/jbc.m109.028316

Beach, J. R., Shao, L., Remmert, K., Li, D., Betzig, E., and Hammer, J. A. III (2014). Nonmuscle myosin II isoforms coassemble in living cells. *Curr. Biol.* 24, 1160–1166. doi: 10.1016/j.cub.2014.03.071

Bezanilla, M., Forsburg, S. L., and Pollard, T. D. (1997). Identification of a second myosin-II in *Schizosaccharomyces pombe*: myp2p is conditionally required for cytokinesis. *Mol. Biol. Cell* 8, 2693–2705. doi: 10.1091/mbc.8.12.2693

Bezanilla, M., and Pollard, T. D. (2000). Myosin-II tails confer unique functions in *Schizosaccharomyces pombe*: characterization of a novel myosin-II tail. *Mol. Biol. Cell* 11, 79–91. doi: 10.1091/mbc.11.1.79

Bezanilla, M., Wilson, J. M., and Pollard, T. D. (2000). Fission yeast myosin-II isoforms assemble into contractile rings at distinct times during mitosis. *Curr. Biol.* 10, 397–400. doi: 10.1016/s0960-9822(00)00420-6

Bhavsar-Jog, Y. P., and Bi, E. (2017). Mechanics and regulation of cytokinesis in budding yeast. *Semin. Cell Dev. Biol.* 66, 107–118. doi: 10.1016/j.semcdb.2016.12.010

Bi, E. (2001). Cytokinesis in budding yeast: the relationship between actomyosin ring function and septum formation. *Cell Struct. Funct.* 26, 529–537. doi: 10.1247/csf.26.529

Bi, E., Maddox, P., Lew, D. J., Salmon, E. D., Mcmillan, J. N., Yeh, E., et al. (1998). Involvement of an actomyosin contractile ring in *Saccharomyces cerevisiae* cytokinesis. *J. Cell Biol.* 142, 1301–1312. doi: 10.1083/jcb.142.5.1301

Billington, N., Wang, A., Mao, J., Adelstein, R. S., and Sellers, J. R. (2013). Characterization of three full-length human nonmuscle myosin II paralogs. *J. Biol. Chem.* 288, 33398–33410. doi: 10.1074/jbc.m113.499848

Boyne, J. R., Yosuf, H. M., Bieganowski, P., Brenner, C., and Price, C. (2000). Yeast myosin light chain, Mlc1p, interacts with both IQGAP and class II myosin to effect cytokinesis. *J. Cell Sci.* 113, 4533–4543.

Bretscher, A. (2003). Polarized growth and organelle segregation in yeast: the tracks, motors, and receptors. *J. Cell Biol.* 160, 811–816. doi: 10.1083/jcb.200301035

Buttery, S. M., Yoshida, S., and Pellman, D. (2007). Yeast formins Bni1 and Bnr1 utilize different modes of cortical interaction during the assembly of actin cables. *Mol. Biol. Cell* 18, 1826–1838. doi: 10.1091/mbc.e06-09-0820

Carvalho, A., Desai, A., and Oegema, K. (2009). Structural memory in the contractile ring makes the duration of cytokinesis independent of cell size. *Cell* 137, 926–937. doi: 10.1016/j.cell.2009.03.021

Cheffings, T. H., Burroughs, N. J., and Balasubramanian, M. K. (2019). Actin turnover ensures uniform tension distribution during cytokinetic actomyosin ring contraction. *Mol. Biol. Cell* 30, 933–941. doi: 10.1091/mbc.e18-08-0511

Chen, X., Wang, K., Svitkina, T., and Bi, E. (2020). Critical roles of a RhoGEF-anillin module in septin architectural remodeling during cytokinesis. *Curr. Biol.* 30, 1477–1490.e3.

Chiaruttini, N., Redondo-Morata, L., Colom, A., Humbert, F., Lenz, M., Scheuring, S., et al. (2015). Relaxation of loaded ESCRT-III spiral springs drives membrane deformation. *Cell* 163, 866–879. doi: 10.1016/j.cell.2015.10.017

Clifford, D. M., Wolfe, B. A., Roberts-Galbraith, R. H., Mcdonald, W. H., Yates, J. R. III, and Gould, K. L. (2008). The Clp1/Cdc14 phosphatase contributes to the robustness of cytokinesis by association with anillin-related Mid1. *J. Cell Biol.* 181, 79–88. doi: 10.1083/jcb.200709060

Conti, M. A., and Adelstein, R. S. (2008). Nonmuscle myosin II moves in new directions. *J. Cell Sci.* 121, 11–18. doi: 10.1242/jcs.007112

Conti, M. A., Even-Ram, S., Liu, C., Yamada, K. M., and Adelstein, R. S. (2004). Defects in cell adhesion and the visceral endoderm following ablation of nonmuscle myosin heavy chain II-A in mice. *J. Biol. Chem.* 279, 41263–41266. doi: 10.1074/jbc.c400352200

Cortes, J. C., Konomi, M., Martins, I. M., Munoz, J., Moreno, M. B., Osumi, M., et al. (2007). The (1,3)beta-D-glucan synthase subunit Bgs1p is responsible for the fission yeast primary septum formation. *Mol. Microbiol.* 65, 201–217. doi: 10.1111/j.1365-2958.2007.05784.x

Cortes, J. C., Ramos, M., Konomi, M., Barragan, I., Moreno, M. B., Alcaide-Gavilan, M., et al. (2018). Specific detection of fission yeast primary septum reveals septum and cleavage furrow ingression during early anaphase independent of mitosis completion. *PLoS Genet.* 14:e1007388. doi: 10.1371/journal.pgen.1007388

Davidson, R., Pontasch, J. A., and Wu, J. Q. (2016). Sbg1 is a novel regulator for the localization of the beta-glucan synthase Bgs1 in fission yeast. *PLoS One* 11:e0167043. doi: 10.1371/journal.pone.0167043

Dema, A., Macaluso, F., Sgro, F., Berto, G. E., Bianchi, F. T., Chiotto, A. A., et al. (2018). Citron kinase-dependent F-actin maintenance at midbody secondary ingression sites mediates abscission. *J. Cell Sci.* 131:jcs209080. doi: 10.1242/jcs.209080

Dobbelaere, J., and Barral, Y. (2004). Spatial coordination of cytokinetic events by compartmentalization of the cell cortex. *Science* 305, 393–396. doi: 10.1126/science.1099892

D'souza, V. M., Naqvi, N. I., Wang, H., and Balasubramanian, M. K. (2001). Interactions of Cdc4p, a myosin light chain, with IQ-domain containing proteins in *Schizosaccharomyces pombe*. *Cell Struct. Funct.* 26, 555–565. doi: 10.1247/csf.26.555

Dundon, S. E. R., and Pollard, T. D. (2020). Microtubule nucleation promoters Mto1 and Mto2 regulate cytokinesis in fission yeast. *Mol. Biol. Cell* 31, 1846–1856. doi: 10.1091/mbc.e19-12-0686

Efimova, N., and Svitkina, T. M. (2018). Branched actin networks push against each other at adherens junctions to maintain cell-cell adhesion. *J. Cell Biol.* 217, 1827–1845. doi: 10.1083/jcb.201708103

Elia, N., Sougrat, R., Spurlin, T. A., Hurley, J. H., and Lippincott-Schwartz, J. (2011). Dynamics of endosomal sorting complex required for transport (ESCRT) machinery during cytokinesis and its role in abscission. *Proc. Natl. Acad. Sci. U.S.A.* 108, 4846–4851. doi: 10.1073/pnas.1102714108

Epp, J. A., and Chant, J. (1997). An IQGAP-related protein controls actin-ring formation and cytokinesis in yeast. *Curr. Biol.* 7, 921–929. doi: 10.1016/s0960-9822(06)00411-8

Fang, X., Luo, J., Nishihama, R., Wloka, C., Dravis, C., Travaglia, M., et al. (2010). Biphasic targeting and cleavage furrow ingression directed by the tail of a myosin-II. *J. Cell Biol.* 191, 1333–1350. doi: 10.1083/jcb.201005134

Fehrenbacher, K. L., Yang, H. C., Gay, A. C., Huckaba, T. M., and Pon, L. A. (2004). Live cell imaging of mitochondrial movement along actin cables in budding yeast. *Curr. Biol.* 14, 1996–2004. doi: 10.1016/j.cub.2004.11.004

Feng, Z., Okada, S., Cai, G., Zhou, B., and Bi, E. (2015). MyosinII heavy chain and formin mediate the targeting of myosin essential light chain to the division site before and during cytokinesis. *Mol. Biol. Cell* 26, 1211–1224. doi: 10.1091/mbc.e14-09-1363

Fenix, A. M., and Burnette, D. T. (2018). Assembly of myosin II filament arrays: network Contraction versus Expansion. *Cytoskeleton* 75, 545–549. doi: 10.1002/cm.21487

Fenix, A. M., Taneja, N., Buttler, C. A., Lewis, J., Van Engelenburg, S. B., Ohi, R., et al. (2016). Expansion and concatenation of non-muscle myosin IIA filaments drive cellular contractile system formation during interphase and mitosis. *Mol. Biol. Cell* 27, 1465–1478. doi: 10.1091/mbc.e15-10-0725

Finnigan, G. C., Booth, E. A., Duvalyan, A., Liao, E. N., and Thorner, J. (2015). The carboxy-terminal tails of septins Cdc11 and Shs1 recruit myosin-II binding factor Bni5 to the bud neck in *Saccharomyces cerevisiae*. *Genetics* 200, 843–862. doi: 10.1534/genetics.115.176503

Frenette, P., Haines, E., Loloyan, M., Kinal, M., Pakarian, P., and Piekny, A. (2012). An anillin-Ect2 complex stabilizes central spindle microtubules at the cortex during cytokinesis. *PLoS One* 7:e34888. doi: 10.1371/journal.pone.0034888

Friend, J. E., Sayyad, W. A., Arasada, R., Mccormick, C. D., Heuser, J. E., and Pollard, T. D. (2018). Fission yeast Myo2: molecular organization and diffusion in the cytoplasm. *Cytoskeleton* 75, 164–173. doi: 10.1002/cm.21425

Fujita, M., Sugiura, R., Lu, Y., Xu, L., Xia, Y., Shuntoh, H., et al. (2002). Genetic interaction between calcineurin and type 2 myosin and their involvement in the regulation of cytokinesis and chloride ion homeostasis in fission yeast. *Genetics* 161, 971–981.

Golomb, E., Ma, X., Jana, S. S., Preston, Y. A., Kawamoto, S., Shoham, N. G., et al. (2004). Identification and characterization of nonmuscle myosin II-C, a new member of the myosin II family. *J. Biol. Chem.* 279, 2800–2808. doi: 10.1074/jbc.m309981200

Guizetti, J., Schermelleh, L., Mantler, J., Maar, S., Poser, I., Leonhardt, H., et al. (2011). Cortical constriction during abscission involves helices of ESCRT-III-dependent filaments. *Science* 331, 1616–1620. doi: 10.1126/science.1201847

Heissler, S. M., and Sellers, J. R. (2015). Four things to know about myosin light chains as reporters for non-muscle myosin-2 dynamics in live cells. *Cytoskeleton* 72, 65–70. doi: 10.1002/cm.21212

Henne, W. M., Buchkovich, N. J., Zhao, Y., and Emr, S. D. (2012). The endosomal sorting complex ESCRT-II mediates the assembly and architecture of ESCRT-III helices. *Cell* 151, 356–371. doi: 10.1016/j.cell.2012.08.039

Henson, J. H., Ditzler, C. E., Germain, A., Irwin, P. M., Vogt, E. T., Yang, S., et al. (2017). The ultrastructural organization of actin and myosin II filaments in the contractile ring: new support for an old model of cytokinesis. *Mol. Biol. Cell* 28, 613–623. doi: 10.1091/mbc.e16-06-0466

Heuze, M. L., Sankara Narayana, G. H. N., D'alessandro, J., Cellerin, V., Dang, T., Williams, D. S., et al. (2019). Myosin II isoforms play distinct roles in adherens junction biogenesis. *eLife* 8:e46599.

Hoffman, C. S., Wood, V., and Fantes, P. A. (2015). An ancient yeast for young geneticists: a primer on the *Schizosaccharomyces pombe* model system. *Genetics* 201, 403–423. doi: 10.1534/genetics.115.181503

Hu, C. K., Coughlin, M., and Mitchison, T. J. (2012). Midbody assembly and its regulation during cytokinesis. *Mol. Biol. Cell* 23, 1024–1034. doi: 10.1091/mbc.e11-08-0721

Hu, S., Dasbiswas, K., Guo, Z., Tee, Y. H., Thiagarajan, V., Hersen, P., et al. (2017). Long-range self-organization of cytoskeletal myosin II filament stacks. *Nat. Cell Biol.* 19, 133–141. doi: 10.1038/ncb3466

Huang, Y., Yan, H., and Balasubramanian, M. K. (2008). Assembly of normal actomyosin rings in the absence of Mid1p and cortical nodes in fission yeast. *J. Cell Biol.* 183, 979–988. doi: 10.1083/jcb.200806151

Huckaba, T. M., Gay, A. C., Pantalena, L. F., Yang, H. C., and Pon, L. A. (2004). Live cell imaging of the assembly, disassembly, and actin cable-dependent movement of endosomes and actin patches in the budding yeast, Saccharomyces cerevisiae. *J. Cell Biol.* 167, 519–530. doi: 10.1083/jcb.200404173

Huckaba, T. M., Lipkin, T., and Pon, L. A. (2006). Roles of type II myosin and a tropomyosin isoform in retrograde actin flow in budding yeast. *J. Cell Biol.* 175, 957–969. doi: 10.1083/jcb.200609155

Jana, S. S., Kawamoto, S., and Adelstein, R. S. (2006). A specific isoform of nonmuscle myosin II-C is required for cytokinesis in a tumor cell line. *J. Biol. Chem.* 281, 24662–24670. doi: 10.1074/jbc.m604606200

Karasmanis, E. P., Hwang, D., Nakos, K., Bowen, J. R., Angelis, D., and Spiliotis, E. T. (2019). A septin double ring controls the spatiotemporal organization of the ESCRT machinery in cytokinetic abscission. *Curr. Biol.* 29, 2174–2187. doi: 10.1016/j.cub.2019.05.050

Kitayama, C., Sugimoto, A., and Yamamoto, M. (1997). Type II myosin heavy chain encoded by the *myo2* gene composes the contractile ring during cytokinesis in *Schizosaccharomyces pombe*. *J. Cell Biol.* 137, 1309–1319. doi: 10.1083/jcb.137.6.1309

Kondo, T., Hamao, K., Kamijo, K., Kimura, H., Morita, M., Takahashi, M., et al. (2011). Enhancement of myosin II/actin turnover at the contractile ring induces slower furrowing in dividing HeLa cells. *Biochem. J.* 435, 569–576. doi: 10.1042/bj20100837

Kondo, T., Isoda, R., Ookusa, T., Kamijo, K., Hamao, K., and Hosoya, H. (2013). Aurora B but not rho/MLCK signaling is required for localization of diphosphorylated myosin II regulatory light chain to the midzone in cytokinesis. *PLoS One* 8:e70965. doi: 10.1371/journal.pone.0070965

Kovacs, M., Thirumurugan, K., Knight, P. J., and Sellers, J. R. (2007). Load-dependent mechanism of nonmuscle myosin 2. *Proc. Natl. Acad. Sci. U.S.A.* 104, 9994–9999. doi: 10.1073/pnas.0701181104

Laplante, C., Berro, J., Karatekin, E., Hernandez-Leyva, A., Lee, R., and Pollard, T. D. (2015). Three myosins contribute uniquely to the assembly and constriction of the fission yeast cytokinetic contractile ring. *Curr. Biol.* 25, 1955–1965. doi: 10.1016/j.cub.2015.06.018

Laplante, C., Huang, F., Tebbs, I. R., Bewersdorf, J., and Pollard, T. D. (2016). Molecular organization of cytokinesis nodes and contractile rings by super-resolution fluorescence microscopy of live fission yeast. *Proc. Natl. Acad. Sci. U.S.A.* 113, E5876–E5885.

Laporte, D., Coffman, V. C., Lee, I. J., and Wu, J. Q. (2011). Assembly and architecture of precursor nodes during fission yeast cytokinesis. *J. Cell Biol.* 192, 1005–1021. doi: 10.1083/jcb.201008171

Le Goff, X., Motegi, F., Salimova, E., Mabuchi, I., and Simanis, V. (2000). The *S. pombe rlc*1 gene encodes a putative myosin regulatory light chain that binds the type II myosins myo3p and myo2p. *J. Cell Sci.* 113, 4157–4163.

Lee, P. R., Song, S., Ro, H. S., Park, C. J., Lippincott, J., Li, R., et al. (2002). Bni5p, a septin-interacting protein, is required for normal septin function and cytokinesis in *Saccharomyces cerevisiae*. *Mol. Cell. Biol.* 22, 6906–6920. doi: 10.1128/mcb.22.19.6906-6920.2002

Lin, C. H., Espreafico, E. M., Mooseker, M. S., and Forscher, P. (1997). Myosin drives retrograde F-actin flow in neuronal growth cones. *Biol. Bull.* 192, 183–185. doi: 10.2307/1542600

Lippincott, J., and Li, R. (1998). Sequential assembly of myosin II, an IQGAP-like protein, and filamentous actin to a ring structure involved in budding yeast cytokinesis. *J. Cell Biol.* 140, 355–366. doi: 10.1083/jcb.140.2.355

Liu, J., Wang, H., Mccollum, D., and Balasubramanian, M. K. (1999). Drc1p/Cps1p, a 1,3-beta-glucan synthase subunit, is essential for division septum assembly in *Schizosaccharomyces pombe*. *Genetics* 153, 1193–1203.

Liu, W., Li, L., Ye, H., Chen, H., Shen, W., Zhong, Y., et al. (2017). From Saccharomyces cerevisiae to human: the important gene co-expression modules. *Biomed. Rep.* 7, 153–158. doi: 10.3892/br.2017.941

Liu, X., Shu, S., and Korn, E. D. (2018). Polymerization pathway of mammalian nonmuscle myosin 2s. *Proc. Natl. Acad. Sci. U.S.A.* 115, E7101–E7108.

Lord, M., Laves, E., and Pollard, T. D. (2005). Cytokinesis depends on the motor domains of myosin-II in fission yeast but not in budding yeast. *Mol. Biol. Cell* 16, 5346–5355. doi: 10.1091/mbc.e05-07-0601

Lord, M., and Pollard, T. D. (2004). UCS protein Rng3p activates actin filament gliding by fission yeast myosin-II. *J. Cell Biol.* 167, 315–325. doi: 10.1083/jcb.200404045

Luo, J., Vallen, E. A., Dravis, C., Tcheperegine, S. E., Drees, B. L., and Bi, E. (2004). Identification and functional analysis of the essential and regulatory light chains of the only type II myosin Myo1p in *Saccharomyces cerevisiae*. *J. Cell Biol.* 165, 843–855. doi: 10.1083/jcb.200401040

Ma, X., Jana, S. S., Conti, M. A., Kawamoto, S., Claycomb, W. C., and Adelstein, R. S. (2010). Ablation of nonmuscle myosin II-B and II-C reveals a role for nonmuscle myosin II in cardiac myocyte karyokinesis. *Mol. Biol. Cell* 21, 3952–3962. doi: 10.1091/mbc.e10-04-0293

Ma, X., Kovacs, M., Conti, M. A., Wang, A., Zhang, Y., Sellers, J. R., et al. (2012). Nonmuscle myosin II exerts tension but does not translocate actin in vertebrate cytokinesis. *Proc. Natl. Acad. Sci. U.S.A.* 109, 4509–4514. doi: 10.1073/pnas.1116268109

Maliga, Z., Junqueira, M., Toyoda, Y., Ettinger, A., Mora-Bermudez, F., Klemm, R. W., et al. (2013). A genomic toolkit to investigate kinesin and myosin motor function in cells. *Nat. Cell Biol.* 15, 325–334. doi: 10.1038/ncb2689

Martin-Garcia, R., Arribas, V., Coll, P. M., Pinar, M., Viana, R. A., Rincon, S. A., et al. (2018). Paxillin-mediated recruitment of calcineurin to the contractile ring is required for the correct progression of cytokinesis in fission yeast. *Cell Rep.* 25, 772–783.e4.

Matsuo, T., Otsubo, Y., Urano, J., Tamanoi, F., and Yamamoto, M. (2007). Loss of the TOR kinase Tor2 mimics nitrogen starvation and activates the sexual development pathway in fission yeast. *Mol. Cell. Biol.* 27, 3154–3164. doi: 10.1128/mcb.01039-06

May, K. M., Watts, F. Z., Jones, N., and Hyams, J. S. (1997). Type II myosin involved in cytokinesis in the fission yeast, *Schizosaccharomyces pombe*. *Cell Motil. Cytoskeleton* 38, 385–396. doi: 10.1002/(sici)1097-0169(1997)38:4<385::aid-cm8>3.0.co;2-2

Mccollum, D., Balasubramanian, M. K., Pelcher, L. E., Hemmingsen, S. M., and Gould, K. L. (1995). *Schizosaccharomyces pombe* cdc4+ gene encodes a novel

EF-hand protein essential for cytokinesis. *J. Cell Biol.* 130, 651–660. doi: 10.1083/jcb.130.3.651

Mcdonald, N. A., Lind, A. L., Smith, S. E., Li, R., and Gould, K. L. (2017). Nanoscale architecture of the *Schizosaccharomyces pombe* contractile ring. *eLife* 6:e28865.

Meitinger, F., and Palani, S. (2016). Actomyosin ring driven cytokinesis in budding yeast. *Semin. Cell Dev. Biol.* 53, 19–27. doi: 10.1016/j.semcdb.2016.01.043

Melli, L., Billington, N., Sun, S. A., Bird, J. E., Nagy, A., Friedman, T. B., et al. (2018). Bipolar filaments of human nonmuscle myosin 2-A and 2-B have distinct motile and mechanical properties. *eLife* 7:e32871.

Mendes Pinto, I., Rubinstein, B., Kucharavy, A., Unruh, J. R., and Li, R. (2012). Actin depolymerization drives actomyosin ring contraction during budding yeast cytokinesis. *Dev. Cell* 22, 1247–1260. doi: 10.1016/j.devcel.2012.04.015

Milberg, O., Shitara, A., Ebrahim, S., Masedunskas, A., Tora, M., Tran, D. T., et al. (2017). Concerted actions of distinct nonmuscle myosin II isoforms drive intracellular membrane remodeling in live animals. *J. Cell Biol.* 216, 1925–1936. doi: 10.1083/jcb.201612126

Mishra, M., Kashiwazaki, J., Takagi, T., Srinivasan, R., Huang, Y., Balasubramanian, M. K., et al. (2013). In vitro contraction of cytokinetic ring depends on myosin II but not on actin dynamics. *Nat. Cell Biol.* 15, 853–859. doi: 10.1038/ncb2781

Mitchison, J. M. (1957). The growth of single cells. I. *Schizosaccharomyces pombe*. *Exp. Cell Res.* 13, 244–262.

Motegi, F., Mishra, M., Balasubramanian, M. K., and Mabuchi, I. (2004). Myosin-II reorganization during mitosis is controlled temporally by its dephosphorylation and spatially by Mid1 in fission yeast. *J. Cell Biol.* 165, 685–695. doi: 10.1083/jcb.200402097

Motegi, F., Nakano, K., Kitayama, C., Yamamoto, M., and Mabuchi, I. (1997). Identification of Myo3, a second type-II myosin heavy chain in the fission yeast *Schizosaccharomyces pombe*. *FEBS Lett.* 420, 161–166. doi: 10.1016/s0014-5793(97)01510-x

Motegi, F., Nakano, K., and Mabuchi, I. (2000). Molecular mechanism of myosin-II assembly at the division site in *Schizosaccharomyces pombe*. *J. Cell Sci.* 113, 1813–1825.

Mullins, J. M., and Biesele, J. J. (1973). Cytokinetic activities in a human cell line: the midbody and the intercellular bridge. *Tissue Cell* 5, 47–61. doi: 10.1016/s0040-8166(73)80005-9

Mullins, J. M., and Biesele, J. J. (1977). Terminal phase of cytokinesis in D-985 cells. *J. Cell Biol.* 73, 672–684. doi: 10.1083/jcb.73.3.672

Mulvihill, D. P., and Hyams, J. S. (2003a). Myosin-cell wall interactions during cytokinesis in fission yeast: a framework for understanding plant cytokinesis? *Cell Biol. Int.* 27, 239–240. doi: 10.1016/s1065-6995(02)00311-6

Mulvihill, D. P., and Hyams, J. S. (2003b). Role of the two type II myosins, Myo2 and Myp2, in cytokinetic actomyosin ring formation and function in fission yeast. *Cell Motil. Cytoskeleton* 54, 208–216. doi: 10.1002/cm.10093

Naqvi, N., Wong, K. C. Y., Tang, X., and Balasubramanian, M. K. (2000). Type II myosin regulatory light chain relieves auto-inhibition of myosin-heavy-chain function. *Nat. Cell Biol.* 2, 855–858. doi: 10.1038/35041107

Nguyen, L. T., Swulius, M. T., Aich, S., Mishra, M., and Jensen, G. J. (2018). Coarse-grained simulations of actomyosin rings point to a nodeless model involving both unipolar and bipolar myosins. *Mol. Biol. Cell* 29, 1318–1331. doi: 10.1091/mbc.e17-12-0736

Niederman, R., and Pollard, T. D. (1975). Human platelet myosin. II. In vitro assembly and structure of myosin filaments. *J. Cell Biol.* 67, 72–92. doi: 10.1083/jcb.67.1.72

Nishihama, R., Schreiter, J. H., Onishi, M., Vallen, E. A., Hanna, J., Moravcevic, K., et al. (2009). Role of Inn1 and its interactions with Hof1 and Cyk3 in promoting cleavage furrow and septum formation in *S. cerevisiae*. *J. Cell Biol.* 185, 995–1012. doi: 10.1083/jcb.200903125

Oelz, D. B., Rubinstein, B. Y., and Mogilner, A. (2015). A combination of actin treadmilling and cross-linking drives contraction of random actomyosin arrays. *Biophys. J.* 109, 1818–1829. doi: 10.1016/j.bpj.2015.09.013

Okada, H., Wloka, C., Wu, J. Q., and Bi, E. (2019). Distinct roles of myosin-II isoforms in cytokinesis under normal and stressed conditions. *iScience* 14, 69–87. doi: 10.1016/j.isci.2019.03.014

Ong, K., Wloka, C., Okada, S., Svitkina, T., and Bi, E. (2014). Architecture and dynamic remodelling of the septin cytoskeleton during the cell cycle. *Nat. Commun.* 5:5698.

Padmanabhan, A., Bakka, K., Sevugan, M., Naqvi, N. I., D'souza, V., Tang, X., et al. (2011). IQGAP-related Rng2p organizes cortical nodes and ensures position of cell division in fission yeast. *Curr. Biol.* 21, 467–472. doi: 10.1016/j.cub.2011.01.059

Palani, S., Chew, T. G., Ramanujam, S., Kamnev, A., Harne, S., Chapa, Y. L. B., et al. (2017). Motor activity dependent and independent functions of myosin II contribute to actomyosin ring assembly and contraction in *Schizosaccharomyces pombe*. *Curr. Biol.* 27, 751–757. doi: 10.1016/j.cub.2017.01.028

Palani, S., Srinivasan, R., Zambon, P., Kamnev, A., Gayathri, P., and Balasubramanian, M. K. (2018). Steric hindrance in the upper 50 kDa domain of the motor Myo2p leads to cytokinesis defects in fission yeast. *J. Cell Sci.* 131:jcs205625. doi: 10.1242/jcs.205625

Paoletti, A., and Chang, F. (2000). Analysis of mid1p, a protein required for placement of the cell division site, reveals a link between the nucleus and the cell surface in fission yeast. *Mol. Biol. Cell* 11, 2757–2773. doi: 10.1091/mbc.11.8.2757

Pathmanathan, S., Hamilton, E., Atcheson, E., and Timson, D. J. (2011). The interaction of IQGAPs with calmodulin-like proteins. *Biochem. Soc. Trans.* 39, 694–699. doi: 10.1042/bst0390694

Pecci, A., Ma, X., Savoia, A., and Adelstein, R. S. (2018). MYH9: structure, functions and role of non-muscle myosin IIA in human disease. *Gene* 664, 152–167. doi: 10.1016/j.gene.2018.04.048

Pelham, R. J., and Chang, F. (2002). Actin dynamics in the contractile ring during cytokinesis in fission yeast. *Nature* 419, 82–86. doi: 10.1038/nature00999

Piekny, A. J., and Glotzer, M. (2008). Anillin is a scaffold protein that links RhoA, actin, and myosin during cytokinesis. *Curr. Biol.* 18, 30–36. doi: 10.1016/j.cub.2007.11.068

Pollard, L. W., Bookwalter, C. S., Tang, Q., Krementsova, E. B., Trybus, K. M., and Lowey, S. (2017). Fission yeast myosin Myo2 is down-regulated in actin affinity by light chain phosphorylation. *Proc. Natl. Acad. Sci. U.S.A.* 114, E7236–E7244.

Pollard, T. D., and O'Shaughnessy, B. (2019). Molecular mechanism of cytokinesis. *Annu. Rev. Biochem.* 88, 661–689. doi: 10.1146/annurev-biochem-062917-012530

Pollard, T. D., Thomas, S. M., and Niederman, R. (1974). Human platelet myosin. I. Purification by a rapid method applicable to other nonmuscle cells. *Anal. Biochem.* 60, 258–266. doi: 10.1016/0003-2697(74)90152-3

Pollard, T. D., and Wu, J. Q. (2010). Understanding cytokinesis: lessons from fission yeast. *Nat. Rev. Mol. Cell Biol.* 11, 149–155. doi: 10.1038/nrm2834

Proctor, S. A., Minc, N., Boudaoud, A., and Chang, F. (2012). Contributions of turgor pressure, the contractile ring, and septum assembly to forces in cytokinesis in fission yeast. *Curr. Biol.* 22, 1601–1608. doi: 10.1016/j.cub.2012.06.042

Pruyne, D., Gao, L., Bi, E., and Bretscher, A. (2004). Stable and dynamic axes of polarity use distinct formin isoforms in budding yeast. *Mol. Biol. Cell* 15, 4971–4989. doi: 10.1091/mbc.e04-04-0296

Ramos, M., Cortes, J. C. G., Sato, M., Rincon, S. A., Moreno, M. B., Clemente-Ramos, J. A., et al. (2019). Two *S. pombe* septation phases differ in ingression rate, septum structure, and response to F-actin loss. *J. Cell Biol.* 218, 4171–4194. doi: 10.1083/jcb.201808163

Rappaport, R. (1996). "Cytokinesis in animal cells," in *Developmental and Cell Biology Series*, eds P. W. Barlow, J. B. Bard, P. B. Green, and D. L. Kirk (Cambridge: Cambridge University Press).

Renshaw, M. J., Liu, J., Lavoie, B. D., and Wilde, A. (2014). Anillin-dependent organization of septin filaments promotes intercellular bridge elongation and Chmp4B targeting to the abscission site. *Open Biol.* 4:130190. doi: 10.1098/rsob.130190

Rodriguez, J. R., and Paterson, B. M. (1990). Yeast myosin heavy chain mutant: maintenance of the cell type specific budding pattern and the normal deposition of chitin and cell wall components requires an intact myosin heavy chain gene. *Cell Motil. Cytoskeleton* 17, 301–308. doi: 10.1002/cm.970170405

Ronen, D., and Ravid, S. (2009). Myosin II tailpiece determines its paracrystal structure, filament assembly properties, and cellular localization. *J. Biol. Chem.* 284, 24948–24957. doi: 10.1074/jbc.m109.023754

Samejima, I., Miller, V. J., Rincon, S. A., and Sawin, K. E. (2010). Fission yeast Mto1 regulates diversity of cytoplasmic microtubule organizing centers. *Curr. Biol.* 20, 1959–1965. doi: 10.1016/j.cub.2010.10.006

Sandquist, J. C., and Means, A. R. (2008). The C-terminal tail region of nonmuscle myosin II directs isoform-specific distribution in migrating cells. *Mol. Biol. Cell* 19, 5156–5167. doi: 10.1091/mbc.e08-05-0533

Schmidt, M., Bowers, B., Varma, A., Roh, D.-H., and Cabib, E. (2002). In budding yeast, contraction of the actomyosin ring and formation of the primary septum at cytokinesis depend on each other. *J. Cell Sci.* 115, 293–302.

Schroeder, T. E. (1972). The contractile ring II: determining its brief existence, volumetric changes, and vital role in cleaving arbacia eggs. *J. Cell Biol.* 53, 419–434.

Sethi, K., Palani, S., Cortes, J. C., Sato, M., Sevugan, M., Ramos, M., et al. (2016). A new membrane protein Sbg1 links the contractile ring apparatus and septum synthesis machinery in fission yeast. *PLoS Genet.* 12:e1006383. doi: 10.1371/journal.pgen.1006383

Shannon, K. B., and Li, R. (2000). A myosin light chain mediates the localization of the budding yeast IQGAP-like protein during contractile ring formation. *Curr. Biol.* 10, 727–730. doi: 10.1016/s0960-9822(00)00539-x

Shutova, M. S., Spessott, W. A., Giraudo, C. G., and Svitkina, T. (2014). Endogenous species of mammalian nonmuscle myosin IIA and IIB include activated monomers and heteropolymers. *Curr. Biol.* 24, 1958–1968. doi: 10.1016/j.cub.2014.07.070

Shutova, M. S., and Svitkina, T. M. (2018). Mammalian nonmuscle myosin II comes in three flavors. *Biochem. Biophys. Res. Commun.* 506, 394–402. doi: 10.1016/j.bbrc.2018.03.103

Sipiczki, M. (2000). Where does fission yeast sit on the tree of life? *Genome Biol.* 1:REVIEWS1011.

Sohrmann, M., Fankhauser, C., Brodbeck, C., and Simanis, V. (1996). The *dmf1/mid1* gene is essential for correct positioning of the division septum in fission yeast. *Genes Dev.* 10, 2707–2719. doi: 10.1101/gad.10.21.2707

Stachowiak, M. R., Laplante, C., Chin, H. F., Guirao, B., Karatekin, E., Pollard, T. D., et al. (2014). Mechanism of cytokinetic contractile ring constriction in fission yeast. *Dev. Cell* 29, 547–561. doi: 10.1016/j.devcel.2014.04.021

Stark, B. C., James, M. L., Pollard, L. W., Sirotkin, V., and Lord, M. (2013). UCS protein Rng3p is essential for myosin-II motor activity during cytokinesis in fission yeast. *PLoS One* 8:e79593. doi: 10.1371/journal.pone.0079593

Stevens, R. C., and Davis, T. N. (1998). Mlc1p is a light chain for the unconventional myosin Myo2p in *Saccharomyces cerevisiae*. *J. Cell Biol.* 142, 711–722. doi: 10.1083/jcb.142.3.711

Straight, A. F., Cheung, A., Limouze, J., Chen, I., Westwood, N. J., Sellers, J. R., et al. (2003). Dissecting temporal and spatial control of cytokinesis with a myosin II Inhibitor. *Science* 299, 1743–1747. doi: 10.1126/science.1081412

Sugiura, R., Toda, T., Shuntoh, H., Yanagida, M., and Kuno, T. (1998). pmp1+, a suppressor of calcineurin deficiency, encodes a novel MAP kinase phosphatase in fission yeast. *EMBO J.* 17, 140–148. doi: 10.1093/emboj/17.1.140

Swaminathan, V., Kalappurakkal, J. M., Mehta, S. B., Nordenfelt, P., Moore, T. I., Koga, N., et al. (2017). Actin retrograde flow actively aligns and orients ligand-engaged integrins in focal adhesions. *Proc. Natl. Acad. Sci. U.S.A.* 114, 10648–10653. doi: 10.1073/pnas.1701136114

Takaine, M., Numata, O., and Nakano, K. (2014). Fission yeast IQGAP maintains F-actin-independent localization of myosin-II in the contractile ring. *Genes Cells* 19, 161–176. doi: 10.1111/gtc.12120

Takaine, M., Numata, O., and Nakano, K. (2015). An actin-myosin-II interaction is involved in maintaining the contractile ring in fission yeast. *J. Cell Sci.* 128, 2903–2918. doi: 10.1242/jcs.171264

Tan, J. L., Ravid, S., and Spudich, J. A. (1992). Control of nonmuscle myosins by phosphorylation. *Annu. Rev. Biochem.* 61, 721–759. doi: 10.1146/annurev.bi.61.070192.003445

Taneja, N., Bersi, M. R., Baillargeon, S. M., Fenix, A. M., Cooper, J. A., Ohi, R., et al. (2020). Precise tuning of cortical contractility regulates cell shape during cytokinesis. *Cell Rep.* 31:107477. doi: 10.1016/j.celrep.2020.03.041

Thiyagarajan, S., Munteanu, E. L., Arasada, R., Pollard, T. D., and O'shaughnessy, B. (2015). The fission yeast cytokinetic contractile ring regulates septum shape and closure. *J. Cell Sci.* 128, 3672–3681. doi: 10.1242/jcs.166926

Thiyagarajan, S., Wang, S., and O'shaughnessy, B. (2017). A node organization in the actomyosin contractile ring generates tension and aids stability. *Mol. Biol. Cell* 28, 3286–3297. doi: 10.1091/mbc.e17-06-0386

Titus, M. A. (2017). Growing, splitting and stacking myosin II filaments. *Nat. Cell Biol.* 19, 77–79. doi: 10.1038/ncb3468

Trybus, K. M. (1991). Assembly of cytoplasmic and smooth muscle myosins. *Curr. Opin. Cell Biol.* 3, 105–111. doi: 10.1016/0955-0674(91)90172-u

Tullio, A. N., Accili, D., Ferrans, V. J., Yu, Z. X., Takeda, K., Grinberg, A., et al. (1997). Nonmuscle myosin II-B is required for normal development of the mouse heart. *Proc. Natl. Acad. Sci. U.S.A.* 94, 12407–12412. doi: 10.1073/pnas.94.23.12407

Vallen, E. A., Caviston, J., and Bi, E. (2000). Roles of Hof1p, Bni1p, Bnr1p, and Myo1p in cytokinesis in *Saccharomyces cerevisiae*. *Mol. Biol. Cell* 11, 593–611. doi: 10.1091/mbc.11.2.593

Vavylonis, D., Wu, J. Q., Hao, S., O'shaughnessy, B., and Pollard, T. D. (2008). Assembly mechanism of the contractile ring for cytokinesis by fission yeast. *Science* 319, 97–100. doi: 10.1126/science.1151086

Verkhovsky, A. B., Svitkina, T. M., and Borisy, G. G. (1995). Myosin II filament assemblies in the active lamella of fibroblasts: their morphogenesis and role in the formation of actin filament bundles. *J. Cell Biol.* 131, 989–1002. doi: 10.1083/jcb.131.4.989

Verkhovsky, A. B., Svitkina, T. M., and Borisy, G. G. (1999). Network contraction model for cell translocation and retrograde flow. *Biochem. Soc. Symp.* 65, 207–222.

Verma, V., Mogilner, A., and Maresca, T. J. (2019). Classical and emerging regulatory mechanisms of Cytokinesis in animal cells. *Biology* 8:55. doi: 10.3390/biology8030055

Verplank, L., and Li, R. (2005). Cell cycle-regulated trafficking of Chs2 controls actomyosin ring stability during cytokinesis. *Mol. Biol. Cell* 16, 2529–2543. doi: 10.1091/mbc.e04-12-1090

Vicente-Manzanares, M., Ma, X., Adelstein, R. S., and Horwitz, A. R. (2009). Non-muscle myosin II takes centre stage in cell adhesion and migration. *Nat. Rev. Mol. Cell Biol.* 10, 778–790. doi: 10.1038/nrm2786

Wang, K., Wloka, C., and Bi, E. (2019). Non-muscle myosin-II is required for the generation of a constriction site for subsequent abscission. *iScience* 13, 69–81. doi: 10.1016/j.isci.2019.02.010

Watanabe, S., Ando, Y., Yasuda, S., Hosoya, H., Watanabe, N., Ishizaki, T., et al. (2008). mDia2 induces the actin scaffold for the contractile ring and stabilizes its position during cytokinesis in NIH 3T3 cells. *Mol. Biol. Cell* 19, 2328–2338. doi: 10.1091/mbc.e07-10-1086

Watts, F. Z., Shiels, G., and Orr, E. (1987). The yeast *MYO1* gene encoding a myosin-like protein required for cell division. *EMBO J.* 6, 3499–3505. doi: 10.1002/j.1460-2075.1987.tb02675.x

Weissbach, L., Bernards, A., and Herion, D. W. (1998). Binding of myosin essential light chain to the cytoskeleton-associated protein IQGAP1. *Biochem. Biophys. Res. Commun.* 251, 269–276. doi: 10.1006/bbrc.1998.9371

Willet, A. H., Mcdonald, N. A., and Gould, K. L. (2015). Regulation of contractile ring formation and septation in *Schizosaccharomyces pombe*. *Curr. Opin. Microbiol.* 28, 46–52. doi: 10.1016/j.mib.2015.08.001

Wloka, C., Vallen, E. A., Thé, L., Fang, X., Oh, Y., and Bi, E. (2013). Immobile myosin-II plays a scaffolding role during cytokinesis in budding yeast. *J. Cell Biol.* 200, 271–286. doi: 10.1083/jcb.201208030

Wu, J. Q., Kuhn, J. R., Kovar, D. R., and Pollard, T. D. (2003). Spatial and temporal pathway for assembly and constriction of the contractile ring in fission yeast cytokinesis. *Dev. Cell* 5, 723–734. doi: 10.1016/s1534-5807(03)00324-1

Wu, J. Q., and Pollard, T. D. (2005). Counting cytokinesis proteins globally and locally in fission yeast. *Science* 310, 310–314. doi: 10.1126/science.1113230

Wu, J. Q., Sirotkin, V., Kovar, D. R., Lord, M., Beltzner, C. C., Kuhn, J. R., et al. (2006). Assembly of the cytokinetic contractile ring from a broad band of nodes in fission yeast. *J. Cell Biol.* 174, 391–402. doi: 10.1083/jcb.200602032

Yamamoto, K., Otomo, K., Nemoto, T., Ishihara, S., Haga, H., Nagasaki, A., et al. (2019). Differential contributions of nonmuscle myosin IIA and IIB to cytokinesis in human immortalized fibroblasts. *Exp. Cell Res.* 376, 67–76. doi: 10.1016/j.yexcr.2019.01.020

Yang, Q., Zhang, X. F., Pollard, T. D., and Forscher, P. (2012). Arp2/3 complex-dependent actin networks constrain myosin II function in driving retrograde actin flow. *J. Cell Biol.* 197, 939–956. doi: 10.1083/jcb.201111052

Yi, J., Wu, X. S., Crites, T., and Hammer, J. A. III (2012). Actin retrograde flow and actomyosin II arc contraction drive receptor cluster dynamics at the immunological synapse in Jurkat T cells. *Mol. Biol. Cell* 23, 834–852. doi: 10.1091/mbc.e11-08-0731

Yonetani, A., Lustig, R. J., Moseley, J. B., Takeda, T., Goode, B. L., and Chang, F. (2008). Regulation and targeting of the fission yeast formin cdc12p in cytokinesis. *Mol. Biol. Cell* 19, 2208–2219. doi: 10.1091/mbc.e07-07-0731

Yuce, O., Piekny, A., and Glotzer, M. (2005). An ECT2-centralspindlin complex regulates the localization and function of RhoA. *J. Cell Biol.* 170, 571–582. doi: 10.1083/jcb.200501097

Zhang, H. M., Ji, H. H., Ni, T., Ma, R. N., Wang, A., and Li, X. D. (2017). Characterization of blebbistatin inhibition of smooth muscle myosin and nonmuscle myosin-2. *Biochemistry* 56, 4235–4243. doi: 10.1021/acs.biochem.7b00311

Zhou, M., and Wang, Y. L. (2008). Distinct pathways for the early recruitment of myosin II and actin to the cytokinetic furrow. *Mol. Biol. Cell* 19, 318–326. doi: 10.1091/mbc.e07-08-0783

Zhou, Z., Munteanu, E. L., He, J., Ursell, T., Bathe, M., Huang, K. C., et al. (2015). The contractile ring coordinates curvature-dependent septum assembly during fission yeast cytokinesis. *Mol. Biol. Cell* 26, 78–90. doi: 10.1091/mbc.e14-10-1441

Zimmermann, D., Homa, K. E., Hocky, G. M., Pollard, L. W., De La Cruz, E. M., Voth, G. A., et al. (2017). Mechanoregulated inhibition of formin facilitates contractile actomyosin ring assembly. *Nat. Commun.* 8:703.

Conflict of Interest: The authors declare that the research was conducted in the absence of any commercial or financial relationships that could be construed as a potential conflict of interest.

Advantages of publishing in Frontiers

OPEN ACCESS
Articles are free to read for greatest visibility and readership

FAST PUBLICATION
Around 90 days from submission to decision

HIGH QUALITY PEER-REVIEW
Rigorous, collaborative, and constructive peer-review

TRANSPARENT PEER-REVIEW
Editors and reviewers acknowledged by name on published articles

Frontiers
Avenue du Tribunal-Fédéral 34
1005 Lausanne | Switzerland

Visit us: www.frontiersin.org
Contact us: frontiersin.org/about/contact

REPRODUCIBILITY OF RESEARCH
Support open data and methods to enhance research reproducibility

DIGITAL PUBLISHING
Articles designed for optimal readership across devices

FOLLOW US
@frontiersin

IMPACT METRICS
Advanced article metrics track visibility across digital media

EXTENSIVE PROMOTION
Marketing and promotion of impactful research

LOOP RESEARCH NETWORK
Our network increases your article's readership